



RESEARCH & DEVELOPMENT

Measurement and Modeling of Spatial Variability in Locomotive Fuel Use and Emission Rates for Piedmont Passenger Rail Service

H. Christopher Frey, Ph.D.

Nikhil Rastogi, Ph.D.

Tongchuan Wei, Ph.D.

North Carolina State University

Department of Civil, Construction, and Environmental

Engineering

Raleigh, NC 27695-7908

NCDOT Project 2020-07

FHWA/NC/2020-07

January 2023

Technical Report Documentation Page

1. Report No. FHWA/NC/2020-07	2. Government Accession No.	3. Recipient's Catalog No.	
4. Title and Subtitle Measurement and Modeling of Spatial Variability in Locomotive Fuel Use and Emission Rates for Piedmont Passenger Rail Service		5. Report Date January 2023	
		6. Performing Organization Code	
7. Author(s) H. Christopher Frey, PhD Nikhil Rastogi, PhD Tongchuan Wei, PhD		8. Performing Organization Report No.	
9. Performing Organization Name and Address North Carolina State University Department of Civil, Construction, and Environmental Engineering Raleigh, North Carolina 27695-7908		10. Work Unit No. (TRAIS)	
		11. Contract or Grant No. FHWA/NC/2020-07	
12. Sponsoring Agency Name and Address North Carolina Department of Transportation Research and Development Unit 104 Fayetteville Street Raleigh, North Carolina 27601		13. Type of Report and Period Covered Final Report Final Report (August 1, 2019 – December 31, 2022)	
		14. Sponsoring Agency Code RP 2020-07	
Supplementary Notes:			
16. Abstract The objectives of this work are to: (1) quantify spatial variability in locomotive fuel use and emission rates (FUERs) and identify factors differentiating emission hotspots from non-hotspots; (2) predict spatially varying real-world locomotive FUERs; (3) develop a software tool for estimating the fuel use and emissions of a typical Piedmont train operation; (4) develop a study design for locomotive exhaust measurements with the Blended After Treatment System (BATS); and (5) develop a study design for quantification of passenger train in-cabin pollutant concentrations. Locomotive FUERs, including CO ₂ , CO, hydrocarbon, NO _x , and particulate matter emission rates, and train speed, train acceleration, track grade, and track curvature were quantified based on over-the-rail measurements, using portable emission measurement systems, for diesel passenger rail service on the Amtrak Piedmont route. A locomotive fuel use and emissions model was developed to estimate FUERs at high spatial resolution. The model was calibrated based on locomotive power demand (LPD), which accounts for the physics of resistive forces opposing train motion such as acceleration, track grade, and track curvature. The model was integrated into the Piedmont Passenger Train Fuel Use and Emission Estimator Software (PPTFUEES) tool in Microsoft Excel. Results show that there is large variability in FUERs over short distances. For example, FUERs among a pair of adjacent 0.25 mile track segments differed on average by a factor of 2 to 60, depending on location and pollutant species. Emission hotspots comprised only 20% of the route length but comprised 40% to 50% of the total fuel use and emissions along the entire route. Acceleration, grade, and speed are key factors in distinguishing segments as hotspots versus non-hotspots. The LPD-based model is capable of predicting precise and accurate FUERs at high spatial resolution. Acceleration, grade, and drag resistances are the highest relative contributors to LPD regardless of train consist. Real-world train speed trajectories are identified that reduce trip fuel use and emissions by 13% to 49% compared to the average. Trip fuel use and emissions can be reduced by dispatching energy-efficient and low-emitting locomotives and operating with 20% blend of biodiesel on trajectories with low LPD. The PPTFUEES is able to estimate fuel use and emissions for each station-to-station segment and the entire route of a typical Piedmont train operation. The software user manual and examples of applications are provided in this final report. In addition, this report also includes a study design for railyard and over-the-rail locomotive exhaust measurements with BATS, and a study design for measurements and modeling of in-cabin air quality for passenger rail.			
17. Key Words Locomotive emissions, fuel consumption, emission hotspots, spatial variability, locomotive power demand, passenger rail		18. Distribution Statement	
19. Security Classif. (of this report) Unclassified	20. Security Classif. (of this page) Unclassified	21. No. of Pages 339	22. Price

Acknowledgement

This work was supported as research project RP 2020-07 by the North Carolina Department of Transportation. This work was made possible by the in-kind technical and logistical support from Lynn Harris, Curtis McDowell, and Derek Ward from McDowell Engineers and the staff at RailPlan International, Inc. Locomotives in over-the-rail service were operated by Amtrak. Dr. Andrew Grieshop in the Department of Civil, Construction, and Environmental Engineering at North Carolina State University played an administrative role on the project since late May in 2022.

Disclaimer

The authors are responsible for the facts and the accuracy of the data presented herein. The contents do not necessarily reflect the official views or policies of either the North Carolina Department of Transportation or the Federal Highway Administration.

Table of Contents

Acknowledgement	ii
Disclaimer	ii
List of Tables	vi
List of Figures	viii
1.0 Introduction	1
1.1 Background.....	1
1.2 Research Needs.....	2
1.3 Objectives	3
1.4 Overview of the Report.....	3
1.5 References Cited in Chapter 1	4
2.0 Characterizing Fuel Use and Emissions Hotspots for a Diesel-operated Passenger Rail Service	7
2.1 Introduction.....	7
2.2 Methods	8
2.2.1 Field Study Design.....	8
2.2.2 Data Analysis	10
2.3 Results and Discussion	13
2.3.1 Segment-Average Activity and Infrastructure Variables.....	13
2.3.2 Segment-Average Fuel Use and Emission Rates.....	15
2.3.3 Hotspot Classification and Location.....	17
2.3.4 Potential Explanatory Variables	17
2.4 Summary of Supporting Information.....	23
2.5 References Cited in Chapter 2	24
3.0 Modeling Spatial Variability in Locomotive Fuel Use and Emission Rates based on Real-World Measurements	30
3.1 Introduction.....	30
3.2 Methods	31
3.2.1 Legacy Data	31
3.2.2 Locomotive Power Demand	35
3.2.3 Modeling Fuel Use and Emission Rates	36
3.2.4 Contribution of Resistive Forces	36

3.2.5 Identification of Emissions Hotspots	37
3.2.6 Identification of Trajectories with Low Fuel Use and Emissions.....	37
3.2.7 Comparison of Delayed versus On-Time Trips	38
3.2.8 Inter-Locomotive, -Consist, and -Fuel Variability	38
3.3 Results and Discussion	39
3.3.1 Locomotive Power Demand Model Calibration and Evaluation.....	39
3.3.2 Contribution of Resistive Forces	43
3.3.3 Identification of Emissions Hotspots.....	43
3.3.4 Identification of Trajectories with Low Fuel Use and Emissions.....	47
3.3.5 Comparison of Delayed versus On-Time Trips.....	48
3.3.6 Inter-Locomotive, -Consist, and -Fuel Variability	48
3.4 Conclusions.....	50
3.5 Summary of Supporting information	51
3.6 References Cited in Chapter 3	51
4.0 Development of a Locomotive Power Demand Software to Estimate Train Fuel Use and Emissions	55
4.1 Introduction.....	55
4.2 System Requirements.....	55
4.3 Calibration Data	56
4.4 Evaluation of the Software Tool.....	57
4.5 Data Input.....	63
4.6 Results Output.....	65
4.7 Software Applications.....	70
4.8 Summary of Supporting Information.....	72
4.9 References Cited in Chapter 4	72
5.0 Study Design for Evaluation of the Effect of the Retrofitted Blended After Treatment System on Locomotive Exhaust Emissions.....	73
5.1 Introduction.....	73
5.2 Benchmarking Two PEMS	73
5.3 Railyard Measurement Study Design	76
5.4 Over-the-Rail Measurement Study Design.....	80
5.5 Summary of Supporting Information.....	81
5.6 References Cited in Chapter 5	81

6.0 Study Design and Modeling Framework for Quantifying Train In-Cabin Air Quality.....	82
6.1 Introduction.....	82
6.2 Railyard Measurement Study Design	82
6.3 Analytical Modeling Framework	83
6.3.1 Methods.....	83
6.3.2 Model Application	86
6.4 Recommendation for Future Work	88
6.5 References Cited in Chapter 6	88
7.0 Conclusions.....	90
7.1 Key Findings	90
7.2 Conclusions.....	91
7.3 Recommendations.....	92
Appendices.....	94
Appendix A. Supporting Information for Chapter 2.....	95
Appendix B. Supporting Information for Chapter 3.....	191
Appendix C. User Manual for Piedmont Passenger Train Fuel Use and Emission Estimator Software	289
Appendix D. Supporting Information for Chapter 5.....	311

List of Tables

Table 3-1. Definitions of Terms for Amtrak-Operated Piedmont Route Passenger Locomotive Consist Types, Emission Hotspots, and Confusion Metrics for Model Performance.	33
Table 3-2. Combinations of Locomotives, Consists, and Fuels (LCF) Measured Over-The-Rail During Revenue-Generating Amtrak-Operated Piedmont Passenger Rail Service	34
Table 3-3. Verification of the Locomotive Power Demand Model to Identify Absolute and Relative Hotspots Based on the Number of True Positives, True Negatives, False Positives, False Negatives, Accuracy, and Precision.	46
Table 4-1. Calibrated Mean Fuel Use and Emission Rates for Sub-Models 1, 2, and 4 based on Measured One-Way Trips for Each Combinations of Locomotives, Consists, and Fuels (LCFs).....	58
Table 4-2. Calibrated Sub-Model 3 Regression Parameters for Fuel Use and Emission Rates based on All One-Way Trips for Measured Combinations of Locomotives, Consists, and Fuels.	59
Table 4-3. Locomotives, Consists, and Fuels (LCF) ID in the Piedmont Passenger Train Fuel Use and Emission Estimator Software.	63
Table 4-4. Train Speed Trajectory ID in the Piedmont Passenger Train Fuel Use and Emission Estimator Software.	64
Table 4-5. Example Output: Train Activity for Each Station-to-Station Segment and Whole Trip for Trajectory ID 15.	66
Table 4-6. Example Output: Total Fuel Use and Emissions for Each Station-to-Station Segment and Whole Trip for Locomotives, Consists, and Fuels (LCF) ID 1 Operating on Speed Trajectory ID 15.....	67
Table 4-7. Example Output: Fuel Economy and Distance-Based Emission Rates for Each Station-to-Station Segment and Whole Trip for Locomotives, Consists, and Fuels (LCF) ID 1 Operating on Speed Trajectory ID 15.....	68
Table 4-8. Example Output: Time-Based Emission Rates for Each Station-to-Station Segment and Whole Trip for Locomotives, Consists, and Fuels (LCF) ID 1 Operating on Speed Trajectory ID 15.....	69
Table 4-9. Example Output: Fuel-Based Emission Rates for Each Station-to-Station Segment and Whole Trip for Locomotives, Consists, and Fuels (LCF) ID 1 Operating on Speed Trajectory ID 15.....	69
Table 4-10. An Example Template for Comparisons of Total Fuel Use and Emissions for a Given Species and a Selected Train Speed Trajectory among 12 Locomotives, Consists, and Fuels (LCFs).....	70

Table 4-11. An Example Template for Comparisons of Total Fuel Use and Emissions for a Given Species and a Selected Locomotive, Consist, and Fuel (LCF) among 45 Speed Trajectories.	71
Table 5-1. Railyard Test Schedule for Prime Mover Engine for One Replicate	78
Table 5-2. Portable Emission Measurement Systems (PEMS) Instrument Assignments for Six Replicates of the Test Schedule.....	79
Table 6-1. Railyard Air Quality Test Schedule for Prime Mover Engine for One Replicate.....	83
Table 6-2. Assumptions on In-Cabin Air Quality Model Input Parameters and Values for the Example Application of a Railyard Test.....	87

List of Figures

Figure 2-1. Segment-Average Speed, Acceleration, Grade and Curvature for the Piedmont Passenger Rail Service Between Raleigh, NC, and Charlotte, NC in the Eastbound Direction based on 14 One-Way Trips.	14
Figure 2-2. Segment-Average Emission Rates for the Piedmont Passenger Rail Service Between Raleigh, NC and Charlotte, NC in the Eastbound Direction based on 14 One-Way Trips.	16
Figure 2-3. Segment-Average Data for Spatially Varying and Average Rates for the Piedmont Passenger Rail Service between Raleigh, NC and Charlotte, NC in Each Travel Direction Based on 35 One-Way Trips.	19
Figure 2-4. Validation of the Classification and Regression Tree-based NO _x and PM Relative Hotspot Prediction Simplified Model with Dynamic Variables including Segment-Average Speed, Acceleration, Grade, and Curvature as Explanatory Variables.	21
Figure 3-1. Variation of Measured Fuel Use Rates, and Emission Rates of NO _x and PM with 12-Second Backwards Moving Average Locomotive Power Demand for 12 combinations of Locomotives, Consists, and Fuels.....	40
Figure 3-2. Calibrated Average Sub-Model 3 Modal Emission Rates of 12 Combinations of Locomotives, Consists, and Fuels.	42
Figure 3-3. Example Time Plot of Variation in Train Speed, Acceleration, Track Grade, and Curvature and Their Effects on Positive Power Demand for Single Locomotive Consist of NC 1797 Operated on B20 from Cary, NC to Durham, NC.....	44
Figure 3-4. Comparison of Modeled versus Measured Fuel Use, NO _x Emissions, and PM Emissions Absolute Hotspots and Non-Hotspots.	45
Figure 3-5. Normalized Model Estimated Trip Emissions for an Average Locomotives, Consists, and Fuels for Each of 45 Complete Trajectories.....	47
Figure 4-1. A Screen Capture of the Piedmont Passenger Train Fuel Use and Emission Estimator Software.	56
Figure 4-2. The Conceptual Diagram of the Key Components of the Piedmont Passenger Train Fuel Use and Emission Estimator Software.....	56
Figure 4-3. Calibrated Average Sub-Model 3 Modal Emission Rates of 12 Combinations of Locomotives, Consists, and Fuels.	62
Figure 5-1. A Schematic Diagram of the Measurement Setup for Benchmark Comparison of Two Portable Emission Measurement Systems (PEMS).	74
Figure 5-2. Benchmarking Axion PEMS Concentration Measurements for Bias-Correction for Future Planned Measurements with Two PEMS.	75
Figure 5-3. Railyard Measurement of Locomotive Prime Mover Engine Emissions Using Portable Emissions Measurement Systems.	76

Figure 5-4. Configuration of Previously Installed Blended After-Treatment System (BATS) Exhaust Channels on Locomotive NC 1859.....	77
Figure 5-5. Conceptual Diagram of Locomotive Prime Mover Engine (PME), Head End Power (HEP) Engine, Blended After-Treatment System (BATS), as well as PEMS Measurement Locations to Sample PME Raw Exhaust, HEP Engine Raw Exhaust, and BATS Outlet Treated Exhaust.	79
Figure 5-6. Schematic Diagram of the Exhaust Sample Hoses Routing Plan and Instrument Locations for Over-The-Rail Measurements.	80
Figure 6-1. An Example of Model-Estimated In-Cabin PM _{2.5} Concentrations Inside a Passenger Car Varied with Time from the Locomotive Prime Mover Engine Start to Off for a Railyard Test.	88

CHAPTER 1: Introduction

This report focuses on development and application of models for inter-city passenger train fuel use and emissions based on real-world data from real-world train emission measurements using Portable Emission Measurement Systems. This report also provides recommendations for future measurements of retrofitted emission controls and implications of locomotive emissions for in-cabin air quality.

1.1 Background

In 2020, the National Railroad Passenger Corporation (Amtrak) provided intercity passenger service over 20,604 miles of routes with an active fleet of 276 diesel locomotives averaging 23 years of age (Amtrak, 2020). Additionally, 731 active diesel-powered locomotives averaging 26 years of age provided commuter rail service in 2018 (APTA, 2020). Thus, the U.S. intercity passenger rail service is comprised of a large share of older diesel locomotives. With rebuilds, these locomotives can be operational for several decades (EPA, 1998). Passenger travel via diesel-powered trains is typically more energy-efficient versus light-duty gasoline vehicles (LDGVs), transit buses, and aircraft (Davis and Boundy, 2018; NCRRP, 2015; Sprung et al., 2018). However, per passenger-mile emission rates of oxides of nitrogen (NO_x) and particulate matter (PM) for older diesel locomotive engines are typically higher than for LDGVs (Graver and Frey, 2016). The US Environmental Protection Agency (EPA) regulates NO_x and PM because of their adverse human health impacts (EPA, 2016, 2009).

Several studies demonstrated methods to modify train activity and were focused on reductions in energy use for a given trip (Feng, 2011; Kim and Chien, 2010; Yuan et al., 2019; Yuan and Frey, 2020). Frey *et al.* (2012) and Vojtisek-Lom *et al.* (2020) measured real-world second-by-second (1 Hz) fuel use and emission rates (FUERs) for passenger rail service. To quantify spatial variability in FUERs, Gould and Niemeier (2011) apportioned annual aggregated fuel use data to local track segments. Emission rates were based on steady-state engine dynamometer measurements. These measurements did not account for realistic train activity, including transients or the effect of track grade and curvature on train operation.

Diesel locomotives used for passenger service typically have a prime mover engine (PME) and a head-end power engine. PME FUERs vary spatially, leading to some locations with emission rates higher than a threshold, known as emission hotspots (Rastogi and Frey, 2021). Spatially resolved FUERs are needed to: (1) quantify the source contribution of railroad sector emissions and to support quantification of local air pollution exposure and health impacts (Bergin et al., 2012; Dick and DiDomenico, 2016); (2) locate emission hotspots (Gould and Niemeier, 2011); and (3) improve train activity, by modifying speed trajectories to reduce fuel use and emission rates (Feng, 2011; Kim and Chien, 2010; Yuan and Frey, 2020). Demonstration of reduction in emissions is needed as a condition of receiving Federal funding for infrastructure changes (EPA, 2004).

One Hz train energy use rates have been estimated based on an assumed linear relationship of fuel use rate with positive locomotive power demand (LPD) (Drish, 1992; NCRRP, 2015; Yuan et al., 2019). LPD is the power provided by the locomotive to overcome resistive forces opposing train motion (Drish, 1992). Some studies quantified emission rates based on steady-state notch-average fuel use and emission rates (Xu et al., 2013, 2018; Yuan and Frey, 2021).

North Carolina Department of Transportation (NCDOT) provides equipment and infrastructure for Amtrak to operate the Piedmont passenger rail service between Raleigh and Charlotte. The NCDOT Rail Division is continually upgrading the equipment, infrastructure, and operational capacity pertaining to the Piedmont service. EPA notes that every county along the Piedmont route has high levels of air pollutants. Thus, NCDOT has been committed to reducing the emissions from the Piedmont service. As service has expanded, NCDOT has had to acquire additional locomotives. Older locomotives do not have the most up-to-date post-combustion emission controls required on new “Tier 4” EPA certified locomotives, including selective catalytic reduction (SCR) for NO_x and diesel particle filters for PM. Thus, in 2015 NCDOT engaged Rail Propulsion Systems, LLC of Fullerton, California to install a prototype, first-of-a-kind post combustion emission control system on an existing F59PH locomotive, NC 1859. This system, referred to as the Blended After Treatment System (BATS), treated blended exhaust from the PME and head end power engines using SCR.

In addition, train in-cabin air quality is of concern because train passengers spend approximately 75% of train travel time inside train cabins and the rest of train travel time at train stations (Kam et al., 2011). In-cabin air quality could be influenced by the exhaust plume of the locomotive, the outdoor ambient air quality, or both.

1.2 Research Needs

Train FUERs vary spatially, leading to some locations with emission rates higher than others, known as emission hotspots. Communities near railroads, ports, and freeways are exposed to elevated levels of air pollutant concentrations contributed by mobile sources such as trucks, ships, and locomotives (Anderson et al., 2018; Hasheminassab et al., 2020; Marshall et al., 2014). Spatially resolved FUERs are needed to accurately quantify local air pollution exposure, health impacts, and the source contribution of railroad sector emissions (Bergin et al., 2012; Fann et al., 2011; Gould and Niemeier, 2011; Hubbell et al., 2009; Lioy and Smith, 2013). Quantification of hotspots and identification of important factors leading to hotspots can be used to prioritize emissions mitigation. Higher spatial resolution is needed to represent more localized spatial variability in train FUERs (Dick and DiDomenico, 2016).

There is need for new work to augment the existing literature with respect to quantification of spatial variability in measured train emission rates, identification of real-world train emissions hotspots, and quantification of the contribution of train activity and track infrastructure to spatial variability in train FUERs.

In the real-world, variations in train FUERs are attributable to variations in locomotives, consists, and fuels (LCFs). Locomotives differ with respect to chassis, engine models, and operation and maintenance history. Consists are defined as the number, model, and type of locomotives, passenger cars, and baggage/café cars that make up a train (APTA, 2019). Fuels vary in their physical and chemical properties (Fritz, 2004; Graver et al., 2016). Inter-LCF variability in FUERs presents an opportunity to reduce system-wide fuel use and emissions for a fleet operator by prioritizing the dispatch of energy-efficient and low-emitting combinations of LCFs (Frey and Rastogi, 2019). A model is needed to predict transient-based fuel use and emission rates for different combinations of LCFs.

The effectiveness of BATS for emissions control will depend on actual passenger rail service for actual duty cycles on the Piedmont route. In addition, the durability of SCR under retrofit conditions for a diesel locomotive has not been quantified. Thus, there is need to develop a

study design to enable future assessment of the performance of a BATS both in the railyard and over-the-rail operations.

To understand whether in-cabin air quality is influenced by the plume from the locomotive or the outdoor ambient air quality, a study design is needed for measurement of passenger train in-cabin pollutant concentrations. An analytical modeling framework to quantify in-cabin air pollutant concentrations is needed to understand how the locomotive exhaust plume and ambient air quality affect the train in-cabin air quality.

1.3 Objectives

The objectives of this work are to: (1) quantify spatial variability in FUERs and identify factors differentiating hotspots from non-hotspots; (2) predict spatially varying real-world fuel use and emission rates; (3) develop a software tool for estimating the fuel use and emissions of a typical Piedmont train operation; (4) develop a study design for locomotive exhaust measurements with BATS; and (5) develop a study design for quantification of passenger train in-cabin pollutant concentrations.

1.4 Overview of the Report

The report consists of seven chapters. The overview of each chapter is briefly described:

Chapter 1 (this chapter) is the introduction that includes research background, research needs, objectives, and overview of the report.

Chapter 2 addresses research objective 1. This chapter is about characterizing fuel use and emissions hotspots for a diesel-operated passenger rail service.

Chapter 3 addresses research objective 2. This chapter is about modeling spatial variability in locomotive fuel use and emission rates based on real-world measurements.

Chapter 4 addresses research objective 3. This chapter is about the development of a locomotive power demand software to estimate train fuel use and emissions.

Chapter 5 addresses research objective 4. This chapter is about the study design for evaluation of the effect of the retrofitted BATS on locomotive exhaust emissions.

Chapter 6 addresses research objective 5. This chapter is about the study design and modeling framework for quantifying train in-cabin air quality.

Chapter 7 includes the key findings, conclusions, and recommendations for future work.

Appendices A-D include supplementary materials for Chapters 2, 3, 4, and 5, respectively.

1.5 References Cited in Chapter 1

- Amtrak, 2020. FY21-26 Five Year Service and Asset Line Plans. National Passenger Rail Corporation (Amtrak), Washington, D.C.
- Anderson, C.M., Kissel, K.A., Field, C.B., Mach, K.J., 2018. Climate change mitigation, air pollution, and environmental justice in California. *Environmental science & technology* 52, 10829–10838.
- APTA, 2020. 2020 Public Transportation Fact Book (No. Edition 71). American Public Transportation Association.
- APTA, 2019. Compendium of Definitions and Acronyms for Rail Systems (No. APTA STD-ADMIN-GL-001-19). American Public Transportation Association, Washington, D.C.
- Bergin, M.S., Harrell, M., Janssen, M., 2012. Locomotive emission inventories for the United States from ERTAC Rail, in: 2012 Annual International Emission Inventory Conference. Tampa, Florida, pp. 13–16.
- Davis, S.C., Boundy, R.G., 2018. Transportation energy data book, 37th ed. Oak Ridge National Laboratory, ORNL-5198, Oak Ridge, TN.
- Dick, C.T., DiDomenico, G., 2016. Factors Affecting Commuter Rail Energy Efficiency (No. NURail2013- UIUC-R12). Report prepared for the U.S. Department of Transportation by University of Illinois at Urbana-Champaign, Washington, D.C.
- Drish, W.F., 1992. Train energy model version 2.0 technical manual. Publication SD-040, Association of American Railroads, Washington, D.C.
- EPA, 2016. Integrated Science Assessment (ISA) for Oxides of Nitrogen - Health Criteria (Final Report, 2016) (No. EPA/600/R-15/068). U.S. Environmental Protection Agency, Washington, DC.
- EPA, 2009. Integrated Science Assessment (ISA) For Particulate Matter (Final Report, Dec 2009) (No. EPA/600/R-08/139F). U.S. Environmental Protection Agency, Washington, DC.
- EPA, 1998. Locomotive Emission Standards: Regulatory Support Document (No. EPA/98-04). U.S. Environmental Protection Agency, Ann Arbor, MI.
- Fann, N., Roman, H.A., Fulcher, C.M., Gentile, M.A., Hubbell, B.J., Wesson, K., Levy, J.I., 2011. Maximizing Health Benefits and Minimizing Inequality: Incorporating Local-Scale Data in the Design and Evaluation of Air Quality Policies. *Risk Analysis* 31, 908–922. <https://doi.org/10.1111/j.1539-6924.2011.01629.x>
- Feng, X., 2011. Optimization of target speeds of high-speed railway trains for traction energy saving and transport efficiency improvement. *Energy Policy* 39, 7658–7665.
- Frey, H.C., Rastogi, N., 2019. Managing Energy and Emissions for Rail Operations (No. FHWA/NC/2018-09). Prepared by North Carolina State University for North Carolina Department of Transportation, Raleigh, NC.
- Fritz, S.G., 2004. Evaluation of Biodiesel Fuel in an EMD GP38-2 Locomotive (No. NREL/SR-510-33436). Prepared for National Renewable Energy Laboratory by Southwest Research Institute, San Antonio, TX. <https://doi.org/10.2172/15009674>

- Gould, G.M., Niemeier, D.A., 2011. Spatial assignment of emissions using a new locomotive emissions model. *Environmental Science & Technology* 45, 5846–5852.
- Graver, B.M., Frey, H.C., 2016. Highway Vehicle Emissions Avoided by Diesel Passenger Rail Service Based on Real-World Data. *Urban Rail Transit* 2, 153–171.
- Graver, B.M., Frey, H.C., Hu, J., 2016. Effect of Biodiesel Fuels on Real-World Emissions of Passenger Locomotives. *Environmental Science & Technology* 50, 12030–12039.
- Hasheminassab, S., Sowlat, M.H., Pakbin, P., Katzenstein, A., Low, J., Polidori, A., 2020. High time-resolution and time-integrated measurements of particulate metals and elements in an environmental justice community within the Los Angeles Basin: Spatio-temporal trends and source apportionment. *Atmospheric Environment: X* 7, 100089.
<https://doi.org/10.1016/j.aeaoa.2020.100089>
- Hubbell, B., Fann, N., Levy, J.I., 2009. Methodological considerations in developing local-scale health impact assessments: balancing national, regional, and local data. *Air Quality, Atmosphere & Health* 2, 99–110. <https://doi.org/10.1007/s11869-009-0037-z>
- Kam, W., Cheung, K., Daher, N., Sioutas, C., 2011. Particulate matter (PM) concentrations in underground and ground-level rail systems of the Los Angeles Metro. *Atmospheric Environment* 45, 1506–1516. <https://doi.org/10.1016/j.atmosenv.2010.12.049>
- Kim, K., Chien, S.I.-J., 2010. Optimal train operation for minimum energy consumption considering track alignment, speed limit, and schedule adherence. *Journal of Transportation Engineering* 137, 665–674.
- Lioy, P.J., Smith, K.R., 2013. A discussion of exposure science in the 21st century: a vision and a strategy. *Environmental Health Perspectives* 121, 405–409.
<https://doi.org/10.1289/ehp.1206170>
- Marshall, J.D., Swor, K.R., Nguyen, N.P., 2014. Prioritizing environmental justice and equality: diesel emissions in Southern California. *Environmental science & technology* 48, 4063–4068.
- NCRRP, 2015. Comparison of Passenger Rail Energy Consumption with Competing Modes, NCRRP Report 3. Prepared for National Cooperative Rail Research Program (NCRRP) by TranSys Research Ltd.; RailTEC at the University of Illinois at Urbana-Champaign; Canadian Pacific Consulting Services Transcom; and Lawson Economics Research Inc., Washington, D.C.
- Rastogi, N., Frey, H.C., 2021. Characterizing Fuel Use and Emission Hotspots for a Diesel-Operated Passenger Rail Service. *Environ. Sci. Technol.* 55, 10633–10644.
<https://doi.org/10.1021/acs.est.1c00273>
- Sprung, M.J., Nguyen, L.X., Riley, D., Zhou, S., Lawson, A., 2018. National Transportation Statistics 2018, Bureau of Transportation Statistics. U.S. Department of Transportation. Washington, D.C.
- U.S. Environmental Protection Agency, 2004. 40 CFR Parts 9, 69, et al., Final Rule for Control of Emissions of Air Pollution From Nonroad Diesel Engines and Fuel [WWW Document]. US EPA. URL <https://www.epa.gov/regulations-emissions-vehicles-and-engines/final-rule-control-emissions-air-pollution-nonroad> (accessed 7.14.22).

- Xu, X., Liu, H., Passmore, R., Patrick, T., Gbologah, F., Rodgers, M.O., Guensler, R., 2018. Fuel and Emissions Calculator (FEC), Version 3.0, Summary Report.
- Xu, Y., Gbologah, F., Cernjul, G., Kumble, A., Guensler, R., Rodgers, M., 2013. Comparison of fuel-cycle emissions per passenger mile from multiple bus and rail technologies, in: Proc., Third International Conference on Urban Public Transportation Systems. pp. 204–216.
- Yuan, W., Frey, H.C., 2021. Multi-scale evaluation of diesel commuter rail fuel use, emissions, and eco-driving. *Transportation Research Part D: Transport and Environment* 99, 102995. <https://doi.org/10.1016/j.trd.2021.102995>
- Yuan, W., Frey, H.C., 2020. Potential for metro rail energy savings and emissions reduction via eco-driving. *Applied Energy* 268, 114944.
- Yuan, W., Frey, H.C., Rastogi, N., 2019. Quantification of Energy Saving Potential for A Passenger Train Based on Inter-Run Variability in Speed Trajectories. *Transportation Research Record* 2673, 153–165.

CHAPTER 2: Characterizing Fuel Use and Emissions Hotspots for a Diesel-operated Passenger Rail Service*

2.1 Introduction

The U.S. freight rail network is distributed over 136,851 miles with Class I freight railroads comprising 93,058 miles. In 2019, U.S. Class I railroads had 24,597 active diesel locomotives. Of these, 47% were manufactured before 2001 and are subject to the least stringent emission standards.¹⁻⁴ In 2020, the National Railroad Passenger Corporation (Amtrak) provided intercity passenger service over 20,604 miles of routes with an active fleet of 276 diesel locomotives averaging 23 years of age.⁵ Additionally, 731 active diesel-powered locomotives averaging 26 years of age provided commuter rail service in 2018.⁶ Thus, the U.S. freight, intercity passenger, and commuter rail service is comprised of a large share of older diesel locomotives. With rebuilds, these locomotives can be operational for several decades.³ Passenger travel via diesel-powered trains is typically more energy-efficient versus light-duty gasoline vehicles (LDGVs), transit buses, and aircraft.⁷⁻⁹ However, per passenger-mile emission rates of oxides of nitrogen (NO_x) and particulate matter (PM) for older diesel locomotive engines are typically higher than for LDGVs.¹⁰ The US Environmental Protection Agency regulates NO_x and PM because of their adverse human health impacts.^{11,12}

Locomotive fuel use and emission rates (FUERs) vary spatially, leading to some locations with emission rates higher than others, known as emission hotspots. Communities near railroads, ports, and freeways are exposed to elevated levels of air pollutant concentrations contributed by mobile sources such as trucks, ships, and locomotives.¹³⁻¹⁵ Spatially resolved FUERs are needed to accurately quantify local air pollution exposure, health impacts, and the source contribution of railroad sector emissions.¹⁶⁻²⁰ Quantification of hotspots and identification of important factors leading to hotspots can be used to prioritize emissions mitigation.

Locomotive FUERs are typically based on static-load steady-state rail-yard (RY)²¹⁻²⁷ or engine dynamometer measurements.²⁸ However, FUERs vary spatially because of variation in train activity and infrastructure variables along a route, and because real-world operation comprises both transient and steady-state operation.²⁹⁻³¹ Train activity variables include speed and acceleration. Infrastructure variables include track grade and curvature. RY and dynamometer data are of limited use in quantifying the spatial variability in FUERs because they do not account for realistic train activity, interactions with infrastructure, and transients. Compared to real-world locomotive FUERs, steady-state operation based NO_x and PM emission rates are typically underestimated by 10%.³²

* This chapter is published as:

Rastogi, N.; Frey, H. C. Characterizing Fuel Use and Emission Hotspots for a Diesel-Operated Passenger Rail Service. *Environ. Sci. Technol.* **2021**, *55* (15), 10633–10644. <https://doi.org/10.1021/acs.est.1c00273>.

Several studies demonstrated methods to modify 1 Hz train activity and were focused on reductions in energy use for a given trip.^{33–36} Frey *et al.*^{10,32,37,38} and Vojtisek-Lom *et al.* (2020)³⁹ measured real-world 1 Hz FUERs for passenger rail service.³⁹ To quantify spatial variability in FUERs, Gould and Niemeier (2011) apportioned annual aggregated fuel use data to local track segments.¹⁹ This study was focused on quantifying spatial variability based on readily available data such as steady-state based FUERs and aggregated train activity. Several models are based on use of localized train activity to estimate FUERs.^{9,40–42} There is need for new work to augment the existing literature with respect to quantification of spatial variability in measured train emission rates, identification of real-world train emissions hotspots, and quantification of the contribution of train activity and track infrastructure to spatial variability in train FUERs.

In prior work, Frey *et al.* conducted over-the-rail (OTR) measurements for a selected Amtrak-operated Piedmont passenger rail service using a Portable Emissions Measurement System (PEMS).^{10,32,37,38} One Hz FUERs, speed, acceleration, position, and elevation for locomotives operated on ultra-low sulfur diesel (ULSD) were measured. However, data were aggregated for each trip. Spatial variability in emission rates and factors leading to emissions hotspots for other transport modes, such as LDGVs, has been quantified.^{43–48} Here, spatial variability in locomotive FUERs is quantified and key sources of spatial variability are identified. The objectives of this work are to: (1) quantify spatial variability in FUERs; and (2) identify factors differentiating hotspots from non-hotspots. This is the first study to systematically quantify spatial variability in locomotive FUERs and associated factors based on real-world data.

2.2 Methods

FUERs were measured in current and prior work using PEMS during OTR operations of the Piedmont passenger rail service.^{10,32,37} Train activity was inferred from an onboard locomotive activity data recorder. Position and elevation were measured using GPS receivers fitted with barometric altimeters (GPS/BA). GPS/BA data were used to infer track grade and curvature. Emission hotspots were characterized for non-overlapping track segments. Key variables affecting hotspot locations were identified using Classification and Regression Trees (CART).

2.2.1 Field Study Design

The study design includes choice of route, locomotives, fuels, and train consists. The approach to field study design was applied to a specific passenger rail service located mostly in the Piedmont area of North Carolina. A similar approach to study design can be applied to other areas that may have different topography, locomotives, fuels, and consists. The Piedmont passenger rail service uses equipment owned by the North Carolina Department of Transportation (NCDOT) (Tables A-1 through A-3). The one-way route length is 173 miles (278 km), the scheduled trip duration is 3h 10m, and the highest allowable speed is 79 mph (Figure A-1).

Six locomotives with a 12 cylinder, 140 L, 2240 kW EMD 12–710, Tier 0+ certified diesel prime move engine (PME) were measured. The PME provides traction to the wheels and has a throttle control with eight non-idle notch positions, a power take-off high idle position, and a low idle position. The locomotive is slowed using the mechanical brake or dynamic brake where the traction motors act as generators and dissipate electricity as heat via an electric resistance grid. Each locomotive has an additional 460 kW to 600 kW head end power (HEP) engine that provides hotel services for passenger cars, such as lighting and space conditioning. Four locomotives have CAT ACERT C-18, and two have CAT ACERT C-15 HEP engines. Each locomotive was operated on ULSD.

The trains operated in four consists (Table A-4): (1) single locomotive consist (SLC); (2) double-powered tandem consist (DP-TC); (3) double-powered push/pull consist (DP-P/PC); and (4) single-powered push/pull consist (SP-P/PC). An SLC comprises one locomotive, placed at the head of the train. A DP-TC comprises two adjacent locomotives at the head of the train, both providing equal power to propel the train. A push/pull consist comprises one locomotive at each end of the train. In DP-P/PC, both locomotives propel the train. In SP-P/PC one locomotive propels and the other idles. Only one HEP engine provided hotel services for each consist. In prior work, four locomotives were measured for SLCs.^{10,32,37} In recent work, measurements were made for DP-TC, DP-P/PC, and SP-P/PC. Nine combinations of locomotives and consists were measured. The typical train length on the Piedmont route varied between 315' (0.06 mile) for SLC and up to 631' (0.12 mile) for consists with two locomotives. The train weighed 344 tons for SLC and between 550 tons and 700 tons for other consists.

2.2.1.1 Portable emissions measurement system

To measure pollutant concentrations required to estimate FUERs, each of the locomotives was instrumented with an OEM-2100AX Axion PEMS manufactured by Global MRV.³² The Axion measures 1 Hz CO₂, CO, HC, nitric oxide (NO), and PM₁₀ concentrations. Similar to Federal Reference Methods (FRMs),⁴⁹ nondispersive infrared (NDIR) detection was used for CO₂ and CO concentrations. HC, NO, and PM₁₀ concentrations were measured using NDIR, an electrochemical sensor, and laser light scattering, respectively (Table A-6). The response of light-scattering to PM is faster than a tapered element oscillating microbalance which provides real-time PM measurements based on Federal Equivalent Method.^{50,51}

The Axion PEMS does not measure NO₂. Therefore, Axion-measured NO concentrations were bias corrected based on simultaneous RY measurements with a Sensors Inc. SEMTECH-DS PEMS. The SEMTECH-DS measures NO, NO₂, and NO_x concentrations based on the same detection methods as specified in 40 CFR 1065 Subpart J.⁵² The bias correction factor for each throttle notch position of each locomotive was estimated as the ratio of notch-average NO_x/NO concentrations measured using a SEMTECH-DS PEMS.^{32,38,53,54} For several heavy-duty diesel engines, the laser light scattering-based PM concentrations were correlated with the FRM. The slope of linear regression of FRM versus laser-light scattering was reported as 5.⁵⁵⁻⁵⁷ Thus laser-light scattering is typically biased low by a factor of 5. Here, each locomotive had the same model PME and was operated on ULSD. A factor of 5 was selected to bias correct Axion PM concentration measurements and estimate average PM emission rates for each notch position for each combination of locomotive and consist. The PM emission rates estimated based on the laser-light scattering PEMS data were compared to reference data reported by the U.S. Environmental Protection Agency³ for the same model of engine. Both data sets have similar trends in relative variations in emission rates among the throttle notch settings and are similar in magnitude (Figure A-5). The bias corrected estimates of PM emission rates based on PEMS are useful for quantifying relative trends in emission rates.

The Axion was evaluated for accuracy and precision based on simultaneous RY measurements versus two reference instruments based on the same detection methods as specified in 40 CFR 1065 Subpart J.⁵² Reference instruments included SEMTECH-DS⁵⁸ and the Ride-Along Vehicle Emission Measurement System (RAVEM) developed by Engine Fuels and Emissions Engineering.⁵⁹ The slope of linear regression of CO₂ concentrations at each throttle notch position for Axion PEMS versus SEMTECH-DS PEMS was 0.951 (Figure A-3). The adjusted R²

was 0.975. The slope of linear regression of NO concentrations for the Axion versus NO_x concentrations for the SEMTECH-DS was 1.02. The adjusted R² was 0.995. The slope of the linear regression and adjusted-R² of fuel use and NO_x emission rates for the Axion PEMS versus RAVEM were each within ±4% of one (Figure A-4). Therefore, Axion based fuel use and NO_x emission rates were accurate and precise.

The Axion measured engine activity variables including engine revolutions per minute, intake air temperature, and manifold absolute pressure. Mass airflow was estimated using the “speed-density method” based on engine activity variables and a previously developed estimate of engine volumetric efficiency.⁶⁰ The speed-density method is based on the ideal gas law.⁶¹ The air to fuel ratio was inferred based on the volume percent of carbon species in the exhaust, including CO₂, CO, and HC, because all carbon in the exhaust comes only from the fuel. Molar exhaust flow rate was estimated from the mass airflow and the air-to-fuel ratio. The 1 Hz FUERs were estimated as the product of molar exhaust flow rate and pollutant concentration.

2.2.1.2 Train fuel use and emission rates

For a given consist, 1 Hz FUERs were estimated based on the sum of FUERs for all powered PME(s) and the operating HEP engine. For double-powered consists, only one PME was measured. The other PME operated identically and with the same assumed FUERs. Typically, three to six one-way trips were measured for each combination of locomotive and consist, for a total of 51 one-way trips. FUERs for CAT ACERT C-18 HEP engines were previously measured.⁶² On average, the electrical load per passenger car was 20 kW.¹⁰ Mass per time-based FUERs were approximately constant for loads up to 200 kW. Given that the measured consists had three to five cars, average loads were ≤100 kW, HEP engine FUERs were not sensitive to load. In the absence of data on the CAT ACERT C15 engine, FUERs of C-18 HEP engines were used.

2.2.1.3 Train activity and infrastructure variables

Locomotive activity recorders logged 1 Hz locomotive speed.³⁰ Acceleration was inferred from difference in speed.

In prior work, track grade and curvature were quantified for 692 non-overlapping quarter-mile track segments.^{38,63} Typically, four to ten GPS/BA receivers were used on each measured one-way trip. The grade for each track segment in the eastbound direction was estimated as the slope of linear regression of elevation versus distance from the start of the segment. The grade in the westbound direction was equal in magnitude but opposite in sign to the grade in the eastbound direction. The GPA-based grade estimates were on average within ±0.3% absolute versus track drawings.⁶³

Curvature was estimated based on circular regression of GPS position data for each track segment.⁶³ Curvature <0.5 degrees was inferred to be straight because the lowest reported curvature >zero degree in the design drawings was 0.5 degrees. The GPA-based curvature estimates were on average within ±0.2 degrees versus track drawings.

2.2.2 Data Analysis

Data from the PEMS, sensor array, locomotive activity recorder, and GPS were time-aligned and screened for errors. Erroneous data were either corrected or excluded from the analysis, as detailed elsewhere.^{32,38,53,60} Typically, less than 3% of the 1 Hz data were excluded.

2.2.2.1 Segment-average fuel use and emission rates

Segment-average FUERs were quantified for the same 0.25-mile track segments for which grade and curvature were estimated. Each one-way train movement on a track segment is a segment-run. For each segment-run, 1 Hz FUERs were summed. Summed 1 Hz FUERs were divided by the measured segment length to estimate mass per distance-based segment-run average FUERs.

Segment-average FUERs for a given track segment were estimated based on average rates of all valid segment-runs on a given track segment. Segment-runs with a large proportion of missing or invalid data may not be representative of segment-average FUERs. The proportion of missing or invalid data was estimated by subtracting the length accounted for by the valid data from the actual segment length. Segment-runs with $\leq 30\%$ missing or invalid data and one-way trips with $< 10\%$ invalid segment-runs were used for analysis.

2.2.2.2 Segment classification: hotspots and non-hotspots

Segments or segment-runs with FUERs above a threshold are hotspots. At present, there are not benchmark thresholds for locomotive FUERs. However, several criteria have been proposed for defining emissions hotspots for LDGVs,⁶⁴⁻⁶⁶ including a threshold of the top 10th percentile of inter-segment variability in segment average rates within a study area.⁴³ A similar approach is adopted here. Segments were classified into hotspots and non-hotspots based on three choices of threshold level: (1) absolute; (2) consist-specific; and (3) relative.

Absolute hotspots indicate segments with FUERs consistently higher than those of other segments. Absolute hotspots are track segments exceeding the 80th percentile of segment-average FUERs based on all measurements combined. Absolute hotspots are directional, because a given track segment may have higher FUERs in one travel direction and lower FUERs in the opposite direction. Absolute hotspots were characterized for each travel direction.

Consist-specific hotspots are defined as the top 20% frequency range of segment-run average FUERs for all one-way trips measured for a given train consist. The sensitivity of hotspot locations to consists was quantified based on the comparison of co-located absolute hotspots and near-hotspots versus consist-specific hotspots and near-hotspots. Absolute near-hotspots are defined as the segments with FUERs between the 70th and 80th percentiles. Consist-specific near-hotspots are defined as the segments with FUERs between the 70th and 80th percentiles for a given consist. The sensitivity is categorized as “weak,” meaning that the identification of hotspots is not highly dependent on the consist, if two conditions were met: (1) the proportion of co-located consist-specific hotspots versus absolute and absolute near-hotspots was $> 80\%$, and (2) the proportion of co-located absolute hotspots versus consist-specific hotspots and consist-specific near-hotspots was $> 80\%$.

Inter-locomotive and inter-consist variability in FUERs may lead to inter-trip variability in segment-run average FUERs for the same values of speed, acceleration, grade, and curvature.⁵³ To account for inter-trip variability in FUERs, relative hotspots were used. Relative hotspots are defined as being in the top 20th percentile segment-run average FUERs for a given one-way trip. The remaining segment-runs are relative non-hotspots. Relative hotspots are useful for identifying controllable operational practices and infrastructure factors that induce relatively high FUERs and to target interventions.

To quantify the minimum number of measured one-way trips required to accurately locate absolute hotspots, bootstrapping was used.^{67,68} For a given travel direction, a selected number of

trips were sampled at random without replacement for 1000 replications. For each species, the number of sampled one-way trips was increased until the selected sample had 90% of the same absolute hotspots with 90% frequency among the replicates as for absolute hotspots based on all one-way trips in that given travel direction.

Trains typically accelerate when leaving a station, operate at near maximum allowable speeds in-between stations, and decelerate when approaching a station. Thus, based on these operations, the track segments were classified into station segments (S), near-station acceleration segments (NSA), near-station deceleration segments (NSD), and intermediate segments (I). S are segments at stations. NSA are segments within 1.25 miles upstream of a station. NSD are segments within 1.25 miles downstream of a station. Segments other than S, NSA, and NSD were designated as intermediate (I).

2.2.2.3 Potential explanatory variables

Explanatory variables affecting segment-run average FUERs were identified based on the physics of motion. One Hz mass per time-based FUERs are directly proportional to locomotive power demand (LPD).^{29,31,53} LPD is the power required to overcome journal, flange, drag, acceleration, grade, and curvature resistances. The proportionality of LPD to each resistance depends on static variables related to the locomotive(s) and consist. For a given locomotive and consist, resistances differ based on variations in train activity and infrastructure variables. Therefore functions of train activity and infrastructure variables are dynamic variables.²⁹⁻³¹ Dynamic variables include sums of 1 Hz speed, speed², and speed³, and sums of product (SOP) of 1-Hz speed and acceleration, 1-Hz speed and segment-average grade, and 1-Hz speed and segment-average curvature. The terms with speed, speed², and speed³ correspond to journal, flange, and drag resistances, respectively. The terms with acceleration, grade, and curvature correspond to acceleration, grade, and curvature resistances.

To assess the strength of the linear relationship among segment-average FUERs, segment-average explanatory variables, and population density, Pearson's correlation coefficients were estimated. Based on their absolute value, correlations <0.60, between 0.61 and 0.75, >0.75 were inferred to be weak, moderate, and strong, respectively. Exposure to a pollutant is directly proportional to emission rates and population density. Although ambient concentration is not modeled here, ambient concentration is a linear function of emission rate. Thus, emission rate is a surrogate for ambient concentration. The product of emission rate with population density is a surrogate indicator of exposure.⁶⁹⁻⁷² This product is used here as an impact index. To assess the impact of spatial variability in emission rates as a contributing factor to hotspots, two cases are compared. A spatially varying case is based on spatial variability in emission rates and population density. An average case is based on route average emission rate applied to all segments and spatially varying population density. For each case, impact hotspots are identified. Impact hotspots are segments in the top 20th percentile of the impact index. The similarity of identified impact hotspots to spatially varying versus average rates was quantified based on a confusion matrix.

To quantify the extent to which static and dynamic variables differentiate relative hotspots from non-hotspots and their importance, CART was used.⁷³ Compared to decision tree-based methods that split data into homogenous groups, such as bagging, boosting, decision stump, and random forests, CART provides simple combinations of variables that distinguish hotspots from non-hotspots.⁷⁴ Therefore, CART was preferred for simplicity. For most splits, CART gives a

combination of variables that leads to hotspots and a complementary combination of variables that leads to non-hotspots. Their comparison enables identification of combinations of variable values that can mitigate hotspots. The importance of each variable in distinguishing hotspots from non-hotspots was quantified based on variable importance (VI). VI was estimated based on the decrease in node impurity at each node in which the predictor variable resulted in a split. The node impurity is a measure of the homogeneity of the split data at the node.⁷³

For each species, four CART models were calibrated: (1) Physical Model with Dynamic Variables (PD); (2) Physical Model with Dynamic and Static Variables (PDS); (3) Simplified Model with Dynamic Variables (SD); and (4) Simplified Model with Dynamic and Static Variables (SDS). Relative hotspots or non-hotspots were the target variable for each model for each species, which included fuel use rate and emission rates of NO_x and PM. The PD models are based on dynamic variables. The PDS models include dynamic and static variables. Terms such as SOP of speed and acceleration, SOP of speed and grade, and SOP of speed and curvature add complexity to a model. Therefore, simpler models with SOP terms replaced by segment-average speed, acceleration, grade, and curvature, were evaluated.

Each CART model was evaluated for accuracy and precision based on calibration and validation data. Calibration data included all but one selected one-way trip for each combination of locomotive and consist. Validation data comprised selected one-way trips for each combination of locomotive and consist.

Model calibration and validation were evaluated in terms of true positives (TP), true negatives (TN), false positives (FP), false negatives (FN), model accuracy (MA), and model precision (MP).⁷³ TP is the number of measured relative hotspots that were modeled as relative hotspots. TN is the number of measured relative non-hotspots that were modeled as relative non-hotspots. FP is the number of measured relative non-hotspots that were modeled as relative hotspots. FN is the number of measured relative hotspots that were modeled as relative non-hotspots. MA is the proportion of correct classifications relative to the total number of observations. MP is the proportion of the modeled relative hotspots that were correctly identified.

2.3 Results and Discussion

The results include inter-segment variation in segment-average speed, acceleration, grade, curvature, and FUERs measured for 35 one-way trips that met the data completeness criterion. These 35 trips included 23,198 valid segment-runs. Valid data comprised 114 h measured over 5,800 miles. The location of hotspots and nearby population density are quantified. The minimum number of one-way trips required to accurately quantify absolute hotspots is estimated. The importance of variables in distinguishing hotspots from non-hotspots is assessed.

2.3.1 Segment-Average Activity and Infrastructure Variables

Segment-average speed, acceleration, grade, and curvature, in the eastbound and westbound direction, are given in Figure 2-1 and Figure A-12, respectively. Segment-average speed varied between 6 mph and 79 mph, with an average of 54 mph in each direction. The average speed was lowest at segments containing stations. For a given track segment, speeds in either travel direction were approximately similar, with a correlation of 0.90.

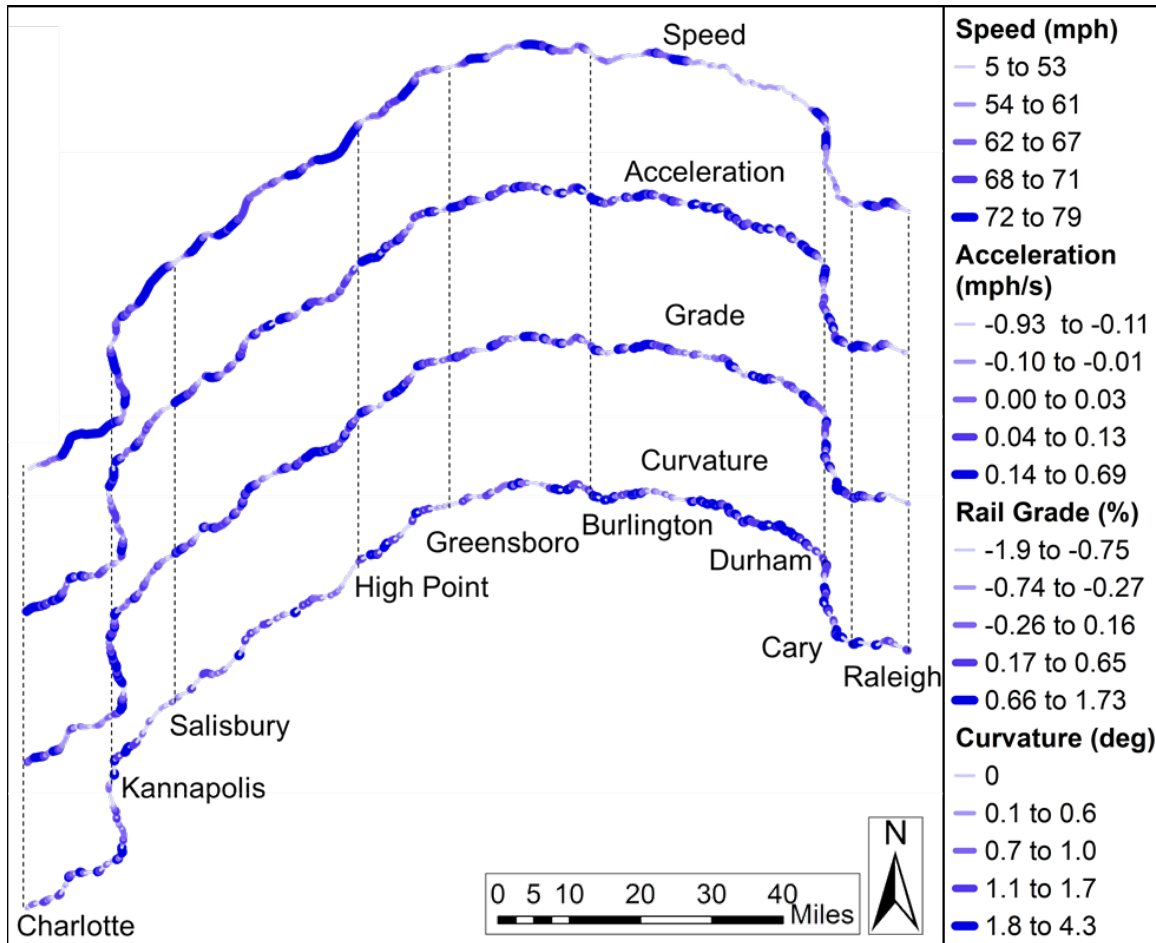


Figure 2-1. Segment-Average Speed, Acceleration, Grade and Curvature for the Piedmont Passenger Rail Service Between Raleigh, NC, and Charlotte, NC in the Eastbound Direction based on 14 One-Way Trips. There are 692 segments, of which each is 0.25 miles long. Segment-average activity was divided into quintiles.

Segment-average acceleration varied between -1.0 mph/s and 0.7 mph/s in each travel direction. Segment-average acceleration in the eastbound direction was negatively correlated, at -0.72, with the westbound direction. Trains decelerated when approaching stations and curves and accelerated when leaving stations and curves. The highest magnitudes of acceleration and deceleration were typically measured when leaving and approaching stations, respectively.

Segment-average grade varied between -2% and 2%. Grades in opposite travel directions were anti-correlated. Because acceleration and grade are negatively correlated by travel direction, a given track segment may have high FUERs in one travel direction and low in the other. Thus, hotspot locations and FUERs may differ based on travel direction.

The cumulative elevation gain, defined as sum of all positive elevation gains, was 784 m and 904 m in the eastbound and westbound direction, respectively. Therefore, westbound trips are typically expected to have higher FUERs than eastbound. Segment-average curvature varied between 0 degrees and 4.3 degrees. Curvature is independent of travel direction. Segments with <0.5 degrees of curvature comprised 54% of total segments.

The ranges of grade and curvature were compared to those of five U.S. passenger rail routes for which such data were available.⁷⁵ The selected routes include the Washington D.C. to Boston along the Northeast Corridor, Buffalo to New York City, Chicago to Detroit, Vancouver to Portland, and Los Angeles to San Diego. For these routes, grades were within $\pm 2.2\%$ and 99% to 100% of track curvature values were < 4.3 degrees. Thus, track infrastructure variables of the Piedmont route are similar to those of other U.S. passenger rail routes.

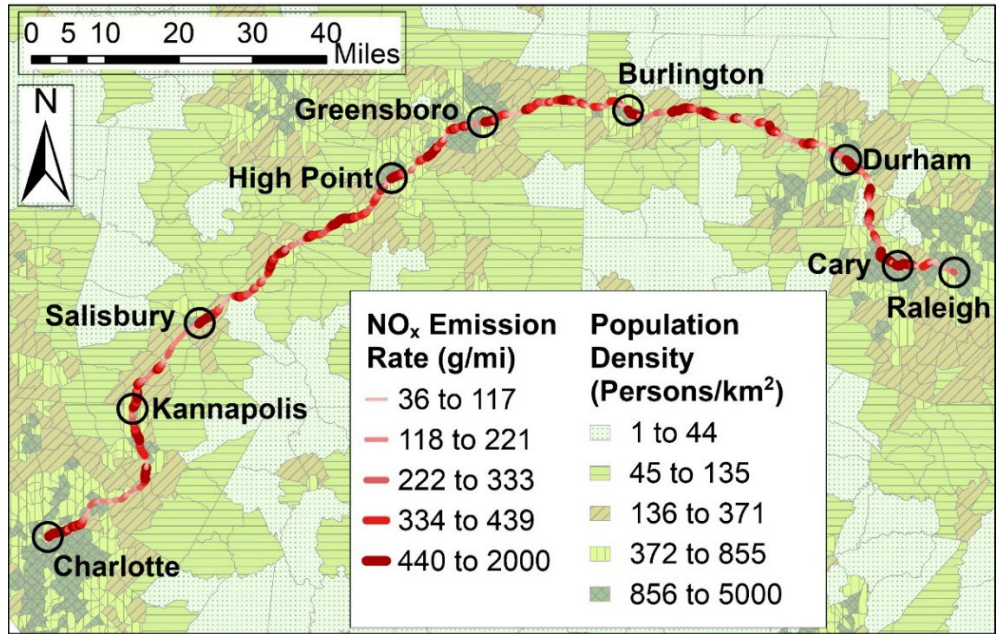
2.3.2 Segment-Average Fuel Use and Emission Rates

Segment-average NO_x and PM emission rates in the eastbound travel direction and US 2010 census tract-based population density are given in Figure 2-2. On average for a given one-way trip, the maximum rates were 24, 21, and 53 times higher than the mean for fuel use, NO_x emissions, and PM emissions, respectively. Thus, FUERs vary over short distances. For example, for each species, the FUERs among a pair of adjacent track segments differed on average by a factor of 2 to 60, depending on location and species.

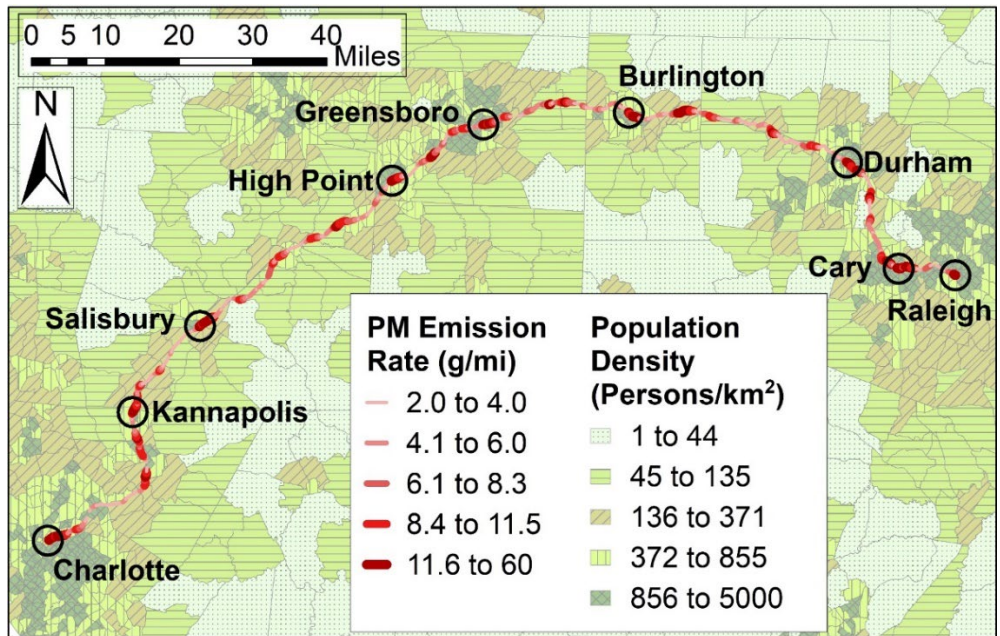
The spatially varying FUERs measured here could not be benchmarked to similar studies because of the lack of such studies. However, in prior work, the measured notch-average mass per time-based FUERs were of the same magnitude as reported by the EPA for the same model PME.^{32,53} The measured notch-average FUERs were based on the same one Hz FUERs from which segment-average FUERs are estimated.

In either direction for each species, S segments consistently had higher average FUERs than other segments. The next highest average FUERs were typically measured at NSA segments. NSD and I segments had the lowest average FUERs. S, NSA, NSD, and I comprised 1%, 6%, 6%, and 87% of all segment-runs, respectively. On average, S, NSA, NSD, and I comprised 4%, 12%, 5%, and 79% of trip fuel use. On average, S, NSA, NSD, and I comprised 3%, 13%, 3%, and 81% of trip NO_x emissions. On average, S, NSA, NSD, and I comprised 5%, 15%, 2%, and 78% of trip PM emissions. Thus, S and NSA segment-runs contributed more to trip total emissions compared to their share of segment-runs.

The severity of the hotspots in one direction may be offset by lower emissions in the other direction because emission rates can be directional. To quantify the effect of both directions combined, a comparison of absolute hotspots was made for each direction and both directions combined. For a given species, 45% to 53% of the absolute hotspots in a given direction were also hotspots for both directions combined. The variation of NO_x emission rates and location of absolute hotspots for each direction, and both directions combined, is given for an example case near the station Salisbury, NC in Figure A-20. Each of the S segments were absolute hotspots in either travel direction and both directions combined. At NSA segments, FUERs were the highest among all segments. However, in the opposite direction, NSA segments were NSD segments and FUERs were the lowest among all segments. Therefore, for both directions combined, average FUERs were typically higher than for other segments. Absolute hotspots based on both directions combined were located on either side of S segments. In contrast, most I segments that were hotspots in one direction, were non-hotspots in the other direction or for combined directions because FUERs for such hotspots were not as high as NSA segments.



(a) NO_x Emission Rate



(b) PM Emission Rate

Figure 2-2. Segment-Average Emission Rates for the Piedmont Passenger Rail Service Between Raleigh, NC and Charlotte, NC in the Eastbound Direction based on 14 One-Way Trips: (a) NO_x Emission Rate; and (b) PM Emission Rate. There are 692 segments, of which each is 0.25 miles long. The map depicts the US 2010 census tract-based population density. Emission rates and population density were divided into quintiles.

Among the average of all consists, SLC had 8%, 18%, and 16% lower segment-average rates of fuel use, NO_x emissions, and PM emissions, respectively. Other consists had 5% to 21% higher FUERs than the average of all consists. Thus, in general, adoption of SLC could reduce the intensity of fuel use and emissions hotspots. However, double-powered consists were preferred by the train operator because they facilitate reliability in the case of one locomotive malfunctioning and they facilitate operation in each direction without having to reconfigure a train.

2.3.3 Hotspot Classification and Location

Absolute fuel use, NO_x emissions, and PM emissions hotspots contributed between 40% and 44% to trip totals in each direction and both directions combined. For each species, the average FUERs for absolute hotspots were approximately three times higher than for non-hotspots. Of the 139 absolute hotspots in a given travel direction, 73% to 82% of the fuel use, NO_x emissions, and PM emissions hotspots were co-located. Of the 553 absolute non-hotspots, 93% to 95% of fuel use, NO_x emissions, and PM emissions non-hotspots were co-located. Therefore, a hotspot for one species was frequently also a hotspot for other species. For a given species and direction, 59% to 69% of the absolute hotspots were located at stations or within 1.25 miles of stations.

Relative fuel use, NO_x emissions, and PM emissions hotspots contributed between 43% and 49% to trip total in each direction and both directions combined. FUERs were five to seven times higher for relative hotspots versus non-hotspots. This ratio was different from the ratio of FUERs for absolute hotspots versus because of differences in the relative rank ordering of the same segments for absolute versus relative hotspots. Of all relative hotspots, 63%, 30%, 6%, and 1% were located on I, NSA, S, and NSD, respectively. All S and 82% of all NSA segment-runs were hotspots. Only 11% and 2% of all I and NSD segment-runs, respectively, were hotspots.

The sensitivity of location of hotspots to consists was evaluated (Table A-9). As an example, the sensitivity was evaluated based on comparing absolute and SLC-specific fuel use hotspots. In the eastbound direction, 68% of SLC-specific fuel use hotspots were co-located with absolute hotspots. An additional 14% of these consist-specific hotspots were absolute near-hotspots. Therefore, 82% of the consist-specific fuel use hotspots were absolute hotspots or absolute near-hotspots. Likewise, 90% of the absolute hotspots were either consist-specific hotspots or consist-specific near-hotspots. Therefore, fuel use hotspots in the eastbound direction were only weakly sensitive to consist. Similar proportions of co-located fuel use hotspots and near-hotspots were estimated for westbound, for other species in either direction, and for other consists in either direction. Hotspots and near-hotspots identified based on one consist were co-located with 80% to 90% of the hotspots for other consists. Therefore, the location of the hotspots in a given travel direction was typically similar among consists.

The minimum number of one-way trips needed to accurately locate absolute hotspots was 13 and 14 for eastbound and westbound, respectively. On average, FUERs in the westbound direction were 5%, 7%, and 20% higher than in the eastbound direction for fuel use, NO_x emissions, and PM emissions rates, respectively. Therefore, FUERs vary with direction.

2.3.4 Potential Explanatory Variables

Instantaneous mass per time-based FUERs were higher at higher speeds, but the distance traveled was also greater. Therefore, mass per distance-based segment-run average FUERs were lower at higher speeds (Tables A-10 and A-11). In contrast, segment-run average FUERs were

higher at slower speeds, typically measured near stations. Because of slower speeds, more time was spent in a given segment resulting in accumulation of fuel use and emissions.

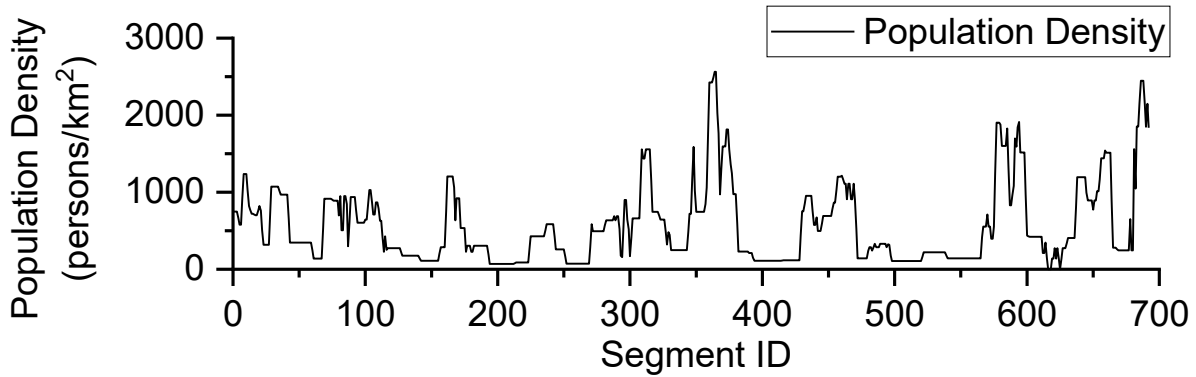
Acceleration was moderately positively correlated with grade and FUERs. However, FUERs were approximately constant among segment-runs with negative acceleration and strongly correlated with acceleration for segment-runs with positive acceleration because the force required to propel a train is directly proportional to positive acceleration.²⁹⁻³¹

Grade was moderately positively correlated with FUERs. Similar to acceleration, the correlation was higher for segment-runs with positive grades than for segment-runs with negative grades because resistive forces are directly proportional to positive grades.²⁹⁻³¹

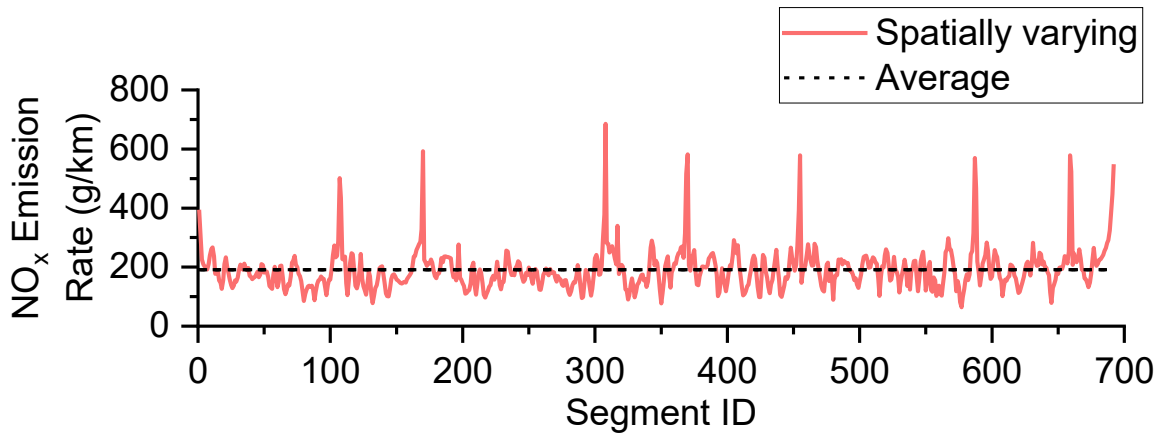
Segment-run average FUERs between species were strongly correlated because FUERs typically increase monotonically with engine power output.³² Therefore, any operational or infrastructural changes designed to intervene to reduce the rate of one species will typically also reduce other species.

FUERs were weakly positively correlated with population density. However, FUERs and population density near stations were consistently higher than at other locations. Fuel use rates and NO_x emission rates were 1.6 to 1.7 times higher near stations versus at other locations, and PM emission rates were 2 times higher. The population density near stations was 2.5 times higher than at other segments. Therefore, people living near stations are potentially exposed to higher pollutant emissions versus other locations. Identification of hotspot locations near populated regions helps target emission reduction measures to improve near-railroad air quality and to reduce human exposure to train-generated air pollution.

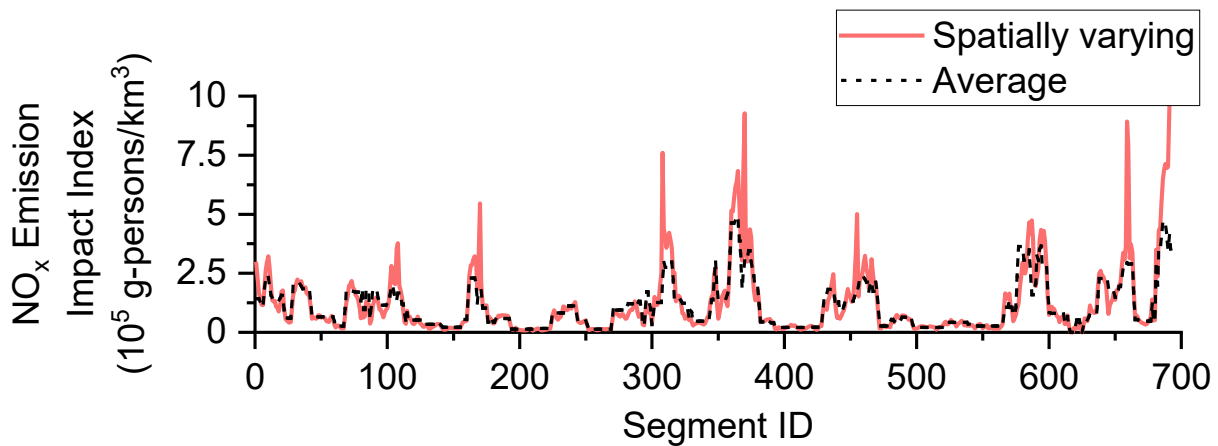
Plots of population density, segment-average emission rates, and pollutant impact index in both travel directions combined versus segment ID are given in Figure 2-3 and Figure A-17 for NO_x and PM emission rates, respectively. Population density varied along the route. The highest population density was typically observed at S, NSA, and NSD segments. Emission rates also varied along the route. The highest emission rates, which averaged at least twice the route average, were at S, NSA, and NSD segments. Consequently, the pollutant impact index for the spatially varying case was $\geq 105\%$ higher versus the average case at S, NSA, and NSD segments. On average for the entire route, the pollutant impact index for the spatially varying case was 11% and 18% higher versus the average case for NO_x and PM emissions, respectively. Therefore, using route average emission rates as opposed to spatially varying emission rates led to underestimation of the impact of emission rates on exposure estimates, especially near densely populated locations. Based on average emission rates, the accuracy of identification of impact hotspots and non-hotspots was 92%. Thus, average emission rates could be used to identify most of the impact hotspots. However, spatially varying emission rates are needed to accurately quantify the intensity of impact hotspots.



(a) Population Density



(b) NO_x Emission Rate



(c) NO_x Emission Impact Index

Figure 2-3. Segment-Average Data for Spatially Varying and Average Rates for the Piedmont Passenger Rail Service between Raleigh, NC and Charlotte, NC in Each Travel Direction Based on 35 One-Way Trips: (a) 2010 CensuA-Tract based Population Density; (b) NO_x Emission Rate; and (c) NO_x Emission Impact Index, which is the Product of Population Density and Emission Rate. There are 692 segments, of which each is 0.25 miles long.

To quantify the effect of combinations of explanatory variables leading to high or low rates, variables corresponding to segment-runs in the top and bottom 20th percentiles of fuel use rates were compared (Table A-13). The top 20% of segments by fuel use had lower average speed, higher mean acceleration, and higher mean grade than segments in the bottom 20%. Speeds in the upper fuel use quintile were typically <20 mph compared to >65 mph in the lower quintile. The upper quintile was associated with a 93.3% frequency of positive accelerations whereas the lower quintile was associated with a 61.2% frequency of negative accelerations. The frequency distributions for grade overlap between the upper and lower quintiles, but there was 83.9% frequency of positive grades for the upper quintile and 85.4% frequency of negative grades for the lower quintile. The frequency distributions for curvature were qualitatively similar between upper and lower quintiles.

Each CART model was calibrated based on 17,332 segment-runs and validated based on 5,866 segment-runs. The calibration data comprised ten and 16 eastbound and westbound one-way trips, respectively. The validation data comprised four and five eastbound and westbound one-way trips, respectively.

The validation of the SD models for NO_x and PM are illustrated in Figure 2-4. MA for the SD models varied between 87% to 89% among the three species. MP varied between 70% and 80%. Thus, there was a high probability of properly categorizing segments and of correctly identifying modeled hotspots. Between 75% and 78% of the FP had segment-run average FUERs between the 70th and 80th percentiles, which is in the top 1/8th of the non-hotspot range. Thus, most of the FP were near-missed hotspots. Between 47% and 53% of the FN had segment-run average FUER in the lower 1/8th of the hotspot range, between the 80th and 82.5th percentile. Thus, these were also near-misses. If the FP and FN near-misses are counted as being true values, MA and MP each increase to 92% to 94%, depending on the species. Similar values of MA and MP were estimated for the calibration data and other three CART models based on calibration and validation data. The SD model is preferred over other models because it has similar performance while being the simplest (Figures A-25 through A-36: Four models for each species).

The SD fuel use, NO_x, and PM models were similar to each other in terms of the number of nodes, the amount of data in each node, the splitting variable identified at each node, and the value of the splitting variable at each node (Figures A-27, A-31, and A-35). VI for each potential variable was also similar among these models (Figure A-37). Since the SD models are similar, one of them, the NO_x model, is used to illustrate the results. The SD model indicates combinations of variables that lead to relative hotspots and the complementary combination of variables that lead to relative non-hotspots. Each of the splits occurred based on speed, or acceleration, or grade. Therefore, speed, acceleration, and grade are key variables that discriminate hotspots from non-hotspots. None of the splits was based on curvature. Train speeds on curves are lower than other locations to prevent overturning and passenger discomfort.⁷⁶ Therefore, trains typically decelerated when approaching a curve, resulting in negative acceleration resistance that compensated for positive curvature resistance. Some segments with curves had grades. However, based on maximum encountered curvature and grade, curvature resistance was only 16% of grade resistance.

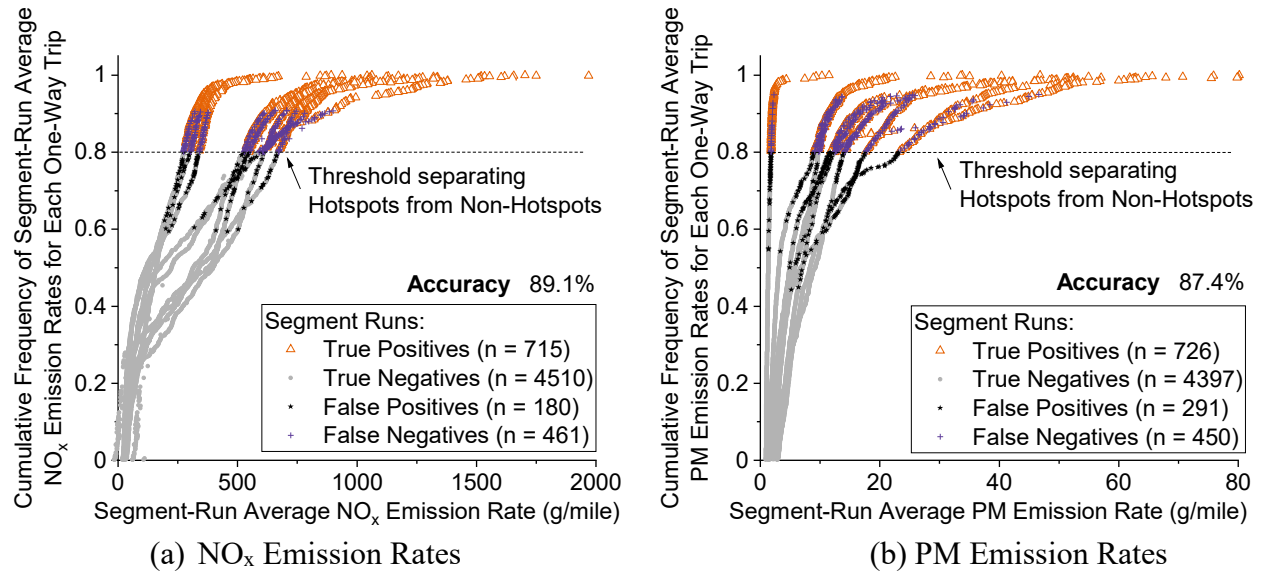


Figure 2-4. Validation of the Classification and Regression Tree-based NO_x and PM Relative Hotspot Prediction Simplified Model with Dynamic Variables including Segment-Average Speed, Acceleration, Grade, and Curvature as Explanatory Variables. Validation data includes one one-way trip from each combination of locomotives and consists for a total of 9 one-way trips comprising 5866 segment-runs. The numbers in parentheses indicate the total number of true positives, true negatives, false positives, and false negatives.

Ranges of segment-run average values of the key variables were classified as low, medium, and high taking into account the cut-points identified for splitting data into branches in the NO_x SD model as follows: (a) low and high average speed is <9.5 mph and >63.8 mph, respectively; (b) low and high acceleration is <0.025 mph/s and >0.18 mph/s, respectively; and (c) low and high grade is <0.08% and >0.72%, respectively. All values equal to or greater than the upper bound of low, and equal to or lower than the upper bound of high, are classified as medium.

Of all relative hotspots, 80%, 75%, and 55% were associated with medium speed, high acceleration, and high grade, respectively. All segment-runs with speed <9.5 mph were hotspots (9% of all hotspots). Such segment-runs were observed for S and NSA. The plurality of relative hotspots (33%) were associated with medium speed and high acceleration combined with medium or high grade. The next highest proportion of hotspots (10%) were associated with medium speed, medium acceleration, and high grade. All S segment-runs were relative hotspots and were associated with either low average speed (<9.5 mph) combined with medium acceleration or average speeds as high as 16 mph combined with high acceleration. Vojtisek-Lom *et al.* (2020) measured real-world passenger train FUERs using PEMS and acknowledged that emissions during departure from stations are of concern for exposure and emissions hotspots.

Segment-run average speed, acceleration, and grade associated with hotspots were 49 mph, 0.3 mph/s, and 0.7%, respectively. In contrast, segment average speed, acceleration, and grade associated with non-hotspots were 65 mph, -0.1 mph/s, and -0.1%, respectively. Therefore, in comparison with non-hotspots, on average, hotspots were associated with lower speed, higher acceleration, and higher grade.

In the order of decreasing VI, acceleration, grade and speed were the key variables in distinguishing hotspots from non-hotspots. Curvature had a negligible VI compared to other variables. Locomotive and consist also had negligible VI based on the comparison of NO_x SD and SDS models.

Dick and DiDomenico (2016) quantified key factors affecting passenger rail energy intensity based on the Rail Traffic Controller (RTC) train movement simulator. Using the simulator, key factors affecting energy intensity were found to include route average grade, route average speed, and number of locomotives.⁷⁷ Here, grade, speed, and number of locomotives were among the key factors affecting segment-average FUEs. The average fuel use rate of 1.4 gal/train-mile for the Piedmont passenger rail route is comparable to the national average Amtrak fuel use rate of 1.7 gal/train-mile⁷⁸ for diesel trains after accounting for the lower power demand of Piedmont trains, with only 3 to 5 passenger cars, compared to the national average of 8 passenger cars per train. Thus, fuel use rates are reasonable compared to reported data.

Gould and Niemeier (2011) estimated link-based variations in freight rail FUEs, based on links with distances of tens to hundreds of miles, and developed fuel use and emissions intensity (FUEI, g/ton-mile) estimates based on steady-state engine dynamometer data.¹⁹ They concluded that inter-link variation in FUEIs for a given train differed by a factor of 3 to 5 depending on species. Dick and DiDomenico (2016) and Gould and Niemeier (2011) recommended that spatially resolved train-specific FUEs, activity, and infrastructure data are needed to more accurately estimate spatially-varying FUEs.^{19,77} Consistent with the recommendations from these studies, this work focused on demonstrating a method for high spatial resolution quantification of FUEs. Although several of the key factors identified here are consistent with prior findings obtained at low spatial resolution (e.g., routes, or long links) using other methods, a distinctive feature of this work is its basis on high resolution (i.e. 0.25 mile segments) train-specific empirical data coupled with analysis focused on elucidating trends at high spatial resolution.

This work demonstrates that PEMS based measurements are useful for quantifying spatial variability in FUEs and associated factors for a given route and operation. Train activity and infrastructure variables can be easily inferred from low-cost GPS devices.^{34,63} The methods and example case study demonstrate that spatial variability in FUEs contributes to high emission rates in populated areas. Intuitively, hotspots are likely to be located on segments with positive grades or positive acceleration. However, the location of hotspots is affected by a combination of key variables such as speed, acceleration, and grade. Segments with positive grades or acceleration may not necessarily be hotspots. For example, some NSA segment-runs were non-hotspots because of low acceleration on high grades. Combinations of values of key variables were identified that could potentially mitigate some of the hotspots via modifications to operation. This information is useful to help operators achieve fuel use and emissions reductions without costly infrastructure modifications such as track realignment.

Results here are based on values measured during typical train operation rather than from controlled experiments aimed at quantifying the efficacy of potential FUEs reduction interventions. Future work is recommended to quantify the efficacy of potential FUEs reduction interventions based on a controlled experiment with lower accelerations on NSA segments, coupled with higher peak speeds on I segments to maintain scheduled travel time between stations. Scheduling constraints, speed limits, rail traffic, delays, and existing track

infrastructure would need to be considered in designing a modified train trajectory that reduces the number of hotspots. Yuan *et al.*, 2020 illustrate that train operations can be varied to reduce energy use and emissions while adhering to a schedule.³³

For hotspots where the modification of train operation may be unachievable, emission reduction interventions such as alternate fuels and retrofitted exhaust aftertreatment technology may be effective. The combined effect of operation, fuels, and technology on FUEs and hotspots are recommended for further evaluation.

Several train trajectory optimization studies report that an ideal strategy to reduce fuel use between adjacent stations is to accelerate rapidly to the maximum allowable or attainable speed, maintain a constant speed, coast without traction forces, and decelerate when approaching stations.^{35,36,42} As shown here segment-runs with acceleration are likely to be emission hotspots. Trajectory optimization algorithms do not currently account for such localized emission hotspots.

The study design demonstrated here to identify hotspots based on key explanatory variables can be applied to other intercity and long-distance passenger train services including Amtrak which is mostly diesel-powered and operates on routes with similar track geometry as the Piedmont route. These routes pass through densely populated cities. Similar to the Piedmont route, hotspots are likely to be located near populated centers resulting in a disproportionately high impact index. However, the cut-points for key variables and their importance could vary among different passenger rail systems because of variations in key variables and distances between stations. For rail services with distances between stations larger than measured here, acceleration away from stations will affect a lower proportion of segment time and distance compared, thereby reducing its importance. Freight trains can be much longer than passenger trains, which increases the importance of inertia management, including challenges with attribution of locomotive emissions to infrastructure for a train that straddles a hilltop, and the importance of factors such as dynamics of coupler slack during acceleration or deceleration that are negligible for much shorter passenger trains.^{79,80}

2.4 Summary of Supporting Information

The supporting information includes: (1) specifications of measured locomotives and consists; (2) description of instrumentation; (3) Amtrak-operated Piedmont passenger rail service route map and schedule; (4) procedure for installation of the PEMS on the PME; (5) procedure for time alignment of data from several sources; (6) procedure for quality assurance and quality control; (7) procedure for estimation of FUEs; (8) procedure for identification of potential explanatory variables; (9) procedure for rail-grade and curvature estimation; (10) characterizing track segments and segment-runs into hotspots and non-hotspots; (11) summary of segment-average activity, FUEs, and population density; and, (12) description of CART model, model calibration and validation, and variable importance. The supporting information to Chapter 2 can be found in Appendix A.

2.5 References Cited in Chapter 2

- (1) AAR. *Railroad Facts 2020*; A66-7305; Association of American Railroads: Washington, DC, 2020.
- (2) Transportation Statistics Annual Report 2020. **2020**. <https://doi.org/10.21949/1520449>.
- (3) EPA. *Locomotive Emission Standards: Regulatory Support Document*; EPA/98-04; U.S. Environmental Protection Agency: Ann Arbor, MI, 1998.
- (4) EPA. Final Rule for Control of Emissions of Air Pollution from Locomotive Engines and Marine Compression-Ignition Engines Less Than 30 Liters per Cylinder. *Federal Register* **2008**, 73 (126), 37096–37350.
- (5) Amtrak. *FY21-26 Five Year Service and Asset Line Plans*; National Passenger Rail Corporation (Amtrak): Washington, D.C., 2020.
- (6) APTA. *2020 Public Transportation Fact Book*; Edition 71; American Public Transportation Association, 2020.
- (7) Davis, S. C.; Boundy, R. G. *Transportation Energy Data Book*, 37th ed.; Oak Ridge National Laboratory, ORNL-5198: Oak Ridge, TN, 2018.
- (8) Sprung, M. J.; Nguyen, L. X.; Riley, D.; Zhou, S.; Lawson, A. *National Transportation Statistics 2018*; Bureau of Transportation Statistics. U.S. Department of Transportation; Washington, D.C., 2018.
- (9) NCRRP. *Comparison of Passenger Rail Energy Consumption with Competing Modes*; NCRRP Report 3; Prepared for National Cooperative Rail Research Program (NCRRP) by TranSys Research Ltd.; RailTEC at the University of Illinois at Urbana-Champaign; Canadian Pacific Consulting Services Transcom; and Lawson Economics Research Inc.: Washington, D.C., 2015.
- (10) Graver, B. M.; Frey, H. C. Highway Vehicle Emissions Avoided by Diesel Passenger Rail Service Based on Real-World Data. *Urban Rail Transit* **2016**, 2 (3–4), 153–171.
- (11) EPA. *Integrated Science Assessment (ISA) For Particulate Matter (Final Report, Dec 2009)*; EPA/600/R-08/139F; U.S. Environmental Protection Agency: Washington, DC, 2009.
- (12) EPA. *Integrated Science Assessment (ISA) for Oxides of Nitrogen - Health Criteria (Final Report, 2016)*; EPA/600/R-15/068; U.S. Environmental Protection Agency: Washington, DC, 2016.
- (13) Marshall, J. D.; Swor, K. R.; Nguyen, N. P. Prioritizing Environmental Justice and Equality: Diesel Emissions in Southern California. *Environmental science & technology* **2014**, 48 (7), 4063–4068.
- (14) Anderson, C. M.; Kissel, K. A.; Field, C. B.; Mach, K. J. Climate Change Mitigation, Air Pollution, and Environmental Justice in California. *Environmental science & technology* **2018**, 52 (18), 10829–10838.
- (15) Hasheminassab, S.; Sowlat, M. H.; Pakbin, P.; Katzenstein, A.; Low, J.; Polidori, A. High Time-Resolution and Time-Integrated Measurements of Particulate Metals and Elements in an Environmental Justice Community within the Los Angeles Basin: Spatio-Temporal

- Trends and Source Apportionment. *Atmospheric Environment: X* **2020**, 7, 100089.
<https://doi.org/10.1016/j.aeaoa.2020.100089>.
- (16) Bergin, M. S.; Harrell, M.; Janssen, M. Locomotive Emission Inventories for the United States from ERTAC Rail. In *2012 Annual International Emission Inventory Conference*; Tampa, Florida, 2012; pp 13–16.
 - (17) Hubbell, B.; Fann, N.; Levy, J. I. Methodological Considerations in Developing Local-Scale Health Impact Assessments: Balancing National, Regional, and Local Data. *Air Quality, Atmosphere & Health* **2009**, 2 (2), 99–110. <https://doi.org/10.1007/s11869-009-0037-z>.
 - (18) Fann, N.; Roman, H. A.; Fulcher, C. M.; Gentile, M. A.; Hubbell, B. J.; Wesson, K.; Levy, J. I. Maximizing Health Benefits and Minimizing Inequality: Incorporating Local-Scale Data in the Design and Evaluation of Air Quality Policies. *Risk Analysis* **2011**, 31 (6), 908–922. <https://doi.org/10.1111/j.1539-6924.2011.01629.x>.
 - (19) Gould, G. M.; Niemeier, D. A. Spatial Assignment of Emissions Using a New Locomotive Emissions Model. *Environmental Science & Technology* **2011**, 45 (13), 5846–5852.
 - (20) Liroy, P. J.; Smith, K. R. A Discussion of Exposure Science in the 21st Century: A Vision and a Strategy. *Environmental Health Perspectives* **2013**, 121 (4), 405–409. <https://doi.org/10.1289/ehp.1206170>.
 - (21) Galvis, B.; Bergin, M.; Russell, A. Fuel-Based Fine Particulate and Black Carbon Emission Factors from a Railyard Area in Atlanta. *Journal of the Air & Waste Management Association* **2013**, 63 (6), 648–658.
 - (22) Bergin, M.; Harrell, M.; McDill, J.; Janssen, M.; Driver, L.; Fronczak, R.; Nath, R.; Seep, D. ERTAC Rail: A Collaborative Effort in Building a Railroad-Related Emissions Inventory Between Eastern States Air Protection Agencies and Participation with the Railroad Industry. In *18th Annual International Emission Inventory Conference, Baltimore, MD*; Citeseer, 2009.
 - (23) Osborne, D.; Fritz, S.; Glenn, D. The Effects of Biodiesel Fuel Blends on Exhaust Emissions from a General Electric Tier 2 Line-Haul Locomotive. *Journal of Engineering for Gas Turbines and Power* **2011**, 133 (10), 102803.
 - (24) Osborne, D. T.; Fritz, S. G.; Iden, M.; Newburry, D. Exhaust Emissions from a 2,850 KW EMD SD60M Locomotive Equipped with a Diesel Oxidation Catalyst. In *ASME/IEEE 2007 Joint Rail Conference and Internal Combustion Engine Division Spring Technical Conference*; American Society of Mechanical Engineers: Pueblo, Colorado, USA, 2007; pp 441–449.
 - (25) Weaver, C. S. *Start-Up And Idling Emissions From Two Locomotives*; Technical Report SCAQMD No. 00112; Prepared for the South Coast Air Quality Management District: Diamond Bar, CA, 2006.
 - (26) Fritz, S. G.; California Environmental Protection Agency.; Air Resources Board.; Fuels Section.; Southwest Research Institute. *Diesel Fuel Effects on Locomotive Exhaust Emissions*; Prepared for California Air Resources Board by Southwest Research Institute: San Antonio, TX; Sacramento, CA, 2000.

- (27) Fritz, S. G. *Evaluation of Biodiesel Fuel in an EMD GP38-2 Locomotive*; NREL/SR-510-33436; Prepared for National Renewable Energy Laboratory by Southwest Research Institute: San Antonio, TX, 2004. <https://doi.org/10.2172/15009674>.
- (28) EPA. *Emission Factors for Locomotives*; EPA420-F-97-051; U.S. Environmental Protection Agency: Ann Arbor, MI, 1997.
- (29) Profillidis, V. A. *Railway Management and Engineering*; Ashgate Publishing, Ltd.: Burlington, VT, 2014.
- (30) Hay, W. W. *Railroad Engineering*; John Wiley & Sons: New York, 1982; Vol. 1.
- (31) AREMA. *American Railway Engineering and Maintenance-of-Way Association Manual for Railway Engineering*; Lanham, MD, 2020.
- (32) Graver, B. M.; Frey, H. C. Comparison of Over-the-Rail and Rail Yard Measurements of Diesel Locomotives. *Environmental Science & Technology* **2015**, *49* (21), 13031–13039.
- (33) Yuan, W.; Frey, H. C. Potential for Metro Rail Energy Savings and Emissions Reduction via Eco-Driving. *Applied Energy* **2020**, *268*, 114944.
- (34) Yuan, W.; Frey, H. C.; Rastogi, N. Quantification of Energy Saving Potential for A Passenger Train Based on Inter-Run Variability in Speed Trajectories. *Transportation Research Record* **2019**, *2673* (5), 153–165.
- (35) Feng, X. Optimization of Target Speeds of High-Speed Railway Trains for Traction Energy Saving and Transport Efficiency Improvement. *Energy Policy* **2011**, *39* (12), 7658–7665.
- (36) Kim, K.; Chien, S. I.-J. Optimal Train Operation for Minimum Energy Consumption Considering Track Alignment, Speed Limit, and Schedule Adherence. *Journal of Transportation Engineering* **2010**, *137* (9), 665–674.
- (37) Frey, H. C.; Choi, H. W.; Kim, K. Portable Emission Measurement System for Emissions of Passenger Rail Locomotives. *Transportation Research Record: Journal of the Transportation Research Board* **2012**, *2289*, 56–63.
- (38) Frey, H. C.; Rastogi, N. *Evaluation of Locomotive Emissions Reduction Strategies*; FHWA/NC/2016-20; Prepared by North Carolina State University for North Carolina Department of Transportation: Raleigh, NC, 2018; p 228.
- (39) Vojtisek-Lom, M.; Jirků, J.; Pechout, M. Real-World Exhaust Emissions of Diesel Locomotives and Motorized Railcars during Scheduled Passenger Train Runs on Czech Railroads. *Atmosphere* **2020**, *11* (6), 582.
- (40) Drish, W. F. *Train Energy Model Version 2.0 Technical Manual*; Publication SD-040, Association of American Railroads: Washington, D.C., 1992.
- (41) Xu, Y.; Gbologah, F.; Cernjul, G.; Kumble, A.; Guensler, R.; Rodgers, M. Comparison of Fuel-Cycle Emissions per Passenger Mile from Multiple Bus and Rail Technologies. In *Proc., Third International Conference on Urban Public Transportation Systems*; 2013; pp 204–216.
- (42) Wang, J.; Ghanem, A.; Rakha, H.; Du, J. A Rail Transit Simulation System for Multi-Modal Energy-Efficient Routing Applications. *International Journal of Sustainable Transportation* **2020**, 1–16. <https://doi.org/10.1080/15568318.2020.1718809>.

- (43) Khan, T.; Frey, H. C.; Rastogi, N.; Wei, T. Geospatial Variation of Real-World Tailpipe Emission Rates for Light-Duty Gasoline Vehicles. *Environ. Sci. Technol.* **2020**, *54* (14), 8968–8979. <https://doi.org/10.1021/acs.est.0c00489>.
- (44) Shu, Y.; Lam, N. S.; Reams, M. A New Method for Estimating Carbon Dioxide Emissions from Transportation at Fine Spatial Scales. *Environmental Research Letters* **2010**, *5* (4), 044008.
- (45) Gately, C. K.; Hutyra, L. R.; Peterson, S.; Sue Wing, I. Urban Emissions Hotspots: Quantifying Vehicle Congestion and Air Pollution Using Mobile Phone GPS Data. *Environmental Pollution* **2017**, *229*, 496–504. <https://doi.org/10.1016/j.envpol.2017.05.091>.
- (46) Zhang, S.; Niu, T.; Wu, Y.; Zhang, K. M.; Wallington, T. J.; Xie, Q.; Wu, X.; Xu, H. Fine-Grained Vehicle Emission Management Using Intelligent Transportation System Data. *Environmental Pollution* **2018**, *241*, 1027–1037. <https://doi.org/10.1016/j.envpol.2018.06.016>.
- (47) Breuer, J. L.; Samsun, R. C.; Peters, R.; Stolten, D. The Impact of Diesel Vehicles on NO_x and PM₁₀ Emissions from Road Transport in Urban Morphological Zones: A Case Study in North Rhine-Westphalia, Germany. *Science of The Total Environment* **2020**, *727*, 138583. <https://doi.org/10.1016/j.scitotenv.2020.138583>.
- (48) Apte, J. S.; Messier, K. P.; Gani, S.; Brauer, M.; Kirchstetter, T. W.; Lunden, M. M.; Marshall, J. D.; Portier, C. J.; Vermeulen, R. C. H.; Hamburg, S. P. High-Resolution Air Pollution Mapping with Google Street View Cars: Exploiting Big Data. *Environ. Sci. Technol.* **2017**, *51* (12), 6999–7008. <https://doi.org/10.1021/acs.est.7b00891>.
- (49) 40 CFR 1065. Engine Testing Procedures. *Federal Register* **2005**, *70* (133), 40516–40612.
- (50) Vojtisek-Lom, M.; Allsop, J. E. Development Of Heavy-Duty Diesel Portable, On-Board Mass Exhaust Emissions Monitoring System With NO_x, CO₂ And Qualitative PM Capabilities; SAE International, 2001. <https://doi.org/10.4271/2001-01-3641>.
- (51) Gilliam, J.; Hall, E. Reference and Equivalent Methods Used to Measure National Ambient Air Quality Standards (NAAQS) Criteria Air Pollutants-Volume IUS Environmental Protection Agency, Washington, DC. *Environmental Protection Agency: Washington, DC, USA* **2016**.
- (52) 40 CFR 1065, S. J. Field Testing and Portable Emission Measurement Systems. *Federal Register* **2005**, *70* (133), 40599–40604.
- (53) Frey, H. C.; Rastogi, N. *Managing Energy and Emissions for Rail Operations*; FHWA/NC/2018-09; Prepared by North Carolina State University for North Carolina Department of Transportation: Raleigh, NC, 2019.
- (54) Graver, B. M.; Frey, H. C.; Hu, J. Effect of Biodiesel Fuels on Real-World Emissions of Passenger Locomotives. *Environmental Science & Technology* **2016**, *50* (21), 12030–12039.
- (55) Johnson, K. C.; Durbin, T. D.; Jung, H.; Cocker, D. R.; Bishnu, D.; Giannelli, R. Quantifying In-Use PM Measurements for Heavy Duty Diesel Vehicles. *Environ. Sci. Technol.* **2011**, *45* (14), 6073–6079. <https://doi.org/10.1021/es104151v>.

- (56) Khan, M. Y.; Johnson, K. C.; Durbin, T. D.; Jung, H.; Cocker, D. R.; Bishnu, D.; Giannelli, R. Characterization of PM-PEMS for in-Use Measurements Conducted during Validation Testing for the PM-PEMS Measurement Allowance Program. *Atmospheric Environment* **2012**, *55*, 311–318. <https://doi.org/10.1016/j.atmosenv.2012.03.004>.
- (57) Durbin, T. D.; Johnson, K.; Cocker, D. R.; Miller, J. W.; Maldonado, H.; Shah, A.; Ensfield, C.; Weaver, C.; Akard, M.; Harvey, N.; Symon, J.; Lanni, T.; Bachalo, W. D.; Payne, G.; Smallwood, G.; Linke, M. Evaluation and Comparison of Portable Emissions Measurement Systems and Federal Reference Methods for Emissions from a Back-Up Generator and a Diesel Truck Operated on a Chassis Dynamometer. *Environ. Sci. Technol.* **2007**, *41* (17), 6199–6204. <https://doi.org/10.1021/es0622251>.
- (58) Sensors Inc. *SEMTECH-DS: On Board Vehicle Emissions Analyzer User Manual*; Revision 2.02; 9510–086; Saline, MI, 2011.
- (59) Weaver, C. S.; Balam-Almanza, M. V. Development of the “RAVEM” Ride-Along Vehicle Emission Measurement System for Gaseous and Particulate Emissions. *SAE Transactions* **2001**, *110*, 2270–2275.
- (60) Graver, B. M.; Frey, H. Comparison of Locomotive Emissions Measured During Dynamometer Versus Rail Yard Engine Load Tests. *Transportation Research Record: Journal of the Transportation Research Board* **2013**, No. 2341, 23–33.
- (61) Vojtisek, M.; Kotek, M. Estimation of Engine Intake Air Mass Flow Using a Generic Speed-Density Method. *Journal of Middle European Construction and Design of Cars* **2014**, *12* (1), 7–15.
- (62) Frey, H. C.; Hu, J. *Measurement of Locomotive Head End Power Engine Fuel and Emissions*; Technical Report 0704–0188; Prepared by North Carolina State University for North Carolina Department of Transportation: Raleigh, NC, 2015.
- (63) Rastogi, N.; Frey, H. C. Estimation of Rail Grade and Horizontal Curvature from Non-Proprietary Data Sources. In *Proceedings of the Transportation Research Board 97th Annual Meeting*; 18-06366; Washington, D.C., 2018.
- (64) Unal, A.; Frey, H. C.; Roupail, N. M. Quantification of Highway Vehicle Emissions Hot Spots Based upon On-Board Measurements. *Journal of the Air & Waste Management Association* **2004**, *54* (2), 130–140.
- (65) Fernandes, P.; Salamati, K.; Roupail, N. M.; Coelho, M. C. Identification of Emission Hotspots in Roundabouts Corridors. *Transportation Research Part D: Transport and Environment* **2015**, *37*, 48–64. <https://doi.org/10.1016/j.trd.2015.04.026>.
- (66) Mudgal, A.; Hallmark, S.; Carriquiry, A.; Gkritza, K. Driving Behavior at a Roundabout: A Hierarchical Bayesian Regression Analysis. *Transportation Research Part D: Transport and Environment* **2014**, *26*, 20–26. <https://doi.org/10.1016/j.trd.2013.10.003>.
- (67) Frey, H. C.; Burmaster, D. E. Methods for Characterizing Variability and Uncertainty: Comparison of Bootstrap Simulation and Likelihood-Based Approaches. *Risk Analysis* **1999**, *19* (1), 109–130.

- (68) Cullen, A. C.; Frey, H. C. *Probabilistic Techniques in Exposure Assessment: A Handbook for Dealing with Variability and Uncertainty in Models and Inputs*; Springer Science & Business Media, 1999.
- (69) Vette, A.; Burke, J.; Norris, G.; Landis, M.; Batterman, S.; Breen, M.; Isakov, V.; Lewis, T.; Gilmour, M. I.; Kamal, A.; Hammond, D.; Vedantham, R.; Bereznicki, S.; Tian, N.; Croghan, C. The Near-Road Exposures and Effects of Urban Air Pollutants Study (NEXUS): Study Design and Methods. *Science of The Total Environment* **2013**, *448*, 38–47. <https://doi.org/10.1016/j.scitotenv.2012.10.072>.
- (70) Kumar, P.; Rivas, I.; Singh, A. P.; Ganesh, V. J.; Ananya, M.; Frey, H. C. Dynamics of Coarse and Fine Particle Exposure in Transport Microenvironments. *npj Climate and Atmospheric Science* **2018**, *1* (1), 11. <https://doi.org/10.1038/s41612-018-0023-y>.
- (71) Snyder, M. G.; Venkatram, A.; Heist, D. K.; Perry, S. G.; Petersen, W. B.; Isakov, V. RLINE: A Line Source Dispersion Model for near-Surface Releases. *Atmospheric Environment* **2013**, *77*, 748–756. <https://doi.org/10.1016/j.atmosenv.2013.05.074>.
- (72) Chang, S. Y.; Vizuete, W.; Valencia, A.; Naess, B.; Isakov, V.; Palma, T.; Breen, M.; Arunachalam, S. A Modeling Framework for Characterizing Near-Road Air Pollutant Concentration at Community Scales. *Science of The Total Environment* **2015**, *538*, 905–921. <https://doi.org/10.1016/j.scitotenv.2015.06.139>.
- (73) Breiman, L.; Friedman, J.; Olshen, R.; Stone, C. *Classification and Regression Trees*; Chapman & Hall/CRC: Boca Raton, FL 33487-2742, 1984.
- (74) Snousy, M. B. A.; El-Deeb, H. M.; Badran, K.; Khlil, I. A. A. Suite of Decision Tree-Based Classification Algorithms on Cancer Gene Expression Data. *Egyptian Informatics Journal* **2011**, *12* (2), 73–82. <https://doi.org/10.1016/j.eij.2011.04.003>.
- (75) Bachman, J.; Marchetti, J.; Meacham Jr, H.; Uher, R.; Watson, R. *Improved Passenger Equipment Evaluation Program - Train System System Review Report Volume I Baseline Data*; FRA/ORD 80/14.I; Prepared by Unified Industries Incorporated for U.S. Department of Transportation, Federal Railroad Administration: Washington, D.C., 1978.
- (76) 49 CFR 213. Track Safety Standards. *Federal Register* **1998**, *63* (119), 34029–34056.
- (77) Dick, C. T.; DiDomenico, G. *Factors Affecting Commuter Rail Energy Efficiency*; NURail2013-UIUC-R12; Report prepared for the U.S. Department of Transportation by University of Illinois at Urbana-Champaign: Washington, D.C., 2016.
- (78) Davis, S. C.; Boundy, R. G. *Transportation Energy Data Book*, 39th ed.; Oak Ridge National Laboratory, ORNL-5198: Oak Ridge, TN, 2020.
- (79) Cole, C.; Spiryagin, M.; Wu, Q.; Sun, Y. Q. Modelling, Simulation and Applications of Longitudinal Train Dynamics. *Vehicle System Dynamics* **2017**, *55* (10), 1498–1571. <https://doi.org/10.1080/00423114.2017.1330484>.
- (80) Wu, Q.; Luo, S.; Cole, C. Longitudinal Dynamics and Energy Analysis for Heavy Haul Trains. *Journal of Modern Transportation* **2014**, *22* (3), 127–136.

CHAPTER 3: Modeling Spatial Variability in Locomotive Fuel Use and Emission Rates based on Real-World Measurements

3.1 Introduction

In 2018, U.S. diesel-powered passenger trains, such as intercity and commuter rail, consumed 22.6 trillion BTUs of energy resulting in 563,000 short tons of carbon dioxide (CO₂) emissions (Amtrak, 2018; Miller, 2020). Diesel-powered passenger trains are typically more energy-efficient and lower emitters of CO₂, carbon monoxide (CO), and hydrocarbons (HC) per passenger-mile than passenger cars, buses, and airplanes (NCRRP, 2015; Sprung et al., 2018). However, diesel-powered passenger trains are typically high emitters of oxides of nitrogen (NO_x) and particulate matter (PM) (Graver and Frey, 2016).

CO₂ is a greenhouse gas and results in climate change (U.S. Environmental Protection Agency [EPA], 2016a). EPA regulates CO, HC, NO_x, and PM because of their adverse human health impacts (EPA, 2016b, 2010, 2009, 2008). Approximately 50% of the 25,604 diesel locomotives used for U.S. freight, intercity passenger, and commuter rail service were manufactured before 2001 (AAR, 2020; Amtrak, 2020; APTA, 2020). With rebuilds, these locomotives can be operational for several decades and, in many cases, certified to the least stringent emission standards taken into effect from 1998 (EPA, 1998). People near rail routes may be exposed to elevated pollutant concentrations because trains pass through densely populated urban corridors (Bergin et al., 2012; Rastogi and Frey, 2021).

Diesel locomotives used for passenger service typically have a prime mover engine (PME) and a head-end power engine. The PME generates direct current electricity that powers traction motors (Dincer et al., 2016). The PME has a throttle control with eight non-idle notch positions, a power take-off high idle position, and a low idle position. The locomotive is slowed using a mechanical brake or dynamic brake. The head-end power engine generates alternating current electricity for hotel services for passenger cars, including lighting and space conditioning (Dincer et al., 2016).

PME fuel use and emission rates vary spatially, leading to some locations with emission rates higher than a threshold, known as emission hotspots (Rastogi and Frey, 2021). Spatially resolved fuel use and emission rates are needed to: (1) quantify the source contribution of railroad sector emissions and to support quantification of local air pollution exposure and health impacts (Bergin et al., 2012; Dick and DiDomenico, 2016); (2) locate emission hotspots (Gould and Niemeier, 2011); and (3) improve train activity, by modifying speed trajectories to reduce fuel use and emission rates (Feng, 2011; Kim and Chien, 2010; Yuan and Frey, 2020). Demonstration of reduction in emissions is needed as a condition of receiving Federal funding for infrastructure changes (EPA, 2004).

Gould and Niemeier (2011) quantified fuel use and emission rates for diesel freight trains based on disaggregating national level fuel consumption data to segments of tens of hundreds of miles. Emission rates were based on steady-state engine dynamometer measurements. These measurements did not account for realistic train activity, including transients or the effect of track grade and curvature on train operation. Higher spatial resolution is needed to represent more localized spatial variability (Dick and DiDomenico, 2016). Diesel locomotive real-world CO₂, NO_x, and PM emission rates measured during real-world transient operation differed by an average of 5% to 10%, depending on pollutant species, compared to steady-state operation (Graver and Frey, 2015).

Based on real-world emission measurements conducted on a diesel passenger intercity rail service using a portable emissions measurement system (PEMS), Rastogi and Frey (2021) defined hotspots as 0.25-mile track segments exceeding the 80th percentile of segment-average fuel use and emission rates for a given species. Hotspots represented 20% of trip distance, contributed 40% to 50% of trip fuel use and emissions, and were located close to densely populated regions. Modifying or choosing alternative trajectories that reduce trip fuel use and emissions can worsen some emission hotspots (Yuan and Frey, 2021). Thus, there is a need to assess the sensitivity of hotspots to variations in trajectories.

Alternatively, 1 Hz train energy use rates have been estimated based on an assumed linear relationship of fuel use rate with positive locomotive power demand (LPD) (Drish, 1992; NCCRP, 2015; Yuan et al., 2019). LPD is the power provided by the locomotive to overcome resistive forces opposing train motion (Drish, 1992). Some studies quantified emission rates based on steady-state notch-average fuel use and emission rates (Xu et al., 2013, 2018; Yuan and Frey, 2021). In the real-world, variations in train fuel use and emission rates are attributable to variations in locomotives, consists, and fuels (LCFs). Locomotives differ with respect to chassis, engine models, and operation and maintenance history. Consists are defined as the number, model, and type of locomotives, passenger cars, and baggage/café cars that make up a train (APTA, 2019). Fuels vary in their physical and chemical properties (Fritz, 2004; Graver et al., 2016). Inter-LCF variability in fuel use and emission rates presents an opportunity to reduce system-wide fuel use and emissions for a fleet operator by prioritizing the dispatch of energy-efficient and low-emitting combinations of LCFs (Frey and Rastogi, 2019). A model is needed to predict transient-based fuel use and emission rates for different combinations of LCFs.

The objectives are to: (1) predict spatially varying real-world fuel use and emission rates; (2) quantify the accuracy and precision of such predictions; and (3) identify key resistive forces, locate hotspots, identify trajectories with low fuel use and emissions, and quantify inter-LCF variability in fuel use and emission rates.

3.2 Methods

Legacy passenger train activity and fuel use and emission rates data were used to calibrate and evaluate a new LPD-based model that accounts for inter-LCF and inter-trajectory variability in fuel use and emission rates, at high spatial and temporal resolution. The model is applied to identify key resistive forces, locate hotspots, identify trajectories with low trip fuel use and emissions, and quantify inter-LCF variability in fuel use and emission rates.

3.2.1 Legacy Data

Over-the-rail fuel use and emission rates, train activity (e.g., speed, acceleration), and track infrastructure (e.g., track grade, curvature) data were previously quantified, using PEMS, for the Piedmont passenger rail service (Frey et al., 2012; Graver and Frey, 2016, 2015; Rastogi and Frey, 2021). The Piedmont rail service is operated by Amtrak between Raleigh, NC and Charlotte, NC using equipment owned by the North Carolina Department of Transportation (NCDOT). Quality assured legacy 1 Hz data are available based on 200 h of measurements over 10,500 miles for 66 one-way trips conducted by 12 combinations of LCFs (Graver et al., 2016; Graver and Frey, 2015; Rastogi and Frey, 2021).

Measurements were conducted for two F59PHI and six F59PH locomotives (Graver and Frey, 2015, 2016; Rastogi and Frey, 2021). Each locomotive has a 12-cylinder, 140 L, 2-stroke 2240

kW EMD 12–710 diesel PME, and a 460 kW to 500 kW Caterpillar ACERT head-end power engine. These locomotives were manufactured between 1988 and 1999 and rebuilt between 2010 and 2016. The PMEs are certified to the U.S. EPA locomotive engine Tier 0+ standard after rebuild (EPA, 2008). These locomotives have similar age and emissions certification as approximately 50% of the U.S. locomotive fleet. The head-end power engines of two F59PHI and four F59PH locomotives are certified to the U.S. EPA nonroad Tier 2 standard (EPA, 2004), and of two F59PH locomotives are certified to the U.S. EPA nonroad Tier 3 standard (EPA, 2004).

One Hz train speed was measured using a locomotive activity recorder. Acceleration was inferred from speed. Speed varied between 0 mph and 79 mph, with an average of 54 mph. Acceleration varied within ± 2.3 mph/s. Grade and horizontal curvature were previously quantified for 692 0.25-mile track segments based on measurements using GPS receivers fitted with barometric altimeter (Rastogi and Frey, 2018). Grade varied within $\pm 1.9\%$. Curvature varied between 0 degrees and 4.3 degrees. The ranges of grade and curvature of the Piedmont route are similar to those of several other U.S. passenger rail routes (Bachman et al., 1978).

The trains operated in four consist types, preferred by the train operator, as described in Table 3-1. The locomotives were operated on ultra-low sulfur diesel (ULSD) or 20% blend of biodiesel in diesel (B20). Each measured combination of LCF was assigned a unique LCF ID (Table 3-2).

For each LCF, one locomotive was instrumented with a PEMS (Global MRV OEM-2100AX Axion). The PEMS measured CO₂, CO, and HC concentrations using nondispersive infrared (NDIR) analyzers, nitric oxide (NO) and oxygen concentrations using electrochemical analyzers, and PM concentration by laser light scattering. Measured HC, NO, and PM concentrations were bias-corrected using previously developed factors to estimate total HC, NO_x, and PM, respectively (Graver and Frey, 2015; Rastogi and Frey, 2021). Bias-corrections are explained in detail in Appendix A Section A.3.

The CO₂ and NO measurements of the PEMS were evaluated for accuracy based on comparison with reference instruments (Rastogi and Frey, 2021). The slopes of parity plots were within $\pm 5\%$ and $\pm 3\%$ of one for CO₂ and NO concentrations, respectively. A similar PEMS was independently evaluated in Vu et al. (2020) in which CO₂, CO, and NO_x concentrations were accurate within $\pm 5\%$. Thus, fuel use and emission rates estimated based on PEMS measurements are accurate.

Table 3-1. Definitions of Terms for Amtrak-Operated Piedmont Route Passenger Locomotive Consist Types, Emission Hotspots, and Confusion Metrics for Model Performance.

Category	Term	Definition
Consist Types ^a	Single Locomotive	One locomotive per train
	Single-Powered Push/Pull	One locomotive at each end of the train, one powered, other idles
	Double-Powered Push/Pull	One locomotive at each end of the train, both powered
	Double-Powered Tandem	Two adjacent locomotives at the head of the train, both powered
Hotspots	Absolute Hotspots	Segments with average mass per distance fuel use and emission rates in the top quintile based on all one-way trips.
	Relative Hotspots	Segments with average mass per distance fuel use and emission rates in the top quintile based on each one-way trip.
	Hotspot Accuracy	The proportion of correctly identified hotspots relative to the total number of estimated hotspots and non-hotspots
	Hotspot Precision	The proportion of the estimated relative hotspots that were correctly identified
Confusion Metrics	True Positives	Number of measured hotspots that were estimated by the model as hotspots
	True Negatives	Number of measured non-hotspots that were estimated by the model as non-hotspots
	False Positives	Number of measured non-hotspots that were estimated by the model as hotspots
	False Negatives	Number of measured hotspots that were estimated by the model as non-hotspots

^a Each consist type has one or two F59PH and/or F59PHI locomotives, a baggage/café car, and passenger cars.

Table 3-2. Combinations of Locomotives, Consists, and Fuels (LCF) Measured Over-The-Rail During Revenue-Generating Amtrak-Operated Piedmont Passenger Rail Service

LCF ID	Locomotive ^a	Locomotive Consist Type	Fuel ^b	One-way Trips	Number of Passenger Cars ^c	Train Weight (metric tons)	Train Length (m)
1	NC1797	Single Locomotive	ULSD	5	3	310	100
2	NC1810	Single Locomotive	ULSD	6	3	310	100
3	NC1859	Single Locomotive	ULSD	6	3	310	100
4	NC1859	Double-Powered Tandem	ULSD	5	6	630	190
5	NC1893	Single Locomotive	ULSD	6	3	310	100
6	NC1871	Single-Powered Push/Pull	ULSD	3	4	500	140
7	NC1871	Double-Powered Push/Pull	ULSD	3	4	500	140
8	NC1984	Single-Powered Push/Pull	ULSD	3	5	570	170
9	NC1984	Double-Powered Push/Pull	ULSD	3	5	570	170
10	NC1797	Single Locomotive	B20	3	3	310	100
11	NC1810	Single Locomotive	B20	3	3	310	100
12	NC1859	Single Locomotive	B20	15	3	310	100

^a Only the measured locomotive is indicated for the train consists with two locomotives. All locomotives have a 2240 kW EMD 12-710 prime mover engine and an additional 460 kW to 600 kW head end power engine. Locomotive NC 1797 is F59PHI. Others are F59PH.

^b Fuel: Ultra-Low Sulfur Diesel (ULSD); B20: 20% blend of biodiesel in diesel.

^c Number of passenger cars includes baggage/café car as they have equal weight and dimensions.

3.2.2 Locomotive Power Demand

LPD is based on resistive forces opposing train motion, including starting, journal, flange, air, wind, curve, grade, acceleration, and internal resistances (AREMA, 2020; Hay, 1982; Profillidis, 2014). LPD was estimated for each powered PME in a consist based on the modified Davis equation specified by the American Railway Engineering and Maintenance-of-Way Association (AREMA, 2020):

$$LPD_t = \left[R_{s,t} + \left\{ \left(0.6 + \frac{20}{w_l} + Bv_t + \frac{C_{d,l}F_l}{w_l n_l} v_t^2 \right) + \sum_{n=1}^N \left(0.6 + \frac{20}{w_l} + Bv_t + \frac{C_{d,p}F_l}{w_l n_l} v_t^2 \right) + \sum_{p=1}^P \left(0.6 + \frac{20}{w_p} + Bv_t + \frac{C_{d,p}F_p}{w_p n_p} v_t^2 \right) \right\} \times \left(\frac{I}{1 + P + N} \right) + Dd_t + Ex_t + Ga_t \right] \times \frac{0.0019 \times v_t \times W}{\eta \times L} \quad (3 - 1)$$

Where,

LPD_t	=	instantaneous locomotive power demand at time t (kW)
$R_{s,t}$	=	starting resistance at time t (18 lb/ton , AREMA, 2020)
w_l	=	weight of locomotive per axle (tons/axle)
B	=	flange resistance coefficient ($= 0.01 \text{ lb/ton-mph}$, AREMA, 2020)
v_t	=	train speed at time t (mph)
$C_{d,l}$	=	drag coefficient of the leading locomotive based on the shape of the front end and the overall configuration, including turbulence from car trucks, air brake fittings under the cars, space between cars, skin friction and eddy currents, and the turbulence and partial vacuum at the rear end ($\text{lb/ft}^2\text{-mph}^2$)
F_l	=	frontal cross-sectional area of the locomotive inferred based on flat rectangular cross-section (ft^2)
n_l	=	number of axles in a locomotive
N	=	number of trailing locomotives
n	=	index for trailing locomotive.
w_p	=	weight of empty passenger per axle (tons/axle)
$C_{d,p}$	=	drag coefficient of the trailing locomotive and passenger cars based on the shape of the front end and the overall configuration, including turbulence from car trucks, air brake fittings under the cars, space between cars, skin friction and eddy currents, and the turbulence and partial vacuum at the rear end ($\text{lb/ft}^2\text{-mph}^2$)
F_p	=	frontal cross-sectional area of the passenger car inferred based on flat rectangular cross-section (ft^2)
n_p	=	number of axles in a passenger car
P	=	number of passenger cars including baggage/café car
p	=	index for passenger cars and baggage/café car
D	=	unit curve resistance ($= 0.8 \text{ lb/ton-degree of curve}$, AREMA, 2020)
d_t	=	degree of a curve at time t (degrees)
E	=	unit grade resistance ($20 \text{ lb/ton-percent grade}$, AREMA, 2020)
x_t	=	rail grade at time t ($\%$)

G	=	unit acceleration resistance (= 200 $lb\text{-}s^2/ton\text{-}m$, AREMA, 2020)
a_t	=	train acceleration at time t (m/s^2)
I	=	factor for modernized train equipment (post-1950) to account for improved train and rail designs (= 0.85, AREMA, 2020)
η	=	locomotive efficiency factor (=0.82 for diesel-electric locomotives, AREMA, 2020)
W	=	total train weight ($tons$)
L	=	number of powered prime move engine

Trains are treated as a point mass because the measured passenger trains were typically 190 meters long or shorter and, thus, could be approximated as occupying a single 400-meter long track segment at a given time where fuel consumption and emissions occur. The model is not formulated to deal with long trains, such as freight trains which could traverse several curves (Wu et al., 2014), coupler slack dynamics of a long train that straddles a hilltop (Wang and Rakha, 2018; Wu et al., 2014), and high-speed trains (AREMA, 2020; Hay, 1982).

The difference in weight and LPD for fully occupied versus empty trains was <3% each (Frey and Rastogi, 2019). Therefore, differences in passenger car weight related to passenger load were neglected.

3.2.3 Modeling Fuel Use and Emission Rates

LPD in the current second is affected by LPD from the past seconds because the PME takes time, typically up to 30s, to transition from one notch position to another (Graver and Frey, 2015). To account for this transition, an n -second backward moving average LPD ($\overline{LPD}_{n,t}$) was estimated for each second, with n varying from 1s to 30s. The value of n with the highest average Pearson's correlation coefficient of $\overline{LPD}_{n,t}$ with fuel use and emission rates was selected.

Based on trends in over-the-rail measurements, sub-models for each LCF corresponding to ranges of LPD with distinct trends in fuel use and emission rates were identified and calibrated. From on-road emissions modeling, fuel use and emission rates are approximately constant for negative, zero, and peak engine loads (Bachman, 1998; Frey et al., 2002). Similar trends are observed for locomotive PMEs. Therefore, locomotive fuel use and emission rates for these ranges were inferred to be constant. Sub-models corresponding to negative, zero, and peak engine load include sub-model 1 (SM1), sub-model 2 (SM2), and sub-model 4 (SM4), respectively. Sub-model 3 (SM3) accounts for all other engine loads. The peak engine load for the EMD 12-701 PMEs is 2519 kW (3378 hp) (General Motors of Canada Limited, 1994). For LCFs with no measured data in SM4, SM4 fuel use and emission rates were inferred to be equal to those estimated by SM3 at the highest observed load.

SM3 was calibrated based on linear regression, quadratic regression, or a modal model. Models used to predict fuel use rates have typically been linear (Drish, 1992; Lukaszewicz, 2009). Quadratic and modal models were added to quantify observations of possible non-linear relationships for fuel use rate because the thermal efficiency of engines typically increases with engine output (Thiruvengadam et al., 2014). Emission rates are correlated with fuel use rates (Frey and Rastogi, 2019) and depend on spatial and temporal variation of chemical kinetics of pollutant formation in the engine cylinder under complex dynamics (Flagan and Seinfeld, 1988). Therefore, emission rates may also have non-linear relationships with engine output. Modal models have been used for on-road emissions modeling to represent complex trends in rates

without imposing an analytical approximation that introduces estimation error (Bachman, 1998; Frey et al., 2002). In a modal model, data are divided into power demand bins and average rates corresponding to each bin are quantified.

For SM3 for a given pollutant species, leave-one-out cross-validation (LOOCV) was employed. In LOOCV, all but one one-way trip was used to calibrate each sub-model. The left-out one-way trip was used for validation. LOOCV was repeated for all combinations of trips for a given LCF. LOOCV reduces bias among available trips in calibration and validation datasets by varying their combinations (Wong, 2015). If the calibrated parameters for a given species and LCF were within $\pm 10\%$ of each other for all possible LOOCV combinations, a final sub-model was calibrated based on all one-way trips combined.

The complete model for a given species and LCF, inclusive of data from all sub-models, was evaluated for accuracy and precision based on parity comparison of estimated versus measured fuel use and emission rates. These evaluations were conducted for three resolutions: 1 Hz, segment-average, and trip-average.

Train fuel use and emission rates include those from all operating PME(s) and head-end power engine(s). However, head-end power engine fuel use and emission rates had $<4\%$ contribution to train fuel use and emission rates and hotspots (Appendix B Section B.4). Thus, the results are based on PME fuel use and emission rates only. Head-end power engine fuel use and emission rates were inferred to be constant with time (Rastogi and Frey, 2021) and are detailed in the Appendix B. The complete model estimated fuel use and emission rates were benchmarked to publicly available fuel use and emission rates for the ULSD-fueled EMD 12-710 PME (EPA, 1998). For double-powered tandem and push/pull consists, the other locomotive was assumed to operate identically with the same fuel use and emission rates. For single-powered consists, the other locomotive PME operated continuously at idle.

3.2.4 Contribution of Resistive Forces

To identify key resistive forces affecting $\overline{LPD}_{n,t}$ and fuel use and emission rates, the contribution of resistive forces to $\overline{LPD}_{n,t}$ was quantified. As shown later, zero or negative $\overline{LPD}_{n,t}$ is associated with idle fuel use and emission rates. Only positive $\overline{LPD}_{n,t}$ leads to average fuel use and emission rates higher than those at idle. Therefore, the contribution of resistive forces to $\overline{LPD}_{n,t}$ was estimated for seconds with each of the resistive forces ≥ 0 kW based on the proportion of positive power to overcome a resistive force to total positive $\overline{LPD}_{n,t}$.

3.2.5 Identification of Emissions Hotspots

Quarter-mile (400-meter) track segments were classified into hotspots and non-hotspots based on two choices of threshold: absolute and relative (Rastogi and Frey, 2021). The accuracy and precision of identification of estimated versus measured hotspots and non-hotspots were quantified based on a confusion matrix (Stehman, 1997) for each hotspot definition. Hotspot definitions, confusion matrix terms, hotspot accuracy, and hotspot precision are described in Table 3-1. Hotspots were identified on absolute and relative bases (Rastogi and Frey, 2021). Absolute hotspots refer to segments with segment-average fuel use and emission rates in the top quintile based on all one-way trips. Absolute hotspots are useful for analyzing near rail-road air quality and exposure to train generated pollution. Relative hotspots refer to segments with segment-average fuel use and emission rates in the top quintile based on each one-way trip.

Relative hotspots are useful for identifying controllable operational practices and infrastructure factors that induce relatively high fuel use and emission rates in each trip.

3.2.6 Identification of Trajectories with Low Fuel Use and Emissions

Estimated train trip fuel use and emissions were compared among observed trajectories to develop insights regarding improvements in operations that can reduce trip fuel use and emissions. Trip fuel use and emissions were estimated as the sum of 1 Hz fuel use and emission rates of all powered PME's for all measured trajectories that met data completeness criteria, including on-time and delayed trips. Any trajectories with more than 10% missing data by time or distance were excluded. Trip fuel use and emissions were estimated separately for each LCF. To quantify the inter-trajectory variability on a consistent basis, model-estimated trip fuel use and emissions were compared among trajectories for an average of 12 LCFs.

3.2.7 Comparison of Delayed versus On-Time Trips

Amtrak passenger trains arriving on time accounted for 78% of total Amtrak trips in 2021 (U.S. Department of Transportation, 2022). Passenger train delays are associated with factors such as freight train interference, passenger and baggage handling at stations, and equipment or engine failure (Amtrak, 2022). Trips delayed by more than 15 minutes of the scheduled time were defined as delayed trips (Federal Railroad Administration, 2020). For measured trajectories that met data completeness criteria, delayed trips were compared with on-time trips to evaluate the effect of delayed trajectories on trip fuel use and emissions as well as the intensity and location of emission hotspots. Model-estimated fuel use and emissions were quantified for each trip and segment for an average of 12 LCFs. For delayed trips, the segments where trains were delayed were identified and referred to as delayed segments. For an average LCF, fuel use and emission rates for delayed segments were compared between delayed versus on-time trips.

Trains can be delayed at or between stations. For delay at stations, the trains dwelled at stations for additional time compared to on-time trips. The delayed segments were located at the associated stations. For delay between stations, the delayed segments were located between stations. Compared to on-time trips, additional deceleration, idling, and acceleration episodes occurred on the associated segments between stations. The delayed segments included speed trajectories associated with induced deceleration, idling, and acceleration. The induced deceleration trajectories started from a segment where the train speed decreased from the naturalistic operating speed and ended at a segment where the speed decreased to zero. The naturalistic operating speed was estimated based on the average speed of on-time trips for the associated segments. The induced acceleration segments started from a segment where the speed increased from zero and ended at a segment where the speed increased to the naturalistic operating speed.

To assess the effect of delays on trip fuel use and emissions on a consistent basis, the delay-associated fuel use and emissions increment was quantified as the difference in mean fuel use and emissions on the delayed segments for delayed versus on-time trips for each species. This increment was then added to each on-time trip to quantify the percentage difference in trip fuel use and emissions with versus without delay increments for an average LCF.

3.2.8 Inter-Locomotive, -Consist, and -Fuel Variability

Inter-LCF variability in estimated trip fuel use and emissions and the number of hotspots were compared based on the average of all trajectories that met data completeness criteria. To quantify

inter-locomotive variability, a comparison was made among different locomotives operated in the same consist and fuel, i.e., LCF IDs 1, 2, 3, and 5 (Table 3-2). To quantify inter-consist variability, comparisons were made among different consists operated with the same locomotive and fuel, i.e., LCF IDs 3 versus 4, 6 versus 7, and 8 versus 9. To quantify inter-fuel variability, comparisons were made among LCF IDs 1, 2, 3 versus 10, 11, and 12, respectively.

3.3 Results and Discussion

The results include: LPD model calibration and evaluation; quantification of the contribution of resistive forces to $\overline{LPD}_{n,t}$; identification of hotspot locations; identification of trajectories with low fuel use and emissions; and effect of LCFs on trip fuel use and emissions and hotspots.

3.3.1 Locomotive Power Demand Model Calibration and Evaluation

This section includes: trends in data used for calibration of the LPD model; model calibration; and model evaluation.

3.3.1.1 Trends in data used for model calibration

On average for each species and LCF, the highest Pearson's correlation coefficient of fuel use and emission rates with $\overline{LPD}_{n,t}$ was for $n = 12s$ (Figure B-3). Therefore, n was determined to be 12s. Fuel use and emission rates were approximately constant for SM1, SM2, and SM4 (Figure 3-1 for fuel use, NO_x, and PM, and Figure B-6 for other species). On average, SM1, SM2, and SM4 comprised 30%, 10%, and 5% of trip duration, respectively.

There was inter-locomotive variability in fuel use and emission rates with respect to $\overline{LPD}_{12,t}$, in part related to differences in year of manufacture, year of rebuild, miles operated, notch-average engine revolutions per minute (RPM), and notch-average manifold absolute pressure (Frey and Rastogi, 2019). A locomotive may be lower-emitting for some species but higher-emitting for others.

PME fuel use rates, and NO_x and PM emission rates were higher for single-powered versus double-powered consists. Two PMEs operated more fuel efficiently and with lower emissions for consists with two locomotives (Frey and Rastogi, 2019). However, the total fuel use and emissions of two PMEs in double-powered consists was typically higher than for single locomotive consists.

On average, for B20 versus ULSD, fuel use rates and CO₂ emission rates were not statistically significantly different, CO, HC, and NO_x emission rates were lower, and PM emission rates were higher.

3.3.1.2 Calibration of locomotive power demand model

The average fuel use and emission rates for SM1, SM2, and SM4 are given in Table B-7. SM1 fuel use and emission rates were compared to steady-state high idle rates because PMEs were operated in high idle for >70% of duration in SM1 or were transitioning to high idle. These transitions were from positive LPD for which associated fuel use and emission rates were elevated. On average over all LCFs, SM1 average fuel use and emission rates were 100% to 400% higher than steady-state high idle rates, and PM emission rates were 90% lower (Table B-8). The difference in absolute PM emission rates was, however, small relative to the highest PM emission rates.

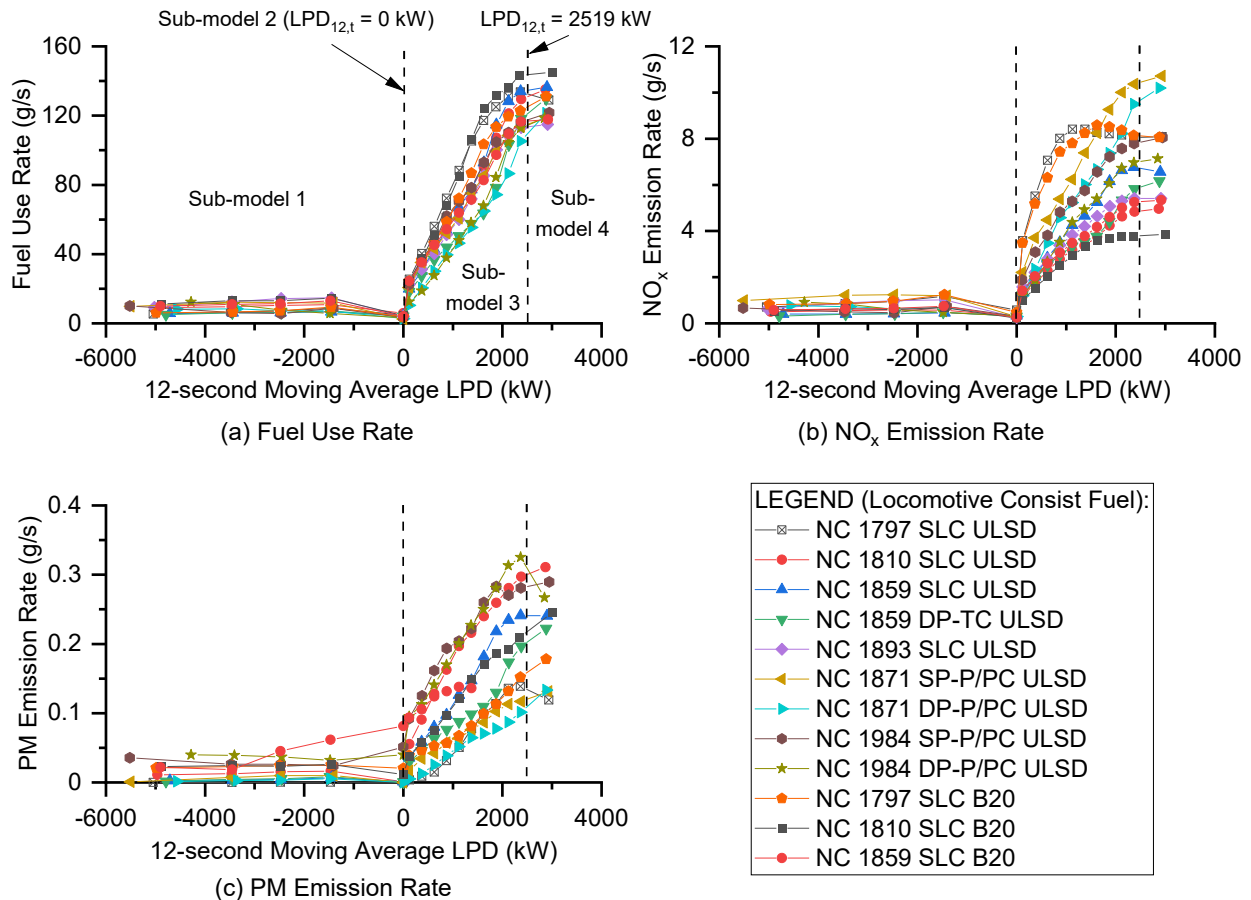


Figure 3-1. Variation of Measured Fuel Use Rates, and Emission Rates of NO_x and PM with 12-Second Backwards Moving Average Locomotive Power Demand ($\overline{LPD}_{12,t}$) for 12 combinations of Locomotives, Consists, and Fuels: (a) Fuel Use Rates; (b) NO_x Emission Rates; and (c) PM Emission Rates. Mean rates are reported for LPD bins: (1) 1000 kW wide bins for negative $\overline{LPD}_{12,t}$; (2) 250 kW wide bins for positive $\overline{LPD}_{12,t}$; and (3) one bin for zero $\overline{LPD}_{12,t}$. Each data point is based on the average of 1134s to 5632s of data in the corresponding LPD bin.

In SM2, the PME is typically operated at low idle or is transitioning to low-idle from high idle. Thus, SM2 average fuel use and emission rates were expected to be lower than steady-state high idle rates. On average of all LCFs, SM2 average fuel use and emission rates were lower than steady-state average rates for each species.

In SM4, the PME is typically operated at notch 8. During a transition to notch 8, fuel use and emission rates are initially lower than steady-state notch 8 average rates but are higher for 5s to 8s before reaching steady-state (Graver and Frey, 2015). Thus, SM4 average fuel use and emission rates can be higher or lower than the steady-state notch 8 average rates. Among all LCFs, fuel use and emission rates were within $\pm 25\%$ of steady-state notch 8 average rates.

The average SM4-to-SM2 ratio was higher for fuel use and CO_2 emission rates than for NO_x , CO, HC, and PM emission rates. Relative variations in fuel use and CO_2 emission rates with respect to $\overline{LPD}_{12,t}$ were more sensitive to relative differences in $\overline{LPD}_{12,t}$ than NO_x , CO, and PM

emission rates. Compared to the other species, relative variations in HC emissions rates were the least sensitive to variations in $\overline{LPD}_{12,t}$.

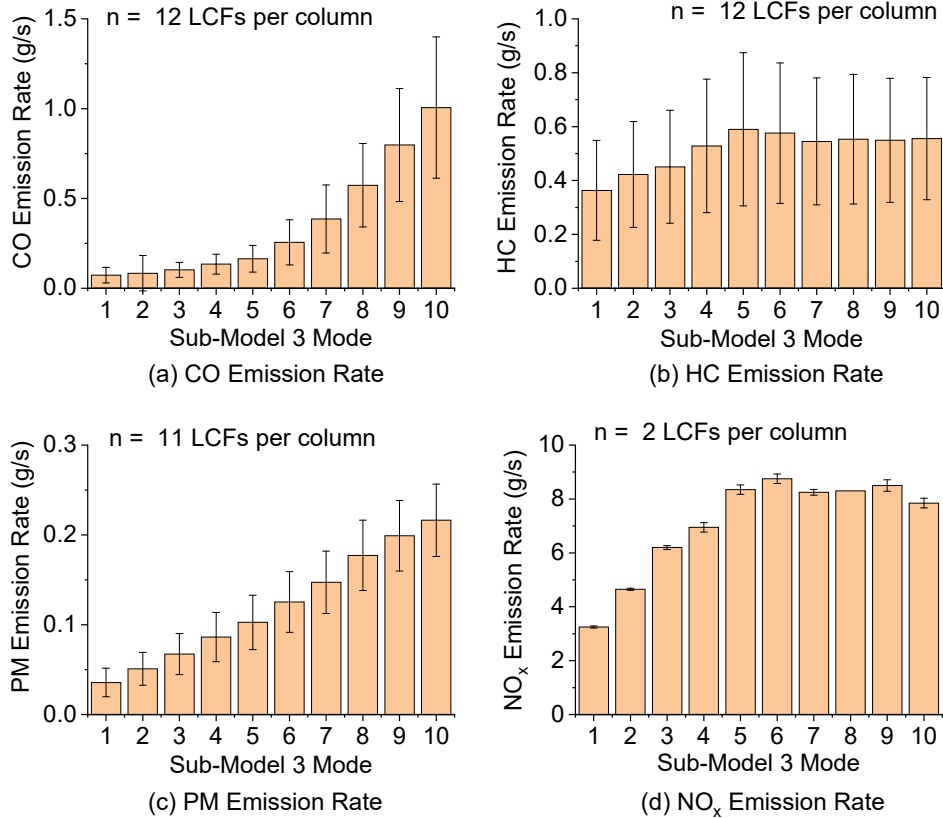
Fuel use rates and CO₂ emission rates are related to engine output (Flagan and Seinfeld, 1988). However, they may not vary linearly with engine output as the thermal efficiency of diesel engines increases with engine output (Frey and Rastogi, 2019; Thiruvengadam et al., 2015). The net effect of factors such as turbocharger, boost pressure, air-to-fuel ratio, combustion efficiency, peak temperature, heat losses, frictional losses, and pumping losses are that engine efficiency tends to increase with load, just above idle, to intermediate loads, and to be relatively constant over a range of moderate to high partial loads and at a full load (Beck and Uyehara, 1987; Flagan and Seinfeld, 1988; Thiruvengadam et al., 2014; Ferguson and Kirkpatrick, 2015; Heywood, 2018). The thermal efficiency can be increased by advancing fuel injector timing. Advancing injector timing gives more time for fuel to combust (Flagan and Seinfeld, 1988).

For SM3, fuel use and emission rates were calibrated using quadratic or modal models depending on LCF and species. On average, SM3 comprised 55% of trip duration. Quadratic models were calibrated for fuel use, CO₂ and NO_x emission rates for each LCF based on LOOCV, except for a modal model for NO_x emission rates for locomotive NC 1797. To ensure continuity with SM2, the quadratic intercept was set to the average fuel use and emission rates estimated for SM2. The LOOCV calibrated SM3 regression parameters and modal-average rates for a given LCF (Table B-10) were within 10% of each other. Therefore, SM3 was re-calibrated based on all one-way trips combined. The relative standard error in linear and quadratic slopes was typically less than 4%, indicating that these parameters were precisely estimated.

The SM3 parameters for each LCF for fuel use, CO₂, and NO_x emission rates are given in Table B-11 based on 3 to 15 measured one-way trips per LCF. For fuel use rates, the quadratic slope was negative for 7 of 12 LCFs, indicating that engine thermal efficiency typically increased with engine output. Although the remaining five quadratic slopes were positive, two were not statistically significantly different from zero and the other three were significantly but not substantially different from zero. The models with quadratic slopes have adjusted R² larger by 1 to 3 percentage points than those without quadratic slopes. Thus, the quadratic models are slightly more precise than the linear models.

For SM3, CO and PM emission rates increased monotonically with $\overline{LPD}_{12,t}$. The marginal increase in CO, HC, and PM emission rates with LPD was not well described by linear or quadratic models. Therefore, a 10-mode modal model was calibrated for these emission rates such that each mode comprised approximately 5% of the trip duration. NO_x emission rates for locomotive NC 1797 (LCF IDs 1 and 10) peaked at intermediate values of $\overline{LPD}_{12,t}$. Therefore, these emission rates were calibrated based on a modal model.

Average SM3 modal emission rates for the pollutants and LCFs for which modal models were calibrated are shown in Figure 3-2. Average CO and PM emission rates increased monotonically with mode. Average HC and NO_x emission rates increased monotonically with modes for output <1000 kW and were approximately constant at higher output.



Sub-Model 3 Mode	12-Second Backwards Moving Average Locomotive Power Demand ($\overline{LPD}_{12,t}$, kW)
1	$0 < \overline{LPD}_{12,t} \leq 164$
2	$164 < \overline{LPD}_{12,t} \leq 354$
3	$354 < \overline{LPD}_{12,t} \leq 568$
4	$568 < \overline{LPD}_{12,t} \leq 794$
5	$794 < \overline{LPD}_{12,t} \leq 1038$
6	$1038 < \overline{LPD}_{12,t} \leq 1298$
7	$1298 < \overline{LPD}_{12,t} \leq 1580$
8	$1580 < \overline{LPD}_{12,t} \leq 1885$
9	$1885 < \overline{LPD}_{12,t} \leq 2190$
10	$2190 < \overline{LPD}_{12,t} < 2519$

Figure 3-2. Calibrated Average Sub-Model 3 Modal Emission Rates of 12 Combinations of Locomotives, Consists, and Fuels (LCFs) for: (a) CO Emission Rates; (b) HC Emission Rates; (c) PM Emission Rates; and (d) NO_x Emission Rates. Error bars in the figures indicate ± one standard deviation on the mean of 12 LCFs for each mode. Sample size (n) indicates number of LCFs. For PM, all LCFs are included except for LCF ID 5. For NO_x, only LCF IDs 1 and 10 are included. The description of each LCF ID is given in Table 3-2.

3.3.1.3 Model evaluation

The accuracy and precision of the complete model for fuel use rates at resolutions of 1 Hz, segment-average, and trip totals were quantified (Tables B-16 and B-17). The parity slope of estimated versus measured fuel use rates and CO₂ emission rates was within 10% of 1 with $R^2 > 0.87$ for each LCF and resolution. For NO_x emission rates, the parity slope was within 7% of 1 with $R^2 > 0.73$ for each LCF. For PM emission rates, the parity slope was within 7% of 1 and R^2 was 0.62 or higher. Thus, the models are accurate and precise. The parity slopes for CO and HC emission rates were typically within 25% of 1 with $R^2 < 0.60$. CO and HC emission rates were typically less precisely estimated compared to other species, in large part because the exhaust CO and HC concentrations were comparable to the gas analyzer detection limit in many cases. However, the average slope based on all LCFs for each species was within 5% of 1.

Model estimated fuel use and emission rates for the nine diesel-fueled LCFs were benchmarked to independent data (Figure B-13). On average, estimated fuel use and emission rates were similar to within 9% of independent data for output <1500 kW. For output >1500 kW, Fuel use and emission rates were typically lower by <33%. Transient-based fuel use and emission rates such as those estimated here are typically lower than steady-state based rates because of transitions from lower notch positions (Yuan and Frey, 2021).

3.3.2 Contribution of Resistive Forces

The contribution of resistive forces to positive LPD varies dynamically during a trip. An example of the contribution of positive resistive forces to positive $\overline{LPD}_{12,t}$ is given in Figure 3-3 for track segments between Cary, NC and Durham, NC. This link was selected because the range of activity and infrastructure is similar to elsewhere on the route and to that of other LCFs. As the train departed Cary, power demand continuously increased because of positive acceleration until reaching peak power output. Typically, for any second with positive acceleration, acceleration resistance was the largest contributor compared to other resistances. During ascent on a grade, grade resistance was the largest contributor for seconds with zero or negative acceleration. Grade resistance was the second-largest contributor for seconds with positive acceleration. Drag resistance was the largest contributor when trains cruised at speeds >50 mph. The journal, flange, and curvature resistances were typically <100 kW each. Their contributions to $\overline{LPD}_{12,t}$ were typically <3% each.

On average for a trip, based on all LCFs and one-way trips, acceleration and grade resistances contributed 37% each to $\overline{LPD}_{12,t}$, and drag resistance contributed 17%. Thus, the acceleration, grade, and drag resistances are major contributors to $\overline{LPD}_{12,t}$ for the Piedmont route.

3.3.3 Identification of Emissions Hotspots

To illustrate the ability of the model to identify hotspots, a map of estimated versus measured absolute hotspots for fuel use, NO_x emissions, and PM emissions is given in Figure 3-4. Measured hotspots are from Rastogi and Frey (2021). Estimated absolute hotspots were typically located at or near segments containing station stops. Fuel use and emission rates near station segments were among the highest over the route because of positive acceleration and slower speeds. Positive acceleration contributed to high power demand, while dwell time at stations and slower average speeds led to the accumulation of emissions within a station segment. Some hotspots were located between stations. These hotspots were mainly due to positive acceleration, positive grade, or both.

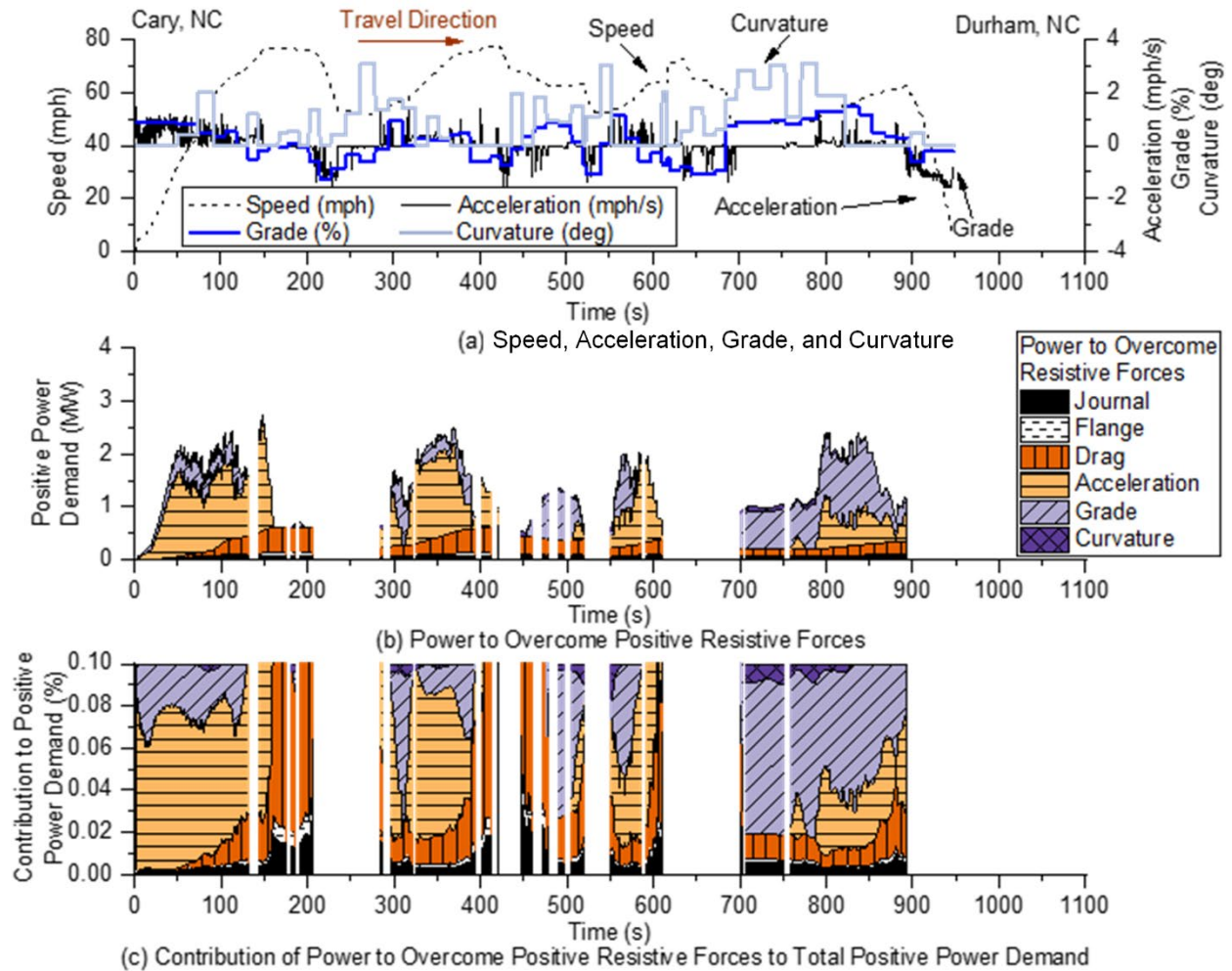


Figure 3-3. Example Time Plot of Variation in Train Speed, Acceleration, Track Grade, and Curvature and Their Effects on Positive Power Demand ($LPD_{12,t}$) for Single Locomotive Consist of NC 1797 Operated on B20 from Cary, NC to Durham, NC: (a) Speed, Acceleration, Grade, and Curvature; (b) Power to Overcome Positive Resistive Forces; and (c) Contribution of Power to Overcome Positive Resistive Forces. The gaps in the time plots are for seconds for which any of the resistive forces were <0 kW.

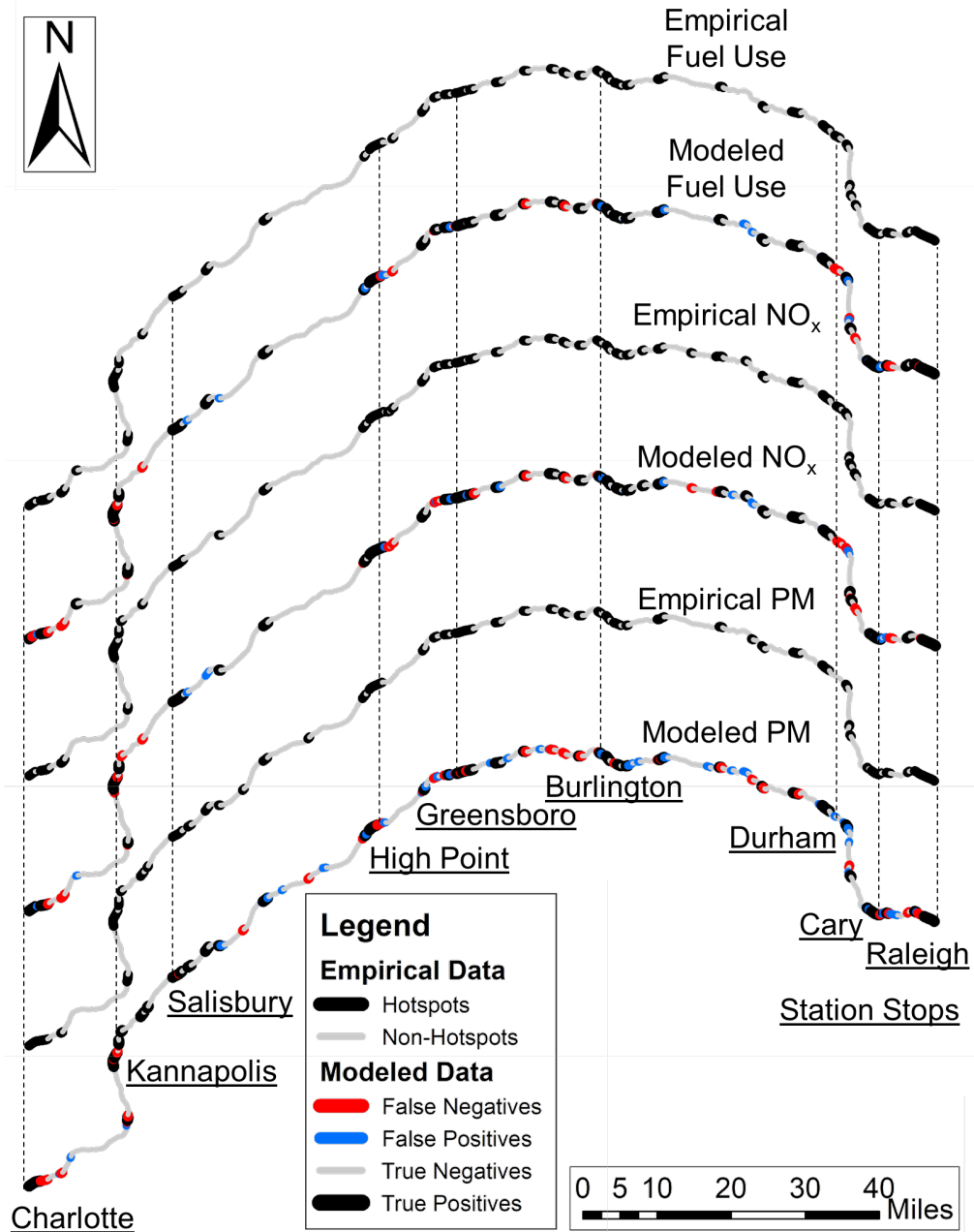


Figure 3-4. Comparison of Modeled versus Measured Fuel Use, NO_x Emissions, and PM Emissions Absolute Hotspots and Non-Hotspots. The model results are based on the locomotive power demand model for all combinations of locomotives, consists, and fuels. Absolute hotspots are the segments with average fuel use or emission rates in the top quintile based on 66 one-way trips. The remaining segments are absolute non-hotspots. Each plot comprises 692 0.25-mile track segments.

For hotspots versus non-hotspots, the average $\overline{LPD}_{12,t}$ was 93% higher. The average contribution of positive acceleration and grade resistance to positive power demand was 6% and 4% higher for hotspots versus non-hotspots, respectively. Other resistive forces contributed 1% to 4% lower for hotspots versus non-hotspots.

Typically, estimated absolute and relative hotspot locations coincided with the measured hotspot locations. Verification of the estimated absolute and relative hotspots is given in Table 3-3. For fuel use, CO₂ emissions, NO_x emissions, and PM emissions, 87% to 93% of the estimated absolute and relative hotspots and non-hotspots were accurately classified. For segments that were misclassified (false positives or false negatives), typically >87% were near misses, defined as segments with fuel use and emission rates between the 70th and 80th percentile but classified as hotspots, and segments with fuel use and emission rates between the 80th and 90th percentile but classified as non-hotspots. The difference in estimated versus measured fuel use and emission rates was within ±6% for each segment. Greater than 93% of false positives and false negatives were within 0.5 miles (2 track segments) of the measured hotspots. Thus, in general, misclassified segments had rates approximately similar to the threshold rates and were located near measured hotspots.

Table 3-3. Verification of the Locomotive Power Demand Model to Identify Absolute and Relative Hotspots Based on the Number of True Positives, True Negatives, False Positives, False Negatives, Accuracy, and Precision.

Hotspot Definition ^a	Metric ^b	Fuel Use	CO ₂	CO	HC	NO _x	PM
Absolute Hotspots (Positives) and Non-Hotspots (Negatives)	True Positives	113	113	102	58	107	92
	True Negatives	527	527	516	472	521	511
	False Positives	27	29	31	93	27	35
	False Negatives	25	23	43	69	37	54
	Accuracy (%)	92.5	92.5	89.3	76.6	90.8	87.1
	Precision (%)	80.7	79.6	76.7	38.4	79.9	72.4
Relative Hotspots (Positives) and Non-Hotspots (Negatives)	True Positives	6820	6818	5925	2992	6410	3423
	True Negatives	34964	34962	30104	30966	34553	17729
	False Positives	2569	2571	3464	6553	2979	906
	False Negatives	2571	2573	7431	6413	2982	2303
	Accuracy (%)	89.0	89.0	76.8	72.4	87.3	86.8
	Precision (%)	72.6	72.6	63.1	31.3	68.3	79.1

^a Absolute hotspots are segments with average fuel use or emission rates in the top quintile of segments based on all one-way trips. Remaining segments are absolute non-hotspots. Relative hotspots are the segments with average fuel use or emission rates in the top quintile of segments based on a given one-way trip. Remaining segments are relative non-hotspots.

^b True positives are the number of hotspots estimated as hotspots. True negatives are the number of non-hotspots estimated as non-hotspots. False positives are the number of non-hotspots estimated as hotspots. False negatives are the number of hotspots estimated as non-hotspots. Accuracy is the proportion of correctly identified hotspots relative to the total number of estimated hotspots and non-hotspots. Precision is the proportion of the estimated hotspots that were correctly identified.

For CO and HC hotspots, the accuracy was 76% and 72%, respectively. CO and HC emission hotspots were less precisely identified than other species, but their emission rates are typically low. HC emission rates did not vary substantially with $\overline{LPD}_{12,t}$, therefore, HC emission hotspots were less precisely estimated than those of other species.

3.3.4 Identification of Trajectories with Low Fuel Use and Emissions

To identify trajectories with low trip fuel use and emissions and, thus, obtain insights regarding improvements in train operations, normalized model-estimated trip fuel use and emissions for an average LCF for each trajectory are shown in Figure 3-5. There were 45 trajectories that met data completeness criteria. Each trajectory was assigned an ID sorted by lowest to highest trip total fuel use. Since the trains operated on the same rail track and typically operated on the same schedule, the distributions of track grade, curvature, train speed, and acceleration were either the same or similar regardless of LCFs.

Trajectory IDs 1 through 13 had relatively low average estimated fuel use and emissions of CO₂, CO, NO_x, and PM compared to other trajectories. The average power demand for these versus other trajectories was 11% to 20% lower. The contribution of acceleration resistance to power demand was 6% to 12% lower for these versus other trajectories. Conversely, the average contribution of grade and drag resistances each was 4% to 10% higher, depending on the one-way trip. For an average LCF, Trajectories IDs 1 through 13 had 28% to 45% lower trip fuel use and emissions than the average of all trajectories, depending on species. Compared to the average of all trajectories, Trajectory IDs 1 through 13 had 11% to 23% fewer absolute hotspots, and 4% to 17% lower average fuel use and emission rates in hotspots, depending on species.

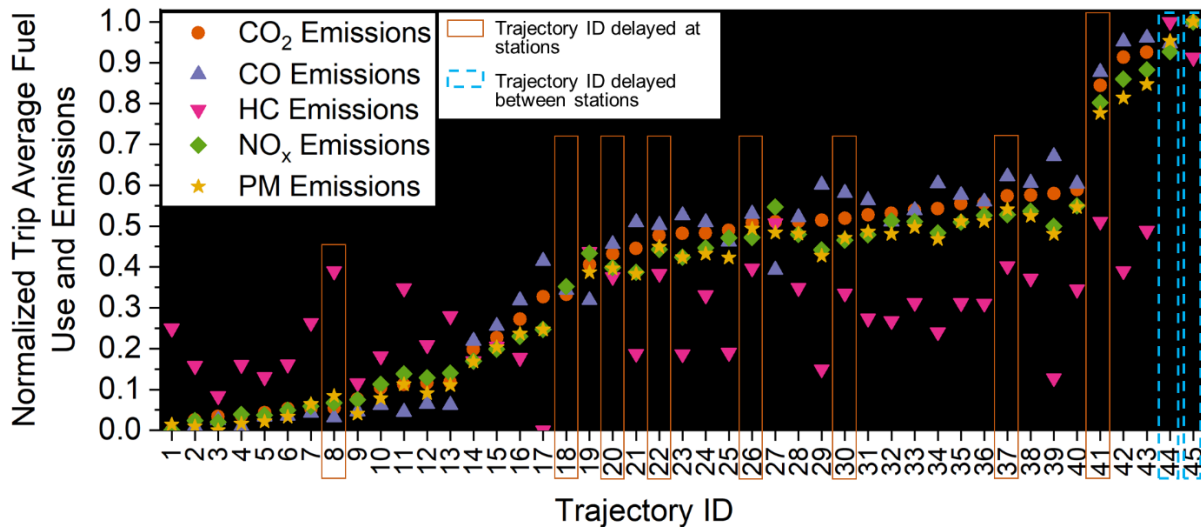


Figure 3-5. Normalized Model Estimated Trip Emissions (TEs) for an Average Locomotive, Consist, and Fuels (LCF) for Each of 45 Complete Trajectories. Each data point is based on the average of trip emissions for 12 LCFs. Each LCF was assumed to be operated on each of 45 trajectories. Trajectory ID and their associated LCF and trip are given in Table B-19. Normalized trip emissions for i^{th} trajectory were estimated as: $(TE_i - TE_{\text{max}})/(TE_{\text{min}} - TE_{\text{max}})$. The trend in normalized model estimated trip fuel use with respect to Trajectory ID is the same as the trend in normalized model estimated trip CO₂ emissions. Trajectory IDs 8, 18, 20, 22, 26, 30, 37, 41, 44, and 45 are delayed trips - Trajectories IDs 44 and 45 are trips delayed only between stations, and others are trips delayed only at stations.

There are inter-species tradeoffs in trajectories with the lowest trip fuel use and emissions. For an average LCF, Trajectory ID 1 had the lowest trip fuel use, CO₂, CO, and NO_x emissions because it had the lowest average power demand. However, HC and PM emissions for Trajectory ID 1 were 12% and 1% higher than the trajectories with the lowest trip HC and PM emissions, respectively. In general, one trajectory may not achieve the lowest trip fuel use and emissions among all species, leading to trade-offs among species. These tradeoffs among species occur because the relative difference in emission rates with engine output differs among species.

Fuel use and emissions reduction potential for each species was estimated as the difference between the average trip fuel use and emissions among all trajectories and the trajectory with the lowest trip fuel use and emissions. The average estimated reduction potential was 34% for fuel use and CO₂ emissions, 49% for CO emissions, 13% for HC emissions, 26% for NO_x emissions, and 25% for PM emissions.

3.3.5 Comparison of Delayed versus On-Time Trips

In general, for an average LCF, delayed trips tend to be at the moderate and high end of trip fuel use and emissions as shown in Figure 3-5. Among 45 trip trajectories that met data completeness criteria, ten were delayed by more than 15 minutes of trip scheduled time. The ratio of delayed to total trips here is similar to that reported in the U.S. Department of Transportation (2022) for Amtrak on-time performance. The delayed trips had 9% to 45% longer travel time than the scheduled travel time, and the average power demand for an average delayed trip was 13% higher than that for an average on-time trip.

Observed train delays typically occurred at stations. Among the ten delayed trips, eight were delayed only at a station. Such delays occurred either at the Durham or Kannapolis stations. On the delayed station segments, the mean fuel use and emissions for such delayed trips were 13% to 100% larger than those for on-time trips depending on species. With these delay increments, the estimated trip fuel use and emissions would increase by less than 1% for all on-time trips and species for an average LCF. For trips with such delays, the trains dwelled at stations for an average of an additional 24 minutes, thus, the emission hotspots due to delays were located at the station segments. These locations were also identified as hotspots for on-time trips. Thus, trips delayed at stations did not add new hotspot locations.

Two trips were delayed only between stations (Trajectory IDs 44 and 45 in Figure 3-5). These two trips had the largest trip fuel use and emissions not only because of delays between stations but also associated with aggressive train operations. Trajectory IDs 41-45 had much higher normalized trip fuel use and emissions (except for HC) than Trajectory IDs 1-40. Trajectory IDs 41-45 had at least 25% higher average power demand than other trajectories except for Trajectory ID 32. Trajectory ID 32 had 3% higher average power demand than Trajectory ID 41 but had 2% to 17% lower average power demand than Trajectory IDs 42-45. Thus, Trajectories IDs 32 and 41-45 are considered to be based on aggressive train operations because of high average power demand. Compared to Trajectories ID 41-45, Trajectory ID 32 had lower normalized trip fuel use and emissions at least in part associated with its lower relative variability in power demand. The coefficient of variation of power demand for Trajectory ID 32 was 5% to 27% lower than that for Trajectory IDs 41-45.

Delay increments for trips with delays between stations were not only associated with train idling on the affected non-station segment, but also associated with creating extra deceleration and acceleration episodes to approach and leave the segment. For example, Trajectory ID 45 was

delayed because the train took 9 minutes to decelerate from 60 mph on Segment ID 642 to 0 mph on Segment ID 631, idled on Segment ID 631 for 28 minutes, and then took 11 minutes to accelerate from 0 mph on Segment ID 631 to 60 mph on Segment ID 616. The total delay, including induced deceleration, idling, and acceleration, was 48 minutes. This delay-included deceleration and acceleration time was much longer than the normal deceleration and acceleration time to approach and leave stations, respectively (e.g., speed trajectory in Figure 3-3). Similar trends were also found for Trajectory ID 44. Thus, although Trajectory IDs 44 and 45 included aggressive operations, the operational driving associated with delays was not aggressive.

With delay increments, trip fuel use and emissions would increase by an estimated 1% to 5% for aggressive on-time trips and increase by an estimated 3% to 14% for non-aggressive on-time trips depending on species. Thus, the effect of delay-associated increments is relatively small on aggressive on-time train operations. Of the delay increments, 62% to 94% was associated with delay-induced acceleration, depending on species.

Trips with delays between stations had larger segment average emission rates on the idling segments and associated downstream acceleration segments than on-time trips. For example, for an average LCF operating on Trajectory ID 45, fuel use and emission rates on Segments ID 616-631 were 2 to 10 times larger than those for on-time trips depending on species. Compared to on-time trips, the observed trips with delays between stations added new relative hotspot locations for idling and associated downstream acceleration segments. For example, Segment IDs 626, 627, and 631 were hotspots for Trajectory ID 45 but were non-hotspots for on-time trips.

3.3.6 Inter-Locomotive, -Consist, and -Fuel Variability

Inter-LCF variability in trip fuel use and emissions and the number of hotspots were quantified (Tables B-22 and B-23). Inter-locomotive variability was quantified based on the same consist and fuel. For a given consist and fuel, such as single locomotive and ULSD, locomotive NC 1893 had lower trip fuel use and CO₂, CO, and HC emissions than locomotives NC 1797, NC 1810, and NC 1859. Compared to the average of the latter three locomotives, trip fuel use and emissions for locomotive NC 1893 were 15% to 38% lower and the average number of absolute hotspots was 15% to 33% lower, depending on species.

Inter-consist variability was quantified based on the same locomotive and fuel. For a given locomotive and fuel, such as locomotive NC 1859 and ULSD, single locomotive consist had 28% to 45% lower trip fuel use and emissions and 27% to 49% lower number of absolute hotspots than double-powered tandem consist, depending on species. PME in single-powered consists ran at higher engine outputs than PMEs in double-powered consists (Rastogi and Frey, 2021). PMEs are typically more energy efficient and have lower emission rates per kilowatt-hour at higher outputs compared to lower outputs.

Inter-fuel variability was quantified based on the same locomotive and consist. For a given locomotive and consist, trip fuel use and CO₂ emissions averaged 0.7% higher for B20 versus ULSD. However, this difference was not statistically significant. Trip average CO, HC, and NO_x emissions were 8% to 19% lower for B20 versus ULSD. In contrast, trip average PM emissions were 6% higher. Graver and Frey (2016) estimated a decrease in CO, HC, and PM emission rates and an increase in fuel use rate, CO₂ emission rate, and NO_x emission rates on average for B20 versus ULSD for the same LCFs measured here. Differences from prior work are because the prior estimates were based on steady-state operation only. The number of absolute hotspots were

0.5% to 8% higher for fuel use, CO₂ emission, and PM emission hotspots for B20 versus ULSD. The number of CO, HC, and NO_x emission hotspots were lower for B20 versus ULSD by 7% to 23%. Thus, using B20 biodiesel can reduce trip CO, HC, and NO_x emissions with the tradeoff of increased PM emissions.

3.4 Conclusions

This work has shown that an LPD-based model for passenger train fuel use and emission rates can be feasibly calibrated based on PEMS and GPS data from 3 to 15 one-way trips for a given locomotive, consist, and fuel. The model can be calibrated to over-the-rail measurements for other passenger rail systems because they are based on the physics of resistive forces opposing train motion. The LPD-based model is able to accurately and precisely estimate passenger rail fuel use and emission rates at high spatial resolution (e.g., quarter-mile track segment) and temporal resolution (e.g., second-by-second). The LPD-based model can be applied to identify key resistive forces, identify trajectories with low fuel use and emissions, locate hotspots, and quantify inter-LCF variability in fuel use and emission rates.

Acceleration, grade, and drag resistances were the highest relative contributors to power demand, regardless of train consist. Track curvature had an insignificant contribution to power demand for the Amtrak-operated Piedmont passenger rail. The same is expected for passenger routes with similar variations in track grade and curvature. This quantification is useful to identify controllable operation practices to reduce power demand and ultimately reduce trip fuel use and emissions, such as controlling acceleration and deceleration.

Trajectories were identified that had lower average acceleration and deceleration per trip with similar trip duration but lower trip fuel use and emissions. However, a trajectory with the lowest trip fuel use or emissions for one species may not necessarily have the lowest trip fuel use or emissions for other species. Nonetheless, a trajectory with the lowest fuel use will also have relatively lower emissions than other trajectories. Thus, depending on the species of concern, a choice among trajectories could be made. These trajectories had fewer absolute hotspots and lower fuel use and emission rates in hotspots than other trajectories. Thus, through trajectory modification, fuel use and emissions can be reduced on a trip and local level.

Delayed trips typically have larger trip fuel use and emissions than on-time trips. Train delays between stations could have larger trip fuel use and emissions than delays at stations because of additional deceleration and acceleration episodes associated with delays between stations. For delay at stations, there is only a small penalty on trip total fuel use and emissions, even though there is a large effect at the station segment where delay occurs. For delays that occur between stations, which leads to an induced acceleration, emission hotspot intensities increase not only on the segment during which the train idles but on associated downstream acceleration segments, which could increase air pollutant exposure in the affected areas.

A particular LCF may not have the lowest rates for all species. By operating fuel-efficient and low-emitting LCFs on trajectories with lower trip fuel use and emissions, system-wide train fuel use and emissions can be reduced. This inter-LCF and inter-trajectory variability in fuel use and emissions can be accurately estimated using the LPD model demonstrated here. Reduction in fuel use will reduce operating costs. Reduction in emission rates will decrease the number and intensity of hotspots resulting in reduced exposure to train-generated pollution near railroad tracks.

3.5 Summary of Supporting Information

The supporting information includes: (1) estimation of LPD; (2) modeling of fuel use and emission rates based on LPD; (3) model benchmarking to independent data; (4) head-end power engine fuel use and emission rates; (5) identification of trajectories with low fuel use and emissions; (6) inter-LCF variability in trip fuel use and emissions and hotspots; (7) sensitivity to passenger cars; and (8) delayed versus on-time trips.

3.6 References Cited in Chapter 3

- AAR, 2020. Railroad Facts 2020 (No. A66-7305). Association of American Railroads, Washington, DC.
- Amtrak, 2022. Delayed by Freight - Measuring On-Time Performance Across Our Network [WWW Document]. Amtrak. URL <https://www.amtrak.com/on-time-performance> (accessed 11.4.22).
- Amtrak, 2020. FY21-26 Five Year Service and Asset Line Plans. National Passenger Rail Corporation (Amtrak), Washington, D.C.
- Amtrak, 2018. FY 2018 Company Profile for the Period October 1, 2017 - September 30, 2018. National Passenger Rail Corporation (Amtrak).
- APTA, 2020. 2020 Public Transportation Fact Book (No. Edition 71). American Public Transportation Association.
- APTA, 2019. Compendium of Definitions and Acronyms for Rail Systems (No. APTA STD-ADMIN-GL-001-19). American Public Transportation Association, Washington, D.C.
- AREMA, 2020. American Railway Engineering and Maintenance-of-way Association Manual for Railway Engineering. Lanham, MD.
- Bachman, J., Marchetti, J., Meacham Jr, H., Uher, R., Watson, R., 1978. Improved Passenger Equipment Evaluation Program - Train System System Review Report Volume I Baseline Data (No. FRA/ORD 80/14.I). Prepared by Unified Industries Incorporated for U.S. Department of Transportation, Federal Railroad Administration, Washington, D.C.
- Bachman, W., 1998. GIS-based modal model of automobile exhaust emissions. Final report, January 1997--May 1998. Georgia Inst. of Tech., School of Civil and Environmental Engineering.
- Bergin, M.S., Harrell, M., Janssen, M., 2012. Locomotive emission inventories for the United States from ERTAC Rail, in: 2012 Annual International Emission Inventory Conference. Tampa, Florida, pp. 13–16.
- Dick, C.T., DiDomenico, G., 2016. Factors Affecting Commuter Rail Energy Efficiency (No. NURail2013- UIUC-R12). Report prepared for the U.S. Department of Transportation by University of Illinois at Urbana-Champaign, Washington, D.C.
- Dincer, I., Hogerwaard, J., Zamfirescu, C., 2016. Locomotive Prime Movers, in: Dincer, I., Hogerwaard, J., Zamfirescu, C. (Eds.), Clean Rail Transportation Options. Springer International Publishing, Cham, pp. 57–73.
- Drish, W.F., 1992. Train energy model version 2.0 technical manual. Publication SD-040, Association of American Railroads, Washington, D.C.
- EPA, 2016. Integrated Science Assessment (ISA) for Oxides of Nitrogen - Health Criteria (Final Report, 2016) (No. EPA/600/R-15/068). U.S. Environmental Protection Agency, Washington, DC.
- EPA, 2016. Endangerment and Cause or Contribute Findings for Greenhouse Gases under the Section 202(a) of the Clean Air Act [WWW Document]. US EPA. URL

- <https://www.epa.gov/ghgemissions/ endangerment-and-cause-or-contribute-findings-greenhouse-gases-under-section-202a-clean> (accessed 10.15.19).
- EPA, 2010. Integrated Science Assessment (ISA) For Carbon Monoxide (Final Report, Jan 2010) (No. EPA/600/R-09/019F). U.S. Environmental Protection Agency, Washington, DC.
- EPA, 2009. Integrated Science Assessment (ISA) For Particulate Matter (Final Report, Dec 2009) (No. EPA/600/R-08/139F). U.S. Environmental Protection Agency, Washington, DC.
- EPA, 2008. Final Rule for Control of Emissions of Air Pollution from Locomotive Engines and Marine Compression-Ignition Engines Less Than 30 Liters per Cylinder. Federal Register, EPA-HQ-OAR-2003-0190 73, 37096-37350.
- EPA, 2004. 40 CFR Parts 9, 69, et al., Final Rule for Control of Emissions of Air Pollution From Nonroad Diesel Engines and Fuel [WWW Document]. US EPA. URL <https://www.epa.gov/regulations-emissions-vehicles-and-engines/final-rule-control-emissions-air-pollution-nonroad> (accessed 7.14.22).
- EPA, 1998. Locomotive Emission Standards: Regulatory Support Document (No. EPA/98-04). U.S. Environmental Protection Agency, Ann Arbor, MI.
- Federal Railroad Administration, 2020. 49 CFR Part 273 Metrics and Minimum Standards for Intercity Passenger Rail Service. Federal Register 85, 32.
- Feng, X., 2011. Optimization of target speeds of high-speed railway trains for traction energy saving and transport efficiency improvement. *Energy Policy* 39, 7658-7665.
- Ferguson, C.R., Kirkpatrick, A.T., 2015. *Internal combustion engines: applied thermosciences*. John Wiley & Sons.
- Flagan, R., Seinfeld, J., 1988. *Fundamentals of air pollution engineering*. Prentice-Hall, Inc., New Jersey.
- Frey, H., Unal, A., Chen, J., Li, S., Xuan, C., 2002. Methodology for developing modal emission rates for EPA's multi-scale motor vehicle & equipment emission system (No. EPA420- R-02-027). Prepared for US Environmental Protection Agency by North Carolina State University, Ann Arbor, Michigan, USA.
- Frey, H.C., Choi, H.W., Kim, K., 2012. Portable Emission Measurement System for Emissions of Passenger Rail Locomotives. *Transportation Research Record: Journal of the Transportation Research Board* 2289, 56-63.
- Frey, H.C., Rastogi, N., 2019. *Managing Energy and Emissions for Rail Operations* (No. FHWA/NC/2018-09). Prepared by North Carolina State University for North Carolina Department of Transportation, Raleigh, NC.
- Fritz, S.G., 2004. Evaluation of Biodiesel Fuel in an EMD GP38-2 Locomotive (No. NREL/SR-510-33436). Prepared for National Renewable Energy Laboratory by Southwest Research Institute, San Antonio, TX.
- General Motors of Canada Limited, 1994. *F59PH Locomotive Service Manual, Third Edition*. Ontario, Canada.
- Gould, G.M., Niemeier, D.A., 2011. Spatial assignment of emissions using a new locomotive emissions model. *Environmental Science & Technology* 45, 5846-5852.
- Graver, B.M., Frey, H.C., 2016. Highway Vehicle Emissions Avoided by Diesel Passenger Rail Service Based on Real-World Data. *Urban Rail Transit* 2, 153-171.
- Graver, B.M., Frey, H.C., 2015. Comparison of Over-the-Rail and Rail Yard Measurements of Diesel Locomotives. *Environmental Science & Technology* 49, 13031-13039.

- Graver, B.M., Frey, H.C., Hu, J., 2016. Effect of Biodiesel Fuels on Real-World Emissions of Passenger Locomotives. *Environmental Science & Technology* 50, 12030–12039.
- Hay, W.W., 1982. *Railroad engineering*. John Wiley & Sons, New York.
- Heywood, J.B., 2018. *Internal combustion engine fundamentals*. McGraw-Hill Education.
- Kim, K., Chien, S.I.-J., 2010. Optimal train operation for minimum energy consumption considering track alignment, speed limit, and schedule adherence. *Journal of Transportation Engineering* 137, 665–674.
- Lukaszewicz, P., 2009. Running resistance and energy consumption of ore trains in Sweden. *Proceedings of the Institution of Mechanical Engineers, Part F: Journal of Rail and Rapid Transit* 223, 189–197.
- Miller, C.A., 2021. Savings in per-passenger CO₂ emissions using rail rather than air travel in the northeastern U.S. *Journal of the Air & Waste Management Association* 71, 1458–1471.
- NCRRP, 2015. *Comparison of Passenger Rail Energy Consumption with Competing Modes*, NCRRP Report 3. Prepared for National Cooperative Rail Research Program (NCRRP) by TranSys Research Ltd.; RailTEC at the University of Illinois at Urbana-Champaign; Canadian Pacific Consulting Services Transcom; and Lawson Economics Research Inc., Washington, D.C.
- Profillidis, V.A., 2014. *Railway management and engineering*. Ashgate Publishing, Ltd., Burlington, VT.
- Rastogi, N., Frey, H.C., 2021. Characterizing Fuel Use and Emission Hotspots for a Diesel-Operated Passenger Rail Service. *Environ. Sci. Technol.* 55, 10633–10644.
- Rastogi, N., Frey, H.C., 2018. Estimation of Rail Grade and Horizontal Curvature from non-Proprietary Data Sources, in: *Proceedings of Transportation Research Board 97th Annual Meeting*. Paper No. TRB 18-06366. Transportation Research Board, Washington, D.C., pp. 1–17.
- Sprung, M.J., Nguyen, L.X., Riley, D., Zhou, S., Lawson, A., 2018. *National Transportation Statistics 2018*, Bureau of Transportation Statistics. U.S. Department of Transportation. Washington, D.C.
- Stehman, S.V., 1997. Selecting and interpreting measures of thematic classification accuracy. *Remote Sensing of Environment* 62, 77–89.
- Thiruvengadam, A., Besch, M.C., Thiruvengadam, P., Pradhan, S., Carder, D., Kappanna, H., Gautam, M., Oshinuga, A., Hogo, H., Miyasato, M., 2015. Emission rates of regulated pollutants from current technology heavy-duty diesel and natural gas goods movement vehicles. *Environmental science & technology* 49, 5236–5244.
- Thiruvengadam, A., Pradhan, S., Thiruvengadam, P., Besch, M., Carder, D., Delgado, O., 2014. *Heavy-duty vehicle diesel engine efficiency evaluation and energy audit (Final Report)*. The International Council on Clean Transportation, Washington, DC.
- U.S. Department of Transportation, 2022. *Amtrak On-Time Performance Trends and Hours of Delay by Cause [WWW Document]*. Bureau of Transportation Statistics. URL <https://www.bts.gov/content/amtrak-time-performance-trends-and-hours-delay-cause> (accessed 11.4.22).
- Vu, D., Szente, J., Loos, M., Maricq, M., 2020. How Well Can mPEMS Measure Gas Phase Motor Vehicle Exhaust Emissions?, in: *WCX SAE World Congress Experience*. Presented at the WCX SAE World Congress Experience, Detroit, MI, pp. 2020-01–0369.
- Wang, J., Rakha, H.A., 2018. Longitudinal train dynamics model for a rail transit simulation system. *Transportation Research Part C: Emerging Technologies* 86, 111–123.

- Wong, T.-T., 2015. Performance evaluation of classification algorithms by k-fold and leave-one-out cross validation. *Pattern Recognition* 48, 2839–2846.
- Wu, Q., Luo, S., Cole, C., 2014. Longitudinal dynamics and energy analysis for heavy haul trains. *Journal of Modern Transportation* 22, 127–136.
- Xu, X., Liu, H., Passmore, R., Patrick, T., Gbologah, F., Rodgers, M.O., Guensler, R., 2018. Fuel and Emissions Calculator (FEC), Version 3.0 (Summary Report). University Transportation Center. Georgia Institute of Technology, Atlanta, GA.
- Xu, Y., Gbologah, F., Cernjul, G., Kumble, A., Guensler, R., Rodgers, M., 2013. Comparison of fuel-cycle emissions per passenger mile from multiple bus and rail technologies, in: Proc., Third International Conference on Urban Public Transportation Systems, Paris, France, November 17-20. pp. 204–216.
- Yuan, W., Frey, H.C., 2021. Multi-scale evaluation of diesel commuter rail fuel use, emissions, and eco-driving. *Transportation Research Part D: Transport and Environment* 99, 102995.
- Yuan, W., Frey, H.C., 2020. Potential for metro rail energy savings and emissions reduction via eco-driving. *Applied Energy* 268, 114944.
- Yuan, W., Frey, H.C., Rastogi, N., 2019. Quantification of Energy Saving Potential for A Passenger Train Based on Inter-Run Variability in Speed Trajectories. *Transportation Research Record* 2673, 153–165.

CHAPTER 4: Development of a Locomotive Power Demand Software to Estimate Train Fuel Use and Emissions

4.1 Introduction

The Piedmont Passenger Train Fuel Use and Emission Estimator Software (PPTFUEES) was developed here for use in estimating trip and station-to-station segment based fuel use and emissions for Piedmont passenger trains. PPTFUEES was developed based on data collected by the Mobile Air Pollutant Emissions Laboratory at North Carolina State University using Portable Emission Measurement Systems (PEMS) from 2013 to 2019 (Rastogi and Frey, 2021, 2018; Graver et al., 2016; Graver and Frey, 2015, 2013). PPTFUEES is applicable to passenger trains with no more than 2 locomotives, no more than 6 passenger cars, and fueled with ultra-low sulfur diesel or 20% blend of biodiesel (B20), for speed limit of no more than 79 mph, for track grade within $\pm 2\%$, and for track curvature within 5 degrees.

PPTFUEES estimates the fuel use and emissions of a typical Piedmont train operation based on second-by-second (1 Hz) train speed, track grade, and track curvature. A screen capture of the user interface for PPTFUEES is shown in Figure 4-1. PPTFUEES is implemented in Microsoft Excel. Input requirements for the user are simplified to the selection of a train consist and a trajectory. The software does the rest.

Figure 4-2 shows a conceptual diagram of the key components of PPTFUEES. PPTFUEES was developed based on a locomotive power demand (LPD) model. LPD accounts for resistive forces opposing train motion, including starting, journal, flange, air, wind, curve, grade, acceleration, and internal resistances (AREMA, 2020; Hay, 1982; Profillidis, 2014). LPD in turn depends on the train speed trajectory and characteristics of the train such as the locomotives, consists, and fuels (LCFs).

PPTFUEES only requires two user inputs, including a LCF ID and a train speed trajectory ID. The outputs include train activities, total fuel use and emissions, and fuel use and emission rates for each station-to-station segment and whole trip for the user-selected LCF ID and speed trajectory ID.

Section 4.2 describes the system requirements for PPTFUEES. Section 4.3 describes the data in PPTFUEES that calibrate the LPD model. Section 4.4 describes the validation of PPTFUEES. Section 4.5 describes the input data required from users. Section 4.6 describes examples of results output from PPTFUEES. Section 4.7 describes applications of PPTFUEES. Details regarding the LPD model development, including model calibration and validation, are documented in Chapter 3 and Appendix B. The software user manual is documented in Appendix C.

4.2 System Requirements

The PPTFUEES requires the following configurations: (1) a computer running Microsoft Windows 10 or 11; (2) Microsoft Excel 2016 and newer (macro-enabled spreadsheet); and (3) at least 300 Megabytes of free hard disk space. The procedure to enable the macro in Microsoft Excel is described in the User Manual in Appendix C.

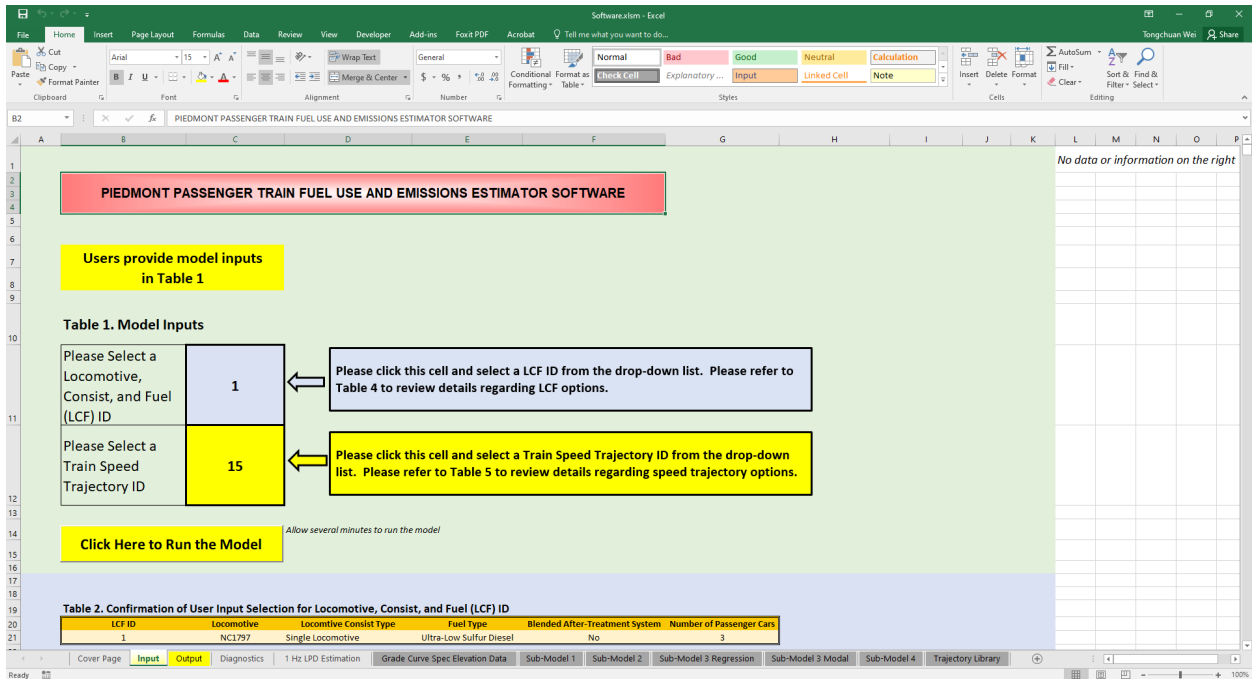


Figure 4-1. A Screen Capture of the Piedmont Passenger Train Fuel Use and Emission Estimator Software. Input worksheet is displayed as an example.

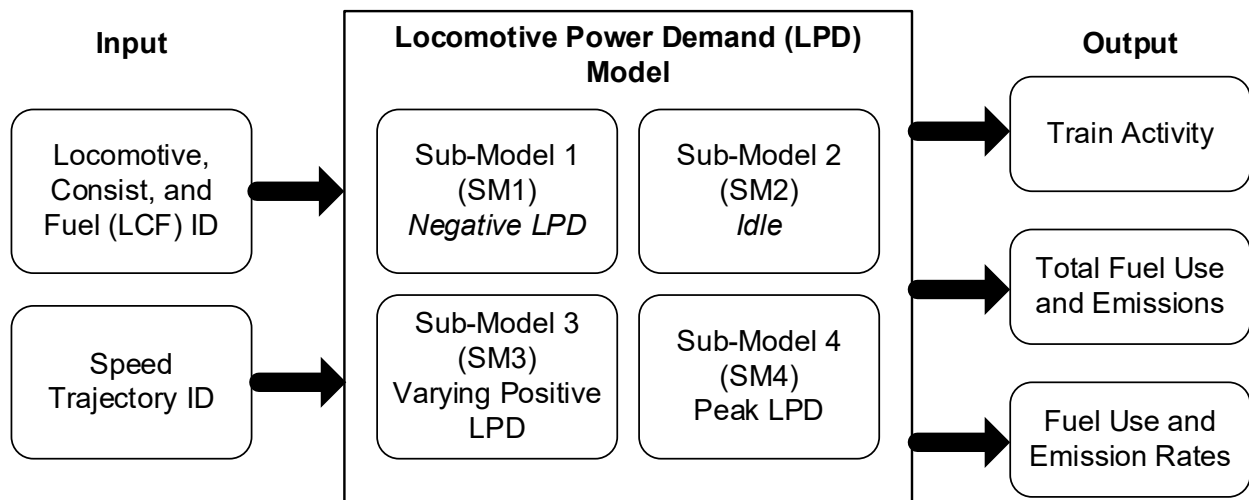


Figure 4-2. The Conceptual Diagram of the Key Components of the Piedmont Passenger Train Fuel Use and Emission Estimator Software.

4.3 Calibration Data

The PPTFUEES was developed based on LPD (AREMA, 2020; Hay, 1982; Profillidis, 2014). One Hz LPD can be quantified based on the 1 Hz train speed trajectory and characteristics of the train, such as the locomotives, consists, and fuels (LCFs).

The LPD model includes four sub-models (Figure 4-2). Sub-models corresponding to negative, zero, and peak engine load include sub-model 1 (SM1), sub-model 2 (SM2), and sub-model 4 (SM4), respectively. Sub-model 3 (SM3) accounts for all other engine loads. Details of the definitions of the sub-models are documented in Chapter 3.

Fuel use and emission rates were calibrated for each LCF ID and each sub-model. The calibrated mean fuel use and emission rates for each LCF ID for SM1, SM2, and SM4 are given in Table 4-1. These calibration data are included in the PPTFUEES in the Sub-Model 1, Sub-Model 2, and Sub-Model 4 sheets, respectively.

For SM3, fuel use and emission rates were calibrated using quadratic or modal models depending on LCF and species. Quadratic models were calibrated for fuel use, CO₂ and NO_x emission rates for each LCF, except for a modal model for NO_x emission rates for locomotive NC 1797. To ensure continuity with SM2, the quadratic intercept was set to the average fuel use and emission rates estimated for SM2. The SM3 parameters for each LCF for fuel use rates, CO₂ emission rates, and NO_x emission rates are given in Table 4-2. These calibrated quadratic regression parameters were included in the PPTFUEES in the Sub-Model 3 Regression sheet. Average SM3 modal emission rates for the pollutants and LCFs for which modal models were calibrated are shown in Figure 4-3. These calibrated modal emission rates data were included in the PPTFUEES in the Sub-Model 3 Modal sheet.

4.4 Evaluation of the Software Tool

The accuracy and precision of the complete LPD model for fuel use rates at resolutions of 1 Hz, segment-average, and trip totals were quantified (Tables B-23 and B-24 in Appendix B). The parity slope of estimated versus measured fuel use rates and CO₂ emission rates was within 10% of 1 with $R^2 > 0.87$ for each LCF and resolution. For NO_x emission rates, the parity slope was within 7% of 1 with $R^2 > 0.73$ for each LCF. For PM emission rates, the parity slope was within 7% of 1 and R^2 was 0.62 or higher. Thus, the models are accurate and precise. The parity slopes for CO and HC emission rates were typically within 25% of 1 with $R^2 < 0.60$. CO and HC emission rates were typically less precisely estimated compared to other species, in large part because the exhaust CO and HC concentrations were comparable to the gas analyzer detection limit in many cases. However, the average slope based on all LCFs for each species was within 5% of 1.

Model estimated fuel use and emission rates for the nine diesel-fueled LCFs were benchmarked to independent data (Figure B-21 in Appendix B). On average, estimated fuel use and emission rates were similar to within 9% of independent data for output <1500 kW. For output >1500 kW, Fuel use and emission rates were typically lower by <33%. Transient-based fuel use and emission rates such as those estimated here are typically lower than steady-state based rates because of transitions from lower notch positions (Yuan and Frey, 2021).

Table 4-1. Calibrated Mean Fuel Use and Emission Rates for Sub-Models 1, 2, and 4 based on Measured One-Way Trips for Each Combinations of Locomotives, Consists, and Fuels (LCFs).

LCF ID	Data Group ^a	Data ^b (%)	$\overline{LPD}_{12,t}$ (kW/s) ^c	Mean Rate (g/s)					
				Fuel Use	CO ₂	CO	HC	NO _x	PM
1	SM1	30	-1460	10.3	31.5	0.1	0.7	1.4	0.01
	SM2	9	-30	4.9	14.5	0.1	0.6	0.6	0.01
	SM4	1	2720	133	422	0.7	0.6	8.1	0.13
2	SM1	32	-1460	11.4	34.9	0.1	0.7	0.6	0.02
	SM2	8	-40	6.1	17.7	0.1	0.9	0.3	0.01
	SM4	7	2780	134	424	1.5	1.1	5.0	0.30
3	SM1	32	-1260	8.6	27.4	0.02	0.1	0.6	0.01
	SM2	11	-20	4.6	14.7	0.03	0.1	0.3	0.01
	SM4	4	2760	136	434	0.6	0.2	6.6	0.24
4	SM1	31	-1340	8.4	26.7	0.01	0.1	0.6	0.01
	SM2	13	-10	4.3	13.5	0.01	0.1	0.3	0.01
	SM4	7	2800	129	411	0.6	0.2	6.1	0.22
5	SM1	28	-1470	14.2	45.2	0.02	0.1	1.0	- ^d
	SM2	6	-50	4.6	14.5	0.02	0.1	0.3	- ^d
	SM4	6	2800	116	370	0.4	0.1	5.5	- ^d
6	SM1	29	-1740	13.3	42.1	0.05	0.1	1.4	0.01
	SM2	8	-40	2.8	8.9	0.05	0.1	0.3	0.01
	SM4	12	2900	119	378	1.0	0.2	10.7	0.13
7	SM1	33	-1040	6.7	21.2	0.01	0.1	0.7	0.01
	SM2	8	-30	3.0	9.5	0.01	0.1	0.3	0.01
	SM4	3	2740	117	373	0.8	0.1	10.2	0.12
8	SM1	26	-1580	11.6	36.4	0.05	0.3	1.0	0.01
	SM2	17	-10	3.3	10.3	0.04	0.1	0.3	0.01
	SM4	11	2980	122	383	2.1	1.1	8.1	0.29
9	SM1	32	-1080	7.0	22.1	0.01	0.2	0.6	0.10
	SM2	14	-10	3.3	10.3	0.01	0.1	0.3	0.08
	SM4	2	2770	118	369	3.0	0.9	7.0	0.34
10	SM1	31	-1500	10.6	32.4	0.02	0.4	1.4	0.01
	SM2	8	-50	3.9	11.6	0.03	0.4	0.5	0.01
	SM4	4	2740	130	404	0.3	0.8	8.1	0.17
11	SM1	28	-1500	14.7	45.4	0.09	0.2	0.7	0.01
	SM2	9	-40	4.5	13.7	0.01	0.2	0.2	0.01
	SM4	1	2790	146	453	1.8	0.1	3.8	0.23
12	SM1	28	-410	16.3	49.8	0.2	0.4	0.9	0.03
	SM2	10	10	4.3	12.6	0.1	0.3	0.3	0.02
	SM4	- ^e	- ^e	- ^e	- ^e	- ^e	- ^e	- ^e	- ^e

^a Data group: Sub-model 1 (SM1) corresponds to data with negative $\overline{LPD}_{12,t}$, sub-model 2 (SM2) corresponds to stationary train, and sub-model 4 (SM4) corresponds to engine operation at peak output. Fuel use and emission rates for high idle and notch 8 correspond to steady-state operation quantified based on over-the-rail measurements (Graver and Frey 2015, 2016; Rastogi and Frey, 2021).

^b Percentage of total seconds that were categorized for each sub-model.

^c $\overline{LPD}_{12,t}$: 12-Second Backwards Moving Average Locomotive Power Demand.

^d Invalid PM data.

^e No measured data in this range.

Table 4-2. Calibrated Sub-Model 3 Regression Parameters for Fuel Use and Emission Rates based on All One-Way Trips for Measured Combinations of Locomotives, Consists, and Fuels: (a) Fuel Use Rate; (b) CO₂ Emission Rate; and (c) NO_x Emission Rate.

(a) Fuel Use Rate

LCF ID ^a	Sample Size	Linear Term			Quadratic Term			Intercept (g/s)	Model R ² without Quadratic Term	Model R ² with Quadratic Term
		Slope ($\times 10^{-2}$ g/kW)	Standard Error ($\times 10^{-3}$ g/kW)	95% Confidence Interval ($\times 10^{-2}$ g/kW)	Slope ($\times 10^{-5}$ g ² /kW ²)	Standard Error ($\times 10^{-6}$ g ² /kW ²)	95% Confidence Interval ($\times 10^{-5}$ g ² /kW ²)			
1	35619	8.54	2.19	[8.10, 8.98]	-1.33	4.38	[-1.42, -1.24]	10.1	0.86	0.89
2	32945	5.51	2.84	[4.94, 6.08]	-0.23	5.32	[-0.34, -0.12]	11.5	0.73	0.76
3	39041	5.22	2.80	[4.66, 5.78]	<i>0.09</i>	<i>4.75</i>	<i>[-0.01, 0.19]</i>	8.6	0.81	0.84
4	29491	3.35	2.57	[2.84, 3.86]	0.43	4.04	[0.35, 0.51]	8.3	0.72	0.74
5	33567	4.30	2.30	[3.84, 4.76]	<i>0.01</i>	<i>5.72</i>	<i>[-0.10, 0.12]</i>	14.3	0.80	0.82
6	18599	4.77	3.57	[4.06, 5.48]	-0.20	7.10	[-0.34, -0.06]	13.5	0.80	0.82
7	19112	3.32	2.24	[2.87, 3.77]	0.23	3.69	[0.16, 0.30]	6.8	0.78	0.79
8	18652	6.33	4.18	[5.49, 7.17]	-0.74	7.95	[-0.90, -0.58]	10.3	0.78	0.81
9	16867	2.88	2.68	[2.35, 3.42]	0.71	5.05	[0.61, 0.81]	7.0	0.74	0.76
10	29461	7.64	5.25	[7.53, 7.74]	-1.06	2.83	[-1.11, -1.00]	10.6	0.83	0.85
11	38212	5.68	5.18	[5.58, 5.78]	-1.09	2.83	[-1.14, -1.03]	14.7	0.86	0.88
12	162304	5.15	3.22	[5.07, 5.24]	-1.36	4.45	[-1.47, -1.25]	16.3	0.76	0.79

^a LCF ID: Each combination of locomotive, consist, and fuel was assigned a unique ID. The description of each LCF ID is given in Table 3-2. Italicized values indicate terms not statistically significantly different than zero.

Table 4-2 Continued on Next Page.

Table 4-2 Continued from Previous Page.

(b) CO₂ Emission Rate

LCF ID ^a	Sample Size	Linear Term			Quadratic Term			Intercept (g/s)	Model R ² without Quadratic Term	Model R ² with Quadratic Term
		Slope ($\times 10^{-1}$ g/kW)	Standard Error ($\times 10^{-2}$ g/kW)	95% Confidence Interval ($\times 10^{-1}$ g/kW)	Slope ($\times 10^{-5}$ g ² /kW ²)	Standard Error ($\times 10^{-6}$ g ² /kW ²)	95% Confidence Interval ($\times 10^{-5}$ g ² /kW ²)			
1	35619	2.71	0.64	[2.58, 2.84]	-4.20	1.85	[-4.57, -3.83]	31	0.87	0.89
2	32945	1.74	0.74	[1.59, 1.89]	-0.72	1.32	[-0.98, -0.46]	35	0.73	0.76
3	39041	1.67	0.88	[1.49, 1.85]	0.27	1.23	[0.02, 0.52]	27	0.83	0.84
4	29491	1.07	0.81	[0.91, 1.23]	1.34	1.83	[0.97, 1.71]	26	0.73	0.74
5	33567	1.37	0.61	[1.25, 1.49]	<i>0.01</i>	<i>1.14</i>	<i>[-0.22, 0.24]</i>	45	0.81	0.82
6	18599	1.52	1.11	[1.30, 1.74]	-0.66	1.88	[-1.04, -0.28]	43	0.80	0.82
7	19112	1.06	0.67	[0.93, 1.19]	0.72	1.48	[0.42, 1.02]	22	0.78	0.80
8	18652	2.01	1.31	[1.75, 2.27]	-2.41	2.55	[-2.92, -1.90]	32	0.78	0.81
9	16867	0.93	1.12	[0.71, 1.15]	2.15	2.01	[1.75, 2.55]	22	0.72	0.76
10	29461	2.37	0.81	[2.21, 2.53]	-0.33	2.38	<i>[-0.80, 0.14]</i>	34	0.83	0.86
11	38212	1.67	0.84	[1.51, 1.84]	-0.33	2.48	<i>[-0.82, 0.16]</i>	38	0.85	0.88
12	162304	1.53	0.52	[1.43, 1.63]	<i>-0.41</i>	3.82	<i>[-1.16, 0.34]</i>	27	0.77	0.80

^a LCF ID: Each combination of locomotive, consist, and fuel was assigned a unique ID. The description of each LCF ID is given in Table 3-2. *Italicized values indicate terms not statistically significantly different than zero.*

Table 4-2 Continued on Next Page.

Table 4-2 Continued from Previous Page.

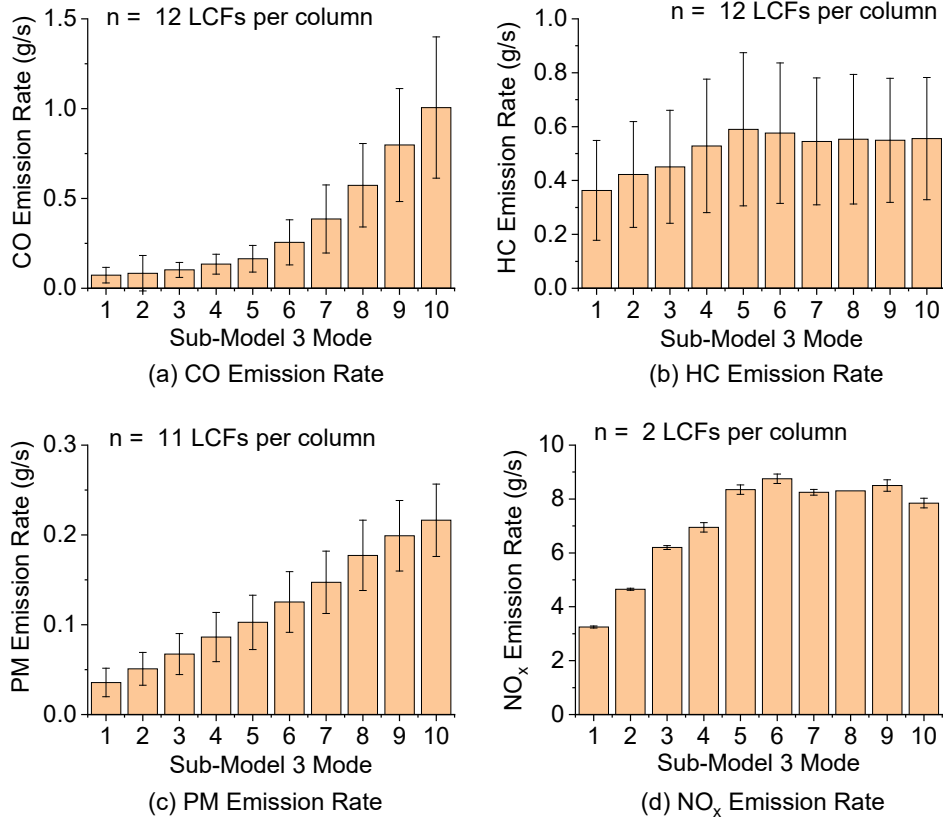
(c) NO_x Emission Rate

LCF ID ^a	Sample Size	Linear Term			Quadratic Term			Intercept (g/s)	Model R ² without Quadratic Term	Model R ² with Quadratic Term
		Slope (×10 ⁻³ g/kW)	Standard Error (×10 ⁻⁴ g/kW)	95% Confidence Interval (×10 ⁻³ g/kW)	Slope (×10 ⁻⁶ g ² /kW ²)	Standard Error (×10 ⁻⁸ g ² /kW ²)	95% Confidence Interval (×10 ⁻⁶ g ² /kW ²)			
1	<i>_b</i>	<i>_b</i>	<i>_b</i>	<i>_b</i>	<i>_b</i>	<i>_b</i>	<i>_b</i>	<i>_b</i>	<i>_b</i>	<i>_b</i>
2	32945	2.75	0.12	[2.73, 2.77]	-0.42	2.52	[-0.47, -0.37]	0.62	0.77	0.80
3	39041	3.81	0.13	[3.78, 3.84]	-0.49	2.18	[-0.53, -0.45]	0.59	0.83	0.84
4	29491	2.84	0.14	[2.81, 2.87]	-0.32	3.29	[-0.39, -0.25]	0.57	0.71	0.74
5	33567	3.16	0.12	[3.14, 3.18]	-0.55	1.56	[-0.58, -0.52]	1.02	0.84	0.85
6	18599	5.21	0.25	[5.16, 5.26]	-0.59	7.19	[-0.73, -0.45]	1.40	0.82	0.82
7	19112	4.54	0.25	[4.49, 4.59]	-0.44	6.58	[-0.57, -0.31]	0.70	0.79	0.79
8	18652	5.04	0.2	[5.00, 5.08]	-0.88	3.58	[-0.95, -0.81]	0.86	0.81	0.84
9	16867	3.82	0.19	[3.78, 3.86]	-0.46	5.78	[-0.58, -0.34]	0.59	0.74	0.77
10	<i>_b</i>	<i>_b</i>	<i>_b</i>	<i>_b</i>	<i>_b</i>	<i>_b</i>	<i>_b</i>	<i>_b</i>	<i>_b</i>	<i>_b</i>
11	38212	3.47	0.11	[3.45, 3.49]	-0.45	3.233	[-0.46, -0.44]	0.55	0.79	0.81
12	112564	3.88	0.23	[3.83, 3.93]	-0.37	2.346	[-0.38, -0.36]	0.59	0.71	0.75

^a LCF ID: Each combination of locomotive, consist, and fuel was assigned a unique ID. The description of each LCF ID is given in Table 3-2.

^b NO_x emission rates for LCF IDs 1 and 10 were modeled based on a 10-mode modal model because they were not modeled properly by the regression model.

Italicized values indicate terms not statistically significantly different than zero.



Sub-Model 3 Mode	12-Second Backwards Moving Average Locomotive Power Demand ($\overline{LPD}_{12,t}$, kW)
1	$0 < \overline{LPD}_{12,t} \leq 164$
2	$164 < \overline{LPD}_{12,t} \leq 354$
3	$354 < \overline{LPD}_{12,t} \leq 568$
4	$568 < \overline{LPD}_{12,t} \leq 794$
5	$794 < \overline{LPD}_{12,t} \leq 1038$
6	$1038 < \overline{LPD}_{12,t} \leq 1298$
7	$1298 < \overline{LPD}_{12,t} \leq 1580$
8	$1580 < \overline{LPD}_{12,t} \leq 1885$
9	$1885 < \overline{LPD}_{12,t} \leq 2190$
10	$2190 < \overline{LPD}_{12,t} < 2519$

Figure 4-3. Calibrated Average Sub-Model 3 Modal Emission Rates of 12 Combinations of Locomotives, Consists, and Fuels (LCFs) for: (a) CO Emission Rates; (b) HC Emission Rates; (c) PM Emission Rates; and (d) NO_x Emission Rates. Error bars in the figures indicate ± one standard deviation on the mean of 12 LCFs for each mode. Sample size (n) indicates number of LCFs. For PM, all LCFs are included except for LCF ID 5. For NO_x, only LCF IDs 1 and 10 are included. The description of each LCF ID is given in Table 3-2.

4.5 Data Input

The PPTFUEES requires two inputs from users, including a LCF ID and a train speed trajectory ID. There are 12 LCF IDs, as shown in Table 4-3, including locomotive name, locomotive consist type, fuel type, number of passenger cars, train weight, and train length.

There are 45 train speed trajectory IDs, as shown in Table 4-4, including origin, destination, travel time, distance, and trip average speed. These 45 speed trajectories met data completeness criteria in which more than 90% of PEMS measured pollutant concentration data were valid.

Table 4-3. Locomotives, Consists, and Fuels (LCF) ID in the Piedmont Passenger Train Fuel Use and Emission Estimator Software.

LCF ID	Locomotive ^a	Locomotive Consist Type	Fuel ^b	One-way Trips	Number of Passenger Cars ^c	Train Weight (metric tons)	Train Length (m)
1	NC1797	Single Locomotive	ULSD	5	3	310	100
2	NC1810	Single Locomotive	ULSD	6	3	310	100
3	NC1859	Single Locomotive	ULSD	6	3	310	100
4	NC1859	Double-Powered Tandem	ULSD	5	6	630	190
5	NC1893	Single Locomotive	ULSD	6	3	310	100
6	NC1871	Single-Powered Push/Pull	ULSD	3	4	500	140
7	NC1871	Double-Powered Push/Pull	ULSD	3	4	500	140
8	NC1984	Single-Powered Push/Pull	ULSD	3	5	570	170
9	NC1984	Double-Powered Push/Pull	ULSD	3	5	570	170
10	NC1797	Single Locomotive	B20	3	3	310	100
11	NC1810	Single Locomotive	B20	3	3	310	100
12	NC1859	Single Locomotive	B20	15	3	310	100

^a Only the measured locomotive is indicated for the train consists with two locomotives. All locomotives have a 2240 kW EMD 12-710 prime mover engine and an additional 460 kW to 600 kW head end power engine. Locomotive NC 1797 is F59PHI. Others are F59PH.

^b Fuel: Ultra-Low Sulfur Diesel (ULSD); B20: 20% blend of biodiesel in diesel.

^c Number of passenger cars includes baggage/café car as they have equal weight and dimensions.

Table 4-4. Train Speed Trajectory ID in the Piedmont Passenger Train Fuel Use and Emission Estimator Software.

(a) Raleigh to Charlotte Trajectories

Speed Trajectory ID	Origin	Destination	Travel Time (min)	Distance (mile)	Average Speed (mph)
1	Raleigh	Charlotte	173	163	57
2	Raleigh	Charlotte	174	160	55
3	Raleigh	Charlotte	174	164	56
4	Raleigh	Charlotte	178	168	56
5	Raleigh	Charlotte	179	164	55
6	Raleigh	Charlotte	180	169	56
7	Raleigh	Charlotte	180	160	53
8	Raleigh	Charlotte	180	159	53
9	Raleigh	Charlotte	180	159	53
10	Raleigh	Charlotte	181	157	52
11	Raleigh	Charlotte	182	160	53
12	Raleigh	Charlotte	187	171	55
13	Raleigh	Charlotte	188	169	54
14	Raleigh	Charlotte	188	171	54
15	Raleigh	Charlotte	190	173	55
16	Raleigh	Charlotte	196	168	51
17	Raleigh	Charlotte	197	166	51
18	Raleigh	Charlotte	197	167	51
19	Raleigh	Charlotte	200	168	50
20	Raleigh	Charlotte	203	162	48
21	Raleigh	Charlotte	204	173	51
22	Raleigh	Charlotte	204	169	50
23	Raleigh	Charlotte	224	170	45
24	Raleigh	Charlotte	242	170	42

Table 4-4 Continued on Next Page

Table 4-4 Continued from Previous Page

(b) Charlotte to Raleigh Trajectories

Speed Trajectory ID	Origin	Destination	Travel Time (min)	Distance (mile)	Average Speed (mph)
25	Charlotte	Raleigh	173	156	54
26	Charlotte	Raleigh	174	156	54
27	Charlotte	Raleigh	175	160	55
28	Charlotte	Raleigh	178	166	56
29	Charlotte	Raleigh	180	166	56
30	Charlotte	Raleigh	183	164	54
31	Charlotte	Raleigh	184	170	56
32	Charlotte	Raleigh	191	161	50
33	Charlotte	Raleigh	191	165	52
34	Charlotte	Raleigh	193	171	53
35	Charlotte	Raleigh	195	173	53
36	Charlotte	Raleigh	196	173	53
37	Charlotte	Raleigh	197	170	52
38	Charlotte	Raleigh	198	163	49
39	Charlotte	Raleigh	201	172	51
40	Charlotte	Raleigh	202	171	51
41	Charlotte	Raleigh	206	165	48
42	Charlotte	Raleigh	207	167	48
43	Charlotte	Raleigh	208	165	48
44	Charlotte	Raleigh	215	169	47
45	Charlotte	Raleigh	228	172	45

4.6 Results Output

For a given speed trajectory ID, the PPTFUEES is able to quantify train activities for each station-to-station segment and whole trip, including travel time, distance, maximum speed, average speed, average positive acceleration, average negative acceleration, idle duration at stations, idle duration during train operations, total idle duration, cumulative elevation gain, cumulative positive elevation gain, and cumulative negative elevation gain. Table 4-5 shows an example output of train activity for each station-to-station segment and whole trip for trajectory ID 15.

Table 4-5. Example Output: Train Activity for Each Station-to-Station Segment and Whole Trip for Trajectory ID 15.

Train Activity	Station-to-Station Segments								Whole Trip
	Raleigh-Cary	Cary-Durham	Durham-Burlington	Burlington-Greensboro	Greensboro-High Point	High Point-Salisbury	Salisbury-Kannapolis	Kannapolis-Charlotte	
Travel Time (minute)	13	19	39	20	15	32	15	27	190
Distance (mile)	8	18	33	21	15	34	16	27	173
Maximum Speed (mph)	78	82	77	80	79	81	79	81	82
Average Speed (mph)	40	56	52	63	63	64	64	60	55
Average Positive Acceleration (mph/s)	1.04	0.68	0.50	0.63	0.38	0.37	0.47	0.47	0.51
Average Negative Acceleration (mph/s)	-1.03	-0.95	-0.66	-0.75	-0.89	-0.68	-0.61	-0.63	-0.75
Idle duration at stations (minute) *	2	2	1	3	1	1	1	0	10
Idle duration during train operations (minute)	0	0	0	0	0	0	0	0	0
Total idle duration (minute)	2	2	1	3	1	1	1	0	11
Cumulative Elevation Gain (feet)	149	-111	271	154	83	-147	80	-100	365
Cumulative Positive Elevation Gain (feet)	314	470	1110	837	457	756	404	594	5093
Cumulative Negative Elevation Gain (feet)	-165	-581	-839	-683	-373	-903	-323	-695	-4729

*Note: Idle duration at stations refers to idling at Cary station for Raleigh-Cary, Durham station for Cary-Durham, Burlington station for Durham-Burlington, Greensboro station for Burlington-Greensboro, High Point station for Greensboro-High Point, Kannapolis station for Salisbury-Kannapolis, and Charlotte station for Kannapolis-Charlotte.

For a given LCF ID and speed trajectory ID, PPTFUEES is able to quantify total fuel use and emissions for CO₂, CO, HC, NO_x, and PM for each station-to-station segment and whole trip. Table 4-6 shows an example output of total fuel use and emissions for each station-to-station segment and whole trip for LCF ID 1 operating on trajectory ID 15. Users can also visualize total fuel use and emissions for each station-to-station segment in the PPTFUEES (see User Manual in Appendix C).

Table 4-6. Example Output: Total Fuel Use and Emissions for Each Station-to-Station Segment and Whole Trip for Locomotives, Consists, and Fuels (LCF) ID 1 Operating on Speed Trajectory ID 15.

Species (unit)	Station-to-Station Segments								Whole Trip
	Raleigh- Cary	Cary- Durham	Durham- Burlington	Burlington- Greensboro	Greensboro- High Point	High Point- Salisbury	Salisbury- Kannapolis	Kannapolis- Charlotte	
Fuel (gallon)	14	20	44	26	20	37	18	31	210
CO ₂ (kg)	137	197	440	262	203	370	179	308	2,106
CO (g)	197	303	670	394	311	572	256	494	3,259
HC (g)	702	1,003	2,054	1,097	774	1,695	846	1,320	9,868
NO _x (g)	4,111	5,603	12,180	6,945	5,122	10,094	5,239	7,932	57,597
PM (g)	26	42	98	61	51	86	37	76	478

For a given LCF ID and speed trajectory ID, PPTFUEES is able to quantify fuel economy (mpg) as well as distance-based emission rates (e.g., g/mile) for CO₂, CO, HC, NO_x, and PM for each station-to-station segment and whole trip. Table 4-7 shows an example output of fuel economy and distance-based emission rates for each station-to-station segment and whole trip for LCF ID 1 operating on trajectory ID 15. Users can also visualize fuel economy and distance-based emission rates for each station-to-station segment and whole trip in the PPTFUEES (see User Manual in Appendix C).

Table 4-7. Example Output: Fuel Economy and Distance-Based Emission Rates for Each Station-to-Station Segment and Whole Trip for Locomotives, Consists, and Fuels (LCF) ID 1 Operating on Speed Trajectory ID 15.

Species (unit)	Station-to-Station Segments								Whole Trip
	Raleigh- Cary	Cary- Durham	Durham- Burlington	Burlington- Greensboro	Greensboro- High Point	High Point- Salisbury	Salisbury- Kannapolis	Kannapolis- Charlotte	
Fuel Economy (mpg)	0.6	0.9	0.8	0.8	0.8	0.9	0.9	0.9	0.8
CO ₂ (kg/mile)	16.2	10.9	13.3	12.2	13.2	10.8	11.4	11.6	12.2
CO (g/mile)	23.2	16.8	20.2	18.4	20.2	16.7	16.3	18.6	18.8
HC (g/mile)	83.0	55.6	61.8	51.3	50.2	49.4	54.0	49.8	57.0
NO _x (g/mile)	486	311	366	325	332	294	334	299	333
PM (g/mile)	3.1	2.3	3.0	2.9	3.3	2.5	2.4	2.9	2.8

For a given LCF ID and speed trajectory ID, PPTFUEES is able to quantify time-based fuel use and emission rates (e.g., g/s) for CO₂, CO, HC, NO_x, and PM for each station-to-station segment and whole trip. Table 4-8 shows an example output of time-based fuel use and emission rates for each station-to-station segment and whole trip for LCF ID 1 operating on trajectory ID 15. Users can also visualize time-based fuel use and emission rates for each station-to-station segment and whole trip in the PPTFUEES (see User Manual in Appendix C).

For a given LCF ID and speed trajectory ID, PPTFUEES is able to quantify fuel-based emission rates (e.g., g/gallon) for CO₂, CO, HC, NO_x, and PM for each station-to-station segment and whole trip. Table 4-9 shows an example output of fuel-based emission rates for each station-to-station segment and whole trip for LCF ID 1 operating on trajectory ID 15. Users can also visualize fuel-based emission rates for each station-to-station segment and whole trip in the PPTFUEES (see User Manual in Appendix C).

Table 4-8. Example Output: Time-Based Emission Rates for Each Station-to-Station Segment and Whole Trip for Locomotives, Consists, and Fuels (LCF) ID 1 Operating on Speed Trajectory ID 15.

Species (unit)	Station-to-Station Segments								Whole Trip
	Raleigh- Cary	Cary- Durham	Durham- Burlington	Burlington- Greensboro	Greensboro- High Point	High Point- Salisbury	Salisbury- Kannapolis	Kannapolis- Charlotte	
Fuel (g/s)	57	54	60	67	73	61	64	61	58
CO ₂ (g/s)	181	170	190	213	230	192	202	194	185
CO (mg/s)	259	260	289	320	352	296	288	310	286
HC (mg/s)	923	861	884	893	876	878	952	829	866
NO _x (mg/s)	5,402	4,814	5,243	5,651	5,800	5,230	5,893	4,983	5,053
PM (mg/s)	35	36	42	50	57	44	42	48	42

Table 4-9. Example Output: Fuel-Based Emission Rates for Each Station-to-Station Segment and Whole Trip for Locomotives, Consists, and Fuels (LCF) ID 1 Operating on Speed Trajectory ID 15.

Species (unit)	Station-to-Station Segments								Whole Trip
	Raleigh- Cary	Cary- Durham	Durham- Burlington	Burlington- Greensboro	Greensboro- High Point	High Point- Salisbury	Salisbury- Kannapolis	Kannapolis- Charlotte	
CO ₂ (kg/gallon)	10.0	10.0	10.0	10.0	10.0	10.0	10.0	10.0	10.0
CO (g/gallon)	14.3	15.4	15.2	15.1	15.3	15.5	14.3	16.1	15.5
HC (g/gallon)	51.1	50.8	46.7	42.0	38.2	45.9	47.2	42.9	46.9
NO _x (g/gallon)	299	284	277	266	253	273	292	258	274
PM (g/gallon)	1.9	2.1	2.2	2.4	2.5	2.3	2.1	2.5	2.3

4.7 Software Applications

PPTFUEES can be applied to inter-LCF comparison of train fuel use and emissions for a selected train speed trajectory. For example, for a selected speed trajectory, a template can be created to compare fuel use and emissions among as many as 12 LCFs for station-to-station segments and the whole trip, as shown in Table 4-10. For a selected trajectory, 12 software runs would be needed. Each run would be done for each LCF of interest. For instance, if a user is interested in comparing total fuel use between LCF 1 versus LCF 2 operating on Trajectory ID 15, after the completion of each software run for LCFs 1 and 2 on Trajectory ID 15, the user would go to Sheet Output, Column V, Row 5, then select and copy Cells V5:AD5, and paste them into the template (Table 4-10). Such comparisons can identify, for example, fuel-efficient and low-emitting LCFs, which would help reduce fuel use and emissions between stations and on the whole Piedmont route.

PPTFUEES can also be applied to compare train fuel use and emissions among speed trajectories for a selected LCF. For example, for a selected LCF, a template can be created to compare fuel use and emissions among up to 45 trajectories for station-to-station segments and the whole trip, as shown in Table 4-11. For a selected LCF, software runs would be needed for each trajectory of interest. Such comparisons can identify, for example, trajectories with low fuel use and emissions for each species on each station-to-station segment and on the whole Piedmont route. These applications will be useful to identify operational practices to reduce trip or segment based fuel use and emissions.

By operating fuel-efficient and low-emitting LCFs on trajectories with lower trip fuel use and emissions, system-wide train fuel use and emissions can be reduced. Reduction in fuel use will reduce operating costs. Reduction in emissions will result in reduced exposure to train-generated air pollution near railroad tracks.

Table 4-10. An example template for comparisons of total fuel use and emissions for a given species and a selected train speed trajectory among multiple locomotives, consists, and fuels (LCFs).

LCF ID	Total Fuel Use and Emissions for a Given Species (g)								
	Station-to-Station Segments								Whole Trip
	Raleigh-Cary	Cary-Durham	Durham-Burlington	Burlington-Greensboro	Greensboro-High Point	High Point-Salisbury	Salisbury-Kannapolis	Kannapolis-Charlotte	
1	<i>14</i>	<i>20</i>	<i>44</i>	<i>26</i>	<i>20</i>	<i>37</i>	<i>18</i>	<i>31</i>	<i>210</i>
2	<i>12</i>	<i>17</i>	<i>39</i>	<i>23</i>	<i>18</i>	<i>33</i>	<i>16</i>	<i>28</i>	<i>187</i>
3									
4									
5									
6									
7									
8									
9									
10									
11									
12									

Note: Data in *italics* in the table are example outputs based on running the software for LCF 1 and LCF 2 on Trajectory ID 15.

Table 4-11. An example template for comparisons of total fuel use and emissions for a given species and a selected locomotive, consist, and fuel (LCF) among up to 45 speed trajectories.

Speed Trajectory ID	Total Fuel Use and Emissions for a Given Species (g)								
	Station-to-Station Segments								Whole Trip
	Raleigh-Cary	Cary-Durham	Durham-Burlington	Burlington-Greensboro	Greensboro-High Point	High Point-Salisbury	Salisbury-Kannapolis	Kannapolis-Charlotte	
1									
2									
3									
4									
5									
6									
7									
8									
9									
10									
11									
12									
13									
14									
15									
16									
17									
18									
19									
20									
21									
22									
23									
24									
25									
26									
27									
28									
29									
30									
31									
32									
33									
34									
35									
36									
37									
38									
39									
40									
41									
42									
43									
44									
45									

4.8 Summary of Supporting Information

A user manual of the PPTFUEES is documented in Appendix C.

4.9 References Cited in Chapter 4

- AREMA, 2020. American Railway Engineering and Maintenance-of-way Association Manual for Railway Engineering. Lanham, MD.
- Graver, B.M., Frey, H.C., 2015. Comparison of Over-the-Rail and Rail Yard Measurements of Diesel Locomotives. *Environ. Sci. Technol.* 49, 13031–13039. <https://doi.org/10.1021/acs.est.5b02497>
- Graver, B.M., Frey, H.C., 2013. Comparison of Locomotive Emissions Measured during Dynamometer versus Rail Yard Engine Load Tests. *Transportation Research Record* 2341, 23–33. <https://doi.org/10.3141/2341-03>
- Graver, B.M., Frey, H.C., Hu, J., 2016. Effect of Biodiesel Fuels on Real-World Emissions of Passenger Locomotives. *Environ. Sci. Technol.* 50, 12030–12039. <https://doi.org/10.1021/acs.est.6b03567>
- Hay, W.W., 1982. *Railroad engineering*. John Wiley & Sons, New York.
- Profillidis, V.A., 2014. *Railway management and engineering*. Ashgate Publishing, Ltd., Burlington, VT.
- Rastogi, N., Frey, H.C., 2021. Characterizing Fuel Use and Emission Hotspots for a Diesel-Operated Passenger Rail Service. *Environ. Sci. Technol.* 55, 10633–10644. <https://doi.org/10.1021/acs.est.1c00273>
- Rastogi, N., Frey, H.C., 2018. Estimation of Rail Grade and Horizontal Curvature from non-Proprietary Data Sources, in: *Proceedings of Transportation Research Board 97th Annual Meeting*. Paper No. TRB 18-06366. Transportation Research Board, Washington, D.C., pp. 1–17.
- Yuan, W., Frey, H.C., 2021. Multi-scale evaluation of diesel commuter rail fuel use, emissions, and eco-driving. *Transportation Research Part D: Transport and Environment* 99, 102995. <https://doi.org/10.1016/j.trd.2021.102995>

CHAPTER 5: Study Design for Evaluation of the Effect of the Retrofitted Blended After Treatment System on Locomotive Exhaust Emissions

5.1 Introduction

North Carolina Department of Transportation (NCDOT) owns diesel locomotives operated by Amtrak for the Piedmont passenger service between Raleigh and Charlotte. The locomotive engines emit nitrogen oxides (NO_x), particulate matter (PM), and other pollutants which are harmful to human health. The Rail Division seeks to quantify the emissions of these locomotives and to identify and evaluate options for reduction in emissions. One such option includes retrofitting Blended After Treatment Systems (BATS) in the locomotives.

In 2015, NCDOT engaged Rail Propulsion Systems, LLC of Fullerton, California to install a prototype, first-of-a-kind post combustion emission control system on an existing F59PH Locomotive NC 1859. This system, referred to as BATS, treated blended exhaust from the prime mover and head end power engines using selective catalytic reduction (SCR). Based on rail yard static load measurements conducted by NC State University in October 2016 and comparison to prior baseline emission tests on the same locomotive conducted as part of a prior project, the retrofitted SCR system was able to reduce NO_x emissions by 80 percent or more when the prime mover engine (PME) was running at high engine load.

The F59PH engine on Locomotive NC 1859 has been retrofitted with an improved second generation production-model BATS. The design of the second generation BATS was based on lessons learned from the first-of-a-kind prototype BATS. The second generation BATS is expected to have a better control system for NO_x reduction.

The BATS treats the blended exhaust from the PME and head end power engine (HEP) before releasing the exhaust to the atmosphere. To quantify BATS efficacy, exhaust gas composition measurements are required upstream and downstream of the BATS. Therefore, there is a need to use two or more instruments (e.g., portable emission measurement systems [PEMS]) to simultaneously measure upstream and downstream emissions of BATS. The two or more instruments should be benchmarked in advance based on simultaneous measurements.

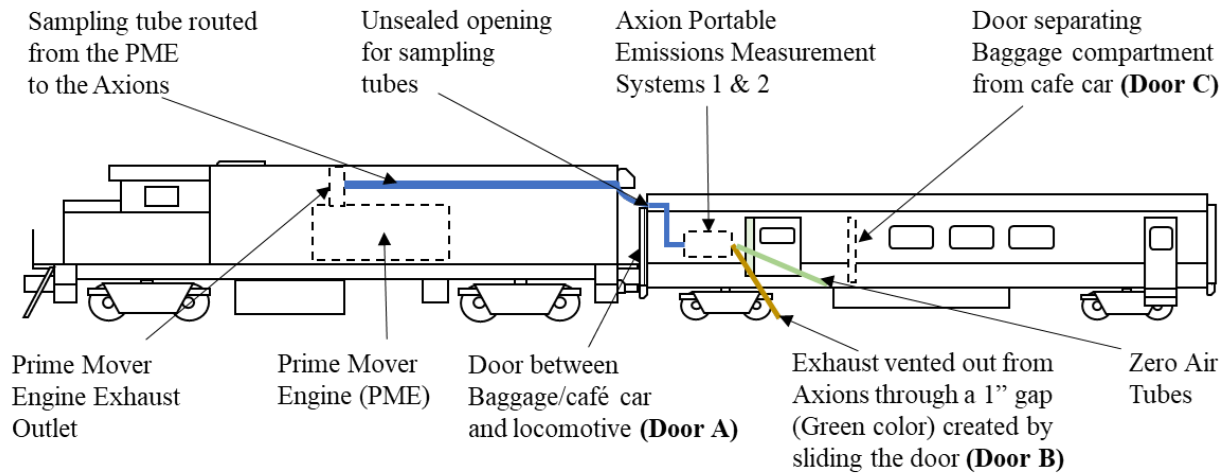
The key objectives of chapter are to: (1) benchmark two PEMS instruments to each other; (2) develop a study design for railyard exhaust emission measurements for a BATS in an F59PH; and (3) develop a study design for over-the-rail exhaust emission measurements for a BATS in an F59PH.

5.2 Benchmarking Two PEMS

To benchmark two PEMS, railyard measurements on an F59PH PME exhaust were conducted on November 17, 2020. Three replicates were conducted. Simultaneous exhaust gas and PM concentration measurements were conducted using two Global MRV Axion PEMS.

A schematic diagram of the measurement setup is given in Figure 5-1. The measurement setup included the placement of PEMS, and routing of exhaust hoses, sensor array cables, and zero air hoses. Two PEMS were placed on the luggage rack inside the baggage compartment. Sixty-foot long engine out exhaust hoses were routed into the baggage car through a small opening created above Door A [Figure 5-1(a)] and connected to the PEMS. PEMS exhaust outlet hoses and zero air inlet hoses were routed outwards from Door B [Figure 5-1(a)] on one side of the baggage

compartment. Door B was slid open to create a 1” gap to let the exhaust outlet and zero air hoses outside the compartment.



(a) A schematic layout of the rail yard measurement



(b) Exhaust hoses and sensor array cables from prime mover engine entering the baggage car



(c) PEMS exhaust outlet hoses and zero air inlet hoses exiting the baggage car

Figure 5-1. A Schematic Diagram of the Measurement Setup for Benchmark Comparison of Two Portable Emission Measurement Systems (PEMS): (a) PEMS Placement and Routing of Exhaust and Zero Air Sample Hoses; (b) Exhaust Hoses and Sensor Array Cables Entering the Baggage Car; and (c) Exhaust Hoses and Zero Air Inlet Hoses Exiting the Baggage Car.

Two Axion PEMS (Axion 1 and Axion 2) were benchmarked to each other. Pollutant concentrations measured with Axion 1 were benchmarked to Axion 2. The comparison is presented in Figure 5-2. The plot of notch-average carbon dioxide (CO₂) concentrations is well described by the line $y=x$. Hence, notch-average CO₂ concentrations measured with both PEMS were comparable to each other. The notch-average CO₂ concentrations were similar to within $\pm 18\%$ for idle and notch 1 and within $\pm 3\%$ for notches 2 and higher. The notch-average CO₂ concentrations at idle and notch 1 were relatively lower than for other notch positions. Therefore, the absolute differences in notch-average CO₂ concentrations were low.

Notch-average carbon (CO) and hydrocarbons (HC) concentrations were typically below the detection limit of both the Axions. Therefore, differences between the average CO and HC concentrations were insignificant.

Notch-average nitric oxide (NO) concentrations were similar to the line $y=x$, except for Replicate 3. The NO concentrations from Axion 2 were systematically underestimated for this replicate, indicating drift or malfunction of Axion 2. Excluding Replicate 3, measured concentrations were typically similar to within $\pm 6\%$ for both Axions.

Notch-average PM concentrations measured with Axion 2 were noisy and did not show a typical trend of monotonically increasing PM concentrations with notch position that was measured for each Replicate of Axion 1, indicating a need for maintenance or repair of the Axion 2 PM sensor.

In general, the concentrations measured with both PEMS were similar to each other, except for PM. Thus, there is no bias in measurements of CO₂, CO, HC, and NO concentrations. A need for maintenance of the PM sensor of Axion 2 was identified.

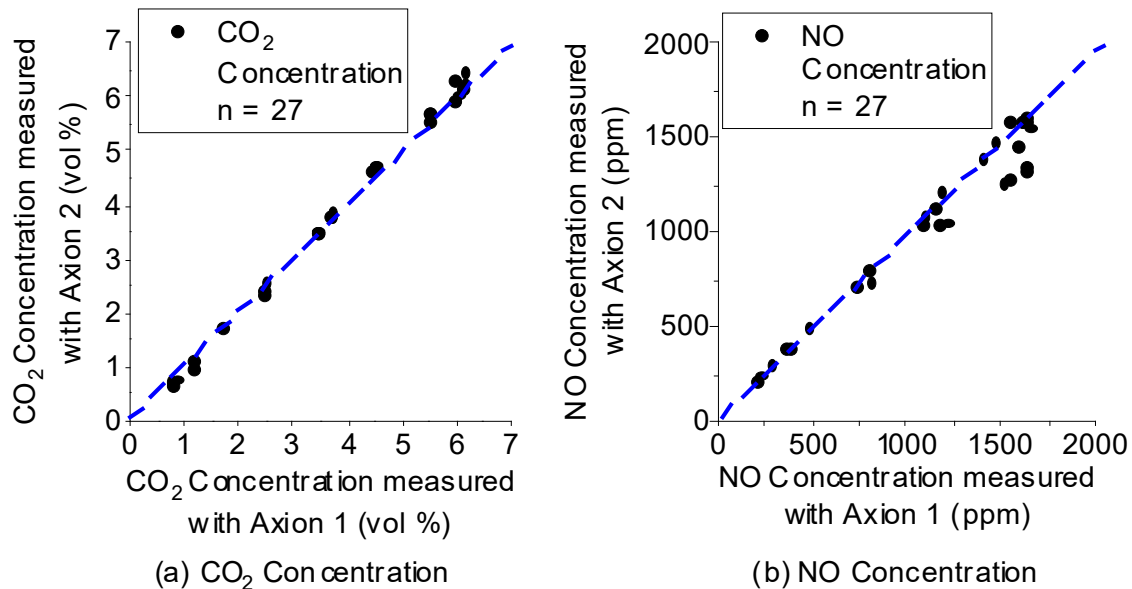


Figure 5-2. Benchmarking Axion PEMS Concentration Measurements for Bias-Correction for Future Planned Measurements with Two PEMS: (a) CO₂; and (b) NO.

The blue dashed line in each panel indicates the line $y = x$.

CO and HC concentrations were typically below the detection limit of both the Axions. Therefore, the differences between the two Axions were insignificant. PM concentrations were noisy indicating a need for maintenance or repair of the PM sensor.

5.3 Railyard Measurement Study Design

The aim of the study design is to have a plan for future measurement of an F59PH locomotive retrofitted with a BATS for the purpose of evaluating the performance of BATS. The study design includes measurement of pollutant concentrations from the PME raw exhaust, HEP engine raw exhausts, and exhaust from the BATS outlet at railyard. The exhaust pollutant concentrations would be measured using PEMS. Measured pollutants include CO₂, CO, HC, NO_x, and PM.

Measurements would be conducted with three PEMS instruments (P1, P2, and P3). Engine activity variables, such as revolutions per minute (RPM), manifold absolute pressure (MAP), and intake air temperature (IAT), would be measured using engine sensors (Figure 5-3). Engine mass air flow would be quantified using a technique known as the “Speed-Density Method”, which depends on RPM, MAP, IAT, engine volumetric efficiency, engine displacement, and engine compression ratio. The engine displacement and compression ratio are known characteristics of each engine to be measured. From engine dynamometer measurements on the same model of PME conducted in a prior study, Graver and Frey (2013) have developed accurate and precise estimates of volumetric efficiency based on the product of RPM and MAP.



(a) Rail Yard Emissions Measurement



(b) Exhaust sample



(c) PEMS



(d) Exhaust sample



(e) Air box pressure and temperature sensors



(f) RPM sensor

Figure 5-3. Railyard measurement of locomotive prime mover engine emissions using Portable Emissions Measurement Systems (Frey and Rastogi, 2018).

For the PME, air/fuel ratio would be inferred from the exhaust composition measured from PEMS located upstream of the BATS. With engine air flow estimated using the speed-density method, and air/fuel ratio, the fuel flow rate and exhaust flow rate would be estimated. Based on exhaust flow rate and measured pollutant concentrations in the exhaust, mass emission rates for each pollutant would be estimated.

NCDOT has a Caterpillar “Electronic Technician” (CAT-ET) electronic control unit (ECU) data logger, which would be requested for use in logging key engine data from the HEP engine ECU. The CAT-ET system includes a communication adapter connected to the HEP engine communication port. Key engine variables that the CAT-ET recorded include fuel flow rate, engine RPM, IAT, boost pressure, and engine load.

BATS outlet flow rates would be estimated based on the exhaust flow of the two engines and SCR chemical reactions. Details of the SCR chemical reactions were documented in a prior NCDOT final report (Frey and Rastogi, 2018). Based on the BATS outlet flow rate and pollutant concentrations, the controlled emission rates and, thus, emission control efficiency of BATS would be quantified for PM and NO_x.

PEMS would be installed at trackside (Figure 5-3). The BATS outlet is comprised of two open channels on the top of the locomotive (Figure 5-4). Stainless steel sample probes would be placed inside the BATS channel to collect exhaust from BATS outlets.



Figure 5-4. Configuration of previously installed blended after-treatment system (BATS) exhaust channels on locomotive NC 1859 (Frey and Rastogi, 2018). NCDOT has fabricated a “sampling rake” that collects exhaust from both channels with ports and fittings for multiple PEMS sample lines. The channel dimensions and sampling geometry may differ in the proposed study.

The F59PH PME with BATS would be run at idle and throttle notch positions 1 through 8 (locomotives have only 8 discrete throttle settings), as indicated in the railyard test schedule given in Table 5-1. Six replicates of the test schedule would be conducted to compare and benchmark the PEMS with each other under various exhaust conditions, including: (1) all three PEMS sample the PME raw exhaust; (2) all three PEMS sample the HEP engine raw exhaust; (3) all three PEMS sample the exhaust from BATS outlet; (4) P1 samples the PME raw exhaust, P2 samples the HEP engine raw exhaust, and P3 samples the exhaust from BATS outlet; (5) P2 samples the PME raw exhaust, P3 samples the HEP engine raw exhaust, and P1 samples the exhaust from BATS outlet; and (6) P3 samples the PME raw exhaust, P1 samples the HEP engine raw exhaust, and P2 samples the exhaust from BATS outlet (Table 5-2). PEMS would be placed downstream of the PME, HEP engine, and BATS to sample the PME raw exhaust, HEP engine raw exhaust, and BATS outlet treated exhaust, respectively (Figure 5-5).

Table 5-1. Railyard Test Schedule for Prime Mover Engine for one replicate

Notch Position	Time (min)
Idle for Warm-up	45
Notch 8	3
Idle for Cooling	5
Notch 7	3
Idle for Cooling	5
Notch 6	3
Idle for Cooling	5
Notch 5	3
Notch 4	3
Notch 3	3
Notch 2	3
Notch 1	3
Idle	3

Table 5-2. Portable emission measurement systems (PEMS) instrument assignments for six replicates of the test schedule.

Sampling Locations	PEMS Assignments for Replicate Number					
	1	2	3	4	5	6
Prime Mover Engine Raw Exhaust	P1, P2, P3	-	-	P1	P2	P3
Head End Power Engine Raw Exhaust	-	P1, P2, P3	-	P2	P3	P1
Blended After Treatment System (BATS) Exhaust	-	-	P1, P2, P3	P3	P1	P2

Note: P1, P2, and P3 represent PEMS instruments 1, 2, and 3, respectively.

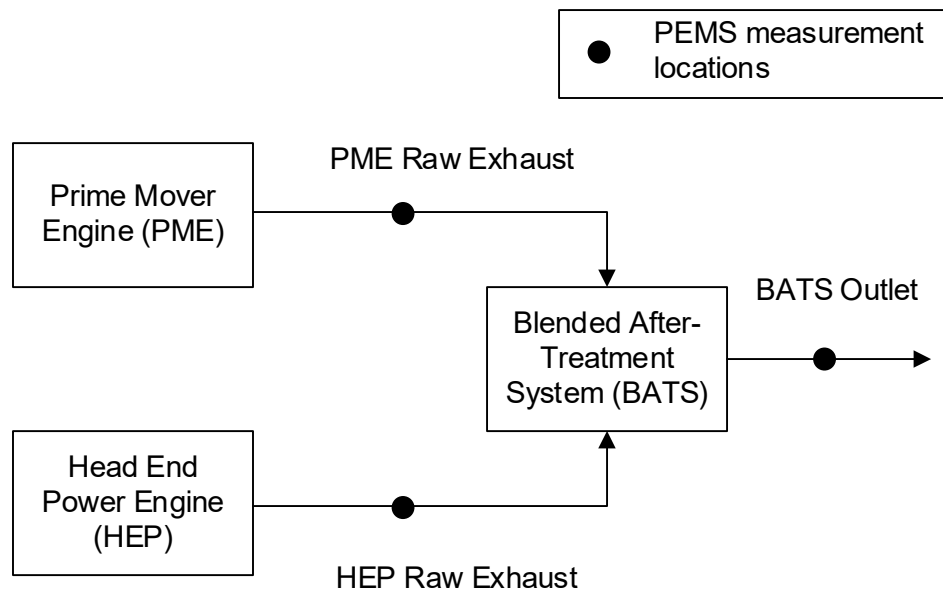


Figure 5-5. Conceptual diagram of locomotive prime mover engine (PME), head end power (HEP) engine, blended after-treatment system (BATS), as well as portable emission measurement systems (PEMS) measurement locations to sample PME raw exhaust, HEP engine raw exhaust, and BATS outlet treated exhaust.

The full set of railyard measurements would be completed in one day, but that it would be advisable to plan on two days per measurement as a contingency for unexpected delays in reconfiguring the placement of PEMS and confirming the best location for sampling exhaust gases.

5.4 Over-the-Rail Measurement Study Design

The aim of the study design is to have a plan for future measurement of an F59PH locomotive retrofitted with a BATS for the purpose of evaluating the performance of BATS during real-world train operations. The study design includes measurement of over-the-rail pollutant concentrations from the PME raw exhaust, HEP engine raw exhaust, and treated exhaust from the BATS outlet. The exhaust pollutant concentrations would be measured using PEMS. Measured pollutants include CO₂, CO, HC, NO_x, and PM. The method for over-the-rail measurement would be similar to railyard measurements, except the PEMS are installed on-board the baggage car of a train (Figure 5-6), and additional data are collected regarding locomotive position using Global Position System (GPS) receivers.

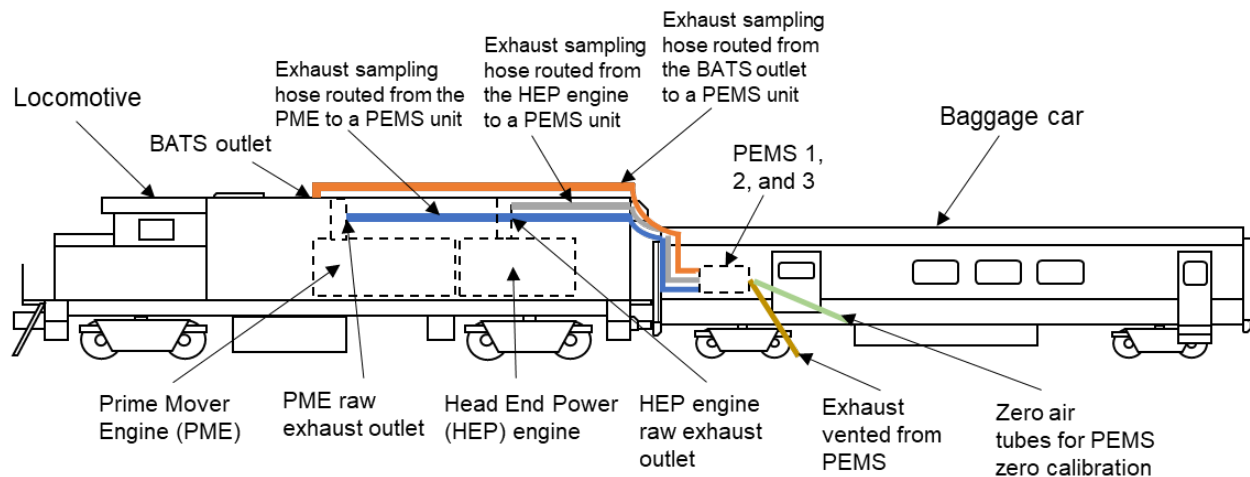


Figure 5-6. Schematic diagram of the exhaust sample hoses routing plan and instrument locations for over-the-rail measurements. BATS: Blended After-Treatment System. HEP: Head End Power Engine. PEMS: Portable Emission Measurement Systems. PME: Prime Mover Engine.

Locomotive speed and acceleration are key factors associated with power produced by the PME. Furthermore, rail track grade and curvature are key factors. To quantify track grade and curvature, GPS receivers with barometric altimeters would be used to record latitude, longitude, and elevation at 1 Hz. Track grades and curvatures have been quantified in prior work, and the method has been found to be accurate (Rastogi and Frey, 2018).

Data would be collected during revenue-generating Piedmont passenger rail service between Raleigh and Charlotte, NC. The one-way travel time is approximately 3 hours and 10 minutes, over a distance of approximately 170 miles. Data would be measured from Raleigh to Charlotte and from Charlotte to Raleigh in the same day. Therefore, two one-way trips can be completed in one day. Based on prior work, we have found that six one-way trips is sufficient to obtain a stable estimate of mean emission rates for each PME notch position and for the trip average. NCDOT and Amtrak typically operate the Piedmont trains with one or two locomotives. Trains with two locomotives typically have one locomotive at each end of the train. With two locomotives, the locomotives are operated in tandem and typically share the tractive load on an equal basis, with one locomotive providing all of the electrical power from one HEP engine for “hotel services” in the train cars. From prior work with other locomotives, we know that the distribution of time in throttle notch settings will be different for single versus tandem operation.

Three PEMS instruments would be deployed for the over-the-rail measurements, with one configured to sample the raw exhaust from the PME, one to sample the raw exhaust from the HEP engine, and the other one to sample the treated exhaust from the BATS outlet. During OTR measurements, PME activity variables, such as RPM, MAP, and IAT, would be measured using engine sensors. One CAT-ET ECU data logger would be installed on the HEP engine to record data engine activity data for the HEP engine.

Over-the-rail measurements are for actual train service. Over-the-rail measurements are observational in that the test cycle is not controlled. Measurements are made for the actual real-world duty cycle during revenue generating passenger service and, therefore, represent actual activity, fuel use, and emissions. Based on prior work, six one-way trips were found to be sufficient to obtain a stable estimate of trip average fuel use and emission rates (Frey and Rastogi, 2018). Given that two one-way trips (inbound and outbound) could be completed in one day, thus, three days of measurements would be required.

5.5 Summary of Supporting Information

Appendix D documented the measurements and results to benchmark two PEMS measurements for F59PH engine exhaust emissions.

5.6 References Cited in Chapter 5

Frey, H.C., Rastogi, N., 2018. Evaluation of Locomotive Emissions Reduction Strategies (Final Report No. FHWA/NC/2016-20). North Carolina State University Research and Development Unit, Raleigh, NC.

Graver, B.M., Frey, H.C., 2013. Comparison of Locomotive Emissions Measured during Dynamometer versus Rail Yard Engine Load Tests. Transportation Research Record 2341, 23–33. <https://doi.org/10.3141/2341-03>

Rastogi, N., Frey, H.C., 2018. Estimation of Rail Grade and Horizontal Curvature from non-Proprietary Data Sources, in: Proceedings of Transportation Research Board 97th Annual Meeting. Paper No. TRB 18-06366. Transportation Research Board, Washington, D.C., pp. 1–17.

CHAPTER 6: Study Design and Modeling Framework for Quantifying Train In-Cabin Air Quality

6.1 Introduction

The research background and needs are described in Chapter 1. In preparation for future work to conduct over-the-rail measurements of locomotive emissions with two or more portable emission measurement systems (PEMS) to be placed in the baggage car or passenger car, baseline background measurements would be needed regarding in-cabin pollutant concentrations. The baseline data would enable later assessment of whether the process of conducting emission measurements with PEMS in the baggage car or passenger car has any measurable impact on in-cabin air quality. Furthermore, the data would provide insight regarding how in-cabin air quality compares to ambient air quality and whether in-cabin air quality is affected by locomotive exhaust. This chapter provides a study design for the railyard in-cabin air quality measurements and an analytical modeling framework to quantify in-cabin air quality.

6.2 Railyard Measurement Study Design

The aim of the study design is to obtain air quality data inside the baggage compartment of the baggage car, lounge compartment of the baggage car, and the passenger car adjacent to the baggage car without any passengers. The baseline air quality measurement would be performed at railyard.

Any uncontrolled locomotive connected to the baggage car and passenger car would be selected for this measurement. The selected locomotive would be requested to be placed upwind of the rest of the train consist.

Five air quality monitors (A1, A2, A3, A4, and A5) would be needed to simultaneously measured air pollutant concentrations:

- A1 would be secured to a tripod or stand and the tripod or stand would be secured on the top shelf of the baggage compartment.
- A2 would be secured to a tripod or stand and the tripod or stand would be secured on the table next to a window in the lounge car.
- A3 would be secured to a tripod or stand and the tripod or stand would be secured on the tray of one of the seats of the passenger car.
- A4 would be secured to a tripod or stand and the tripod or stand would be placed on the ground upwind of the selected locomotive to measure ambient air quality.
- A5 would be secured to a tripod or stand and the tripod or stand would be placed on the ground downwind of the selected locomotive to measure ambient air quality.

During the air quality test, lighting and space conditioning of the baggage car and passenger cars would be operated at the same settings expected during revenue-generating service. The selected locomotive would be run at idle and throttle notch positions 1 through 8, as indicated in the railyard test schedule given in Table 6-1. Three replicates of the test schedule are recommended.

Table 6-1. Railyard Air Quality Test Schedule for Prime Mover Engine for one replicate

Notch Position	Time (min)
Idle for Warm-up	45
Notch 8	3
Idle for Cooling	5
Notch 7	3
Idle for Cooling	5
Notch 6	3
Idle for Cooling	5
Notch 5	3
Notch 4	3
Notch 3	3
Notch 2	3
Notch 1	3
Idle	3

6.3 Analytical Modeling Framework

The objective is to develop an analytical modeling framework for estimating train in-cabin pollutant concentrations. An example of model application is also provided in this section.

6.3.1 Methods

The in-cabin AQ model includes three phases: (I) from the locomotive prime mover engine (PME) start to exhaust plume reaching to each in-cabin location; (II) exhaust plume penetration; and (III) after the PME shuts off.

6.3.1.1 Phase I - from the engine start to exhaust plume reaching to in-cabin locations

Phase I models in-cabin pollutant concentrations before the locomotive exhaust plume reaches to train cabins. After PME starts, exhaust plume needs time to be transported from the exhaust outlet to each in-cabin location, including baggage compartment, lounge compartment, and passenger car. The modeling framework for Phase I is:

$$C_{in,p,l,t} = BC_{in,p,l}, \text{ when } 0 \leq t \leq \frac{D_l}{S} \quad (6-1)$$

Where,

- $C_{in,p,l,t}$ = in-cabin concentrations for pollutant p at location l and time t (e.g., $\mu\text{g}/\text{m}^3$)
- $BC_{in,p,l}$ = baseline in-cabin concentrations for pollutant p at location l (e.g., $\mu\text{g}/\text{m}^3$)
- D_l = distance from the locomotive exhaust outlet to the in-cabin location l (mile)
- S = wind speed (mph)

- p = pollutants, such as carbon dioxide (CO₂), formaldehyde (HCHO), particulate matter with an aerodynamic diameter of 2.5 μm or less (PM_{2.5}), and particulate matter with an aerodynamic diameter of 10 μm (PM₁₀)
- l = in-cabin locations, including baggage compartment, lounge compartment, and passenger car
- t = min-by-min measurement duration (min)

The measured locomotive is requested to be placed upwind of the rest of the train consist. The predominant wind direction in the study area is from the south, but the actual wind direction on a given day can be variable. Within a few days prior to the measurement, we will check weather reports to ascertain the preferred placement of the locomotive.

For Phase I, the baseline concentrations for each in-cabin location (BC_{in,p,l}) will be measured using an AQ monitor (e.g., Temtop 2000c) for 30 minutes before the PME starts. The distance from the exhaust outlet to each in-cabin location (D_l) will be measured using a tape measure for the measured train. The wind speed (S) will be measured using a wind monitor (e.g., Kestrel 5500 Weather Meter) at the upwind AQ monitor sampling location.

6.3.1.2 Phase II - exhaust plume penetration

When the exhaust plume reaches to an in-cabin location, air pollutants will start to penetrate into the train cabin and, thus, lead to in-cabin pollutant concentrations increase. A mass balance model is used to model the in-cabin pollutant concentrations, assuming the pollutants are well mixed and uniformly distributed in the cabin:

$$V_l \frac{dC_{in,p,l,t}}{dt} = P_{p,l} Q_l C_{out,p,t} + E_{in,p,l} - Q_l C_{in,p,l,t} - k_{p,l} V_l C_{in,p,l,t} - \eta Q_{f,l} C_{in,p,l,t},$$

when $\frac{D_l}{S} \leq t \leq t_{engine-off}$ (6-2)

Where,

- V_l = in-cabin volume for location *l* (m³)
- P_{p,l} = penetration factor for pollutant *p* at location *l* (dimensionless)
- Q_l = volumetric air flow rate at location *l* (m³/min)
- C_{out,p,t} = out-cabin concentrations for pollutant *p* at time *t* (e.g., μg/m³)
- E_{in,p,l} = in-cabin emission rate for pollutant *p* at location *l* (e.g., μg/min)
- k_{p,l} = deposition rate for pollutant *p* at location *l* (min⁻¹)
- η = air filter removal efficiency for the fresh air intake system (fraction)
- Q_{f,l} = airflow rate through the air filter at location *l* (m³/min)
- t_{engine-off} = time when the locomotive engine shuts off (min)

The differential equation for the mass balance model [Equation (6-2)] was solved to estimate in-cabin pollutant concentrations, as follows:

$$C_{in,p,l,t} = BC_{in,p,l} \times e^{-\left(\lambda_l + k_{p,l} + \frac{\eta Q_{f,l}}{V_l}\right)\left(t - \frac{D_l}{S}\right)} + \left(\frac{P_{p,l} C_{out,p,t} + BC_{in,p,l}}{1 + \frac{k_{p,l}}{\lambda_l} + \frac{\eta Q_{f,l}}{\lambda_l V_l}}\right) \left[1 - e^{-\left(\lambda_l + k_{p,l} + \frac{\eta Q_{f,l}}{V_l}\right)\left(t - \frac{D_l}{S}\right)}\right],$$

when $\frac{D_l}{S} \leq t \leq t_{engine-off}$ (6-3)

Where,

$$\begin{aligned}\lambda_l &= \text{air exchange rate at location } l \text{ (min}^{-1}\text{), which is } \frac{Q_l}{V_l} \\ BC_{in,p,l} &= \text{baseline in-cabin concentrations for pollutant } p \text{ at location } l \text{ (e.g., } \mu\text{g/m}^3\text{),} \\ &\text{which is } \frac{E_{in,p,l}}{\lambda_l V_l}\end{aligned}$$

For Phase II, the out-cabin concentrations ($C_{out,p,t}$) will be measured using an AQ monitor at the downwind AQ monitor sampling location near to the train passenger car. The air exchange rate (λ_l), deposition rate ($k_{p,l}$), and air filter removal efficiency (η) can be referred from the literature. The in-cabin volume (V_l) and airflow rate through the air filter ($Q_{f,l}$) for the measured train can be provided by North Carolina Department of Transportation (NCDOT). The penetration factor ($P_{p,l}$) will be quantified based on the slope of the linear least squares regression of in-cabin versus out-cabin pollutant concentrations:

$$C_{in,p,l,t} = P_{p,l}C_{out,p,t} + BC_{in,p,l} \quad (6-4)$$

6.3.1.3 Phase III - after the engine off

Phase III models in-cabin pollutant concentrations after the PME shuts off and before in-cabin concentrations back to the baseline. The estimated in-cabin pollutant concentrations are assumed to follow a first order decay after the PME shuts off:

$$C_{in,p,l,t} = C_{in,p,l,t=t_{engine-off}} e^{-(\lambda_l + D_{p,l} + \frac{\eta Q_{f,l}}{V_l})(t - t_{engine-off})}, \text{ when } t \geq t_{engine-off} \quad (6-5)$$

Where,

$$\begin{aligned}C_{in,p,l,t=t_{engine-off}} &= \text{in-cabin concentrations for pollutant } p \text{ at location } l \text{ and time} \\ &t = t_{engine-off} \text{ (e.g., } \mu\text{g/m}^3\text{)}\end{aligned}$$

For Phase III, the in-cabin concentrations at each location when the PME shuts off ($C_{in,p,l,t=t_{engine-off}}$) can be estimated based on Equation (6-3) in Phase II.

6.3.1.4 Overall - final combined model

The final combined model is a combination of the models in Phases I, II, and III to estimate in-cabin pollutant concentrations:

$$\left\{ \begin{array}{ll} C_{in,p,l,t} = BC_{in,p,l}, & \text{when } 0 \leq t \leq \frac{D_l}{S} \\ C_{in,p,l,t} = BC_{in,p,l} \times e^{-(\lambda_l + k_{p,l} + \frac{\eta Q_{f,l}}{V_l})(t - \frac{D_l}{S})} + \left(\frac{P_{p,l}C_{out,p,t} + BC_{in,p,l}}{1 + \frac{k_{p,l}}{\lambda_l} + \frac{\eta Q_{f,l}}{\lambda_l V_l}} \right) [1 - e^{-(\lambda_l + k_{p,l} + \frac{\eta Q_{f,l}}{V_l})(t - \frac{D_l}{S})}], & \text{when } \frac{D_l}{S} \leq t \leq t_{engine-off} \\ C_{in,p,l,t} = C_{in,p,l,t=t_{engine-off}} e^{-(\lambda_l + D_{p,l} + \frac{\eta Q_{f,l}}{V_l})(t - t_{engine-off})}, & \text{when } t \geq t_{engine-off} \end{array} \right.$$

Where,

$$BC_{in,p,l} = \text{baseline in-cabin concentrations for pollutant } p \text{ at location } l \text{ (e.g., } \mu\text{g/m}^3\text{)}$$

$C_{in,p,l,t}$	=	in-cabin concentrations for pollutant p at location l and time t (e.g., $\mu\text{g}/\text{m}^3$)
$C_{in,p,l,t=t_{\text{engine-off}}}$	=	in-cabin concentrations for pollutant p at location l and time $t = t_{\text{engine-off}}$ (e.g., $\mu\text{g}/\text{m}^3$)
$C_{out,p,t}$	=	out-cabin concentrations for pollutant p at time t (e.g., $\mu\text{g}/\text{m}^3$)
D_l	=	length from the locomotive exhaust outlet to the in-cabin location l (mile)
$k_{p,l}$	=	deposition rate for pollutant p at location l (min^{-1})
$P_{p,l}$	=	penetration factor for pollutant p at location l (dimensionless)
$Q_{f,l}$	=	airflow rate through the air filter at location l (m^3/min)
Q_l	=	volumetric air flow rate at location l (m^3/min)
S	=	wind speed (mph)
$t_{\text{engine-off}}$	=	time when the locomotive engine shuts off (min)
V_l	=	in-cabin volume for location l
λ_l	=	air exchange rate at location l (min^{-1})
η	=	air filter removal efficiency for the fresh air intake system (fraction)
l	=	in-cabin locations, including baggage compartment, lounge compartment, and passenger car
p	=	pollutants, such as CO_2 , HCHO, $\text{PM}_{2.5}$, and PM_{10}
t	=	min-by-min measurement duration (min)

6.3.2 Example Model Application

An example of the application of the in-cabin AQ model is given in this section. The application scenario is specific to a railyard test in which the train is stationary, so it is not representative of train operation during passenger service. The AQ model was used to estimate in-cabin $\text{PM}_{2.5}$ concentrations inside a passenger car. The model results are grouped into the three phases, as described previously in Section 6.3.1.

Assumptions on model input parameters and values for the example application are summarized in Table 6-2, including wind speed, baseline in-cabin $\text{PM}_{2.5}$ concentrations, out-cabin $\text{PM}_{2.5}$ concentrations, air exchange rate, deposition rate, penetration factor, and distance from the locomotive exhaust outlet to the in-cabin location. Wind speed here is the annual average wind speed reported from the Raleigh-Durham International Airport in 2022. Out-cabin concentrations are the ambient $\text{PM}_{2.5}$ concentrations reported from the Millbrook, NC site AQ monitor, which is the closest site AQ monitor to the railyard. In this example, a value of $7.5 \mu\text{g}/\text{m}^3$ is selected to represent typical ambient $\text{PM}_{2.5}$ concentrations in Raleigh. In future work, the out-cabin concentration would be measured to account for the combination of ambient background concentration and any contribution from the locomotive plume. The AQ model assumes the ability to measure out-cabin concentrations. The out-cabin concentration is intended to represent the combined contribution from the locomotive exhaust plume as well as other sources of ambient $\text{PM}_{2.5}$. Other values for input parameters are either based on reported data in peer-reviewed literature (e.g., baseline in-cabin concentration, air exchange rate, deposition rate, penetration factor) or empirical measurement (e.g., distance from the locomotive exhaust outlet to the passenger car).

Table 6-2. Assumptions on in-cabin air quality model input parameters and values for the example application of a railyard test ^a.

Input Parameters	Values	References
Wind speed ^b	6.0 mph	North Carolina Climate Office, 2023
Baseline in-cabin PM _{2.5} concentrations	2.0 µg/m ³	Otuyo et al., 2022
Out-cabin PM _{2.5} concentrations	7.5 µg/m ³	North Carolina Department of Environmental Quality, 2023
Air exchange rate	0.083 min ⁻¹ (equivalent to 5.0 hr ⁻¹)	Liu and Frey, 2011
PM _{2.5} deposition rate	0.067 min ⁻¹ (equivalent to 4.0 hr ⁻¹)	He et al., 2005
PM _{2.5} penetration factor	0.40	Li et al., 2018
Distance from the locomotive exhaust outlet to the passenger car ^c	220 feet (equivalent to 0.042 mile)	Empirical measurement ^d

- Notes: ^a Train is assumed to be stationary during the railyard test for the example application.
^b The wind speed here is the annual average wind speed reported from the Raleigh-Durham International Airport in 2022.
^c The passenger car here refers to the first passenger car located at the downwind side of the powered locomotive.
^d The distance from the locomotive exhaust outlet to the passenger car was measured using a tape measure.

Figure 6-1 shows variation in model-estimated in-cabin PM_{2.5} concentrations inside a passenger car with time from the locomotive PME start to off. The passenger car here refers to the first passenger car located at the downwind side of the powered locomotive. In this example, the time duration for the exhaust plume reaching the passenger car is 25 seconds (Phase I). During Phase I, the model-estimated in-cabin PM_{2.5} concentrations are constant at the baseline in-cabin concentration (2.0 µg/m³). Starting from the 26th second, the out-cabin concentration starts to penetrate into the passenger car (Phase II). The estimated in-cabin PM_{2.5} concentrations increase from the baseline concentration (2.0 µg/m³) to the steady-state concentration (2.8 µg/m³) in 26 minutes. Then, the estimated in-cabin concentrations are constant at the steady-state concentration for 109 minutes until the PME shuts off. The accumulated time duration for Phase II is 135 minutes (26 min + 109 min). The PME shuts off at the 136th minute from the PME starts. The estimated in-cabin concentrations decrease from the steady-state concentration (2.8 µg/m³) back to the baseline concentration (2.0 µg/m³) in 3 minutes (Phase III).

The in-cabin AQ model can be applied to train operation during passenger service in which the train is moving. If the train were moving, the wind speed could be up to 79 mph head wind relative to the train, assuming no or negligible ambient wind.

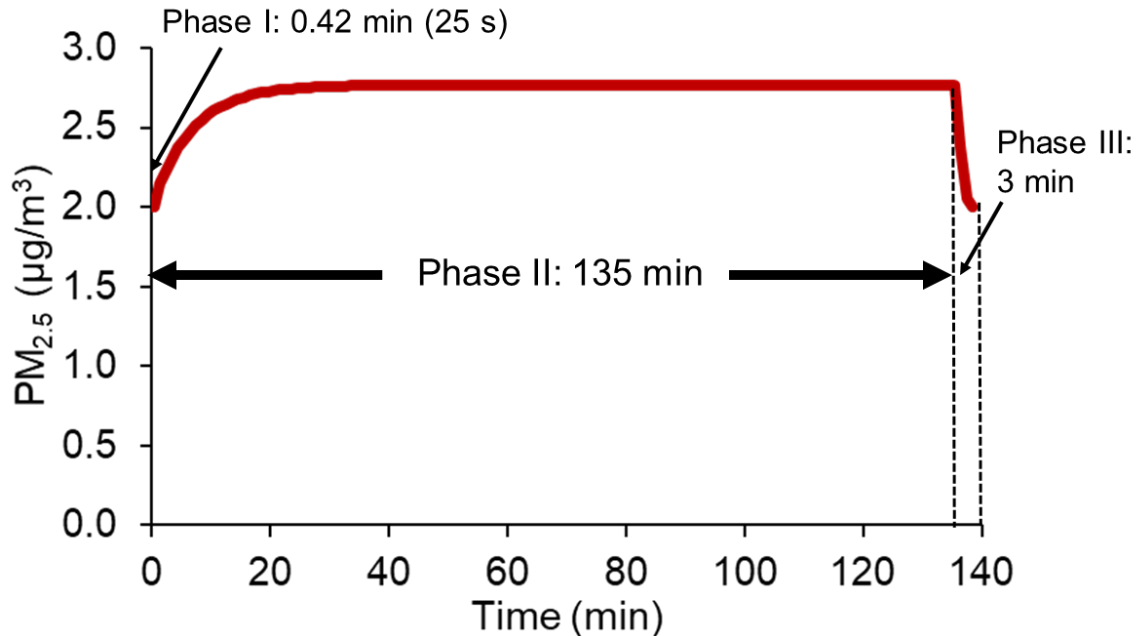


Figure 6-1. An example of model-estimated in-cabin PM_{2.5} concentrations inside a passenger car varied with time from the locomotive prime mover engine start to off for a railyard test. Phase I: from the engine start to exhaust plume reaching the passenger car; Phase II: out-cabin PM_{2.5} concentrations penetrate into the passenger car; Phase III: after the engine shuts off.

6.4 Recommendation for Future Work

The final combined in-cabin AQ model can be calibrated and validated based on the railyard AQ measurement. Three replicates of the test schedule are recommended to conduct for the railyard AQ measurement. Two replicates can be used to calibrate the in-cabin AQ model. The remaining one replicate can be used to validate the model.

6.5 References Cited in Chapter 6

- He, C., Morawska, L., Gilbert, D., 2005. Particle deposition rates in residential houses. *Atmospheric Environment* 39, 3891–3899. <https://doi.org/10.1016/j.atmosenv.2005.03.016>
- Li, Z., Che, W., Frey, H.C., Lau, A.K.H., 2018. Factors affecting variability in PM_{2.5} exposure concentrations in a metro system. *Environmental Research* 160, 20–26. <https://doi.org/10.1016/j.envres.2017.09.006>
- Liu, X., Frey, H.C., 2011. Modeling of in-vehicle human exposure to ambient fine particulate matter. *Atmospheric Environment* 45, 4745–4752. <https://doi.org/10.1016/j.atmosenv.2011.04.019>
- North Carolina Climate Office, 2023. Wind Rose [WWW Document]. North Carolina Climate Office. URL <https://legacy.climate.ncsu.edu/windrose?state=NC&station=KRDU> (accessed 1.17.23).
- North Carolina Department of Environmental Quality, 2023. Available Ambient Data by Site [WWW Document]. Available Ambient Data by Site. URL

<https://xapps.ncdenr.org/aq/ambient/AmbtSiteEnvista.jsp?site=371830014> (accessed 1.22.23).

Otuyo, M.K., Mohd Nadzir, M.S., Latif, M.T., Saw, L.H., 2022. In-train particulate matter (PM10 and PM2.5) concentrations: Level, source, composition, mitigation measures and health risk effect – A systematic literature review. *Indoor and Built Environment* 1420326X221131947. <https://doi.org/10.1177/1420326X221131947>

CHAPTER 7: Conclusions

This chapter includes a summary of key findings and conclusions for this project and recommendations for future work.

7.1 Key Findings

There is large spatial variability in segment-average fuel use and emission rates (FUERs). For example, FUERs among a pair of adjacent track segments differed on average by a factor of 2 to 60, depending on location and species. On average for a given one-way trip, the maximum rates were 24, 21, and 53 times higher than the mean for fuel use, NO_x emissions, and PM emissions, respectively.

Station segments, consistently had higher average FUERs than other segments. The next highest average FUERs were typically measured at segments within 1.25 miles downstream of a station, designated as near-station acceleration segments where trains accelerated. Station and near-station acceleration segment-runs contributed more to trip total emissions compared to their share of segment-runs.

The hotspots comprised only 20% of the route length but comprised between 40% to 50% of the total fuel use and emissions along the entire route. The majority of the fuel use, NO_x emissions, and PM emissions hotspots were co-located and were located at stations or within 1.25 miles of stations. Hotspots and near-hotspots identified based on one consist were co-located with 80% to 90% of the hotspots for other consists. Therefore, the location of the hotspots in a given travel direction was typically similar among consists. The minimum number of one-way trips needed to accurately locate absolute hotspots was 13 and 14 for eastbound and westbound, respectively.

Segment-run average FUERs were negatively correlated with speed, positively correlated with positive acceleration and grade, and uncorrelated with curvature. FUERs and population density near stations were consistently higher than at other locations. Intuitively, hotspots are likely to be located on segments with positive grades or positive acceleration. However, the location of hotspots is affected by a combination of key variables such as speed, acceleration, and grade. Segments with positive grades or acceleration may not necessarily be hotspots. For example, some near station acceleration segment-runs were non-hotspots because of low acceleration on high grades. Therefore, on segments with high grades, acceleration might be restricted but would require a tradeoff of faster travel time on other segments to maintain the train schedule.

In the order of decreasing importance, acceleration, grade, and speed were the key variables in distinguishing hotspots from non-hotspots. Curvature, locomotive, and consist had negligible importance compared to other variables.

This project has shown that LPD models can be feasibly calibrated based on PEMS and GPS data from 3-15 one-way trips. These models can be calibrated to OTR measurements for other passenger rail systems because they are based on the physics of resistive forces opposing train motion.

Acceleration, grade, and drag resistances were the highest relative contributors to power demand, regardless of train consist. While, theoretically it was qualitatively known what resistances affected power demand, prior work did not quantify which resistances were the highest relative contributors for an actual passenger rail service. This quantification is useful to identify

controllable operation practices to reduce power demand and ultimately reduce trip fuel use and emissions (TFUEs).

Trajectories were identified that had similar trip duration but lower TFUEs. These trajectories had lower average acceleration and deceleration per trip resulting in lower average positive power demand and TFUEs. However, a trajectory with the lowest TFUEs for one species may not necessarily have the lowest TFUEs for other species. Nonetheless, a trajectory with the lowest fuel use will also have relatively lower emissions than other trajectories. Thus, depending on the species of concern, a choice among trajectories could be made. These trajectories had lower number of absolute hotspots and lower FUERs in hotspots than other trajectories. Thus, through trajectory modification, fuel use and emissions can be reduced on a trip and local level.

Inter-locomotive, inter-consist, and inter-fuel variability in FUERs presents an opportunity to reduce FUERs for train operators by prioritizing the dispatch of more energy-efficient and low emitting LCFs. However, a particular LCF may not have the lowest rates for all species. Inter-LCF variability in FUERs and inter-trajectory variability in TTFUEs was accurately estimated using the LPD model demonstrated here. Reduction in fuel use will reduce operating costs. Reduction in emission rates will decrease the number and intensity of hotspots resulting in reduced exposure to train-generated pollution near railroad tracks.

Adding passenger cars and passengers to a train reduces energy use and emissions intensity, defined as grams of fuel or pollutant/passenger-mile. However, the maximum number of passenger cars that can be added is determined by the capacity of the locomotive to propel the train for a desired speed trajectory.

In general, the concentrations measured with two PEMS were similar to each other. There is no bias in measurements of CO₂, CO, HC, and NO concentrations with long exhaust sample lines.

7.2 Conclusions

There is large variability in FUERs over short distances. Thus, finely resolved FUERs are needed to accurately quantify localized fuel use and emissions. Such an analysis is needed to accurately quantify localized air quality and exposure and identify disparities in air pollution impacts leading to environmental injustice.

People living near stations are potentially exposed to higher pollutant emissions versus other locations. Identification of hotspot locations near populated regions helps target emission reduction measures to improve near-railroad air quality and to reduce human exposure to train-generated air pollution.

Several train trajectory optimization studies report that an ideal strategy to reduce fuel use between adjacent stations is to accelerate rapidly to the maximum allowable or attainable speed, maintain a constant speed, coast without traction forces, and decelerate when approaching stations. However, segment-runs with acceleration are likely to be emission hotspots. Trajectory optimization algorithms do not currently account for such localized emission hotspots and could worsen hotspots. Thus, finely-resolved FUERs must also be considered while evaluating trajectories with lower TFUEs.

Quantification of hotspot locations enables operators to prioritize emission reduction interventions. Making changes to train operation could potentially mitigate some of the hotspots. For example, some near station acceleration segment-runs that were non-hotspots had low

acceleration on high grades. Therefore, on segments with high grades, acceleration might be restricted but would require a tradeoff of faster travel time on other segments to maintain the train schedule. This information is useful to help operators achieve fuel use and emissions reductions without costly infrastructure modifications such as track realignment.

Track curvature had an insignificant contribution to power demand for the Amtrak-operated Piedmont passenger rail. The same is expected for passenger routes with similar variations in track grade and curvature. However, curvature resistance could be significant for freight and high-speed trains. The model was not formulated to deal with freight and high-speed trains.

This work demonstrates that PEMS based measurements are useful for quantifying spatial variability in FUERs and associated factors for a given route and operation. Train activity and infrastructure variables can be inferred from low-cost GPS devices.

To better capture the variation of FUERs with n -second backward moving average power demand ($\overline{LPD}_{n,t}$), trends inferred from finely resolved real-world measurements were used for model formulation. FUERs were found to be more strongly correlated with a 12-second backward moving average ($\overline{LPD}_{12,t}$) than any other period. Four different trends of FUERs versus $\overline{LPD}_{12,t}$ were inferred for different $\overline{LPD}_{12,t}$ ranges. The calibrated sub-models were continuous at boundaries, captured the variations in FUERs, and were consistent with the underlying assumptions. The sub-models typically described the observed trends in FUERs. Several models based on 1 Hz LPD are in use at present. These models are used to estimate trip fuel use and emissions or optimize trajectory to lower trip fuel use and emissions for inter-city trains, commuter trains, metro trains, and freight trains. Therefore, the model demonstrated here could be applied to these trains as well. However, FUERs are needed to calibrate the model.

Trajectory optimization algorithms do not account for localized FUERs, which can be concentrated in populated areas. The model demonstrated here was precise and accurate at several resolutions, including one Hz, 0.25-mile, and trip total. FUERs at different resolutions facilitate different applications. FUERs at one Hz resolution were used to evaluate the effect on FUERs for a hypothetical case of replacing a small track segment comprising of an ascent followed by a descent with a flat track. This hypothetical replacement led to an estimated reduction in fuel use and emissions. This quantification of emission reductions is useful to seek Federal funding for infrastructure modification projects. The knowledge of the location of hotspots is useful to prioritize emission reduction interventions. The model was accurate and precise for distinguishing hotspots from non-hotspots.

7.3 Recommendations

Future work is needed to assess the control efficiency of blended-exhaust after treatment system (BATS) under dynamic real-world operating conditions, during which there are periodic transitions from one throttle notch position to another, leading to transients in engine load and engine-out emissions. Assessment of the ability of the emission control system to respond to such transients could be evaluated as part of real-world measurements. Real-world measurements will provide the ability to assess emission control performance under realistic operating conditions typical of actual operations. The effects of combinations of interventions such as technology - operation, technology - fuel, and technology - operation - fuel should also be verified based on real-world measurements. In addition, future work is needed to assess the in-

cabin air quality for Piedmont trains, and calibrate and validate the in-cabin air quality model developed in this project.

Appendices

Appendix A. Supporting Information for Chapter 2

A.1 Locomotive and Consist Description

In this section, locomotives and consists measured for Over-the-rail (OTR) measurements are described.

A.1.1 Locomotive specifications

The North Carolina Department of Transportation (NCDOT) has a fleet of two F59PHIs and six F59PHs series locomotives configured for passenger service. Each of the locomotives has a prime mover engine (PME) and a head end power (HEP) engine. The PME drives an electrical generator or alternator. The generator provides electricity to the traction motors, which in turn drive the locomotive wheels. Therefore, diesel locomotives are also referred to as “diesel-electric” locomotives. The PME has a throttle control with eight positions, a high idle, and a low idle position. Each of the throttle positions is called a notch (Hay, 1982). The locomotive is slowed using the mechanical brake or dynamic brake. In a dynamic brake, the traction motors act as generators, and electricity is dissipated as heat through an electric resistance grid.

The HEP engine is used to generate alternating current electricity for hotel services in passenger cars, such as lighting and space conditioning (Hay, 1982; Profillidis, 2014). The load on the HEP engine is dependent on the number of passenger cars connected (Graver and Frey, 2016). The baggage/café car has a separate space for baggage and café. The café includes vending machines, refrigerated water, hot coffee, and seating space. Thus, although the baggage/café car has less passenger space than a passenger car, and therefore proportionally less space conditioning load, it has more electrical load for other accessories. Therefore, as an approximation, the baggage/café car is assumed to have the same electrical load as a passenger car. In addition to the passenger car load, some of the power produced by the HEP is consumed to charge locomotive batteries. However, the electrical load to charge batteries is typically less than one percent of the full HEP engine load capacity. Based on prior rail yard measurements of the electrical load for 0 to 4 connected passenger cars, the electrical load per passenger car varied between 13 and 24 kW. The average electrical load per passenger car was 20 kW (Graver and Frey, 2016).

The names, year of manufacture, and year of the last rebuild of the NCDOT locomotives are given in Table A-1. The specifications of the PMEs of the locomotives in the NCDOT fleet are given in Table A-2. Each of the locomotives was built by General Motors Electro-Motive Division (GM-EMD). Two of the F59PHs, NC 1871 and NC 1984, are among the locomotives most recently acquired and rebuilt by NCDOT. The F59PHIs and the two most recently acquired F59PHs have an electronic fuel injection system. The older F59PHs have a mechanically governed fuel injection system.

The specifications of the HEP engines of the locomotives in the NCDOT fleet are given in Table A-3. Six of the locomotives, except for the two recently acquired locomotives, have a Caterpillar Advanced Combustion Emissions Reduction Technology (CAT ACERT) C18 HEP engine. However, there are two variations of the CAT ACERT C18 engine that differ in engine shaft power. Locomotives NC 1755, NC 1797, and NC 1893 have CAT ACERT C18 831 hp HEP engines, and locomotives NC 1810, NC 1859, and NC 1869 have CAT ACERT C18 766 HEP engine. The two recently acquired locomotives have CAT ACERT C-15 626 hp HEP engines.

Table A-1. Description of the NCDOT Locomotive Fleet

Locomotive	Name	Year of Manufacture	Last Rebuild	Rebuilder
NC 1755	City of Salisbury	1999	2011	Unknown to the Author
NC 1797	City of Asheville			
NC 1810	City of Greensboro	1988	2010	American Motive Power
NC 1859	City of High Point			
NC 1869	City of Durham		2011	Amtrak
NC 1893	City of Burlington	1990		
NC 1871	Town of Cary	1988	2016	Norfolk Southern Thoroughbred Mechanical Services
NC 1984	City of Kannapolis			

All of these locomotives were manufactured by General Motors Electro-Motive Division.

Table A-2. Prime Mover Engine Specifications

Locomotive Model	F59PHI		F59PH	
	Electronically governed	Mechanically governed	Electronically governed	Electronically governed
Locomotives	NC 1755, NC 1797	NC 1810, NC 1859, NC 1869, NC 1893	NC 1871, NC 1984	
Prime Mover Diesel Engine	EMD	EMD	EMD	
Engine Model	12N-710G3B-EC	12N-710G3	12N-710G3	
Aspiration	Turbocharged	Turbocharged	Turbocharged	
Total Displacement	139.6 L (8,520 in ³)	139.6 L (8,520 in ³)	139.6 L (8,520 in ³)	
Number of Cylinders	12	12	12	
Cylinder Arrangement	45° “V”	45° “V”	45° “V”	
Compression Ratio	16:1	16:1	16:1	
Displacement per Cylinder	11,635 cm ³ (710 in ³)	11,635 cm ³ (710 in ³)	11,635 cm ³ (710 in ³)	
Cylinder Bore	230.19 mm (9.06 in)	230.19 mm (9.06 in)	230.19 mm (9.06 in)	
Cylinder Stroke	279.4 mm (11.0 in)	279.4 mm (11.0 in)	279.4 mm (11.0 in)	
Operating Principle	2 Stroke Cycle	2 Stroke Cycle	2 Stroke Cycle	
Rotation (Facing Flywheel End)	Counterclockwise	Counterclockwise	Counterclockwise	
Full Speed	904 RPM	904 RPM	904 RPM	
High Idle Speed	343 RPM	371 RPM	268 RPM	
Low Idle Speed	200 RPM	238 RPM	219 RPM	
Rated speed of traction motors	110 mph	83 mph	83 mph	
Weight	13,700 kg (30,200 lbs)	13,700 kg (30,200 lbs)	13,700 kg (30,200 lbs)	
Rated power	3,000 hp (2,240 kW)	3,000 hp (2,240 kW)	3,000 hp (2,240 kW)	
Emission Standard	U.S. EPA Tier 0+	U.S. EPA Tier 0+	U.S. EPA Tier 0+	

Table A-3. Head End Power Engine Specifications

HEP Engine Model	CAT ACERT C-18		CAT ACERT C-15
Rated power	831 hp (620 kW)	766 hp (571 kW)	626 hp (467 kW)
Locomotives	NC 1755, NC 1797, and NC 1893	NC 1810, NC 1859, and NC 1869	NC 1871, NC 1984
Rated Speed	1800-1900 RPM	1800-1900 RPM	1800-2100 RPM
Emission Standards	U.S. EPA Tier 2 Final Nonroad	U.S. EPA Tier 2 Final Nonroad	U.S. EPA Tier 3 Final Nonroad
Engine Configuration	In-Line 6, 4-Stroke-Cycle Diesel	In-Line 6, 4-Stroke-Cycle Diesel	In-Line 6, 4-Stroke-Cycle Diesel
Stroke	183 mm (7.2 in)	183 mm (7.2 in)	171 mm (6.73 in)
Bore	145 mm (5.71 in)	145 mm (5.71 in)	137 mm (5.4 in)
Displacement	18.1 L (1104.5 in ³)	18.1 L (1104.5 in ³)	15.2 L (927.6 in ³)
Aspiration	Turbocharged-After cooled	Turbocharged-After cooled	Turbocharged-After cooled
Compression Ratio	16.0:1	16.0:1	17.0:1
Combustion System	Direct Injection	Direct Injection	Direct Injection
Length	1438 mm (56.6 in)	1438 mm (56.6 in)	1438 mm (56.6 in)
Width	1132 mm (44.6 in)	1132 mm (44.6 in)	1132 mm (44.6 in)
Height	1356 mm (53.4 in)	1356 mm (53.4 in)	1356 mm (53.4 in)
Weight - Net Dry (Basic Operating Engine Without Optional Attachments)	1717 kg (3785 lb)	1717 kg (3785 lb)	1666 kg (3673 lb)

The PMEs and HEP engines of locomotives in the U.S. are typically operated on ultra-low sulfur diesel (ULSD) (Amtrak, 2018; Elgowainy et al., 2018; Graver and Frey, 2015). Therefore, this work is focused on ULSD. Over-the-rail (OTR) and rail yard (RY) measurements were conducted for PMEs. OTR measurements were conducted during the actual revenue-generating Piedmont passenger rail service. Fuel use and emission rates (FUERs) for HEP engines were measured at steady state for several loads in the RY. HEP engines operate at approximately constant loads during OTR operation. Therefore, FUERs for HEP engines were not measured for OTR operation.

PEMA-based FUER were estimated for the HEP engines of NCDOT owned locomotives NC 1755, NC 1797, NC 1810, NC 1859, NC 1869, and NC 1893 operated on ULSD and B20 based on RY measurements (Frey and Hu, 2015). An external load box was used to simulate a wide range of loads on the HEP engine. Simulated loads include 50kW, 125 kW, 250 kW, 375 kW, and 500 kW. Measured emission rates were compared with the EPA emission standards for non-road engines. Mass per time-based FUER increased with increasing load for each engine and fuel. Cycle average PM emission rates for B20 were 23 percent lower than for ULSD. Cycle

average CO emission rates and HC emission rates for B20 were 3 percent and 6 percent lower than for ULSD. However, these differences were not statistically significant. Cycle average NO_x emissions rates for B20 were 3 percent higher than for ULSD, but the difference was not statistically significant. Cycle average CO and HC emission rates were 90 percent and 30 percent lower than the level of EPA nonroad Tier 2 standards for all locomotives for both fuels, respectively. Cycle average NO_x emission rates were higher than the level of Tier 2 standards for NC 1797 and NC 1810 on ULSD, and for NC 1869 on B20. Cycle average PM emission rates were comparable to the level of the Tier 2 standards for only the HEP engine of NC 1859 operated on B20. For all other locomotive-fuel combinations, cycle average PM emission rates were higher than the level of Tier 2 standard.

A.1.2 Consist specifications

Trains were operated in four consists during OTR measurements:

- (1) single locomotive consist (SLC);
- (2) double-powered tandem consist (DP-TC);
- (3) double-powered push/pull consist (DP-P/PC); and
- (4) single-powered push/pull consist (SP-P/PC).

An SLC comprises one locomotive, placed at the head of the train that propels the entire train. A DP-TC comprises two adjacent locomotives at the head of the train. A push/pull consist comprises one locomotive at each end of the train. Tandem and push/pull consists are double-powered if both PMEs provide equal power to propel the train. In an SP-P/PC, only one locomotive provides tractive effort. For tandem and push/pull consists, only one HEP engine was powered, while the other was shut-off. Additionally, each train comprised one baggage/café car and 2 to 4 passenger cars. The push/pull consist is preferred by the operator because it allows the train to run in either direction without having to turn around a locomotive between directions. In prior work, four locomotives were measured for SLCs (Frey et al., 2012; Graver and Frey, 2016, 2015). In recent work, measurements were made for DP-TC, DP-P/PC, and SP-P/PC. Measured PMEs and consists are given in Table A-4. Each of the locomotives is 58'2" in length measured from coupler to coupler. Each passenger car and baggage/café car are 85'8" in length measured from coupler to coupler. Between adjacent locomotive or passenger car pairs, the couplers overlap but the length of overlap is negligible compared to the length of the locomotive or the passenger car. Thus, the train length was estimated as the sum of lengths measured from coupler to coupler of each locomotive(s), baggage/café car(s), and passenger car(s). The typical train length on the Piedmont route varied between 315' (0.06 mile) and 631' (0.12 mile).

A.2 Piedmont Rail Route

The selected route is the Amtrak-operated Piedmont passenger rail service, which uses equipment owned by the North Carolina Department of Transportation (NCDOT). The one-way route length is 173 miles (278 km), the scheduled trip duration is 3h 10m and the highest operating speed is restricted to 79 mph. The Piedmont route has nine stations. Trains running from Raleigh to Charlotte are westbound and trains from Charlotte to Raleigh are eastbound. The route map is presented in Figure A-1.

Table A-4. Locomotives and Consists Measured For Over-The-Rail Operation

Locomotive ^a	Consist ^b	Number of Passenger Cars ^c	One-way Trips	Source ^d
NC 1797	SLC	3	5	Prior Work
NC 1810	SLC	3	6	Prior Work
NC 1859	SLC	3	6	Current Work
NC 1859	DP-T	6	5	Current Work
NC 1871	DP-P/PC	4	8	Current Work
NC 1871	SP-P/PC	4	4	Current Work
NC 1893	SLC	3	6	Prior Work
NC 1984	DP-P/PC	3	5	Current Work
NC 1984	SP-P/PC	5	2	Current Work
NC 1984	DP-P/PC	5	2	Current Work
NC 1984	SP-P/PC	4	1	Current Work
NC 1984	DP-P/PC	4	1	Current Work

Total: 51

^a Only the measured locomotive is indicated for the train consists with two locomotives.

^b Consist: (1) SLC: Single Locomotive Consist; (2) DP-TC: Double-powered Tandem Consist; (3) DP-P/PC: Double-powered Push/Pull Consist; and (4) SP-P/PC: Single-powered Push/Pull Consist

^c Number of passenger cars includes baggage/café car as they have equal weight and dimensions.

^d Prior work: (Graver and Frey, 2015).

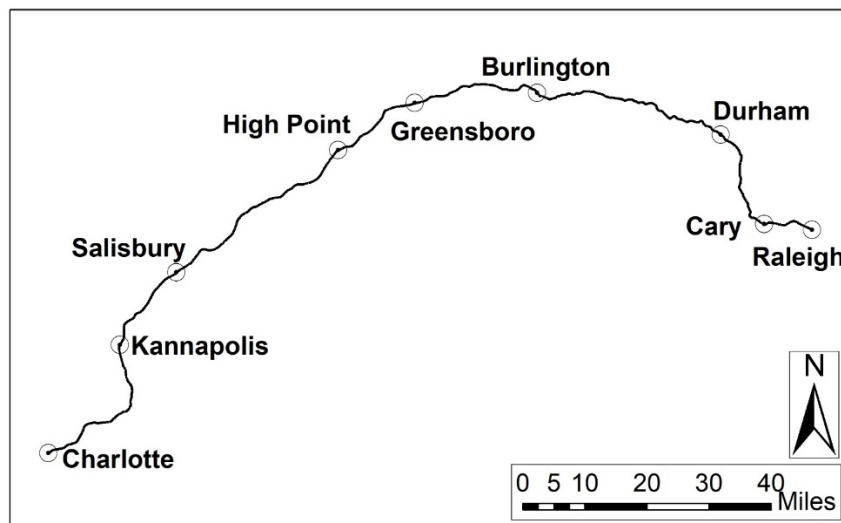


Figure A-1. Amtrak-Operated Piedmont Rail Route between Raleigh, NC and Charlotte, NC.

The schedule of the Piedmont passenger rail service is given in Table A-5. Raleigh and Charlotte are the terminal stations. The Piedmont passenger rail service begins from the terminal station of Raleigh where it dwells for about 15 minutes before leaving westbound towards Charlotte. Upon reaching Charlotte, the train dwells at Charlotte for approximately 15 minutes to 2 hours depending on the difference in the time of arrival at Charlotte and the departure for the eastbound trip. At each intermediate station, the train dwells for about 1 minute to 2 minutes each. The terminal station for the eastbound trip is Raleigh, where the train dwells for about 2 minutes to 5 minutes. The locomotives idle during dwelling and emissions accumulate.

Table A-5. North Carolina Amtrak Piedmont Passenger Rail Service Daily Timetable For: (a) Westbound Trains from Raleigh to Charlotte; and (b) Eastbound Trains from Charlotte to Raleigh.

(a) Westbound Trains			
Station	Train 73	Train 75	Train 77
Raleigh (RGH)	06:30	10:00	15:00
Cary (CYN)	06:42	10:12	15:12
Durham (DNC)	07:02	10:32	15:32
Burlington (BNC)	07:38	11:08	16:08
Greensboro (GRO)	08:03	11:33	16:33
High Point (HPT)	08:19	11:49	16:49
Salisbury (SAL)	08:53	12:23	17:23
Kannapolis (KAN)	09:09	12:39	18:10
Charlotte (CLT)	(arrival) 09:40	(arrival) 13:10	(arrival) 18:41
(b) Eastbound Trains			
Station	Train 74	Train 76	Train 78
Charlotte (CLT)	10:30	15:15	19:00
Kannapolis (KAN)	10:55	15:40	19:25
Salisbury (SAL)	11:11	15:56	19:41
High Point (HPT)	11:44	16:29	20:14
Greensboro (GRO)	12:03	16:48	20:33
Burlington (BNC)	12:24	17:09	20:54
Durham (DNC)	13:03	17:48	21:33
Cary (CYN)	13:23	18:08	21:53
Raleigh (RGH)	(arrival) 13:41	(arrival) 18:26	(arrival) 22:10

Timetable reflects the timetable during the study period. The current timetable may be different. Times are departure times unless indicated.

A.3 Instrumentation

Locomotive exhaust gas and particulate matter concentrations measurements are typically based on engine dynamometer measurements, trackside measurement systems, and PEMS. This section describes the characteristics of these instruments, the selection of instruments for OTR measurements, and the procedure for deployment of these instruments.

A.3.1 Engine dynamometer measurements

Engine dynamometer facilities use the Federal Reference Method (FRM) or Federal Equivalent Method (FEM) test procedures to measure emissions as the basis for regulatory certification of the engine. Engine dynamometer facilities provide 40 CFR 1065 and 1033-complaint measurements under standard test conditions (40 CFR 1033, 1998; 40 CFR 1065, 2005). However, there are only a few engine dynamometer facilities in the U.S. where the engine could be shipped to for measurements. Examples of such facilities are the Southwest Research Institute's Locomotive Technology Center (SwRI, 2016) and the Locomotive Emissions Testing Facility of Norfolk Southern and the Center for Alternative Fuels Engines and Emissions of West Virginia University (Norfolk Southern and Center for Alternative Fuels Engines and Emissions, n.d.). The shipping of the engine to the measurement facility and measurement itself is costly and leads to loss of revenue during the period that the locomotive is out of service.

The certification locomotive exhaust emission test procedure is based on discrete load steady-state engine operation (40 CFR 1033, 1998; 40 CFR 1065, 2005). However, real-world engine operation involves steady-state operation and transition among steady-state load levels. Steady-state load-based measurements are not an accurate representation of real-world operation (Graver and Frey, 2013, 2015).

A.3.2 Trackside emission measurement systems for certification

Alternatives to shipping the locomotive to the test facility include measurement based on trackside emission systems and PEMS. An example of a trackside measurement system is the Ride-Along Vehicle Emission Measurement System (RAVEM) developed by Engine Fuels and Emissions Engineering (Weaver and Balam-Almanza, 2001; Weaver and Petty, 2004). The RAVEM measures CO₂ and CO concentrations using nondispersive infrared (NDIR), total hydrocarbon (THC) concentration using flame-ionization detection FID, NO_x concentration using chemiluminescent analyzer (Weaver and Balam-Almanza, 2001) and gravimetric filter-based particulate matter mass. Thus, RAVEM is based on the same detection methods as specified in 40 CFR 1065.

A.3.3 Portable Emissions Measurement System

PEMS are compact and lightweight compared to the engine dynamometer facilities and RAVEM. The PEMS may provide 1065-compliant measurements for some or all pollutants. Therefore, the PEMS were evaluated for accuracy and precision versus 1065-compliant measurement systems. PEMS were used for static load trackside measurements and OTR measurements. Two commercially available PEMS were used for RY measurements, including a SEMTECH-DS manufactured by Sensors Inc. and an Axion manufactured by Global MRV. Specifications of both of these PEMS are given in Table A-6. The Axion was used for OTR measurements. The Axion was compared and evaluated for accuracy and precision with the SEMTECH-DS PEMS and RAVEM.

A.3.3.1 SEMTECH-DS portable emissions measurement system

The SEMTECH-DS measures CO₂ and CO concentrations using NDIR, THC concentration using heated FID, and NO_x concentration using nondispersive ultraviolet (NDUV) (Sensors Inc., 2011). These detection methods are specified in 40 CFR 1065 for the corresponding exhaust gas measurements. FID is ignited using H/He fuel. The NCDOT and Amtrak do not allow FID fuel onboard. As an alternative, SEMTECH-DS measures HC concentration using NDIR. However, The SEMTECH-DS does not measure PM. Therefore, a SEMTECH-DS was not used for OTR measurements.

A.3.3.2 Axion portable emissions measurement system

The Axion PEMS is composed of two parallel five-gas analyzers, a laser light scattering PM detection system, an engine sensor array, and an onboard computer. The Axion measures CO₂, CO, and HC concentrations using nondispersive infrared (NDIR) analyzer, NO concentration using an electrochemical cell, and PM using laser light scattering (GlobalMRV, 2014). For Axion, only CO₂ and CO concentration measurements are based on detection methods specified in 40 CFR 1065.

NDIR is well known to respond only partially to the total loading of hydrocarbon species in the exhaust, because it responds well to alkanes but is less responsive to other aromatics (Singer et al., 1998; Stephens et al., 1996b, 1996a). Thus, HC may not be representative of Total Hydrocarbons (THC) (Butler et al., 1995; Nakamura et al., 2003; Vojtisek-Lom and Allsop, 2001). Correction factors were estimated for each throttle notch position for each locomotive based on simultaneous exhaust gas measurements with SEMTECH-DS PEMS of the same locomotive in a rail yard.

For OTR measurements, NO concentration was measured with the Axion using electrochemical sensors. The Axion PEMS does not measure NO₂. RY SEMTECH-DS measurements of NO and NO₂ using NDUV were used to estimate the notch-average NO_x/NO concentration ratio for each locomotive. These ratios were used to bias correct Axion measured NO to estimate NO_x. The bias correction factors are explained later in Section 5.3.3.

The laser light scattering-based PM measurement is typically biased low by a factor of 5 as shown by Durbin *et. al.*, 2007 (Miller et al., 2006). Typically, scattering detects particles greater than 100 nm in diameter. The amount of light scattered is different for elemental carbon versus organic carbon particles and varies by particle shape (Miller et al., 2006). The Axion PEMS measured PM concentrations were bias corrected by a factor of 5.

Table A-6. Specifications of the Gas Analyzers for the Global MRV Axion and Sensors Inc. SEMTECH-DS Portable Emissions Measurement Systems

Attribute	Global MRV Axion	Sensors Inc. SEMTECH-DS
CO ₂	Method	Non-Dispersive Infrared
	Resolution	0.01 %
	Range	0.01 % to 16.00 %
	Accuracy	± 0.30 % absolute
	Precision	± 0.30 % absolute
	Response	T ₉₀ & T ₁₀ < 3 s
CO	Method	Non-Dispersive Infrared
	Resolution	0.001 %
	Range	0.001 % to 10.000 %
	Accuracy	± 0.02 % absolute
	Precision	± 0.02 % absolute
	Response	T ₉₀ & T ₁₀ < 3 s
HC	Method	Non-Dispersive Infrared
	Resolution	1 ppmC
	Range	1 ppmC to 2,000 ppmC
	Accuracy	± 4 ppmC
	Precision	± 4 ppmC
	Response	T ₉₀ & T ₁₀ < 3 s
NO	Method	Heated Flame Ionization Detection
	Resolution	0.1 ppmC
	Range	0.1 ppmC to 100 ppmC ^c
	Accuracy	± 5 ppmC or ± 2 %
	Precision	± 2 ppmC or ± 1 %
	Response	T ₉₀ < 2 s
NO ₂	Method	Electrochemical cell
	Resolution	1 ppm
	Range	1 ppm to 4000 ppm
	Accuracy	± 25 ppm
	Precision	± 25 ppm
	Response	T ₉₀ & T ₁₀ < 6 s
PM	Method	Non-Dispersive Ultra Violet
	Resolution	1 ppm
	Range	1 ppm to 500 ppm
	Accuracy	± 10 ppm or ± 3 %
	Precision	± 5 ppm or ± 2 %
	Response	T ₉₀ < 2 s
PM	Method	Laser light scattering
	Resolution	NA ^b
	Range	NA
	Accuracy	NA
	Precision	NA
	Response	NA
Dimensions	21.7"L × 16.9"W × 8.5"H	24.5"L × 20.3" W × 15.9"H
Weight	38 lbs (17.2 kg)	78 lbs (35.4 kg)

^a Instrument not capable of measuring the selected attribute

^b Data not available for the selected attribute

^c Higher concentration measurements are also possible at reduced resolution, accuracy, and precision

Both the PEMS were span calibrated to BAR 97 Low calibration gas mixture for all gaseous pollutants before each set of OTR measurements. For PM, the detector was calibrated by the manufacturer. During measurements, the two Axion gas analyzers (referred to as “benches”), worked simultaneously. Periodically, one bench was taken offline for zeroing to prevent drift. While zeroing, the gas analyzer intakes ambient air instead of engine exhaust and switches back to exhaust when finished. Although zero air stored in bottles or generated using an external zero air generator can be used, ambient air pollutant levels are negligible compared to those found in the undiluted exhaust. Ambient air contains 20.9 vol % O₂ and contains levels of HC, CO, and NO that are below the detection limit of the gas analyzers. CO₂ levels in ambient air are approximately 400 parts per million (400 ppm or 0.04 vol %), which are negligible compared to the typical levels of CO₂ in the engine exhaust (e.g., 0.60 vol % to 7.2 vol %). Therefore, ambient air was used for zeroing the gas analyzers for all measured pollutants.

A sensor array was installed on the engine and connected to the Axion PEMS. The sensor array includes sensors to record engine activity variables including engine revolutions per minute (RPM), the intake air temperature (IAT), and the manifold absolute pressure (MAP). MAP is also referred to as the “airbox pressure.” These data are required to estimate dry molar exhaust flow rate which is an important variable to estimate FUEP. The details are presented in Section 8.

A light sensor measured engine RPM, a thermocouple measured the temperature in the engine intake air manifold, and a pressure sensor measured pressure in the engine intake air manifold. Reflective tape was put on the engine flywheel and a light beam was aimed towards the flywheel. The RPM sensor counted the number of times light was reflected from the flywheel to the sensor to quantify engine RPM. A sensor array box received signals from these sensors and routed them to the PEMS. The PEMS also has a GPS receiver that recorded 1 Hz position. The components of the Axion PEMS are shown in Figure A-2.

For OTR measurements, the PEMS cannot be placed in the engine compartment because of the high temperature and vibrations inside the compartment. The PEMS cannot be placed outside the locomotive because it may affect locomotive clearance and could be damaged because of protruding tree branches. Thus, the PEMS was installed in the locomotive cab. Limited space inside the locomotive cab constrains the choice of PEMS. The Axion is the smaller of the two PEMS and provides measurements of all pollutants at 1 Hz. Additionally, the engine sensor array of the Axion allows measurement of engine activity variables which are required to estimate fuel use and emission rates from exhaust gas and PM concentration measurements. Also, FID fuel required for SEMTECH-DS was not allowed on board by the NCDOT and Amtrak. Thus, the Axion PEMS was used for OTR measurements.



Figure A-2. The Global MRV Axion PEMS And Components: (a) GPS Receiver; (b) Meteorology Sensor; (c) Intake Air Temperature Sensor; (d) Exhaust Sample Lines; (e) Axion PEMS; (f) Engine Sensor Array; (g) Zero Air And Exhaust-Out Lines; (h) Manifold Absolute Pressure Sensor; and (i) Engine Revolutions Per Minute Sensor.

A.3.3.3 Axion portable emissions measurement system evaluation

The accuracy and precision of the PEMS for fuel use rate, CO₂, CO, HC, and NO concentrations were evaluated based on simultaneous exhaust gas measurements with RAVEM and SEMTECH-DS conducted at a RY for several diesel passenger locomotives. Bias correction factors for THC and NO_x were estimated. Vu et al., 2020 evaluated Axion PEMS versus a PEMS used for regulatory purposes.

A.3.3.3.1 Versus SEMTECH-DS portable emissions measurement system

Simultaneous exhaust gas measurements with the Axion and SEMTECH-DS PEMS were conducted for eight NCDOT owned-locomotives between 2010 and 2018 at a RY (Frey and

Rastogi, 2019, 2018; Graver et al., 2016; Graver and Frey, 2015). Each measurement comprised three repetitions of operating the locomotive at 9 or 10 throttle notch positions, for 3 minutes to 5 minutes each. Two locomotives were measured twice. Axion measured notch-average CO₂ and NO concentrations were compared to the SEMTECH-DS measured CO₂ and NO_x concentrations. Diesel engines are low emitters of CO and HC and these concentrations were typically below the detection limit of the Axion. Therefore, CO and HC concentrations were not compared. However, from SEMTECH-DS concentration measurements of HC, THC, NO, and NO₂, bias correction factors were estimated. Notch-average CO₂ and NO_x concentrations measured with Axion and SEMTECH-DS PEMS are compared in Figure A-3.

For diesel exhaust, notch-average CO₂ concentrations typically varied between 0.60 vol% and 6.72 vol%, and between 0.55 vol% and 6.62 vol%, based on measurements with the Axion and SEMTECH-DS PEMS, respectively. The slope of the linear regression of CO₂ concentrations for Axion PEMS versus SEMTECH-DS PEMS was 0.951. On average, the Axion-measured notch-average CO₂ concentrations were 0.09 vol% lower than SEMTECH-DS based notch-average CO₂ concentrations. The 95% confidence interval of difference in the mean concentration measured by the Axion compared to the SEMTECH-DS ranged between -0.13 vol% and -0.05 vol%. For Axion-measured CO₂ concentrations <4 vol%, the average difference from SEMTECH-DS was -0.05 vol%. For Axion-measured CO₂ concentrations ≥4 vol%, the average difference from SEMTECH-DS was -0.15 vol%. Thus, differences in measured CO₂ concentrations between the Axion and the SEMTECH-DS were negligible compared to the magnitude of the measured concentrations. The 95% confidence interval on the slope was within ±2% of the mean slope. Thus, the slope was precisely estimated. The adjusted R² was 0.975, indicating very high precision.

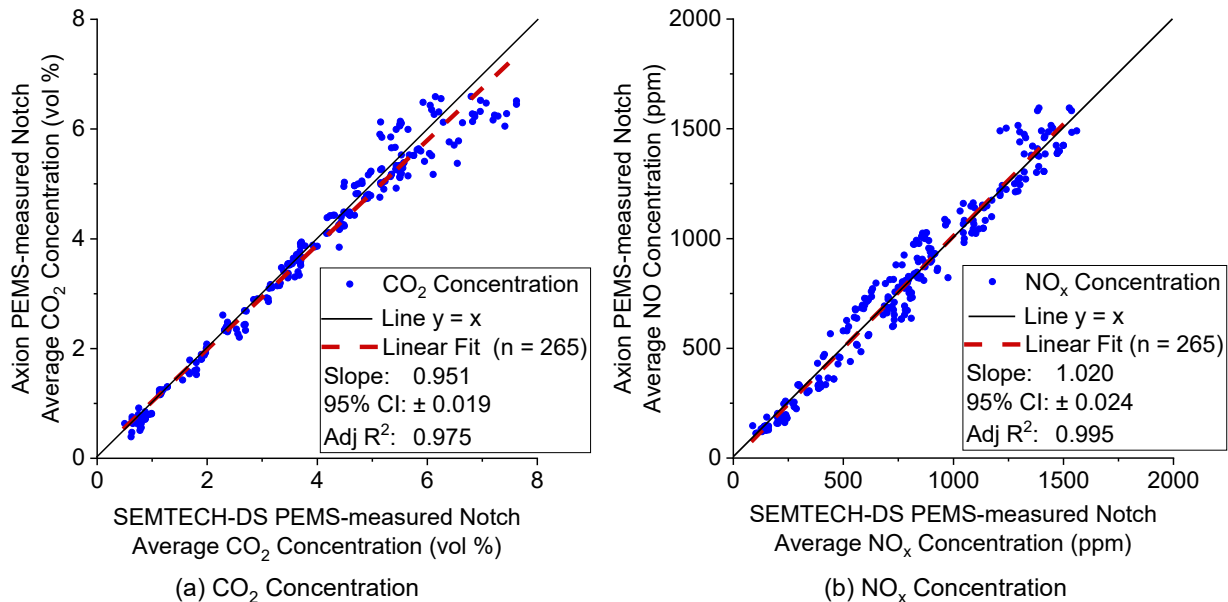


Figure A-3. Comparison of CO₂ and NO_x Concentrations Measured in Diesel Locomotive Exhaust Based on Simultaneous Rail Yard Measurements Conducted Using Axion and SEMTECH-DS Portable Emission Measurement Systems (PEMS): (a) CO₂ Concentration; and (b) NO_x Concentration.

SEMTECH-DS PEMS measures NO_x concentration comprising NO and NO₂. Axion PEMS measures NO concentration only. Thus, only NO concentrations are reported for Axion PEMS.

Notch-average NO concentration varied between 170 ppm and 1545 ppm based on measurements with the Axion PEMS. Notch-average NO_x concentration varied between 181 ppm and 1651 ppm based on measurements with the SEMTECH-DS PEMS. The slope of the linear regression of NO and NO_x concentrations for Axion PEMS versus SEMTECH-DS PEMS was 1.02. On average, the Axion-measured notch-average NO concentrations were 16.7 ppm lower than SEMTECH-DS measured notch-average NO_x concentrations. The 95% confidence interval of difference in the mean concentrations measured by the Axion compared to the SEMTECH-DS ranged between -16 ppm and 2.9 ppm. For Axion-measured NO concentrations <700 ppm, the average difference compared to the SEMTECH-DS was -14 ppm. For Axion-measured NO concentrations ≥700 ppm, the average difference compared to the SEMTECH-DS was -19 ppm. Thus, differences in Axion-measured CO₂ concentrations compared to SEMTECH-DS measured concentrations were negligible compared to the magnitude of the measured concentrations. The 95% confidence interval on the slope was within ±2% of the mean slope. Thus, the slope was precisely estimated. The adjusted R² was 0.995, indicating very high precision. Thus, compared to the SEMTECH-DS, the Axion measurements of exhaust CO₂ and NO_x concentrations are precise and accurate.

For OTR measurements, only the Axion was used. HC and NO concentrations measured by the Axion were bias corrected based on measurements made in the rail yard using the SEMTECH-DS. To correct the Axion HC concentrations to a THC basis, notch-average THC and HC concentrations measured in the rail yard using the SEMTECH-DS were used to estimate notch-specific THC/HC concentration ratios. Likewise, to correct the Axion NO concentrations to a total NO_x basis, notch-average NO_x and NO concentrations measured in the rail yard using the SEMTECH-DS were used to estimate notch-specific NO_x/NO concentration ratios.

For a given locomotive, notch-average THC/HC concentration ratio typically varied between 2 and 5. The overall response to NDIR to a mixture of hydrocarbons in engine exhaust is approximately 23% to 68% of the actual total HC (Stephens et al., 1996b). The THC/HC ratio in typical diesel exhaust was expected to range between 1.5 and 4.3. Thus, the observed THC/HC ratios were consistent with expectations based on prior studies. For a given locomotive, notch-average NO_x/NO concentration ratio typically varied between 1.03 and 1.07 based on 3 replicates measured for a given locomotive and notch position. These ratios are comparable to the expected NO_x/NO ratio of 1.053 based on a typical diesel exhaust composition of 95 percent NO and 5 percent NO₂ (Flagan and Seinfeld, 2012; Fritz et al., 2000; Tsolakis et al., 2007).

A.3.3.3.2 Versus ride-along vehicle emission measurement system

In 2017, simultaneous exhaust gas measurements were conducted using the Axion PEMS and RAVEM (Frey and Rastogi, 2018). The RAVEM was installed and operated by Engine Fuels and Emissions Engineering (EF&EE). EF&EE also analyzed data collected from RAVEM to provide notch-average FUEP. Measurements were conducted on the treated exhaust of locomotive NC 1859 retrofitted with a NO_x control exhaust after-treatment device. The locomotive operated at 10 throttle notch positions for 3 m to 5 min each for 4 repetitions. An external tank was used to supply fuel to the locomotive. The external tank was weighed gravimetrically by EF&EE at each notch change. The fuel consumption rate for a notch position was inferred as the difference of the weight of the tank before and after notch change divided by the time spent in that notch change.

The comparison of Axion PEMS measurement-based versus RAVEM measurement-based fuel use rates and NO_x emission rates is presented in Figure A-4. The slope of the linear regression of fuel use rates for the Axion PEMS versus gravimetrically measured fuel use rate was 1.02. The 95% confidence interval on the slope was within ±2% of the mean slope. Thus, the slope was precisely estimated. The Axion measurement-based fuel use rates differed from gravimetrically measured fuel use rates by an average of only 2.2 percent. The adjusted R² was 0.99. Thus, the Axion measurement-based fuel use rates were highly precise and accurate compared to gravimetrically measured fuel use rates.

The slope of the linear regression of NO_x emission rates for bias corrected Axion PEMS measurements versus RAVEM was 0.972. The 95% confidence interval on the slope was within ±6% of the mean slope. Thus, the slope was precisely estimated. On average, Axion measurement-based NO_x emission rates were lower by 1.2% relative to RAVEM measurement-based NO_x emission rates. The adjusted R² was 0.963. Thus, the Axion measurement-based NO_x emission rates were highly precise and accurate compared to the RAVEM measurement-based rates. NO_x emission rates are reported as NO₂ equivalent.

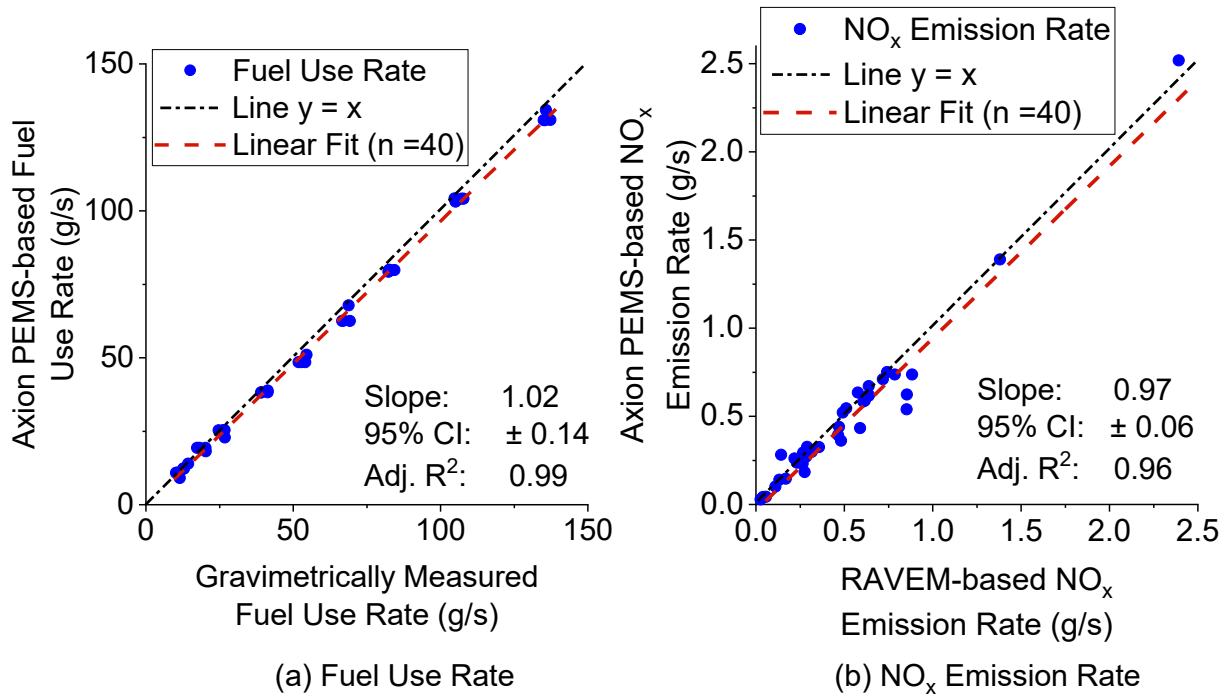


Figure A-4. Comparison of CO₂ and NO_x Emission Rates for Diesel Locomotive Exhaust Based On Simultaneous Rail Yard Measurements Conducted Using Axion Portable Emission Measurement Systems (PEMS) And Ride-Along Vehicle Emission Measurement System (RAVEM): (a) CO₂ Emission Rates; and (b) NO_x Emission Rates.

RAVEM measures NO_x concentrations comprising NO and NO₂. Axion PEMS measures NO concentrations only. For both RAVEM and Axion, emission rates are reported as equivalent NO₂ emission rates. RAVEM based rates were based on NO_x concentrations, and Axion rates were based on bias corrected NO concentrations.

A.3.3.3.3 Versus regulatory portable emissions measurement system

Vu et al., 2020 evaluated five commercially available PEMS versus chassis dynamometer-based laboratory emission measurement system. The Axion PEMS was one of the PEMS evaluated. Evaluations were performed for a light-duty gasoline vehicle (LDGV) and a light-duty diesel truck (LDDT). The vehicles were operated on a chassis dynamometer over several regulatory test cycles. Axion PEMS concentration measurements of CO₂, CO, HC, and NO were benchmarked to laboratory analyzer measured CO₂, CO, and NO_x. The laboratory analyzer was Horiba MEXA 7000 series which uses NDIR for CO₂, and CO concentrations, FID for HC concentration, and chemiluminescence for NO_x concentration.

For a given species, Vu et al., 2020 compared concentration and cycle average emission rates based on all PEMS, categorized by the type of detection method, versus laboratory grade analyzer measurements. Emission rates were compared based on several regulatory driving cycles. The specific PEMS for each measurement data series was not identified. However, in several cases there was either only one PEMS that has the same detection method as the Axion, or only a few PEMS with the same detection method as the Axion. Thus, comparisons of PEMS with the same detection method as the Axion are summarized versus regulatory PEMS and lab grade analyzer measurements.

Vu et al., 2020 included three PEMS with NDIR measurement capabilities for CO₂, including the Axion. The slope of the parity plot of three NDIR-based PEMS versus lab grade analyzer measurements was 0.88. The low slope was because of overestimation of CO₂ concentrations for exhaust concentrations of 4 vol% or lower. With the intercept set to zero, the parity plot slope increased to 0.95. The single value of slope presented here corresponds to the average of three NDIR based PEMS and not just the Axion. The slope for the Axion may have been higher or lower, but this cannot be inferred from the data presented. However, as explained earlier in Section 2.3.3, CO₂ concentrations measured with the Axion were accurate based on comparison with SEMTECH-DS PEMS. For Axion-measured CO₂ concentrations <4 vol%, the average difference from SEMTECH-DS was -0.05 vol%. Thus, differences in measured CO₂ concentrations between the Axion and the SEMTECH-DS were negligible compared to the magnitude of the measured concentrations. NDIR-measurement based cycle-average CO₂ emission rates were within ±4% of the lab grade analyzer measurements. Thus, the CO₂ measurement has adequate accuracy and precision.

Vu et al., 2020 included only one PEMS with NDIR for CO concentration measurements. Therefore, the PEMS compared here was the Axion. The Axion-measured CO concentration had a parity slope of 1.02 and R² of 0.96 versus the laboratory analyzer. These results indicate a high degree of accuracy and precision.

HC concentration was measured only using the Axion PEMS and a laboratory grade analyzer. The Axion -measured HC concentrations were lower than the laboratory grade analyzer by two to four times. As explained earlier in Section 2.3.3, NDIR-measured HC concentrations were expected to be lower than the laboratory grade analyzer. Thus, this result is consistent with expectations.

Vu et al., 2020 included two PEMS with electrochemical cell-based detection for NO_x concentration, including the Axion. However, the specific PEMS for each measurement data series was not identified. The parity slope for the two PEMS was 1.1 and 0.97 with and R² ≥0.97. Thus, irrespective of which data series was for the Axion, the results are adequately accurate and

are highly precise. Overall, the measurements from the Axion PEMS compare well with the laboratory analyzer measurements for CO₂, CO, and NO concentration measurements.

A.3.3.3.4 Versus regulatory data

For several heavy-duty diesel engines, the laser light scattering-based PM concentrations were correlated with the FRM. The slope of linear regression of FRM versus laser-light scattering was reported as 5 (Durbin et al., 2007; Johnson et al., 2011; Khan et al., 2012). Thus laser-light scattering is typically biased low by a factor of 5. Here, each locomotive had the same model PME and was operated on ULSD. A factor of 5 was selected to bias correct Axion PM concentration measurements and estimate average PM emission rates for each notch position for each combination of locomotive and consist. The PM emission rates estimated based on the laser-light scattering PEMS data were compared to reference data reported by the U.S. Environmental Protection Agency (EPA, 1998) for the same model of engine. Both data sets have similar trends in relative variations in emission rates among the throttle notch settings and are similar in magnitude (Figure A-5). The bias corrected estimates of PM emission rates based on PEMS are useful for quantifying relative trends in emission rates.

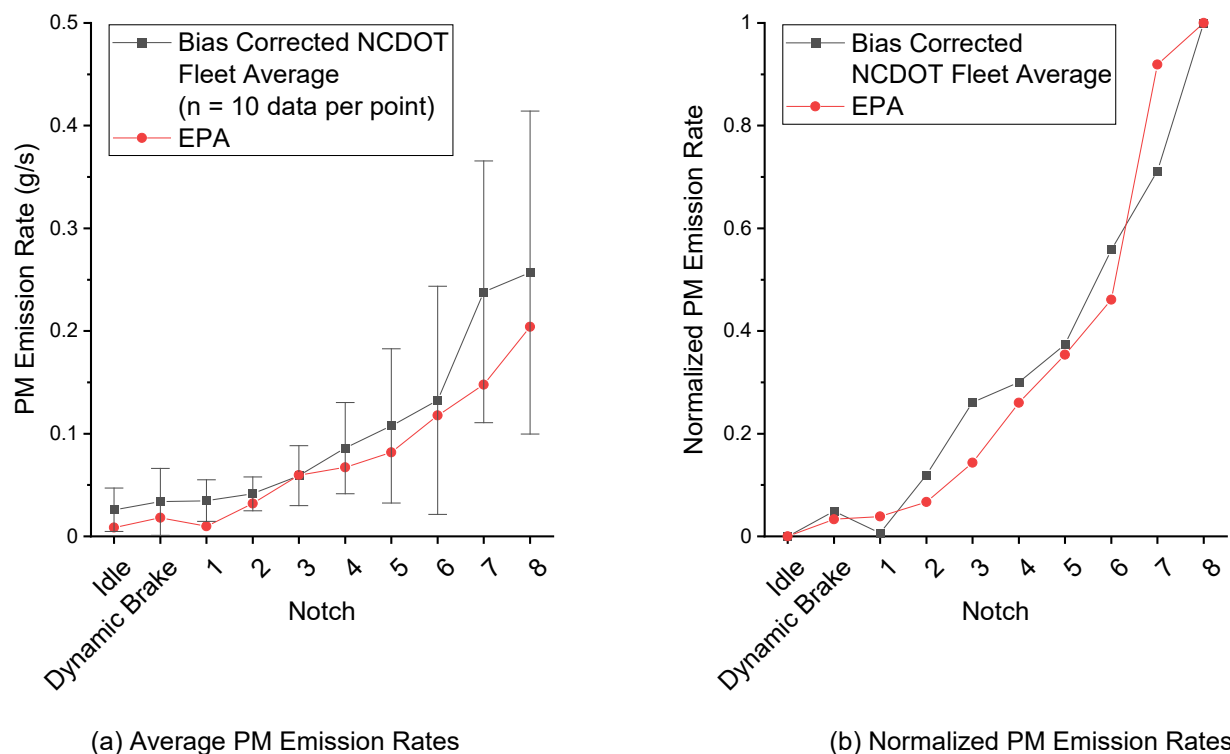


Figure A-5. Relative Trends of Bias Corrected Axion-Based Notch-Average PM Emission Rates Based on Over-the-Rail Measurements Conducted for the NCDOT Fleet Versus the EPA Reported Notch-Average PM Emission Rates for the Same Model Prime Mover Engine: (a) Average PM Emission Rates; and (b) Normalized PM Emission Rates.

Source for EPA Data: (EPA, 1998). The error bars in (a) indicate 95% confidence interval on mean of PM emission rates for a given notch position. Normalized rates in (b) were estimated as the ratio of difference of given rate with minimum rate to the difference of maximum rate and minimum rate.

A.3.4 Locomotive activity data recorder

The throttle notch position for each second of data was inferred from solenoid valve settings (solenoid valves A, B, C, and D) and Generator, and Dynamic Brake indicators recorded by the locomotive activity recorder. The values for each are either 0 or 1. Unique combinations of these indicators were used to identify the notch position of the locomotive as given in Table A-7.

Table A-7. Notch Indicators Recorded by Locomotive Activity Recorder Used to Infer Throttle Notch Position

Notch Indicators						Inferred Throttle Notch Position
Solenoid Valve A	Solenoid Valve B	Solenoid Valve C	Solenoid Valve D	Generator	Dynamic Brake	
0	0	0	0	1	0	Idle
0	0	0	0	0	1	Dynamic Brake
0	0	0	0	1	0	1
1	0	0	0	1	0	2
0	0	1	0	1	0	3
1	0	1	0	1	0	4
0	1	1	1	1	0	5
1	1	1	1	1	0	6
0	1	1	0	1	0	7
1	1	1	0	1	0	8

A.4 PEMS Installation

The installation of the Axion PEMS is illustrated in Figure A-6. The PEMS was placed inside the locomotive cab, as shown in Figure A-6(a). Exhaust gases and PM were continuously sampled from the PME exhaust duct, as shown in Figure A-6(b). Pressure and temperature sensors were installed on a modified airbox access port as shown in Figure A-6(c). The engine RPM sensor was placed near the flywheel, as shown in Figure A-6(d).

A.5 Time Alignment

Each instrument may have slightly different clock times and some instruments or sensors may have different measurement response times. Thus, the recorded time in each instrument may not correspond to the actual time of the measurement. Hence, it is necessary to align the data from multiple data sources such that each row of data corresponds to the same event. Time alignment between two measurement sources involves identification of a reference event from each source which is known to be simultaneous. The reference data were aligned such that peaks and troughs in one dataset aligned with the peaks and troughs in the other dataset. For example, a peak in engine RPM typically corresponds to a peak in CO₂ and NO concentrations.



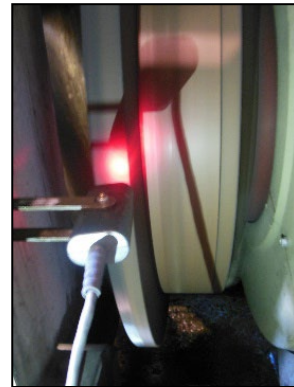
(a) Axion PEMS



(b) Exhaust Sampling Port



(c) Manifold Absolute Pressure And Temperature Sensor



(d) Engine RPM sensor

Figure A-6. Installation of Axion PEMS for Measuring Prime Mover Engine Exhaust for Over-The-Rail Measurements: (a) Axion PEMS Placed Inside the Locomotive Cab; (b) Exhaust Sampling Lines from the Prime Mover Engine Exhaust to the PEMS; (c) Manifold Absolute Pressure And Temperature Sensor; and (d) Engine Revolutions Per Minute Sensor.

Axion PEMS measured exhaust gas and PM concentrations were aligned to engine RPM using CO₂ concentration as a reference measurement. Typically, an increase in engine RPM corresponds to a simultaneous increase in CO₂ concentration. Locomotive speed recorded by the locomotive activity recorder was aligned to the engine RPM at station stops. The locomotive idles at a station stop. Hence, RPM is at its lowest operating value, and speed is zero. As the train prepares to depart, the PME is switched to a higher notch, at which time RPM increases as does train speed. The GPS data were aligned to the locomotive activity data. GPS inferred speed was used as a reference and aligned to locomotive activity recorder measured speed. Thus, data from the engine sensor array, PEMS, locomotive activity recorder, and GPS were time-aligned.

Examples of time plots of unaligned CO₂ concentrations and engine RPM, and CO₂ concentrations aligned to engine RPM, are shown in Figure A-7(a) and Figure A-7(b), respectively. In Figure A-7(a), the dashed red line indicates the start of a rise in the engine RPM. An example of the corresponding start of a rise in the CO₂ concentration is indicated by a dashed blue line. The difference between the two lines is the difference in the recorded timestamps of the two measurements. Using the engine RPM as primary reference data, CO₂ concentrations were shifted by a time equal to the difference of the times between the two dashed lines, in this

case, 18 seconds, such that the dashed lines fell exactly on top of each other, as shown in Figure A-7(b). Exhaust gas and PM measurements from the same dataset were also shifted by the same period.

Engine activity data were aligned with locomotive activity recorder data. Engine RPM was again chosen as a primary reference data and locomotive speed recorded by the activity recorder was chosen as the secondary reference data. Example time plot of unaligned locomotive speed and engine RPM, and locomotive speed aligned to engine RPM, are shown in Figure A-8(a) and Figure A-8 (b), respectively. These two datasets are typically aligned based on comparing locomotive speed and RPM at station stops. At such a stop, speed is zero, and RPM is low. As the train leaves a station, both speed and RPM increase simultaneously. In this example, the locomotive activity recorder data was shifted by 11 seconds to align with the engine activity data.

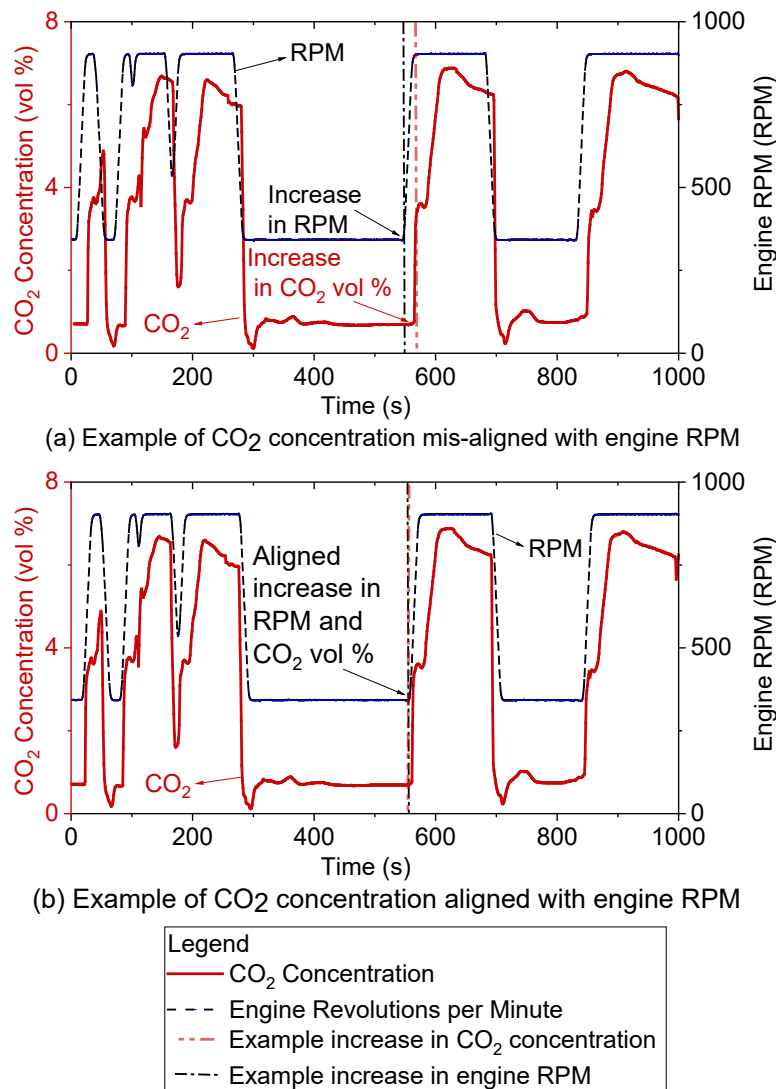
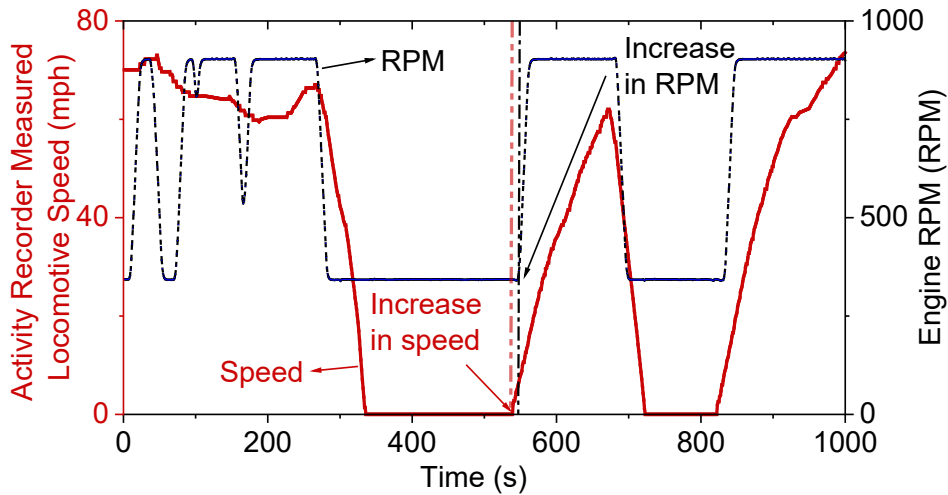
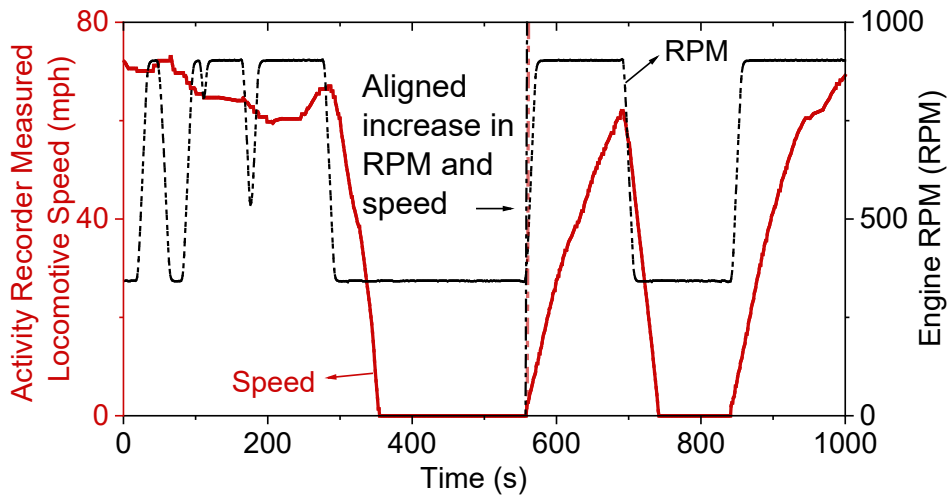


Figure A-7. Example Time Plots of CO₂ Concentration and Engine RPM measured with PEMS for: (a) Unaligned CO₂ Concentrations and Engine RPM; and (b) CO₂ Concentrations Aligned to Engine RPM.



(a) Example of Locomotive Speed mis-aligned with engine RPM



(b) Example of Locomotive Speed aligned with engine RPM

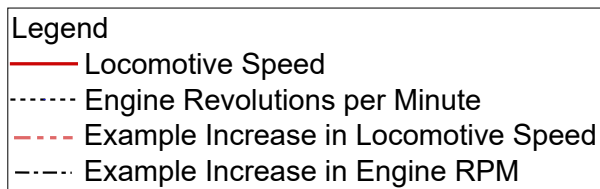


Figure A-8. Example Time Plots of Locomotive Speed measured with Locomotive Activity Recorder and Engine RPM measured with PEMS for: (a) Unaligned Locomotive Speed and Engine RPM; and (b) Locomotive Speed Aligned to Engine RPM.

The time-aligned locomotive speed from the activity recorder was used as the primary reference to align the GPS data using locomotive speed inferred from a GPS receiver as secondary reference data. For this particular case, the data are aligned to obtain the maximum correlation between the two reference data as they both measure the same thing. Example time plots of unaligned locomotive speed and GPS inferred speed, and GPS inferred speed aligned to locomotive speed, are shown in Figure A-9(a) and Figure A-9 (b), respectively. The correlation was 0.95 for the raw data and 0.99 for the aligned data. The GPS data were shifted by 7 seconds to align with the locomotive activity recorder data.

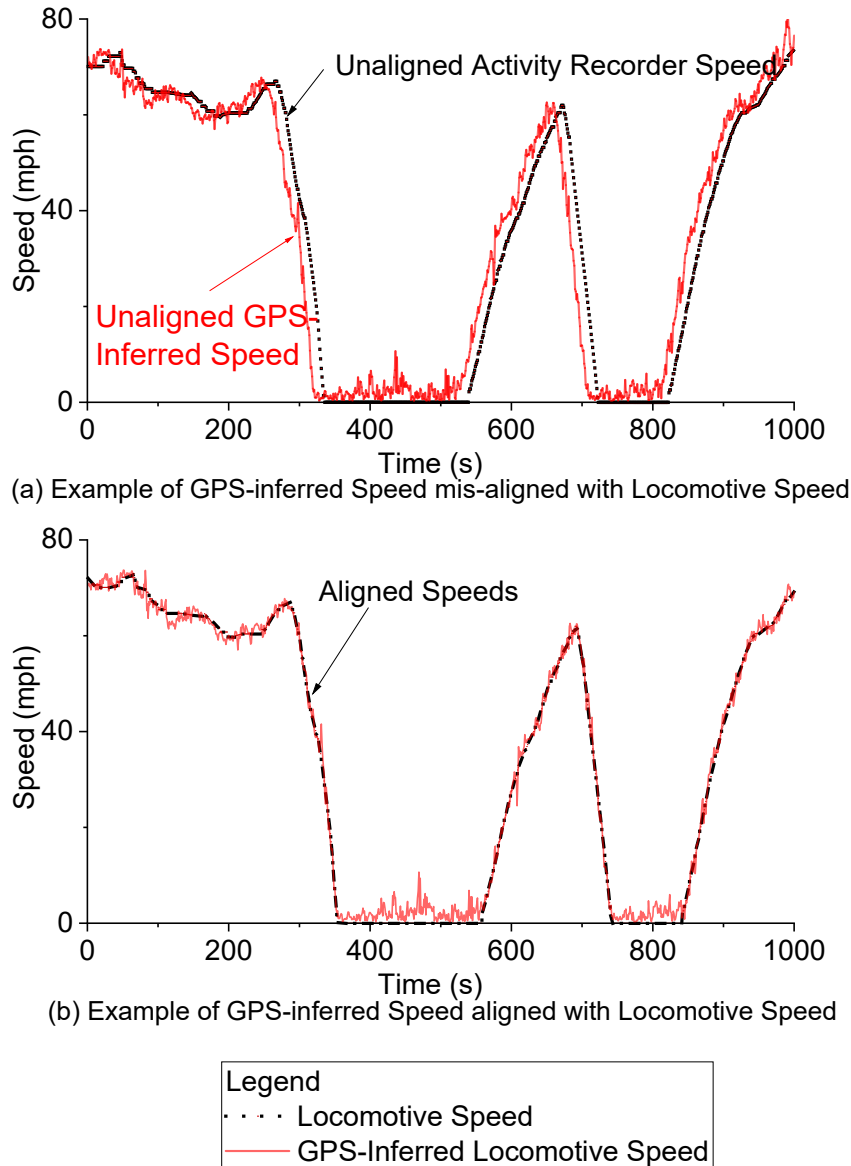


Figure A-9. Example Time Plots of Locomotive Speed measured with Locomotive Activity Recorder and inferred with GPS Receiver for: (a) Unaligned Locomotive Speeds; and (b) Aligned Locomotive Speeds.

A.6 Quality Assurance

Erroneous data were either corrected or rejected from the data analysis. Typical errors in the data include: (1) Errors in engine sensor array data; and (2) errors in gas analyzer data. Errors in engine sensor data were identified based on deviations from credible ranges of RPM, IAT, and MAP. The engine RPM of the locomotives measured varied between 268 RPM at idle to 901 RPM at Notch 8. The IAT typically varied between 10 °C and 125 °C. The MAP typically varied between 90 kPa and 250 kPa. Thus, any data outside these ranges were excluded from further analysis.

Errors in gas analyzer data were identified by comparing the measurements of both of the benches of an Axion PEMS when they operated simultaneously. If the relative error between the measurements was within a Maximum Allowable Difference (MAD), an average of the two values was taken. However, if the relative error exceeded the MAD, then further assessment of data quality was required. The MAD is based on twice the detection limit of each sensor. The MAD for CO₂, CO, HC, NO and O₂ are 0.6 %, 0.04 %, 28 ppm, 50 ppm and 0.5 %, respectively. Discrepancies in measurements might be due to: (1) leakage in the sample exhaust line leading to a bench; (2) overheating of a bench; or (3) problems with the sampling pump of a bench, leading to inadequate flow. In such cases, only the data from the properly working bench was used and the data from the erroneous bench were rejected. Negative values of concentrations are physically implausible. Negative concentrations that were lower than zero by less than the magnitude of the detection limit of the instrument were assumed to be zero. Negative concentrations that were lower than zero by more than the magnitude of the detection limit of the instrument typically tend to occur from time to time for the HC concentrations and were excluded. Additional details on quality assurance are provided elsewhere (Frey and Graver, 2012; Graver and Frey, 2013; Sandhu and Frey, 2013).

A.7 Fuel Use and Emission Rates

Fuel use and CO₂, CO, HC, NO_x, and PM emission rates are typically expressed as mass per time or mass per unit of engine power output. Mass per time emission rates of gases are estimated as the product of dry molar exhaust flow rate and the measured volumetric pollutant exhaust concentration. PM is measured using Axion PEMS as mass per unit volume and converted to mass per mole of the exhaust based on ideal gas law. Mass per time-based PM emission rate was estimated as a product of PM molar concentration and dry molar exhaust flow rate. Mass per distance based FUER were estimated as sum of all measured 1 Hz mass per time based FUER in a given track segment divided by the measured segment length.

A.7.1 Mass per time-based rates

Molar exhaust flow rate was estimated from the mass airflow rate and the air-to-fuel ratio. Mass airflow was estimated using the “speed-density method” based on the measurement of engine activity variables and a previously developed estimate of engine volumetric efficiency (Graver and Frey, 2013). The speed-density method is based on the ideal gas law (Vojtisek and Kotek, 2014). The engine activity variables required include engine revolutions per minute (RPM), intake air temperature (IAT), manifold absolute pressure (MAP), and engine volumetric efficiency (η_{ev}). Volumetric efficiency is the ratio of the actual volume of air that flows through the engine cylinders versus the physical cylinder displacement. Volumetric efficiency accounts for factors that affect airflow such as engine design and operation. Volumetric efficiency was found to be well correlated with the product of MAP and RPM from prior dynamometer

measurements on similar EMD 12-710 PME's (Graver and Frey, 2013). Thus, the volumetric efficiency of a PME was estimated based on measured RPM and MAP. The air to fuel ratio was inferred based on the volume percent of carbon species in the exhaust, including CO₂, CO, and HC because all of the carbon in the exhaust comes only from the fuel.

The PME volumetric efficiency was estimated as (Graver and Frey, 2013):

$$\eta_{ev,t} = 4.3648 \times \left(\frac{ES_t \times P_{M,t}}{1000} \right)^{-0.298} \quad (A-1)$$

Where,

$$\begin{aligned} \eta_{ev,t} &= \text{engine volumetric efficiency of the engine at time } t \\ ES_t &= \text{engine speed at time } t \text{ (RPM)} \\ P_{M,t} &= \text{engine manifold absolute pressure at time } t \text{ (kPa)} \end{aligned}$$

The intake air molar flow rate for a PME for each second was estimated as:

$$M_{a,t} = \frac{\left(\frac{P_{M,t} - P_B}{ER} \right) \times EV \times \left(\frac{ES_t}{30 \times EC} \right)}{R \times T_{int,t}} \quad (A-2)$$

Where,

$$\begin{aligned} M_{a,t} &= \text{intake molar air flow rate at time } t \text{ (gmol/s)} \\ EC &= \text{engine strokes per cycle (1 for two-stroke engines and 2 for four-stroke engines)} \\ ER &= \text{engine compression ratio} \\ EV &= \text{engine displacement (L)} \\ P_B &= \text{barometric pressure assumed to be constant during a measurement (101 kPa)} \\ T_{int,t} &= \text{intake air temperature at time } t \text{ (K)} \\ R &= \text{universal gas constant (8.314 J mol}^{-1} \text{ K}^{-1}) \end{aligned}$$

Exhaust molar flow rate on a dry basis was estimated based on $M_{a,t}$ and air to fuel ratio (AFR) inferred from exhaust gas composition (Sandhu and Frey, 2013):

$$M_{e,t,dry} = \frac{2 \times 0.21 \times M_{a,t}}{\left(2 + \frac{x}{2} + z \right) y_{CO_2,t,dry} + \left(1 + \frac{x}{2} - z \right) y_{CO,t,dry} + 2y_{O_2,t,dry} + y_{NO,t,dry} + \left(\frac{3x - 8 - 6z}{2} \right) y_{HC,t,dry}} \quad (A-3)$$

Where,

- $M_{e,t,dry}$ = molar exhaust flow rate at time t on a dry basis ($gmol/s$)
 $y_{s,t,dry}$ = mole fraction of pollutant species s at time t for a PME on a dry basis ($gmol/gmol$ of dry exhaust)
 x,z = elemental composition of fuel CH_xO_z where x is $gmol$ of hydrogen per $gmol$ of carbon in the fuel, and y is the $gmol$ of oxygen per $gmol$ of carbon in the fuel

For each second, mass emission rates of gaseous pollutants were estimated based upon the pollutant mole fraction on a dry basis, dry exhaust molar flow rate, and molecular weight of the gaseous pollutant, except for NO_x for which the molecular weight of NO_2 was used:

$$m_{s,t} = y_{s,t,dry} \times M_{e,t,dry} \times MW_s \quad (A-4)$$

Where,

- $m_{s,t}$ = mass emission rate of pollutant species s at time t (g/s)
 MW_s = equivalent molecular weight of all pollutant species except for NO_x . NO_x was reported as equivalent NO_2 . Therefore, for NO_x emission rates, the equivalent weight of NO_2 was used ($g/gmol$)

Assuming that all the carbon in the exhaust is coming from the carbon content of the fuel and that carbon in fuel is distributed among CO_2 , CO and HC in the exhaust, the mass per time fuel use rate was estimated as:

$$m_{f,t} = M_{e,t,dry} \times MW_f \times (y_{CO_2,t,dry} + y_{CO,t,dry} + m \times y_{HC,t,dry}) \quad (A-5)$$

Where,

- $m_{f,t}$ = mass fuel use rate by the engine at time t (g/s)
 MW_f = equivalent molecular weight of fuel ($g/gmolC$)
 m = moles of carbon per gram mole of the hydrocarbon

The PM mass emission rate ($m_{PM,t,dry}$) was estimated as:

$$m_{PM,t,dry} = C_{PM,t,dry} \times M_{e,t,dry} \times \left(\frac{R T}{P_B} \right) \quad (A-6)$$

Where,

- $m_{PM,t,dry}$ = PM mass emission rate at time t on a dry basis (mg/s)
 $C_{PM,t,dry}$ = measured PM concentration in the exhaust at time t on a dry basis (mg/m^3)
 T = standard temperature ($298 K$)

A.7.2 Segment-average rates

Segment-average FUERs were estimated as mass per distance-based FUERs. Segment-average FUERs were estimated from 1 Hz rates by summing all 1 Hz rates in a given segment divided by the measured segment length. For the sake of simplicity, regardless of the position of the locomotive(s) in a consist, the train was assumed to be a point emitting source with the emissions of all locomotives in the consist occurring at the location of measured locomotive. Given that the length of a train is typically 0.08 miles, which is much less than the length of a 0.25-mile segment, this assumption is not expected to lead to a substantial segment classification error.

At the terminal stations, the dwell time for the train was much larger than at the intermediate stations. Longer dwell time is associated with greater cumulative idling emissions. Therefore, FUERs at the terminal stations were expected to be higher than intermediate stations. Mass per distance-based FUERs were estimated at the terminal stations for two cases: (1) assuming an average dwell time of 2 minutes at each terminal station to be consistent with other stations for comparison; and (2) assuming the usual average dwell time of 15 minutes at Raleigh and 1 hour at Charlotte for each one-way trip to account for actual emissions at these locations.

Each one-way trip is called a run. For each segment in a given run, mass per distance-based fuel use and emission rates were estimated and called as segment-run average FUERs. For a given segment, average rates were based on a given travel direction and based on both directions combined. These rates were called as segment-average rates. Segment-average rates are average rates without excess dwell time at the terminal stations. Rates with additional dwell time included at the terminal stations are quantified as a sensitivity case.

A.8 Potential Explanatory Variables

In this section, explanatory variables potentially affecting segment-run average FUERs based on physics of motion are discussed. Based on resistances opposing train motion, 1 Hz mass per time-based fuel use and emission rates are directly proportional to locomotive power demand (LPD) (AREMA, 2020; Frey and Rastogi, 2019; Profillidis, 2014). LPD is the power required to overcome journal, flange, drag, curvature, grade and acceleration resistances. LPD is a function of train speed and acceleration, and track grade and curvature (AREMA, 2020; Hay, 1982; Profillidis, 2014):

$$LPD_{i,j,t,L,C} = c_{1,L,C} v_{i,j,t,L,C} + c_{2,L,C} v_{i,j,t,L,C}^2 + c_{3,L,C} v_{i,j,t,L,C}^3 + c_{4,L,C} v_{i,j,t,L,C} d_i + c_{5,L,C} v_{i,j,t,L,C} x_i + c_{6,L,C} v_{i,j,t,L,C} a_{i,j,t,L,C} \quad (A-7)$$

Where,

$LPD_{i,j,t,L,C}$	=	instantaneous locomotive power demand for the i^{th} track segment of the j^{th} one-way trip at time t for locomotive L operated in consist C (kW/ton).
$v_{i,j,t,L,C}$	=	train speed for the i^{th} track segment of the j^{th} one-way trip at time t for locomotive L operated in consist C (mph)
d_i	=	curvature of the i^{th} track segment ($degrees$)
x_i	=	grade i^{th} track segment ($\%$)
$a_{i,j,t,L,C}$	=	acceleration for the i^{th} track segment of the j^{th} one-way trip at time t for locomotive L operated in consist C (mph/s)

$c_{k,L,C}$ = unit resistance coefficients depending on static factors including train consist, locomotive(s), train weight, lead locomotive frontal shape, and the number of passenger cars for locomotive L operated in consist C . $k \in [1, 2, 3, 4, 5, 6]$ for journal, flange, drag, curvature, grade and acceleration resistance, respectively.

PME(s) idle when LPD is zero or negative. For seconds with positive LPD, FUERs over idle FUERs are hypothesized to be directly proportional to LPD. The unit resistance coefficients depend on static factors. One-Hz mass per time-based FUER as a function of LPD are:

$$M_{p,i,j,t,L,C} = M_{p,L,C}^0 + C_{p,L,C} \times LPD_{i,j,t,L,C} \quad (A-8)$$

Where,

$M_{p,i,j,t,L,C}$ = One Hz mass per time-based fuel use rate or emission rate of pollutant p for the i^{th} track segment of the j^{th} one-way trip at time t for locomotive L operated in consist C (g/s)

$M_{p,L,C}^0$ = One Hz mass per time-based idle fuel use rate or emission rate of pollutant p for locomotive L operated in consist C (g/s)

$C_{p,L,C}$ = proportionality constant for fuel use rate or emission rates of pollutant p for locomotive L operated in consist C (g-ton/A-kW)

PME(s) idle when LPD is zero or negative. For seconds with positive LPD, FUER in excess of idle rates are hypothesized to be directly proportional to LPD. The unit resistance coefficients depend on static factors. Mass per distance-based segment-average FUERs as a function of LPD are:

$$\begin{aligned} \bar{M}_{p,i,j,t,L,C} = & \frac{1}{\sum_{t=1}^{n_{i,j,L,C}} v_{i,j,t,L,C}} \left\{ \sum_{t=1}^{n_{i,j,L,C}} M_{p,L,C}^0 + c_{1,L,C} \sum_{t=1}^{n_{i,j,L,C}} v_{i,j,t,L,C} + c_{2,L,C} \sum_{t=1}^{n_{i,j,L,C}} v_{i,j,t,L,C}^2 \right. \\ & + c_{3,L,C} \sum_{t=1}^{n_{i,j,L,C}} v_{i,j,t,L,C}^3 + c_{4,L,C} \sum_{t=1}^{n_{i,j,L,C}} v_{i,j,t,L,C} d_i \\ & \left. + c_{5,L,C} \sum_{t=1}^{n_{i,j,L,C}} v_{i,j,t,L,C} x_i + c_{6,L,C} \sum_{t=1}^{n_{i,j,L,C}} v_{i,j,t,L,C} a_{i,j,t,L,C} \right\} \quad (A-9) \end{aligned}$$

Where,

$\bar{M}_{p,i,j,t,L,C}$ = Mass per distance-based segment-run average fuel use or emission rate of pollutant p for the i^{th} track segment of the j^{th} one-way trip at time t for locomotive L operated in consist C (g/mile)

$n_{i,j,L,C}$ = Time spent in the i^{th} track segment of the j^{th} one-way trip for locomotive L operated in consist C (s)

The dynamic variables affecting segment-run average FUEs are time in each segment, sum of speeds, the sum of squares of speed, the sum of cubes of speed, the sum of product (SOP) of speed and acceleration, SOP of speed and grade, SOP of speed and curvature. The static variables include locomotive and consist.

A.9 Rail-Grade and Curvature

Rail- grade and horizontal curvature were inferred from prior GPS measurements for eight locomotives operated on ULSD and biodiesel blends (Frey and Rastogi, 2018; Rastogi and Frey, 2018). GPS receivers record position and elevation data. However, each recorded position is subject to random errors. The typical horizontal position precision of a low-cost GPS receiver is ± 9 feet or more. The vertical precision of altimeter measurements is ± 1 m. The imprecision of the position and elevation data can be compensated for by a large sample size of data. A method to estimate road grade using low-cost GPS receivers with barometric altimeters has previously been demonstrated (Boroujeni et al., 2013; Boroujeni and Frey, 2014).

Position and elevation data were collected at 1 Hz using Garmin 76CSx and Garmin Oregon 500 receivers. The GPS receivers were installed near the window in the locomotive cab. Grade and curve radii estimates were found to be independent of the position of the GPS receivers with respect to rail elevation and the centerline of the track. Grade is based on relative changes in elevation. The estimated grade is unaffected by the location of the GPS receiver within the train as long as the position is the same throughout the trip. On curves, the inner rail has a shorter radius than the outer rail. However, the difference between the two radii was less than the precision of the GPS receivers. Thus, the positioning of receivers with respect to the centerline is an insignificant source of error. It was also assumed that the longitudinal grade is approximately similar regardless of the superelevation of the track. Although the latter is an approximation, differences in elevation of just a few inches are smaller than the precision of the GPS receivers.

Segment length was selected to be long enough to include sufficient 1 Hz data to obtain precise estimates of average grade and curve radii, and short enough such that actual changes in elevation were approximately linear and the horizontal curves were approximately arcs of a circle (Boroujeni et al., 2013; Boroujeni and Frey, 2014; Frey and Rastogi, 2018; Rastogi and Frey, 2018). Boroujeni and Frey (2014) found a distance of 0.1 miles to be appropriate for quantifying road grade based on GPS data (Boroujeni and Frey, 2014). However, for railroad tracks, elevation changes are typically more gradual than for roads. Therefore, a segment length of 0.25 mile is used here. The number of GPS data points in a segment depends upon train speed. For example, for the Piedmont route which has a speed limit of 79 mph, at least 11 data points were recorded at 1 Hz for a 0.25-mile segment per GPS receiver. The selected segment length was also larger than the longest train length measured on this route (0.12 mile).

Typically, 4 to 10 GPS receivers fitted with barometric altimeters were used per one-way trip. Any receiver that lost signal or that could not record data for some part of a trip was excluded from further analysis. Data from 180 GPS measurements were used. Each GPS measurement represents one GPS receiver that recorded 1 Hz data for a complete one-way trip. The 173-mile rail route was divided into 692 0.25-mile segments. Grade estimation is based on relative changes in elevation. The barometric pressure varies from run-to-run depending on weather conditions. Thus, while the change in elevation along a segment is repeatable, the recorded absolute barometric pressure may vary on average from one run to another. Because grade is based on relative changes in elevation, it is not necessary to know the actual absolute elevation.

However, statistical precision of grade estimates from multiple GPS runs was improved by vertically aligning data points from each run to an arbitrary average reference elevation for each segment.

Rail grade was quantified for non-overlapping adjacent equal-length track segments based on a method developed by Boroujeni and Frey (2014) for road segments. This method included the following steps:

- (1) projecting position-elevation data from 180 GPS measurements onto the segmented line representing the location of the track using ArcGIS (ESRI, 2004);
- (2) combining 1 Hz measurements from multiple GPS measurements into a single dataset regardless of the travel direction;
- (3) aligning each GPS measurement to have the same average elevation for each track segment to improve the statistical precision of grade estimates;
- (4) using Geographic Information System (GIS), calculating the distance of each point from the start point of each segment in the travel direction from Charlotte to Raleigh;
- (5) fitting a linear regression for elevation versus distance in each segment; and
- (6) inferring grade from the slope of the linear regression.

The Piedmont rail route comprises single and double tracks. Double tracks run parallel to each other. Therefore, grade and curvature are not dependent on the track. Grade was estimated in the travel direction from Charlotte, NC to Raleigh, NC. For the reverse travel direction, grade was assumed to have the same magnitude but opposite sign.

In prior work, rail grade estimated using GPS receivers was compared with track design drawings available for a 40-mile section of the route and with grade estimated based on Light Detection and Ranging (LIDAR)-based Digital Elevation Models (DEMs) (Rastogi and Frey, 2018). The GPA-based grade estimates were accurate compared to these other data sources. The GPA-based grade estimates were compared with the grade from the track design drawings. The grade in the track design drawings was for segments typically 0.5 miles or longer. Based on the design drawings for a 40-mile section of the route, the grade varied between -2 percent and 2 percent. The GPA-based grade estimates were on average within ± 0.3 percent absolute versus the track drawings. The grade estimated based on GPS data for the entire Piedmont route varied between -1.9 percent and 1.9 percent. Thus, the range of grades included in the design drawings is representative of grades for the entire route.

Track curvature was estimated based on circular regression of GPS position data and the GIA-based track shapefile for each segment (Rastogi and Frey, 2018). Track curvature estimated using GPS data and the GIS shapefile were compared to design drawings for 0.25-mile track segments of the Piedmont route. The track design drawings were labeled with curvature in degrees at a resolution of 0.5 degrees for a 40-mile section of the route for every 0.1-mile track segment. Thus, every 0.25-mile segment on the Piedmont route comprised three 0.1-mile track segments corresponding to track design drawings. To enable consistent comparison, an average curvature of three 0.1-mile track segments was compared with the overlapping 0.25-mile track segment. Based on average track curvature inferred from track design drawings, curvature varied between 0.0 degrees and 4.0 degrees. The GPA-based curvature estimates were on average within ± 0.2 degrees versus track drawings. Curvature estimated based on GPS data for the entire

Piedmont route varied between 0 degrees and 4.3 degrees. Thus, the range of curvature included in the design drawings are representative of curvatures for the entire route.

For a given track segment, curvature estimated based on the GIS shapefile was within ± 0.1 degrees of curvature estimated based on GPS data. The GIA-based curvature estimates were on average within ± 0.2 degrees versus track drawings. Therefore, curvature estimated from either GPS data or the GIS shapefile is comparable and suitable for estimating curvature for segments for which design drawings are not available. Here, track curvature was estimated based on GPS data.

A.10 Characterizing Track Segments and Segment-Runs

In this section, the track segments were characterized based on location where trains typically dwell, accelerate, decelerate, or cruise. The track segments and segment-runs were classified based on FUEP into hotspots and non-hotspots. Segment classification based on location and FUEP is presented in Table A-8.

Trains typically accelerate when leaving a station, operate at near maximum allowable speeds in-between stations, and decelerate when approaching a station. Thus, based on these operations, the track segments were classified into (1) station segments (S); (2) near station acceleration segments (NSA); (3) near station deceleration segments (NSD); and (4) intermediate segments (I). NSA and NSD are also collectively referred to as near stations segments (NS). NSA in one travel direction are NSD in the opposite direction.

The S segments are track segments that include a station. Each station was enclosed within a single track segment. None of the stations were split into two adjoining segments. The segment ID's 1, 108, 170, 308, 370, 455, 588, 660, and 692 were station segments for Charlotte, Kannapolis, Salisbury, High Point, Greensboro, Burlington, Durham, Cary, and Raleigh, respectively.

Based on measured data for this route, trains typically accelerated within 1.25 mile (five track segments) downstream of a station. Thus, track segments within 1.25 mile downstream of each S segment were classified as NSA segments. Track segments within 1.25 mile upstream of each station segment were classified as NSD segments because the trains typically decelerated in these segments. Segments other than S, NSA, and NSD segments were classified as I segments.

Table A-8. Segment and Segment-Run Classification Based on Location and Fuel Use and Emission Rates

Classification By	Applicability	Classification	Definition
Location	Segment	Station (S)	Segments containing a station
		Near Station Acceleration (NSA)	Five adjacent segments downstream of a station where trains typically accelerate
		Near Station Deceleration (NSD)	Five adjacent segments upstream of a station where trains typically decelerate
		Intermediate (I)	Segments other than <i>S</i> , <i>NSA</i> and <i>NSD</i> .
		Near Station (NS)	<i>NSA</i> and <i>NSD</i> constitute <i>NS</i> .
Fuel Use or Emission Rate (FUER)	Segment	Absolute Hotspot ($AH_{i,S,D} = 1$) ^a	Segment-average rate for i^{th} segment for species <i>S</i> in the top 20 th percentile based on all segment-runs for all consists in direction <i>D</i> .
		Absolute Non-Hotspot ($AH_{i,S,D} = 0$) ^a	Segment-average rate for i^{th} segment for species <i>S</i> in the bottom 80 th percentile based on all segment-runs for all consists in direction <i>D</i> .
		Consist-Specific Hotspot ($CH_{i,S,C,D} = 1$) ^{a,b}	Segment-average rate for i^{th} segment for species <i>S</i> in the top 20 th percentile based on all segment-runs for consist <i>C</i> in direction <i>D</i> .
		Consist-Specific Non-Hotspot ($CH_{i,S,C,D} = 0$) ^{a,b}	Segment-average rate for i^{th} segment for species <i>S</i> in the bottom 80 th percentile based on all segment-runs for consist <i>C</i> in direction <i>D</i> .
	Segment-Run	Relative Hotspot ($RH_{i,j,S} = 1$) ^{a,c}	Segment-run rate for i^{th} segment of j^{th} one-way trip for species <i>S</i> in the top 20 th percentile for a given one-way trip
		Relative Non-Hotspot ($RH_{i,j,S} = 0$) ^{a,c}	Segment-run rate for i^{th} segment of j^{th} one-way trip for species <i>S</i> in the bottom 80 th percentile for a given one-way trip

^a *S*: index for species = fuel for fuel use rate, = NO_x for NO_x emission rate, = *PM* for *PM* emission rate; *D*: index for direction = *e* for eastbound, = *w* for westbound, and = *b* for both directions combined; *i*: index for segment, $i \in [1, 2, 3, \dots, 692]$; *j*: index for one-way trip, $j \in [1, 2, 3, \dots, 35]$

^b *C*: Index for consist. *C* \in single locomotive consist (*SLC*), double-powered tandem consist (*DP-TC*), double-powered push/pull consist (*DP-P/PC*), or single-powered push/pull consist (*SP-P/PC*).

^c Relative hotspots in each travel direction were used as input to the model described in Section 11. Relative hotspots were not averaged for both directions combined.

Segments were classified into hotspots and non-hotspots based on segment-average FUEP as: (1) Absolute; and (2) Consist-specific. Segment-runs were classified into relative hotspots and relative non-hotspots based on segment-run average FUEP. Absolute hotspots indicate locations with FUEP consistently higher than other locations. Absolute hotspots included the track segments in the top 20th percentile of segment-average FUEP based on all measurements combined. Remaining segments were classified as absolute non-hotspots. Because a given track segment may have higher rates in one travel direction and lower in the other, absolute definition was based on travel direction. Hotspots in one travel direction only indicate a potential for higher exposure to pollutants during the passing of one train. Hotspots in both directions indicate the location with higher exposure per round trip. Therefore, a given track segment i for species S and direction D was classified as an absolute hotspot ($AH_{i,S,D} = 1$) or absolute non-hotspot ($AH_{i,S,D} = 0$). i is the ID of the track segment. S is *fuel*, NO_x or PM for fuel use rate, NO_x emission rate, or PM emission rate, respectively. D is e , w , or b for eastbound, westbound, or both directions combined, respectively. Segment-average speed, acceleration, grade, and curvature were also assessed.

Consist-specific hotspots indicate the top 20th percent frequency range of segment-run average FUEP all one-way trips measured for a given train consist. Based on this definition, one-way trips with a fewer number of hotspots compared to other trips are indicative of trips with better operational practices. This definition can also be used to support assessment of inter-consist variability in segment-average FUEP. A given track segment i for species S , consist C , and direction D was classified into consist-specific hotspot ($CH_{i,S,C,D} = 1$) or consist-specific non-hotspot ($CH_{i,S,C,D} = 0$). Measured consists include SLC , $DP-TC$, $DP-P/PC$, and $SP-P/PC$. Measured consists were described in Section 1.2.

Inter-locomotive and inter-consist variability in FUEP may lead to differences in segment-run average FUEP for the same values of speed, acceleration, grade, and curvature. For example, a locomotive with higher FUEP than other locomotives will have a larger number of hotspots. Conversely, a low emitting locomotive may have fewer hotspots. The low emitting locomotive will still have operating practices that will lead to higher FUEP at some locations relative to others. Absolute hotspots are useful for identifying operational practices leading to spatial variability for an average of many runs from multiple consists. However, absolute hotspots are not applicable to identifying whether hotspots differ among individual trips by trains with different locomotives and consists. To account for inter-trip variability in FUEP, segment-runs were classified on a relative basis. The threshold was chosen as the 80th percentile segment-run FUEP for each one-way trip. A given segment-run for i^{th} segment of j^{th} trip for species S was classified as a relative hotspot ($RH_{i,j,S} = 1$) or relative non-hotspot ($RH_{i,j,S} = 0$). Each segment-run is one-directional. Relative hotspots are useful for identifying controllable operational practices and infrastructure factors that induce relatively high FUEP and to target interventions. Relative hotspots also differ by travel direction. However, as discussed later in Section 11, relative hotspots in each travel direction were used to quantify the effect and importance of potential explanatory variables in differentiating hotspots from non-hotspots. Relative hotspots in each direction were not averaged for both directions. Rather, relative hotspots in each direction were used as input to a model. Separate models for each direction or both directions combined were not needed.

A.11 Segment-Average Activity, Fuel Use Rate, Emission Rates, and Population Density

In this section, the variation of segment-average activity, and FUER based on travel direction, and both travel directions are presented. The variation of population density along the route based on census tracts enclosing the track segments is also presented.

The variation of segment-average dynamic variables and FUERs along the route is compared. Segment-average dynamic variables based on 14 one-way trips in eastbound direction are presented in Figure A-10. Dynamic variables include speed, acceleration, grade, and curvature. Segment-average NO_x and PM emission rates in the eastbound direction and the US 2010 census tract-based population density are presented in Figure A-11. Segment-average dynamic variables based on 21 one-way trips in westbound direction are presented in Figure A-12. Segment-average NO_x and PM emission rates in the westbound direction and the US 2010 census tract-based population density are presented in Figure A-13.

To quantify the sensitivity of the location of hotspots to consists, the number of co-located absolute hotspots and absolute near-hotspots versus consist-specific hotspots were compared. Near-hotspots are defined as the segments with average rates in a given direction between 70th and 80th percentile. Near-hotspots were quantified for each of absolute hotspots ($AH_{i,S,D} = 1$) and consist-specific hotspots ($CH_{i,S,C,D} = 1$) as absolute near-hotspots ($NAH_{i,S,D} = 1$) and consist-specific near-hotspots ($NCH_{i,S,C,D} = 1$), respectively. Based on the definition of hotspots, there were 139 hotspots and 70 near-hotspots for a given species in a given travel direction. The sensitivity is categorized as “weak,” meaning that the identification of hotspots is not highly dependent on the type of consist, if the proportion of co-located consist-specific hotspots versus absolute and absolute near-hotspots was >80%, and the proportion of co-located absolute hotspots versus consist-specific hotspots and consist-specific near-hotspots was >80%.

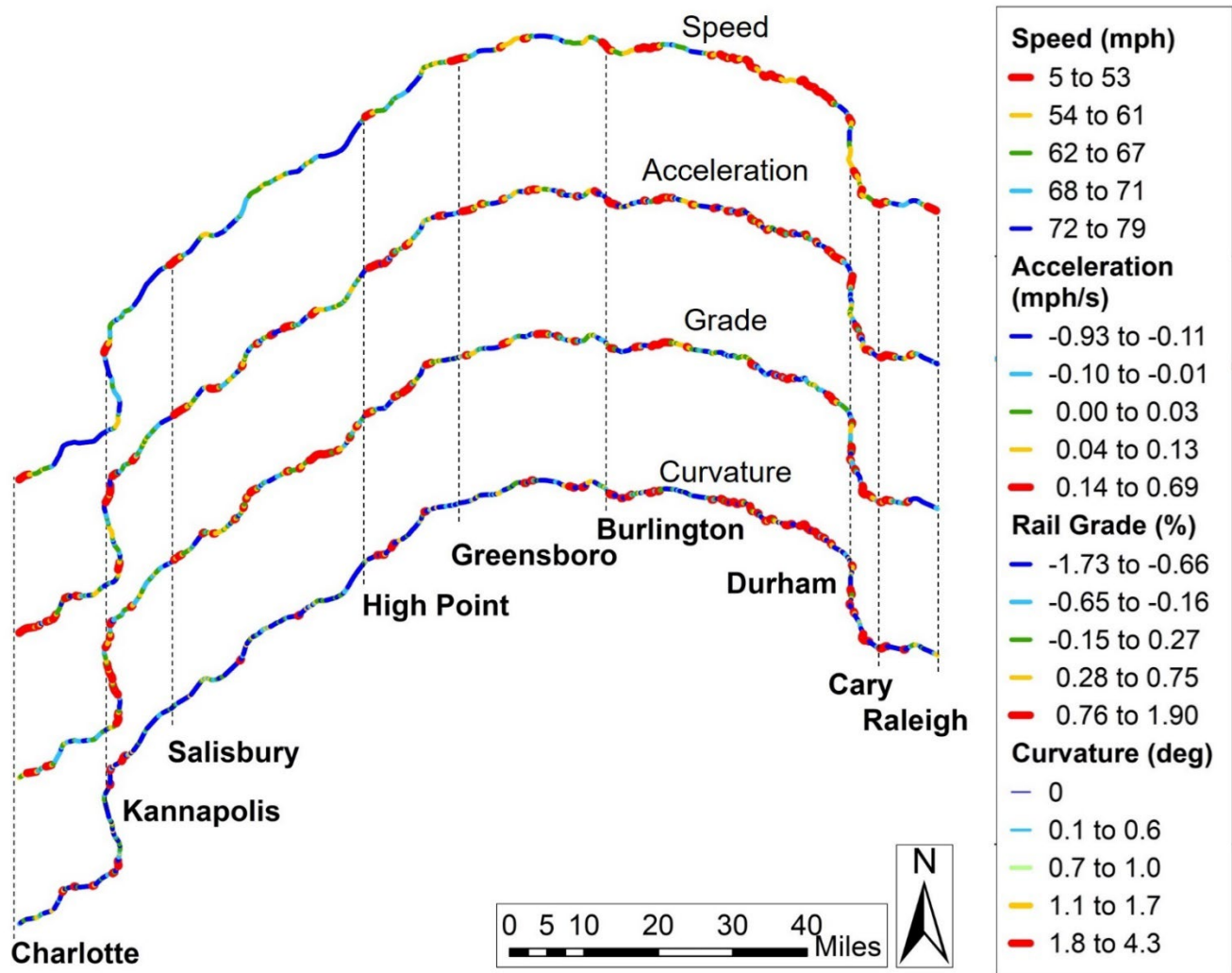
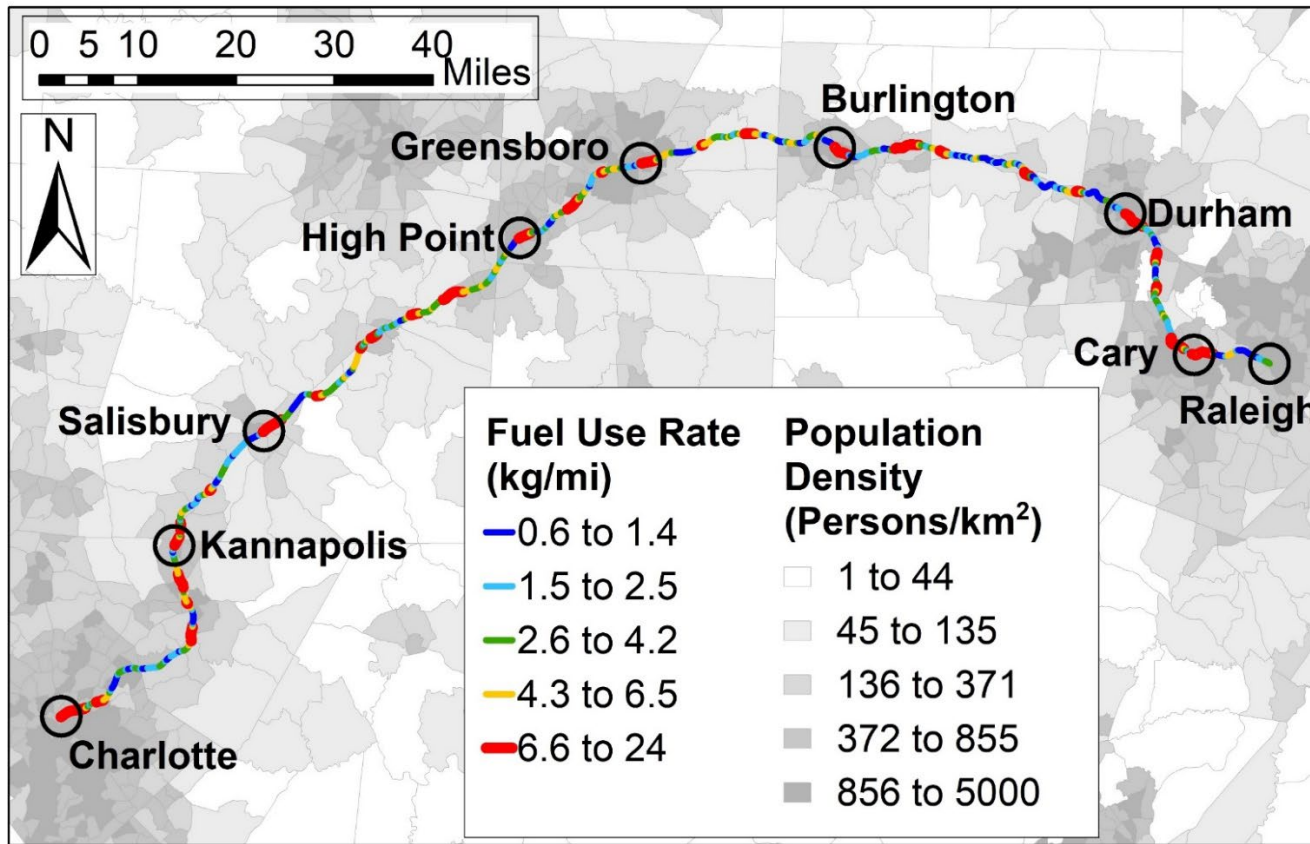


Figure A-10. Segment-Average Speed, Acceleration, Grade, and Curvature for the Piedmont Passenger Rail Service between Raleigh, NC and Charlotte, NC in the Eastbound Direction Based on 14 One-Way Trips.

Segment-average activity are divided in five 20th percentile groups. The groups are colored from cool blues to warm red. The values in blue are expected to likely result in lower fuel use and emission rates, whereas the values in red are expected to result in higher fuel use and emission rates. This is the same as Figure 2-1 in the main text and is given here for completeness.



(a) Fuel Use Rates

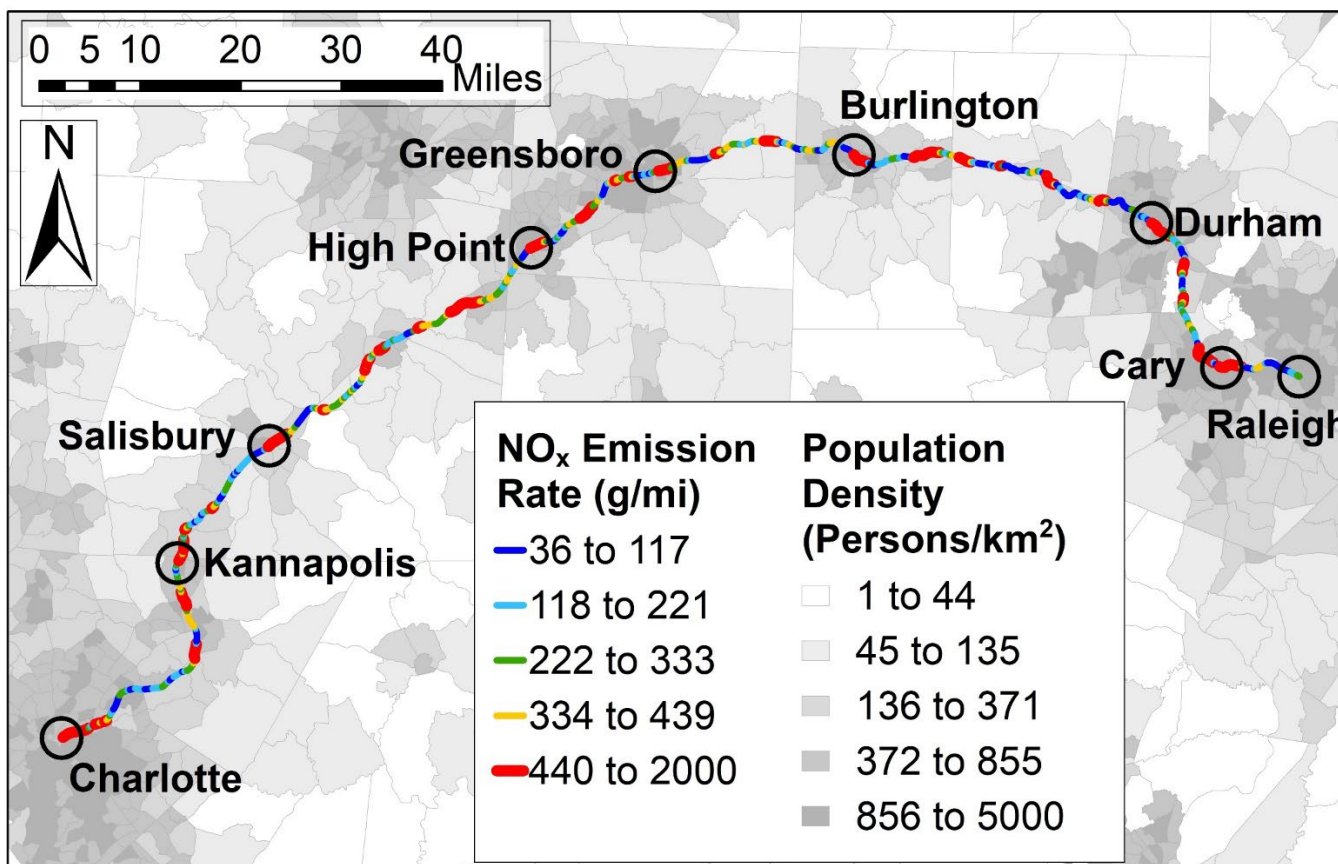
Figure A-11. Segment-Average Fuel Use and Emission Rates For The Piedmont Passenger Rail Service Between Raleigh, NC And Charlotte, NC In The Eastbound Direction Based On 14 One-Way Trips: (a) Fuel Use Rate; (b) NO_x Emission Rate; And (c) PM Emission Rate.

The map depicts the US 2010 census tract-based population density.

Fuel use rate, emission rates, and population density are divided into five 20th percentile groups. The groups are colored from cool blues indicating low values to warm red indicating high values. NO_x emission rates are reported as the equivalent of NO₂ emission rates.

Figure A-11 Continued on Next Page.

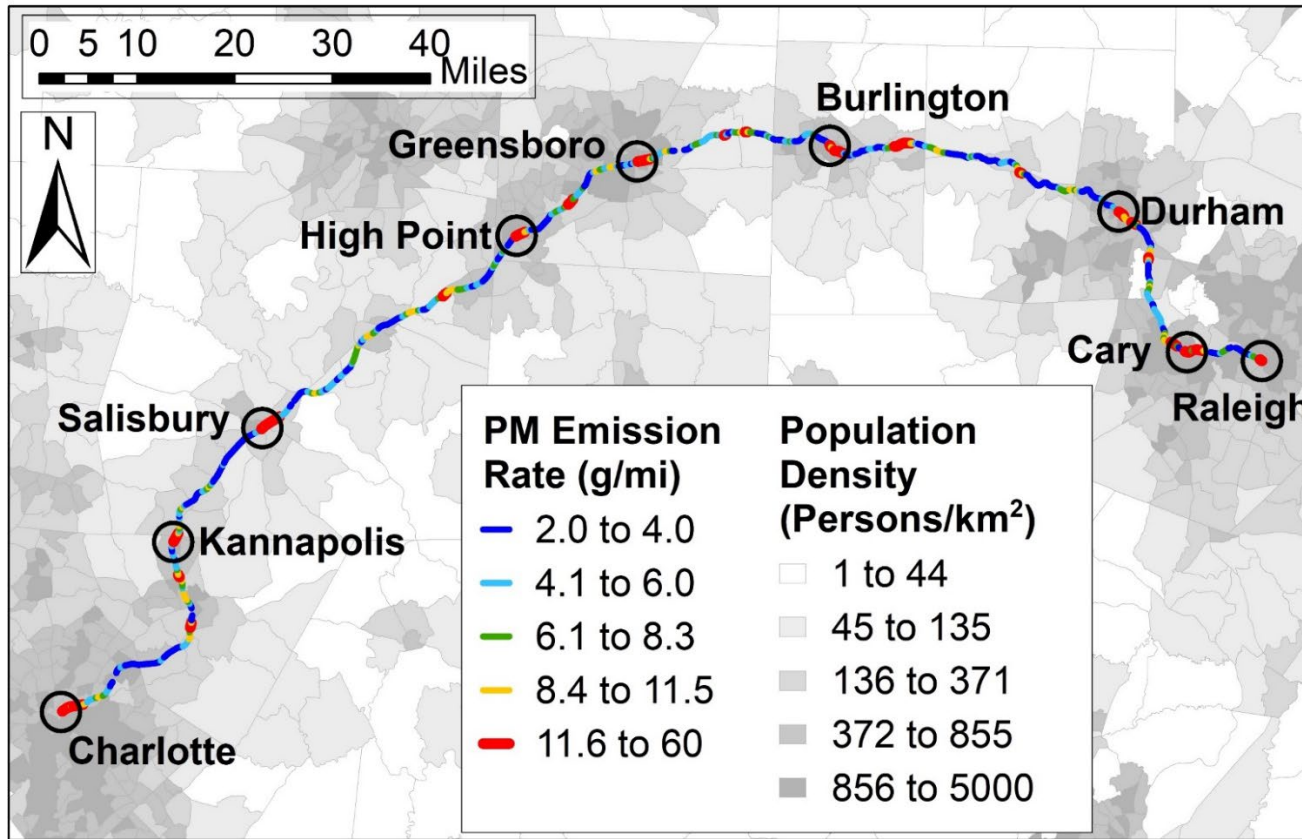
Figure A-11 Continued From Previous Page.



(b) NO_x Emission Rates

Figure A-11 Continued on Next Page.

Figure A-11 Continued From Previous Page.



(c) PM Emission Rates

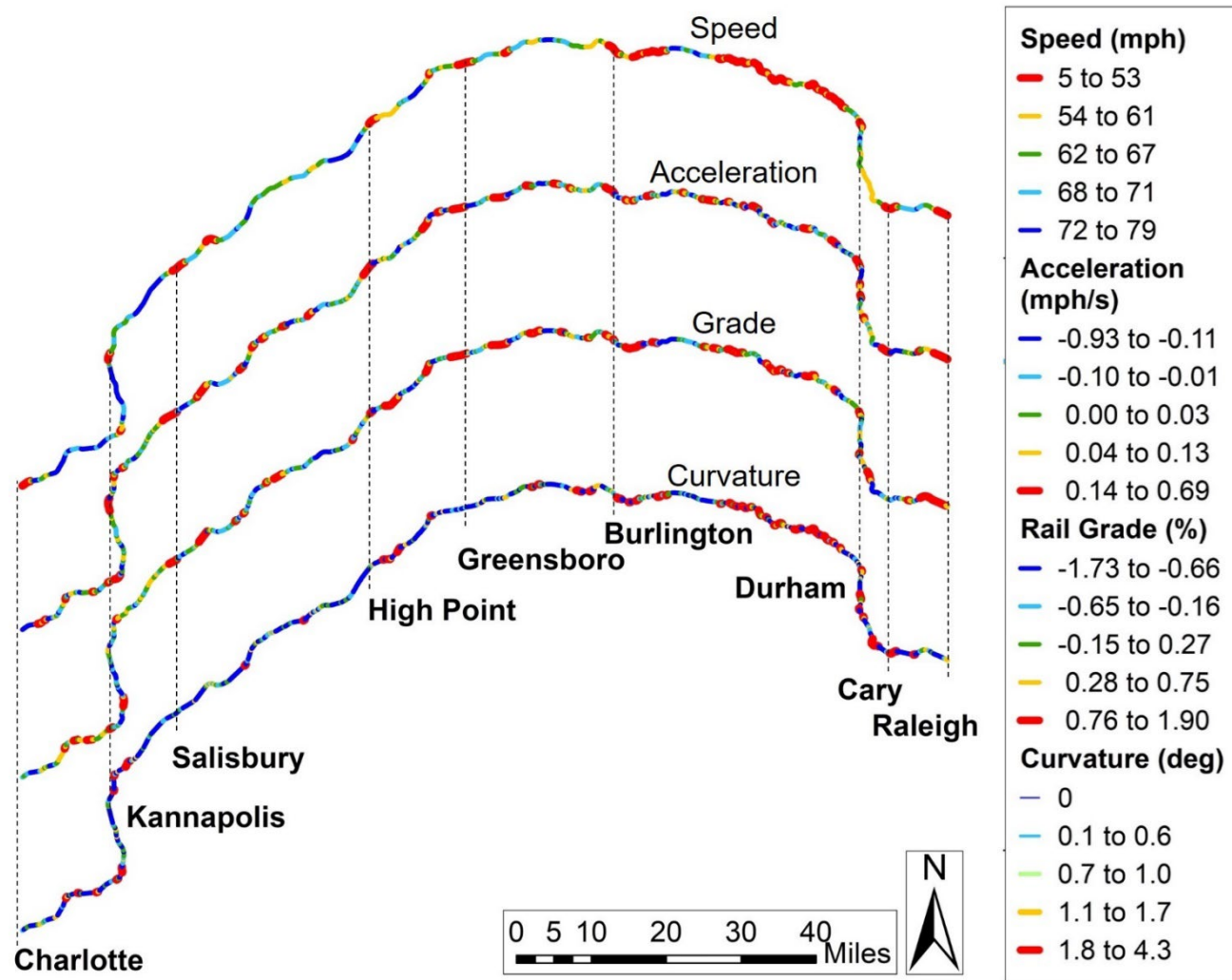
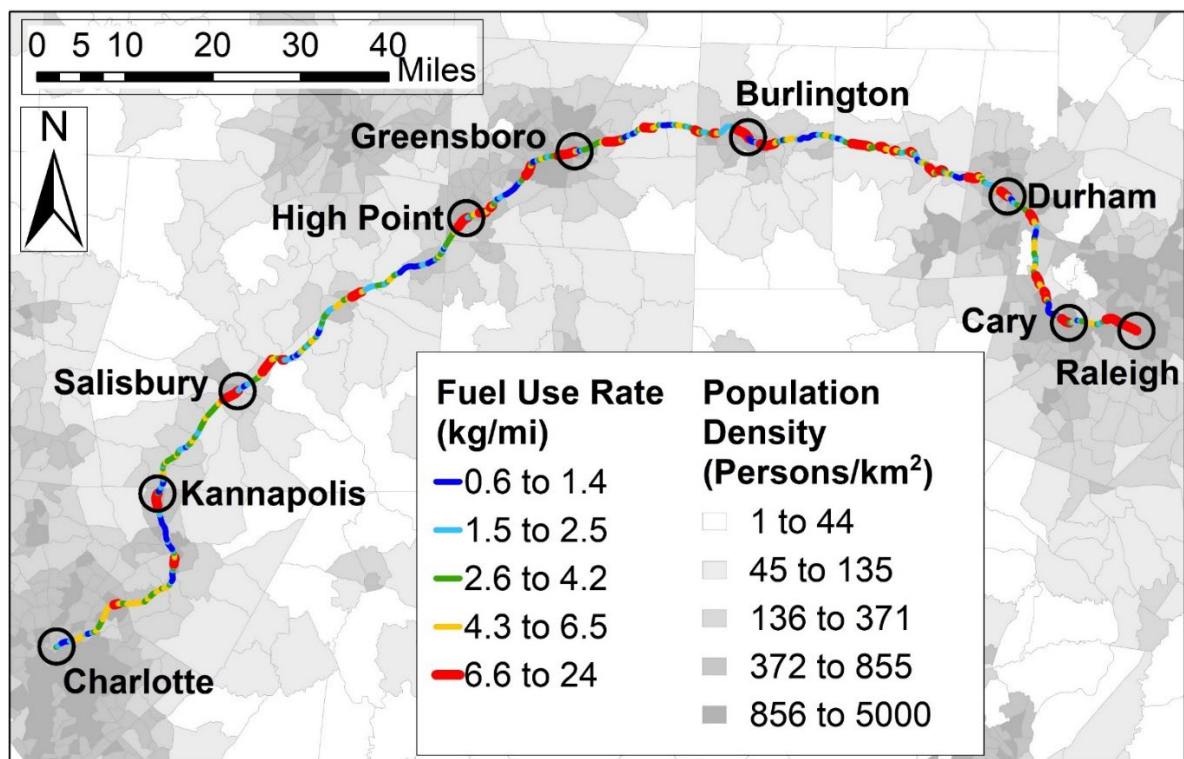


Figure A-12. Segment-Average Speed, Acceleration, Grade, and Curvature for the Piedmont Passenger Rail Service between Raleigh, NC and Charlotte, NC in the Westbound Direction Based on 21 One-Way Trips.

Segment-average activity are divided in five 20th percentile groups. The groups are colored from cool blues to warm red. The values in blue are expected to likely result in lower fuel use and emission rates, whereas the values in red are expected to result in higher fuel use and emission rates.



(a) Fuel Use Rates

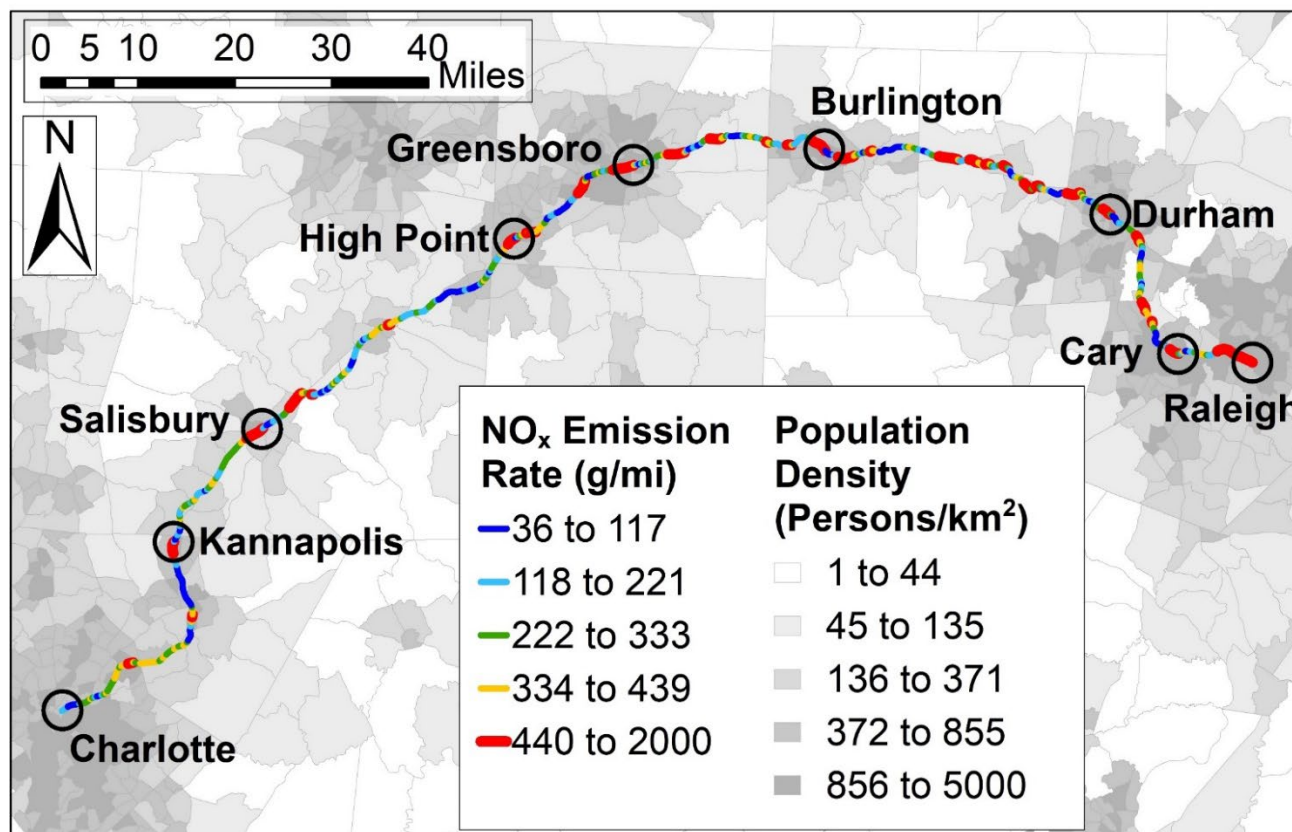
Figure A-13. Segment-Average fuel use and emission rates for the Piedmont passenger rail service between Raleigh, NC and Charlotte, NC in the westbound direction based on 21 one-way trips: (a) Fuel Use Rates; (b) NO_x Emission Rate; and (c) PM Emission Rate.

The map depicts the US 2010 census tract-based population density.

Fuel use rate, emission rates, and population density are divided in five 20th percentile groups. The groups are colored from cool blues indicating low values to warm red indicating high values. NO_x emission rates are reported as equivalent of NO₂ emission rates.

Figure A-13 Continued on Next Page

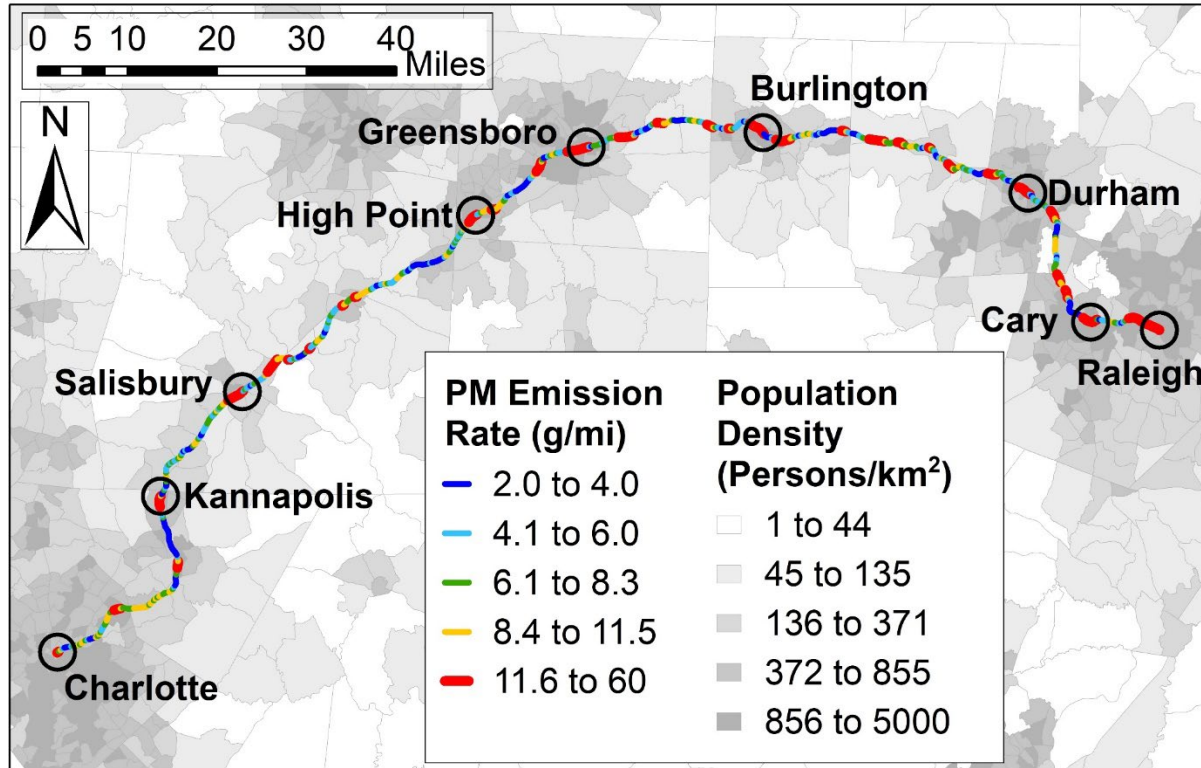
Figure A-13 Continued from Previous Page



(b) NO_x Emission Rates

Figure A-13 Continued on Next Page

Figure A-13 Continued from Previous Page



(c) PM Emission Rates

The number of co-located absolute hotspots and absolute near-hotspots versus consist-specific hotspots based on each travel direction and both directions combined are given in Table A-9. As an example, the sensitivity of the location of hotspots to consists is evaluated based on the comparison among absolute and single locomotive consist-specific fuel hotspots. For fuel hotspots for the single locomotive consist versus absolute fuel hotspots in the eastbound direction:

- 68% of the consist-specific hotspots ($CH_{i,fuel,SLC,e} = 1$) were co-located with absolute hotspots ($AH_{i,fuel,e} = 1$).
- The proportion of all consist-specific hotspots ($CH_{i,fuel,SLC,e} = 1$) that were absolute near-hotspots ($NAH_{i,fuel,e} = 1$) was 14%.
- Based on the two bullets immediately above, 82% of the consist-specific hotspots ($CH_{i,fuel,SLC,e} = 1$) were either absolute hotspots ($AH_{i,fuel,e} = 1$) or absolute near-hotspots ($NAH_{i,fuel,e} = 1$).
- The proportion of all absolute hotspots ($AH_{i,fuel,e} = 1$) that were consist-specific near-hotspots ($NCH_{i,fuel,SLC,e} = 1$) was 22%.
- 90% of the absolute hotspots were either consist-specific hotspots or consist-specific near-hotspots for the single locomotive consist.

Therefore, fuel hotspots in the eastbound direction were weakly sensitive to consist.

In the westbound direction:

- The proportion of all consist-specific hotspots ($CH_{i,fuel,SLC,w} = 1$) co-located with absolute hotspots ($AH_{i,fuel,w} = 1$) and absolute near-hotspots ($NAH_{i,fuel,w} = 1$) was 82% and 11%, respectively.
- Therefore, 93% of the consist-specific hotspots ($CH_{i,fuel,SLC,w} = 1$) were co-located with absolute hotspots ($AH_{i,fuel,w} = 1$) and absolute near-hotspots ($NAH_{i,fuel,w} = 1$).
- The proportion of all absolute hotspots ($AH_{i,fuel,w} = 1$) co-located with consist-specific near-hotspots ($NCH_{i,fuel,SLC,w} = 1$) was 13%.
- 95% of all absolute hotspots ($AH_{i,fuel,w} = 1$) were co-located with consist-specific hotspots ($CH_{i,fuel,SLC,w} = 1$) and consist-specific near-hotspots ($NCH_{i,fuel,SLC,w} = 1$).

Therefore, fuel hotspots in the westbound direction were weakly sensitive to consist. In either direction, the location of absolute fuel hotspots was weakly sensitive to the single locomotive consist-specific hotspots. Similarly, the location of consist-specific fuel hotspots was weakly sensitive to absolute hotspots. Therefore, fuel hotspots in either direction are weakly sensitive to consists.

Table A-9. Number of Co-Located Hotspots and Near-Hotspots for Absolute Hotspots versus Consist-Specific Hotspots based on Each Travel Direction and Both Directions Combined to Quantify the Sensitivity of Location of Hotspots to Consists

Direction	Specie	Absolute and Absolute Near-hotspots ^a	Consist-Specific and Consist-Specific Near-Hotspots ^b							
			$CH_{i,S,DP-P/PC,D}$	$NCH_{i,S,DP-P/PC,D}$	$CH_{i,S,SP-P/PC,D}$	$NCH_{i,S,SP-P/PC,D}$	$CH_{i,S,DP-TC,D}$	$NCH_{i,S,DP-TC,D}$	$CH_{i,S,SLC,D}$	$NCH_{i,S,SLC,D}$
Both	Fuel	$AH_{i,fuel,b}$	92	22	94	16	95	16	96	21
		$NAH_{i,fuel,b}$	23	13	26	13	11	15	22	21
	NO _x	$AH_{i,NOx,b}$	79	27	97	16	82	18	82	22
		$NAH_{i,NOx,b}$	30	5	19	12	18	10	13	13
	PM	$AH_{i,PM,b}$	98	23	87	23	90	19	84	28
		$NAH_{i,PM,b}$	24	11	15	14	15	15	9	9
Eastbound	Fuel	$AH_{i,fuel,e}$	115	18	78	22	104	18	95	30
		$NAH_{i,fuel,e}$	14	27	20	18	17	18	19	13
	NO _x	$AH_{i,NOx,e}$	122	14	83	16	98	20	88	26
		$NAH_{i,NOx,e}$	11	35	15	19	14	13	14	14
	PM	$AH_{i,PM,e}$	113	11	75	23	103	10	85	24
		$NAH_{i,PM,e}$	19	25	22	14	13	13	11	11
Eastbound	Fuel	$AH_{i,fuel,w}$	111	14	106	17	98	21	114	15
		$NAH_{i,fuel,w}$	12	24	21	13	18	25	18	29
	NO _x	$AH_{i,NOx,w}$	111	20	112	17	57	11	107	19
		$NAH_{i,NOx,w}$	13	25	12	19	21	14	26	26
	PM	$AH_{i,PM,w}$	111	17	93	25	99	17	96	23
		$NAH_{i,PM,w}$	12	18	20	11	22	22	17	17

^a Absolute Hotspot for i^{th} segment for species S in direction D ($AH_{i,S,D}$) is defined as the segment in the top 20th percentile rates based on all trips for all consists; Absolute Near-Hotspot for i^{th} segment for species S in direction D ($NAH_{i,S,D}$) is defined as the segment in the top 70th percentile rates excluding absolute hotspots. S : index for species = fuel for fuel use rate, = NO_x for NO_x emission rate, = PM for PM emission rate; D : index for direction = e for eastbound, = w for westbound, and = b for both directions combined; i : index for segment, $i \in [1, 2, 3, \dots, 692]$.

^b Consist-Specific Hotspot for i^{th} segment for species S and consist C in direction D ($CH_{i,S,C,D}$) is defined as the segment in the top 20th percentile rates based on all trips for a given consist; Consist-Specific Near-Hotspot for i^{th} segment for species S and consist C in direction D ($NCH_{i,S,C,D}$) is defined as the segment in the top 70th percentile rates excluding consist-specific hotspots. Measured consists include single locomotive consist (SLC), double-powered tandem consist (DP-TC), double-powered push/pull consist (DP-P/PC), and single-powered push/pull consist (SP-P/PC).

Similar proportions of co-located hotspots and near-hotspots were measured for other species in each direction. Similar results were obtained for consist-specific hotspots, for other consists, versus absolute hotspots. Other consists included double-powered tandem, double-powered push/pull, and single-powered push/pull. Therefore, the location of the hotspots in a given travel direction was weakly sensitive to the choice of consists. Hotspots and near-hotspots identified based on one consist accounted for about 80% to 90% of the hotspots for each of the other consists. Therefore, hotspots identified based on one consist were typically hotspots or near-hotspots for other consists.

A.11.1 Relationship among variables

To understand the relationship among segment-average speed, acceleration, grade, curvature, FUERs, and population density, Pearson's and Spearman's correlation coefficients among these were estimated. Pearson's and Spearman's correlation coefficient among segment-average speed, acceleration, grade, curvature, FUERs, and population density are presented in Table A-10 and Table A-11, respectively. Pearson's correlation coefficients among a given pair of variables, except for FUERs versus population density were within ± 0.05 of each other for eastbound versus westbound travel direction. Based on their absolute value, correlations lower than 0.60 are inferred to be weak, between 0.61 and 0.75 are inferred to be moderate, and between 0.76 and 1.0 are inferred to be strong. Correlations with absolute value less than 0.10 were typically found to be statistically insignificant. Spearman's correlation coefficients were typically within ± 0.05 of the Pearson's correlation coefficient between the same pair of variables. Because the Spearman's correlation coefficient were comparable to Spearman's, only results for Pearson's correlation coefficient are discussed and interpreted.

Speed was uncorrelated with acceleration and was negatively correlated with grade, curvature, FUERs, and population density. Segment-average acceleration varied between -0.99 mph/s and 0.68 mph/s. An example plot of segment-average acceleration versus speed for one one-way trip each in eastbound and westbound directions for single locomotive consist is illustrated in Figure A-14. The plot is oval-shaped with the largest magnitude accelerations and decelerations observed near mid-speeds of 40 mph. The maximum observed values of acceleration were lower at speeds less than 10 mph or greater than 50 mph compared to acceleration at speeds between 10 mph and 50 mph.

An example plot of segment-average curvature versus speed and grade for one one-way trip each in eastbound and westbound directions for single locomotive consist is illustrated in Figure A-15. Trains typically operate at lower speeds on curves and positive grades than on straight and level track segments. For curves > 2.5 degrees, train speed was < 50 mph. For grades $> 1.5\%$, speed was < 60 mph. Speeds > 60 mph were measured for curves < 2.5 degree and grade $< 1.5\%$.

Instantaneous mass per time-based FUERs are higher at higher speeds, but the distance traveled is also greater. Therefore, mass per distance-based segment-run average FUERs were lower at higher speeds. The population density near stations was on average higher than at other locations.

Table A-10. Pearson’s Correlation Coefficient among Segment-Average Speed, Acceleration, Grade, Curvature, Fuel Use Rate, NO_x and PM Emission Rates, and Population Density Based On 692 Segments In Each Travel Direction.

Variable	Direction ^a	Acceleration (mph/s) ^c	Grade (%) ^d	Curvature (deg) ^e	Fuel Use Rate (g/mi) ^f	NO _x Emission Rate (g/mi) ^f	PM Emission Rate (g/mi) ^f	Population Density (persons/km ²)
Speed (mph) ^b	Eastbound	0.01	-0.05	-0.29	-0.35	-0.36	-0.53	-0.30
	Westbound	-0.01	-0.19	-0.27	-0.48	-0.48	-0.57	-0.31
Acceleration (mph/s) ^c	Eastbound		0.42	0.04	0.57 (0.82)	0.57 (0.81)	0.40 (0.76)	-0.05
	Westbound		0.42	-0.06	0.61 (0.83)	0.58 (0.82)	0.43 (0.77)	0.04
Grade (%) ^d	Eastbound			0.02	0.66 (0.71)	0.68 (0.77)	0.44 (0.71)	-0.13
	Westbound			-0.02	0.71 (0.76)	0.72 (0.79)	0.52 (0.75)	0.13
Curvature (deg) ^e	Eastbound				-0.05	-0.03	-0.04	-0.01
	Westbound				-0.06	-0.05	-0.06	-0.01
Fuel Use Rate (g/mi) ^f	Eastbound					0.99	0.90	0.10
	Westbound					0.99	0.91	0.29
NO _x Emission Rate (g/mi) ^f	Eastbound						0.89	0.08
	Westbound						0.90	0.26
PM Emission Rate (g/mi) ^f	Eastbound							0.17
	Westbound							0.31

^a Direction: Eastbound direction from Charlotte, NC to Raleigh, NC. Westbound direction from Raleigh, NC to Charlotte, NC.

^b Speed: Average speed based on all one-way trips measured for a given segment in the given direction.

^c Acceleration: Average acceleration based on all one-way trips measured for a given segment in the given direction.

^d Grade: Segment-average grade in the given travel direction estimated based on 160 GPS measurements.

^e Curvature: Segment-average curvature estimated based on 160 GPS measurements.

^f Average rates estimated as average rates for all one-way trips measured in a given travel direction

^g Population Density: Population density for the given track segment was estimated as the average population density of all US 2010 census tracts in which the segment was located.

Statistically significant correlations are highlighted in bold.

Numbers in parentheses correspond to correlation coefficients for segment-runs that had positive values of the variable on the left.

Table A-11. Spearman’s Correlation Coefficient among Segment-Average Speed, Acceleration, Grade, Curvature, Fuel Use Rate, NO_x and PM Emission Rates, And Population Density Based on 692 Segments In Each Travel Direction.

Variable	Direction ^a	Acceleration (mph/s) ^c	Grade (%) ^d	Curvature (deg) ^e	Fuel Use Rate (g/mi) ^f	NO _x Emission Rate (g/mi) ^f	PM Emission Rate (g/mi) ^f	Population Density (persons/km ²) ^g
Speed (mph) ^b	Eastbound	-0.07	-0.06	-0.35	-0.31	-0.13	-0.27	-0.21
	Westbound	-0.04	-0.22	-0.31	-0.43	-0.30	-0.35	-0.22
Acceleration (mph/s) ^c	Eastbound		0.38	0.02	0.56	0.64	0.59	-0.01
	Westbound		0.38	-0.12	0.62	0.64	0.62	0.06
Grade (%) ^d	Eastbound			0.01	0.63	0.76	0.63	-0.08
	Westbound			-0.01	0.70	0.79	0.70	0.08
Curvature (deg) ^e	Eastbound				-0.05	-0.05	-0.05	0.03
	Westbound				-0.07	-0.06	-0.06	0.03
Fuel Use Rate (g/mi) ^f	Eastbound					0.99	0.91	0.11
	Westbound					0.98	0.89	0.31
NO _x Emission Rate (g/mi) ^f	Eastbound						0.91	0.02
	Westbound						0.92	0.15
PM Emission Rate (g/mi) ^f	Eastbound							0.08
	Westbound							0.18

^a Direction: Eastbound direction from Charlotte, NC to Raleigh, NC. Westbound direction from Raleigh, NC to Charlotte, NC.

^b Speed: Average speed based on all one-way trips measured for a given segment in the given direction.

^c Acceleration: Average acceleration based on all one-way trips measured for a given segment in the given direction.

^d Grade: Segment-average grade in the given travel direction estimated based on 160 GPS measurements.

^e Curvature: Segment-average curvature estimated based on 160 GPS measurements.

^f Average rates estimated as average rates for all one-way trips measured in a given travel direction

^g Population Density: Population density for the given track segment was estimated as the average population density of all US 2010 census tracts in which the segment was located.

Statistically significant correlations are highlighted in bold.

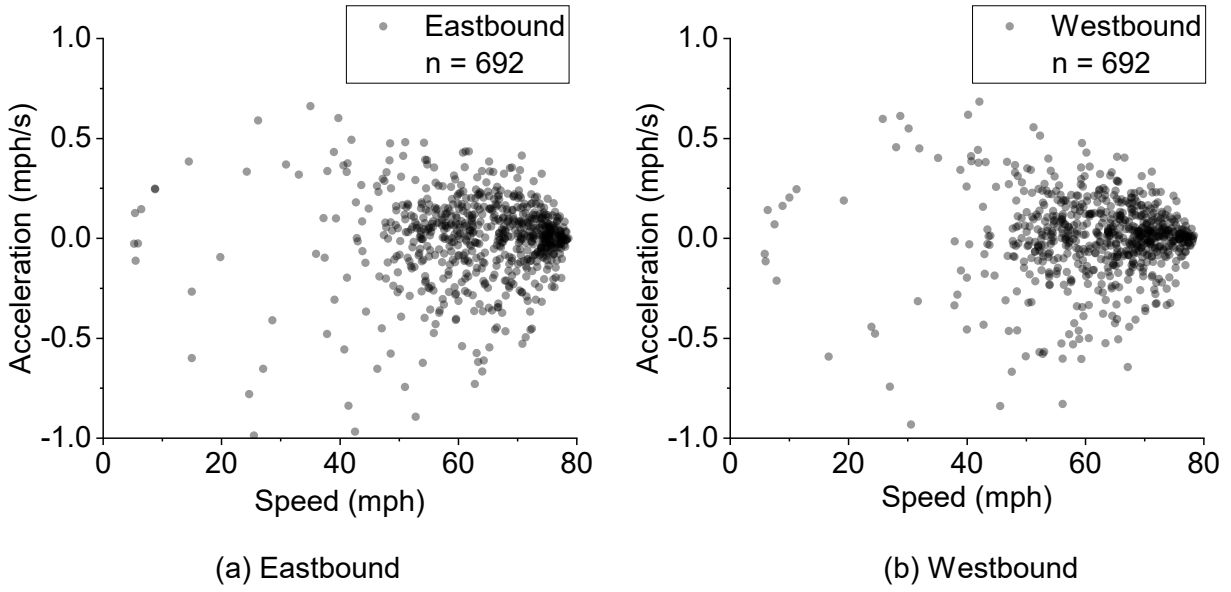


Figure A-14. Example Segment-Average Acceleration Versus Speed Based on One One-Way Trip Each Travel Direction for Single Locomotive Consist: (a) Eastbound; and (b) Westbound.

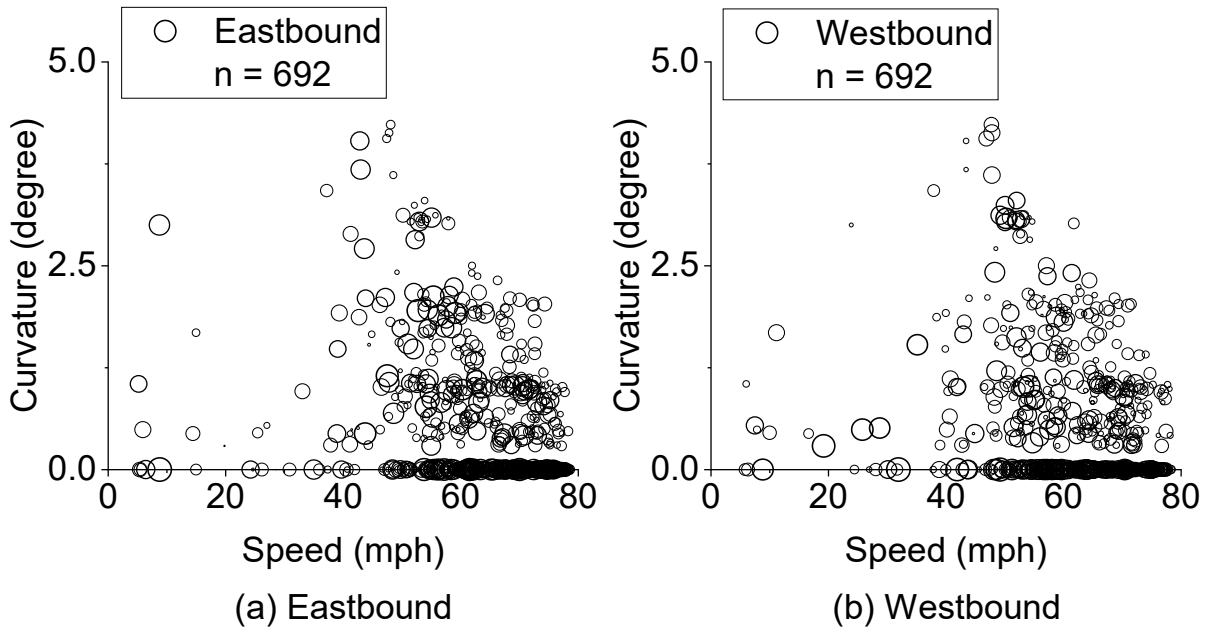


Figure A-15. Example Segment-Average Curvature Versus Speed and Grade Based on One One-Way Trip Each Travel Direction for Single Locomotive Consist: (a) Eastbound; and (b) Westbound.

Symbol size is indicative of grade. The smallest size indicates the route minimum grade of -1.9% and the largest size indicates the route maximum grade of 1.9%.

Acceleration was moderately positively correlated with grade and FUERs, and uncorrelated with curvature and population density. Positive correlation between acceleration and grade indicates that trains typically accelerated during ascent and decelerated during descent. For segment-runs that had negative accelerations, FUERs were approximately constant. For segment-runs that had positive accelerations, acceleration was strongly correlated with FUERs. Therefore, overall, acceleration was weakly correlated with FUERs.

Grade was uncorrelated with curvature and moderately positively correlated with FUERs. Similar to acceleration, correlation was higher for segment-runs with positive grades than for segment-runs with positive and negative grades. Grade was weakly correlated with population density. Curvature was uncorrelated with FUERs and population density. Therefore, high FUERs were typically associated with low train speeds, positive acceleration and positive grades.

Segment-run average fuel use rate and emission rates of NO_x and PM had strong correlations among them. This indicates that locations with high segment-average rates of multiple species typically coexist. Therefore, any operational or infrastructural changes designed for intervening to reduce the rate of one specie will also reduce other species. FUERs were weakly positively correlated with population density. However, at stations and the adjacent five upstream and downstream segments, FUERs and population density were each among the highest of the observed values.

Exposure to a pollutant is directly proportional to emission rates and population density. Although we do not model the ambient concentration, ambient concentration is a linear function of emission rate. Thus, emission rate is a surrogate for ambient concentration, and the product of emission rate with population density is a surrogate indicator of exposure. Therefore, the product of emission rates and population density is used here as a pollutant impact index:

$$I_{p,i} = R_{p,i} \times P_i \tag{A-10}$$

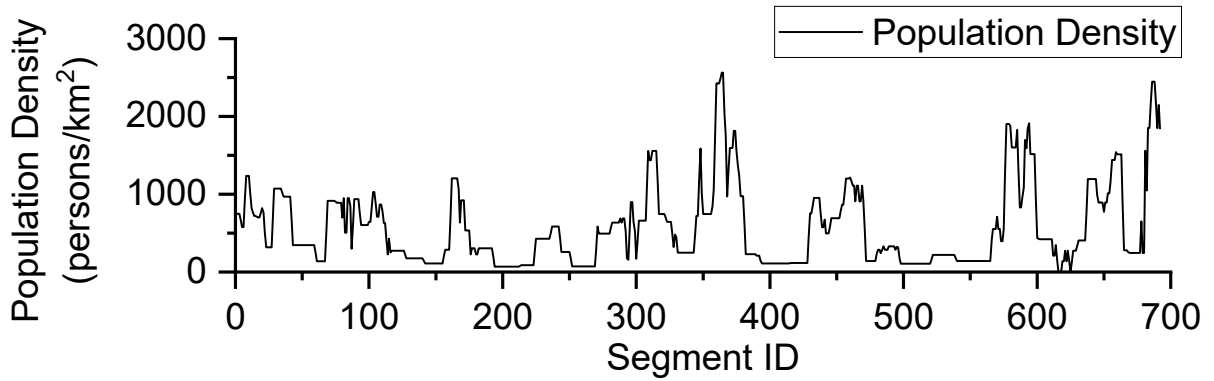
Where,

- $I_{p,i}$ = Impact index of pollutant p in i^{th} segment ($g\text{-persons}/km^3$)
- $R_{p,i}$ = Emission rate of pollutant p in i^{th} segment (g/km)
- P_i = population density near the i^{th} segment ($persons/km^2$)

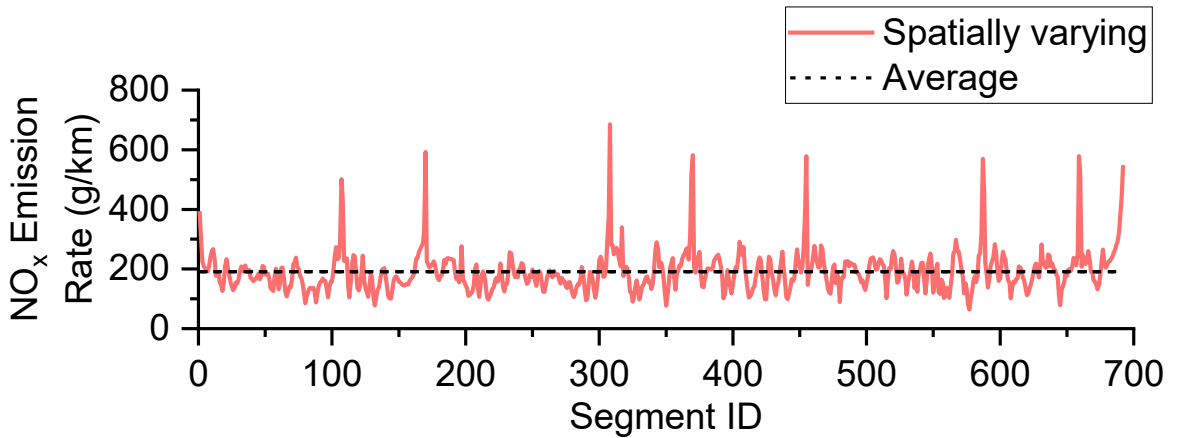
Both the emission rate and population density vary with location along the route. Thus, both are quantified for each segment of the route. However, to assess the impact of spatial variability in emission rates as a contributing factor to impact hotspots, sensitivity analysis was conducted. In the sensitivity analysis, one case was quantified based on spatial variability in emission rates and population density, and a sensitivity case was quantified based on a route average emission rate and spatially varying population density. The difference between the two cases, for a given segment, provides insight regarding whether impact hotspots are mostly related to variation in emission rates versus variation in population density.

Plots of population density, segment-average emission rates, and pollutant impact index in both travel directions combined versus segment ID are given in Figures A-16 and A-17 for NO_x and PM emission rates, respectively. The population density, given in Figure A-16(a), varied along the route. The highest population density was typically observed at S, NSA, and NSD segments. Likewise, emission rates given in Figures A-16(b) and A-17(b), varied along the route. The highest emission rates, which averaged at least twice the route average, were at S, NSA, and NSD segments. Consequently, the pollutant impact index for the spatially varying case was 105% or higher versus average case at S, NSA, and NSD segments. On average for the entire route, the pollutant impact index for the spatially varying case was 11% and 18% higher versus average case for NO_x and PM emissions, respectively. Therefore, using route average emission rates as opposed to spatially varying emission rates led to underestimation of the impact of emission rates on exposure estimates, especially near densely populated locations. A parity comparison of pollutant emissions impact index is presented in Figure A-18 also shows that the impact index based on average emission rates was underestimated.

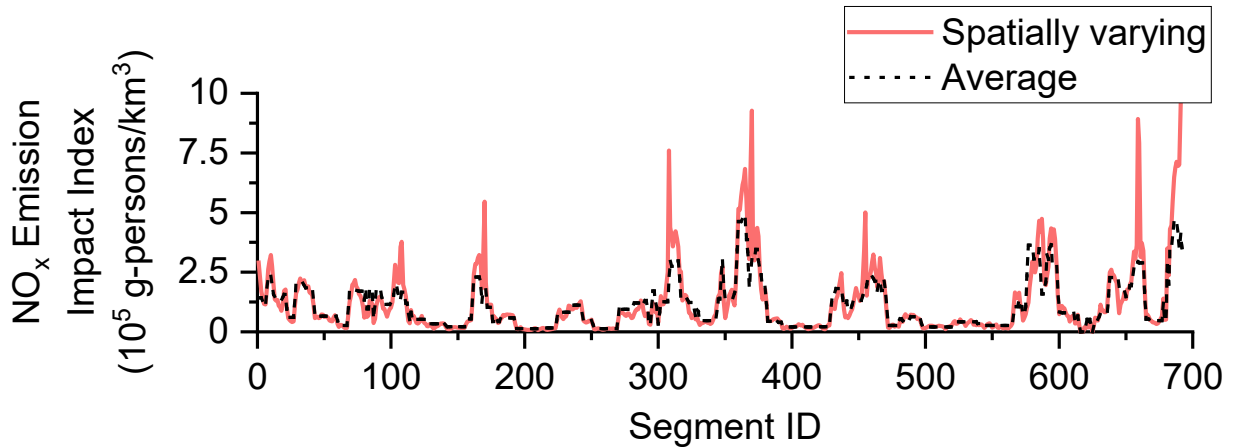
To quantify if the identification of top impact hotspots is sensitive to spatially varying versus average emissions rates, a parity plot of rank of segments based on impact index for both cases are given in Figure A-19. For NO_x and PM, the parity slope was 1.03 and 1.02 respectively. Similar to emission rates, segments with impact index in the top 20th percentile were classified as impact hotspots and the remaining segments were classified as impact non-hotspots. This was done for spatially varying and average emissions rates cases. The classification of the same segments based on these two cases were evaluated in terms of true positives, true negatives, false positives, and false negatives to quantify accuracy and precision for impact hotspot identification based on average rates. The accuracy was 92% and 91% for NO_x and PM emissions, respectively. The precision was 81% and 78% for NO_x and PM emissions, respectively. Thus, average emission rates could be used to identify most of the impact hotspots. However, spatially varying emission rates are needed to accurately quantify the intensity of impact hotspots.



(a) Population Density

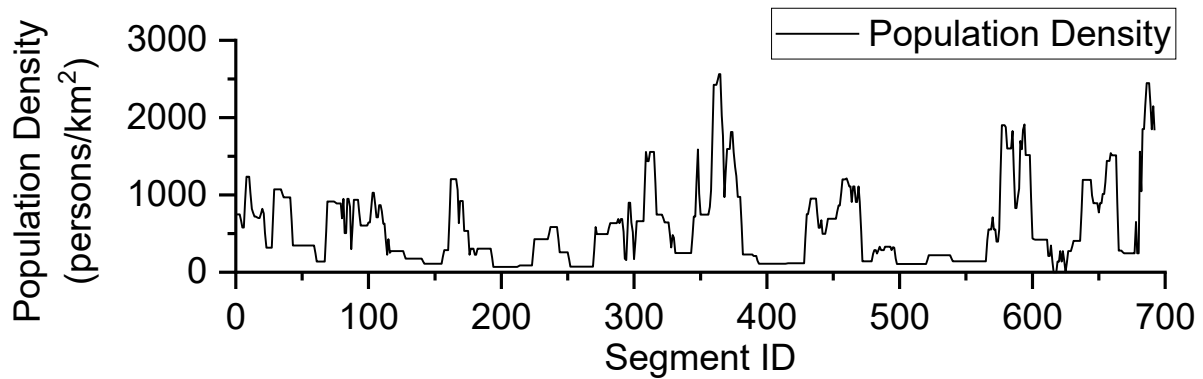


(b) NO_x Emission Rate

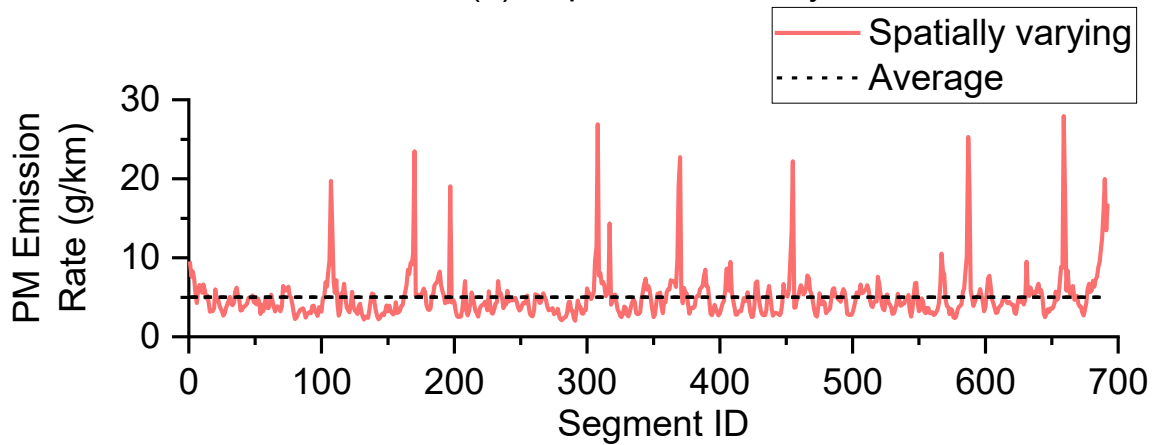


(c) NO_x Emission Impact Index

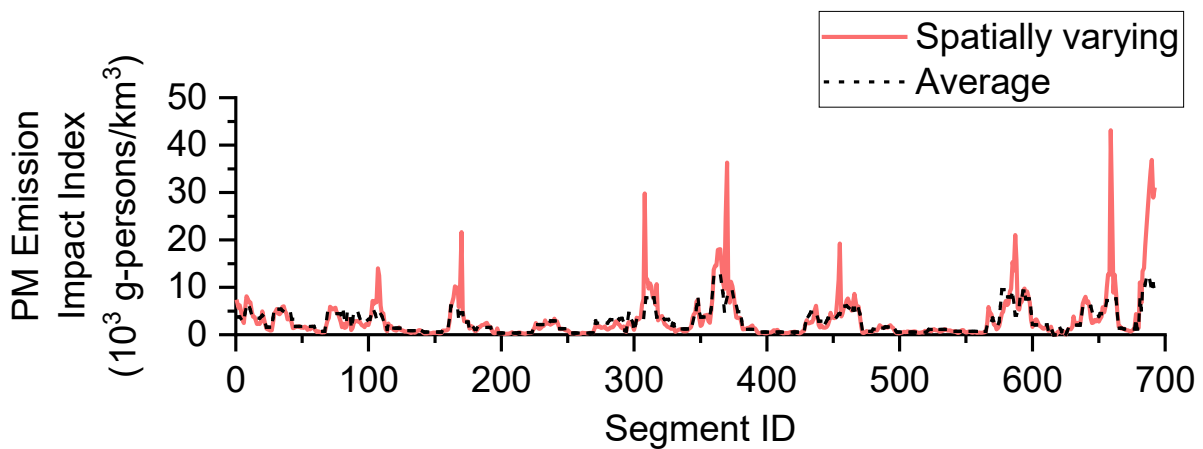
Figure A-16. Segment-Average Data for Spatially Varying and Average Rates for the Piedmont Passenger Rail Service between Raleigh, NC and Charlotte, NC in Both Travel Directions Based on 35 One-Way Trips: (a) 2010 CensA-Tract based Population Density; (b) NO_x Emission Rate; and (c) NO_x Emission Impact Index.



(a) Population Density



(b) PM Emission Rate



(c) PM Emission Impact Index

Figure A-17. Segment-Average Data for Spatially Varying and Average Rates for the Piedmont Passenger Rail Service between Raleigh, NC and Charlotte, NC in Both Travel Directions Based on 35 One-Way Trips: (a) 2010 CensA-Tract based Population Density; (b) PM Emission Rate; and (c) PM Emission Impact Index.

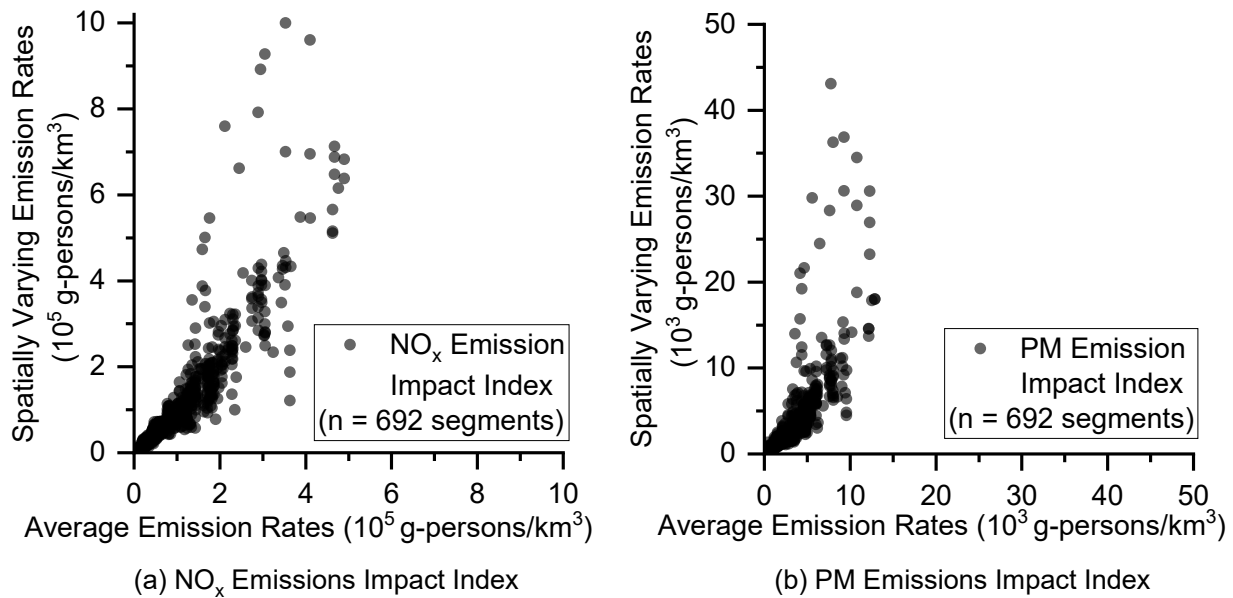


Figure A-18. Segment-Average Impact Index for Spatially Varying and Average Rates for the Piedmont Passenger Rail Service between Raleigh, NC and Charlotte, NC in Both Travel Directions Based on 35 One-Way Trips for: (a) NO_x Emissions; and (b) PM Emissions.

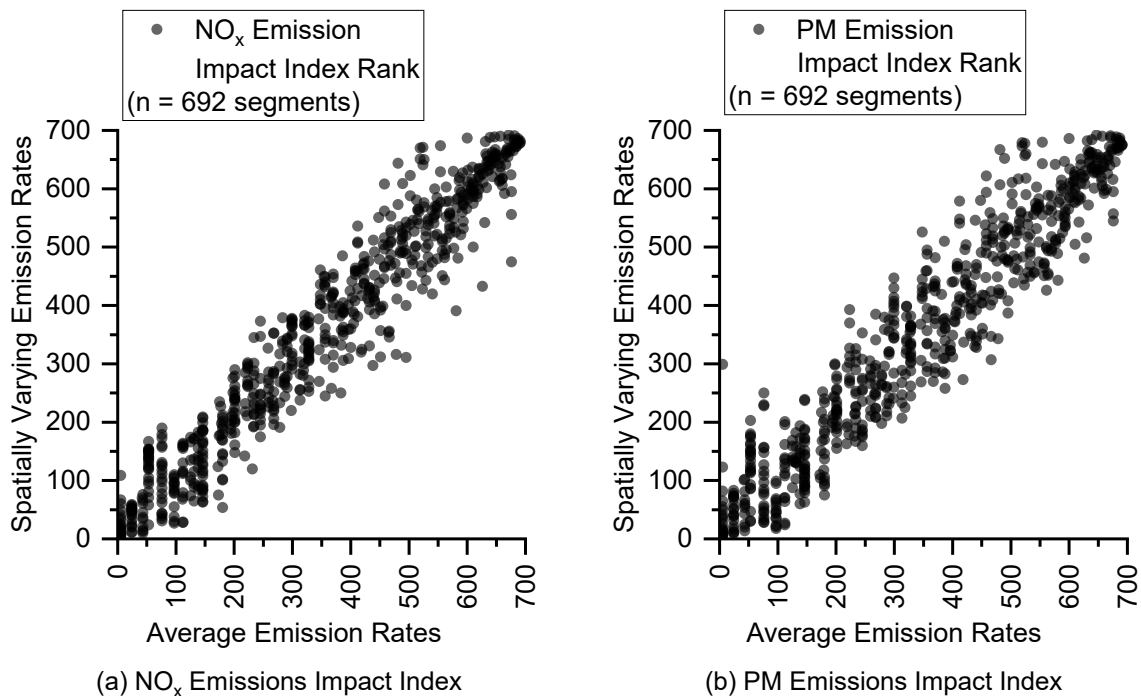


Figure A-19. Rank of Segment-Average Impact Index for Spatially Varying and Average Rates for the Piedmont Passenger Rail Service between Raleigh, NC and Charlotte, NC in Both Travel Directions Based on 35 One-Way Trips for: (a) NO_x Emissions; and (b) PM Emissions.

A.11.2 Absolute hotspots by direction

As discussed in Section 10, absolute hotspots are directional. Therefore, the severity of the hotspots in one direction may be offset by lower emissions in the other direction. To quantify the effect of both directions combined, a comparison of absolute hotspots was made for each direction and both directions combined. For a given species, 45% to 53% of the absolute hotspots in a given direction were also hotspots for both directions combined. Conversely, 49% to 61% of the absolute hotspots were non-hotspots in both directions. Therefore, absolute hotspots in one direction may not always be mitigated in the opposite direction. The variation of NO_x emission rates and location of absolute hotspots for each direction and both directions combined for an example case near the station Salisbury, NC is given in Figure A-20. Each of the station segments were always absolute hotspots in either travel direction and both directions combined. Downstream of a station segment, trains accelerated rapidly and FUERs were among the highest among all segments. However, in the opposite direction for the same segments, trains decelerated when approaching the stations and FUERs were the lowest among all segments. The cumulative effect of both directions combined was that the average emission rates were typically higher than other segments. Thus, near stations, hotspots in one direction were not mitigated by non-hotspots in the opposite direction. Thus, absolute hotspots based on both directions combined were located on either side of station segments. On the contrary, for most intermediate segments, hotspots in one direction were mitigated by non-hotspots in the opposite direction because the emission rates for such hotspots were not as high as near stations.

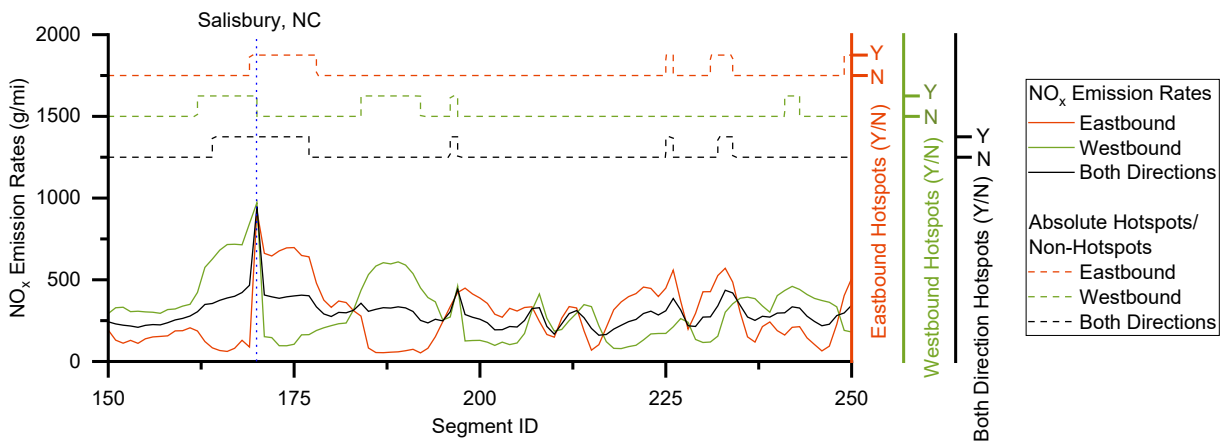


Figure A-20. Variation of NO_x Emission Rates and Location of Absolute Hotspots for Each Direction and Both Directions Combined for an Example Case Near the Station Salisbury, NC.

A.11.3 Segment-run average rates binned by explanatory variables

Ranges of variables resulting in highest and lowest segment-average FUERs are discussed. Variation of segment-run average FUERs with explanatory variables is also discussed.

To identify the values of variables associated with the highest and lowest segment-average rates, the five segments with the top and bottom fuel use rates and emission rates of NO_x and PM, and their corresponding segment-average variables, are presented in Table A-12. The segments with the top five fuel use and emission rates of NO_x and PM were all station segments. These segments were associated with average speeds typically <10 mph, average acceleration >0.13 mph/s, grade >0.23%. The curvature was 0 degrees for four of these segments and 3 degrees for one of these segments. For the segments with the lowest rates, average speeds were typically >74 mph, acceleration was negative or close to zero, grades were <-0.78 and curvature was <1 degree. Therefore, for this small selection of segments, speeds typically <10 mph, positive acceleration and positive grade led to high FUERs. Conversely, high speeds, negative acceleration and negative grade resulted in low FUERs. Curvature had a negligible impact.

Table A-12. Track Segments with the Top and Bottom Five Average Fuel Use Rates and Emission Rates of NO_x and PM and Corresponding Segment-Average Speed, Acceleration, Grade and Curvature based on Both Travel Directions.

(a) Top 5 Segment-Average Rates

Species	Segment ID	Direction	Rate (g/mi)	Speed (mph)	Acceleration (mph/s)	Grade (%)	Curvature (deg)
Fuel	370	Eastbound	24465	5.4	0.13	0.34	0.0
	660	Eastbound	23005	8.7	0.25	1.16	3.0
	587	Westbound	21246	8.8	0.16	1.49	0.0
	108	Eastbound	20406	8.8	0.25	1.73	0.0
	588	Eastbound	19259	6.4	0.15	0.89	0.0
NO _x	370	Eastbound	1738	5.4	0.13	0.34	0.0
	660	Eastbound	1667	8.7	0.25	1.16	3.0
	108	Eastbound	1425	8.8	0.25	1.73	0.0
	587	Westbound	1391	8.8	0.16	1.49	0.0
	588	Eastbound	1389	6.4	0.15	0.89	0.0
PM	370	Eastbound	67.5	5.4	0.13	0.34	0.0
	587	Westbound	59.5	8.8	0.16	1.49	0.0
	659	Westbound	57.1	6.3	0.14	0.23	0.0
	660	Eastbound	54.8	8.7	0.25	1.16	3.0
	588	Eastbound	51.3	6.4	0.15	0.89	0.0

Table A-12 Continued on Next Page.

Table A-12 Continued From Previous Page.

(b) Bottom 5 Segment-Average Rates

Species	Segment ID	Direction	Rate (g/mi)	Speed (mph)	Acceleration (mph/s)	Grade (%)	Curvature (deg)
Fuel	680	Eastbound	617	74.4	0.00	-0.79	1.0
	416	Westbound	620	77.6	-0.03	-0.78	0.0
	334	Westbound	632	76.7	-0.02	-0.78	1.0
	92	Westbound	638	78.0	-0.02	-1.05	0.0
	93	Westbound	652	78.1	0.01	-0.95	1.0
NO _x	334	Westbound	38	76.7	-0.02	-0.78	1.0
	680	Eastbound	40	74.4	0.00	-0.79	1.0
	416	Westbound	41	77.6	-0.03	-0.78	0.0
	92	Westbound	41	78.0	-0.02	-1.05	0.0
	89	Westbound	42	75.9	-0.05	-0.55	0.0
PM	388	Eastbound	2.1	76.4	-0.20	-0.89	0.0
	387	Eastbound	2.1	77.3	-0.02	-0.99	0.4
	77	Eastbound	2.1	75.8	-0.24	-1.01	0.9
	76	Eastbound	2.1	77.0	0.01	-1.03	0.7
	30	Eastbound	2.1	77.4	-0.20	-0.87	0.0

For a more comprehensive analysis, cumulative frequency plots of segment-run average speed, acceleration, grade and curvature corresponding to segment-runs in the top and bottom 20th percentile of fuel use rates are given in Figure A-21. The top and bottom 20th percentile segment-runs comprised 4647 runs each. The fuel use rates have a 95 percent frequency range from 6600 g/mile to 13700 g/mile in the top 20% compared to 135 g/mile to 310 g/mile in the bottom 20%. The 95 percent frequency range of NO_x emission rates, for the segments that have the top 20% of fuel use rates, is 317 g/mile to 1010 g/mile, compared to a range of 12.4 g/mile to 37.7 g/mile for segments that have the bottom 20% of fuel use rates. Thus, the NO_x emission rates for segments with high fuel use rates are substantially higher than those for segments with low fuel use rates. Segment-average fuel use and NO_x emission rates have a correlation of 0.99. Thus, segments that have high fuel use rate tend to have high emission rates.

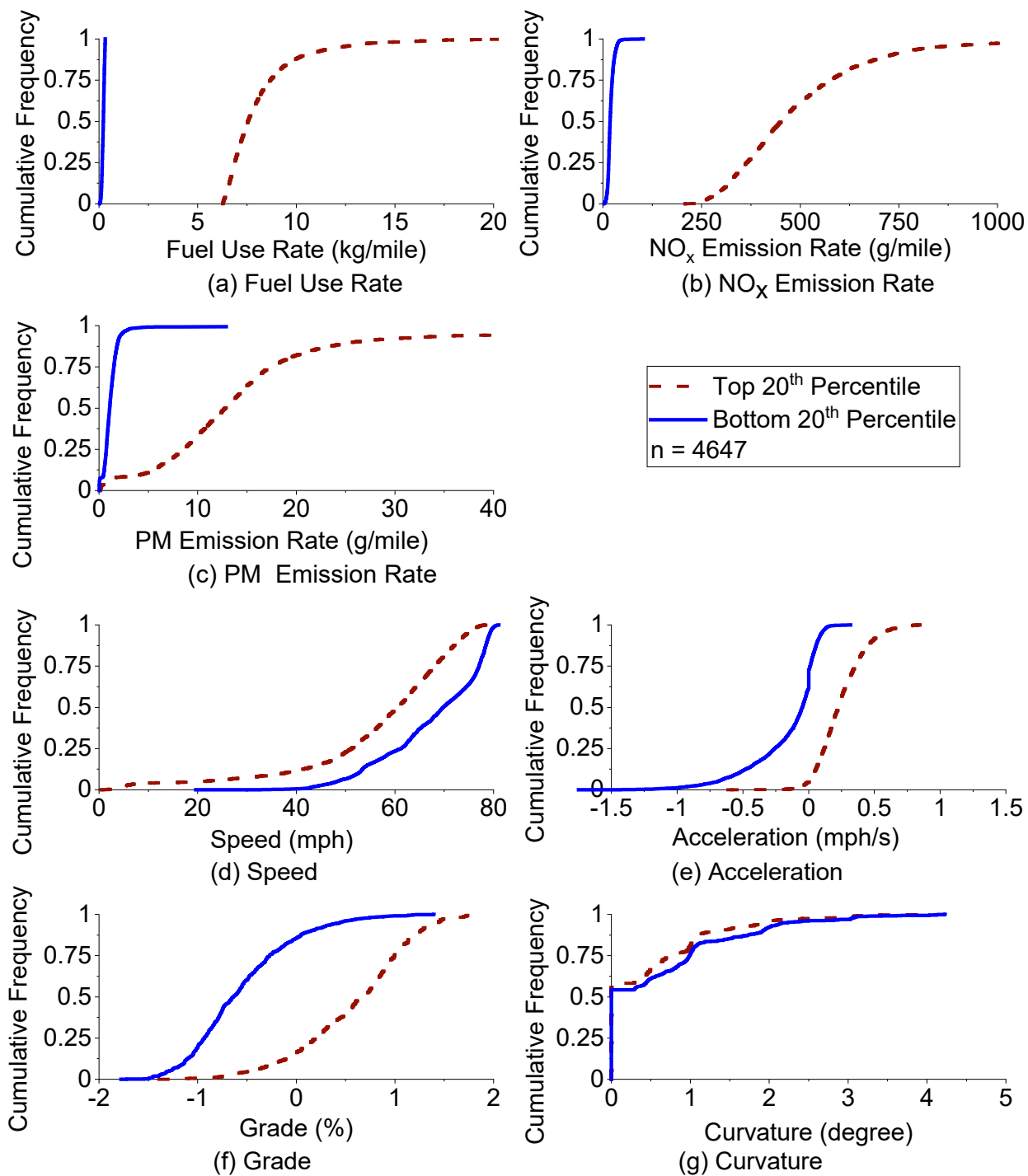


Figure A-21. Cumulative Frequency Plots of Fuel Use Rate, Emission Rates, and Activity Variables for Segment-Runs in the Top and Bottom 20th Percentile Fuel Use Rates Based on Measured All One-Way Trips: (a) Fuel Use Rate; (b) NO_x Emission Rate; (c) PM Emission Rate; (d) Speed; (e) Acceleration; (f) Grade; and (g) Curvature.

The 95 percent frequency range of PM emission rates, for the segments that have the top 20% of fuel use rates, is 5.38 g/mile to 35.63 g/mile, compared to a range of 0.53 g/mile to 2.65 g/mile for segments that have the bottom 20% of fuel use rates. Unlike fuel use rate and NO_x emission rate, there was some overlap of PM emission rates in the top and bottom 20 percent of fuel use rates. The overlap of PM emission rates occurred due to inter-locomotive and inter-consist variability in FUERs. Among the NCDOT locomotives, the relative ranking of locomotives and consists by mass per time-based notch-average fuel use rate and NO_x emission rate was similar to each other. Therefore, locomotives and consists with low fuel use rates also had low NO_x emission rates. However, the relative rank ordering of locomotives and consists for PM emission rates was different than for fuel use rate and NO_x emission rate (Frey and Rastogi, 2019). For example, locomotives NC 1810, NC 1859, NC 1869, and NC 1893 operated in single locomotive consists typically had lower fuel use rate and NO_x emission rate versus other locomotives and consists. However, PM emission rates for these locomotives were approximately twice as high as other locomotives. Therefore, for similar fuel use, these locomotives had higher PM emission rates versus other locomotives. Because of this difference in relative rank-ordering, segment-runs with the lowest fuel use rate were not always the segment-runs with the lowest PM emission rate. Likewise, segment-runs with the highest fuel use rate were not always the segment-runs with the highest PM emission rate. PM emission rates also had lower correlation versus fuel use rate compared to the correlation between NO_x emission rate versus fuel use rate.

The mean and 95 percent confidence interval on the mean for fuel use rates, NO_x and PM emission rates, and values of key activity variables are given in Table A-13, based on segments with the top 20 percent and bottom 20 percent of fuel use rates. The average fuel use rates in the top 20% of segments are nearly 39 times higher than in the bottom 20% of segments and are significantly different. The NO_x and PM emission rates for the segments with high fuel use rate are 25 and 12 times, respectively, larger than for the segments with low fuel use rate. There are significant differences in the mean values of speed, acceleration, grade, and curvature between the two groups of segments, with the top 20% of segments by fuel use having lower average speed, higher mean acceleration, higher mean grade, and lower mean curvature than segments in the bottom 20%. Furthermore, the higher rates are associated with positive acceleration and positive grade, whereas the lower rates are associated with negative acceleration and negative grade. NO_x and PM emission rates had a correlation of 0.90 or higher with the fuel use rate. Because the correlations are high, there is concordance between the top 20 percent of fuel use rates and the top 20 percent of NO_x emission rates, and likewise for fuel use rates versus PM emission rates. For example, 88% of the segment-runs in the top 20 percent of fuel use rate were also in the top 20% of the NO_x emission rate. For the segment-runs in the bottom 20% of fuel use rate, 67% were also in the bottom 20% of the NO_x emission rate. For PM emission rates versus fuel use rates, 85% and 71% of the segment-runs were concordant for the top and bottom 20 percent, respectively.

Table A-13. Summary of Segment-Run Average Fuel Use Rate, Emission Rates, Speed, Acceleration, Grade, and Curvature for Segment-Runs in the Top and Bottom 20th Percentile Segment-Run Average Fuel Use Rate

Percentile	Top 20 th		Bottom 20 th		Statistically Significant Difference of Means
	Mean	95% Confidence Interval	Mean	95% Confidence Interval	
Fuel Use Rate (g/mile)	8169	±59.9	212	±1.8	Yes
NO _x Emission Rate (g/mile)	498	±6.0	20	±0.2	Yes
PM Emission Rate (g/mile)	13.7	±0.39	1.1	±0.02	Yes
Speed (mph)	56.9	±0.46	67.7	±0.30	Yes
Acceleration (mph/s)	0.24	±0.01	-0.15	±0.01	Yes
Grade (%)	0.58	±0.02	-0.56	±0.01	Yes
Curvature (degree)	0.45	±0.02	0.59	±0.02	Yes

The cumulative distributions in Figure A-21 indicate that there is substantial inter-segment variability in activity variables associated with each of the top 20% and bottom 20% of segment-average fuel use rates. For speed, there is considerable overlap, ranging from 20 mph and 78 mph, between the upper and lower fuel use quintiles. However, the distribution of speed for the upper fuel use quintile is skewed toward lower speeds, including speeds below 20 mph. Although there is some overlap between the upper and lower fuel use quintiles in the cumulative distributions of acceleration, the higher fuel use rates are associated with a 93.3 percent frequency of positive accelerations whereas the lower fuel use rates are associated with a 61.2 percent frequency of negative accelerations. The frequency distributions for grade overlap between the two quintiles, but there is 83.9 percent frequency of positive grades for the higher fuel use rates and 85.4 percent frequency of negative grades for the lower fuel use rates. Although there is a significant numerical difference in the mean curvature between the two quintiles, the frequency distributions for curvature are qualitatively similar.

To explain the variation of FUERs, average rates were estimated for various ranges of explanatory variables based on variability among all segment-runs. For this purpose, the data were stratified for each potential explanatory variable, and comparisons were made between combinations of strata. Segment-run average speed, acceleration, and grade were each binned into four quartiles. Segment-runs with 0 degree curvature comprised 56%. Segment-runs with curvature >0 degree but <0.9 degree comprised 21% of all segment-runs. Segment-runs with curvature >0.9 degree comprised 25% of all segment-runs. These curvature values were selected

as cut-points for three curvature bins. The number of such combinations of groups of four variables is 192, based on 4 bins for speed, 4 bins for acceleration, 4 bins for grade, and 3 bins for curvature ($4 \times 4 \times 4 \times 3 = 192$). The cumulative frequency plots for each of these variables and their cutoff values are given in Figure A-22.

Average fuel use and emission rates for the 192 combinations of speed, acceleration, grade, and curvature bins are summarized in Table A-14. The average rates are shaded in colors from blue to red in increasing order. The highest three rates were associated with the same combination of lowest speed quartile, highest acceleration quartile, and highest grade quartile corresponding to rows 46 through 48. Each of these rows belonged to a different curvature bin.

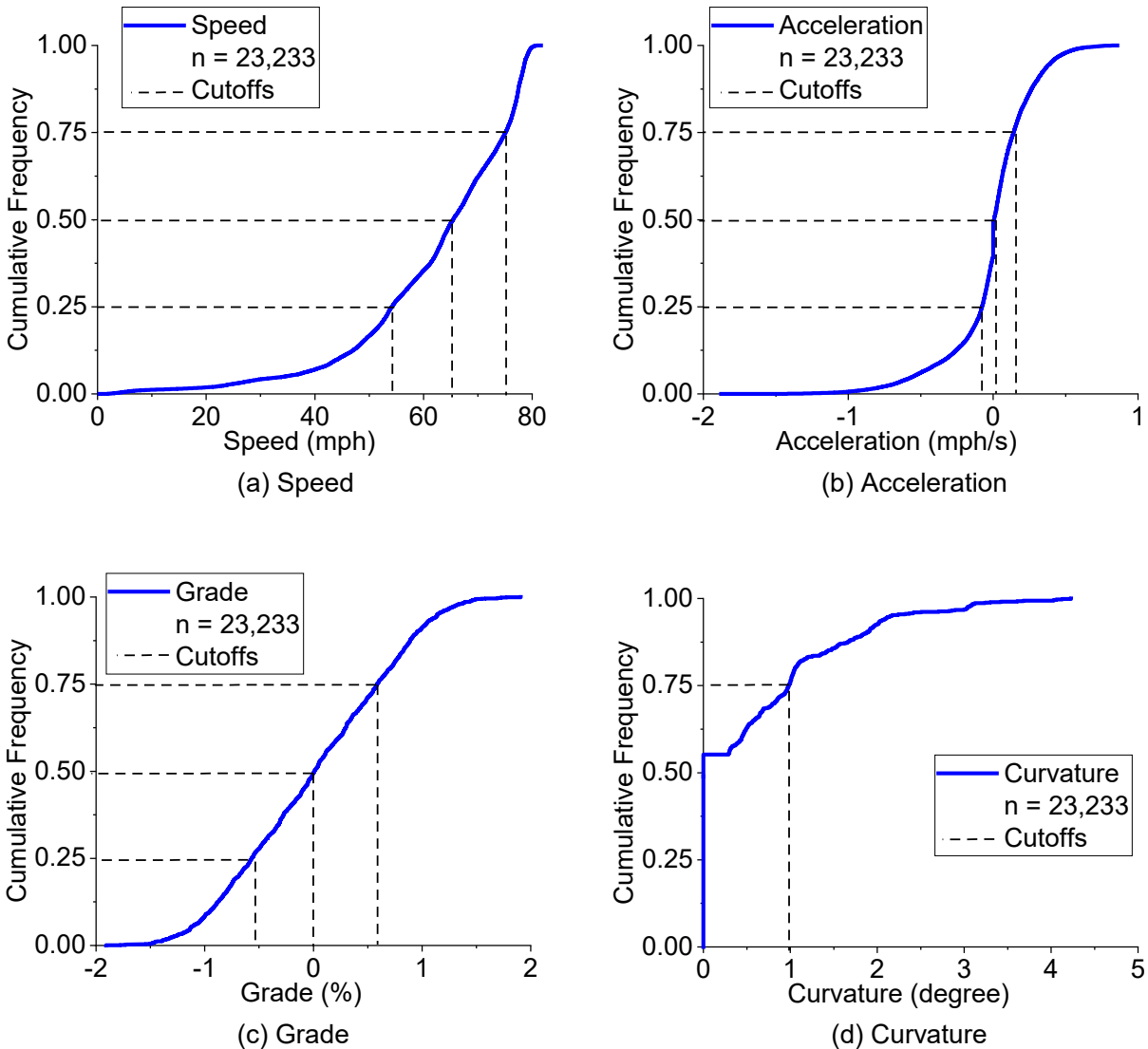


Figure A-22. Cumulative Frequency Plots of Segment-Run Average Speed, Acceleration, Grade, and Curvature to Bin the Data into Groups of Quartiles of these Variables: (a) Speed; (b) Acceleration; (c) Grade; and (d) Curvature.

For curvature, one of the bin comprised only 0 degree curvature. Second bin comprise curvature >0 degree but <0.9 degree. There is a cut-off at curvature >0 obscured by the y-axis.

Conversely, the lowest three FUERs were measured for the highest or second highest speed quartiles and lowest negative acceleration, and lowest grade quartiles corresponding to rows 101, 146, and 159. On average, the highest three FUERs were 8 to 12 times higher than the lowest three FUERs.

To assess the sensitivity of FUERs to curvature, FUERs corresponding to the lowest speed quartile, highest acceleration, and highest grade quartiles were compared versus different curvature bins. For rows 46 through 48, fuel use rates, NO_x emission rates, and PM emission rates were within $\pm 4\%$, $\pm 5\%$, and $\pm 2\%$ of each other, respectively. Likewise, FUERs were similar to each other for rows 94 through 96, each belonging to the same speed quartile, acceleration quartile and grade quartile, but different curvature bins. Similar results were typically obtained for other combinations with the same speed, acceleration, and grade quartiles but different curvature bins. Therefore, FUERs were typically similar to each other for different curvature bins within the same speed, acceleration, and grade quartiles.

Table A-14. Segment-Run Average Fuel Use and Emission Rates Grouped by Quartile Bins of Segment-Run Average Speed, Acceleration, Grade, and Curvature.

Row	Speed (mph)	Acceleration (mph/s)	Grade (%)	Curvature (deg)	Number of Segment-Runs	Average Fuel Use Rate (g/mi)	Average NO _x Emission Rate (g/mi)	Average PM Emission Rate (g/mi)
1	(0, 54.2]	(-1.9, -0.076]	(-1.91, -0.57]	0	291	1830	120	6.5
2	(0, 54.2]	(-1.9, -0.076]	(-1.91, -0.57]	(0, 0.98]	183	2400	160	7.7
3	(0, 54.2]	(-1.9, -0.076]	(-1.91, -0.57]	(0.98, 4.23]	239	1980	130	6.8
4	(0, 54.2]	(-1.9, -0.076]	(-0.57, 0.01]	0	207	2540	170	8.3
5	(0, 54.2]	(-1.9, -0.076]	(-0.57, 0.01]	(0, 0.98]	121	1840	120	6.1
6	(0, 54.2]	(-1.9, -0.076]	(-0.57, 0.01]	(0.98, 4.23]	75	1350	80	4.6
7	(0, 54.2]	(-1.9, -0.076]	(0.01, 0.59]	0	145	2620	180	7.2
8	(0, 54.2]	(-1.9, -0.076]	(0.01, 0.59]	(0, 0.98]	33	2960	210	8.2
9	(0, 54.2]	(-1.9, -0.076]	(0.01, 0.59]	(0.98, 4.23]	68	1790	130	4.7
10	(0, 54.2]	(-1.9, -0.076]	(0.59, 1.91]	0	134	2980	240	6.7
11	(0, 54.2]	(-1.9, -0.076]	(0.59, 1.91]	(0, 0.98]	58	2120	150	6.1
12	(0, 54.2]	(-1.9, -0.076]	(0.59, 1.91]	(0.98, 4.23]	201	3210	250	6.5
13	(0, 54.2]	(-0.076, 0.007]	(-1.91, -0.57]	0	58	1910	130	6.8
14	(0, 54.2]	(-0.076, 0.007]	(-1.91, -0.57]	(0, 0.98]	50	2360	180	7.6
15	(0, 54.2]	(-0.076, 0.007]	(-1.91, -0.57]	(0.98, 4.23]	142	2300	160	7.7
16	(0, 54.2]	(-0.076, 0.007]	(-0.57, 0.01]	0	88	2620	200	8.0
17	(0, 54.2]	(-0.076, 0.007]	(-0.57, 0.01]	(0, 0.98]	64	3080	200	18.3
18	(0, 54.2]	(-0.076, 0.007]	(-0.57, 0.01]	(0.98, 4.23]	85	1400	90	4.3
19	(0, 54.2]	(-0.076, 0.007]	(0.01, 0.59]	0	103	4920	370	12.9
20	(0, 54.2]	(-0.076, 0.007]	(0.01, 0.59]	(0, 0.98]	45	6250	470	14.5
21	(0, 54.2]	(-0.076, 0.007]	(0.01, 0.59]	(0.98, 4.23]	95	3680	310	6.9
22	(0, 54.2]	(-0.076, 0.007]	(0.59, 1.91]	0	87	6040	480	11.8
23	(0, 54.2]	(-0.076, 0.007]	(0.59, 1.91]	(0, 0.98]	76	6360	500	12.1

Table A-14 Continued on Next Page.

Table A-14 Continued from Previous Page.

Row	Speed (mph)	Acceleration (mph/s)	Grade (%)	Curvature (deg)	Number of Segment-Runs	Average Fuel Use Rate (g/mi)	Average NO _x Emission Rate (g/mi)	Average PM Emission Rate (g/mi)
24	(0, 54.2]	(-0.076, 0.007]	(0.59, 1.91]	(0.98, 4.23]	207	6870	550	12.2
25	(0, 54.2]	(0.007, 0.142]	(-1.91, -0.57]	0	98	2130	140	6.7
26	(0, 54.2]	(0.007, 0.142]	(-1.91, -0.57]	(0, 0.98]	56	2880	190	10.9
27	(0, 54.2]	(0.007, 0.142]	(-1.91, -0.57]	(0.98, 4.23]	214	1660	120	5.0
28	(0, 54.2]	(0.007, 0.142]	(-0.57, 0.01]	0	85	2510	200	6.4
29	(0, 54.2]	(0.007, 0.142]	(-0.57, 0.01]	(0, 0.98]	28	3160	250	8.7
30	(0, 54.2]	(0.007, 0.142]	(-0.57, 0.01]	(0.98, 4.23]	87	2970	230	8.0
31	(0, 54.2]	(0.007, 0.142]	(0.01, 0.59]	0	80	10580	750	28.6
32	(0, 54.2]	(0.007, 0.142]	(0.01, 0.59]	(0, 0.98]	69	7440	550	15.9
33	(0, 54.2]	(0.007, 0.142]	(0.01, 0.59]	(0.98, 4.23]	80	4730	380	8.5
34	(0, 54.2]	(0.007, 0.142]	(0.59, 1.91]	0	167	10140	730	21.8
35	(0, 54.2]	(0.007, 0.142]	(0.59, 1.91]	(0, 0.98]	96	8820	710	15.3
36	(0, 54.2]	(0.007, 0.142]	(0.59, 1.91]	(0.98, 4.23]	168	8250	620	12.4
37	(0, 54.2]	(0.142, 0.86]	(-1.91, -0.57]	0	77	6420	420	12.1
38	(0, 54.2]	(0.142, 0.86]	(-1.91, -0.57]	(0, 0.98]	48	5750	390	10.7
39	(0, 54.2]	(0.142, 0.86]	(-1.91, -0.57]	(0.98, 4.23]	111	4450	320	8.3
40	(0, 54.2]	(0.142, 0.86]	(-0.57, 0.01]	0	144	7270	530	12.6
41	(0, 54.2]	(0.142, 0.86]	(-0.57, 0.01]	(0, 0.98]	24	8210	580	13.0
42	(0, 54.2]	(0.142, 0.86]	(-0.57, 0.01]	(0.98, 4.23]	35	7040	470	13.0
43	(0, 54.2]	(0.142, 0.86]	(0.01, 0.59]	0	203	9300	660	15.2
44	(0, 54.2]	(0.142, 0.86]	(0.01, 0.59]	(0, 0.98]	154	9250	630	15.4
45	(0, 54.2]	(0.142, 0.86]	(0.01, 0.59]	(0.98, 4.23]	136	9770	640	16.2
46	(0, 54.2]	(0.142, 0.86]	(0.59, 1.91]	0	396	11750	750	20.9

Table A-14 Continued on Next Page.

Table A-14 Continued from Previous Page.

Row	Speed (mph)	Acceleration (mph/s)	Grade (%)	Curvature (deg)	Number of Segment-Runs	Average Fuel Use Rate (g/mi)	Average NO _x Emission Rate (g/mi)	Average PM Emission Rate (g/mi)
47	(0, 54.2]	(0.142, 0.86]	(0.59, 1.91]	(0, 0.98]	173	11960	790	20.3
48	(0, 54.2]	(0.142, 0.86]	(0.59, 1.91]	(0.98, 4.23]	246	11550	740	19.9
49	(54.2, 65.4]	(-1.9, -0.076]	(-1.91, -0.57]	0	337	1070	70	3.3
50	(54.2, 65.4]	(-1.9, -0.076]	(-1.91, -0.57]	(0, 0.98]	116	1120	70	3.3
51	(54.2, 65.4]	(-1.9, -0.076]	(-1.91, -0.57]	(0.98, 4.23]	247	1010	70	3.0
52	(54.2, 65.4]	(-1.9, -0.076]	(-0.57, 0.01]	0	147	1220	90	3.9
53	(54.2, 65.4]	(-1.9, -0.076]	(-0.57, 0.01]	(0, 0.98]	74	1380	100	3.3
54	(54.2, 65.4]	(-1.9, -0.076]	(-0.57, 0.01]	(0.98, 4.23]	88	1110	80	3.2
55	(54.2, 65.4]	(-1.9, -0.076]	(0.01, 0.59]	0	120	1660	130	3.8
56	(54.2, 65.4]	(-1.9, -0.076]	(0.01, 0.59]	(0, 0.98]	54	1570	110	4.0
57	(54.2, 65.4]	(-1.9, -0.076]	(0.01, 0.59]	(0.98, 4.23]	131	1690	130	3.8
58	(54.2, 65.4]	(-1.9, -0.076]	(0.59, 1.91]	0	99	2710	200	5.7
59	(54.2, 65.4]	(-1.9, -0.076]	(0.59, 1.91]	(0, 0.98]	57	3100	230	6.0
60	(54.2, 65.4]	(-1.9, -0.076]	(0.59, 1.91]	(0.98, 4.23]	101	2750	210	5.1
61	(54.2, 65.4]	(-0.076, 0.007]	(-1.91, -0.57]	0	76	1010	80	3.1
62	(54.2, 65.4]	(-0.076, 0.007]	(-1.91, -0.57]	(0, 0.98]	48	1100	80	3.5
63	(54.2, 65.4]	(-0.076, 0.007]	(-1.91, -0.57]	(0.98, 4.23]	126	1170	80	3.3
64	(54.2, 65.4]	(-0.076, 0.007]	(-0.57, 0.01]	0	104	1830	150	4.1
65	(54.2, 65.4]	(-0.076, 0.007]	(-0.57, 0.01]	(0, 0.98]	50	1370	110	3.0
66	(54.2, 65.4]	(-0.076, 0.007]	(-0.57, 0.01]	(0.98, 4.23]	158	1620	130	3.5
67	(54.2, 65.4]	(-0.076, 0.007]	(0.01, 0.59]	0	84	3030	240	5.0
68	(54.2, 65.4]	(-0.076, 0.007]	(0.01, 0.59]	(0, 0.98]	48	2970	260	6.0
69	(54.2, 65.4]	(-0.076, 0.007]	(0.01, 0.59]	(0.98, 4.23]	161	3030	260	5.1

Table A-14 Continued on Next Page.

Table A-14 Continued from Previous Page.

Row	Speed (mph)	Acceleration (mph/s)	Grade (%)	Curvature (deg)	Number of Segment-Runs	Average Fuel Use Rate (g/mi)	Average NO _x Emission Rate (g/mi)	Average PM Emission Rate (g/mi)
70	(54.2, 65.4]	(-0.076, 0.007]	(0.59, 1.91]	0	158	5340	410	8.6
71	(54.2, 65.4]	(-0.076, 0.007]	(0.59, 1.91]	(0, 0.98]	70	5560	410	7.6
72	(54.2, 65.4]	(-0.076, 0.007]	(0.59, 1.91]	(0.98, 4.23]	120	5780	440	8.4
73	(54.2, 65.4]	(0.007, 0.142]	(-1.91, -0.57]	0	101	1650	130	3.7
74	(54.2, 65.4]	(0.007, 0.142]	(-1.91, -0.57]	(0, 0.98]	57	1200	90	3.3
75	(54.2, 65.4]	(0.007, 0.142]	(-1.91, -0.57]	(0.98, 4.23]	135	1300	90	3.5
76	(54.2, 65.4]	(0.007, 0.142]	(-0.57, 0.01]	0	96	2770	230	5.8
77	(54.2, 65.4]	(0.007, 0.142]	(-0.57, 0.01]	(0, 0.98]	43	2600	220	4.5
78	(54.2, 65.4]	(0.007, 0.142]	(-0.57, 0.01]	(0.98, 4.23]	108	2640	220	4.9
79	(54.2, 65.4]	(0.007, 0.142]	(0.01, 0.59]	0	119	5100	400	8.7
80	(54.2, 65.4]	(0.007, 0.142]	(0.01, 0.59]	(0, 0.98]	44	5130	390	9.1
81	(54.2, 65.4]	(0.007, 0.142]	(0.01, 0.59]	(0.98, 4.23]	80	4370	340	7.3
82	(54.2, 65.4]	(0.007, 0.142]	(0.59, 1.91]	0	276	6940	500	10.1
83	(54.2, 65.4]	(0.007, 0.142]	(0.59, 1.91]	(0, 0.98]	113	7650	520	11.3
84	(54.2, 65.4]	(0.007, 0.142]	(0.59, 1.91]	(0.98, 4.23]	123	7240	560	9.2
85	(54.2, 65.4]	(0.142, 0.86]	(-1.91, -0.57]	0	95	5410	390	9.1
86	(54.2, 65.4]	(0.142, 0.86]	(-1.91, -0.57]	(0, 0.98]	32	4750	330	7.8
87	(54.2, 65.4]	(0.142, 0.86]	(-1.91, -0.57]	(0.98, 4.23]	60	4060	270	7.3
88	(54.2, 65.4]	(0.142, 0.86]	(-0.57, 0.01]	0	222	7230	500	12.1
89	(54.2, 65.4]	(0.142, 0.86]	(-0.57, 0.01]	(0, 0.98]	53	5970	450	8.3
90	(54.2, 65.4]	(0.142, 0.86]	(-0.57, 0.01]	(0.98, 4.23]	106	5880	410	8.6
91	(54.2, 65.4]	(0.142, 0.86]	(0.01, 0.59]	0	308	8820	560	14.2
92	(54.2, 65.4]	(0.142, 0.86]	(0.01, 0.59]	(0, 0.98]	101	8410	510	12.5

Table A-14 Continued on Next Page.

Table A-14 Continued from Previous Page.

Row	Speed (mph)	Acceleration (mph/s)	Grade (%)	Curvature (deg)	Number of Segment-Runs	Average Fuel Use Rate (g/mi)	Average NO _x Emission Rate (g/mi)	Average PM Emission Rate (g/mi)
93	(54.2, 65.4]	(0.142, 0.86]	(0.01, 0.59]	(0.98, 4.23]	73	8000	470	13.9
94	(54.2, 65.4]	(0.142, 0.86]	(0.59, 1.91]	0	380	10120	600	17.4
95	(54.2, 65.4]	(0.142, 0.86]	(0.59, 1.91]	(0, 0.98]	137	10040	560	17.3
96	(54.2, 65.4]	(0.142, 0.86]	(0.59, 1.91]	(0.98, 4.23]	129	9820	580	15.0
97	(65.4, 75.1]	(-1.9, -0.076]	(-1.91, -0.57]	0	466	1110	80	2.9
98	(65.4, 75.1]	(-1.9, -0.076]	(-1.91, -0.57]	(0, 0.98]	147	880	60	2.6
99	(65.4, 75.1]	(-1.9, -0.076]	(-1.91, -0.57]	(0.98, 4.23]	55	970	70	3.0
100	(65.4, 75.1]	(-1.9, -0.076]	(-0.57, 0.01]	0	262	1390	110	3.4
101	(65.4, 75.1]	(-1.9, -0.076]	(-0.57, 0.01]	(0, 0.98]	47	870	60	2.6
102	(65.4, 75.1]	(-1.9, -0.076]	(-0.57, 0.01]	(0.98, 4.23]	78	1310	100	3.1
103	(65.4, 75.1]	(-1.9, -0.076]	(0.01, 0.59]	0	170	2170	180	4.2
104	(65.4, 75.1]	(-1.9, -0.076]	(0.01, 0.59]	(0, 0.98]	69	1610	120	4.1
105	(65.4, 75.1]	(-1.9, -0.076]	(0.01, 0.59]	(0.98, 4.23]	82	2030	160	4.3
106	(65.4, 75.1]	(-1.9, -0.076]	(0.59, 1.91]	0	109	2970	250	6.2
107	(65.4, 75.1]	(-1.9, -0.076]	(0.59, 1.91]	(0, 0.98]	48	2220	170	4.6
108	(65.4, 75.1]	(-1.9, -0.076]	(0.59, 1.91]	(0.98, 4.23]	23	2870	230	5.4
109	(65.4, 75.1]	(-0.076, 0.007]	(-1.91, -0.57]	0	97	1350	110	3.0
110	(65.4, 75.1]	(-0.076, 0.007]	(-1.91, -0.57]	(0, 0.98]	52	1140	90	3.1
111	(65.4, 75.1]	(-0.076, 0.007]	(-1.91, -0.57]	(0.98, 4.23]	38	1020	70	3.2
112	(65.4, 75.1]	(-0.076, 0.007]	(-0.57, 0.01]	0	133	2180	190	4.2
113	(65.4, 75.1]	(-0.076, 0.007]	(-0.57, 0.01]	(0, 0.98]	49	1750	140	4.5
114	(65.4, 75.1]	(-0.076, 0.007]	(-0.57, 0.01]	(0.98, 4.23]	111	2240	170	4.3
115	(65.4, 75.1]	(-0.076, 0.007]	(0.01, 0.59]	0	151	4090	340	6.8

Table A-14 Continued on Next Page.

Table A-14 Continued from Previous Page.

Row	Speed (mph)	Acceleration (mph/s)	Grade (%)	Curvature (deg)	Number of Segment-Runs	Average Fuel Use Rate (g/mi)	Average NO _x Emission Rate (g/mi)	Average PM Emission Rate (g/mi)
116	(65.4, 75.1]	(-0.076, 0.007]	(0.01, 0.59]	(0, 0.98]	50	3350	280	6.3
117	(65.4, 75.1]	(-0.076, 0.007]	(0.01, 0.59]	(0.98, 4.23]	107	3370	290	5.9
118	(65.4, 75.1]	(-0.076, 0.007]	(0.59, 1.91]	0	162	5180	410	7.9
119	(65.4, 75.1]	(-0.076, 0.007]	(0.59, 1.91]	(0, 0.98]	75	4770	360	8.1
120	(65.4, 75.1]	(-0.076, 0.007]	(0.59, 1.91]	(0.98, 4.23]	47	5380	400	9.1
121	(65.4, 75.1]	(0.007, 0.142]	(-1.91, -0.57]	0	138	1590	130	4.1
122	(65.4, 75.1]	(0.007, 0.142]	(-1.91, -0.57]	(0, 0.98]	78	2000	170	3.6
123	(65.4, 75.1]	(0.007, 0.142]	(-1.91, -0.57]	(0.98, 4.23]	68	1080	80	3.0
124	(65.4, 75.1]	(0.007, 0.142]	(-0.57, 0.01]	0	168	3010	230	6.3
125	(65.4, 75.1]	(0.007, 0.142]	(-0.57, 0.01]	(0, 0.98]	32	2560	240	4.0
126	(65.4, 75.1]	(0.007, 0.142]	(-0.57, 0.01]	(0.98, 4.23]	61	3270	270	5.4
127	(65.4, 75.1]	(0.007, 0.142]	(0.01, 0.59]	0	186	5560	400	8.7
128	(65.4, 75.1]	(0.007, 0.142]	(0.01, 0.59]	(0, 0.98]	81	5460	400	9.8
129	(65.4, 75.1]	(0.007, 0.142]	(0.01, 0.59]	(0.98, 4.23]	68	3820	320	6.3
130	(65.4, 75.1]	(0.007, 0.142]	(0.59, 1.91]	0	305	6730	420	10.3
131	(65.4, 75.1]	(0.007, 0.142]	(0.59, 1.91]	(0, 0.98]	94	7270	450	11.2
132	(65.4, 75.1]	(0.007, 0.142]	(0.59, 1.91]	(0.98, 4.23]	41	6830	430	11.7
133	(65.4, 75.1]	(0.142, 0.86]	(-1.91, -0.57]	0	107	4930	390	8.7
134	(65.4, 75.1]	(0.142, 0.86]	(-1.91, -0.57]	(0, 0.98]	43	4640	330	8.3
135	(65.4, 75.1]	(0.142, 0.86]	(-1.91, -0.57]	(0.98, 4.23]	38	3760	290	7.1
136	(65.4, 75.1]	(0.142, 0.86]	(-0.57, 0.01]	0	472	6590	420	11.1
137	(65.4, 75.1]	(0.142, 0.86]	(-0.57, 0.01]	(0, 0.98]	86	7170	460	12.3
138	(65.4, 75.1]	(0.142, 0.86]	(-0.57, 0.01]	(0.98, 4.23]	70	6030	430	9.2

Table A-14 Continued on Next Page.

Table A-14 Continued from Previous Page.

Row	Speed (mph)	Acceleration (mph/s)	Grade (%)	Curvature (deg)	Number of Segment-Runs	Average Fuel Use Rate (g/mi)	Average NO _x Emission Rate (g/mi)	Average PM Emission Rate (g/mi)
139	(65.4, 75.1]	(0.142, 0.86]	(0.01, 0.59]	0	424	7940	500	12.1
140	(65.4, 75.1]	(0.142, 0.86]	(0.01, 0.59]	(0, 0.98]	121	7370	470	10.8
141	(65.4, 75.1]	(0.142, 0.86]	(0.01, 0.59]	(0.98, 4.23]	65	8400	520	13.8
142	(65.4, 75.1]	(0.142, 0.86]	(0.59, 1.91]	0	308	9490	550	16.5
143	(65.4, 75.1]	(0.142, 0.86]	(0.59, 1.91]	(0, 0.98]	107	9330	560	16.2
144	(65.4, 75.1]	(0.142, 0.86]	(0.59, 1.91]	(0.98, 4.23]	51	10290	620	19.1
145	(75.1, 80]	(-1.9, -0.076]	(-1.91, -0.57]	0	194	940	70	2.5
146	(75.1, 80]	(-1.9, -0.076]	(-1.91, -0.57]	(0, 0.98]	75	870	70	2.1
147	(75.1, 80]	(-1.9, -0.076]	(-1.91, -0.57]	(0.98, 4.23]	26	1030	80	2.9
148	(75.1, 80]	(-1.9, -0.076]	(-0.57, 0.01]	0	194	1420	110	3.3
149	(75.1, 80]	(-1.9, -0.076]	(-0.57, 0.01]	(0, 0.98]	42	1030	80	2.6
150	(75.1, 80]	(-1.9, -0.076]	(-0.57, 0.01]	(0.98, 4.23]	27	1540	140	3.1
151	(75.1, 80]	(-1.9, -0.076]	(0.01, 0.59]	0	210	2080	170	4.4
152	(75.1, 80]	(-1.9, -0.076]	(0.01, 0.59]	(0, 0.98]	31	1870	170	3.3
153	(75.1, 80]	(-1.9, -0.076]	(0.01, 0.59]	(0.98, 4.23]	29	2660	220	4.5
154	(75.1, 80]	(-1.9, -0.076]	(0.59, 1.91]	0	70	2720	220	5.2
155	(75.1, 80]	(-1.9, -0.076]	(0.59, 1.91]	(0, 0.98]	25	2820	240	4.9
156	(75.1, 80]	(-1.9, -0.076]	(0.59, 1.91]	(0.98, 4.23]	5	3140	230	5.9
157	(75.1, 80]	(-0.076, 0.007]	(-1.91, -0.57]	0	368	1000	80	2.5
158	(75.1, 80]	(-0.076, 0.007]	(-1.91, -0.57]	(0, 0.98]	122	970	80	2.4
159	(75.1, 80]	(-0.076, 0.007]	(-1.91, -0.57]	(0.98, 4.23]	59	770	60	2.1
160	(75.1, 80]	(-0.076, 0.007]	(-0.57, 0.01]	0	613	1880	160	3.5
161	(75.1, 80]	(-0.076, 0.007]	(-0.57, 0.01]	(0, 0.98]	171	1820	150	3.6

Table A-14 Continued on Next Page.

Table A-14 Continued from Previous Page.

Row	Speed (mph)	Acceleration (mph/s)	Grade (%)	Curvature (deg)	Number of Segment-Runs	Average Fuel Use Rate (g/mi)	Average NO _x Emission Rate (g/mi)	Average PM Emission Rate (g/mi)
162	(75.1, 80]	(-0.076, 0.007]	(-0.57, 0.01]	(0.98, 4.23]	84	1980	170	3.6
163	(75.1, 80]	(-0.076, 0.007]	(0.01, 0.59]	0	538	3410	290	5.2
164	(75.1, 80]	(-0.076, 0.007]	(0.01, 0.59]	(0, 0.98]	123	3230	280	4.9
165	(75.1, 80]	(-0.076, 0.007]	(0.01, 0.59]	(0.98, 4.23]	71	2750	240	4.1
166	(75.1, 80]	(-0.076, 0.007]	(0.59, 1.91]	0	184	4870	420	6.6
167	(75.1, 80]	(-0.076, 0.007]	(0.59, 1.91]	(0, 0.98]	55	4830	420	7.5
168	(75.1, 80]	(-0.076, 0.007]	(0.59, 1.91]	(0.98, 4.23]	45	6200	530	9.0
169	(75.1, 80]	(0.007, 0.142]	(-1.91, -0.57]	0	358	1340	110	3.2
170	(75.1, 80]	(0.007, 0.142]	(-1.91, -0.57]	(0, 0.98]	114	1070	90	2.8
171	(75.1, 80]	(0.007, 0.142]	(-1.91, -0.57]	(0.98, 4.23]	91	1430	120	4.1
172	(75.1, 80]	(0.007, 0.142]	(-0.57, 0.01]	0	511	2350	190	5.0
173	(75.1, 80]	(0.007, 0.142]	(-0.57, 0.01]	(0, 0.98]	91	2320	190	4.2
174	(75.1, 80]	(0.007, 0.142]	(-0.57, 0.01]	(0.98, 4.23]	65	3610	300	6.4
175	(75.1, 80]	(0.007, 0.142]	(0.01, 0.59]	0	398	4040	320	6.3
176	(75.1, 80]	(0.007, 0.142]	(0.01, 0.59]	(0, 0.98]	98	4080	310	6.9
177	(75.1, 80]	(0.007, 0.142]	(0.01, 0.59]	(0.98, 4.23]	53	3790	320	6.1
178	(75.1, 80]	(0.007, 0.142]	(0.59, 1.91]	0	140	5800	420	8.3
179	(75.1, 80]	(0.007, 0.142]	(0.59, 1.91]	(0, 0.98]	41	6970	490	10.6
180	(75.1, 80]	(0.007, 0.142]	(0.59, 1.91]	(0.98, 4.23]	32	6900	510	12.1
181	(75.1, 80]	(0.142, 0.86]	(-1.91, -0.57]	0	65	4100	300	9.1
182	(75.1, 80]	(0.142, 0.86]	(-1.91, -0.57]	(0, 0.98]	18	4130	310	7.4
183	(75.1, 80]	(0.142, 0.86]	(-1.91, -0.57]	(0.98, 4.23]	12	4600	340	9.1
184	(75.1, 80]	(0.142, 0.86]	(-0.57, 0.01]	0	126	5120	330	9.7

Table A-14 Continued on Next Page.

Table A-14 Continued from Previous Page.

Row	Speed (mph)	Acceleration (mph/s)	Grade (%)	Curvature (deg)	Number of Segment-Runs	Average Fuel Use Rate (g/mi)	Average NO _x Emission Rate (g/mi)	Average PM Emission Rate (g/mi)
185	(75.1, 80]	(0.142, 0.86]	(-0.57, 0.01]	(0, 0.98]	20	5820	370	9.7
186	(75.1, 80]	(0.142, 0.86]	(-0.57, 0.01]	(0.98, 4.23]	20	5350	370	7.6
187	(75.1, 80]	(0.142, 0.86]	(0.01, 0.59]	0	93	7020	470	12.1
188	(75.1, 80]	(0.142, 0.86]	(0.01, 0.59]	(0, 0.98]	42	6280	350	12.0
189	(75.1, 80]	(0.142, 0.86]	(0.01, 0.59]	(0.98, 4.23]	11	9350	710	13.6
190	(75.1, 80]	(0.142, 0.86]	(0.59, 1.91]	0	23	8430	500	14.8
191	(75.1, 80]	(0.142, 0.86]	(0.59, 1.91]	(0, 0.98]	10	9270	650	14.5
192	(75.1, 80]	(0.142, 0.86]	(0.59, 1.91]	(0.98, 4.23]	5	7970	460	17.1

Speed, acceleration, and grade were each divided into quartiles. Curvature was binned into three bins. Average rates and the number of segment-runs in each possible combination of bins of these variables are given in this Table.

Fuel use and emission rates are color-coded from dark blue to white to dark red. Dark blue indicates the lowest rates, whereas, dark red indicates the highest rates.

To assess the sensitivity of FUERs to speed quartiles, average FUERs corresponding to the highest acceleration and grade quartiles were compared versus different quartiles of speed. Compared to the FUERs for the lowest speed quartile among species, FUERs were 9% to 13%, 14% to 17%, and 23% to 27% lower for the second, third, and fourth lowest speed quartiles, respectively.

To assess the sensitivity of FUERs to acceleration quartiles, average FUERs for the slowest speed quartile and highest grade quartile are compared to FUERs for different acceleration quartiles. Compared to the FUERs for the highest acceleration quartile among species, FUERs were 21% to 23%, 43% to 55%, and 85% to 93% lower for the second, third, and fourth lowest acceleration quartiles, respectively.

To assess the sensitivity of FUERs to grade quartiles, average FUERs for the slowest speed quartile and highest acceleration quartile are compared to FUERs for different grade quartiles. Compared to the FUERs for the highest grade quartile among species, FUERs were 8% to 12%, 26% to 31%, and 35% to 41% lower for the second, third, and fourth lowest grade quartiles, respectively.

Typically, FUERs were the most sensitive to changes in acceleration quartiles, followed by grade quartiles, speed quartiles, and curvature bins.

The combination of variables associated with the lowest FUERs typically included the highest two speed quartiles, lowest two acceleration quartiles, lowest two grade quartiles and all curvature bins. As discussed earlier, variation in curvature had the least effect on variability in FUERs compared to variations in speed, acceleration, and grade. Therefore, these low FUERs were due to higher speeds, negative acceleration, and negative grade.

A.11.4 Segment-average rates by location

Segment-average FUER among segments characterized by location are compared. Segment-characterization by location was discussed in Section 9. Segment-average rates stratified by location are given in Table A-15.

FUERs in either direction were the highest for station segments. On average in either direction, station segments had average speeds <15 mph combined with positive acceleration and grade. Average fuel use rates and NO_x and PM emission rates in either direction were the lowest for NSD. Average PM emission rates were similar and low for NSD and I segment locations compared to either NSA or S locations. Compared to NSD, FUERs for station segments were 7.6 to 8.4 times and 4.6 to 5.6 times higher in the eastbound and westbound direction, respectively. For eastbound versus westbound, average speed for NSA was 3 mph higher and average speed for S was 5 mph lower. Average acceleration and grade were lower for eastbound versus westbound for each of NSD and S. Because of differences in speed for eastbound versus westbound, FUERs for NSD were lower and FUERs for S were higher. Therefore, the ratio of FUERs for NSD and S was higher for eastbound than for westbound. FUERs at stations were consistently higher than at any other locations.

Table A-15. Segment-Average Fuel Use and Emission Rates by Segment Location based on All One-Way Trips and All consists

Variable	Travel Direction	Segment Location ^a				
		Intermediate (I)	Near Station Acceleration (NSA)	Near Station Deceleration (NSD)	Near Station Segments (NS)	Station (S)
Speed (mph)	Eastbound	65.9	48.4	49.4	48.8	8.4
	Westbound	64.8	49.4	46.4	47.3	13.4
Acceleration (mph/s)	Eastbound	0.00	0.32	-0.42	-0.04	0.08
	Westbound	0.00	0.34	-0.34	0.01	0.15
Grade (%)	Eastbound	-0.05	0.56	-0.72	-0.02	0.54
	Westbound	0.04	0.60	-0.65	0.05	0.72
Curvature (degree)	Eastbound	0.57	0.54	0.40	0.50	0.74
	Westbound	0.57	0.40	0.60	0.50	0.46
Fuel Use Rate (g/mile)	Eastbound	3840	9340	1990	6710	16000
	Westbound	4030	9880	2680	7180	15200
NO _x Emission Rate (g/mile)	Eastbound	288	649	141	475	1180
	Westbound	280	603	182	456	1020
PM Emission Rate (g/mile)	Eastbound	6.0	14.8	5.5	13.3	41.7
	Westbound	7.7	18.6	8.3	15.9	38.3
Population Density (persons/km ²)	Eastbound	470	1110	1260	1179	1140
	Westbound	470	1290	1110	1185	1050

^a Segment Location: station segments (S) defined as segments containing stations near station acceleration segments (NSA) defined as segments within 1.25 mile downstream of station segments where trains typically accelerate; near station deceleration segments (NSD) defined as segments within 1.25 mile upstream of station segments where trains typically decelerate; intermediate segments (I) defined as segments other than S, NSA and NSD; near station segments (NS) defined as segments comprising NSA and NSD since NSA in one direction is NSD in the opposite direction.

NSA had the second-highest FUERs among different segment location types. In each direction, for NSA versus S, fuel use rate and NO_x emission rates were 35% to 45%, and PM emission rates were 50% to 65% lower for PM emission rates. NSA had the highest average acceleration among segments, but the speed was faster than for stations, at 49 mph versus 10 mph, respectively. As discussed in Section 10.1, segment-average FUERs were positively correlated with acceleration and negatively correlated with speed. Therefore, even with greater positive

acceleration, NSA had lower rates than S. For NSA, FUERs were within $\pm 12\%$ for eastbound versus westbound. The relatively smaller difference in NSA rates by direction compared to S are associated with smaller differences in speed, acceleration, and grade between the directions.

Intermediate segments had FUERs within $\pm 5\%$ of each other for eastbound versus westbound. For eastbound versus westbound, average speed was within ± 1.1 mph, average acceleration was within ± 0.004 mph/s, grade was within $\pm 0.1\%$ absolute, and curvature was the same. Comparable average speed, acceleration, grade, and curvature for each direction lead to comparable FUERs.

To quantify if high emission rates tend to be located near populated regions, the population density near the segment-runs was compared with segment-average rates. The population density was within $\pm 6\%$ for NSA, NSD and S. The population density was approximately 2.5 times higher for these three segment types than for I. Station segments had the highest average FUERs and were among the locations with the highest population density on the Piedmont rail route. Therefore, more people are potentially exposed to higher pollutant emission rates. NSA and NSD are the same segments as NSA in one direction are NSD in the opposite direction; therefore, average rates and population density for NSA and NSD combined are estimated. For NSA and NSD, average FUERs were 52% to 68% lower than for S but the population density was similar to S. Therefore, population exposures for NSA and NSD are likely to be lower than S. Population exposures are likely to be lowest in proximity to I segments because of the combination of low FUERs and low population density at these locations.

A.11.5 Segment-average rates inclusive of dwell time at terminal stations

The sensitivity of NO_x and PM emission rates to dwell time at Raleigh and Charlotte was assessed based on average idle fuel use rate and NO_x and PM emission rates of 3.0 g/s, 0.3 g/s and 0.02 g/s, respectively (Frey and Rastogi, 2019). Dwell time at stations leads to accumulation of emissions at a given location. With the dwell time included, the segment-average fuel use rate, NO_x and PM rates at Charlotte increased by 191%, 183% and 277% for a given segment to 43000 g/mile, 3409 g/mile and 196 g/mile. At Raleigh, the segment-average fuel use rate, NO_x and PM rates increased by 29%, 31% and 37%, respectively. Since the dwell time at Raleigh was shorter than Charlotte, the percent increase was lower.

A.11.6 Minimum trips to accurately locate absolute hotspots

To quantify the minimum number of one-way trips required to accurately locate absolute emission hotspots, bootstrapping was used (Cullen and Frey, 1999; Frey and Burmaster, 1999). For a given travel direction, a selected number of trips were sampled at random without replacement for 1000 replications. For each pollutant, the number of sampled one-way trips was increased until the selected sample had 90% of the same absolute hotspots with 90% frequency among the replicates as for absolute hotspots based on all one-way trips in that given travel direction. The results of the bootstrapping are given in Figure A-23. The minimum number of one-way trips needed to accurately locate absolute hotspots is 13 and 14 for eastbound and westbound, respectively. As discussed in Section 10.3, FUERs in westbound direction were higher than eastbound because the average grade in westbound direction is positive versus negative for eastbound. Therefore, FUERs vary with direction, resulting in different number of trips for eastbound versus westbound.

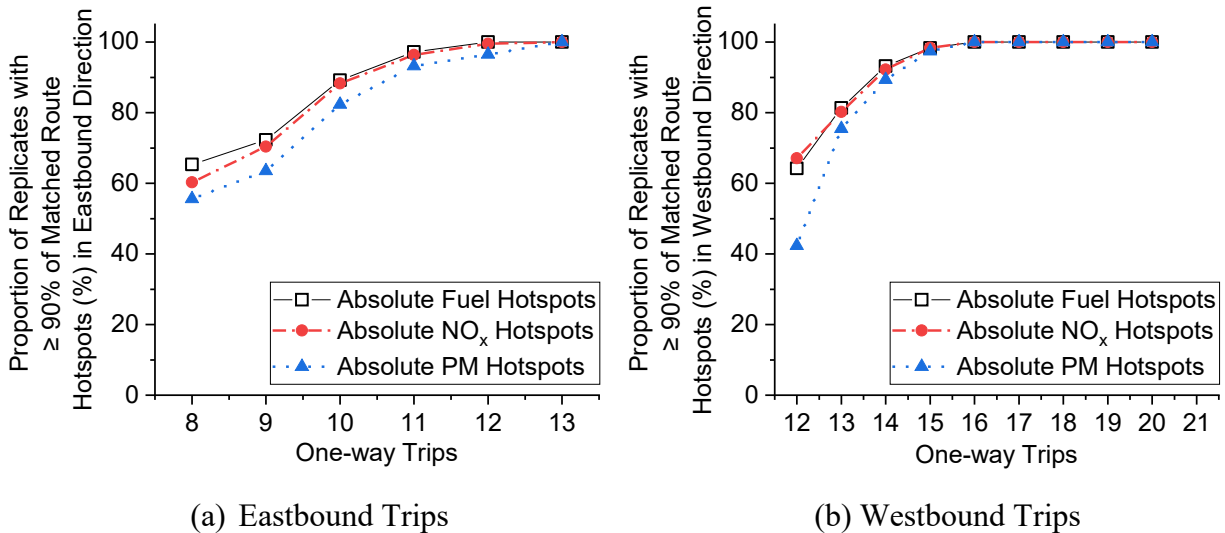


Figure A-23. Minimum One-Way Trips Needed to Locate Fuel Use, NO_x And PM Absolute Hotspots With A Frequency $\geq 90\%$ Based On 1000 Random Replications Without Replacement For A Given Number Of One-Way Trips: (a) For Eastbound Trips Based On 14 Measured One-Way Trips; And (b) For Westbound Trips Based On 21 Measured One-Way Trips.

A.12 Quantifying the Importance of Potential Explanatory Variables

This section explains Classification and Regression Trees (CART) based models used to identify the combinations of potential explanatory variables that distinguish relative hotspots from relative not hotspots. CART was also used to identify the importance of variables in distinguishing relative hotspots from relative not hotspots.

A.12.1 Classification and regression trees

CART is a form of a decision tree that seeks to divide a data set into subsets, each of which is more homogeneous compared to the entire data set (Breiman et al., 1984). A decision tree is a type of supervised learning algorithm that can be used for classification and regression. A decision tree can account for both categorical and continuous predictor variable(s) and a target variable. The CART decision tree is a binary recursive partitioning tree. Decision trees are not based on the assumptions of normality, the relationship between variables (linear, non-linear, or monotonic), provide easier to interpret results as simple functions of input variables and are resistant to outliers and missing data. They are also useful to identify important variables.

A decision tree consists of a root node, decision nodes, and terminal nodes as shown in Figure A-24. A root node represents the entire sample which gets divided into two homogeneous sub-nodes. The process of dividing a node into sub-nodes is called splitting. The sub-nodes that further split into sub-nodes are called decision nodes. The sub-nodes that do not split further are called terminal nodes or leaf. The tree is constructed by repeatedly splitting the data based on a single predictor variable at each split. Each split partitions the data into two mutually exclusive groups that are more homogenous than the decision node. At each decision node, all possible splits of all predictor variables are made. Of these splits, the split that maximizes the homogeneity among the two resultant nodes is used. The homogeneity of each node is quantified in terms of node impurity. Node impurity is zero for a completely homogenous split. Splitting

continues until all the terminal nodes are homogenous or until the terminal nodes meet a pre-defined criterion. In many practical applications, splitting to get all homogenous groups results in an overgrown tree and results in overfitting. Such a tree is complex to interpret. Therefore, the tree is pruned to a smaller tree. Trees may be pruned to yield low cost-complexity or higher prediction accuracy.

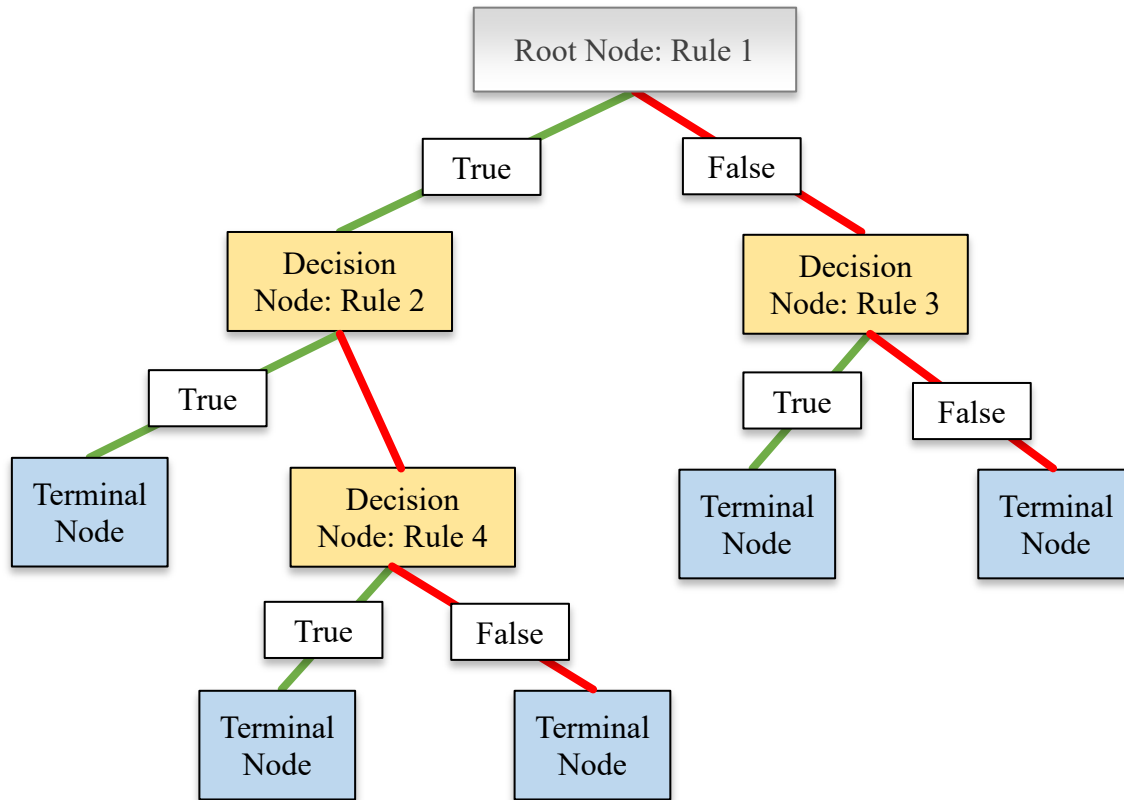


Figure A-24. A Typical Layout of a Binary Decision Tree.

The CART prediction accuracy was evaluated based on cross-validation in which a subset of data is used to train the tree and another mutually exclusive data is used for prediction. CART models are robust to an imbalance in target variable classes in the training data. For example, a target variable may have only two categories, with one category comprising 80 percent of the data and the other 20 percent. Such an imbalance does not affect CART performance. However, the training and validation data should have approximately the same distribution for better model performance.

The CART also quantifies the importance of each predictor variable. Variable importance is based on the decrease in node impurity at each node in which the predictor variable resulted in a split. The importance is estimated for the primary splitting variable as well as the surrogate variable(s). Two correlated variables may have equal variable importance but in the decision

tree, one variable may be more prominent, or one variable may not appear at all if they provide similar splits. Therefore, in such cases, one variable may mask the other variable. However, for prediction, these two variables can be used interchangeably. In the case of one missing variable, the other can be used. The variable importance accounts for these surrogate variables. Over an entire tree, the variable that splits the highest proportion of data into homogenous groups will have the highest variable importance.

A.12.2 Potential Variables Distinguishing Hotspots from Non-Hotspots

For each species, four CART models were evaluated for calibration and validation. Among the models, the most appropriate model was identified. Relative fuel use, NO_x and PM emission hotspots were the target variable for four CART models.

Four models are described in Table A-16. The first model was based on dynamic variables affecting FUEP identified in Equation A-9. Since this model is based on physics of motion, this model is referred to as the Physical Model with Dynamic Variables (PD). The second model included the dynamic variables and static variables to account for proportionality coefficients in Equation A-9. Therefore, this model is referred to as Physical Model with Dynamic and Static Variables (PDS). Two simplified models based on segment-average speed, acceleration, grade and curvature as dynamic variables were also evaluated with and without static variables. The former model only included simplified dynamic variables and is referred to as the Simplified Model with Dynamic Variables (SD). The latter model included simplified dynamic variables and static variables and is referred to as the Simplified Model with Dynamic and Static Variables (SDS).

Table A-16. Description of Models Used for Quantifying Key Variables Used to Distinguish Relative Hotspots from Relative Non-Hotspots

Model	Abbreviation	Definition	Dynamic Variables	Static Variables
Physical Model with Dynamic Variables	PD	Physical Model based on Equation A-9 including all dynamic variables affecting train resistance	Speed, Sum of Product of Speed and Acceleration, Sum of Product of Speed and Grade, and Sum of Product of Speed and Curvature	None
Physical Model with Dynamic and Static Variables	PDS	Physical Model based on Equation A-9 including all dynamic and static variables affecting train resistance		Locomotive and Consist
Simplified Model with Dynamic Variables	SD	Model with simplified dynamic variables	Segment-run average speed, acceleration, grade, and curvature	None
Simplified Model with Dynamic and Static Variables	SDS	Model with static variables and simplified dynamic variables		Locomotive and Consist

Each CART model was calibrated based on 17,332 segment-runs and validated based on 5,866 segment-runs. The calibration data comprised 10 and 16 eastbound and westbound one-way trips, respectively. The validation data comprised 4 and 5 eastbound and westbound one-way trips, respectively.

The CART models for fuel use relative hotspots are presented in Figure A-25 through Figure A-28 for PD, PDS, SD, and SDS, respectively. The CART models for NO_x emission hotspots are presented in Figure A-29 through Figure A-32 for PD, PDS, SD, and SDS, respectively. The CART models for PM emission hotspots are presented in Figure A-33 through Figure A-36 for PD, PDS, SD, and SDS, respectively.

Similarities among models across species are identified. The PD model for fuel use was similar to NO_x model in terms of the number of nodes, the number of data in each node, the splitting variable identified at each node, and the value of the splitting variable at each node. For example, for each model the first split occurred for SOP of speed and acceleration at 630 mph²/s. Data were divided identically at this split among the models. Although, the likelihood of the data being classified as hotspot and non-hotspot differed, the difference was small relative to the likelihood. For example, for the split related to SOP of speed and acceleration >630 mph²/s, the likelihood of a segment-run being a hotspot was 63% for fuel and 59% for NO_x. The values of splitting variables for further splits were also generally within 2% to 5% of each other. The PM PD model was also similar to the PD fuel model.

Since the PD models are similar, the NO_x model is used as a representative example to describe the key findings and insights that are representative of each of the species. Insights from the model include what combinations of variables result in relative hotspots versus non-hotspots.

The plurality of hotspots (45% of all hotspots) were associated with:

- Speed <10 mph;
- SOP of speed and acceleration >630 mph²/s; and
- SOP of speed and grade >286 mph%.

Segment-runs meeting these conditions had an 85% likelihood of being a hotspot. Other combinations of variables accounted for 15% or fewer of the hotspots each.

The maximum proportion of NO_x non-hotspots (80% of all non-hotspots) were associated with:

- Speed >10 mph;
- SOP of speed and acceleration <630 mph²/s; and
- SOP of speed and grade <2574 mph%.

Segment-runs meeting these conditions had a 97% likelihood of being a non-hotspot.

In the model, none of the splits were based on SOP of speed and curvature, which was the only physically-based curvature term included in the model. Therefore, curvature was not a key variable in distinguishing hotspots from non-hotspots.

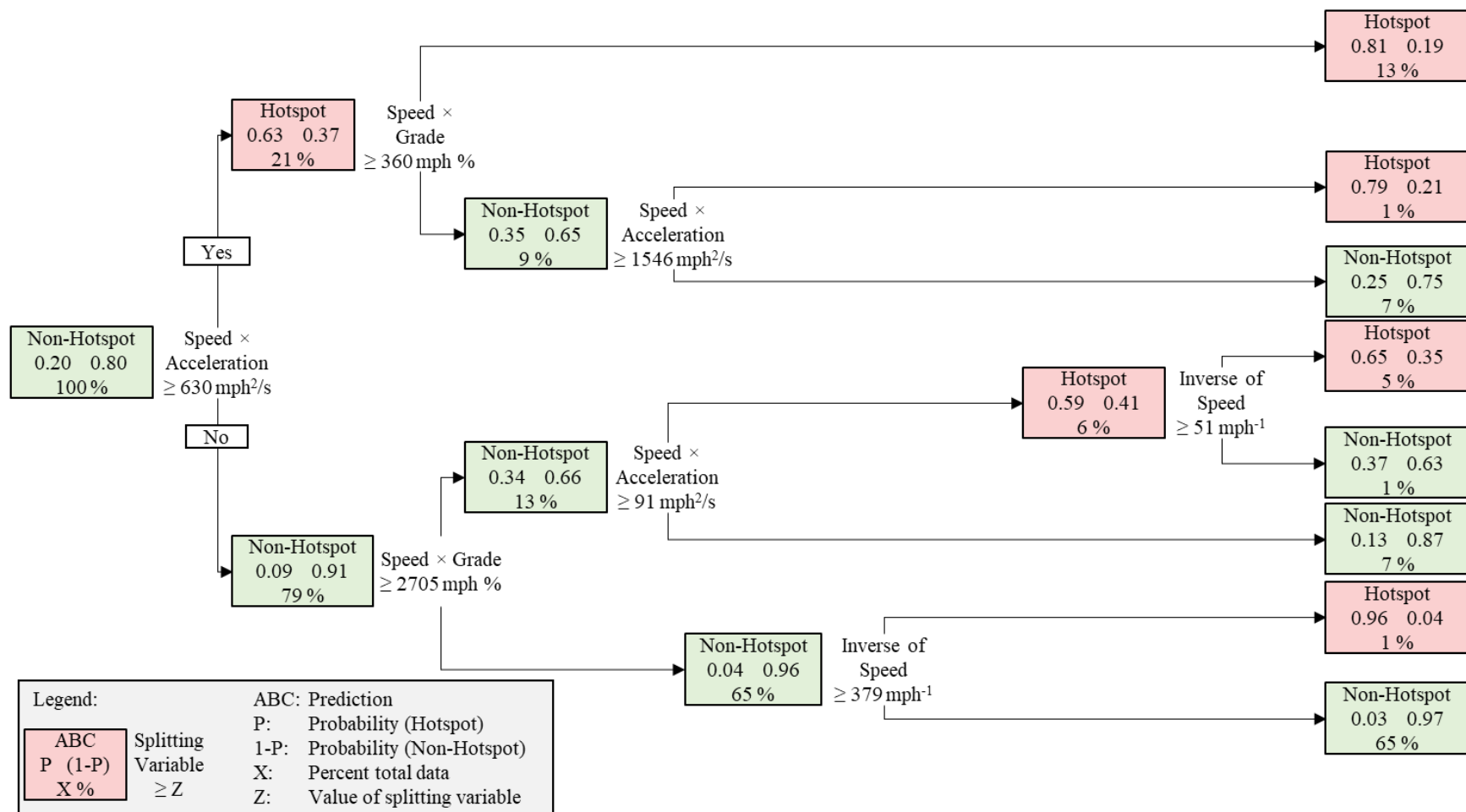


Figure A-25. Fuel Physical Model with Dynamic Variables: Calibration of Classification and Regression TreeA-Based Fuel Hotspot Model Including Dynamic Variables in the Physical Model without Locomotive and Consist as Static Variables Based on 26 One-Way Trips in Either Travel Direction.

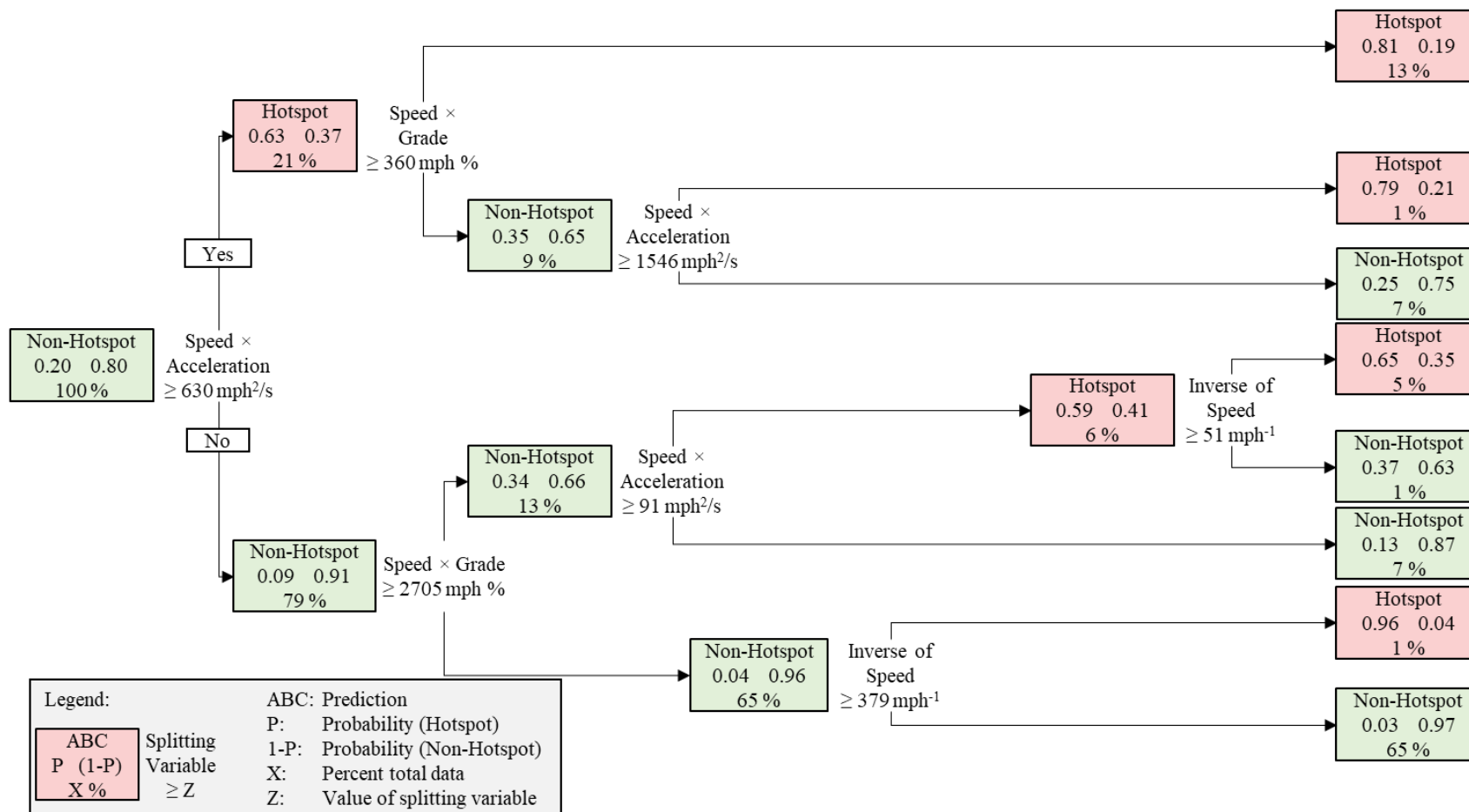


Figure A-26. Fuel Physical Model with Dynamic and Static Variables: Calibration of Classification and Regression Tree-based Fuel Hotspot Model including Dynamic Variables in the Physical model with Locomotive and Consist as Static Variables based on 26 One-way Trips in Either Travel Direction.

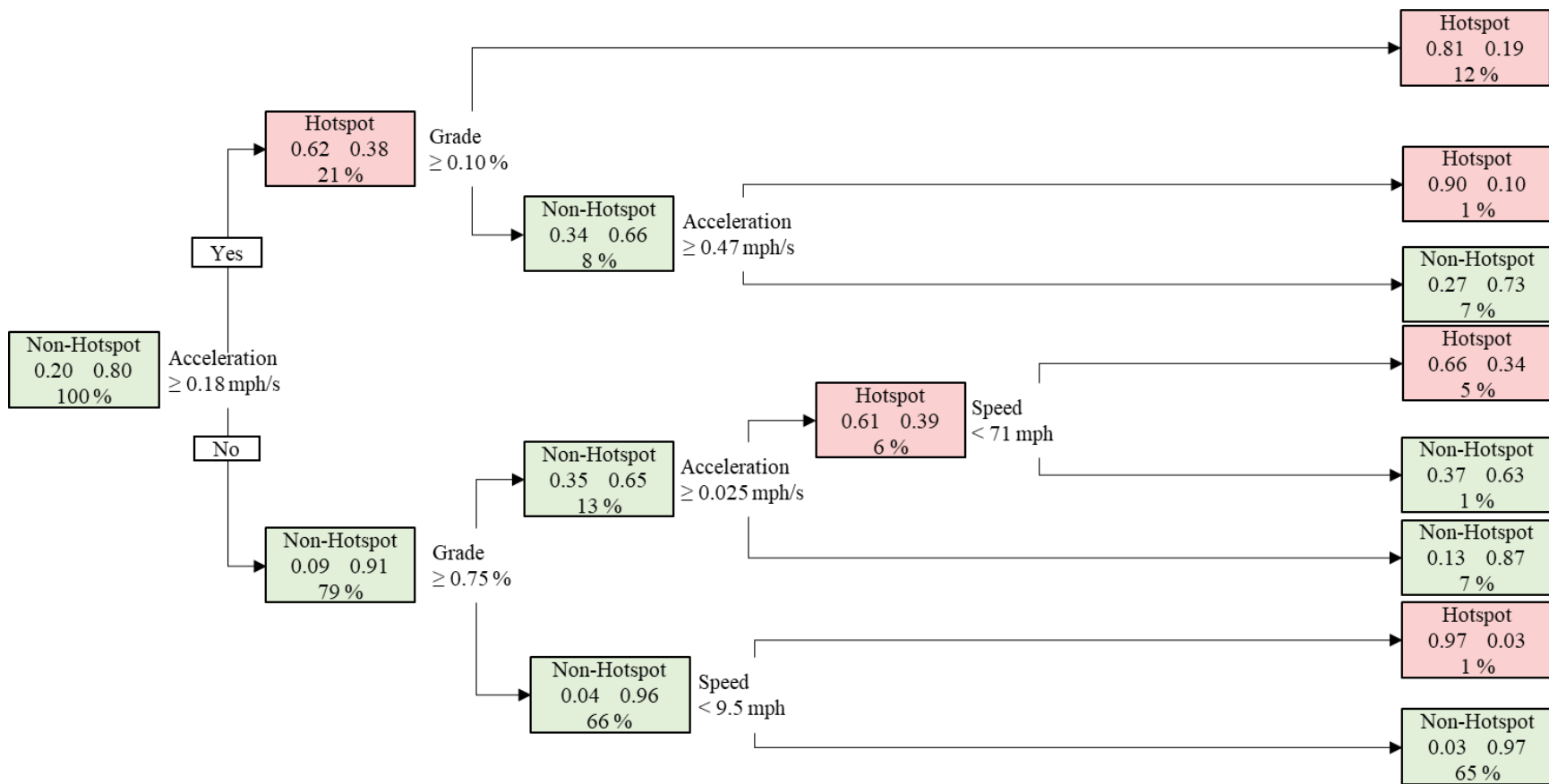


Figure A-27. Fuel Simplified Model with Dynamic Variables: Calibration of Classification and Regression TreeA-based Fuel Hotspot Simplified Model including Segment-Run Average Speed, Acceleration, Grade, and Curvature as Dynamic Variables without Locomotive and Consist based on 26 One-Way Trips in Either Travel Direction.

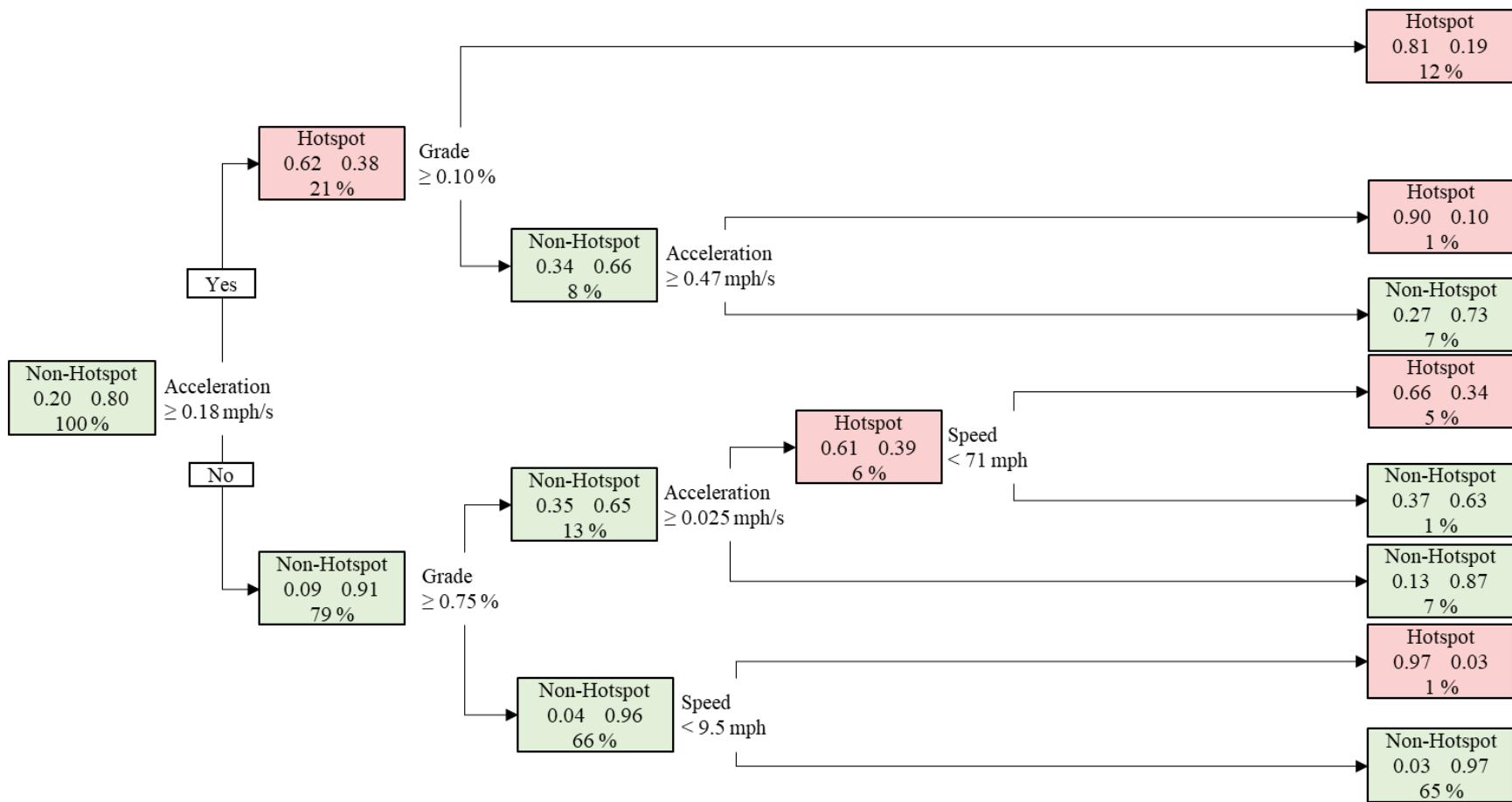


Figure A-28. Fuel Simplified Model with Dynamic and Static Variables: Calibration of Classification and Regression Tree-based Fuel Hotspot Simplified Model including Segment-Run Average Speed, Acceleration, Grade, and Curvature as Dynamic Variables with Locomotive and Consist based on 26 One-Way Trips in Either Travel Direction.

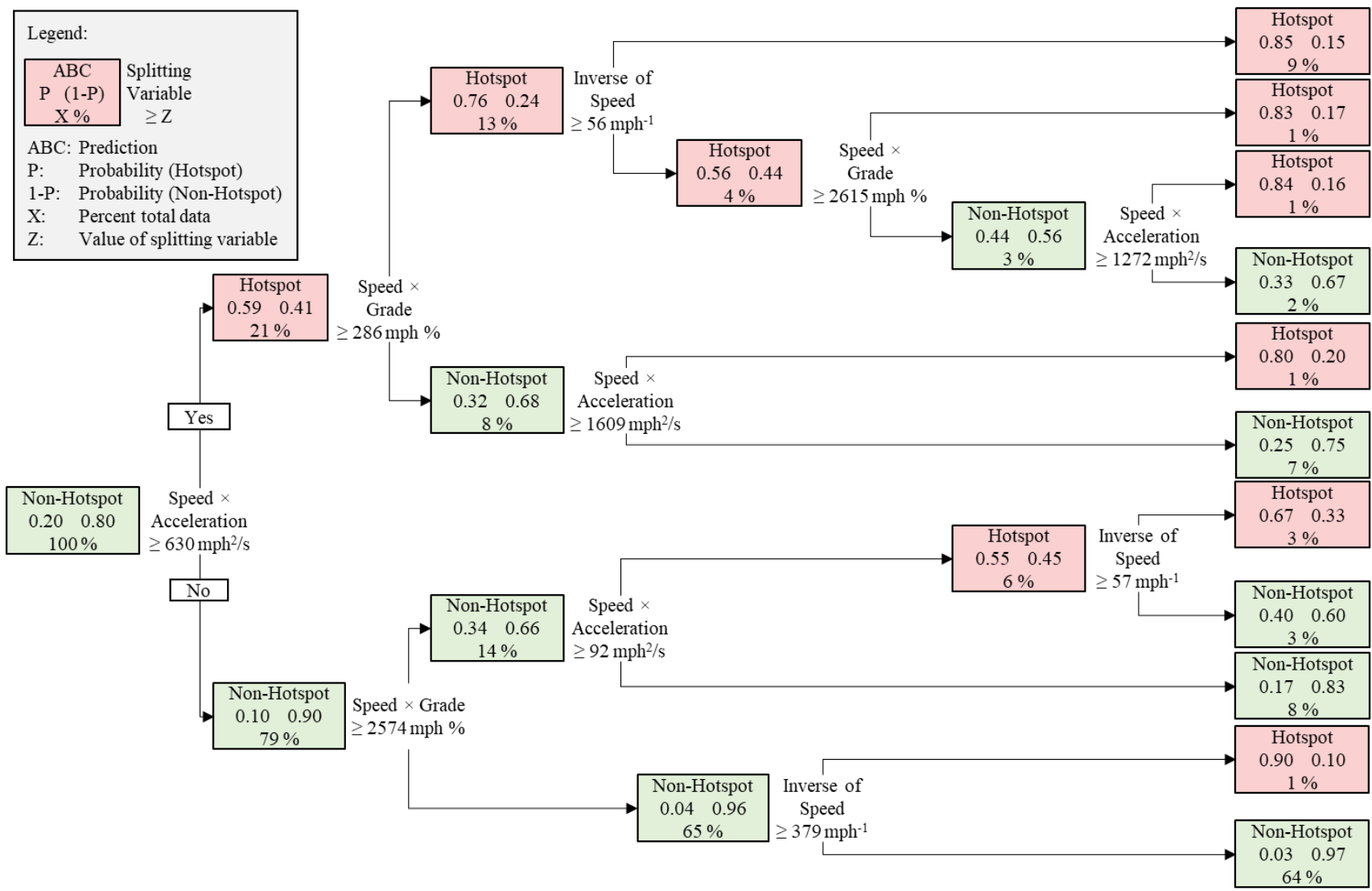


Figure A-29. NO_x Physical Model with Dynamic Variables: Calibration of Classification and Regression TreeA-based NO_x Hotspot Model including Dynamic Variables in the Physical Model without Locomotive and Consist as Static Variables based on 26 One-Way Trips in Either Travel Direction.

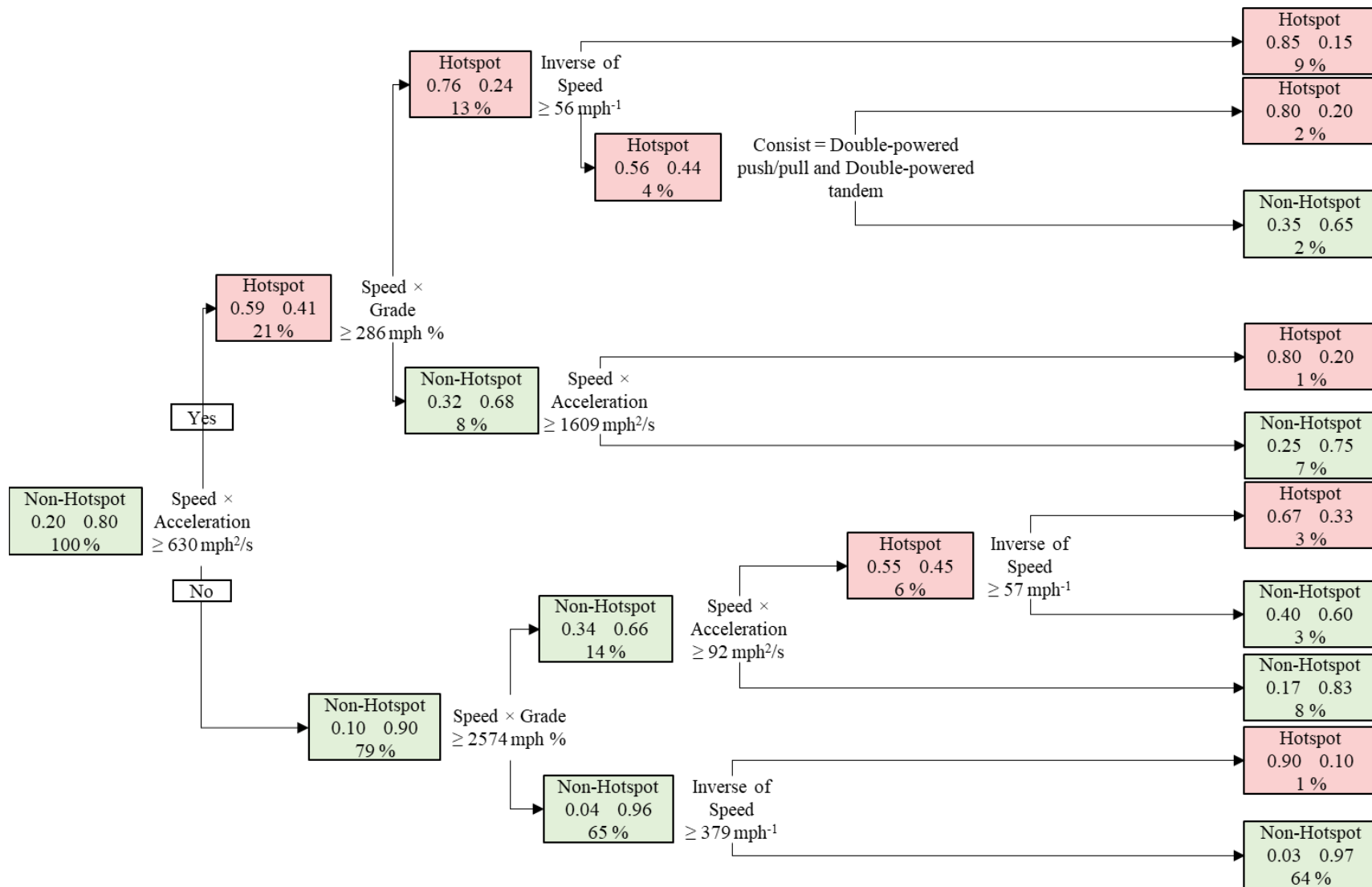


Figure A-30. NO_x Physical Model with Dynamic and Static Variables: Calibration of Classification and Regression TreeA-based NO_x Hotspot Model including Dynamic Variables in the Physical Model with Locomotive and Consist as Static Variables based on 26 One-Way Trips in Either Travel Direction.

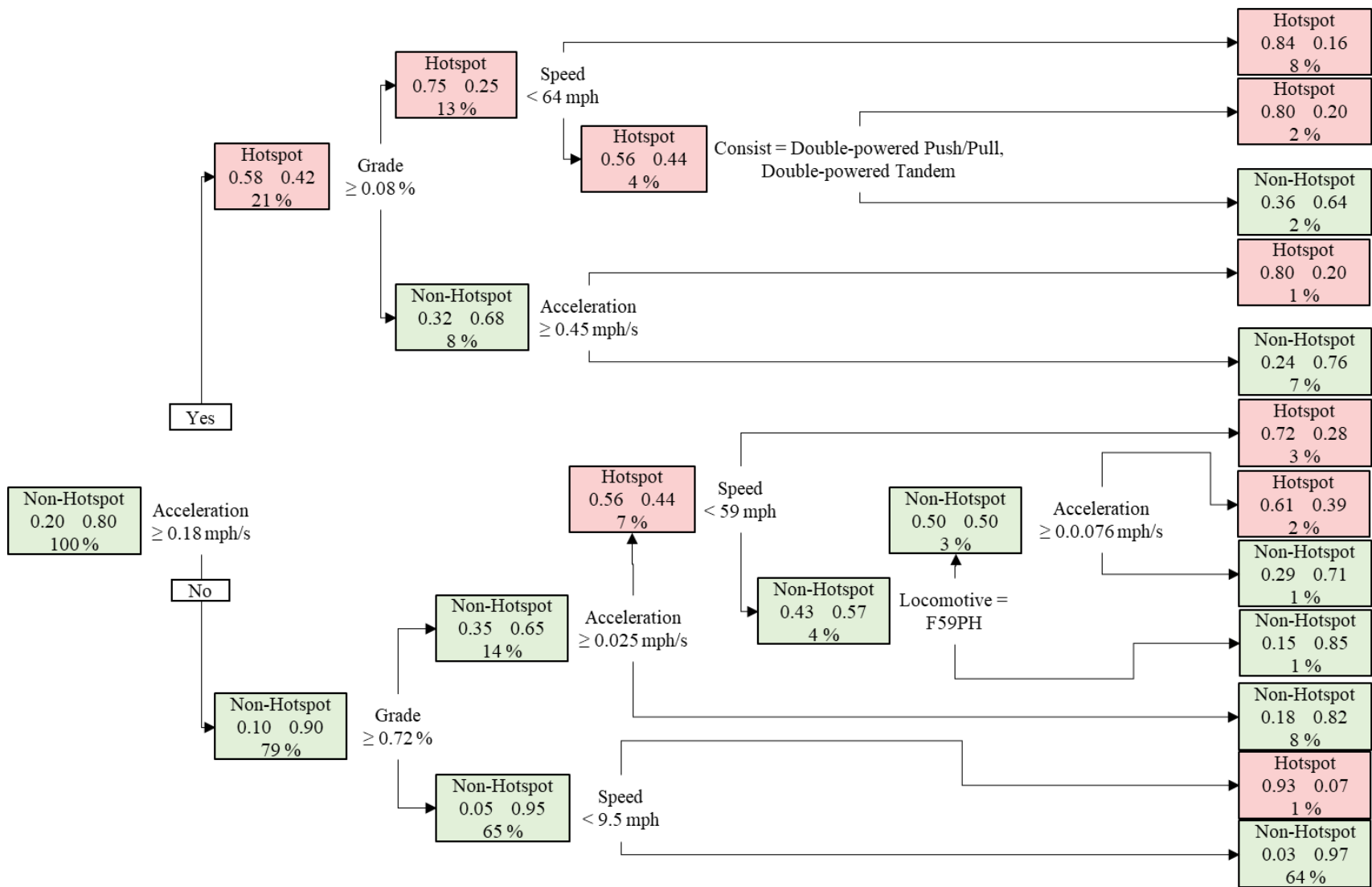


Figure A-32. NO_x Simplified Model with Dynamic and Static Variables: Calibration of Classification and Regression Tree-based NO_x Hotspot Simplified Model including Segment-Run Average Speed, Acceleration, Grade, and Curvature as Dynamic Variables with Locomotive and Consist based on 26 One-Way Trips in Either Travel Direction.

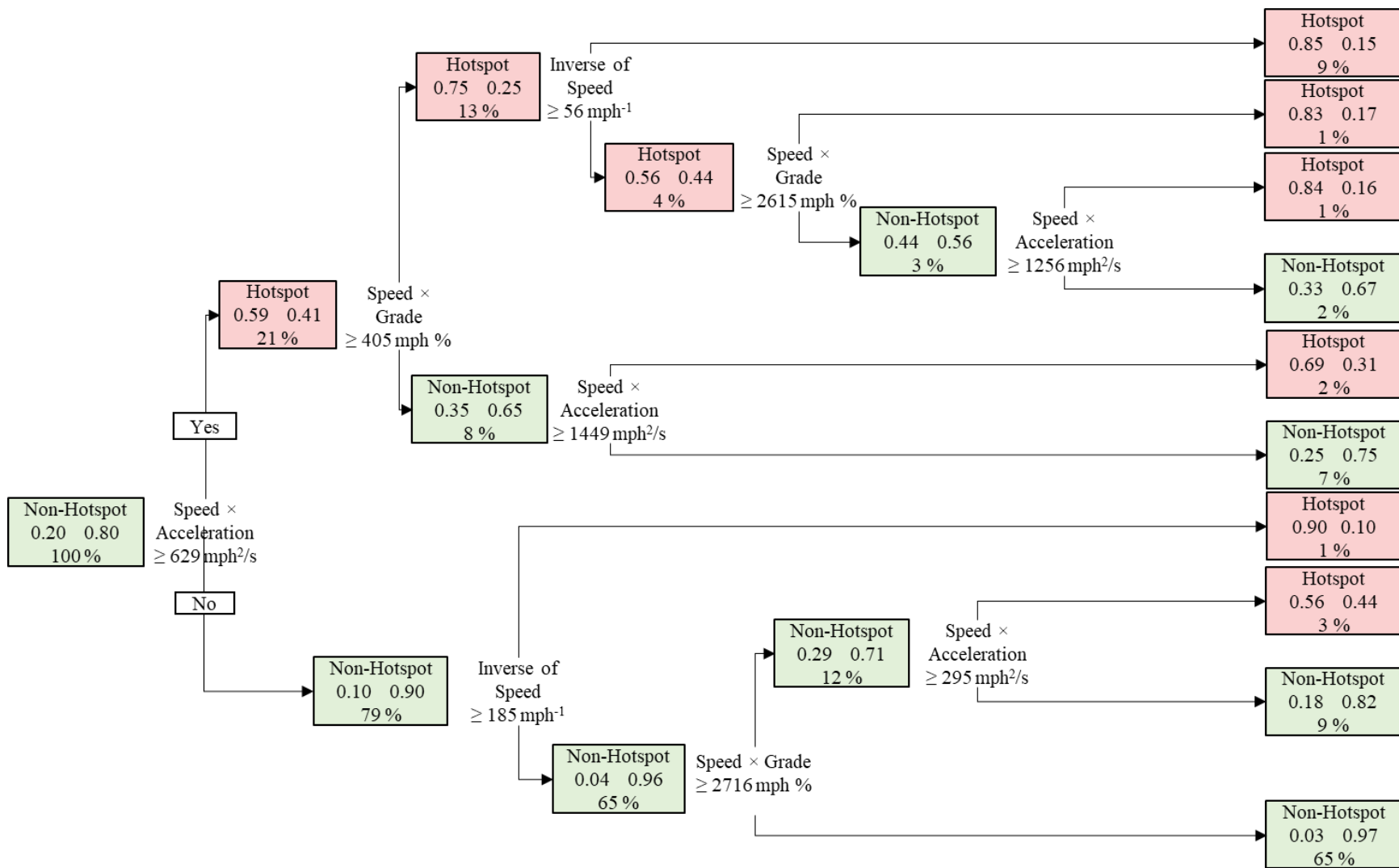


Figure A-33. PM Physical Model with Dynamic Variables: Calibration of Classification and Regression TreeA-Based PM Hotspot Model Including Dynamic Factors from the Full Physical Model Without Locomotive and Consist as Static Factors Based on 26 One-Way Trips in Either Travel Direction.

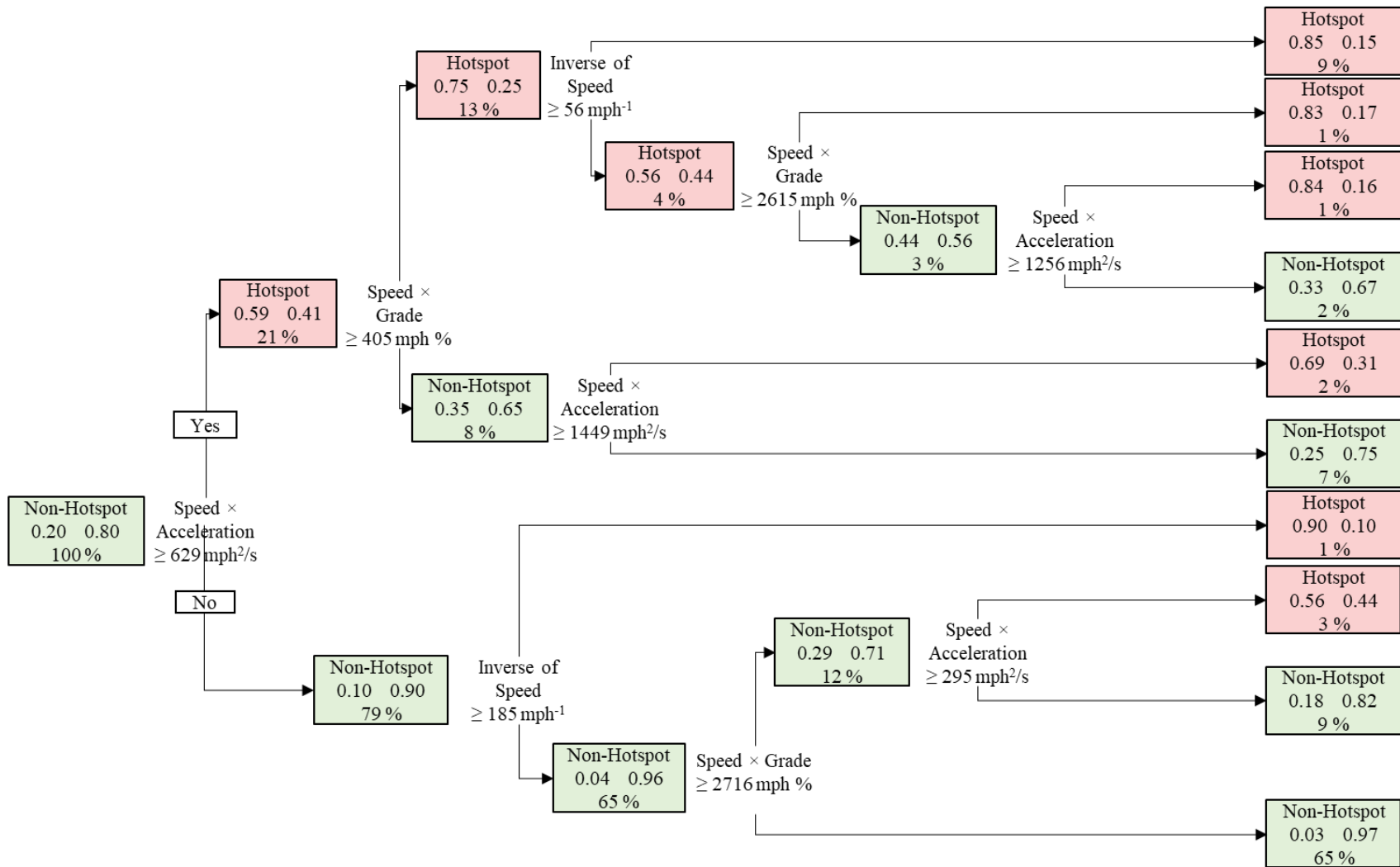


Figure A-34. PM Physical Model with Dynamic and Static Variables: Calibration of Classification and Regression Tree-Based PM Hotspot Model Including Dynamic Factors from the Full Physical Model with Locomotive and Consist as Static Factors based on 26 One-Way Trips in Either Travel Direction.

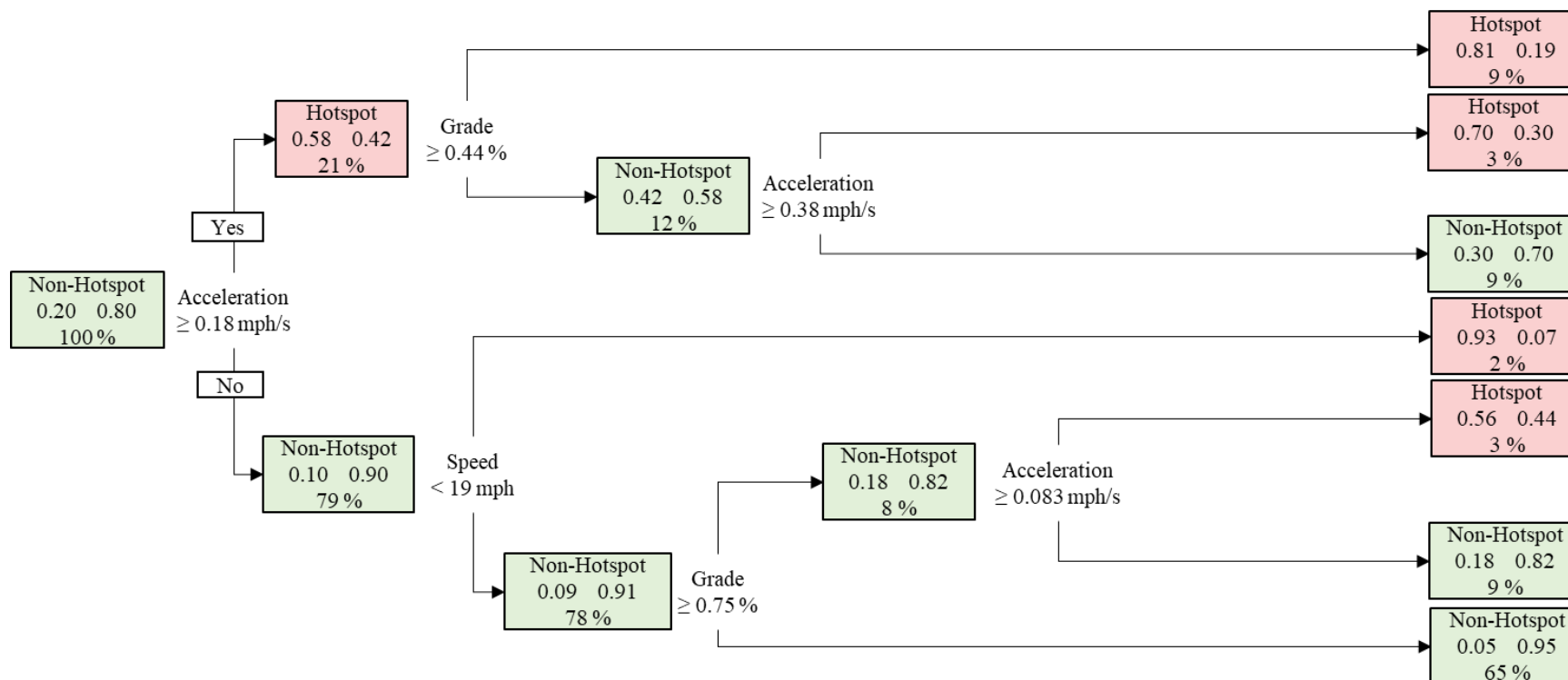


Figure A-35. PM Simplified Model with Dynamic Variables: Calibration of Classification and Regression TreeA-Based PM Hotspot Model Including Segment-Run Average Speed, Acceleration, Grade, and Curvature as Dynamic Factors Without Locomotive and Consist based on 26 One-Way Trips in Either Travel Direction.

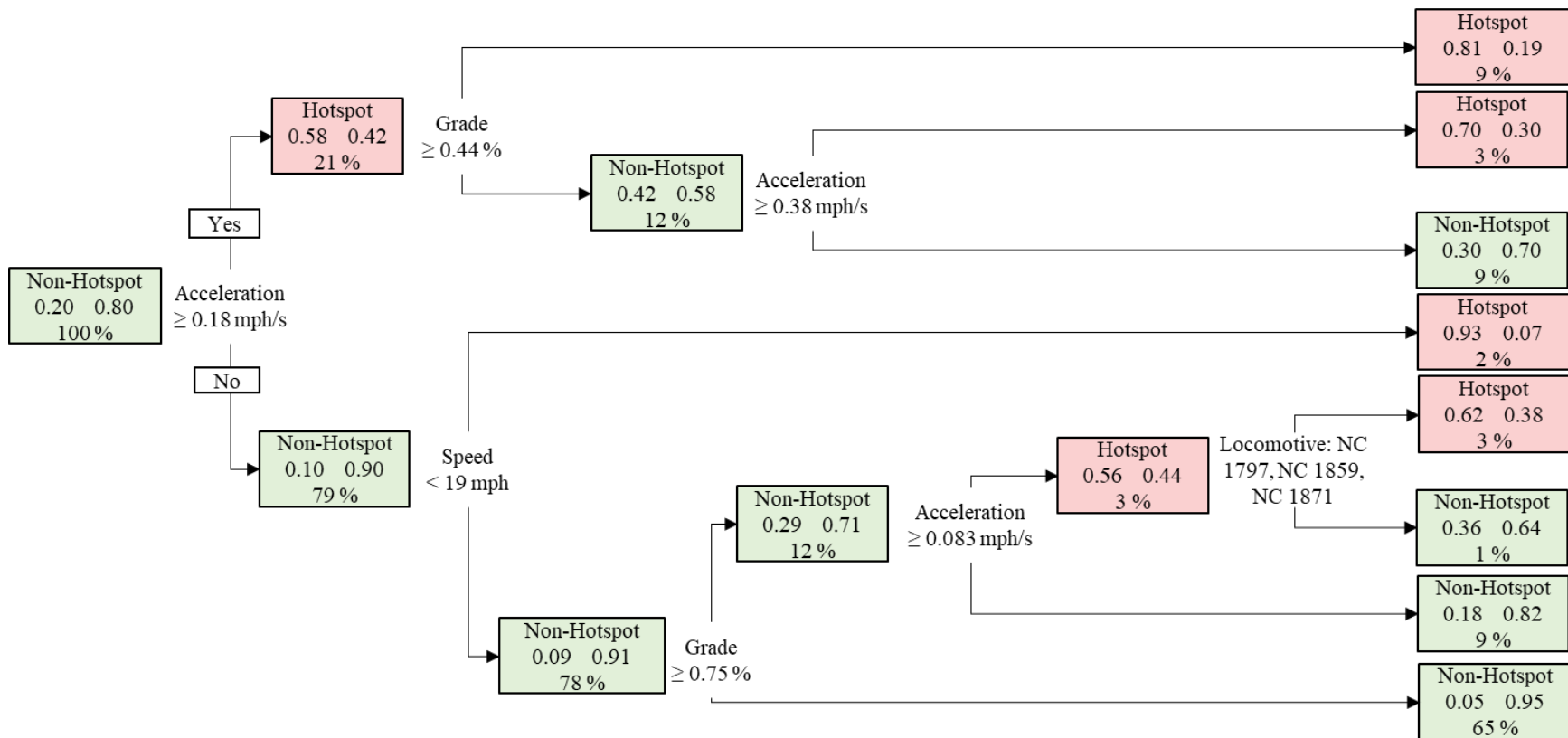


Figure A-36. PM Simplified Model with Static and Dynamic Variables: Calibration of Classification and Regression Tree-Based PM Hotspot Model Including Segment-Run Average Speed, Acceleration, Grade, and Curvature as Dynamic Factors with Locomotive and Consist based on 26 One-Way Trips in Either Travel Direction.

To quantify the sensitivity of the location of hotspots to locomotives and consists, the PD models were compared with PDS models for the corresponding species. The PDS fuel model was identical to PD fuel model. The PDS NO_x model was typically similar to the PD NO_x model, except for one split. For this split, the splitting variable of SOP of speed and acceleration in the PD model was replaced by consist in the PDS model. This split accounted for only 4% of all segment-runs, 2% each for hotspots and non-hotspots. No split occurred for locomotive as a distinguishing variable. Therefore, the addition of two static variables did not change the model substantially. Therefore, locomotives and consists were not key variables in distinguishing hotspots from non-hotspots. For PM, the PDS model was identical to the PD model. For each species, curvature, locomotives, and consists were not key variables. Key variables were speed, SOP of speed and acceleration, and SOP of speed and grade.

Terms such as SOP of speed and acceleration and SOP of speed and grade add complexity, which may not be essential to distinguishing between hotspots and non-hotspots. Therefore, models with simplified variables, that are not based on sums of products, including segment-run average speed, acceleration, grade, curvature, locomotives, and consists were evaluated. For each specie, the SD model was typically similar to the PD model in terms of the number of nodes and the number of data in each node. For some of the branches, variables used for splitting in the SD model were closely related to the PD model. For example, for a split occurring based on SOP of speed and acceleration in the PD model, a similar split occurred in the SD model based on segment-average acceleration. Similarly, the splits based on SOP of speed and grade in the PD model occurred based on segment-average grade in the SD model. With these substitutions, the trees were similar for SD versus PD models. Since the SD models for fuel, NO_x and PM were similar to each other, model insights based on NO_x are described. For easier cross-referencing, the terminal nodes in Figure A-31 are numbered from 1 to 11.

Based on the NO_x SD model, the plurality of hotspots (34% of all hotspots) were associated with Node 1:

- speed <64 mph;
- acceleration ≥ 0.18 mph/s; and
- grade $\geq 0.08\%$.

Segment-runs with these conditions had an 84% likelihood of being a hotspot.

The maximum proportion of NO_x non-hotspots (80% of all non-hotspots) were associated with Node 11:

- speed >9 mph;
- acceleration <0.18 mph/s; and
- grade <0.72 %.

Segment-runs meeting these conditions had a 97% likelihood of being a non-hotspot. None of the splits were based on curvature. Therefore, curvature was not a key variable.

To identify the combinations of variables associated with hotspots and non-hotspots at S, NSA, NSD, and I, the number of segment-runs corresponding to each location were quantified for each node. The number of segment-runs that were S, NSA, NSD, or I within each node are given in Table A-17.

Table A-17. Number of Segment-Runs Corresponding to Station, Near Station Acceleration, Near Station Deceleration, and Intermediate Segments within Each Node of the Simplified Model with Dynamic Variables for NO_x.

Node ^a	Number of Segment-Runs					Percentage of all Segment-Runs (%)
	S ^b	NSA ^b	NSD ^b	I ^b	Total	
1	26	658	4	773	1461	8.4
2	0	12	0	169	181	1.0
3	0	13	0	88	101	0.6
4	0	3	4	420	427	2.5
5	0	40	4	155	199	1.1
6	0	51	22	1139	1212	7.0
7	24	44	0	430	498	2.9
8	0	4	0	641	645	3.7
9	0	31	0	1274	1305	7.5
10	105	15	15	13	148	0.9
11	0	88	1033	10034	11155	64.4
Total	155	959	1082	15136		
Percentage of all Segment-Runs (%)	0.9	5.5	6.2	87.3		

^a Node number mentioned here corresponds to the node number of the terminal branch of Simplified Model with Dynamic Variables for NO_x (SD NO_x Model, Figure A-31).

^b Segment Location: station segments (S) defined as segments containing stations near station acceleration segments (NSA) defined as segments within 1.25 mile downstream of station segments where trains typically accelerate; near station deceleration segments (NSD) defined as segments within 1.25 mile upstream of station segments where trains typically decelerate; and, intermediate segments (I) defined as segments other than S, NSA and NSD.

The sensitivity of hotspot locations to locomotives and consists was quantified based on the comparison of SD models to SDS models. Similar to the comparison of PD and PDS models, locomotives and consists were not key variables in distinguishing hotspots from non-hotspots.

A.12.3 Importance of variables

In this section, the importance of potential explanatory variables in distinguishing hotspots from non-hotspots is quantified. Variable importance is described in Section 11.1. The importance of each variable in distinguishing hotspots from non-hotspots is presented in Figure A-37. For NO_x PD and PDS models, the importance of a given dynamic variable was approximately the same in either model. For example, the SOP of speed and acceleration had an importance of 54% in the

PD model and 51% in the PDS model. In the PDS model, the importance of static variables, including locomotives and consists, was <2% each. Therefore, locomotive and consists had a negligible effect on distinguishing hotspots from non-hotspots. Likewise, for SD and SDS models, importance of dynamic variables was similar among the models and the importance of static variables was <2% each.

The importance of variables among the four models for each species are compared. For each species and model, the variables based on acceleration were the most important. In the PD and PDS models, the importance of SOP of speed and acceleration was 54% and 51%, respectively. In the SD and SDS models, the importance of segment-average acceleration was 57% and 54%, respectively. Variables based on grade had the second-highest VI in each model. In the PD and PDS models, the VI of SOP of speed and grade varied between 18% and 24%. In the SD and SDS models, the VI of segment-average grade varied between 20% and 28%. Variables based solely on speed, such as sum of speed, sum of speed², sum of speed³, and segment-average speed were the third most important group of variables. In the PD and PDS models, the VI of the sum of speed, sum of speed², sum of speed³ varied between 17% and 23%. In the SD and SDS models, the VI of segment-average speed varied between 13% and 17%. For each species and model, the variables based on curvature, locomotive and consist had lower VIs than the variables based on speed, acceleration, or grade. In each model, VI for curvature was 0.3% or lower. In the PDS and SDS models, the VI of each of locomotive and consist was 3% or lower.

A.12.4 Model Evaluation

This section describes the evaluation of CART models for accuracy and precision based on calibrated and validated data. The classification models are evaluated in terms of exact matches and misclassification for modeled versus measured hotspots. For a binary classification among *N* segment-runs with complete data, such as “Hotspots” and “Non-Hotspots,” models were compared in terms of:

- True positives (TP) is the number of measured hotspots that were also modeled as hotspots.
- True negatives (TN) is the number of measured non-hotspots that were modeled as non-hotspots.
- False positives (FP) is the number of measured non-hotspots that were modeled as hotspots.
- False negatives (FN) is the number of measured hotspots that were modeled as non-hotspots.

The model accuracy (MA) is the proportion of correct classifications with respect to the total number of observations. The model accuracy was estimated as:

$$MA = \frac{TP + TN}{N} \times 100 \tag{A-11}$$

Where,

- | | | |
|-----------|---|--|
| <i>MA</i> | = | Model Accuracy |
| <i>TP</i> | = | True positives: number of measured hotspots modeled as hotspots. |
| <i>TN</i> | = | True negatives: number of measured non-hotspots modeled as not hotspots. |
| <i>N</i> | = | Number of segment-runs with complete data |

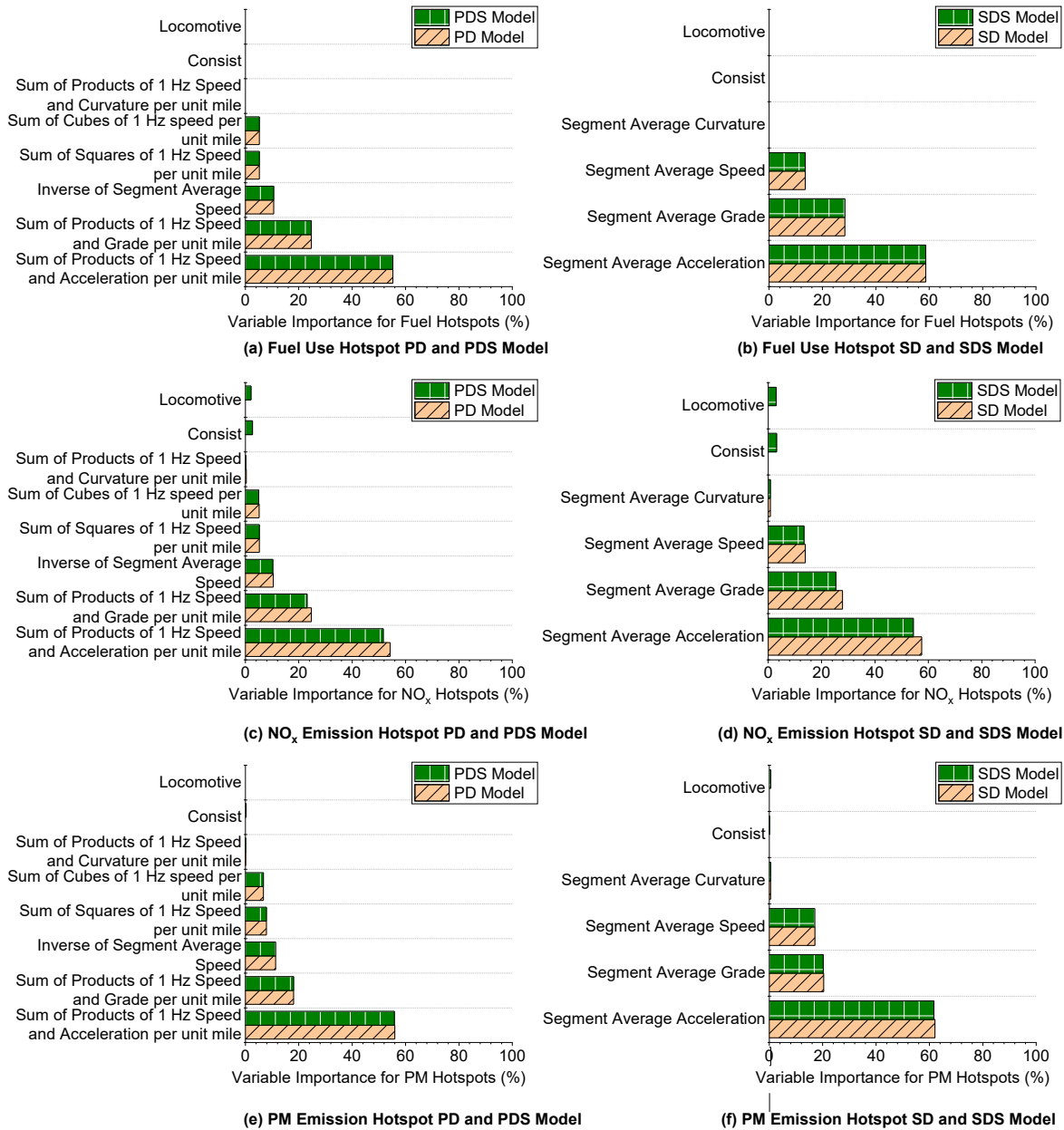


Figure A-37. Importance of Variables Used in Four Classification and Regression Tree Models in Distinguishing Hotspots from Non-Hotspots based on Calibration Data: (a) Fuel Use PD and PDS Model; (b) Fuel Use Model SD and SDS Model; (c) NO_x PD and PDS Model; (d) NO_x SD and SDS Model; (e) PM PD and PDS Model; and (f) PM SD and SDS Model.

Physical model with dynamic variables (PD) includes all dynamic variables specified in Equation A-9. Physical model with dynamic and static variables (PDS) includes both static and dynamic variables. Static variables include locomotive and consist. Simplified model with dynamic variables (SD) includes simplified dynamic variables such as segment-average speed, acceleration, grade, and curvature. Simplified model with dynamic and static variables (SDS) includes simplified dynamic variables and static variables.

Variable Importance for a given model was estimated based on 17,332 segment-runs each used for fuel use and NO_x model calibration, and 16,602 segment-runs used for PM model calibration.

The model precision (MP) is the proportion of the modeled hotspots that are correctly identified.

The model precision was estimated as:

$$MP = \frac{TP}{TP + FP} \times 100 \quad (A-12)$$

Where,

MP = Model precision

MA and MP vary between 0% and 100%. The ideal value of MA and MP is 100% for a perfect model. Therefore, values of MA and MP close to 100% indicate a good model. The four CART models each for fuel use, NO_x, and PM hotspot models are evaluated in Table A-18. Each of the four NO_x Models had approximately similar TP, TN, FP, and FN. Therefore, MA and MP were also approximately similar. MA varied between 89.6 % and 90 % for the calibration data and 88.4 % and 89.2 % for the validation data. Thus, all models are similarly accurate and precise. The PM and fuel use model performance was similar to NO_x hotspot Models.

Since SD has the least number of variables, all of which are simple and easy to interpret for practitioners, SD is most appropriate for identifying emission hotspots. Simplified rules in terms of segment-average speed, acceleration, and grade can be conveyed to train operators for better managing their operations to reduce fuel use and emission rates and hotspots. For future track designs, designers could be informed of grades that will result in lower emissions.

Table A-18. Comparison of Classification and Regression Tree Models for NO_x and PM Emission Hotspots

Pollutant	Model ^a	Calibration Data ^b						Validation Data ^c					
		TP ^d	TN ^d	FP ^d	FN ^d	MA ^d (%)	MP ^d (%)	TP ^d	TN ^d	FP ^d	FN ^d	MA ^d (%)	MP ^d (%)
Fuel	PD	2111	13441	538	1242	89.7	79.7	766	4461	203	436	89.1	79.1
	PDS	2194	13340	561	1237	89.6	79.6	780	4406	223	457	88.4	77.8
	SD	2086	13441	468	1337	89.6	81.7	751	4474	185	456	89.1	80.2
	SDS	2332	13262	613	1125	90.0	79.2	704	4528	181	453	89.2	79.5
NO _x	PD	2222	13330	527	1253	89.7	80.8	744	4483	207	432	89.1	78.2
	PDS	2216	13318	539	1259	89.6	80.4	765	4421	212	468	88.4	78.3
	SD	2129	13398	459	1346	89.6	82.3	715	4510	180	461	89.1	79.9
	SDS	2356	13238	619	1119	90.0	79.2	733	4499	189	445	89.2	79.5
PM	PD	2270	12372	893	1067	88.2	71.8	771	4324	364	405	86.9	67.9
	PDS	2270	12372	893	1067	88.2	71.8	754	4354	351	405	87.1	68.2
	SD	2110	12556	709	1227	88.3	74.8	726	4397	291	450	87.4	71.4
	SDS	2067	12633	632	1270	88.5	76.6	743	4299	306	516	86.0	70.8

^a Physical model with dynamic variables (PD) includes all dynamic variables specified in Equation A-9. Physical model with dynamic and static variables (PDS) includes both static and dynamic variables. Static variables include locomotive and consist. Simplified model with dynamic variables (SD) includes simplified dynamic variables such as segment-average speed, acceleration, grade, and curvature. Simplified model with dynamic and static variables (SDS) includes simplified dynamic variables and static variables.

^b Calibration data comprises segment-runs from all but one one-way trip for a given combination of locomotive and consist.

^c Validation data comprises the one-way trip left out from the calibration data.

^d TP: number of true positives; TN: number of true negatives; FP: number of false positives; FN: number of false negatives; MA: model accuracy; and MP: model precision.

A.13 References Cited in Appendix A

- 40 CFR 1033, 1998. Control of Emissions from Locomotives. Fed. Regist. 63, 18978–19084.
- 40 CFR 1065, S.J., 2005. Field Testing and Portable Emission Measurement Systems. Fed. Regist. 70, 40599–40604.
- Amtrak, 2018. Amtrak Sustainability Report 2016-17. National Passenger Rail Corporation (Amtrak).
- AREMA, 2020. American Railway Engineering and Maintenance-of-way Association Manual for Railway Engineering. Lanham, MD.
- Boroujeni, B.Y., Frey, H.C., 2014. Road grade quantification based on global positioning system data obtained from real-world vehicle fuel use and emissions measurements. Atmos. Environ. 85, 179–186.
- Boroujeni, B.Y., Frey, H.C., Sandhu, G.S., 2013. Road grade measurement using in-vehicle, stand-alone GPS with barometric altimeter. J. Transp. Eng. 139, 605–611.
- Breiman, L., Friedman, J., Olshen, R., Stone, C., 1984. Classification and Regression Trees. Chapman & Hall/CRC, Boca Raton, FL 33487-2742.
- Butler, J., Gierczak, C., Liscombe, P., Lesko, J., New, D., 1995. Factors Affecting the NDIR Measurement of Exhaust Hydrocarbons, in: Published by the Coordinating Research Council, Published for the CRC 5th On-Road Vehicle Emissions Workshop.
- Cullen, A.C., Frey, H.C., 1999. Probabilistic techniques in exposure assessment: a handbook for dealing with variability and uncertainty in models and inputs. Springer Science & Business Media.
- Durbin, T.D., Johnson, K., Cocker, D.R., Miller, J.W., Maldonado, H., Shah, A., Ensfield, C., Weaver, C., Akard, M., Harvey, N., Symon, J., Lanni, T., Bachalo, W.D., Payne, G., Smallwood, G., Linke, M., 2007. Evaluation and Comparison of Portable Emissions Measurement Systems and Federal Reference Methods for Emissions from a Back-Up Generator and a Diesel Truck Operated on a Chassis Dynamometer. Environ. Sci. Technol. 41, 6199–6204. <https://doi.org/10.1021/es0622251>
- Elgowainy, A., Vyas, A., Biruduganti, M., Shurland, M., 2018. Railroad Energy Intensity and Criteria Air Pollutant Emissions (No. DOT/FRA/ORD-18/34). Argonne National Laboratory, Argonne, IL United States 60439.
- EPA, 1998. Locomotive Emission Standards: Regulatory Support Document (No. EPA/98-04). U.S. Environmental Protection Agency, Ann Arbor, MI.
- Flagan, R.C., Seinfeld, J.H., 2012. Fundamentals of air pollution engineering. Courier Corporation.
- Frey, H.C., Burmaster, D.E., 1999. Methods for characterizing variability and uncertainty: comparison of bootstrap simulation and likelihood-based approaches. Risk Anal. 19, 109–130.
- Frey, H.C., Choi, H.W., Kim, K., 2012. Portable Emission Measurement System for Emissions of Passenger Rail Locomotives. Transp. Res. Rec. J. Transp. Res. Board 2289, 56–63.

- Frey, H.C., Graver, B.M., 2012. Measurement and evaluation of fuels and technologies for passenger rail service in North Carolina. Prepared by North Carolina State University for North Carolina Department of Transportation.
- Frey, H.C., Hu, J., 2015. Measurement of Locomotive Head End Power Engine Fuel and Emissions (Technical Report No. 0704–0188). Prepared by North Carolina State University for North Carolina Department of Transportation, Raleigh, NC.
- Frey, H.C., Rastogi, N., 2019. Managing Energy and Emissions for Rail Operations (No. FHWA/NC/2018-09). Prepared by North Carolina State University for North Carolina Department of Transportation, Raleigh, NC.
- Frey, H.C., Rastogi, N., 2018. Evaluation of Locomotive Emissions Reduction Strategies (No. FHWA/NC/2016-20). Prepared by North Carolina State University for North Carolina Department of Transportation, Raleigh, NC.
- Fritz, S.G., California Environmental Protection Agency., Air Resources Board., Fuels Section., Southwest Research Institute., 2000. Diesel fuel effects on locomotive exhaust emissions. Prepared for California Air Resources Board by Southwest Research Institute, San Antonio, TX; Sacramento, CA.
- GlobalMRV, 2014. Axion R/S™ Basic User's Manual.
- Graver, B.M., Frey, H., 2013. Comparison of Locomotive Emissions Measured During Dynamometer Versus Rail Yard Engine Load Tests. *Transp. Res. Rec. J. Transp. Res. Board* 23–33.
- Graver, B.M., Frey, H.C., 2016. Highway Vehicle Emissions Avoided by Diesel Passenger Rail Service Based on Real-World Data. *Urban Rail Transit* 2, 153–171.
- Graver, B.M., Frey, H.C., 2015. Comparison of Over-the-Rail and Rail Yard Measurements of Diesel Locomotives. *Environ. Sci. Technol.* 49, 13031–13039.
- Graver, B.M., Frey, H.C., Hu, J., 2016. Effect of Biodiesel Fuels on Real-World Emissions of Passenger Locomotives. *Environ. Sci. Technol.* 50, 12030–12039.
- Hay, W.W., 1982. *Railroad engineering*. John Wiley & Sons, New York.
- Johnson, K.C., Durbin, T.D., Jung, H., Cocker, D.R., Bishnu, D., Giannelli, R., 2011. Quantifying In-Use PM Measurements for Heavy Duty Diesel Vehicles. *Environ. Sci. Technol.* 45, 6073–6079. <https://doi.org/10.1021/es104151v>
- Khan, M.Y., Johnson, K.C., Durbin, T.D., Jung, H., Cocker, D.R., Bishnu, D., Giannelli, R., 2012. Characterization of PM-PEMS for in-use measurements conducted during validation testing for the PM-PEMS measurement allowance program. *Atmos. Environ.* 55, 311–318. <https://doi.org/10.1016/j.atmosenv.2012.03.004>
- Miller, J.W., Durbin, T., Johnson, K., Cocker III, D., 2006. Evaluation of Portable Emissions Measurement Systems (PEMS) for Inventory Purposes and the Not-To-Exceed Heavy-Duty Diesel Engine Regulation (No. 03–345). Prepared for California Air Resources Board by University of California Riverside, Riverside, CA.

- Nakamura, H., Kihara, N., Adachi, M., Nakamura, S., Ishida, K., 2003. Development of hydrocarbon analyzer using heated-NDIR method and its application to on-board mass emission measurement system. *JSAE Rev.* 24, 127–133.
- Norfolk Southern, Center for Alternative Fuels Engines and Emissions, n.d. Locomotive Emissions Testing Facility. Altoona, Pennsylvania.
- Profillidis, V.A., 2014. *Railway management and engineering*. Ashgate Publishing, Ltd., Burlington, VT.
- Rastogi, N., Frey, H.C., 2018. Estimation of Rail Grade and Horizontal Curvature from Non-Proprietary Data Sources, in: *Proceedings of the Transportation Research Board 97th Annual Meeting*, 18-06366. Washington, D.C.
- Sandhu, G., Frey, H., 2013. Effects of errors on vehicle emission rates from portable emissions measurement systems. *Transp. Res. Rec. J. Transp. Res. Board* 10–19.
- Sensors Inc., 2011. SEMTECH-DS: On Board Vehicle Emissions Analyzer User Manual (No. 9510–086), Revision 2.02. Saline, MI.
- Singer, B.C., Harley, R.A., Littlejohn, D., Ho, J., Vo, T., 1998. Scaling of infrared remote sensor hydrocarbon measurements for motor vehicle emission inventory calculations. *Environ. Sci. Technol.* 32, 3241–3248.
- Stephens, R.D., Cadle, S.H., Qian, T.Z., 1996a. Analysis of remote sensing errors of omission and commission under FTP conditions. *J. Air Waste Manag. Assoc.* 46, 510–516.
- Stephens, R.D., Mulawa, P.A., Giles, M.T., Kennedy, K.G., Grobiicki, P.J., Cadle, S.H., Knapp, K.T., 1996b. An experimental evaluation of remote sensing-based hydrocarbon measurements: A comparison to FID measurements. *J. Air Waste Manag. Assoc.* 46, 148–158.
- SwRI, 2016. *SwRI Upgrades Locomotive Technology Center to Meet EPA Certification Guidelines*. San Antonio, TX.
- Tsolakis, A., Megaritis, A., Wyszynski, M.L., Theinnoi, K., 2007. Engine performance and emissions of a diesel engine operating on diesel-RME (rapeseed methyl ester) blends with EGR (exhaust gas recirculation). *Energy* 32, 2072–2080.
- Vojtisek, M., Kotek, M., 2014. Estimation of Engine Intake Air Mass Flow Using a Generic Speed-Density Method. *J. Middle Eur. Constr. Des. Cars* 12, 7–15.
- Vojtisek-Lom, M., Allsop, J.E., 2001. Development of Heavy-Duty Diesel Portable, On-Board Mass Exhaust Emissions Monitoring System with NO_x, CO₂ and Qualitative PM Capabilities. SAE Technical Paper.
- Vu, D., Szente, J., Loos, M., Maricq, M., 2020. How Well Can mPEMS Measure Gas Phase Motor Vehicle Exhaust Emissions? SAE Technical Paper.
- Weaver, C.S., Balam-Almanza, M.V., 2001. Development of the ‘RAVEM’ Ride-Along Vehicle Emission Measurement System for Gaseous and Particulate Emissions. SAE Technical Paper.
- Weaver, C.S., Petty, L.E., 2004. Reproducibility and accuracy of on-board emission measurements using the RAVEMTM System. SAE Technical Paper.

Appendix B. Supporting Information for Chapter 3

B.1 Locomotive Power Demand

Locomotive FUERs are directly proportional to the tractive effort of the locomotive. The tractive effort, known as locomotive power demand (LPD), is estimated based on the resistive forces opposing train motion. Locomotive FUERs vary spatially due to differences in speed, acceleration, grade, and curvature along a railroad route (AREMA, 2020; Hay, 1982; Profillidis, 2014). Therefore, some locations may have higher emissions than others, leading to emissions hotspots. This section describes the resistive forces, key variables affecting the magnitude and direction of resistive forces, and estimation of LPD based on these variables.

B.1.1 Resistive forces

The motion of a train is opposed by several resistive forces, including: (1) starting resistance; (2) journal resistance; (3) flange resistance; (4) air resistance; (5) wind resistance; (6) curve resistance; (7) grade resistance; (8) acceleration resistance; and (9) internal resistance (Hay, 1982; Profillidis, 2014). The higher the magnitude of resistive forces, the higher is the required tractive effort and, thus, the higher will be the FUERs for a locomotive.

Starting resistance is typically encountered when the train begins to move from a stop. Starting resistance depends on the inertia of the train and the low temperature of journal lubricants. Starting resistance is typically estimated at 18 lbs/ton, although it can be up to 50 lbs/ton due to cold temperatures, long halts, or poor lubrication:

$$R_{s,t} = \begin{cases} 18 \frac{\text{lbs}}{\text{ton}} & \text{if } v_{t-1} = 0 \text{ and } v_t > 0 \\ 0 & \text{otherwise} \end{cases} \quad (\text{B-1})$$

Where,

$$\begin{aligned} R_{s,t} &= \text{Starting resistance at time } t \text{ (lbs/ton)} \\ v_t &= \text{Train speed at time } t \text{ (mph)} \\ v_{t-1} &= \text{Train speed at time } t-1 \text{ (mph)} \end{aligned}$$

Journal resistance includes journal friction, rolling resistance, and track resistance, and varies with axle load. Journal resistance is independent of train speed. For locomotives and passenger cars with different weight per unit axles, the journal resistance was estimated individually for each locomotive and passenger car as:

$$R_{j,t} = \left(0.6 + \frac{20}{w} \right) \quad (\text{B-2})$$

Where,

$$\begin{aligned} R_{j,t} &= \text{journal resistance (lbs/ton)} \\ w &= \text{weight of locomotive per axle } (w_l) \text{ or passenger car per axle } (w_p) \text{ (tons/axle)} \end{aligned}$$

Flange resistance includes flange friction between the track and wheel flange, and oscillation (swaying and concussion). Flange resistance varies directly with train speed. The coefficient of proportionality between flange resistance and train speed is the flange resistance coefficient. Flange resistance was estimated as:

$$R_{f,t} = B \times v_t \quad (\text{B-3})$$

Where,

$$\begin{aligned} R_{f,t} &= \text{flange resistance at time } t \text{ (lbs/ton)} \\ B &= \text{flange resistance coefficient (lbs/ton-mph)} \end{aligned}$$

Air resistance is the drag on a train due to still air and varies with the square of train speed. Train air resistance is the sum of air resistance for each locomotive and each passenger car. Since the drag is different for the lead locomotive versus trailing locomotives and passenger cars, the drag resistance should be estimated separately for each. For a train consist with multiple locomotives, the front and sides of the lead locomotive are fully exposed to the atmosphere. In contrast, for the trailing locomotive(s), the sides are fully exposed, similar to passenger cars. Thus, for estimating drag, any trailing locomotive(s) is assumed to be similar to passenger cars. Air resistance of locomotive or a passenger car for speeds up to 60 mph is estimated as (Hay, 1982; Profillidis, 2014):

$$R_{d,t} = \frac{C_d \times F \times v_t^2}{w \times n} \quad (\text{B-4})$$

Where,

$$\begin{aligned} R_{d,t} &= \text{air resistance for a locomotive or a passenger car with speeds less than 60 mph at time } t \text{ (lbs/ton)} \\ C_d &= \text{drag coefficient of the locomotive or a passenger car based on the shape of the front end and the overall configuration, including turbulence from car trucks, air brake fittings under the cars, space between cars, skin friction and eddy currents, and the turbulence and partial vacuum at the rear end (lbs/ft}^2\text{-mph}^2\text{)}. \text{ See Table B-1 for typical values.} \\ F &= \text{frontal cross-sectional area of the locomotive } (F_l) \text{ or passenger car } (F_p) \text{ in (ft}^2\text{)}. \\ n &= \text{number of axles in a locomotive } (n_l) \text{ or a passenger car } (n_p) \end{aligned}$$

For speeds greater than 60 mph, more complex and data-intensive calculations than Equation B-10 are sometimes used to estimate air resistance more accurately. For example, estimation of the drag coefficient requires a streamline design factor, the value of which is based on the combination of shapes of different exterior parts of a locomotive or a passenger car. However, the data for such calculations may not be available. Hence, most studies only use Equation B-10 as an estimate for air resistance to simplify the calculations for train speeds typically up to 100 mph (Drish, 1992; Kim et al., 2006; Lukaszewicz, 2009). The drag coefficient for locomotives, freight cars, and passenger cars is given in Table B-1.

Table B-1. Drag Coefficients and Frontal Area for Typical Diesel Locomotives and Passenger Cars in the U.S. (Source: Hay, 1984)

Equipment Type	Drag coefficient, C_d (lbs/ft ² -mph ²)
Lead Locomotive	0.0024
Streamlined Lead Locomotive	0.0017
Freight cars	0.0005
Trailing Locomotive(s) and Passenger cars	0.00034 ^a

^a *The passenger car is always behind the locomotive. Thus, only a part of the full frontal area of the passenger car leads to the drag resistance. Therefore, a passenger car and a locomotive with similar frontal areas do not create the same drag. The drag coefficient for passenger cars is 7 to 10 times lower than that of locomotives with similar frontal areas. Therefore, the effect of reduced exposed or effective frontal area is included in the drag coefficient of the passenger car. For a train consist with more than one locomotive, drag resistance is based on the leading locomotive. All trailing locomotive(s) and passenger cars are quantified in the same way as passenger cars because trailing units are not completely exposed to the atmosphere.*

Wind resistance ($R_{w,t}$) occurs due to the wind blowing over the tracks and can be accounted for by incorporating wind speed into Equation B-10. However, the effect of wind is typically ignored as the trains travel back and forth on a given route, thereby negating the net impact of wind direction over time. Therefore, wind speed is set to 0 and only air resistance is considered as a source of drag. Drag resistance, including air and wind resistance for a locomotive or a passenger car was estimated as:

$$R_{w,t} = \frac{C_d \times F \times (v_t + v_w)^2}{w \times n} \quad (\text{B-5})$$

Where,

$$\begin{aligned} R_{w,t} &= \text{drag resistance for trains with directly opposing wind at time } t \text{ (lbs/ton)} \\ v_{w,t} &= \text{wind speed opposite to train motion at time } t \text{ (mph)} \end{aligned}$$

Curve resistance is encountered on a horizontal curve. Curve resistance occurs due to the longitudinal and transverse sliding between the wheel and rail on a curve and the increased friction on the surface of the flange and inner rail because of the effect of lateral forces (Hay, 1982; Profillidis, 2014). Curve resistance is directly proportional to the degree of curve, also known as track curvature. The degree of a curve is the angle subtended by a 100-ft chord at the center of a curve. Curve resistance per unit train weight was estimated as (AREMA, 2020):

$$R_{c,t} = D \times d_t \quad (\text{B-6})$$

Where,

$$\begin{aligned} R_{c,t} &= \text{curvature resistance at time } t \text{ (lbs/ton)} \\ D &= \text{unit curve resistance (lbs/ton-degree of curve)} = 0.8 \\ d_t &= \text{degree of a curve at time } t \text{ (degrees)} \end{aligned}$$

Grade resistance is encountered while ascending a vertical curve. Grade resistance can be negative while descending a curve as the gravitational force assists the train motion. Grade resistance is directly proportional to rail grade. Rail grade is defined as the change in elevation per unit length of the horizontal projection of the track on a level surface. However, for small relative grades typically observed on railroad tracks, the horizontal projection of the track on a level surface is approximately equal to the track length. Grade was estimated based on the change in elevation per unit track length. The error in estimated grade based on this assumption for a 2% grade, which is the maximum observed grade on the Piedmont route, is 0.02%. Therefore, the error in the grade estimates based on track length rather than projected length on a level surface is negligible. The grade resistance per unit train weight was estimated as (AREMA, 2020; Hay, 1982; Profillidis, 2014):

$$R_{x,t} = E \times x_t \quad (\text{B-7})$$

Where,

$$\begin{aligned} R_{x,t} &= \text{grade resistance at time } t \text{ (lbs/ton)} \\ E &= \text{unit grade resistance (lbs/ton-percent grade)} = 20 \\ x_t &= \text{rail grade at time } t \text{ (\%)} \end{aligned}$$

Acceleration resistance is encountered when the train speed is increasing, which results in a change in kinetic energy. Based on Newton's second law, the force required to accelerate a body is directly proportional to its acceleration. The acceleration resistance per unit train weight was estimated as:

$$R_{a,t} = G \times a_t \quad (\text{B-8})$$

Where,

$$\begin{aligned} R_{a,t} &= \text{acceleration resistance at time } t \text{ (lbs/ton)} \\ G &= \text{unit acceleration resistance} = 200 \text{ (lbB- } s^2/\text{ton-m)} \\ a_t &= \text{train acceleration at time } t \text{ (m/s}^2\text{)} \end{aligned}$$

B.1.2 Traction resistance

The resistances associated with train movement are called traction resistance. Traction resistance includes starting, journal, flange, air, wind, curve, grade, and acceleration resistances. Journal, flange, and air resistance are always present during train movement. The American Railway Engineering and Maintenance-of-way Association (AREMA) recommended multiplying the journal, flange, and air resistance by a factor of 0.85 to account for improved train and rail designs (AREMA, 2020). Other resistances are only encountered intermittently, e.g., starting resistance is only encountered when the train starts to move after a stop. Curve and grade resistances are only encountered while traversing curves and grades, respectively. Acceleration resistance is only present during train acceleration. The traction resistance was estimated as:

$$R_{T,t} = R_{s,t} + (R_j + R_{f,t} + R_{w,t}) \times I + R_{c,t} + R_{x,t} + R_{a,t} \quad (\text{B-9})$$

Where,

$$R_{T,t} = \text{traction resistance at time } t \text{ (lbs/ton)}$$

I = factor for modernized train equipment (post-1950) to account for improved train and rail designs = 0.85

B.1.3 Internal resistance

The internal resistance (R_i) arises from forces inside the locomotive, including engine and shaft losses, cylinder friction, bearing friction, windage in motors and generators, and power used by auxiliaries for lighting, heating, and space conditioning inside the locomotive cab. Thus, a part of the tractive effort produced by the locomotive is needed to overcome internal resistance. For diesel-electric locomotives, a locomotive efficiency factor of 0.82 was used to account for internal resistance (Hay, 1982; Profillidis, 2014). Lighting, heating, and space conditioning for passenger cars is provided by the HEP engine.

B.1.4 Gross resistance

Gross resistance is the sum of all of the resistive forces. The locomotive efficiency factor is used to account for the internal resistance of a train. The gross resistance was estimated as:

$$R_{g,t} = \frac{R_{T,t}}{\eta} \quad (\text{B-10})$$

Where,

$R_{g,t}$ = gross resistance at time t (*lbs/ton*)
 η = locomotive efficiency factor = 0.82 for diesel-electric locomotives

Substituting the value of $R_{T,t}$ from Equation B-15,

$$R_{g,t} = \frac{R_{s,t} + (R_j + R_{f,t} + R_{w,t}) \times I + R_{c,t} + R_{x,t} + R_{a,t}}{\eta} \quad (\text{B-11})$$

Ignoring wind resistance and substituting the expressions for $R_{j,t}$, $R_{f,t}$, $R_{d,t}$, $R_{c,t}$, $R_{x,t}$ and $R_{a,t}$, from Equations B-8, B-9, B-10, B-11, B-12, and B-13, respectively, Equation B-17 becomes:

$$R_{g,t} = \frac{R_s + \left(\left(0.6 + \frac{20}{w} \right) + Bv_t + \frac{C_d \times F}{w \times n} v_t^2 \right) \times I + Dd_t + Ex_t + Ga_t}{\eta} \quad (\text{B-12})$$

Equation B-18 is applicable for the lead locomotive, trailing locomotive(s), or passenger cars. However, the parameters w , F , C_d , and n may differ among lead locomotive, trailing locomotives, and passenger cars. Therefore, the gross train resistance was estimated individually for each. Each of the locomotive owned by the NCDOT has the same corresponding value for w , F , and n , which was obtained from the locomotive manual. C_d differs among locomotive based on the shape of the frontal cross-section and the position of the locomotive in a consist. The locomotives owned by NCDOT have two distinct shapes of the frontal cross-section. The F59PHI locomotives have a more aerodynamic frontal cross-section versus F59PH locomotives. If the lead locomotive was an F59PH, C_d equal to $0.0024 \text{ lbs/ft}^2\text{-mph}^2$ was used for estimating drag resistance. For a lead F59PHI locomotive, C_d equal to $0.0017 \text{ lbs/ft}^2\text{-mph}^2$ was used for estimating drag resistance (Table B-1).

Passenger cars are not fully exposed to the atmosphere. Therefore, the drag resistance is lower versus lead locomotive, as indicated by a relatively lower C_d of $0.00034 \text{ lbs/ft}^2\text{-mph}^2$ for passenger cars (Table B-1). Since trailing locomotive(s) are also not fully exposed to the atmosphere, they were assumed to have the same drag coefficient as a passenger car. Parameters w , F , and n corresponding to trailing locomotive(s) or passenger cars were used.

The gross train resistance for a consist was estimated as the sum of resistances for the lead locomotive, trailing locomotive(s), and passenger cars:

$$R_{g,t} = \frac{1}{\eta} \times \left[R_{s,t} + \left\{ \left(0.6 + \frac{20}{w_l} + Bv_t + \frac{C_{d,l}F_l}{w_l n_l} v_t^2 \right) + N \left(0.6 + \frac{20}{w_l} + Bv_t + \frac{C_{d,p}F_l}{w_l n_l} v_t^2 \right) + P \left(0.6 + \frac{20}{w_p} + Bv_t + \frac{C_{d,p}F_p}{w_p n_p} v_t^2 \right) \right\} \times \left(\frac{I}{1 + P + N} \right) + Dd_t + Ex_t + Ga_t \right] \quad (\text{B-13})$$

Where,

N	=	number of locomotives per train other than the lead locomotive
P	=	number of passenger cars per train
n_l	=	number of axles per locomotive
n_p	=	number of axles per passenger car
w_l	=	weight per unit axle of locomotive (<i>tons</i>)
w_p	=	weight per unit axle of passenger car (<i>tons</i>)
$C_{d,l}$	=	drag coefficient for lead locomotive from Table B-1 ($\text{lbs/ft}^2\text{-mph}^2$)
$C_{d,p}$	=	drag coefficient for trailing locomotive(s) and passenger cars from Table B-1 ($\text{lbs/ft}^2\text{-mph}^2$)
F_l	=	frontal area of locomotive (ft^2)
F_p	=	frontal area of passenger car (ft^2)

The coefficients R_s, B, I, D, E, G, η and v_w are constant. These coefficients, independent of the train system, are given in Table B-2. The coefficients $N, w_l, n_l, C_{d,l}, F_l, P, w_p, n_p, C_{d,p}$ and F_p depend on the type of locomotive or passenger car, and the train consist. The weight of passenger car per unit axle (w_p) is also affected by the number of passengers onboard a train. However, the weight of each passenger car at full seating capacity versus an empty passenger car differs only by 7% for the passenger cars used on the Amtrak Piedmont train. Therefore, differences in passenger car weight related to passenger load were neglected. The coefficients $N, w_l, n_l, C_{d,l}, F_l, P, w_p, n_p, C_{d,p}$ and F_p for the Amtrak Piedmont train are shown in Table B-3.

Table B-2. Train Resistance Equation Parameters Independent of the Train System Based On Gross Train Resistance Equation

Coefficient	Significance	Value (Hay, 1984)
$R_{s,t}$	Starting resistance	18 <i>lbs/ton</i>
B	Flange resistance coefficient	0.01 <i>lbs/ton-mph</i>
I	Adjustment factor for modern trains	0.85
D	Unit curve resistance	0.8 <i>lbs/ton-degree of curve</i>
E	Train resistance per unit grade	20 <i>lbs/ton-percent grade</i>
G	Train resistance per unit acceleration	200 <i>lbB-s²/ton-m</i>
η	Locomotive efficiency factor	0.82
$v_{w,t}$	Wind speed	Typically assumed zero

Table B-3. Train Resistance Equation Parameters for the Amtrak-Operated Piedmont Passenger Rail Service between Raleigh, NC, and Charlotte, NC based On Gross Train Resistance Equation.

Coefficient	Significance	Value for Amtrak Piedmont
N	Number of locomotives	1
w_l	Locomotive weight per unit axle (<i>tons</i>)	33.5
n_l	Number of axles per locomotive	4
$C_{d,l}$	Locomotive drag coefficient (<i>lbs/ft²-mph²</i>) ^c	0.0024 (F59PH) 0.0017 (F59PHI)
F_l	Locomotive frontal cross-sectional area (<i>ft²</i>)	165.35
P	Number of passenger cars ^a	3
w_p	Passenger car weight per unit axle (<i>tons</i>) ^b	17.5 (Empty) 18.8 (Full Capacity)
n_p	Number of axles per passenger car	4
$C_{d,p}$	Trailing locomotive(s) or passenger car drag coefficient (<i>lbs/ft²-mph²</i>)	0.00034
F_p	Passenger car frontal cross-sectional area (<i>ft²</i>)	142

^a The number of passenger cars includes baggage/café car. For the sake of simplicity, all cars are assumed to be equivalent to a passenger car with respect to w_p , n_p , $C_{d,p}$ and F_p .

^b The weight of an empty passenger car used on the Piedmont rail route is 70 tons. Assuming an average weight of 70 kgs per person (Gbologah et al., 2014), the weight of a passenger car with a seating capacity of 66 persons fully occupied by passengers is 75 tons. To simplify calculations, the weight of an empty passenger car was used.

^c F59PHI locomotives have more aerodynamic frontal cross-section compared to F59PH locomotives. Therefore, two different values of drag coefficients are used.

B.1.5 Locomotive power demand

Power is defined as work done per unit time and is estimated as the product of force and speed. LPD was estimated as the product of gross train resistance, train speed, and train weight. For the Piedmont passenger service with double-powered consists, the tractive power was provided equally by both the locomotives. However, FUERs were measured for only one locomotive. Therefore, LPD per unit locomotive was estimated for modeling FUERs. Taking into account unit conversions, LPD per unit powered locomotive for each second of train operation was estimated as (Profillidis, 2014):

$$LPD_t = 0.0019 \times R_{g,t} \times v_t \times W \quad (B-14)$$

Where,

$$\begin{aligned} LPD_t &= \text{locomotive power demand at time } t \text{ (kW)} \\ W &= \text{total train weight (tons)} \end{aligned}$$

$R_{g,t}$ was estimated using Equation B-13. Train weight was estimated as:

$$W = w_l \times n_l \times (1 + N) + w_p \times n_p \times P \quad (B-15)$$

B.2 Modeling Fuel Use and Emission Rates

Modeling FUERs comprised describing variations in FUERs, train activity, track geometry, and LPD; inferring trends of FUERs with LPD; calibrating and validating sub-models for each trend; evaluating continuity at the sub-model boundaries; and quantifying accuracy and precision of the complete model, inclusive of all sub-models.

B.2.1 Variation in empirical fuel use and emission rates

The distribution of 1 Hz empirical PME FUERs for each measured combination of locomotive, consist, and fuel (LCF) is given in Figure B-1. Each series corresponds to all 1 Hz FUERs measured for all trips for a given observed combination of locomotive, consist, and fuel. The 95th percentile FUERs differed for each combination of locomotive, consist, and fuel because of inter-locomotive, inter-consist, and inter-fuel variability in FUERs. For example in Figure B-1(a), for locomotives operated on ULSD in SLC, locomotive NC 1797 had lower 95th percentile FUERs than NC 1810 indicating that locomotive NC 1797 is more fuel-efficient. Among consists for locomotive NC 1871 operated on ULSD, 95th percentile FUERs were lower for DP-P/PC than for SP-P/PC. Among fuels, for locomotive NC 1797 operated in SLC, the 95th percentile fuel use rate was lower for B20 than for ULSD. For the same measurements, Graver *et al.*, 2016 also reported 4% lower cycle-average fuel use rate for B20 versus ULSD. These inter-locomotive, inter-consist, and inter-fuel variability in FUERs indicate a potential to reduce FUERs for the Piedmont passenger rail service by prioritizing the operations based on combinations of locomotives, consists, and fuels with lower FUERs.

Plots of fuel use rate and NO_x emission rate shown in Figure B-1(a) and Figure B-1(d), respectively, have two steep slopes. As an example, steep slopes were observed for fuel use rates ranging between 2 g/s and 9 g/s and between 110 g/s and 150 g/s. These ranges correspond to engine operation under relatively lower and higher power demand, respectively. Data in these two ranges typically comprised 55% to 88% of the trip duration. This is consistent with prior measurements where the operators typically spend 60% to 87% of the trip duration in the notch

positions with the lowest and highest engine power output (Graver and Frey, 2015). Similar trends were observed for CO₂ emission rates. CO, HC, and PM emission rates change gradually with load relative to fuel use rates, and take relatively longer to reach the highest emission rates for a given engine load. Therefore, no steep slopes were observed for CO, HC, and PM emission rates. A good model should capture this variation in FUERs.

B.2.2. Variation in train activity and track infrastructure

The distribution of measured speed, acceleration, grade, and curvature for each second of data for each combination of locomotive, consist, and fuel is given in Figure B-2. The train was stopped for about 10% of the total time for an average one-way trip. Speeds between 60 mph and 80 mph accounted for about 50% of the measured data. The average speed on this route was 52.6 mph. The acceleration varied between -2.3 mph/s and 2.3 mph/s. The train cruised at a constant speed or stopped (no acceleration) for about 50% of the average trip duration. At speeds greater than 50 mph, speed changes were gradual or the train cruised at a constant speed for short periods (e.g., 25 seconds or less) before speed changed and the train cruised at a new speed. About 80% of the accelerations were between -0.5 mph/s and 0.5 mph/s.

The grade varied between -1.9% and 1.9%. More than 90% of the trip duration was typically spent on track segments with grades between -1% and 1%. The segment-average curvature varied between 0.2 degrees and 4.3 degrees. Fifty percent of the segments did not have horizontal curvature. Curves with less than 1 degree of curvature accounted for about 25% of the track segments. Curves exceeding 2 degrees accounted for less than 10% of the track segments.

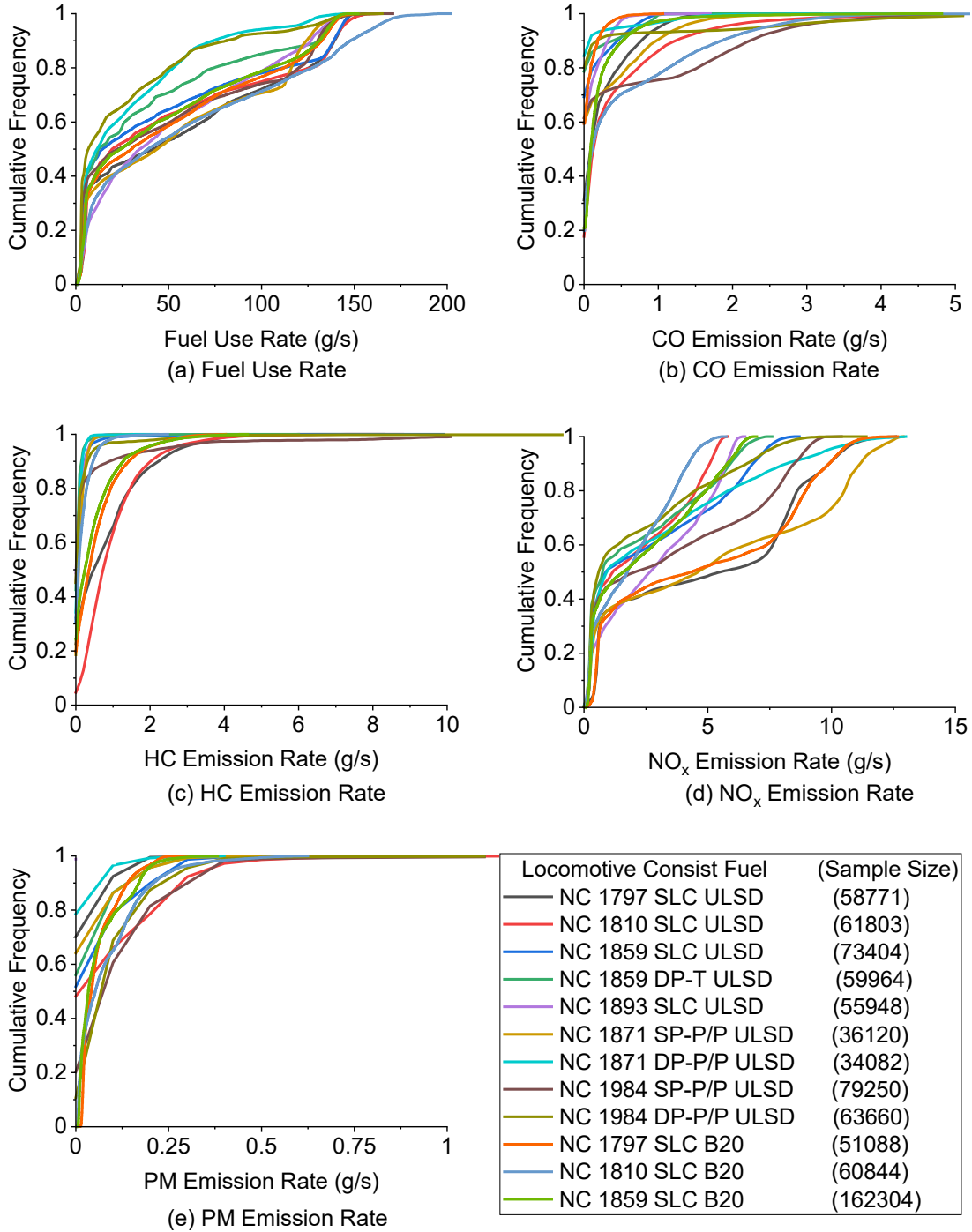
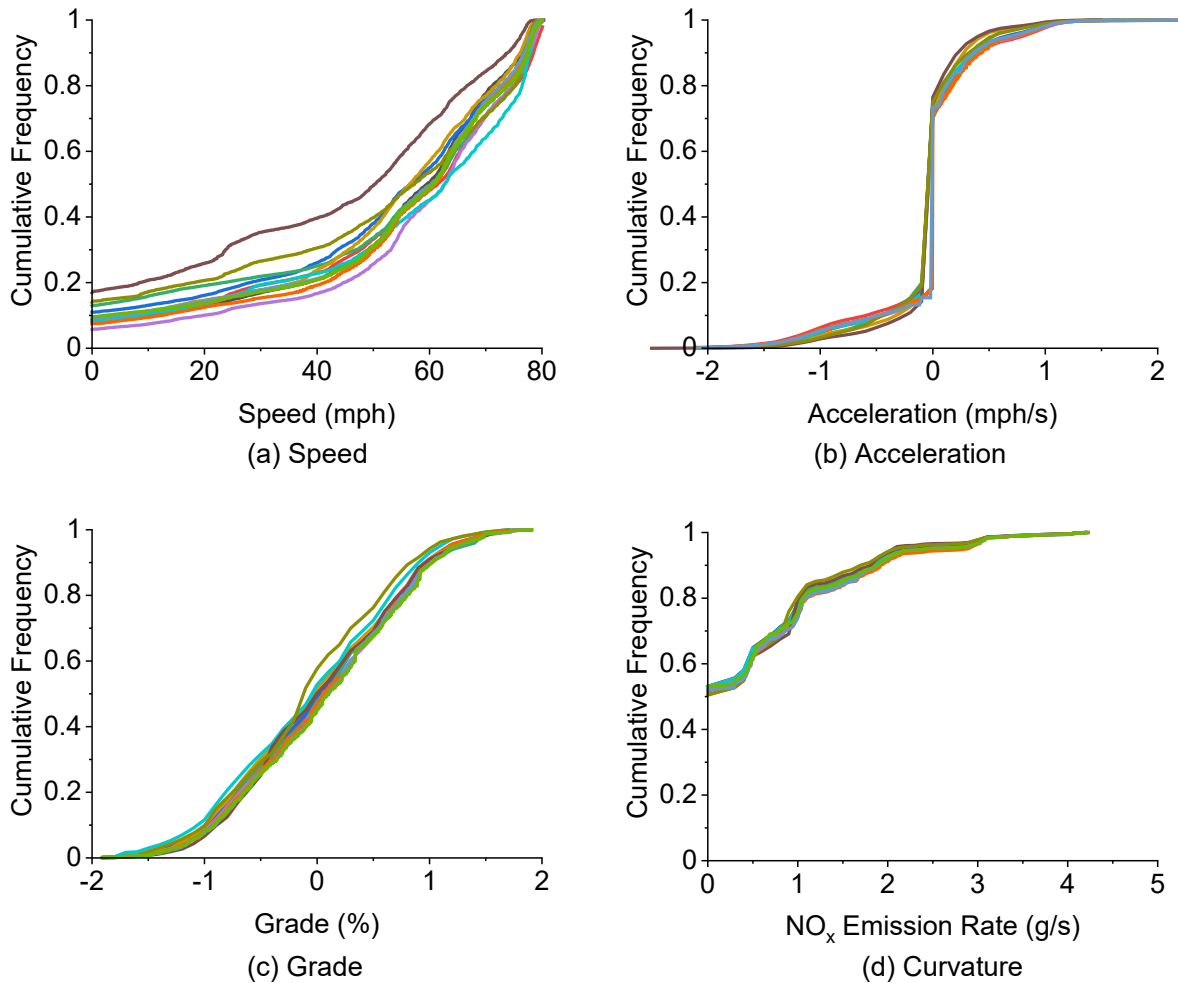


Figure B-1. Cumulative Frequency Plots of Empirical Fuel Use and Emission Rates Measured for Combinations of Locomotives, Consists, and Fuels: (a) Fuel Use Rate; (b) CO Emission Rate; (c) HC Emission Rate; (d) NO_x Emission Rate; and (e) PM Emission Rate.

Each series corresponds to all 1 Hz FUERs measured for all trips for a given observed combination of locomotive, consist, and fuel. CO₂ emission rates have similar trends as fuel use rates because 99% of the carbon in fuel is emitted as CO₂. Therefore, plot for CO₂ is not shown.



Locomotive Consist Fuel	(Sample Size)
NC 1797 SLC ULSD	(58771)
NC 1810 SLC ULSD	(61803)
NC 1859 SLC ULSD	(73404)
NC 1859 DP-T ULSD	(59964)
NC 1893 SLC ULSD	(55948)
NC 1871 SP-P/P ULSD	(36120)
NC 1871 DP-P/P ULSD	(34082)
NC 1984 SP-P/P ULSD	(79250)
NC 1984 DP-P/P ULSD	(63660)
NC 1797 SLC B20	(51088)
NC 1810 SLC B20	(60844)
NC 1859 SLC B20	(162304)

Figure B-2. Cumulative Frequency Plots of Train Activity and Track Infrastructure Measured for the Combinations of Locomotives, Consists, and Fuels: (a) Speed; (b) Acceleration; (c) Grade; and (d) Curvature.

Each series corresponds to all 1 Hz FUEs measured for all trips for a given observed combination of locomotive, consist, and fuel.

B.2.3 Backward moving average locomotive power demand

LPD in the current second is affected by LPD from the past seconds because the PME operation takes time, typically up to 30 s, to respond to throttle notch changes. To account for this transition, an n -second backward moving average LPD ($\overline{LPD}_{n,t}$) was used. n was varied from 1 to 30. The period that gave the highest Pearson's correlation coefficient of $\overline{LPD}_{n,t}$ with FUERs was selected as the most appropriate period. $\overline{LPD}_{n,t}$ is defined as an average of the LPD at time t , and the LPD_t in the past ($n-1$) seconds:

$$\overline{LPD}_{n,t} = \frac{1}{n} \sum_{i=0}^{n-1} LPD_{t-i} \quad (\text{B-16})$$

Where,

$\overline{LPD}_{n,t}$ = average of the locomotive power demand at time t and the past ($n-1$) seconds

n = backward moving average period (s)

To determine the most appropriate backward moving average LPD period to account for engine transitions, the variation of Pearson's correlation coefficient of FUERs versus n -second backward moving average LPD ($\overline{LPD}_{n,t}$) is presented in Figure B-3. For each species, the correlation coefficient was lowest for $n = 1$ s and increased monotonically with n . A sharp increase was observed between 1s and 10s, followed by a relatively gradual increase peaking at around 11s to 13s after which the coefficient was approximately constant. Therefore, n was selected as 12s. As shown in Figure B-4, the variation in empirical fuel use rate was more appropriately captured by the variation in $\overline{LPD}_{12,t}$ as the rise and fall in fuel use rate typically coincided with the rise and fall in $\overline{LPD}_{12,t}$, and the peaks were proportional to each other. In contrast, the values of instantaneous LPD often changed more frequently than the observed changes in fuel use rate and often exceeded the locomotive capacity. In the real-world, locomotives typically operate at steady-state with approximately constant FUERs because of approximately constant engine load. Therefore, instantaneous LPD is not an accurate indicator of real-world operation. $\overline{LPD}_{12,t}$ is a better indicator of observed trends in fuel use rates and therefore, more representative of real-world operation.

The cumulative frequency distribution of $\overline{LPD}_{12,t}$ for all trips measured for a given combination of locomotive, consist, and fuel is given in Figure B-5. The PMEs have a rated net horsepower of 3000 hp (2240 kW) and a gross horsepower of 3200 hp (2386 kW). However, during the engine load standardization tests, the expected gross horsepower at notch 8 when controlled by a governor is 3378 hp (2519 kW) (General Motors of Canada Limited, 1994). Typically, 92% to 99% of the data had $\overline{LPD}_{12,t} < 2519$ kW. Therefore, most of the measured data had $\overline{LPD}_{12,t}$ within the locomotive capacity. The estimated $\overline{LPD}_{12,t}$ were realistic.

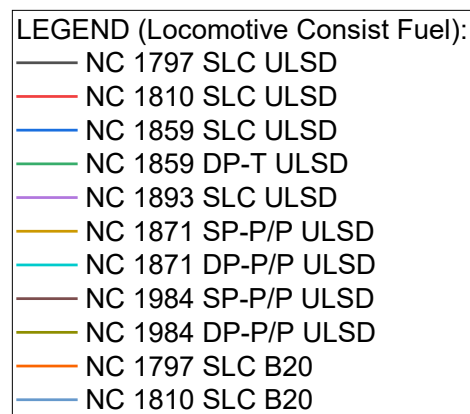
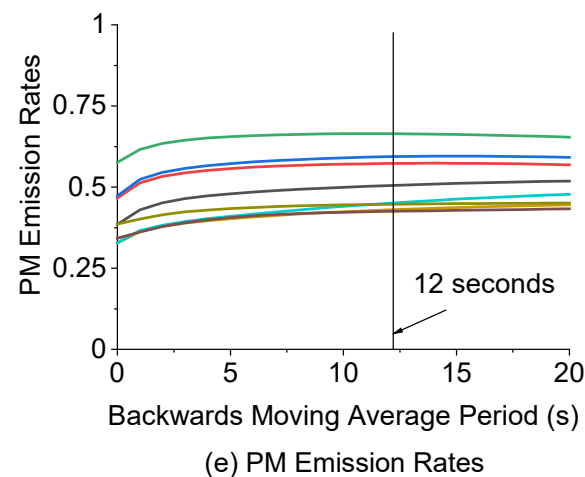
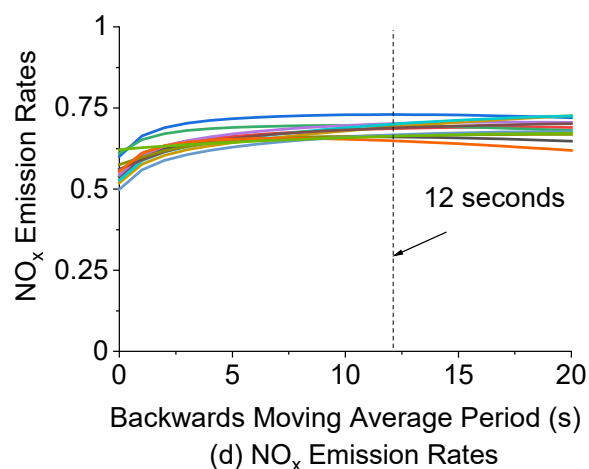
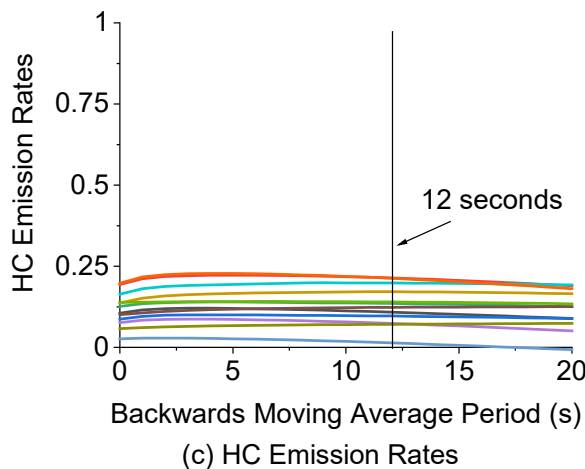
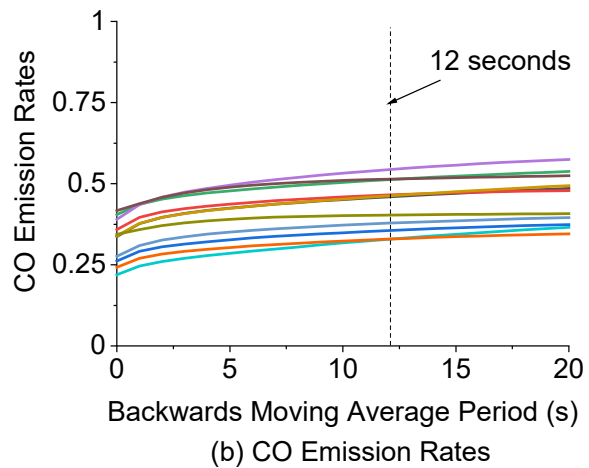
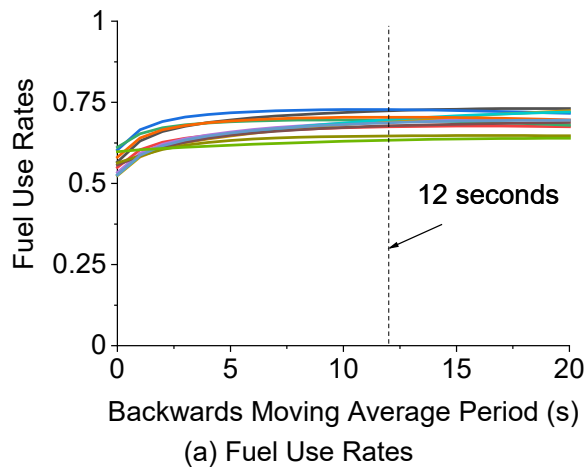


Figure B-3. Variation of Pearson's Correlation Coefficient of Fuel Use and Emission Rates for Different Moving Average Locomotive Power Demand for the Measured Combinations of Locomotives, Consists, and Fuels: (a) Fuel Use Rate; (b) CO Emission Rate; (c) HC Emission Rate; (d) NO_x Emission Rate; and (e) PM Emission Rate.

CO₂ emission rates have similar trends as fuel use rates because 99% of the carbon in fuel is emitted as CO₂. Therefore, plot for CO₂ is not shown.

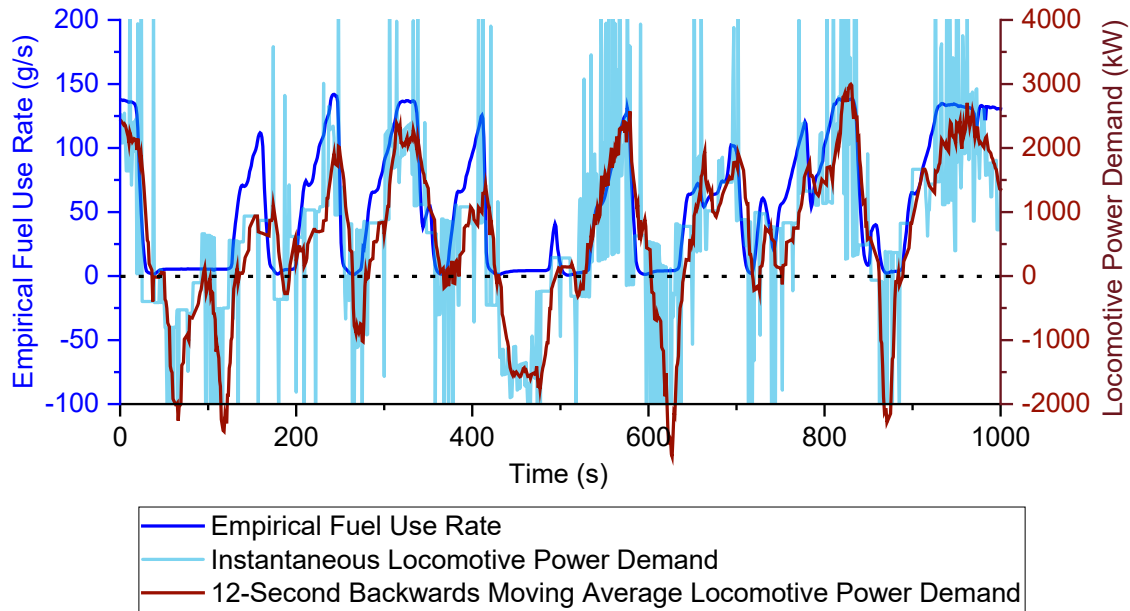


Figure B-4. Example Time Plot of Variation in Empirical Fuel Use Rate with Instantaneous Locomotive Power Demand (LPD) and 12-Second Backwards Moving Average LPD.

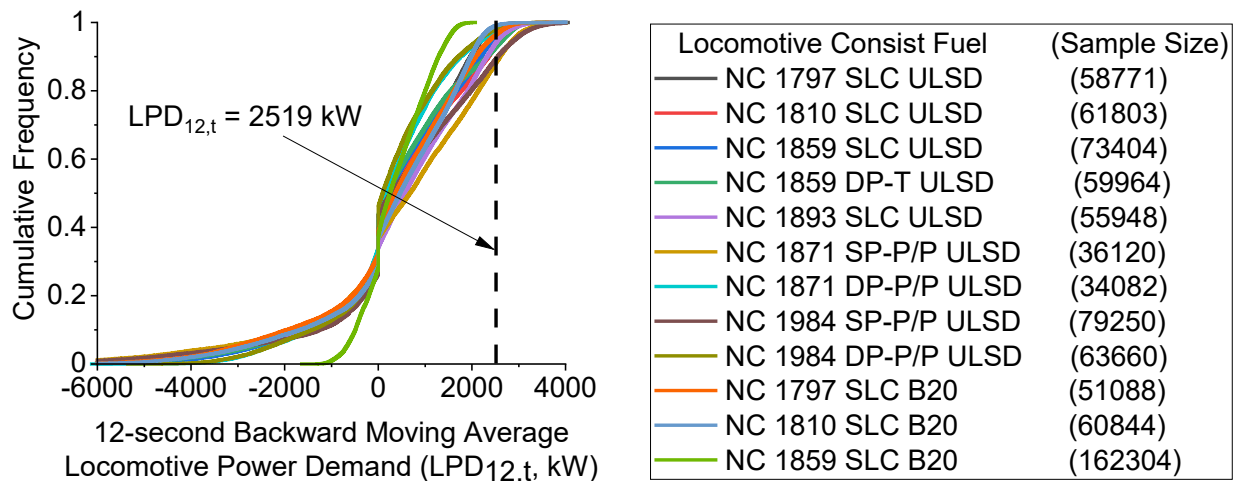


Figure B-5. Cumulative Frequency Plots of 12-Second Backwards Moving Average Locomotive Power Demand for the Measured Combinations of Locomotives, Consists, and Fuels.

The prime mover engines have a rated net horsepower of 3000 hp (2240 kW) and a gross horsepower of 3200 hp (2386 kW). However, during the engine load standardization tests, the highest expected gross horsepower when controlled by a governor is 3378 hp (2519 kW) (General Motors of Canada Limited, 1994). Therefore, the frequency of data > 2519 kW was quantified to ensure that such events are rare.

B.2.4 Trends of fuel use and emission rates with locomotive power demand

Operators operate PMEs differently for different ranges of $\overline{LPD}_{12,t}$. Therefore, several different trends of FUERs with $\overline{LPD}_{12,t}$ may exist. To infer the trends of FUERs with $\overline{LPD}_{12,t}$, average FUERs for data binned into 10 groups for $0 < \overline{LPD}_{12,t} < 2519$ kW were estimated. Average FUERs were also estimated for $\overline{LPD}_{12,t} < 0$, $= 0$, and > 2519 kW.

The variation of FUERs with $\overline{LPD}_{12,t}$ is shown in Figure B-6. Based on measured data, four trends of FUERs with $\overline{LPD}_{12,t}$ were inferred. For each trend, a sub-model was defined. Sub-model 1 (SM1) corresponds to a moving train under negative $\overline{LPD}_{n,t}$. For SM1, FUERs were approximately constant with FUERs higher than high-idle FUERs. The PMEs are operated at idle for negative $\overline{LPD}_{12,t}$, however, FUERs are slightly higher because of the transition from a notch with higher FUERs. Sub-model 2 (SM2) corresponds to a stationary train with zero $\overline{LPD}_{12,t}$. FUERs for SM2 were approximately constant, with average FUERs between low and high idle FUERs.

B.2.4.1 Sub-model 1

For seconds with $v_t > 0$ mph and $\overline{LPD}_{12,t} \leq 0$ kW, the operators typically transition to idle from higher notch positions. The PME operates at high idle during such transitions. FUERs also transition to lower levels of idle from higher levels of prior notch position until FUERs reach a steady-state is reach for high idle. Thus, average FUERs for sub-model 1 are typically expected to be higher than high idle steady-state rates. For this sub-model, FUERs were inferred as average FUERs of all seconds with $v_t > 0$ mph and $\overline{LPD}_{12,t} \leq 0$ kW.

B.2.4.2 Sub-model 2

For a stationary train, the PME operates at idle and reaches steady-state operation at high idle after a short duration. If the train stops for longer durations, the PME transitions to steady-state at low idle, after operating at high idle for 30 seconds to 5 minutes. This duration varies with locomotives depending on the PME configuration. The operator transitions to high idle a few seconds before the intended departure. Thus, depending on the duration of the stop, locomotives may or may not reach low idle. Also, on some occasions when locomotive stops, some initial seconds had FUERs higher than steady-state idle levels because FUERs were transitioning from the levels of higher notch positions in which locomotive operated before stopping. Depending on the duration of the stop, the average rates in this sub-model were higher or lower than the steady-state high idle rate. All seconds with $v_t = 0$ mph were inferred to have constant FUERs estimated as average of FUERs with $v_t = 0$ mph.

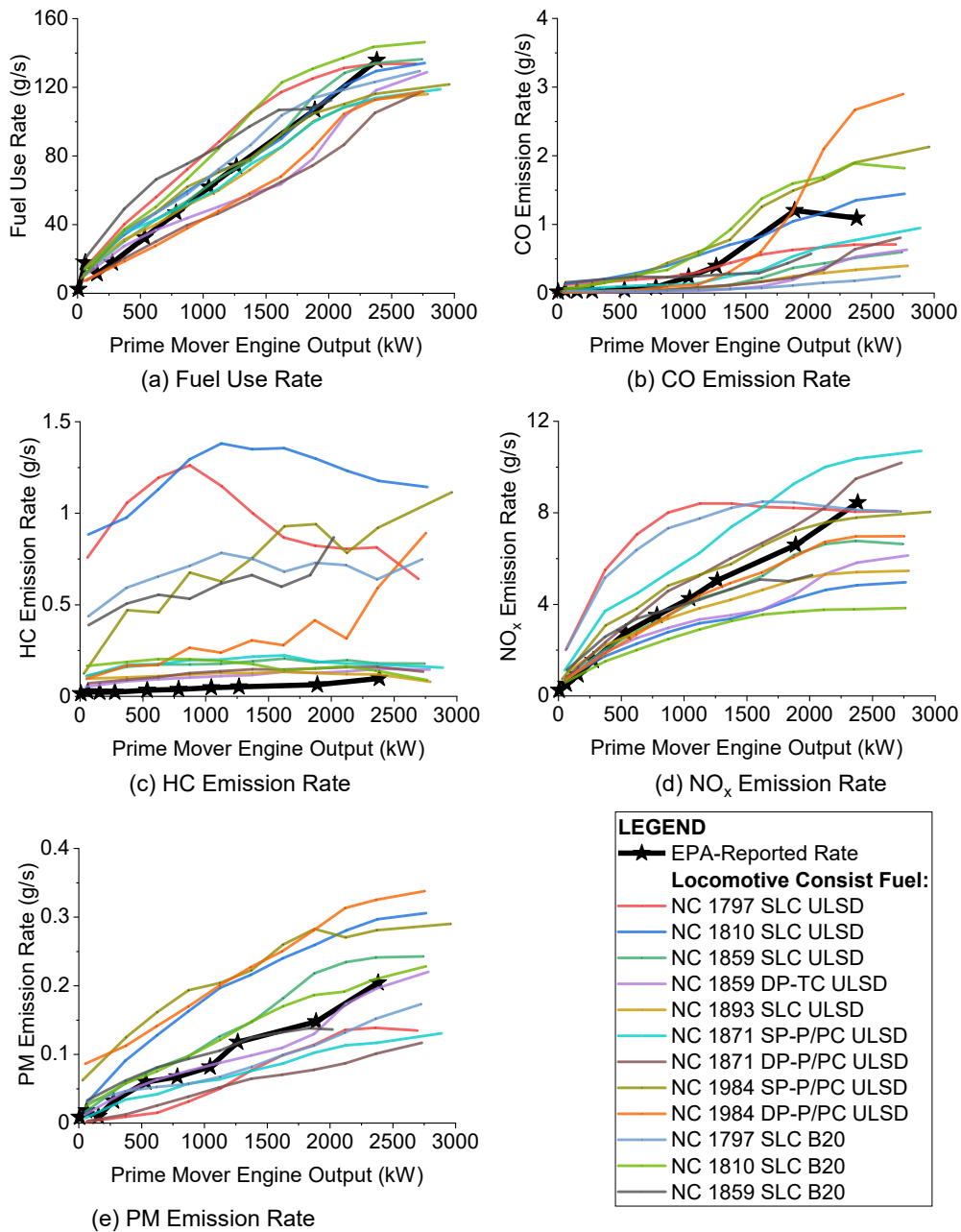


Figure B-6. Variation of Fuel Use Rate and Emission Rates with 12-Second Backwards Moving Average Locomotive Power Demand for 12 Combinations of Locomotives, Consists, and Fuels and Comparison with EPA-Reported Notch-Average Rates for the Same Model Prime Mover Engine: (a) Fuel Use Rate; (b) CO Emission Rate; (c) HC Emission Rate; (d) NO_x Emission Rate; and (e) PM Emission Rate.

To visualize the average trend for each combination of locomotive, consist, and fuel, data were divided into 250 kW bins and average rates corresponding to each bin are shown, connected by straight lines. CO₂ emission rates have similar trends as fuel use rates because 99% of the carbon in fuel is emitted as CO₂. Therefore, plot for CO₂ is not shown. EPA-reported data comprises notch-average rates and corresponding engine output for the same model prime mover engine measured in this study connected by straight lines (EPA, 1998).

B.2.4.3 Sub-model 3

This sub-model applies to $\overline{LPD}_{12,t} \geq 0$ kW but less than a threshold. The threshold was determined as the $\overline{LPD}_{12,t}$ beyond which FUERs become approximately constant regardless of $\overline{LPD}_{12,t}$. Based on Figure B-6, this threshold varied among FUERs and LCF IDs but was typically between 3000 hp to 3500 hp. The PMEs have a rated net horsepower of 3000 hp (2240 kW) and a gross horsepower of 3200 hp (2386 kW). However, during the engine load standardization tests, the load expected gross horsepower at notch 8 when controlled by a governor is 3378 hp (2519 kW) (General Motors of Canada Limited, 1994). Thus, the threshold was determined to be 3378 hp (2519 kW) based on the expected upper bound of peak horsepower during PME load standardization tests.

Within this $\overline{LPD}_{12,t}$ range, fuel use, and emission rates of CO₂ and NO_x varied approximately linearly with $\overline{LPD}_{12,t}$, except for LCF ID 1 and 10 for NO_x emission rates. For LCF ID 1 and 10, NO_x emission rates peaked at around 1200 hp and decreased thereafter. The locomotive NC1797 was an unusually high NO_x emitter relative to other locomotives (Frey and Rastogi, 2019).

For fuel use and emission rates of CO₂ and NO_x (except for LCF ID 1 and 10 for NO_x), an ordinary least squares regression was fit for FUERs versus $\overline{LPD}_{12,t}$ with the intercept set to average FUERs inferred for sub-model 2. The regression was conducted with just the linear $\overline{LPD}_{12,t}$ term, and with linear and quadratic $\overline{LPD}_{12,t}$ terms. To determine the contribution of the quadratic term, model R² for each of the linear regressions were compared.

CO, HC, and PM emission rates typically increased monotonically with $\overline{LPD}_{12,t}$. However, the variation was not a simple regression. Thus, a 10-mode modal model was calibrated for CO, HC, and PM emission rates. $\overline{LPD}_{12,t}$ between 0 kW and 2519 kW was divided into 10 modes such that each mode had equal data based on all LCF IDs combined. Modal models with the same $\overline{LPD}_{12,t}$ modes as for CO, HC, and PM emission rates were also calibrated for LCF ID 1 and 10 for NO_x emission rates.

B.2.4.4 Sub-model 4

Sub-model 4 corresponds to $\overline{LPD}_{12,t} \geq 2519$ kW. For this sub-model, FUERs were inferred to be constant, equal to the average of 1 Hz FUERs in this LPD range. Such $\overline{LPD}_{12,t}$ range is expected to be less frequent than other sub-models. The inferred rates are expected to be close to average notch 8 steady-state rates.

B.2.4.5. Fuel use and emission rates based on all sub-models

Each sub-model, identified in previous sections, is summarized in Table B-4. The basis of sub-model parameters is given in Table B-5.

Table B-4. Locomotive Power Demand Sub-Model Definition

Sub-Model	Speed (v_t mph)	12-Second Backwards Moving Average Locomotive Power Demand ($LPD_{12,t}$ kW)
1	> 0	≤ 0
2	= 0	= 0
3	> 0	$0 < LPD_{12,t} < 2519$
4	> 0	≥ 2519

Fuel use rate and emission rates of CO₂, and NO_x for all locomotives except for NO_x emission rates for locomotive NC 1797 (LCF ID 1 and 10) were modeled as:

$$R_{ID,SM,s,t} = \begin{cases} I_{ID,SM,s} & SM \in 1,2,4 \\ I_{ID,SM,s} + \alpha_{ID,SM,s} \times \overline{LPD}_{12,t} + \beta_{ID,SM,s} \times \overline{LPD}_{12,t}^2 + \epsilon_{ID,SM,s,t} & SM \in 3 \end{cases} \quad (B-17)$$

Where,

- $R_{ID,SM,s,t}$ = Fuel use or emission rate of species s at time t for a given LCF ID and a given sub-model SM (g/s)
- s = index for species. $s \in$ Fuel use rate, and emission rates of CO₂ and NO_x
- ID = index for LCF ID. $ID \in 1,2,3,\dots,12$
- SM = index for sub-model. $SM \in 1,2,3,4$
- $\bar{R}_{ID,SM,s}$ = average of fuel use and emission rates within the sub-model
- $I_{ID,SM,s}$ = intercept of regression of species s at time t for a given LCF ID based on given sub-model SM (g/s)
- $\alpha_{ID,SM,s}$ = linear slope of the regression of species s at time t for a given LCF ID based on given sub-model SM (g/kW-s)
- $\beta_{ID,SM,s}$ = quadratic slope of the regression of species s at time t for a given LCF ID based on given sub-model SM (g²/kW²-s)
- $\epsilon_{ID,SM,s,t}$ = Residual error of species s at time t for a given LCF ID on given sub-model SM (g/s)
- $\overline{LPD}_{n,t}$ = n -second backwards moving average locomotive power demand (kW)

Since FUERs and $\overline{LPD}_{12,t}$ are a part of time series they could be autocorrelated. The residual errors corresponding to sub-model 3 of Equation B-17 could be auto correlated as well. In such a case, the parameters, including slopes and intercept, model variance, and model R² would be unbiased. However, the standard error in slopes and intercept of the regression and the statistical significance of slopes and intercept could be biased (Tsay, 2010; Wooldridge, 2016). The standard errors of slopes and intercept can be bias corrected. The corrected standard errors are known as Heteroscedasticity and Autocorrelation Consistent (HAC) standard errors. The HAC standard error is robust to autocorrelation among residual errors.

Table B-5. Basis of Sub-Model Parameters for Fuel Use and Emission Rates.

Species	Sub-Model	$I_{ID,SM,s}$ (g/s)	$\alpha_{ID,SM,s}$ (g/kW-s)	$\beta_{ID,SM,s}$ (g ² /kW ² -s ²)	Number of Modes	$\bar{r}_{ID,SM,s',m}$ (g/s)
Fuel Use Rate	1	Average rate of sub-model 1	NA	NA	NA	NA
	2	Average rate of sub-model 2	NA	NA	NA	NA
	3	Average rate of sub-model 1	Regression	Regression	NA	NA
	4	Average rate of sub-model 4	NA	NA	NA	NA
CO ₂ Emission Rate	1	Average rate of sub-model 1	NA	NA	NA	NA
	2	Average rate of sub-model 2	NA	NA	NA	NA
	3	Average rate of sub-model 1	Regression	Regression	NA	NA
	4	Average rate of sub-model 4	NA	NA	NA	NA
NO _x Emission Rate	1	Average rate of sub-model 1	NA	NA	NA	NA
	2	Average rate of sub-model 2	NA	NA	NA	NA
	3	Average rate of sub-model 1	Regression ^a	Regression ^a	10 ^b	Average rate for each mode ^b
	4	Average rate of sub-model 4	NA	NA	NA	NA
CO Emission Rate	1	Average rate of sub-model 1	NA	NA	NA	NA
	2	Average rate of sub-model 2	NA	NA	NA	NA
	3	NA	NA	NA	10	Average rate for each mode
	4	Average rate of sub-model 4	NA	NA	NA	NA
HC Emission Rate	1	Average rate of sub-model 1	NA	NA	NA	NA
	2	Average rate of sub-model 2	NA	NA	NA	NA
	3	NA	NA	NA	10	Average rate for each mode
	4	Average rate of sub-model 4	NA	NA	NA	NA
PM Emission Rate	1	Average rate of sub-model 1	NA	NA	NA	NA
	2	Average rate of sub-model 2	NA	NA	NA	NA
	3	NA	NA	NA	10	Average rate for each mode
	4	Average rate of sub-model 4	NA	NA	NA	NA

^a Regression part for NO_x emission rates is applicable for all LCF IDs except 1 and 10.

^b Modal model part for NO_x emission rates is applicable for LCF IDs 1 and 10.

The unbiased standard errors were estimated from the biased standard errors as:

$$se(\hat{\beta}_i) = \left\{ \frac{se(\hat{\beta}_i)'}{\hat{\sigma}} \right\}^2 \times \sqrt{\hat{v}} \quad (\text{B-18})$$

Where,

- $se(\hat{\beta}_i)$ = vector of unbiased estimators of regression parameters with the size equal to the number of parameters
- $se(\hat{\beta}_i)'$ = vector of biased estimators of regression parameters with the size equal to the number of parameters estimated using the ordinary least squares regression without accounting for autocorrelated residual errors
- i = size of vector = 2 here
- $\hat{\sigma}$ = standard error of regression, also known as root mean squared error
- \hat{v} = metric to bias correct heteroskedasticity and autocorrelation

The metric to bias correct heteroscedasticity and autocorrelation was estimated as:

$$\hat{v} = \sum_{t=1}^d \hat{a}_t^2 + 2 \sum_{h=1}^g \left(1 - \frac{h}{g+1}\right) \left(\sum_{t=h+1}^d \hat{a}_t \hat{a}_{t-h} \right) \quad (\text{B-19})$$

Where,

- d = number of seconds of data in sub-model 3 (s)
- g = maximum lag to account for autocorrelation (s)
- h = index for lags (s). $h \in 1, 2, 3, \dots, g$
- \hat{a}_t = $\hat{r}_t \times \hat{\epsilon}_t$
- $\hat{\epsilon}_t$ = vector of residuals of Equation B-17 corresponding to sub-model 3 with size d
- \hat{r}_t = vector of residuals of an auxiliary regression with size d

The auxiliary regression corresponds to regression with any one of the independent variables chosen as a dependent variable versus other independent variables. In this case:

$$\overline{LPD}_{12,t} = \partial_2 \times \overline{LPD}_{12,t}^2 + r_t \quad (\text{B-20})$$

Where,

- ∂_2 = Estimated slope of the auxiliary regression
- r_t = residual of the auxiliary regression

g was estimated, rounded to the nearest integer as:

$$g = 4 \times \left(\frac{d}{100} \right)^{\frac{2}{9}} \quad (\text{B-21})$$

Emission rates of CO, HC, and PM for all LCF IDs, and NO_x emission rates for LCF ID 1 and 10 were modeled as:

$$R_{ID,SM,s',t} = \begin{cases} I_{ID,SM,s'} & SM \in 1,2,4 \\ \bar{r}_{ID,SM,s',m} & SM \in 3 \end{cases} \quad (\text{B-22})$$

Where,

- $R_{ID,SM,s',t}$ = Emission rate of species s' at time t for a given LCF ID and sub-model SM (g/s)
- $I_{ID,SM,s'}$ = Intercept of regression of species s' at time t for a given LCF ID and sub-model SM (g/s)
- s' = Index for species. $s' \in$ CO emission rate, HC emission rate, and PM emission rate
- m = Index for mode m at time t of sub-model SM for species s' . $m \in 1,2,3,\dots,10$ for sub-model 3.
- $\bar{r}_{ID,SM,s',m}$ = Average rate for a given LCF ID for species s' based on given mode m of sub-model 3 SM (g/s).

B.2.5 Contribution of resistances to power demand

Higher FUERs are typically associated with higher power demand as shown in Figure B-6. Therefore, to quantify key resistive forces leading to high power demand and FUERs, the contribution of each resistances to the power demand for each trip was estimated. Based on Equation B-19, LPD can be negative, zero, or positive. Likewise, $\overline{LPD}_{12,t}$ can also be negative, zero, or positive. As discussed in Section 0, FUERs for negative and $\overline{LPD}_{12,t}$ are typically approximately equal to idle FUERs. Only $\overline{LPD}_{12,t} \geq 0$ kW leads to higher FUERs. Therefore, the contribution of resistances to $\overline{LPD}_{12,t}$ was quantified only for $\overline{LPD}_{12,t} \geq 0$ kW.

The average contribution of each resistive force to $\overline{LPD}_{12,t}$ for a given one-way trip is given in Table B-6. For a given one-way trip, starting resistance comprised <0.01% of the power demand. Starting resistance is typically only applicable for the first second during which the train departs a station stop. Therefore, the average contribution of starting resistance to power demand for a trip was negligible compared to other resistances. The contribution of journal resistance varied between 3.6% and 8.2% with a mean of 5.1%. The contribution of flange and curvature resistances was <2.5% each on average. Therefore, for the Piedmont passenger rail service, starting, journal, flange, and curvature resistances typically have a small effect on power demand and, consequently, on FUERs. Drag resistance typically contributed 10% to 20% of the power demand. Acceleration and grade resistances each contributed between 28% and 49% to the power demand with an average of 37% each. Therefore, acceleration and grade resistances are the highest contributors to power demand and FUERs. Inter-trip variability in the contributions of resistive forces indicates differences in operator behavior leading to inter-trip variability in power demand and FUERs. Therefore, there is potential to reduce FUERs for given rail service by controlling train acceleration and speeds on grades.

Table B-6. Average Contribution of Each Resistive Force to 12-Second Backwards Moving Average Locomotive Power Demand for a Given One-Way Trip.

LCF ID	Trip	Average Contribution of Resistive Forces to Power Demand (%) ^a					
		Journal	Flange	Drag	Acceleration	Grade	Curvature
1	1	4.7	1.7	14.0	42.2	36.2	1.3
1	2	5.4	1.9	14.7	38.8	37.4	1.8
1	3	4.8	1.7	14.3	42.5	35.3	1.4
1	4	4.9	1.8	15.3	42.7	33.6	1.6
1	5	5.0	1.8	14.6	37.2	40.0	1.4
2	1	4.5	1.5	14.6	43.5	34.4	1.4
2	2	4.6	1.6	16.1	44.1	32.1	1.5
2	3	4.3	1.6	15.2	43.8	33.9	1.2
2	4	5.6	1.7	15.3	39.9	35.6	1.8
2	5	4.2	1.5	15.1	45.0	32.9	1.2
2	6	5.1	1.8	17.7	41.9	32.1	1.4
3	1	4.5	1.7	15.9	40.8	35.5	1.7
3	2	4.5	1.6	15.7	42.0	34.5	1.7
3	3	4.7	1.7	15.8	40.9	35.5	1.5
3	4	4.7	1.7	16.3	41.5	34.1	1.7
3	5	4.5	1.5	13.4	44.0	35.4	1.3
3	6	4.4	1.5	14.6	45.6	32.4	1.5
4	1	4.7	1.8	14.3	41.3	36.2	1.7
4	2	4.8	1.8	14.7	41.5	35.4	1.8
4	3	4.2	1.5	12.0	47.2	33.8	1.3
4	4	4.5	1.6	12.6	48.6	31.1	1.5
4	5	4.9	1.8	14.3	39.8	37.3	1.8
5	1	4.5	1.7	17.4	39.7	35.0	1.7
5	2	4.5	1.7	17.0	42.9	32.2	1.6
5	3	4.5	1.7	16.8	39.8	36.0	1.1
5	4	4.9	1.6	14.1	40.3	37.2	1.9
5	5	4.1	1.6	15.2	44.2	33.7	1.2
5	6	4.9	1.6	15.6	43.1	33.3	1.5
6	1	5.7	2.0	15.2	35.8	39.6	1.7
6	3	5.1	1.8	13.2	38.6	39.7	1.6
6	5	5.3	1.8	13.6	37.1	40.5	1.7
7	2	5.0	2.0	17.1	41.6	32.5	1.8
7	4	5.4	2.1	17.6	39.7	33.4	1.8
7	6	6.0	1.9	15.7	42.3	32.4	1.7
8	1	8.2	2.0	12.4	29.7	45.5	2.2
8	3	6.6	2.0	12.9	34.6	41.9	2.1
8	5	6.4	2.2	16.7	28.3	44.3	2.1

Table B-6 Continued on Next Page.

Table B-6 Continued from Previous Page.

LCF ID	Trip	Average Contribution of Resistive Forces to Power Demand (%) ^a					
		Journal	Flange	Drag	Acceleration	Grade	Curvature
9	2	7.0	2.1	14.3	35.7	38.4	2.5
9	4	5.8	2.3	20.4	34.8	35.1	1.6
9	6	5.5	2.0	16.2	39.2	35.0	2.1
10	1	4.5	1.5	12.4	44.8	35.2	1.6
10	2	4.9	1.9	15.8	40.6	35.0	1.8
10	4	5.0	1.8	14.3	43.5	33.6	1.8
10	5	4.9	1.8	14.4	38.4	39.0	1.6
10	6	4.9	1.7	14.0	40.9	36.7	1.7
11	1	5.9	1.6	15.4	38.4	37.2	1.6
11	2	4.8	1.9	18.3	38.4	34.8	1.8
11	3	4.8	1.7	15.7	38.9	37.5	1.6
11	4	4.6	1.7	16.0	40.4	35.8	1.6
11	5	4.8	1.7	15.8	37.0	39.1	1.7
11	6	4.8	1.7	16.2	39.4	36.2	1.7
12	1	6.6	1.0	18.6	37.0	34.3	2.5
12	2	3.6	1.9	10.4	36.3	45.5	2.3
12	3	6.1	1.5	12.9	42.5	34.7	2.3
12	4	4.3	1.2	14.0	34.4	43.8	2.3
12	5	4.5	1.6	10.3	41.8	40.4	1.3
12	6	5.8	1.7	17.4	33.6	39.2	2.2
12	7	5.9	2.4	12.7	31.0	45.9	2.1
12	8	5.5	1.2	15.3	34.0	42.1	1.9
12	9	5.6	2.3	17.8	44.4	28.4	1.5
12	10	6.9	1.2	12.5	35.9	41.8	1.7
12	11	5.0	2.0	11.5	33.5	46.9	1.2
12	12	4.1	1.3	17.3	40.1	35.6	1.7
12	13	3.8	2.6	16.6	33.7	41.6	1.8
12	14	5.7	2.2	10.9	42.0	38.2	1.0
12	15	5.1	1.2	15.4	39.0	37.6	1.7
Minimum		3.6	1.0	10.3	28.3	28.4	1.0
Maximum		8.2	2.6	20.4	48.6	46.9	2.5
Average		5.1	1.7	15.0	39.7	36.8	1.7

^a The average contribution of resistive forces was estimated based on data with 12-Second Backwards Moving Average Locomotive Power Demand ($\overline{LPD}_{12,t}$) > 0 kW. The contribution of starting resistance was < 0.01% and is therefore not shown in this Table.

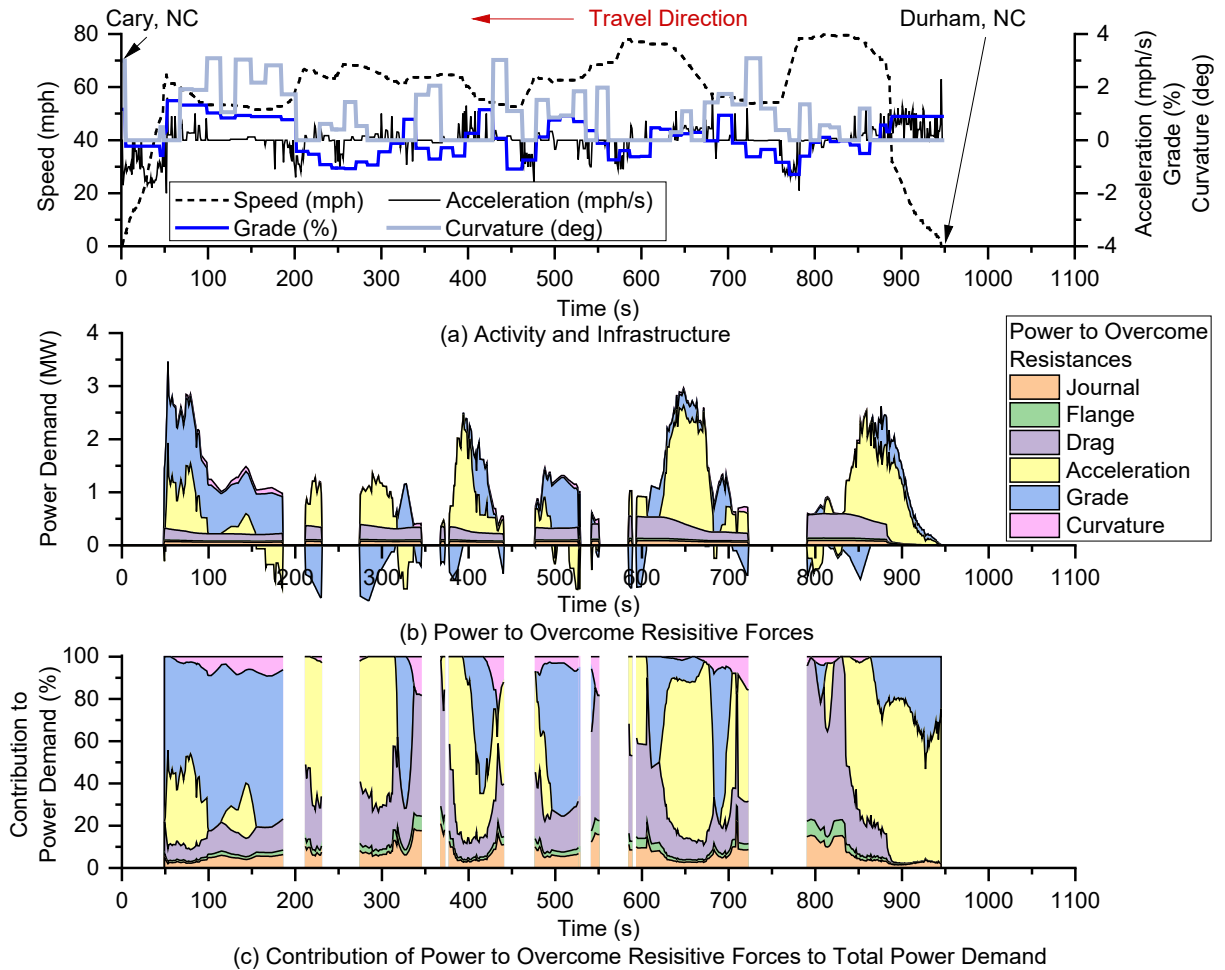


Figure B-7. Example Time Plot of Variation in Activity and Infrastructure and Their Effect on Power Demand ($LPD_{12,t}$) for Single Locomotive Consist of NC 1797 Operated on B20 from Durham, NC to Cary, NC: (a) Activity and Infrastructure, (b) Power to Overcome Resistive Forces, and (c) Contribution of Power to Overcome Resistive Forces.

The gaps in the time plots are for seconds with $LPD_{12,t} < 0$ kW. For the remaining data, negative resistive forces were inferred as 0 kW.

The variation of fuel use rates with deciles of speed, acceleration, and grade is given in Figure B-8. These mean fuel use rates are based on 488 combinations of speed, acceleration, and grade deciles measured in the real-world. These combinations correspond to all measured combinations of deciles of speed, acceleration, and grade. Fuel use rate was typically the lowest, close to idle fuel use rate when acceleration, grade, or both were negative. While positive values of acceleration or grade lead to high power demand, negative resistance of one of these variables compensates for the positive resistance of the other. The highest values of fuel use rate were measured for the combinations with relatively higher deciles of speed, acceleration, and grade.

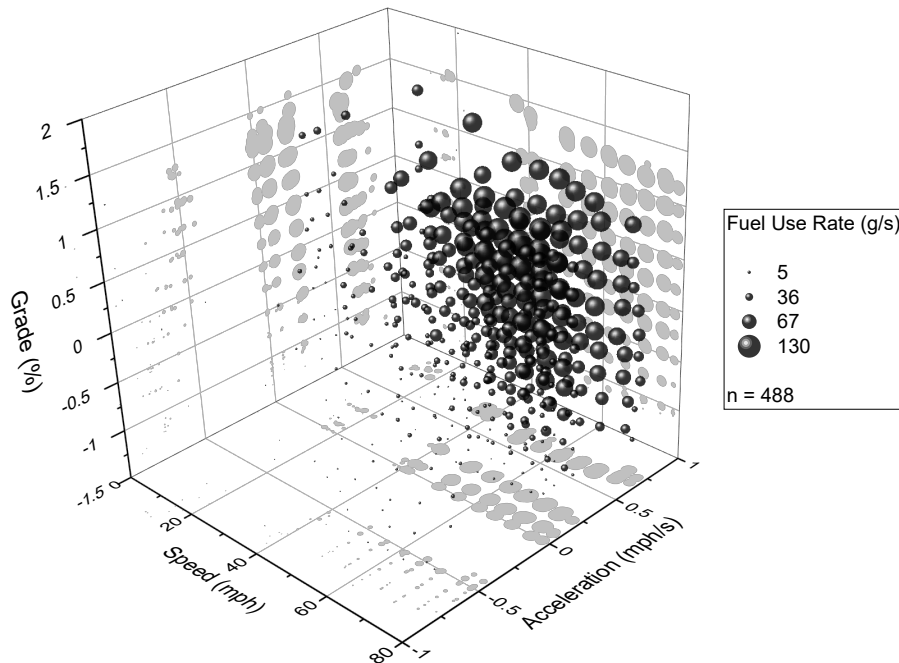


Figure B-8. Variation of Fuel Use Rate with Deciles of Speed, Acceleration, and Grade.

Since the trains typically run on the same schedule unless delayed, the distributions of speed, acceleration, and grade were similar regardless of locomotives or consists. Therefore, speed, acceleration, and grade for all combinations of locomotives, consists, and fuels were binned into deciles for a maximum possible combinations equal to 1000. However, 488 combinations were measured in real-world for the Piedmont passenger rail service.

B.2.6 Model calibration

The calibration involved estimating the average FUERs for sub-models 1, 2, and 4 and sub-model 3 parameters described in Table B-5. Data in each sub-model and average FUERs corresponding to each sub-model are given in Table B-7. FUERs for SM1 were expected to vary between low and high idle FUERs. FUERs for SM2 were expected to be slightly higher than high idle FUERs because SM2 typically comprised idle operation and transition from a notch with higher FUERs. FUERs for SM4 were expected to be close to or higher than notch 8 average FUERs because SM4 and notch 8 correspond to the highest PME load. The sub-model inferred rates were compared to steady-state low idle, high idle, and notch 8 rates in Table B-8. Typically, sub-model inferred rates were within the range of expected notch-average rates.

The calibration also comprised ensuring the continuity of FUERs at each sub-model boundary. To evaluate model continuity at the boundary of sub-models 3 and 4, sub-model 3 estimated FUERs at 2519 kW were compared with sub-model 4 inferred FUERs. The comparison is given in Table B-9. For fuel use rates and emission rates of CO₂ and NO_x, this difference was typically less than 10%, indicating good model continuity. For CO and PM emission rates, mode 10 average rates were typically 2% to 20% lower than sub-model 4 inferred rates. Lower rates were expected because the average $\overline{LPD}_{12,t}$ in mode 10 was lower than 2519 kW because mode 10 included $\overline{LPD}_{12,t}$ between 2190 kW and 2519 kW. On average, mode 9 rates were 10% lower

than mode 10 rates. The differences of adjacent modes indicate a monotonic increasing trend, which is consistent with the observed at the boundary between the two models.

For HC emission rates, mode 10 rates range from -44% lower to 51% higher than the sub-model 4 rates. By comparison, mode 9 rates range from 8% lower to 20% higher than the mode 10 rates. The variability among LCF IDs in the trend in emission rates at high power demand, among modes 9 and 10 and sub-model 4, is influenced in part by the fact that HC emission rates were based on low measured exhaust concentrations that are either below detection limit or that were not substantially higher than the detection limit, such that the measurements were imprecise, coupled with a general pattern that the HC emission rates tend to be similar, on average, for modes 6 through 10. For several LCF IDs, the differences at sub-model boundaries were large but were within the noise of the data. Since HC rates were low, large percentage differences can be associated with a small absolute difference in rates. Hence, the sub-models were inferred to be continuous.

Table B-7. Average Power Demand, Fuel Use Rate, and Emission Rates in Each Sub-Model.

LCF ID	Sub-model	Data Count (sec)	Percentage of Total Data (%) ^a	Mean LPD-12 (kW)	Mean Fuel Use Rate (g/s)	Mean CO ₂ Emission Rate (g/s)	Mean CO Emission Rate (g/s)	Mean HC Emission Rate (g/s)	Mean NO _x Emission Rate (g/s)	Mean PM Emission Rate (g/s)
1	2	5068	8.6	-33	4.9	14.5	0.10	0.60	0.59	0.0002
	1	17368	29.6	-1459	10.3	31.5	0.10	0.67	1.39	0.001
	3	35596	60.6	1151	85.3	270	0.38	1.00	7.26	0.061
	4	739	1.3	2715	133	422	0.70	0.62	8.07	0.135
2	2	4828	7.8	-36	6.1	17.7	0.10	0.89	0.32	0.001
	1	19649	31.8	-1459	11.4	34.9	0.14	0.73	0.62	0.020
	3	33056	53.5	1105	69.2	218	0.60	1.17	2.95	0.176
	4	4270	6.9	2776	134	424	1.45	1.14	4.97	0.307
3	2	8049	11.0	-21	4.6	14.7	0.00	0.09	0.34	0.001
	1	23248	31.7	-1260	8.6	27.4	0.02	0.10	0.59	0.011
	3	39217	53.4	1138	70.6	225	0.17	0.18	4.05	0.132
	4	2890	3.9	2764	136	434	0.60	0.18	6.63	0.242
4	2	7760	12.9	-10	4.3	13.5	0.00	0.05	0.31	0.001
	1	18305	30.5	-1342	8.4	26.7	0.01	0.07	0.57	0.009
	3	29565	49.3	1040	51.7	165	0.10	0.11	3.10	0.088
	4	4334	7.2	2795	129	411	0.63	0.15	6.14	0.221
5	2	3186	5.7	-47	4.6	14.5	0.00	0.10	0.28	- ^a
	1	15832	28.3	-1470	14.2	45.2	0.02	0.08	1.01	- ^a
	3	33646	60.1	1193	66.0	210	0.13	0.12	3.73	- ^a
	4	3284	5.9	2803	116	370	0.40	0.08	5.46	- ^a
6	2	2734	7.6	-38	2.8	8.9	0.00	0.10	0.30	0.001
	1	10476	29.0	-1738	13.3	42.1	0.05	0.11	1.37	0.009
	3	18653	51.6	1269	70.2	223	0.32	0.19	6.79	0.072
	4	4257	11.8	2902	119	378	0.95	0.16	10.71	0.131

Table B-7 Continued on Next Page

Table B-7 Continued from Previous Page

LCF ID	Sub-model	Data Count (sec)	Percentage of total data in sub-model (%)	Mean LPD-12 (kW)	Mean Fuel Use Rate (g/s)	Mean CO ₂ Emission Rate (g/s)	Mean CO Emission Rate (g/s)	Mean HC Emission Rate (g/s)	Mean NO _x Emission Rate (g/s)	Mean PM Emission Rate (g/s)
7	2	2756	8.1	-26	3.0	9.5	0.01	0.06	0.31	0.0003
	1	11326	33.2	-1044	6.7	21.2	0.01	0.07	0.69	0.003
	3	19145	56.2	899	39.9	127	0.10	0.12	4.26	0.039
	4	855	2.5	2743	117	373	0.81	0.13	10.20	0.117
8	2	13410	16.9	-5	3.3	10.3	0.00	0.07	0.30	0.051
	1	20884	26.4	-1575	11.6	36.4	0.05	0.29	0.97	0.084
	3	36582	46.2	1191	71.4	225	0.82	0.67	5.20	0.203
	4	8374	10.6	2975	122	383	2.13	1.10	8.05	0.290
9	2	8894	14.0	-5	3.3	10.3	0.00	0.06	0.31	0.080
	1	20269	31.8	-1083	7.0	22.1	0.01	0.18	0.60	0.098
	3	33306	52.3	913	42.4	134	0.39	0.24	3.48	0.176
	4	1191	1.9	2770	118	369	3.04	0.90	6.96	0.338
10	2	3848	7.5	-50	3.9	11.6	0.03	0.36	0.48	0.020
	1	15945	31.2	-1503	10.6	32.4	0.02	0.37	1.44	0.026
	3	29461	57.7	1119	72.3	224	0.07	0.67	6.92	0.078
	4	1834	3.6	2736	130	404	0.25	0.75	8.07	0.174
11	2	5238	8.6	-42	4.5	13.7	0.01	0.18	0.24	0.011
	1	16840	27.7	-1501	14.7	45.4	0.09	0.15	0.67	0.027
	3	38212	62.8	1162	86.2	267	0.83	0.17	2.71	0.123
	4	554	0.9	2790	146	453	1.83	0.09	3.82	0.228
12	2	15627	9.6	2	4.3	12.6	0.12	0.31	0.26	0.018
	1	45187	27.8	-414	16.3	49.8	0.16	0.39	0.90	0.029
	3	10149	62.5	743	67.3	208	0.23	0.55	3.37	0.084
	4	^a	^b	^b	^b	^b	^b	^b	^b	^b

^a Invalid PM data. ^b No measured data in this range

Table B-8. Comparison of Sub-Model 1, 2, and 4 Inferred Fuel Use and Emission Rates With The Steady-State Over-The-Rail Measurement-Based Notch-Average Rates at Low Idle, High Idle and Notch 8: (a) Fuel Use Rates; (b) CO₂ Emission Rates; (c) CO Emission Rates; (d) HC Emission Rates; (e) NO_x Emission Rates; and (f) PM Emission Rates.

(a) Fuel Use Rate (g/s)

LCF ID	Low Idle (g/s)	Sub-model 2 (SM2) (g/s)	High Idle (g/s)	SM2 versus High Idle ^a (%)	Sub-model 1 (SM1) (g/s)	SM1 versus High Idle ^a (%)	Sub-model 4 (SM4) (g/s)	Notch 8 (g/s)	SM4 versus Notch 8 ^a (%)
1	2.2	4.9	3.7	32	10.1	174	133	115	15
2	2.6	6.1	4.6	32	11.5	149	134	133	1
3	2.3	4.6	4.0	16	8.6	116	136	125	9
4	2.9	4.3	5.7	-25	8.3	46	129	106	22
5	2.3	4.6	5.8	-21	14.3	147	116	128	-10
6	2.2	2.8	2.6	9	13.5	419	119	105	13
7	2.0	3.0	3.0	1	6.8	128	117	94	24
8	2.6	3.3	3.0	9	10.3	243	123	109	13
9	2.1	3.3	2.8	17	7.0	151	117	104	12
10	- ^b	3.9	4.1	-5	10.6	172	130	112	16
11	4.0	4.5	8.7	-48	14.7	227	146	128	14
12	2.5	4.3	6.2	-31	16.3	279	137	114	20

(b) CO₂ Emission Rate (g/s)

LCF ID	Low Idle (g/s)	Sub-model 2 (SM2) (g/s)	High Idle (g/s)	SM2 versus High Idle ^a (%)	Sub-model 1 (SM1) (g/s)	SM1 versus High Idle ^a (%)	Sub-model 4 (SM4) (g/s)	Notch 8 (g/s)	SM4 versus Notch 8 ^a (%)
1	7	14	12	21	31	159	421	359	17
2	8	18	15	18	35	134	424	407	4
3	7	15	12	22	27	128	433	365	19
4	9	13	18	-25	26	46	411	332	24
5	7	14	17	-15	45	168	368	373	-1
6	6	9	8	11	43	435	377	327	15
7	6	10	9	6	22	140	371	294	26
8	6	10	9	15	32	258	387	339	14
9	7	10	9	14	22	145	366	322	14
10	-b	12	12	0	32	167	404	347	16
11	12	14	27	-48	45	221	453	395	15
12	7	13	19	-32	50	285	433	355	22

Table B-8 Continued on Next Page

Table B-8 Continued from Previous Page

(c) CO Emission Rate (g/s)									
LCF ID	Low Idle (g/s)	Sub-model 2 (SM2) (g/s)	High Idle (g/s)	SM2 versus High Idle ^a (%)	Sub-model 1 (SM1) (g/s)	SM1 versus High Idle ^a (%)	Sub-model 4 (SM4) (g/s)	Notch 8 (g/s)	SM4 versus Notch 8 ^a (%)
1	0.11	0.10	0.02	410	0.10	396	0.74	0.73	-5
2	0.08	0.10	0.12	-19	0.14	20	1.45	1.73	-16
3	0.03	0.002	0.11	-98	0.02	-83	0.67	0.88	-32
4	0.01	0.001	0.02	-95	0.01	-61	0.69	0.36	73
5	0.02	0.0002	0.05	-100	0.02	-65	0.46	0.60	-35
6	0.01	0.002	0.01	-79	0.05	446	0.94	0.63	50
7	0.003	0.01	0.01	-43	0.01	47	0.81	0.46	73
8	0.01	0.0002	0.01	-98	0.03	219	2.24	1.62	34
9	0.01	0.001	0.01	-89	0.01	29	3.06	1.82	64
10	^{-b}	0.03	0.02	50	0.02	-33	0.28	0.10	180
11	0.22	0.01	0.33	-97	0.09	800	1.85	3.38	-45
12	0.09	0.12	0.14	-14	0.16	33	0.92	0.35	163
(d) HC Emission Rate (g/s)									
LCF ID	Low Idle (g/s)	Sub-model 2 (SM2) (g/s)	High Idle (g/s)	SM2 versus High Idle ^a (%)	Sub-model 1 (SM1) (g/s)	SM1 versus High Idle ^a (%)	Sub-model 4 (SM4) (g/s)	Notch 8 (g/s)	SM4 versus Notch 8 ^a (%)
1	0.76	0.60	0.17	254	0.66	290	0.65	1.45	-53
2	0.51	0.89	0.83	7	0.73	-12	1.15	1.73	-34
3	0.26	0.09	0.77	-88	0.10	-87	0.19	2.66	-93
4	0.04	0.05	0.07	-34	0.07	2	0.15	0.18	12
5	0.16	0.10	0.26	-61	0.08	-69	0.08	0.56	-85
6	0.08	0.10	0.08	21	0.11	35	0.16	0.24	-12
7	0.01	0.06	0.06	3	0.07	23	0.13	0.12	1
8	0.02	0.07	0.22	-69	0.28	28	1.01	1.25	-16
9	0.003	0.06	0.12	-47	0.18	51	0.98	0.51	113
10	^{-b}	0.36	0.35	3	0.37	3	0.75	0.92	-18
11	0.23	0.18	0.53	-66	0.15	-17	0.09	0.45	-80
12	0.47	0.31	0.51	-39	0.39	26	0.23	0.91	-75

Table B-8 Continued on Next Page

Table B-8 Continued from Previous Page

(e) NO_x Emission Rate (g/s)

LCF ID	Low Idle (g/s)	Sub-model 2 (SM2) (g/s)	High Idle (g/s)	SM2 versus High Idle ^a (%)	Sub-model 1 (SM1) (g/s)	SM1 versus High Idle ^a (%)	Sub-model 4 (SM4) (g/s)	Notch 8 (g/s)	SM4 versus Notch 8 ^a (%)
1	0.4	0.6	0.7	-16	1.4	95	8.1	11.1	-27
2	0.2	0.3	0.4	-21	0.6	56	5.0	6.4	-23
3	0.2	0.3	0.3	13	0.6	97	6.6	5.6	18
4	0.2	0.3	0.4	-21	0.6	42	6.1	5.1	20
5	0.2	0.3	0.4	-30	1.0	154	5.4	6.6	-17
6	0.2	0.3	0.3	-1	1.4	366	10.7	9.4	14
7	0.2	0.3	0.3	4	0.7	133	10.1	8.4	21
8	0.3	0.3	0.3	1	0.9	188	8.2	6.9	18
9	0.2	0.3	0.3	3	0.6	96	7.0	6.5	7
10	^{-b}	0.5	0.5	20	1.4	180	8.1	8.7	-7
11	0.2	0.2	0.3	-33	0.7	250	3.8	3.4	12
12	0.2	0.3	0.4	-25	0.9	200	7.4	5.2	42

(f) PM Emission Rate (g/s)

LCF ID	Low Idle (g/s)	Sub-model 2 (SM2) (g/s)	High Idle (g/s)	SM2 versus High Idle ^a (%)	Sub-model 1 (SM1) (g/s)	SM1 versus High Idle ^a (%)	Sub-model 4 (SM4) (g/s)	Notch 8 (g/s)	SM4 versus Notch 8 ^a (%)
1	0.01	0.0002	0.01	-98	0.001	-93	0.1	0.2	-16
2	0.01	0.0009	0.01	-91	0.02	99	0.3	0.3	-7
3	0.03	0.001	0.03	-97	0.01	-64	0.2	0.4	-45
4	0.03	0.0007	0.03	-98	0.01	-69	0.2	0.2	10
5	^{-c}	^{-c}	^{-c}	^{-c}	^{-c}	^{-c}	^{-c}	^{-c}	^{-c}
6	0.01	0.0003	0.01	-97	0.01	-6	0.1	0.2	-27
7	0.01	0.0003	0.02	-99	0.004	-82	0.1	0.1	-17
8	0.03	0.05	0.07	-27	0.08	14	0.03	0.05	0.07
9	0.06	0.08	0.07	14	0.10	40	0.3	0.2	38
10	^{-b}	0.02	0.01	100	0.03	50	0.2	0.1	100
11	0.02	0.01	0.03	-67	0.03	200	0.2	0.3	-33
12	0.01	0.02	0.01	100	0.03	50	0.3	0.2	50

^a Percentage difference of X versus Y was estimated as $(X-Y) \times 100/Y$ ^b No data for the corresponding notch position^c No valid PM data

Table B-9. Comparison of Sub-Model 3 Fitted Fuel Use and Emission Rates at 2519 kW with Sub-Model 4 Inferred Fuel Use and Emission Rates to Evaluate Continuity at Sub-Model Boundary: (a) Fuel Use Rates; (b) CO₂ Emission Rates; (c) CO Emission Rates; (d) HC Emission Rates; (e) NO_x Emission Rates; and (f) PM Emission Rates.

(a) Fuel Use Rate

LCF ID	Fitted Rate at 2519 kW (g/s)	Sub-Model 4 Inferred Rate (g/s)	Percentage Difference of Fitted Rate at 2519 kW Versus Sub-Model 4 Inferred Rate (%) ^a
1	141	133	5.7
2	135	134	1.1
3	146	136	7.3
4	120	129	-7.1
5	123	116	6.1
6	121	119	1.6
7	105	117	-10.1
8	123	123	-0.3
9	125	117	6.8
10	123	130	-5.4
11	150	146	2.7
12	131	137	-4.4

(b) CO₂ Emission Rate

LCF ID	Fitted Rate at 2519 kW (g/s)	Sub-Model 4 Inferred Rate (g/s)	Percentage Difference of Fitted Rate at 2519 kW Versus Sub-Model 4 Inferred Rate (%) ^a
1	446	421	6.1
2	428	424	0.9
3	464	433	7.2
4	381	411	-7.3
5	392	368	6.5
6	384	377	1.9
7	334	371	-9.9
8	386	387	-0.4
9	393	366	7.3
10	397	404	-1.7
11	458	453	1.1
12	427	433	-1.4

Table B-9 Continued on Next Page.

Table B-9 Continued from Previous Page.

(c) CO Emission Rate

LCF ID	Fitted Rate at 2519 kW (g/s)	Sub-Model 4 Inferred Rate (g/s)	Percentage Difference of Sub-Model 3 Inferred Rate Versus Sub-Model 4 Inferred Rate (%) ^a
1	0.69	0.69	-1
2	1.34	1.45	-8
3	0.50	0.59	-16
4	0.52	0.62	-16
5	0.33	0.39	-15
6	0.76	0.94	-19
7	0.60	0.8	-24
8	1.97	2.16	-9
9	2.70	2.99	-10
10	0.17	0.28	-39.3
11	1.88	1.85	1.6
12	0.61	0.92	-33.7

(d) HC Emission Rate

LCF ID	Fitted rate at 2519 kW (g/s)	Sub-Model 4 Inferred Rate (g/s)	Percentage Difference of Fitted Rate at 2519 kW Versus Sub-Model 4 Inferred Rate (%) ^a
1	0.81	0.65	25
2	1.21	1.15	5
3	0.18	0.19	-8
4	0.15	0.15	1
5	0.12	0.08	51
6	0.17	0.16	8
7	0.17	0.13	27
8	1.05	1.01	4
9	0.55	0.98	-44
10	0.75	0.75	0.0
11	1.31	1.22	6.3
12	0.20	0.23	-13.0

Table B-9 Continued on Next Page.

Table B-9 Continued from Previous Page.

(e) NO_x Emission Rate

LCF ID	Fitted Rate at 2519 kW (g/s)	Sub-Model 4 Inferred Rate (g/s)	Percentage Difference of Fitted Rate at 2519 kW Versus Sub-Model 4 Inferred Rate (%) ^a
1	8.1 ^b	8.1	0
2	4.9	5.0	-2.1
3	7.1	6.6	6.4
4	5.7	6.1	-7.5
5	5.5	5.5	1.1
6	10.8	10.7	0.7
7	9.3	10.1	-8.1
8	8.0	8.2	-2.1
9	7.3	7.0	5.0
10	9.2 ^b	8.1	14.0
11	3.6	3.8	-6.2
12	8.0	7.4	2.1

^a Percentage difference of *X* versus *Y* was estimated as $(X-Y) \times 100/Y$

^b For LCF ID 2 and 10 for NO_x emission rates, a modal model was used instead of a regression-based model

(f) PM Emission Rate

LCF ID	Fitted Rate at 2519 kW (g/s)	Sub-Model 4 Inferred Rate (g/s)	Percentage Difference of Fitted Rate at 2519 kW Versus Sub-Model 4 Inferred Rate (%) ^a
1	0.14	0.13	8
2	0.30	0.31	-3
3	0.24	0.24	0
4	0.20	0.22	-9
5	- ^b	- ^b	- ^b
6	0.11	0.13	-15
7	0.10	0.12	-17
8	0.29	0.29	0
9	0.32	0.33	-3
10	0.15	0.26	-42.3
11	0.29	0.25	16.0
12	0.24	0.33	-27.3

^a Percentage difference of *X* versus *Y* was estimated as $(X-Y) \times 100/Y$

^b Invalid PM data

SM3 is comprised of two parts: regression and modal. The regression part is applicable to fuel use rate and emission rates of CO₂ and NO_x, except for NO_x emission rates for LCF IDs 1 and 10. The regression part of SM3 was calibrated based on leave-one-out cross-validation (LOOCV) for each LCF (Wong, 2015). In a LOOCV, all but one one-way trip were used to calibrate each sub-model. The left-out one-way trip was used for validation. All possible LOOCV combinations were calibrated. The models were weakly sensitive to the choice of one-way trips if the parameters were within 10% of each other for all LOOCV combinations. For such cases, a final model based on all one-way trips combined was calibrated and validated.

Calibrated parameters for each LOOCV case of the regression part of SM3 are given in Table B-10. The calibrated parameters for a given species and LCF were within 10% of each other for all LOOCV combinations. Therefore, a final model was fit to data from all the one-way trips combined for a given species and LCF. The final model was later evaluated and modeled. The standard error in linear and quadratic slope was typically less than 4% relative to the slope and had narrow confidence intervals, indicating that these parameters were precisely estimated. The model R² with the quadratic term included for each LCF ID and species was 0.74 or higher, indicating high model precision. For each LCF ID, model R² was higher for the model with linear and quadratic terms than for the model with the linear term only. The increase in model R² was small relative to the model R² without the quadratic term. Thus, the models were approximately linear. The addition of the quadratic term reduced the difference from sub-model 4 inferred rates at 2519 kW versus the linear model. Therefore, a model with both linear and quadratic terms is more suitable for the data.

Table B-10. Calibrated Sub-Model 3 Regression Parameters for Fuel Use Rate based on All Combinations of Leave-One-Out Calibration Validation Cases for Measured Combinations of Locomotives, Consists, and Fuels: (a) Fuel Use Rate; (b) CO₂ Emission Rate; and (c) NO_x Emission Rate.

(a) Fuel Use Rate

ID ^a	Trips	Sample Size	Linear Term			Quadratic Term			Intercept (g/s)	Model R ²
			Slope (×10 ⁻² g/kW)	Standard Error (×10 ⁻³ g/kW)	95% Confidence Interval (×10 ⁻² g/kW)	Slope (×10 ⁻⁵ g ² /kW ²)	Standard Error (×10 ⁻⁶ g ² /kW ²)	95% Confidence Interval (×10 ⁻⁵ g ² /kW ²)		
1	2,3,4,5	28590	9.05	2.39	[8.58, 9.52]	-1.33	4.56	[-1.54, -1.12]	9.7	0.83
	1,3,4,5	28230	9.22	2.41	[8.75, 9.70]	-1.34	4.16	[-1.53, -1.15]	11.0	0.88
	1,2,4,5	28560	8.88	2.06	[8.48, 9.29]	-1.46	4.20	[-1.66, -1.27]	9.6	0.88
	1,2,3,5	28976	8.97	2.39	[8.50, 9.43]	-1.42	4.20	[-1.62, -1.23]	9.4	0.86
	1,2,3,4	28028	9.05	2.26	[8.61, 9.49]	-1.44	4.29	[-1.63, -1.24]	10.2	0.86
2	2,3,4,5,6	27620	5.90	2.67	[5.37, 6.42]	-0.21	5.69	[-0.47, 0.05]	11.4	0.72
	1,3,4,5,6	28652	5.01	2.78	[4.47, 5.56]	-0.21	5.69	[-0.47, 0.05]	10.6	0.73
	1,2,4,5,6	26805	5.40	2.56	[4.90, 5.90]	-0.23	4.84	[-0.45, -0.01]	11.3	0.72
	1,2,3,5,6	26894	5.73	3.01	[5.14, 6.32]	-0.22	5.64	[-0.48, 0.04]	11.3	0.75
	1,2,3,4,6	27612	5.23	2.73	[4.70, 5.77]	-0.24	5.48	[-0.49, 0.01]	11.8	0.72
	1,2,3,4,5	27697	5.12	2.78	[4.58, 5.67]	-0.23	4.79	[-0.45, -0.01]	11.6	0.74
3	2,3,4,5,6	32999	5.64	2.97	[5.06, 6.22]	0.10	4.80	[-0.13, 0.32]	8.2	0.83
	1,3,4,5,6	32850	4.96	2.66	[4.44, 5.48]	0.08	4.94	[-0.15, 0.31]	8.0	0.82
	1,2,4,5,6	32531	4.70	2.80	[4.15, 5.25]	0.08	4.70	[-0.13, 0.30]	8.4	0.81
	1,2,3,5,6	32473	4.75	2.86	[4.19, 5.31]	0.09	4.47	[-0.11, 0.30]	8.5	0.83
	1,2,3,4,6	32786	5.53	2.52	[5.04, 6.03]	0.10	5.08	[-0.13, 0.33]	7.8	0.79
	1,2,3,4,5	32446	4.85	2.88	[4.29, 5.42]	0.09	4.32	[-0.11, 0.29]	9.3	0.81

Table B-10(a) Continued on Next Page.

Table B-10(a) Continued from Previous Page.

ID ^a	Trips	Sample Size	Linear Term			Quadratic Term			Intercept (g/s)	Model R ²
			Slope ($\times 10^{-2}$ g/kW)	Standard Error ($\times 10^{-3}$ g/kW)	95% Confidence Interval ($\times 10^{-2}$ g/kW)	Slope ($\times 10^{-5}$ g ² /kW ²)	Standard Error ($\times 10^{-6}$ g ² /kW ²)	95% Confidence Interval ($\times 10^{-5}$ g ² /kW ²)		
4	2,3,4,5	23906	3.69	2.65	[3.17, 4.20]	0.46	4.36	[0.26, 0.66]	8.8	0.73
	1,3,4,5	23533	3.25	2.31	[2.80, 3.70]	0.41	4.32	[0.21, 0.61]	8.2	0.71
	1,2,4,5	23804	3.48	2.83	[2.93, 4.04]	0.44	4.00	[0.25, 0.62]	8.0	0.70
	1,2,3,5	23599	3.69	2.49	[3.20, 4.17]	0.44	3.80	[0.27, 0.62]	8.5	0.70
	1,2,3,4	23418	3.62	2.47	[3.13, 4.10]	0.41	3.72	[0.24, 0.58]	8.0	0.73
5	2,3,4,5,6	28564	4.43	2.46	[3.95, 4.91]	0.01	5.89	[-0.26, 0.28]	14.6	0.82
	1,3,4,5,6	28362	3.91	2.37	[3.45, 4.38]	0.01	5.72	[-0.25, 0.27]	14.6	0.78
	1,2,4,5,6	27573	4.17	2.53	[3.68, 4.67]	0.01	6.23	[-0.28, 0.30]	13.9	0.78
	1,2,3,5,6	29779	4.60	2.28	[4.15, 5.05]	0.01	6.12	[-0.27, 0.29]	15.7	0.80
	1,2,3,4,6	27159	3.87	2.21	[3.44, 4.30]	0.01	5.78	[-0.26, 0.27]	14.9	0.78
	1,2,3,4,5	26793	4.34	2.44	[3.87, 4.82]	0.01	6.29	[-0.28, 0.30]	15.3	0.82
6	1,3	12546	5.10	3.89	[4.34, 5.87]	-0.18	7.10	[-0.51, 0.14]	14.6	0.79
	1,5	12255	4.67	3.36	[4.02, 5.33]	-0.19	6.89	[-0.50, 0.13]	13.6	0.78
	3,5	12505	4.63	3.25	[3.99, 5.26]	-0.20	7.74	[-0.56, 0.15]	12.6	0.81
7	2,4	12999	3.09	2.37	[2.62, 3.55]	0.23	3.65	[0.06, 0.40]	6.9	0.78
	2,6	12544	2.99	2.40	[2.52, 3.46]	0.21	3.73	[0.04, 0.38]	6.3	0.80
	4,6	12747	3.59	2.02	[3.19, 3.98]	0.22	3.87	[0.04, 0.40]	6.7	0.78
8	1,3	21882	6.08	4.05	[5.28, 6.87]	-0.68	8.03	[-1.05, -0.31]	9.8	0.78
	1,5	23475	6.08	3.85	[5.32, 6.83]	-0.75	8.75	[-1.16, -0.35]	10.9	0.77
	3,5	27807	5.89	4.60	[4.99, 6.79]	-0.75	7.23	[-1.08, -0.41]	9.3	0.78

Table B-10(a) Continued on Next Page.

Table B-10(a) Continued from Previous Page.

ID ^a	Trips	Sample Size	Linear Term			Quadratic Term			Intercept (g/s)	Model R ²
			Slope ($\times 10^{-2}$ g/kW)	Standard Error ($\times 10^{-3}$ g/kW)	95% Confidence Interval ($\times 10^{-2}$ g/kW)	Slope ($\times 10^{-5}$ g ² /kW ²)	Standard Error ($\times 10^{-6}$ g ² /kW ²)	95% Confidence Interval ($\times 10^{-5}$ g ² /kW ²)		
9	2,4	23717	2.68	2.92	[2.11, 3.25]	0.75	5.50	[0.49, 1.00]	7.4	0.73
	2,6	22692	2.76	2.76	[2.22, 3.31]	0.65	5.35	[0.40, 0.89]	6.9	0.73
	4,6	20203	3.00	2.73	[2.46, 3.53]	0.74	4.80	[0.52, 0.96]	6.4	0.76
10	2,3,4,5	24011	8.25	5.62	[7.15, 9.35]	-0.95	2.69	[-1.08, -0.83]	9.8	0.83
	1,3,4,5	24273	7.03	4.73	[6.10, 7.95]	-1.16	2.91	[-1.29, -1.02]	10.8	0.84
	1,2,4,5	24030	8.40	5.30	[7.36, 9.44]	-1.03	2.77	[-1.16, -0.90]	9.9	0.85
	1,2,3,5	22588	7.64	5.46	[6.57, 8.71]	-0.96	2.77	[-1.09, -0.84]	11.6	0.81
	1,2,3,4	22942	8.25	5.30	[7.21, 9.29]	-1.02	2.66	[-1.14, -0.90]	11.1	0.82
11	2,3,4,5,6	32665	5.11	4.92	[4.15, 6.08]	-1.06	3.06	[-1.20, -0.92]	13.2	0.85
	1,3,4,5,6	32228	5.74	5.59	[4.64, 6.83]	-1.11	2.55	[-1.23, -0.99]	15.9	0.84
	1,2,4,5,6	30991	5.28	5.34	[4.24, 6.33]	-1.13	2.80	[-1.26, -1.00]	13.2	0.86
	1,2,3,5,6	31683	5.68	5.44	[4.61, 6.75]	-1.19	2.63	[-1.31, -1.07]	15.7	0.88
	1,2,3,4,6	31458	6.02	5.02	[5.04, 7.01]	-1.07	2.77	[-1.20, -0.94]	16.0	0.89
	1,2,3,4,5	32035	5.28	5.23	[4.26, 6.31]	-1.10	2.58	[-1.22, -0.98]	13.5	0.85

Table B-10(a) Continued on Next Page.

Table B-10(a) Continued from Previous Page.

ID ^a	Trips	Sample Size	Linear Term			Quadratic Term			Intercept (g/s)	Model R ²
			Slope ($\times 10^{-2}$ g/kW)	Standard Error ($\times 10^{-3}$ g/kW)	95% Confidence Interval ($\times 10^{-2}$ g/kW)	Slope ($\times 10^{-5}$ g ² /kW ²)	Standard Error ($\times 10^{-6}$ g ² /kW ²)	95% Confidence Interval ($\times 10^{-5}$ g ² /kW ²)		
12	2,3,4,5,6,7,8,9,1 0,11,12,13,14,15	97803	5.10	3.22	[4.47, 5.73]	-1.39	4.81	[-1.61, -1.17]	16.8	0.74
	1,3,4,5,6,7,8,9,1 0,11,12,13,14,15	95034	5.00	3.25	[4.36, 5.63]	-1.29	4.41	[-1.49, -1.09]	16.6	0.74
	1,2,4,5,6,7,8,9,1 0,11,12,13,14,15	94499	4.94	3.28	[4.30, 5.59]	-1.26	4.36	[-1.47, -1.06]	16.8	0.75
	1,2,3,5,6,7,8,9,1 0,11,12,13,14,15	94547	5.61	2.93	[5.04, 6.19]	-1.47	4.23	[-1.66, -1.27]	16.6	0.77
	1,2,3,4,6,7,8,9,1 0,11,12,13,14,15	94974	4.74	3.16	[4.12, 5.36]	-1.22	4.67	[-1.44, -1.01]	15.5	0.78
	1,2,3,4,6,7,8,9,1 0,11,12,13,14,15	94085	4.79	3.19	[4.16, 5.41]	-1.25	4.18	[-1.44, -1.06]	16.1	0.78
	1,2,3,4,5,6,8,9,1 0,11,12,13,14,15	94171	4.69	3.28	[4.04, 5.33]	-1.32	4.32	[-1.52, -1.12]	16.0	0.74
	1,2,3,4,5,6,7,9,1 0,11,12,13,14,15	94073	4.89	3.35	[4.24, 5.55]	-1.43	4.90	[-1.65, -1.20]	17.9	0.78
	1,2,3,4,5,6,7,8,1 0,11,12,13,14,15	94653	5.46	2.90	[4.89, 6.03]	-1.29	4.54	[-1.5, -1.08]	17.9	0.77
	1,2,3,4,5,6,7,8,9, 11,12,13,14,15	94258	4.84	3.38	[4.18, 5.50]	-1.36	4.58	[-1.57, -1.15]	17.8	0.75
1,2,3,4,5,6,7,8,9, 10,12,13,14,15	94678	5.67	2.96	[5.08, 6.25]	-1.33	4.63	[-1.55, -1.12]	16.8	0.74	

Table B-10 (a) Continued on Next Page.

Table B-10 (a) Continued from Previous Page.

ID ^a	Trips	Sample Size	Linear Term			Quadratic Term			Intercept (g/s)	Model R ²
			Slope ($\times 10^{-2}$ g/kW)	Standard Error ($\times 10^{-3}$ g/kW)	95% Confidence Interval ($\times 10^{-2}$ g/kW)	Slope ($\times 10^{-5}$ g ² /kW ²)	Standard Error ($\times 10^{-6}$ g ² /kW ²)	95% Confidence Interval ($\times 10^{-5}$ g ² /kW ²)		
12	1,2,3,4,5,6,7,8,9,10,11,13,14,15	94615	4.89	3.25	[4.26, 5.53]	-1.40	4.27	[-1.60, -1.20]	17.4	0.74
	1,2,3,4,5,6,7,8,9,10,11,12,14,15	94687	5.30	3.38	[4.64, 5.97]	-1.41	4.63	[-1.63, -1.20]	15.2	0.75
	1,2,3,4,5,6,7,8,9,10,11,12,13,15	94381	4.94	3.03	[4.35, 5.54]	-1.33	4.18	[-1.53, -1.14]	17.1	0.78
	1,2,3,4,5,6,7,8,9,10,11,12,13,14	94402	5.67	3.09	[5.06, 6.27]	-1.40	4.14	[-1.59, -1.21]	17.6	0.78

^a LCF ID: Each combination of locomotive, consist, and fuel was assigned a unique ID. The description of each LCF ID is given in the supporting information Table B-4.

Italicized values indicate terms not statistically significantly different than zero.

Table B-10 Continued on Next Page.

Table B-10 Continued from Previous Page.

(b) CO₂ Emission Rate

ID ^a	Trips	Sample Size	Linear Term			Quadratic Term			Intercept (g/s)	Model R ²
			Slope (×10 ⁻¹ g/kW)	Standard Error (×10 ⁻² g/kW)	95% Confidence Interval (×10 ⁻¹ g/kW)	Slope (×10 ⁻⁵ g ² /kW ²)	Standard Error (×10 ⁻⁶ g ² /kW ²)	95% Confidence Interval (×10 ⁻⁵ g ² /kW ²)		
1	2,3,4,5	28590	2.53	0.61	[2.41, 2.65]	-1.28	4.07	[-1.46, -1.09]	32	0.89
	1,3,4,5	28230	2.56	0.65	[2.43, 2.69]	-1.32	4.60	[-1.53, -1.11]	29	0.82
	1,2,4,5	28560	2.63	0.58	[2.52, 2.75]	-1.32	4.69	[-1.53, -1.10]	33	0.84
	1,2,3,5	28976	2.58	0.60	[2.46, 2.70]	-1.21	4.60	[-1.42, -1.0]	34	0.89
	1,2,3,4	28028	2.66	0.58	[2.55, 2.77]	-1.26	4.60	[-1.48, -1.05]	31	0.86
2	2,3,4,5,6	27620	1.59	0.71	[1.45, 1.73]	-0.25	5.37	[-0.50, -0.01]	34	0.74
	1,3,4,5,6	28652	1.88	0.77	[1.72, 2.03]	-0.23	5.80	[-0.49, 0.04]	39	0.71
	1,2,4,5,6	26805	1.70	0.71	[1.57, 1.84]	-0.21	5.59	[-0.46, 0.05]	35	0.75
	1,2,3,5,6	26894	1.72	0.75	[1.58, 1.87]	-0.25	5.75	[-0.51, 0.02]	37	0.72
	1,2,3,4,6	27612	1.91	0.76	[1.76, 2.06]	-0.25	5.32	[-0.50, -0.01]	35	0.75
	1,2,3,4,5	27697	1.89	0.81	[1.73, 2.05]	-0.23	5.48	[-0.49, 0.02]	34	0.73
3	2,3,4,5,6	32999	1.51	0.85	[1.35, 1.68]	0.10	4.32	[-0.10, 0.30]	27	0.84
	1,3,4,5,6	32850	1.74	0.84	[1.58, 1.90]	0.09	4.47	[-0.12, 0.29]	30	0.80
	1,2,4,5,6	32531	1.87	0.91	[1.70, 2.05]	0.10	4.80	[-0.12, 0.32]	27	0.85
	1,2,3,5,6	32473	1.78	0.91	[1.60, 1.96]	0.08	4.28	[-0.11, 0.28]	27	0.79
	1,2,3,4,6	32786	1.59	0.83	[1.43, 1.75]	0.09	5.13	[-0.14, 0.33]	31	0.86
	1,2,3,4,5	32446	1.80	0.92	[1.62, 1.98]	0.09	5.04	[-0.14, 0.32]	25	0.85

Table B-10 (b) Continued on Next Page.

Table B-10 (b) Continued from Previous Page.

ID ^a	Trips	Sample Size	Linear Term			Quadratic Term			Intercept (g/s)	Model R ²
			Slope ($\times 10^{-1}$ g/kW)	Standard Error ($\times 10^{-2}$ g/kW)	95% Confidence Interval ($\times 10^{-1}$ g/kW)	Slope ($\times 10^{-5}$ g ² /kW ²)	Standard Error ($\times 10^{-6}$ g ² /kW ²)	95% Confidence Interval ($\times 10^{-5}$ g ² /kW ²)		
4	2,3,4,5	23906	0.95	0.85	[0.79, 1.12]	0.45	4.20	[0.25, 0.64]	24	0.69
	1,3,4,5	23533	1.07	0.79	[0.92, 1.22]	0.41	4.00	[0.22, 0.59]	25	0.76
	1,2,4,5	23804	1.01	0.83	[0.85, 1.17]	0.42	4.32	[0.22, 0.62]	26	0.78
	1,2,3,5	23599	1.01	0.86	[0.84, 1.18]	0.39	4.08	[0.2, 0.57]	24	0.72
	1,2,3,4	23418	1.01	0.83	[0.85, 1.17]	0.42	3.72	[0.25, 0.59]	28	0.72
5	2,3,4,5,6	28564	1.30	0.61	[1.18, 1.42]	0.01	5.32	[-0.24, 0.25]	46	0.81
	1,3,4,5,6	28362	1.48	0.66	[1.35, 1.61]	0.01	6.29	[-0.28, 0.30]	45	0.85
	1,2,4,5,6	27573	1.37	0.57	[1.26, 1.48]	0.01	5.38	[-0.24, 0.26]	45	0.85
	1,2,3,5,6	29779	1.24	0.63	[1.12, 1.37]	0.01	6.29	[-0.28, 0.30]	42	0.82
	1,2,3,4,6	27159	1.57	0.63	[1.44, 1.69]	0.01	5.95	[-0.26, 0.28]	43	0.86
	1,2,3,4,5	26793	1.32	0.60	[1.20, 1.43]	0.01	5.72	[-0.25, 0.27]	43	0.80
6	1,3	12546	1.41	1.17	[1.18, 1.64]	-0.18	6.46	[-0.48, 0.12]	41	0.82
	1,5	12255	1.57	1.12	[1.35, 1.79]	-0.18	7.17	[-0.51, 0.15]	42	0.85
	3,5	12505	1.55	1.05	[1.34, 1.76]	-0.20	7.03	[-0.52, 0.13]	48	0.81
7	2,4	12999	1.16	0.66	[1.03, 1.29]	0.23	3.51	[0.06, 0.39]	22	0.80
	2,6	12544	1.20	0.68	[1.07, 1.33]	0.22	3.80	[0.05, 0.40]	24	0.75
	4,6	12747	0.98	0.64	[0.86, 1.11]	0.24	3.87	[0.07, 0.42]	22	0.80
8	1,3	21882	2.13	1.39	[1.86, 2.41]	-0.81	7.31	[-1.14, -0.47]	34	0.78
	1,5	23475	2.01	1.28	[1.76, 2.26]	-0.81	7.47	[-1.15, -0.46]	31	0.77
	3,5	27807	2.12	1.44	[1.83, 2.40]	-0.78	8.27	[-1.16, -0.40]	37	0.75

Table B-10 (b) Continued on Next Page.

Table B-10 (b) Continued from Previous Page.

ID ^a	Trips	Sample Size	Linear Term			Quadratic Term			Intercept (g/s)	Model R ²
			Slope ($\times 10^{-1}$ g/kW)	Standard Error ($\times 10^{-2}$ g/kW)	95% Confidence Interval ($\times 10^{-1}$ g/kW)	Slope ($\times 10^{-5}$ g ² /kW ²)	Standard Error ($\times 10^{-6}$ g ² /kW ²)	95% Confidence Interval ($\times 10^{-5}$ g ² /kW ²)		
9	2,4	23717	1.01	1.16	[0.78, 1.24]	0.73	5.56	[0.48, 0.99]	22	0.73
	2,6	22692	0.95	1.08	[0.74, 1.16]	0.67	5.25	[0.43, 0.92]	23	0.76
	4,6	20203	0.88	1.19	[0.65, 1.12]	0.70	4.90	[0.48, 0.93]	24	0.67
10	2,3,4,5	24011	2.19	0.80	[2.04, 2.35]	-0.96	2.77	[-1.09, -0.84]	38	0.86
	1,3,4,5	24273	2.50	0.83	[2.33, 2.66]	-1.17	3.08	[-1.31, -1.02]	34	0.82
	1,2,4,5	24030	2.11	0.76	[1.96, 2.26]	-1.12	3.08	[-1.27, -0.98]	38	0.82
	1,2,3,5	22588	2.34	0.86	[2.18, 2.51]	-1.07	3.11	[-1.21, -0.93]	32	0.85
	1,2,3,4	22942	2.28	0.83	[2.12, 2.44]	-0.96	2.75	[-1.09, -0.84]	33	0.83
11	2,3,4,5,6	32665	1.78	0.85	[1.62, 1.95]	-1.10	3.08	[-1.24, -0.96]	42	0.89
	1,3,4,5,6	32228	1.69	0.77	[1.54, 1.84]	-1.06	2.58	[-1.18, -0.94]	36	0.90
	1,2,4,5,6	30991	1.84	0.79	[1.68, 1.99]	-1.12	2.89	[-1.26, -0.99]	43	0.88
	1,2,3,5,6	31683	1.64	0.88	[1.47, 1.81]	-1.00	2.66	[-1.13, -0.88]	34	0.86
	1,2,3,4,6	31458	1.53	0.82	[1.37, 1.69]	-1.01	3.08	[-1.16, -0.87]	34	0.80
	1,2,3,4,5	32035	1.87	0.91	[1.69, 2.05]	-1.13	3.08	[-1.28, -0.99]	43	0.86

Table B-10 (b) Continued on Next Page.

Table B-10 (b) Continued from Previous Page.

ID ^a	Trips	Sample Size	Linear Term			Quadratic Term			Intercept (g/s)	Model R ²
			Slope ($\times 10^{-1}$ g/kW)	Standard Error ($\times 10^{-2}$ g/kW)	95% Confidence Interval ($\times 10^{-1}$ g/kW)	Slope ($\times 10^{-5}$ g ² /kW ²)	Standard Error ($\times 10^{-6}$ g ² /kW ²)	95% Confidence Interval ($\times 10^{-5}$ g ² /kW ²)		
12	2,3,4,5,6,7,8,9,10,11,12,13,14,15	97803	1.50	0.53	[1.40, 1.61]	-1.39	4.05	[-1.57, -1.20]	27	0.77
	1,3,4,5,6,7,8,9,10,11,12,13,14,15	95034	1.59	0.51	[1.49, 1.69]	-1.47	4.41	[-1.67, -1.27]	27	0.78
	1,2,4,5,6,7,8,9,10,11,12,13,14,15	94499	1.53	0.49	[1.44, 1.63]	-1.25	4.23	[-1.45, -1.06]	27	0.77
	1,2,3,5,6,7,8,9,10,11,12,13,14,15	94547	1.46	0.51	[1.36, 1.56]	-1.37	4.09	[-1.56, -1.19]	27	0.73
	1,2,3,4,6,7,8,9,10,11,12,13,14,15	94974	1.67	0.55	[1.56, 1.77]	-1.29	4.05	[-1.48, -1.11]	28	0.77
	1,2,3,4,6,7,8,9,10,11,12,13,14,15	94085	1.65	0.52	[1.55, 1.75]	-1.46	4.63	[-1.67, -1.24]	28	0.75
	1,2,3,4,5,6,8,9,10,11,12,13,14,15	94171	1.65	0.48	[1.56, 1.74]	-1.36	4.72	[-1.58, -1.14]	27	0.78
	1,2,3,4,5,6,7,9,10,11,12,13,14,15	94073	1.57	0.50	[1.47, 1.66]	-1.33	4.76	[-1.55, -1.11]	24	0.74
	1,2,3,4,5,6,7,8,10,11,12,13,14,15	94653	1.42	0.51	[1.32, 1.52]	-1.26	4.18	[-1.46, -1.07]	24	0.75
	1,2,3,4,5,6,7,8,9,11,12,13,14,15	94258	1.57	0.50	[1.47, 1.66]	-1.44	4.27	[-1.64, -1.25]	25	0.81
1,2,3,4,5,6,7,8,9,10,12,13,14,15	94678	1.42	0.51	[1.32, 1.52]	-1.32	4.90	[-1.54, -1.09]	27	0.81	

Table B-10 (b) Continued on Next Page.

Table B-10 (b) Continued from Previous Page.

ID ^a	Trips	Sample Size	Linear Term			Quadratic Term			Intercept (g/s)	Model R ²
			Slope ($\times 10^{-1}$ g/kW)	Standard Error ($\times 10^{-2}$ g/kW)	95% Confidence Interval ($\times 10^{-1}$ g/kW)	Slope ($\times 10^{-5}$ g ² /kW ²)	Standard Error ($\times 10^{-6}$ g ² /kW ²)	95% Confidence Interval ($\times 10^{-5}$ g ² /kW ²)		
12	1,2,3,4,5,6,7,8,9,10,11,13,14,15	94615	1.65	0.54	[1.54, 1.75]	-1.44	4.18	[-1.63, -1.25]	26	0.76
	1,2,3,4,5,6,7,8,9,10,11,12,14,15	94687	1.46	0.53	[1.35, 1.56]	-1.44	4.18	[-1.63, -1.25]	29	0.80
	1,2,3,4,5,6,7,8,9,10,11,12,13,15	94381	1.58	0.52	[1.48, 1.68]	-1.36	4.14	[-1.55, -1.17]	26	0.75
	1,2,3,4,5,6,7,8,9,10,11,12,13,14	94402	1.38	0.48	[1.28, 1.47]	-1.48	4.27	[-1.68, -1.29]	25	0.76

^a LCF ID: Each combination of locomotive, consist, and fuel was assigned a unique ID. The description of each LCF ID is given in the supporting information Table B-4.

Italicized values indicate terms not statistically significantly different than zero.

Table B-10 Continued on Next Page.

Table B-10 Continued from Previous Page.

(c) NO_x Emission Rate

ID ^a	Trips	Sample Size	Linear Term			Quadratic Term			Intercept (g/s)	Model R ²
			Slope (×10 ⁻³ g/kW)	Standard Error (×10 ⁻⁴ g/kW)	95% Confidence Interval (×10 ⁻³ g/kW)	Slope (×10 ⁻⁶ g ² /kW ²)	Standard Error (×10 ⁻⁸ g ² /kW ²)	95% Confidence Interval (×10 ⁻⁶ g ² /kW ²)		
1	2,3,4,5	_b	_b	_b	_b	_b	_b	_b	_b	_b
	1,3,4,5	_b	_b	_b	_b	_b	_b	_b	_b	_b
	1,2,4,5	_b	_b	_b	_b	_b	_b	_b	_b	_b
	1,2,3,5	_b	_b	_b	_b	_b	_b	_b	_b	_b
	1,2,3,4	_b	_b	_b	_b	_b	_b	_b	_b	_b
2	2,3,4,5,6	27620	2.53	0.13	[2.50, 2.56]	-0.46	2.49	[-0.47, -0.45]	0.65	0.75
	1,3,4,5,6	28652	2.70	0.13	[2.67, 2.72]	-0.39	2.34	[-0.41, -0.38]	0.64	0.77
	1,2,4,5,6	26805	2.83	0.12	[2.81, 2.86]	-0.39	2.42	[-0.40, -0.38]	0.58	0.76
	1,2,3,5,6	26894	2.92	0.11	[2.89, 2.94]	-0.40	2.70	[-0.42, -0.39]	0.61	0.79
	1,2,3,4,6	27612	3.03	0.11	[3.00, 3.05]	-0.42	2.55	[-0.43, -0.41]	0.56	0.75
	1,2,3,4,5	27697	2.64	0.13	[2.61, 2.67]	-0.44	2.39	[-0.45, -0.43]	0.63	0.79
3	2,3,4,5,6	32999	4.15	0.13	[4.13, 4.18]	-0.47	1.96	[-0.48, -0.46]	0.64	0.85
	1,3,4,5,6	32850	3.73	0.12	[3.71, 3.76]	-0.47	2.05	[-0.48, -0.46]	0.63	0.83
	1,2,4,5,6	32531	3.66	0.13	[3.63, 3.68]	-0.47	2.07	[-0.48, -0.46]	0.60	0.82
	1,2,3,5,6	32473	3.43	0.14	[3.40, 3.46]	-0.46	2.40	[-0.47, -0.44]	0.56	0.82
	1,2,3,4,6	32786	4.11	0.14	[4.09, 4.14]	-0.46	1.98	[-0.46, -0.45]	0.57	0.85
	1,2,3,4,5	32446	3.47	0.13	[3.44, 3.49]	-0.48	2.05	[-0.49, -0.47]	0.55	0.85

Table B-10 (c) Continued on Next Page.

Table B-10 (c) Continued from Previous Page.

ID ^a	Trips	Sample Size	Linear Term			Quadratic Term			Intercept (g/s)	Model R ²
			Slope ($\times 10^{-3}$ g/kW)	Standard Error ($\times 10^{-4}$ g/kW)	95% Confidence Interval ($\times 10^{-3}$ g/kW)	Slope ($\times 10^{-6}$ g ² /kW ²)	Standard Error ($\times 10^{-8}$ g ² /kW ²)	95% Confidence Interval ($\times 10^{-6}$ g ² /kW ²)		
4	2,3,4,5	23906	2.75	0.13	[2.73, 2.78]	-0.33	3.06	[-0.35, -0.32]	0.57	0.72
	1,3,4,5	23533	2.78	0.15	[2.75, 2.81]	-0.34	3.52	[-0.35, -0.32]	0.54	0.72
	1,2,4,5	23804	2.75	0.14	[2.73, 2.78]	-0.34	2.96	[-0.36, -0.33]	0.54	0.72
	1,2,3,5	23599	2.81	0.14	[2.78, 2.84]	-0.35	2.96	[-0.37, -0.34]	0.62	0.70
	1,2,3,4	23418	2.70	0.14	[2.67, 2.73]	-0.32	3.19	[-0.33, -0.30]	0.54	0.73
5	2,3,4,5,6	28564	3.13	0.12	[3.10, 3.15]	-0.59	1.44	[-0.60, -0.58]	1.12	0.81
	1,3,4,5,6	28362	3.22	0.13	[3.20, 3.25]	-0.61	1.47	[-0.61, -0.60]	1.09	0.83
	1,2,4,5,6	27573	3.29	0.12	[3.26, 3.31]	-0.54	1.44	[-0.55, -0.53]	1.08	0.84
	1,2,3,5,6	29779	3.35	0.13	[3.32, 3.38]	-0.56	1.59	[-0.56, -0.55]	1.04	0.83
	1,2,3,4,6	27159	3.35	0.13	[3.32, 3.37]	-0.50	1.53	[-0.51, -0.49]	1.11	0.81
	1,2,3,4,5	26793	3.03	0.13	[3.01, 3.06]	-0.57	1.61	[-0.58, -0.56]	0.99	0.83
6	1,3	12546	5.52	0.26	[5.47, 5.57]	-0.62	7.62	[-0.65, -0.58]	1.53	0.83
	1,5	12255	4.79	0.26	[4.74, 4.84]	-0.53	7.84	[-0.57, -0.49]	1.29	0.80
	3,5	12505	4.85	0.24	[4.80, 4.89]	-0.55	7.41	[-0.59, -0.52]	1.50	0.81
7	2,4	12999	4.13	0.26	[4.08, 4.18]	-0.46	6.71	[-0.49, -0.43]	0.66	0.81
	2,6	12544	4.63	0.27	[4.58, 4.68]	-0.42	6.91	[-0.45, -0.39]	0.71	0.77
	4,6	12747	4.18	0.27	[4.12, 4.23]	-0.44	6.58	[-0.47, -0.41]	0.75	0.81
8	1,3	21882	4.94	0.19	[4.90, 4.98]	-0.94	3.47	[-0.96, -0.93]	0.94	0.83
	1,5	23475	5.44	0.20	[5.40, 5.48]	-0.95	3.33	[-0.97, -0.94]	0.88	0.83
	3,5	27807	5.24	0.20	[5.20, 5.28]	-0.81	3.94	[-0.83, -0.79]	0.95	0.79

Table B-10 (c) Continued on Next Page.

Table B-10 (c) Continued from Previous Page.

ID ^a	Trips	Sample Size	Linear Term			Quadratic Term			Intercept (g/s)	Model R ²
			Slope ($\times 10^{-3}$ g/kW)	Standard Error ($\times 10^{-4}$ g/kW)	95% Confidence Interval ($\times 10^{-3}$ g/kW)	Slope ($\times 10^{-6}$ g ² /kW ²)	Standard Error ($\times 10^{-8}$ g ² /kW ²)	95% Confidence Interval ($\times 10^{-6}$ g ² /kW ²)		
9	2,4	23717	4.09	0.17	[4.05, 4.12]	-0.45	5.95	[-0.48, -0.42]	0.55	0.72
	2,6	22692	4.01	0.19	[3.97, 4.05]	-0.45	5.38	[-0.48, -0.43]	0.61	0.76
	4,6	20203	3.51	0.19	[3.48, 3.55]	-0.49	6.01	[-0.52, -0.46]	0.63	0.75
10	2,3,4,5	<i>_b</i>	<i>_b</i>	<i>_b</i>	<i>_b</i>	<i>_b</i>	<i>_b</i>	<i>_b</i>	<i>_b</i>	<i>_b</i>
	1,3,4,5	<i>_b</i>	<i>_b</i>	<i>_b</i>	<i>_b</i>	<i>_b</i>	<i>_b</i>	<i>_b</i>	<i>_b</i>	<i>_b</i>
	1,2,4,5	<i>_b</i>	<i>_b</i>	<i>_b</i>	<i>_b</i>	<i>_b</i>	<i>_b</i>	<i>_b</i>	<i>_b</i>	<i>_b</i>
	1,2,3,5	<i>_b</i>	<i>_b</i>	<i>_b</i>	<i>_b</i>	<i>_b</i>	<i>_b</i>	<i>_b</i>	<i>_b</i>	<i>_b</i>
	1,2,3,4	<i>_b</i>	<i>_b</i>	<i>_b</i>	<i>_b</i>	<i>_b</i>	<i>_b</i>	<i>_b</i>	<i>_b</i>	<i>_b</i>
11	2,3,4,5,6	32665	3.68	0.10	[3.66, 3.70]	-0.41	2.94	[-0.42, -0.40]	0.59	0.81
	1,3,4,5,6	32228	3.40	0.12	[3.38, 3.42]	-0.47	3.27	[-0.49, -0.46]	0.50	0.77
	1,2,4,5,6	30991	3.71	0.11	[3.69, 3.73]	-0.42	3.20	[-0.44, -0.41]	0.50	0.81
	1,2,3,5,6	31683	3.82	0.10	[3.80, 3.84]	-0.41	3.14	[-0.42, -0.40]	0.61	0.77
	1,2,3,4,6	31458	3.82	0.11	[3.80, 3.84]	-0.44	3.20	[-0.45, -0.42]	0.56	0.78
	1,2,3,4,5	32035	3.12	0.12	[3.10, 3.15]	-0.41	3.36	[-0.43, -0.40]	0.59	0.81

Table B-10 (c) Continued on Next Page.

Table B-10 (c) Continued from Previous Page.

ID ^a	Trips	Sample Size	Linear Term			Quadratic Term			Intercept (g/s)	Model R ²
			Slope ($\times 10^{-3}$ g/kW)	Standard Error ($\times 10^{-4}$ g/kW)	95% Confidence Interval ($\times 10^{-3}$ g/kW)	Slope ($\times 10^{-6}$ g ² /kW ²)	Standard Error ($\times 10^{-8}$ g ² /kW ²)	95% Confidence Interval ($\times 10^{-6}$ g ² /kW ²)		
12	2,3,4,5,6,7,8,9,10,11,12,13,14,15	97803	3.88	0.26	[3.83, 3.93]	-0.37	2.13	[-0.38, -0.36]	0.58	0.73
	1,3,4,5,6,7,8,9,10,11,12,13,14,15	95034	3.65	0.22	[3.60, 3.69]	-0.36	2.49	[-0.37, -0.35]	0.55	0.72
	1,2,4,5,6,7,8,9,10,11,12,13,14,15	94499	3.96	0.25	[3.91, 4.01]	-0.37	2.51	[-0.39, -0.36]	0.58	0.73
	1,2,3,5,6,7,8,9,10,11,12,13,14,15	94547	3.49	0.25	[3.44, 3.54]	-0.34	2.53	[-0.35, -0.33]	0.61	0.72
	1,2,3,4,6,7,8,9,10,11,12,13,14,15	94974	3.96	0.23	[3.91, 4.00]	-0.35	2.53	[-0.36, -0.34]	0.64	0.70
	1,2,3,4,6,7,8,9,10,11,12,13,14,15	94085	3.57	0.25	[3.52, 3.62]	-0.40	2.30	[-0.41, -0.39]	0.62	0.70
	1,2,3,4,5,6,8,9,10,11,12,13,14,15	94171	4.04	0.25	[3.99, 4.08]	-0.33	2.18	[-0.34, -0.32]	0.54	0.72
	1,2,3,4,5,6,7,9,10,11,12,13,14,15	94073	3.57	0.21	[3.53, 3.61]	-0.39	2.51	[-0.40, -0.38]	0.57	0.69
	1,2,3,4,5,6,7,8,10,11,12,13,14,15	94653	3.80	0.22	[3.76, 3.85]	-0.33	2.32	[-0.34, -0.32]	0.54	0.72
	1,2,3,4,5,6,7,8,9,11,12,13,14,15	94258	3.65	0.24	[3.60, 3.69]	-0.37	2.51	[-0.38, -0.36]	0.64	0.72
1,2,3,4,5,6,7,8,9,10,12,13,14,15	94678	3.76	0.21	[3.72, 3.80]	-0.35	2.49	[-0.36, -0.34]	0.63	0.72	

Table B-10 (c) Continued on Next Page.
 Table B-10 (c) Continued from Previous Page.

ID ^a	Trips	Sample Size	Linear Term			Quadratic Term			Intercept (g/s)	Model R ²
			Slope ($\times 10^{-3}$ g/kW)	Standard Error ($\times 10^{-4}$ g/kW)	95% Confidence Interval ($\times 10^{-3}$ g/kW)	Slope ($\times 10^{-6}$ g ² /kW ²)	Standard Error ($\times 10^{-8}$ g ² /kW ²)	95% Confidence Interval ($\times 10^{-6}$ g ² /kW ²)		
12	1,2,3,4,5,6,7,8,9,10,11,13,14,15	94615	4.04	0.24	[3.99, 4.08]	-0.34	2.18	[-0.35, -0.33]	0.54	0.69
	1,2,3,4,5,6,7,8,9,10,11,12,14,15	94687	3.53	0.25	[3.48, 3.58]	-0.38	2.20	[-0.39, -0.37]	0.57	0.70
	1,2,3,4,5,6,7,8,9,10,11,12,13,15	94381	3.61	0.23	[3.56, 3.65]	-0.38	2.18	[-0.39, -0.37]	0.62	0.69
	1,2,3,4,5,6,7,8,9,10,11,12,13,14	94402	3.57	0.24	[3.52, 3.62]	-0.36	2.49	[-0.37, -0.35]	0.64	0.70

^a LCF ID: Each combination of locomotive, consist, and fuel was assigned a unique ID. The description of each LCF ID is given in the supporting information Table B-4.

Italicized values indicate terms not statistically significantly different than zero.

^b NO_x emission rates for LCF IDs 1 and 10 were modeled based on a 10-mode modal model because they were not modeled properly by the regression model.

The final SM3 model for fuel use rate and emission rates of CO₂ and NO_x calibrated based on all one-way trips is given in Table B-11. The standard error in linear and quadratic slope was typically less than 4% relative to the slope and had narrow confidence intervals, indicating that these parameters were precisely estimated. The model R² with the quadratic term included for each LCF ID and species was 0.74 or higher, indicating high model precision. For each LCF ID, model R² was higher for the model with linear and quadratic terms than for the model with the linear term only. The increase in model R² was small relative to the model R² without the quadratic term. Thus, the models were approximately linear. The addition of the quadratic term reduced the difference from sub-model 4 inferred rates at 2519 kW versus the linear model. Therefore, a model with both linear and quadratic terms is more suitable for the data. For each regression model, residuals were uniformly distributed around mean 0 and were normally distributed. The variance was also uniformly distributed along a horizontal line.

For the modal model part of sub-model 3, the cutoffs for each model are given in Table B-12. The number of seconds of data in each mode is given in Table B-13. The average number of seconds of data for all LCF IDs combined in each mode was between 2646 and 2771. Thus, each mode comprised of approximately similar amounts of data.

The estimated sub-model 3 parameters for the modal model for CO, HC, and PM emission rates for all LCF IDs and NO_x emission rates for LCF IDs 1 and 10 are given in Table B-14. For modal average CO emission rates for all LCF IDs, modal average rates for a given mode were compared with the modal rate of the preceding adjacent mode to evaluate the monotonic increase in rates with modes. For 12 LCF IDs and 10 modes, the total possible adjacent paired comparisons were 108. Out of 108 pairs, 89 pairs had higher rates for the higher adjacent mode. Thus, in general, CO emission rates increased monotonically with mode. For modes 1 through 5, only 30 pairs out of 48 had higher rates than the preceding mode. CO emission rates in these modes were typically based on CO concentrations below the detection limit of the Axion PEMS and are, thus, noisy. For modes 6 through 10, 59 pairs out of 60 had higher rates than the preceding mode. Thus, for CO concentrations above the detection limit, CO emission rates increased monotonically with mode. On average over all LCF IDs, CO emission rates increased monotonically with mode from 0.10 g/s to 2.70 g/s. CO emission rates were typically good indicated by model R² of 0.44 or higher.

For modal average HC emission rates, 70 pairs of adjacent modes out of 108 had higher rates for the next higher mode. HC emission rates were typically based on HC concentrations below the detection limit of the Axion PEMS. For modes 1 through 5, 41 pairs out of 48 had higher rates than the preceding mode. Thus, the HC emission rates are typically monotonic for modes 1 through 5. For modes 6 through 10, only 29 out of 60 pairs had higher rates than the preceding mode. For modes 6 through 10, 45 out of 60 pairs had HC emission rates within 10% of each other. Therefore, for modes 6 through 10, HC emission rates were approximately constant in most cases. On average over all LCF IDs, HC emission rates increased monotonically with mode from 0.07 g/s to 1.44 g/s for modes 1 through 5. For modes 6 through 10, HC emission rates were approximately constant at 0.48 g/s. HC emission rates had low model precision because most rates were low and noisy.

Table B-11. Calibrated Sub-Model 3 Regression Parameters for Fuel Use Rate based on All One-Way Trips (Final Sub-Model 3) for Measured Combinations of Locomotives, Consists, and Fuels: (a) Fuel Use Rate; (b) CO₂ Emission Rate; and (c) NO_x Emission Rate.

(a) Fuel Use Rate

LCF ID ^a	Sample Size	Linear Term			Quadratic Term			Intercept (g/s)	Model R ² without Quadratic Term	Model R ² with Quadratic Term
		Slope ($\times 10^{-2}$ g/kW)	Standard Error ($\times 10^{-3}$ g/kW)	95% Confidence Interval ($\times 10^{-2}$ g/kW)	Slope ($\times 10^{-5}$ g ² /kW ²)	Standard Error ($\times 10^{-6}$ g ² /kW ²)	95% Confidence Interval ($\times 10^{-5}$ g ² /kW ²)			
1	35619	8.54	2.19	[8.10, 8.98]	-1.33	4.38	[-1.42, -1.24]	10.1	0.86	0.89
2	32945	5.51	2.84	[4.94, 6.08]	-0.23	5.32	[-0.34, -0.12]	11.5	0.73	0.76
3	39041	5.22	2.80	[4.66, 5.78]	<i>0.09</i>	<i>4.75</i>	<i>[-0.01, 0.19]</i>	8.6	0.81	0.84
4	29491	3.35	2.57	[2.84, 3.86]	0.43	4.04	[0.35, 0.51]	8.3	0.72	0.74
5	33567	4.30	2.30	[3.84, 4.76]	<i>0.01</i>	<i>5.72</i>	<i>[-0.10, 0.12]</i>	14.3	0.80	0.82
6	18599	4.77	3.57	[4.06, 5.48]	-0.20	7.10	[-0.34, -0.06]	13.5	0.80	0.82
7	19112	3.32	2.24	[2.87, 3.77]	0.23	3.69	[0.16, 0.30]	6.8	0.78	0.79
8	18652	6.33	4.18	[5.49, 7.17]	-0.74	7.95	[-0.90, -0.58]	10.3	0.78	0.81
9	16867	2.88	2.68	[2.35, 3.42]	0.71	5.05	[0.61, 0.81]	7.0	0.74	0.76
10	29461	7.64	5.25	[7.53, 7.74]	-1.06	2.83	[-1.11, -1.00]	10.6	0.83	0.85
11	38212	5.68	5.18	[5.58, 5.78]	-1.09	2.83	[-1.14, -1.03]	14.7	0.86	0.88
12	162304	5.15	3.22	[5.07, 5.24]	-1.36	4.45	[-1.47, -1.25]	16.3	0.76	0.79

^a LCF ID: Each combination of locomotive, consist, and fuel was assigned a unique ID. The description of each LCF ID is given in the supporting information Table B-4.

Italicized values indicate terms not statistically significantly different than zero.

Table B-11 Continued on Next Page.

Table B-11 Continued from Previous Page.

(b) CO₂ Emission Rate

LCF ID ^a	Sample Size	Linear Term			Quadratic Term			Intercept (g/s)	Model R ² without Quadratic Term	Model R ² with Quadratic Term
		Slope ($\times 10^{-1}$ g/kW)	Standard Error ($\times 10^{-2}$ g/kW)	95% Confidence Interval ($\times 10^{-1}$ g/kW)	Slope ($\times 10^{-5}$ g ² /kW ²)	Standard Error ($\times 10^{-6}$ g ² /kW ²)	95% Confidence Interval ($\times 10^{-5}$ g ² /kW ²)			
1	35619	2.71	0.64	[2.58, 2.84]	-4.20	1.85	[-4.57, -3.83]	31	0.87	0.89
2	32945	1.74	0.74	[1.59, 1.89]	-0.72	1.32	[-0.98, -0.46]	35	0.73	0.76
3	39041	1.67	0.88	[1.49, 1.85]	0.27	1.23	[0.02, 0.52]	27	0.83	0.84
4	29491	1.07	0.81	[0.91, 1.23]	1.34	1.83	[0.97, 1.71]	26	0.73	0.74
5	33567	1.37	0.61	[1.25, 1.49]	<i>0.01</i>	<i>1.14</i>	<i>[-0.22, 0.24]</i>	45	0.81	0.82
6	18599	1.52	1.11	[1.30, 1.74]	-0.66	1.88	[-1.04, -0.28]	43	0.80	0.82
7	19112	1.06	0.67	[0.93, 1.19]	0.72	1.48	[0.42, 1.02]	22	0.78	0.80
8	18652	2.01	1.31	[1.75, 2.27]	-2.41	2.55	[-2.92, -1.90]	32	0.78	0.81
9	16867	0.93	1.12	[0.71, 1.15]	2.15	2.01	[1.75, 2.55]	22	0.72	0.76
10	29461	2.37	0.81	[2.21, 2.53]	-0.33	2.38	<i>[-0.80, 0.14]</i>	34	0.83	0.86
11	38212	1.67	0.84	[1.51, 1.84]	-0.33	2.48	<i>[-0.82, 0.16]</i>	38	0.85	0.88
12	162304	1.53	0.52	[1.43, 1.63]	<i>-0.41</i>	3.82	<i>[-1.16, 0.34]</i>	27	0.77	0.80

^a LCF ID: Each combination of locomotive, consist, and fuel was assigned a unique ID. The description of each LCF ID is given in the supporting information Table B-4.

Italicized values indicate terms not statistically significantly different than zero.

Table B-11 Continued on Next Page.

Table B-11 Continued from Previous Page.

(c) NO_x Emission Rate

LCF ID ^a	Sample Size	Linear Term			Quadratic Term			Intercept (g/s)	Model R ² without Quadratic Term	Model R ² with Quadratic Term
		Slope (×10 ⁻³ g/kW)	Standard Error (×10 ⁻⁴ g/kW)	95% Confidence Interval (×10 ⁻³ g/kW)	Slope (×10 ⁻⁶ g ² /kW ²)	Standard Error (×10 ⁻⁸ g ² /kW ²)	95% Confidence Interval (×10 ⁻⁶ g ² /kW ²)			
1	<i>_b</i>	<i>_b</i>	<i>_b</i>	<i>_b</i>	<i>_b</i>	<i>_b</i>	<i>_b</i>	<i>_b</i>	<i>_b</i>	<i>_b</i>
2	32945	2.75	0.12	[2.73, 2.77]	-0.42	2.52	[-0.47, -0.37]	0.62	0.77	0.80
3	39041	3.81	0.13	[3.78, 3.84]	-0.49	2.18	[-0.53, -0.45]	0.59	0.83	0.84
4	29491	2.84	0.14	[2.81, 2.87]	-0.32	3.29	[-0.39, -0.25]	0.57	0.71	0.74
5	33567	3.16	0.12	[3.14, 3.18]	-0.55	1.56	[-0.58, -0.52]	1.02	0.84	0.85
6	18599	5.21	0.25	[5.16, 5.26]	-0.59	7.19	[-0.73, -0.45]	1.40	0.82	0.82
7	19112	4.54	0.25	[4.49, 4.59]	-0.44	6.58	[-0.57, -0.31]	0.70	0.79	0.79
8	18652	5.04	0.2	[5.00, 5.08]	-0.88	3.58	[-0.95, -0.81]	0.86	0.81	0.84
9	16867	3.82	0.19	[3.78, 3.86]	-0.46	5.78	[-0.58, -0.34]	0.59	0.74	0.77
10	<i>_b</i>	<i>_b</i>	<i>_b</i>	<i>_b</i>	<i>_b</i>	<i>_b</i>	<i>_b</i>	<i>_b</i>	<i>_b</i>	<i>_b</i>
11	38212	3.47	0.11	[3.45, 3.49]	-0.45	3.233	[-0.46, -0.44]	0.55	0.79	0.81
12	112564	3.88	0.23	[3.83, 3.93]	-0.37	2.346	[-0.38, -0.36]	0.59	0.71	0.75

^a LCF ID: Each combination of locomotive, consist, and fuel was assigned a unique ID. The description of each LCF ID is given in the supporting information Table B-4.

^b NO_x emission rates for LCF IDs 1 and 10 were modeled based on a 10-mode modal model because they were not modeled properly by the regression model.

Italicized values indicate terms not statistically significantly different than zero.

Table B-12. Sub-Model 3 Modal Model Locomotive Power Demand Ranges for CO, HC, and PM Emission Rates for All LCF IDs and NO_x Emission Rates for LCF IDs 1 and 10.

Sub-Model 3 Mode	12-Second Backwards Moving Average Locomotive Power Demand ($\overline{LPD}_{12,t}$, kW)	Average Data in Each Mode (s) ^a
1	$0 < \overline{LPD}_{12,t} \leq 164$	2710
2	$164 < \overline{LPD}_{12,t} \leq 354$	2710
3	$354 < \overline{LPD}_{12,t} \leq 568$	2712
4	$568 < \overline{LPD}_{12,t} \leq 794$	2708
5	$794 < \overline{LPD}_{12,t} \leq 1038$	2710
6	$1038 < \overline{LPD}_{12,t} \leq 1298$	2710
7	$1298 < \overline{LPD}_{12,t} \leq 1580$	2710
8	$1580 < \overline{LPD}_{12,t} \leq 1885$	2710
9	$1885 < \overline{LPD}_{12,t} \leq 2190$	2710
10	$2190 < \overline{LPD}_{12,t} < 2519$	2710

^a Average number of seconds of data in each mode based on data from all LCF IDs.

Table B-13. Number of Seconds of Data in Each Mode for the Modal Model part of Sub-Model 3 for Emission Rates for CO, HC, and PM based on All LCF IDs and NO_x Emission Rate for LCF ID 1 and 10.

LCF ID	Number of Seconds of Data in Each Mode (s)									
	1	2	3	4	5	6	7	8	9	10
1	2850	3023	3197	3537	3434	3872	4570	4723	3844	2569
2	3364	3642	3421	3356	3111	3152	3015	2926	3236	3722
3	4116	3900	3821	3599	3689	3487	3594	3980	4430	4425
4	3169	3331	3148	3119	3161	3258	2944	2371	2194	2796
5 ^a	2717	3016	3109	3328	3277	3276	3177	3428	4203	4036
6	1326	1376	1387	1641	1973	1865	1949	2244	2306	2532
7	2595	2427	2445	2227	2211	2063	1659	1403	1070	1012
8	1939	1379	1660	1715	1747	1792	1883	2056	2032	2449
9	2313	2295	2221	1847	1787	1624	1598	1258	1074	849
10	2181	3034	2356	2119	2503	2957	2104	3048	2704	3303
11	2942	2379	2881	3155	2121	2987	3178	2281	2914	2056
12	3127	3311	3006	3058	2739	2906	2405	3222	3242	3201
Average	2720	2759	2721	2725	2646	2770	2673	2745	2771	2746

^a For PM, no valid data in any mode.

Table B-14. Sub-Model 3 Inferred Modal Average Emission Rates for CO, HC, and PM based on All LCF IDs and NO_x Emission Rate for LCF IDs 1 and 10.

(a) CO Emission Rates

LCF ID	Modal Average Rates for Sub-Model-3 Mode (g/s)										Model R ²
	1	2	3	4	5	6	7	8	9	10	
1	0.13	0.15	0.17	0.20	0.24	0.32	0.47	0.59	0.66	0.69	0.66
2	0.16	0.45	0.23	0.32	0.41	0.56	0.72	0.93	1.11	1.34	0.45
3	0.02	0.67	0.03	0.04	0.05	0.08	0.13	0.30	0.41	0.50	0.67
4	0.01	0.71	0.02	0.02	0.02	0.04	0.06	0.13	0.30	0.52	0.71
5	0.01	0.56	0.03	0.04	0.05	0.08	0.12	0.20	0.28	0.33	0.56
6	0.06	0.62	0.10	0.11	0.11	0.16	0.26	0.44	0.63	0.76	0.62
7	0.01	0.59	0.03	0.05	0.05	0.09	0.13	0.18	0.26	0.60	0.59
8	0.06	0.44	0.15	0.28	0.33	0.64	0.95	1.34	1.66	1.97	0.44
9	0.01	0.54	0.03	0.06	0.08	0.13	0.36	0.90	1.97	2.70	0.54
10	0.03	0.12	0.03	0.03	0.04	0.04	0.06	0.10	0.15	0.17	0.68
11	0.08	0.33	0.21	0.27	0.42	0.74	1.20	1.41	1.60	1.88	0.48
12	0.30	0.67	0.20	0.19	0.17	0.19	0.17	0.36	0.54	0.61	0.61

(b) HC Emission Rates

LCF ID	Modal Average Rates for Sub-Model-3 Mode (g/s)										Model R ²
	1	2	3	4	5	6	7	8	9	10	
1	0.91	0.99	1.08	1.22	1.26	1.13	0.97	0.85	0.83	0.81	0.22
2	0.88	0.92	1.01	1.18	1.32	1.37	1.33	1.36	1.25	1.21	0.15
3	0.13	0.15	0.17	0.18	0.17	0.18	0.19	0.20	0.19	0.18	0.16
4	0.07	0.07	0.09	0.10	0.11	0.11	0.11	0.14	0.13	0.15	0.26
5	0.09	0.10	0.11	0.11	0.12	0.13	0.13	0.13	0.12	0.12	0.23
6	0.13	0.16	0.17	0.18	0.19	0.21	0.22	0.20	0.19	0.17	0.13
7	0.08	0.09	0.09	0.11	0.13	0.14	0.15	0.15	0.16	0.17	0.14
8	0.18	0.44	0.45	0.54	0.58	0.71	0.76	0.89	1.07	1.05	0.24
9	0.11	0.17	0.16	0.20	0.23	0.26	0.31	0.34	0.40	0.55	0.24
10	0.87	0.89	0.98	1.10	1.34	1.18	0.93	0.77	0.82	0.75	0.22
11	0.79	0.95	0.94	1.22	1.44	1.30	1.26	1.40	1.25	1.31	0.14
12	0.12	0.14	0.16	0.20	0.19	0.19	0.18	0.21	0.18	0.20	0.16

Table B-14 Continued on Next Page

Table B-14 Continued from Previous Page

(c) PM Emission Rates

LCF ID	Modal Average Rates for Sub-Model-3 Mode (g/s)										Model R ²
	1	2	3	4	5	6	7	8	9	10	
1	0.004	0.01	0.01	0.02	0.03	0.05	0.08	0.11	0.13	0.14	0.67
2	0.05	0.07	0.10	0.14	0.17	0.20	0.22	0.25	0.27	0.30	0.63
3	0.03	0.05	0.07	0.08	0.10	0.13	0.15	0.20	0.23	0.24	0.57
4	0.03	0.04	0.05	0.07	0.08	0.09	0.10	0.12	0.16	0.20	0.54
5	- ^a	- ^a	- ^a	- ^a	- ^a	- ^a	- ^a	- ^a	- ^a	- ^a	- ^a
6	0.01	0.03	0.04	0.05	0.06	0.07	0.08	0.09	0.11	0.11	0.57
7	0.005	0.01	0.02	0.03	0.04	0.05	0.07	0.07	0.08	0.10	0.65
8	0.09	0.12	0.14	0.16	0.18	0.22	0.24	0.27	0.28	0.29	0.54
9	0.09	0.10	0.12	0.15	0.18	0.20	0.24	0.28	0.30	0.32	0.59
10	0.004	0.01	0.01	0.02	0.03	0.05	0.08	0.11	0.13	0.15	0.68
11	0.05	0.07	0.11	0.15	0.16	0.19	0.21	0.24	0.27	0.29	0.60
12	0.03	0.05	0.07	0.08	0.10	0.13	0.15	0.21	0.23	0.24	0.55

^a Invalid PM data.

(d) NO_x Emission Rates for LCF IDs 1 and 10

LCF ID	Modal Average Rates for Sub-Model-3 Mode (g/s)										Model R ²
	1	2	3	4	5	6	7	8	9	10	
1	3.2	4.6	6.1	7.2	8.1	8.5	8.4	8.3	8.2	8.1	0.71
10	3.3	4.7	6.3	6.7	8.6	9.0	8.1	8.3	8.8	7.6	0.72

For PM emission rates, 95 out of 99 pairs had higher modal rates than the preceding mode. For the remaining 4 of 99 cases for which there was not an increase, the rate was the same for the higher versus adjacent lower mode. Thus, PM emission rates typically increased monotonically with mode. On average over all LCF IDs, PM emission rates increased monotonically from 0.004 g/s at model 1 to 0.32 g/s at mode 10. PM emission rates had a moderate model precision of 0.54 or higher.

For NO_x emission rates for LCF IDs 1 and 10, emission rates increased monotonically with modes, and model precision was 0.71 on average.

B.2.7 Model validation and verification

Model validation comprised parity comparison of the model predicted FUERs versus empirical FUERs. Comparisons were made for the regression part of SM3 based on all possible LOOCV combinations. The entire model comprising data from all sub-models was verified based on comparison of FUERs predicted based on the average model versus empirical FUERs. The regression part of SM3 was validated based on LOOCV as discussed in Section 0. The validation parameters for each LOOCV combination and their average including slope, standard error of slope, 95% confidence interval, and model R² are given in Table B-15.

Table B-15. Validation of the Regression Part of Sub-Model 3 Based on Parity Comparison of Model Predicted versus Empirical Fuel Use and Emission Rates without Intercept for all Leave-One-Out Cross-Validation Combinations: (a) Fuel Use Rates; (b) CO₂ Emission Rates; and (c) NO_x Emission Rates.

(a) Fuel Use Rate

ID ^a	Trips	Sample Size	Slope	95 % Confidence Interval on Slope	Standard Error in Slope	Goodness of Fit (R ²)
1	1	7006	1.05	[0.95, 1.15]	0.05	0.83
	2	7366	0.99	[0.93, 1.05]	0.03	0.88
	3	7036	0.96	[0.93, 0.99]	0.01	0.90
	4	6620	0.98	[0.89, 1.07]	0.04	0.87
	5	7568	0.93	[0.92, 0.94]	0.00	0.88
	Average			0.98	[0.93, 1.04]	0.03
2	1	5436	1.06	[0.97, 1.15]	0.05	0.73
	2	4404	0.96	[0.92, 1.00]	0.02	0.73
	3	6251	0.97	[0.91, 1.03]	0.03	0.72
	4	6162	0.93	[0.88, 0.98]	0.02	0.75
	5	5444	0.93	[0.87, 0.99]	0.03	0.73
	6	5359	1.04	[0.98, 1.10]	0.03	0.75
Average			0.98	[0.92, 1.04]	0.03	0.73
3	1	6218	1.01	[0.96, 1.06]	0.03	0.82
	2	6367	0.93	[0.85, 1.01]	0.04	0.80
	3	6686	1.02	[1.01, 1.03]	0.01	0.81
	4	6744	1.02	[0.95, 1.09]	0.04	0.85
	5	6431	0.99	[0.91, 1.07]	0.04	0.78
	6	6771	1.03	[1.02, 1.04]	0.01	0.81
Average			1.00	[0.95, 1.05]	0.03	0.81
4	1	5659	1.06	[0.98, 1.14]	0.04	0.74
	2	6032	1.02	[1.00, 1.04]	0.01	0.70
	3	5761	0.93	[0.86, 1.00]	0.04	0.70
	4	5966	1.06	[1.00, 1.12]	0.03	0.71
	5	6147	1.01	[0.92, 1.10]	0.05	0.73
	Average			1.02	[0.95, 1.08]	0.03

Table B-15 Continued on Next Page

Table B-15 Continued from Previous Page

ID ^a	Trips	Sample Size	Slope	95 % Confidence Interval on Slope	Standard Error in Slope	Goodness of Fit (R ²)
5	1	5082	1.07	[1.04, 1.10]	0.02	0.84
	2	5284	0.95	[0.94, 0.96]	0.00	0.77
	3	6073	1.04	[0.99, 1.09]	0.03	0.79
	4	3867	0.95	[0.91, 0.99]	0.02	0.80
	5	6487	1.08	[0.98, 1.18]	0.05	0.77
	6	6853	0.93	[0.92, 0.94]	0.00	0.82
	Average			1.00	[0.96, 1.04]	0.02
6	5	6107	1.05	[0.96, 1.14]	0.05	0.79
	3	6398	1.08	[1.06, 1.10]	0.01	0.79
	1	6148	0.98	[0.97, 0.99]	0.00	0.82
	Average			1.04	[1.00, 1.08]	0.02
7	6	6146	0.94	[0.87, 1.01]	0.04	0.79
	4	6601	0.99	[0.90, 1.08]	0.04	0.82
	2	6398	0.93	[0.92, 0.94]	0.00	0.79
	Average			0.95	[0.90, 1.01]	0.03
8	5	14700	0.99	[0.97, 1.01]	0.01	0.79
	3	13107	0.97	[0.96, 0.98]	0.00	0.78
	1	8775	1.06	[0.99, 1.13]	0.04	0.78
	Average			1.01	[0.97, 1.04]	0.02
9	6	9589	1.04	[0.97, 1.11]	0.04	0.73
	4	10614	1.00	[0.95, 1.05]	0.03	0.74
	2	13103	0.95	[0.87, 1.03]	0.04	0.76
	Average			1.00	[0.93, 1.06]	0.03
10	1	5450	1.00	[0.91, 1.09]	0.05	0.81
	2	5188	0.99	[0.94, 1.04]	0.02	0.85
	3	5431	0.96	[0.86, 1.06]	0.05	0.84
	4	6873	0.94	[0.89, 0.99]	0.02	0.80
	5	6519	0.96	[0.93, 0.99]	0.01	0.83
	Average			0.97	[0.91, 1.03]	0.03

Table B-15 Continued on Next Page

Table B-15 Continued from Previous Page

ID ^a	Trips	Sample Size	Slope	95 % Confidence Interval on Slope	Standard Error in Slope	Goodness of Fit (R ²)
11	1	5547	0.98	[0.92, 1.04]	0.03	0.86
	2	5984	1.06	[1.04, 1.08]	0.01	0.84
	3	7221	1.04	[0.95, 1.13]	0.05	0.88
	4	6529	1.06	[1.00, 1.12]	0.03	0.88
	5	6754	1.08	[1.03, 1.13]	0.03	0.89
	6	6177	0.99	[0.90, 1.08]	0.04	0.86
	Average			1.04	[0.97, 1.10]	0.03
12	1	3687	1.00	[0.93, 1.07]	0.04	0.75
	2	6456	0.97	[0.94, 1.00]	0.01	0.73
	3	6991	0.96	[0.95, 0.97]	0.00	0.74
	4	6943	1.07	[1.06, 1.08]	0.01	0.79
	5	6516	1.03	[0.99, 1.07]	0.02	0.78
	6	7405	1.01	[0.97, 1.05]	0.02	0.79
	7	7319	1.01	[0.95, 1.07]	0.03	0.74
	8	7417	1.08	[0.97, 1.19]	0.05	0.78
	9	6837	1.08	[0.98, 1.18]	0.05	0.78
	10	7232	0.99	[0.93, 1.05]	0.03	0.76
	11	6812	0.93	[0.83, 1.03]	0.05	0.74
	12	6875	1.04	[0.95, 1.13]	0.05	0.75
	13	6803	1.02	[1.00, 1.04]	0.01	0.76
	14	7109	1.05	[1.03, 1.07]	0.01	0.80
	15	7088	0.97	[0.96, 0.98]	0.00	0.80
Average			1.01	[0.96, 1.06]	0.03	0.77

Table B-15 Continued on Next Page

Table B-15 Continued from Previous Page

(b) CO₂ Emission Rate

ID ^a	Trips	Sample Size	Slope	95 % Confidence Interval on Slope	Standard Error in Slope	Goodness of Fit (R ²)
1	1	7006	1.03	[0.95, 1.15]	0.05	0.83
	2	7366	1.01	[0.93, 1.05]	0.03	0.89
	3	7036	0.96	[0.93, 0.99]	0.01	0.91
	4	6620	0.97	[0.89, 1.07]	0.04	0.88
	5	7568	0.93	[0.92, 0.94]	0.00	0.87
	Average			0.98	[0.92, 1.04]	0.03
2	1	5436	1.05	[0.97, 1.15]	0.05	0.74
	2	4404	0.97	[0.92, 1.00]	0.02	0.72
	3	6251	0.97	[0.91, 1.03]	0.03	0.71
	4	6162	0.92	[0.88, 0.98]	0.02	0.76
	5	5444	0.92	[0.87, 0.99]	0.03	0.75
	6	5359	1.04	[0.98, 1.10]	0.03	0.76
Average			0.97	[0.92, 1.03]	0.03	0.74
3	1	6218	1.00	[0.96, 1.06]	0.03	0.83
	2	6367	0.93	[0.85, 1.01]	0.04	0.79
	3	6686	1.01	[1.01, 1.03]	0.01	0.79
	4	6744	1.01	[0.95, 1.09]	0.04	0.83
	5	6431	1.00	[0.91, 1.07]	0.04	0.79
	6	6771	1.03	[1.02, 1.04]	0.01	0.81
Average			1.00	[0.95, 1.05]	0.03	0.81
4	1	5659	1.07	[0.98, 1.14]	0.04	0.74
	2	6032	1.04	[1.00, 1.04]	0.01	0.71
	3	5761	0.94	[0.86, 1.00]	0.04	0.70
	4	5966	1.05	[1.00, 1.12]	0.03	0.72
	5	6147	1.00	[0.92, 1.10]	0.05	0.71
	Average			1.02	[0.95, 1.08]	0.03

Table B-15 Continued on Next Page

Table B-15 Continued from Previous Page

ID ^a	Trips	Sample Size	Slope	95 % Confidence Interval on Slope	Standard Error in Slope	Goodness of Fit (R ²)
5	1	5082	1.05	[1.04, 1.10]	0.02	0.85
	2	5284	0.96	[0.94, 0.96]	0.00	0.77
	3	6073	1.02	[0.99, 1.09]	0.03	0.80
	4	3867	0.94	[0.91, 0.99]	0.02	0.79
	5	6487	1.08	[0.98, 1.18]	0.05	0.77
	6	6853	0.91	[0.92, 0.94]	0.00	0.83
	Average			0.99	[0.96, 1.03]	0.02
6	5	6107	1.07	[0.96, 1.14]	0.05	0.78
	3	6398	1.06	[1.06, 1.10]	0.01	0.78
	1	6148	0.96	[0.97, 0.99]	0.00	0.82
	Average			1.03	[0.99, 1.07]	0.02
7	6	6146	0.96	[0.87, 1.01]	0.04	0.79
	4	6601	1.00	[0.90, 1.08]	0.04	0.82
	2	6398	0.92	[0.92, 0.94]	0.00	0.81
	Average			0.96	[0.90, 1.02]	0.03
8	5	14700	1.00	[0.97, 1.01]	0.01	0.80
	3	13107	0.98	[0.96, 0.98]	0.00	0.76
	1	8775	1.07	[0.99, 1.13]	0.04	0.77
	Average			1.02	[0.98, 1.05]	0.02
9	6	9589	1.03	[0.97, 1.11]	0.04	0.74
	4	10614	1.00	[0.95, 1.05]	0.03	0.74
	2	13103	0.95	[0.87, 1.03]	0.04	0.74
	Average			0.99	[0.93, 1.06]	0.04
10	1	5450	1.01	[0.91, 1.09]	0.04	0.82
	2	5188	0.98	[0.94, 1.04]	0.02	0.87
	3	5431	0.94	[0.86, 1.06]	0.05	0.84
	4	6873	0.93	[0.89, 0.99]	0.02	0.78
	5	6519	0.94	[0.93, 0.99]	0.01	0.83
	Average			0.96	[0.90, 1.03]	0.03

Table B-15 Continued on Next Page

Table B-15 Continued from Previous Page

ID ^a	Trips	Sample Size	Slope	95 % Confidence Interval on Slope	Standard Error in Slope	Goodness of Fit (R ²)
11	1	5547	0.98	[0.92, 1.04]	0.03	0.87
	2	5984	1.06	[1.04, 1.08]	0.01	0.83
	3	7221	1.04	[0.95, 1.13]	0.05	0.89
	4	6529	1.06	[1.00, 1.12]	0.03	0.89
	5	6754	1.08	[1.03, 1.13]	0.03	0.88
	6	6177	0.99	[0.90, 1.08]	0.05	0.88
	Average			1.04	[0.97, 1.10]	0.03
12	1	3687	1.00	[0.93, 1.07]	0.03	0.76
	2	6456	0.97	[0.94, 1.00]	0.01	0.74
	3	6991	0.96	[0.95, 0.97]	0.00	0.75
	4	6943	1.07	[1.06, 1.08]	0.01	0.80
	5	6516	1.03	[0.99, 1.07]	0.02	0.77
	6	7405	1.01	[0.97, 1.05]	0.02	0.80
	7	7319	1.01	[0.95, 1.07]	0.03	0.73
	8	7417	1.08	[0.97, 1.19]	0.05	0.79
	9	6837	1.08	[0.98, 1.18]	0.05	0.78
	10	7232	0.99	[0.93, 1.05]	0.03	0.76
	11	6812	0.93	[0.83, 1.03]	0.05	0.75
	12	6875	1.04	[0.95, 1.13]	0.05	0.74
	13	6803	1.02	[1.00, 1.04]	0.01	0.76
	14	7109	1.05	[1.03, 1.07]	0.01	0.81
	15	7088	0.97	[0.96, 0.98]	0.00	0.79
Average			1.01	[0.96, 1.06]	0.03	0.77

Table B-15 Continued on Next Page

Table B-15 Continued from Previous Page

(c) NO_x Emission Rate

ID ^a	Trips	Sample Size	Slope	95 % Confidence Interval on Slope	Standard Error in Slope	Goodness of Fit (R ²)
1	1	<i>_b</i>	<i>_b</i>	<i>_b</i>	<i>_b</i>	<i>_b</i>
	2	<i>_b</i>	<i>_b</i>	<i>_b</i>	<i>_b</i>	<i>_b</i>
	3	<i>_b</i>	<i>_b</i>	<i>_b</i>	<i>_b</i>	<i>_b</i>
	4	<i>_b</i>	<i>_b</i>	<i>_b</i>	<i>_b</i>	<i>_b</i>
	5	<i>_b</i>	<i>_b</i>	<i>_b</i>	<i>_b</i>	<i>_b</i>
	Average		<i>_b</i>	<i>_b</i>	<i>_b</i>	<i>_b</i>
2	1	5436	0.98	[0.88, 1.08]	0.05	0.77
	2	4404	1.04	[1.03, 1.05]	0.01	0.76
	3	6251	0.99	[0.90, 1.08]	0.04	0.75
	4	6162	0.98	[0.93, 1.03]	0.02	0.79
	5	5444	0.92	[0.84, 1.00]	0.04	0.74
	6	5359	1.03	[1.00, 1.06]	0.02	0.81
Average			0.99	[0.93, 1.05]	0.03	0.77
3	1	6218	1.05	[0.94, 1.16]	0.06	0.87
	2	6367	1.07	[1.02, 1.12]	0.03	0.82
	3	6686	0.95	[0.92, 0.98]	0.01	0.83
	4	6744	1.07	[0.98, 1.16]	0.05	0.80
	5	6431	0.98	[0.91, 1.05]	0.03	0.84
	6	6771	0.96	[0.95, 0.97]	0.00	0.85
Average			1.01	[0.95, 1.07]	0.03	0.83
4	1	5659	0.92	[0.88, 0.96]	0.02	0.70
	2	6032	0.92	[0.83, 1.01]	0.05	0.71
	3	5761	0.97	[0.88, 1.06]	0.04	0.72
	4	5966	0.94	[0.93, 0.95]	0.00	0.70
	5	6147	1.00	[0.91, 1.09]	0.05	0.74
	Average			0.95	[0.89, 1.01]	0.03

Table B-15 Continued on Next Page

Table B-15 Continued from Previous Page

ID ^a	Trips	Sample Size	Slope	95 % Confidence Interval on Slope	Standard Error in Slope	Goodness of Fit (R ²)
5	1	5082	1.07	[1.06, 1.08]	0.01	0.82
	2	5284	1.02	[1.01, 1.03]	0.01	0.84
	3	6073	1.02	[0.98, 1.06]	0.02	0.86
	4	3867	1.00	[0.99, 1.01]	0.01	0.83
	5	6487	0.93	[0.83, 1.03]	0.05	0.82
	6	6853	1.01	[0.90, 1.12]	0.06	0.84
	Average			1.01	[0.96, 1.05]	0.02
6	5	6107	0.97	[0.88, 1.06]	0.04	0.84
	3	6398	0.92	[0.87, 0.97]	0.02	0.82
	1	6148	0.99	[0.89, 1.09]	0.05	0.80
	Average			0.96	[0.88, 1.04]	0.04
7	6	6146	1.07	[1.04, 1.10]	0.02	0.80
	4	6601	1.00	[0.92, 1.08]	0.04	0.76
	2	6398	1.03	[0.96, 1.10]	0.04	0.81
	Average			1.03	[0.97, 1.09]	0.03
8	5	14700	0.92	[0.87, 0.97]	0.02	0.84
	3	13107	1.00	[0.99, 1.01]	0.01	0.84
	1	8775	0.92	[0.86, 0.98]	0.03	0.78
	Average			0.95	[0.91, 0.99]	0.02
9	6	9589	0.93	[0.83, 1.03]	0.05	0.73
	4	10614	1.03	[0.94, 1.12]	0.05	0.75
	2	13103	0.97	[0.89, 1.05]	0.04	0.75
	Average			0.98	[0.89, 1.07]	0.05
10	1	_b	_b	_b	_b	_b
	2	_b	_b	_b	_b	_b
	3	_b	_b	_b	_b	_b
	4	_b	_b	_b	_b	_b
	5	_b	_b	_b	_b	_b
	Average			_b	_b	_b

Table B-15 Continued on Next Page

Table B-15 Continued from Previous Page

ID ^a	Trips	Sample Size	Slope	95 % Confidence Interval on Slope	Standard Error in Slope	Goodness of Fit (R ²)
11	1	5547	0.96	[0.95, 0.97]	0.00	0.82
	2	5984	0.97	[0.87, 1.07]	0.05	0.76
	3	7221	1.06	[1.02, 1.10]	0.02	0.82
	4	6529	0.97	[0.96, 0.98]	0.00	0.78
	5	6754	0.95	[0.93, 0.97]	0.01	0.78
	6	6177	0.99	[0.93, 1.05]	0.03	0.82
	Average			0.98	[0.94, 1.02]	0.02
12	1	3687	1.05	[0.94, 1.16]	0.06	0.73
	2	6456	1.05	[0.95, 1.15]	0.05	0.72
	3	6991	0.93	[0.86, 1.00]	0.04	0.73
	4	6943	0.97	[0.95, 0.99]	0.01	0.73
	5	6516	0.96	[0.87, 1.05]	0.05	0.69
	6	7405	1.00	[0.97, 1.03]	0.02	0.70
	7	7319	1.03	[0.99, 1.07]	0.02	0.73
	8	7417	1.02	[1.00, 1.04]	0.01	0.68
	9	6837	0.93	[0.86, 1.00]	0.04	0.73
	10	7232	1.02	[0.93, 1.11]	0.05	0.71
	11	6812	0.96	[0.93, 0.99]	0.01	0.72
	12	6875	1.04	[0.98, 1.10]	0.03	0.70
	13	6803	1.02	[1.01, 1.03]	0.01	0.70
	14	7109	1.07	[0.99, 1.15]	0.04	0.70
	15	7088	1.04	[0.96, 1.12]	0.04	0.71
Average			1.01	[0.94, 1.07]	0.03	0.71

^a LCF ID: Each combination of locomotive, consist, and fuel was assigned a unique ID. The description of each LCF ID is given in the supporting information Table B-4.

^b NO_x emission rates for LCF IDs 1 and 10 were modeled based on a 10-mode modal model because they were not modeled properly by the regression model.

The parity slope for fuel use rate for a given LOOCV combination for a given LCF ID was typically within a narrow range of $\pm 10\%$ of 1. The standard error in slope was typically $< 5\%$ of the slope indicating that the slope was precisely estimated. The 95% confidence intervals were also narrow because of the precisely estimated slope and enclosed the slope for $> 70\%$ of the LOOCV cases. Model R^2 for validation data was typically within ± 0.05 of the model R^2 of the corresponding calibration data indicating similar model precision. For fuel use rates, model R^2 was typically 0.70 or higher indicating good model precision. Each of these estimated parameters were within $\pm 10\%$ of each other for a given LOOCV combination. Therefore, the model is insensitive to the choice of trips used for calibration and validation. The average slope for a given LOOCV combination was within $\pm 3\%$ of 1 indicating good model accuracy. Therefore, the regression part of SM3 for fuel use rate was precise and accurate. Similar results were also measured for emission rates of CO_2 and NO_x .

The model evaluation parameters based on the parity comparison of fitted versus actual rates for all sub-Models combined are presented in Table B-16. For each species and LCF ID, the intercept was found to be statistically insignificant. Thus, the intercept was set to zero for all parity comparisons. For fuel use rate and emission rates of CO_2 and NO_x , the standard error relative to the slope was less than 1% and confidence intervals on the slope were narrow indicating that the slope was precisely estimated for each LCF ID. For these species, the model R^2 varied between 0.63 and 0.86 with an average of 0.76. For the 36 cases comprised of 3 species and 12 LCF IDs, the model R^2 was 0.70 or higher for 32 cases. Model R^2 was lower than 0.70 for four LCF IDs for NO_x emission rates. For these four LCF IDs, model R^2 for NO_x emission rates varied between 0.63 and 0.68. Thus, the models were typically precise. The average slope was within 10% of the ideal value of 1 and on average was within 4% of 1, indicating good model accuracy.

CO and HC emission rates for sub-models 1, 2, and several modes of sub-model 3 were based on CO and HC concentrations below the detection limit of the Axion PEMS. Thus, the trends in average rates of these species among sub-models and with the modes of sub-model 3 were noisy relative to other species. This noise resulted in larger deviations from an ideal slope of 1 and model R^2 of 1 than for other species. However, on average over all LCF IDs, the slopes were within 2% of 1 for HC emission rates and 7% of 1 for CO emission rates. The average R^2 for CO and HC emission rates was lower than the average R^2 for fuel use rates and emission rates of CO_2 and NO_x . Thus, CO and HC models were accurate but less precise than fuel use rates and emission rates of CO_2 and NO_x .

The estimated slope for PM emission rates varied within 8% of 1. On average, the slope was within 3% of 1. On average, the PM model was accurate for all sub-models combined. Model R^2 for PM emission rates varied from 0.64 to 0.80 and was 0.73 on average, indicating good model precision.

Table B-16. Model Evaluation Based on Parity Comparison of Model Predicted versus Empirical Fuel Use and Emission Rates without Intercept for all Sub-Models Combined: (a) Fuel Use Rates; (b) CO₂ Emission Rates; (c) CO Emission Rates; (d) HC Emission Rates; (e) NO_x Emission Rates; and (f) PM Emission Rates.

(a) Fuel Use Rate

LCF ID	Sample Size	Slope	Standard Error	95% Confidence Interval	Model R ²
1	58760	1.043	0.00173	[1.039, 1.046]	0.76
2	61803	1.007	0.00184	[1.003, 1.010]	0.76
3	73404	1.068	0.00149	[1.065, 1.071]	0.85
4	59964	1.038	0.00178	[1.035, 1.042]	0.82
5	55948	0.934	0.00185	[0.931, 0.938]	0.70
6	36120	1.015	0.00235	[1.011, 1.020]	0.76
7	34082	1.031	0.00226	[1.026, 1.035]	0.77
8	39625	1.080	0.00219	[1.075, 1.084]	0.77
9	31830	0.959	0.00240	[0.955, 0.964]	0.72
10	51088	1.030	0.0017	[1.027, 1.033]	0.71
11	60844	0.970	0.0018	[0.966, 0.974]	0.71
12	162304	1.070	0.0015	[1.067, 1.073]	0.82
Average		1.020			0.76
Minimum		0.934			0.70
Maximum		1.080			0.85

(b) CO₂ Emission Rate

LCF ID	Sample Size	Slope	Standard Error	95% Confidence Interval	Model R ²
1	58760	1.053	0.00173	[1.049, 1.056]	0.77
2	61803	1.007	0.00184	[1.003, 1.010]	0.77
3	73404	1.078	0.00149	[1.075, 1.081]	0.84
4	59964	1.041	0.00178	[1.038, 1.045]	0.81
5	55948	0.943	0.00185	[0.940, 0.947]	0.72
6	36120	1.018	0.00235	[1.014, 1.023]	0.75
7	34082	1.033	0.00226	[0.985, 0.994]	0.77
8	39625	1.083	0.00219	[1.078, 1.087]	0.79
9	31830	0.956	0.00240	[0.952, 0.961]	0.73
10	51088	0.940	0.0018	[0.937, 0.943]	0.81
11	60844	0.960	0.0019	[0.956, 0.964]	0.80
12	162304	1.010	0.0015	[1.007, 1.013]	0.86
Average		1.010			0.78
Minimum		0.940			0.72
Maximum		1.083			0.86

Table B-16 Continued on Next Page

Table B-16 Continued from Previous Page

(c) CO Emission Rate

LCF ID	Sample Size	Slope	Standard Error	95% Confidence Interval	Model R ²
1	58760	1.096	0.0158	[1.065, 1.127]	0.43
2	61803	0.897	0.0185	[0.861, 0.933]	0.49
3	73404	1.086	0.0337	[1.020, 1.152]	0.54
4	59964	1.031	0.0177	[0.996, 1.066]	0.53
5	55948	1.122	0.0424	[1.039, 1.205]	0.57
6	36120	1.138	0.0204	[1.098, 1.178]	0.42
7	34082	1.134	0.0402	[1.055, 1.213]	0.59
8	39625	1.145	0.0276	[1.091, 1.199]	0.48
9	31830	0.982	0.0281	[0.927, 1.037]	0.41
10	51088	0.930	0.0164	[0.898, 0.962]	0.43
11	60844	0.960	0.0192	[0.922, 0.998]	0.47
12	162304	0.940	0.0347	[0.872, 1.008]	0.56
Average		1.038			0.49
Minimum		0.897			0.41
Maximum		1.145			0.59

(d) HC Emission Rate

LCF ID	Sample Size	Slope	Standard Error	95% Confidence Interval	Model R ²
1	58760	1.145	0.0318	[1.083, 1.207]	0.08
2	61803	1.099	0.0296	[1.041, 1.157]	0.13
3	73404	1.138	0.0486	[1.043, 1.233]	0.05
4	59964	1.017	0.0576	[0.904, 1.130]	0.08
5	55948	1.107	0.0316	[1.045, 1.169]	0.05
6	36120	0.929	0.0169	[0.896, 0.962]	0.14
7	34082	0.886	0.0217	[0.843, 0.929]	0.22
8	39625	0.968	0.0156	[0.937, 0.999]	0.12
9	31830	0.880	0.0413	[0.799, 0.961]	0.09
10	51088	1.060	0.0296	[1.002, 1.118]	0.08
11	60844	1.050	0.0305	[0.990, 1.110]	0.12
12	162304	0.990	0.0505	[0.891, 1.089]	0.05
Average		1.022			0.10
Minimum		0.880			0.05
Maximum		1.145			0.22

Table B-16 Continued on Next Page

Table B-16 Continued from Previous Page

(e) NO_x Emission Rate

LCF ID	Sample Size	Slope	Standard Error	95% Confidence Interval	Model R ²
1	58760	1.022	0.00173	[1.019, 1.025]	0.74
2	61803	1.050	0.00193	[1.047, 1.054]	0.65
3	73404	1.082	0.00159	[1.079, 1.085]	0.77
4	59964	1.026	0.00194	[1.022, 1.030]	0.73
5	55948	1.006	0.00205	[1.002, 1.010]	0.63
6	36120	1.035	0.00244	[1.030, 1.039]	0.76
7	34082	1.056	0.00243	[1.051, 1.060]	0.73
8	39625	1.084	0.00224	[1.080, 1.088]	0.84
9	31830	1.011	0.00256	[1.006, 1.016]	0.68
10	51088	0.950	0.0016	[0.947, 0.953]	0.75
11	60844	1.020	0.0019	[1.016, 1.024]	0.64
12	162304	1.020	0.0016	[1.017, 1.023]	0.81
Average		1.030			0.73
Minimum		0.950			0.63
Maximum		1.084			0.84

(f) PM Emission Rate

LCF ID	Sample Size	Slope	Standard Error	95% Confidence Interval	Model R ²
1	58760	1.088	0.0292	[1.031, 1.145]	0.72
2	61803	1.088	0.0271	[1.035, 1.141]	0.64
3	73404	0.996	0.0151	[0.966, 1.026]	0.64
4	59964	0.972	0.0202	[0.932, 1.012]	0.80
5	^a	^a	^a	^a	^a
6	36120	1.020	0.0246	[0.972, 1.068]	0.77
7	34082	1.064	0.0173	[1.030, 1.098]	0.76
8	39625	0.933	0.0117	[0.910, 0.956]	0.75
9	31830	1.089	0.0184	[1.053, 1.125]	0.78
10	51088	0.980	0.0292	[0.923, 1.037]	0.74
11	60844	0.930	0.0276	[0.876, 0.984]	0.65
12	162304	1.010	0.0151	[0.980, 1.040]	0.65
Average		1.015			0.72
Minimum		0.930			0.64
Maximum		1.089			0.80

^a Invalid PM data

The entire model, inclusive of all sub-models for each species and LCF IDs was verified for three resolutions: one Hz, 0.25-mile, and trip based on comparison of FUERs estimated based on average model versus empirical FUERs. Thus, model predictions were compared to the same data used to calibrate the model. An example time plot of empirical, modeled, and EPA-reported fuel use rate and PM emission rate for locomotive NC 1797 operated in SLC on ULSD is given in Figure B-17. At approximately 280 s, the operator switched the throttle notch position from high idle to notch 8. After this switch, empirical and modeled rates fuel use and PM emission rates increased simultaneously for the next 35 s. At 305 s, both empirical and modeled rates became approximately constant. At 350 s, the PME was switched to notch 5 and fuel use rate and PM emission rates started to decrease simultaneously. Thus, modeled FUERs rates closely resembled the rise and fall in empirical FUERs.

A typical practice for estimating locomotive emissions for a duty cycle or trip is based on weighing steady-state based notch-average FUERs to the time spent in each notch position (Bergin et al., 2012; Caretto, 2008; EPA, 1998). EPA reported notch-average mass per time-based FUERs for EMD 12-710 PMEs which are the same model PMEs measured here (EPA, 1998). Because PME real-world operation comprises steady-state operation in a given notch position, and transitions in operations when notch positions are changed, differences in empirical one Hz, segment-average, and trip-based FUERs were quantified relative to those estimated based on steady-state. A transition starts when the predecessor notch position is switched to a successor notch position and ends when the PME reaches steady state in the successor notch or the notch is changed before steady-state could be reached. The transition is referred to as upshift when the successor notch is higher than predecessor notch and downshift when the successor notch is lower. Upshifts take 5B-30s to reach steady-state, whereas downshifts only take <4s to reach steady-state. Transient rates during upshift are higher than the predecessor steady-state notch-average rate but lower than the steady-state average rate for the successor notch. On average, because of longer duration of upshifts relative to downshifts, FUERs based on steady-state are typically higher than transient rates for a given notch-position. Therefore, using steady-state FUERs such as those reported by the EPA are likely to overestimate one Hz FUERs on average.

The cumulative frequency distribution of modeled and empirical one Hz FUERs, segment-average FUERs, and PTFUEs are given in Figure B-10, Figure B-11, and Figure B-12, respectively. For each plot for each species, the distribution of modeled FUERs were approximately similar to the empirical FUERs. In Figure B-10(a) for one Hz fuel use rates, the distribution of modeled rates was approximately identical to empirical rates up to 150 g/s. Empirical rates exceeding 150 g/s were rare (typically <1% of the entire trip duration). These rare rates cannot be described by a mean-based model such as SM3, which represents mean trends, and SM4, which is a simple mean of rates. Similar results were obtained for other species, where emission rates greater than a threshold were measured but not modeled. The range of model predicted FUERs covers 99% or higher of the range of empirical FUERs. The range of EPA-reported data does not cover the entire range of empirical FUERs. Additionally, as shown in Figure B-14, EPA-reported data do not account for inter-locomotive, and inter-consist variability in FUERs.

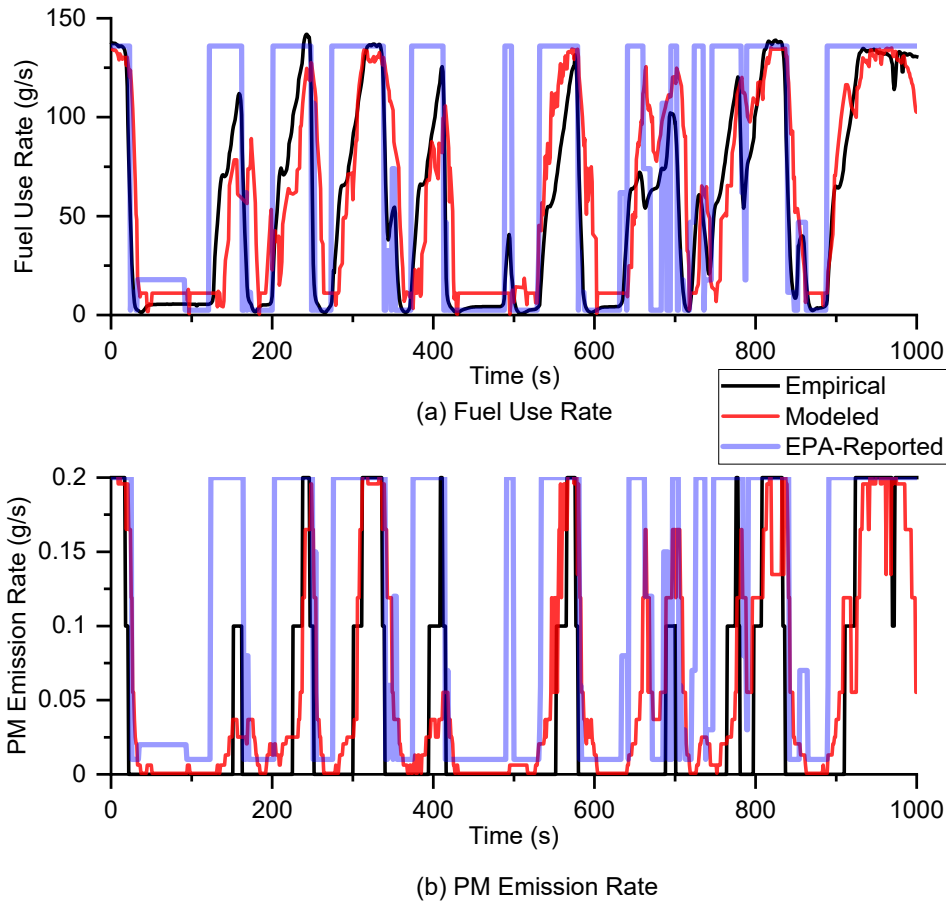


Figure B-9. Comparison of Time Plot of One Hz Empirical, Modeled, and EPA-Reported Fuel Use and Emission Rates Based on Over-the-Rail Measurements for Locomotive NC 1797 Operated in Single Locomotive Consist on Diesel: (a) Fuel Use Rate; and (b) PM Emission Rate.

EPA-reported data comprises notch-average rates for the same model prime mover engine measured in this study operated on diesel (EPA, 1998). EPA-reported rates were applied to each second of data based on the throttle notch position on which the PME was operating.

In Figure B-11 (a) for segment-average fuel use rates, modeled and empirical rates cover approximately similar ranges with approximately similar distributions. The effects of rare cases of higher one Hz empirical rates averaged out at a segment-level resolution. Therefore, modeled FUERs had approximately similar distributions as empirical FUERs. Likewise, modeled PTFUEs also had approximately similar distributions as empirical PTFUEs. Segment-average FUERs estimated based on EPA-reported data are likely to overestimate FUERs in the mid-range of empirical FUERs as these segments are largely comprised of transient operation. The segments with relatively lower or higher emission rates typically comprise of steady-state operation. As shown in Figure B-17, EPA-reported rates were similar to empirical FUERs for several locomotives during steady-state operation.

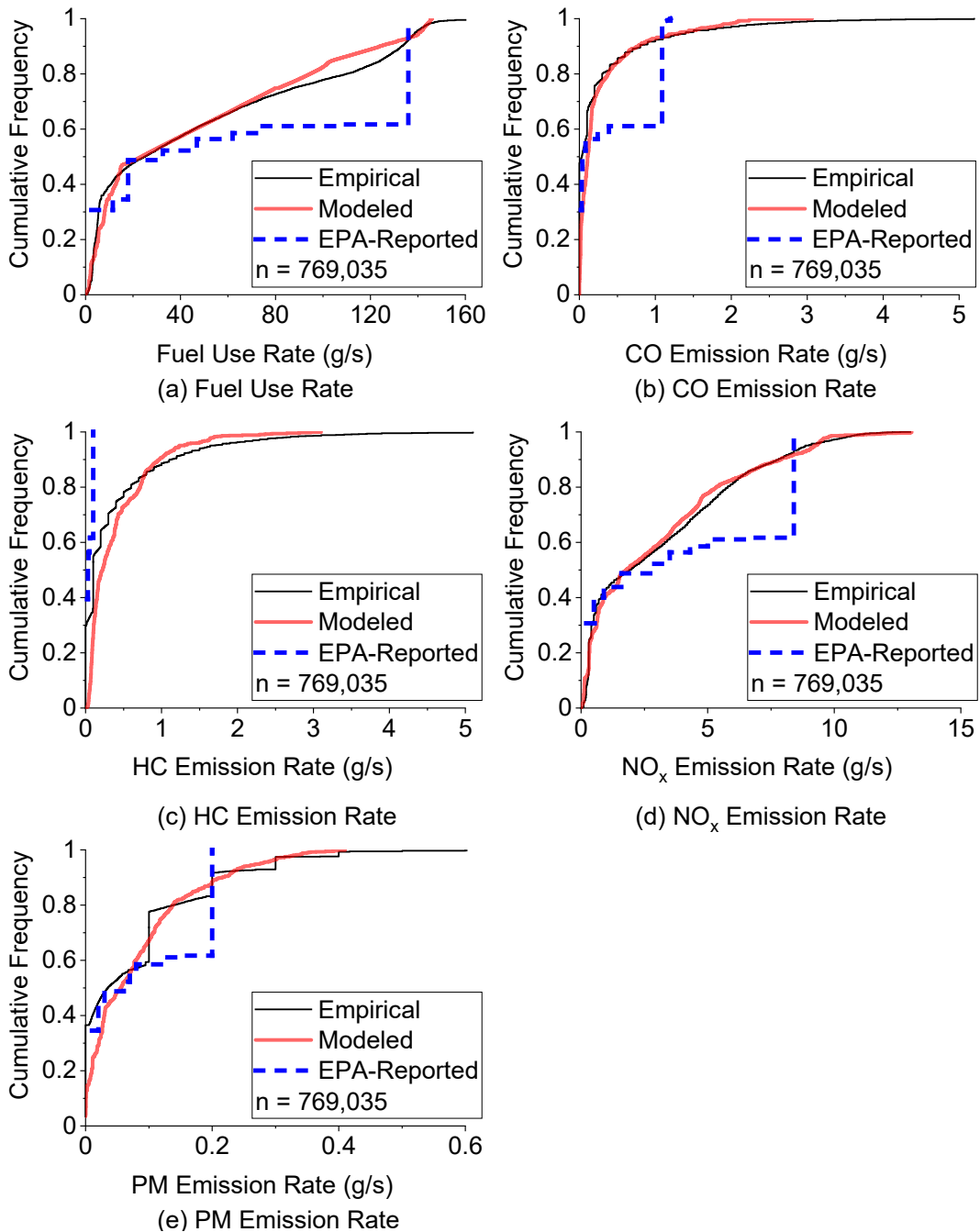


Figure B-10. Comparison of Distributions of One Hz Empirical, Modeled, and EPA-reported Fuel Use and Emission Rates based on All LCF IDs: (a) Fuel Use Rate; (b) CO Emission Rate; (c) HC Emission Rate; (d) NO_x Emission Rate; and (e) PM Emission Rate.

CO₂ emission rates have similar trends as fuel use rates because 99% of the carbon in fuel is emitted as CO₂. Therefore, plot for CO₂ is not shown. In each plot, n is the number of data points for each of empirical and modeled rates corresponding to total valid one Hz data for all LCF IDs combined. EPA-reported data comprises notch-average rates for the same model prime mover engine measured in this study operated on diesel (EPA, 1998). EPA-reported rates were applied to each second of data based on the throttle notch position on which the PME was operating.

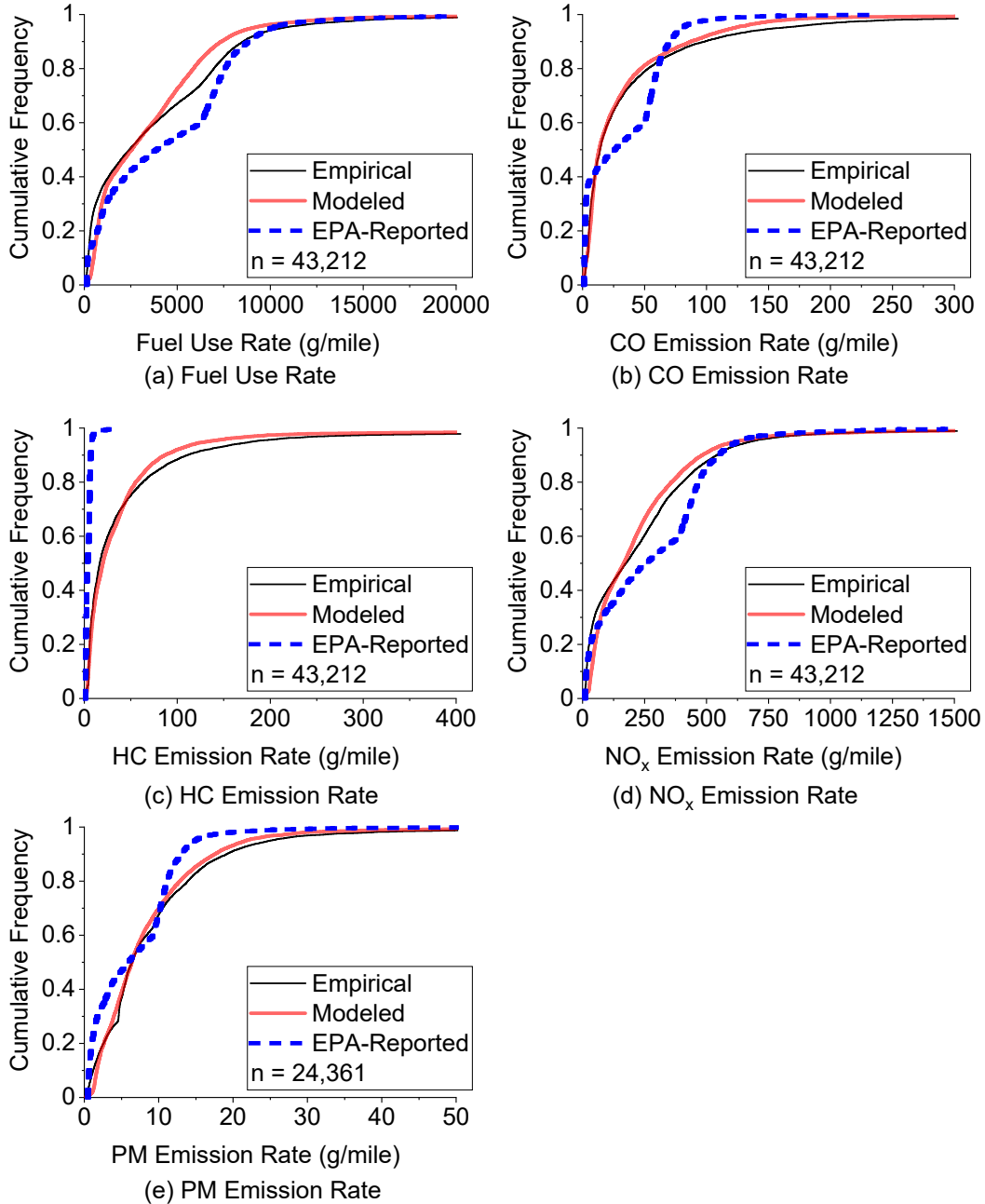


Figure B-11. Comparison of Distributions of Segment-Average Fuel Use and Emission Rates among Modeled, Empirical, and Those Estimated for the Piedmont Passenger Rail based on EPA-reported Data for All LCF IDs: (a) Fuel Use Rate; (b) CO Emission Rate; (c) HC Emission Rate; (d) NO_x Emission Rate; and (e) PM Emission Rate.

CO₂ emission rates have similar trends as fuel use rates because 99% of the carbon in fuel is emitted as CO₂. Therefore, plot for CO₂ is not shown. In each plot, n is the number of data points for each of empirical and modeled rates corresponding to all valid 0.25-mile segment average data for all LCF IDs. EPA-reported data comprises notch-average rates for the same model prime mover engine measured in this study operated on diesel (EPA, 1998). EPA-reported rates were applied to each second of data based on the throttle notch position on which the PME was operating and were summed for each segment to estimate segment-average rates.

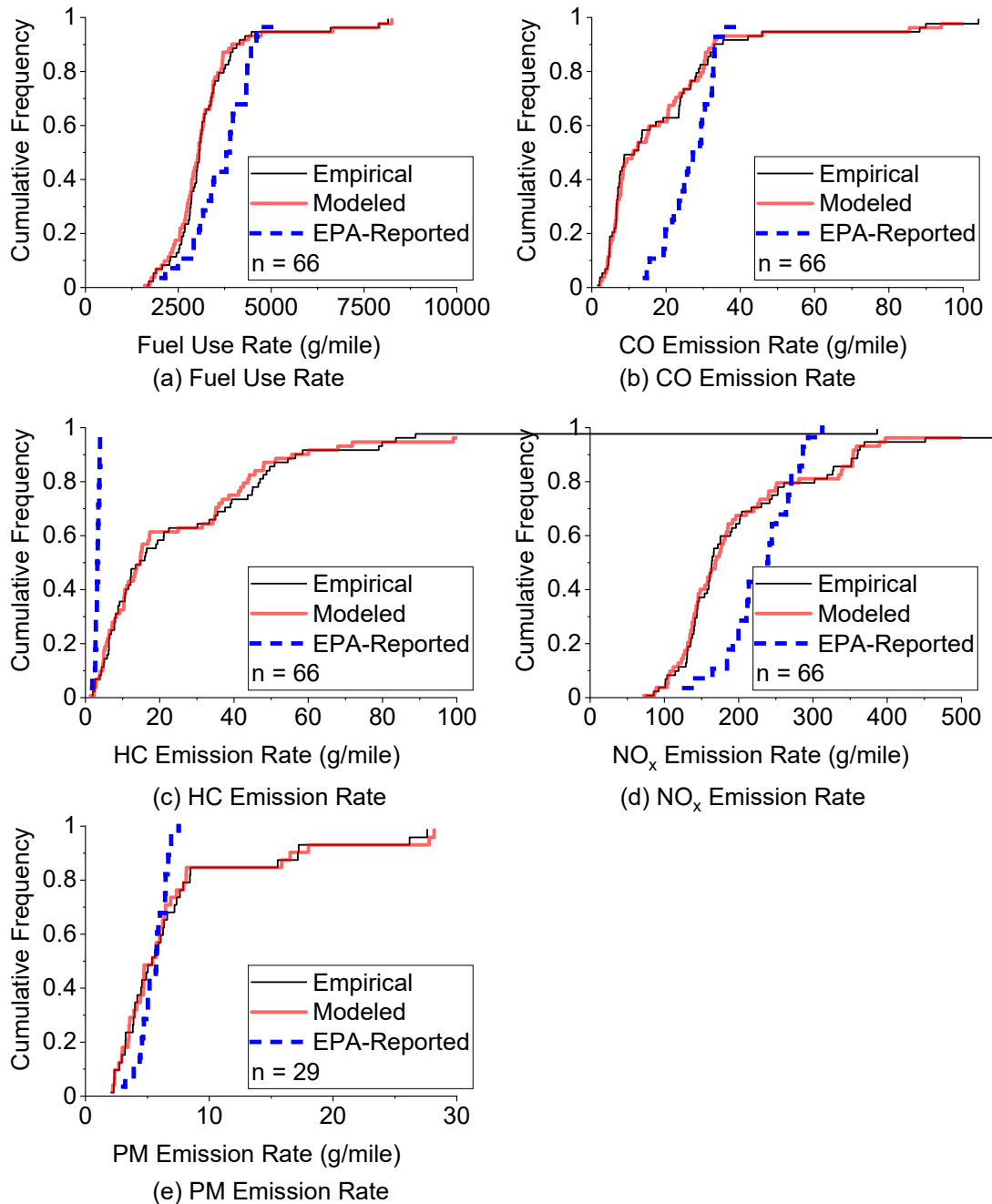


Figure B-12. Comparison of Distributions of Prime Mover Engine Trip Average Fuel Use and Emissions among Modeled, Empirical, and Those Estimated for the Piedmont Passenger Rail based on EPA-reported Data for All LCF IDs: (a) Fuel Use; (b) CO Emissions; (c) HC Emissions; (d) NO_x Emissions; and (e) PM Emissions.

CO₂ emission rates have similar trends as fuel use rates because 99% of the carbon in fuel is emitted as CO₂. Therefore, plot for CO₂ is not shown. In each plot, n is the number of one-way trips for each of empirical and modeled data. EPA-reported data comprises notch-average rates for the same model prime mover engine measured in this study operated on diesel (EPA, 1998). EPA-reported rates were applied to each second of data based on the throttle notch position on which the PME was operating and were summed for each one-way trip to estimate trip-average rates.

In Figure B-20, empirical and modeled PTFUEs had similar distributions. However, based on the EPA-reported data, some locomotives had consistently higher PTFUEs estimated because steady-state FUERs are generally higher than transient FUERs. For other locomotives, FUERs based on EPA-reported data were lower than empirical PTFUEs, because there were higher emitting locomotives than the average.

Parity comparisons of FUERs estimated based on average model versus empirical FUERs were made for each species inclusive of all LCF IDs. Model predictions were compared to the same data used to calibrate the model. For each of the parity comparisons, the slope was within 10% of one and the intercept was not statistically significantly different from zero. The slope was within 10%, 7%, and 4% of one for one Hz FUERs, segment-average FUERs, and PTFUEs, respectively. Therefore, the model is accurate at predicting FUERs at several temporal and spatial resolutions. The model accuracy increases as the FUERs are aggregated over larger resolutions.

B.3 Model Benchmarking to Independent Data

To benchmark the model, publicly available FUERs for the same model PME were used. EPA reported notch-average engine output and corresponding FUERs for an EMD 12-710 PME operated on ULSD are given in Table B-24 (EPA, 1998). The model predicted FUERs at the same engine output for LCF IDs 1 through 9 for each species were compared to independent data. Modeled FUERs for the nine LCFs measured on ULSD corresponding to the same engine output as independent data are given in Figure B-21. This figure is interpreted in Chapter 3.

Table B-17. Notch-Average Engine Output, Fuel Use Rates, and Emission Rates for EMD 12-701 PME reported by the EPA (EPA 1998).

Throttle Notch Position	Engine Output		Notch-Average Rate (g/s)				
	(bhp)	(kW)	Fuel Use	CO	HC	NO _x	PM
Idle	8	6	2.4	0.02	0.02	0.2	0.01
Dynamic Brake	84	63	18	0.03	0.03	0.5	0.02
1	209	156	11	0.03	0.02	0.9	0.01
2	372	277	18	0.04	0.02	1.6	0.03
3	717	535	33	0.05	0.03	2.8	0.06
4	1053	785	47	0.08	0.04	3.5	0.07
5	1402	1045	62	0.24	0.05	4.3	0.08
6	1696	1265	74	0.39	0.05	5.0	0.12
7	2534	1890	107	1.20	0.06	6.6	0.15
8	3196	2383	136	1.09	0.10	8.4	0.20

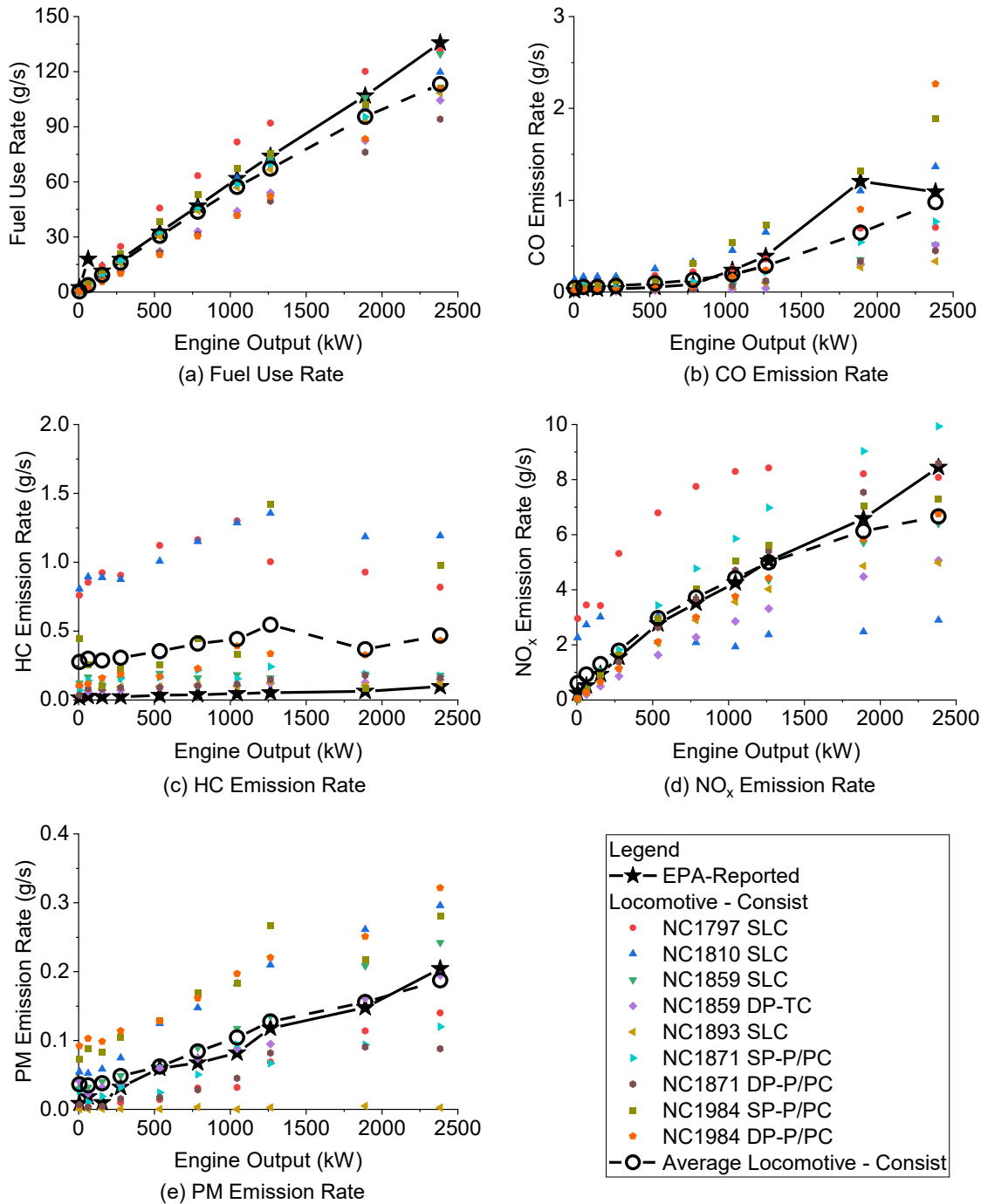


Figure B-13. Benchmarking of Locomotive Power Demand Model Predicted Fuel Use and Emission Rates (FUERs) for NCDOT Locomotives and Consists Operated on Ultra-Low Sulfur Diesel to FUERs Reported by the EPA for the Same Model Prime Mover Engine as NCDOT Locomotives and the Same Engine Output.

Source for EPA-reported FUERs: (EPA 1998). Only the measured locomotive is indicated for the train consists with two locomotives. Consist: (1) SLC: Single Locomotive Consist; (2) DP-TC: Double-powered Tandem Consist; (3) DP-P/PC: Double-powered Push/Pull Consist; and (4) SP-P/PC: Single-powered Push/Pull Consist.

B.4 Head End Power Engine Fuel Use and Emission Rates

HEP Engine FUERs of the NCDOT fleet are expected to be lower compared to the PME FUERs because the HEP engines are certified to more stringent emission standards and operate at lower loads than PMEs as explained in Section 1.1, and 1.4, respectively. The contribution of HEP engine FUERs to train FUERs, estimated as the sum of PME(s) FUERs and HEP engine FUERs was quantified.

For one Hz resolution, the contribution of HEP engine FUERs decreased with increasing PME load because HEP engine FUERs were constant whereas PME FUERs increased with load. The HEP engine FUERs contribution was lowest, between 2% and 4%, at the highest PME load, depending on species, and combination of LCF (Figure B-22). The highest HEP engine FUERs contributions were estimated when PME idled. For idle PME, HEP engine FUERs contributed between 45% and 57% to train fuel use rates, and emission rates of CO₂ and NO_x, and between 11% and 24% to CO, HC, and PM emission rates (Figure B-22).

Similar to 1 Hz FUERs, the contribution of HEP engine FUERs decreased with increasing PME load within a segment. At segments with positive grade or acceleration, LPD was among the highest resulting in the highest segment-average PME FUERs and, consequently, the lower contribution of HEP engine FUERs. On a segment-average resolution, the HEP engine FUERs had contributions of >60% when the train was idling, decelerating, or descending a hill such that PME was typically operating at idle throughout the segment (Figure B-23). Such segments comprised <20% of the trip.

On a trip total resolution, the contribution of HEP engine FUERs was low at <3% for each LCF, one-way trip, and species (Table B-25). This was because a large share of trip duration for a given species and one-way trip, typically >70%, was from data with HEP engine FUERs contributing <4% to train FUERs.

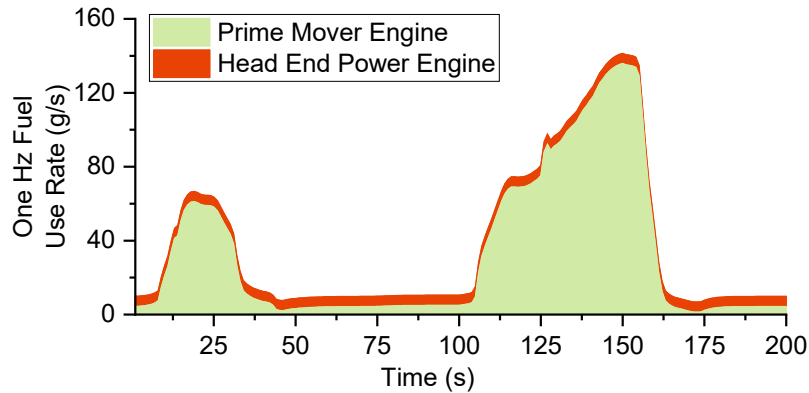
The classification of segments into hotspots and non-hotspots based on train FUERs was similar to that based on PME FUERs (Figure B-24). For each species, the plots closely resembled the line $y = x$, showing that segment-average FUERs were approximately similar and the hotspots classification was independent of the choice of train FUERs versus PME FUERs. Hotspots can be accurately identified based on PME FUERs only because HEP engine FUERs have a low contribution to train FUERs. However, this contribution of HEP engine FUERs to TTFUEs depends on the difference in certification and operating load between PME and HEP engine and could affect the location of hotspots. In this work, HEP engines certified to were Tier 2 or Tier 3 whereas PMEs were certified to Tier 0+ standard. The HEP engines also operated at loads <120 kW compared to loads ~2519 kW for the PME. More stringent standard certification standards and low load for the HEP engine resulted in low HEP engine FUERs relative to PME.

Table B-18. Contribution of Head End Power Engine Fuel Use and Emissions to Train Fuel Use and Emissions for Measured Combinations of Locomotives, Consists, and Fuels.

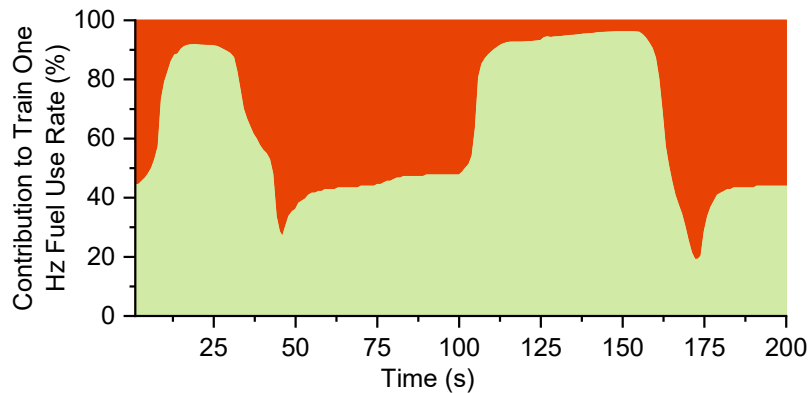
LCF ID ^a	Average Contribution (%)					
	Fuel Use	CO ₂ Emissions	CO Emissions	HC Emissions	NO _x Emissions	PM Emissions
1	3.7	3.8	2.9	2.7	3.5	2.7
2	3.6	3.6	2.6	2.6	3.9	2.7
3	3.4	3.4	2.4	2.4	3.1	2.4
4	2.7	2.7	1.7	1.8	2.5	1.6
5	3.9	4.0	3.0	3.0	3.4	3.1
6	3.0	3.0	2.0	2.0	2.3	2.0
7	2.6	2.6	1.5	1.7	2.0	1.7
8	2.9	2.9	1.9	1.8	1.9	2.0
9	2.6	2.7	1.8	1.7	2.4	1.8
10	3.8	3.8	2.9	2.7	2.7	2.7
11	3.9	3.8	2.9	2.9	3.3	2.8
12	3.6	3.5	2.6	2.6	3.2	2.4
Average	3.3	3.3	2.4	2.3	2.9	2.3
CV ^b	0.2	0.2	0.2	0.2	0.2	0.2

^a LCF ID: Each combination of locomotive, consist, and fuel was assigned a unique ID. The description of each LCF ID is given in the supporting information Table B-4.

^b CV = Coefficient of variation, defined as the ratio of standard deviation to mean.



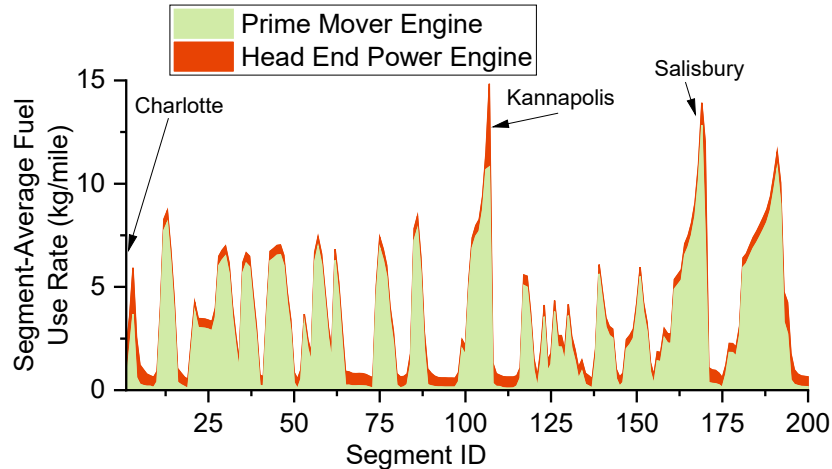
(a) One Hz Fuel Use Rate



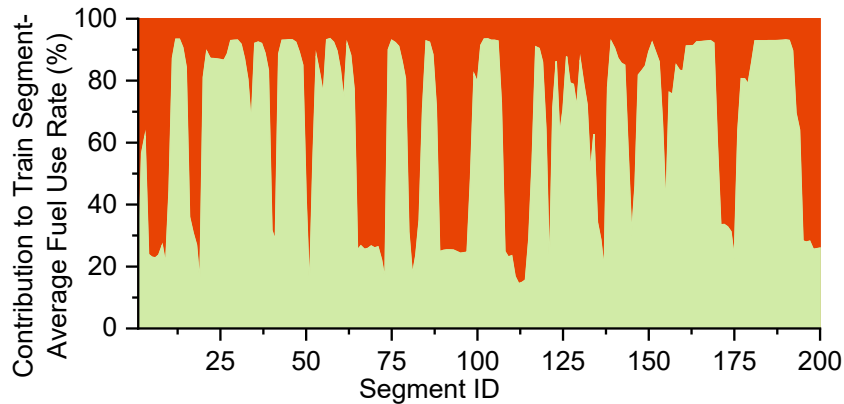
(b) Contribution to Train One Hz Fuel Use Rate

Figure B-14. Example Time Plot of One Hz Prime Mover Engine and Head End Power Engine Fuel Use Rates and Their Contribution to One Hz Train Fuel Use Rate for During a Select Portion of One One-Way Trip from Raleigh, NC to Charlotte, NC Measured For Locomotive NC 1797 Operated in Single Locomotive Consist on Ultra-Low Sulfur Diesel: (a) One Hz Fuel Use Rate; and (b) Contribution to Train One Hz Fuel Use Rate.

Train fuel use rates was estimated as the sum of prime mover engine and head end power engine fuel use rates. This portion was selected because the prime mover engine fuel use rate shown here covered the entire range of fuel use rates measured for the entire route. The head end power (HEP) engine fuel use rate was inferred to be constant per unit time for the entire trip. For the selected portion, HEP engine fuel use rate contributed 3.2% of train total fuel use rate on average.



(a) Segment-Average Fuel Use Rate



(b) Contribution to Train Segment-Average Fuel Use Rate

Figure B-15. Example Segment-Average Prime Mover Engine and Head End Power Engine Fuel Use Rates and Their Contribution to Train Fuel Use Rate for 200 Selected 0.25-Mile Track Segments Between Charlotte, NC and High Point, NC Measured For Locomotive NC 1797 Operated in Single Locomotive Consist on Ultra-Low Sulfur Diesel: (a) Segment-Average Fuel Use Rate; and (b) Contribution to Train Segment-Average Fuel Use Rate.

Train fuel use rates was estimated as the sum of prime mover engine and head end power engine fuel use rates. 0.25-mile track segments were given IDs from 1 to 692 corresponding to Charlotte, NC and Raleigh, NC, respectively. Here, segments are shown for only a part of the route between Charlotte and High Point because the selected part covers range of segment-average fuel use rates measured elsewhere. For the selected segments, the average contribution of head end power engine fuel use rate to train total was 3.5%.

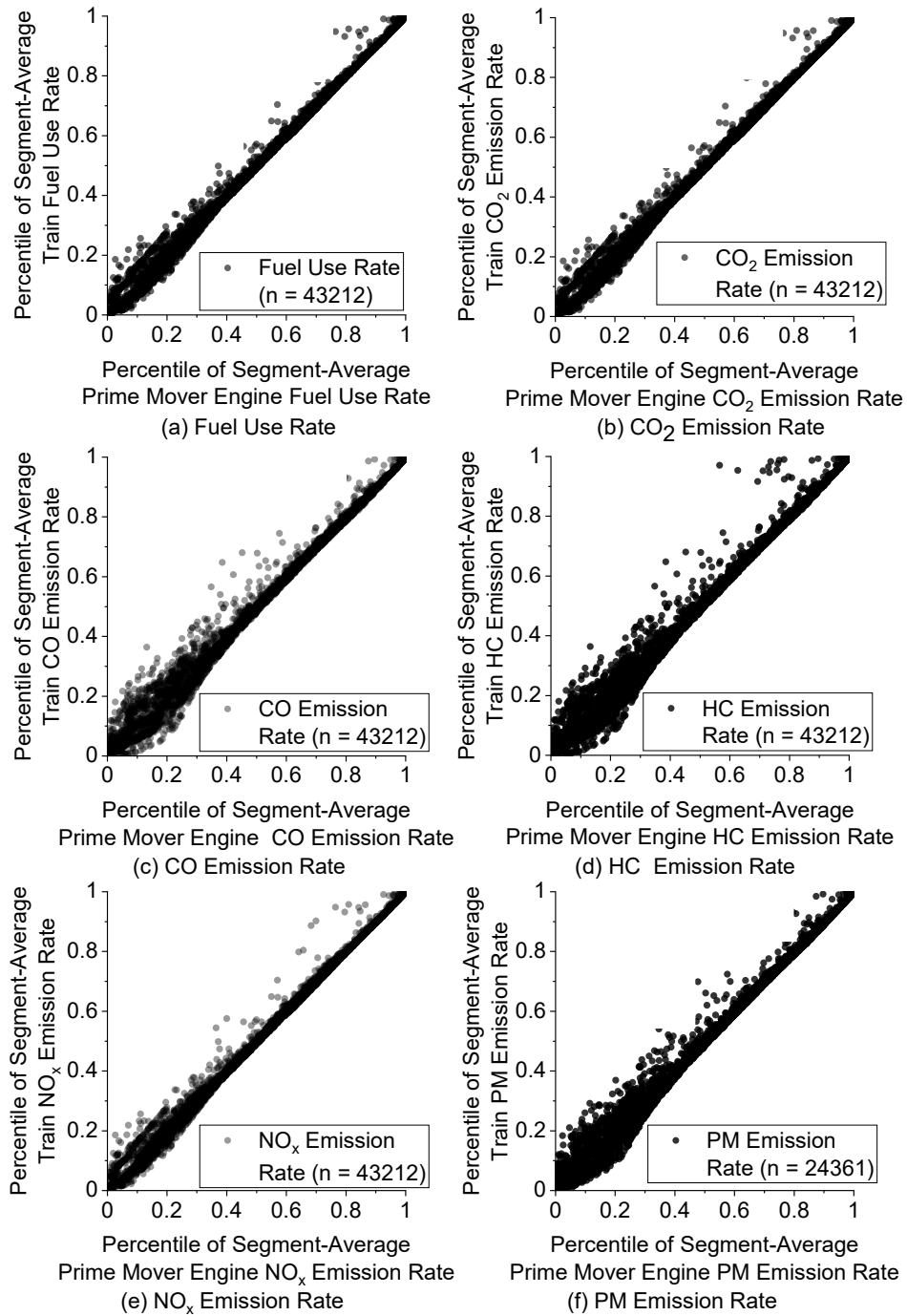


Figure B-16. Comparison of Percentiles Estimated for Train Versus Prime Mover Engine Segment-Average Fuel Use and Emission Rates based on Relative Hotspot Definition for 12 combinations of Locomotives, Consists, and Fuels: (a) Fuel Use Rate; (b) CO₂ Emission Rate; (c) CO Emission Rate; (d) HC Emission Rate; (e) NO_x Emission Rate; and (f) PM Emission Rate.

Not all one-way trips had valid PM data. Therefore, the number of segments for PM emission rates was lower than for other species.

B.5 Identification of Trajectories with Low Fuel Use and Emissions

This section provides information related to Trajectory IDs referred to in Figure 3-5 of Chapter 3. Missing data by time for each Trajectory ID was estimated as the difference of travel time between origin and destination less valid 1 Hz data. Missing data by distance was estimated as the route length less the distance accounted for by the valid 1 Hz data. Trajectory IDs and their corresponding LCF and one-way trip are given in Table B-26. The maximum and minimum TTFUEs among 45 one-way trips, used to normalize TTFUEs, are given in Table B-27.

Table B-19. ID Assigned to the Trajectory Measured for the Corresponding One-Way Trip

Trajectory ID	Locomotive	Consist	Fuel	Trip ID ^a
1	NC 1859	Single Locomotive Consist	B20	12-4
2	NC 1859	Single Locomotive Consist	B20	12-10
3	NC 1859	Single Locomotive Consist	B20	12-2
4	NC 1859	Single Locomotive Consist	B20	12-3
5	NC 1859	Single Locomotive Consist	B20	12-14
6	NC 1859	Single Locomotive Consist	B20	12-12
7	NC 1859	Single Locomotive Consist	B20	12-8
8	NC 1859	Single Locomotive Consist	B20	12-16
9	NC 1859	Single Locomotive Consist	B20	12-13
10	NC 1859	Single Locomotive Consist	B20	12-15
11	NC 1859	Single Locomotive Consist	B20	12-9
12	NC 1859	Single Locomotive Consist	B20	12-11
13	NC 1859	Single Locomotive Consist	B20	12-7
14	NC 1871	Double-Powered Push/Pull Consist	ULSD	7-6
15	NC 1871	Double-Powered Push/Pull Consist	ULSD	7-4
16	NC 1871	Double-Powered Push/Pull Consist	ULSD	7-2
17	NC 1797	Single Locomotive Consist	B20	10-4
18	NC 1984	Double-Powered Push/Pull Consist	ULSD	9-6
19	NC 1797	Single Locomotive Consist	ULSD	1-2
20	NC 1859	Double-Powered Tandem Consist	ULSD	4-2
21	NC 1859	Double-Powered Tandem Consist	ULSD	4-4
22	NC 1859	Single Locomotive Consist	ULSD	3-2
23	NC 1810	Single Locomotive Consist	ULSD	2-3
24	NC 1859	Double-Powered Tandem Consist	ULSD	4-5
25	NC 1797	Single Locomotive Consist	ULSD	1-5
26	NC 1859	Single Locomotive Consist	ULSD	3-6
27	NC 1797	Single Locomotive Consist	ULSD	1-5
28	NC 1859	Single Locomotive Consist	ULSD	3-4
29	NC 1810	Single Locomotive Consist	ULSD	2-1
30	NC 1859	Double-Powered Tandem Consist	ULSD	4-1
31	NC 1859	Single Locomotive Consist	ULSD	3-3
32	NC 1810	Single Locomotive Consist	B20	11-3
33	NC 1797	Single Locomotive Consist	ULSD	1-1
34	NC 1859	Double-Powered Tandem Consist	ULSD	4-3
35	NC 1797	Single Locomotive Consist	ULSD	1-4
36	NC 1797	Single Locomotive Consist	ULSD	1-3
37	NC 1859	Single Locomotive Consist	ULSD	3-5
38	NC 1859	Single Locomotive Consist	ULSD	3-1
39	NC 1810	Single Locomotive Consist	ULSD	2-5
40	NC 1893	Single Locomotive Consist	ULSD	5-6
41	NC 1871	Single-Powered Push/Pull Consist	ULSD	6-5
42	NC 1871	Single-Powered Push/Pull Consist	ULSD	6-1
43	NC 1871	Single-Powered Push/Pull Consist	ULSD	6-3
44	NC 1984	Single-Powered Push/Pull Consist	ULSD	8-3
45	NC 1984	Single-Powered Push/Pull Consist	ULSD	8-1

^a Trip ID X-Y is defined as the Yth measurement for Locomotive, Consist, and Fuel (LCF) ID X. For example, Trip ID 12-4 indicates the 4th measurement for LCF ID 12. The LCF ID is defined in Table 3-2.

Table B-20. The Maximum and Minimum Train Trip Fuel Use and Emissions (TTFUEs) Estimated for each Measured Trajectory Used to Normalize TTFUEs Given in Figure 3-5 of Chapter 3.

Specie	Train Trip Fuel Use and Emissions	
	Minimum (g) ^a	Maximum (g) ^a
Fuel Use	309000	524000
CO ₂ Emissions	974000	1650000
CO Emissions	1840	4000
HC Emissions	4030	6000
NO _x Emissions	24000	36500
PM Emissions	694	1194

^a These numbers are minimum and maximum among the 45 trajectory IDs given in Table B-25.

B.6 Inter-Locomotive, -Consist, and -Fuel Variability

To quantify inter-LCF variability in fuel use and emissions, estimated TTFUEs and the number of hotspots were compared. These LCFs were compared based on all trajectories that met data completeness criteria. To quantify inter-locomotive variability, a comparison was made among different locomotives operated in the same consist and fuel, e.g., LCF IDs 1, 2, 3, and 5. To quantify inter-consist variability, a comparison was made among different consists operated with the same locomotive and fuel, e.g., LCF IDs 3 versus 4, 6 versus 7, and 8 versus 9. To quantify inter-fuel variability, a comparison was made among LCF IDs 1, 2, 3 versus 10, 11, and 12, respectively. TTFUEs and the number of absolute hotspots are given in Table B-28, and Table B-29, respectively. These tables are interpreted in Chapter 3.

Table B-21. Comparison Among Average Estimated Train Total Fuel Use and Emissions for 12 Combinations of Locomotives, Consist Types, and Fuels Each Assumed to Operate on the 45 Real-World Trajectories that Met Data Completeness Criteria.

LCF ID	Locomotive ^a	Consist Type ^b	Fuel ^c	Average Train Total Fuel Use and Emissions					
				Fuel Use (kg)	CO ₂ Emissions (kg)	CO Emissions (g)	HC Emissions (g)	NO _x Emissions (g)	PM Emissions (g)
1	NC1797	Single Locomotive Consist	ULSD	587	1860	3430	7110	50800	840
2	NC1810	Single Locomotive Consist	ULSD	483	1520	3720	7480	20900	920
3	NC1859	Single Locomotive Consist	ULSD	486	1550	2840	3810	28200	880
4	NC1859	Double-Powered Tandem	ULSD	674	2150	5050	6580	40200	1590
5	NC1893	Single Locomotive Consist	ULSD	422	1340	2500	3400	24700	N/A
6	NC1871	Single-Powered Push/Pull	ULSD	533	1690	3050	3000	50600	700
7	NC1871	Double-Powered Push/Pull	ULSD	520	1660	5570	7150	56400	1610
8	NC1984	Single-Powered Push/Pull	ULSD	587	1850	5760	5530	41200	1380
9	NC1984	Double-Powered Push/Pull	ULSD	602	1900	6160	8040	49100	2540
10	NC1797	Single Locomotive Consist	B20	507	1570	2770	5540	49200	970
11	NC1810	Single Locomotive Consist	B20	433	1360	3110	5170	23100	870
12	NC1859	Single Locomotive Consist	B20	564	1800	3710	4190	19500	980

^a Only the measured locomotive is indicated for the train consists with two locomotives.

^b Consist: (1) SLC: Single Locomotive Consist; (2) DP-TC: Double-powered Tandem Consist; (3) DP-P/PC: Double-powered Push/Pull Consist; and (4) SP-P/PC: Single-powered Push/Pull Consist.

^c Fuel: Ultra-Low Sulfur Diesel (ULSD); B20: 20% blend of biodiesel in diesel.

Table B-22. Comparison Among Estimated Average Number of Absolute Hotspots for 12 Combinations of Locomotives, Consist Types, and Fuels Each Assumed to Operate on the 45 Real-World Trajectories that Met Data Completeness Criteria.

LCF ID	Locomotive ^a	Consist Type ^b	Fuel ^c	Number of Absolute Hotspots ^d					
				Fuel Use	CO ₂ Emissions	CO Emissions	HC Emissions	NO _x Emissions	PM Emissions
1	NC1797	Single Locomotive Consist	ULSD	111	111	110	109	110	108
2	NC1810	Single Locomotive Consist	ULSD	91	91	122	118	45	117
3	NC1859	Single Locomotive Consist	ULSD	92	92	92	59	62	112
4	NC1859	Double-Powered Tandem	ULSD	179	180	144	115	95	153
5	NC1893	Single Locomotive Consist	ULSD	79	81	56	77	53	N/A
6	NC1871	Single-Powered Push/Pull	ULSD	143	141	112	49	164	85
7	NC1871	Double-Powered Push/Pull	ULSD	121	122	180	154	183	230
8	NC1984	Single-Powered Push/Pull	ULSD	149	147	157	98	132	181
9	NC1984	Double-Powered Push/Pull	ULSD	155	154	203	137	154	287
10	NC1797	Single Locomotive Consist	B20	96	93	92	87	108	122
11	NC1810	Single Locomotive Consist	B20	82	82	102	81	50	112
12	NC1859	Single Locomotive Consist	B20	117	115	122	66	44	124

^a Only the measured locomotive is indicated for the train consists with two locomotives.

^b Consist: (1) SLC: Single Locomotive Consist; (2) DP-TC: Double-powered Tandem Consist; (3) DP-P/PC: Double-powered Push/Pull Consist; and (4) SP-P/PC: Single-powered Push/Pull Consist.

^c Fuel: Ultra-Low Sulfur Diesel (ULSD); B20: 20% blend of biodiesel in diesel.

^d Absolute Hotspots: Segments with fuel use and emission rates (FUERs) in the top quintile based on all real-world measurements combined for all combinations of locomotives, consists, and fuels. For a route with 692 segments, typically there were expected to be 135 absolute hotspots.

B.7 Sensitivity to Passenger Cars

The average number of passenger cars for Amtrak is eight (Davis and Boundy, 2020), which is larger than the number of cars in the measured consists (Table 3-2 of Chapter 3). Therefore, the effect of a larger number of passenger cars on FUERs and hotspots was estimated. For the Piedmont rail, it is not possible to operate an eight-car train at 79 mph peak speed with only one locomotive. Thus, only double-powered consists including DP-TC and DP-P/P (LCF IDs 4, 7, and 9) can operate with 8 passenger cars. To assess the sensitivity of these three LCFs to variations in the number of passenger cars, these LCFs were compared based on all trajectories that met data completeness criteria. The base case comprised of LCF IDs 4, 7, and 9 were operated with 6, 4, and 5 passenger cars respectively. In Case 1, 2 and 1 passenger cars were added to LCF IDs 7 and 9, respectively such that the number of passenger cars in each of these three consists was 6. In case 2, 2 passenger cars were added to each consist to take the number of passenger cars to 8. TTFUEs and the number of absolute hotspots for base case versus 6 passenger cars, and for eight versus six passenger cars are given in Table B-30.

The sensitivity of TTFUEs and hotspots to the number of passenger cars for 3 selected LCFs are given in Table B-30. For Case 1 versus Base Case for LCF ID 7, train weight and average $\overline{LPD}_{12,t}$ were estimated to increase by 26% and 25%, respectively. However, 1 Hz and segment-average FUERs were estimated to increase between 5% and 20%, depending on species. The lowest percentage increase was estimated for HC emissions, whereas the highest percentage increase was estimated for PM emissions. As explained in Section 3.1, HC emission rates are least sensitive to change in $\overline{LPD}_{12,t}$, whereas PM emission rates are most sensitive to change in $\overline{LPD}_{12,t}$. The relative increase in FUERs was lower than the relative increase in $\overline{LPD}_{12,t}$ because, as explained in Section 3.1, engines are typically more thermodynamically efficient at higher $\overline{LPD}_{12,t}$. The estimated number of absolute hotspots increased between 2% for HC and 9% for PM. The percentage increase in the number of hotspots was lower than the corresponding percentage increase in segment-average FUERs. This was because segment-average FUERs increased for all segments, including those which were already hotspots, whereas the increase in segment-average FUERs for only a few non-hotspots was sufficient enough to cross the 80th percentile threshold quantified for absolute hotspots. For Case 1 versus Base Case for LCF ID 9, train weight and average $\overline{LPD}_{12,t}$ were estimated to each increase by 11%. However, 1 Hz and segment-average FUERs were estimated to increase between 2% and 9%, depending on species. The estimated number of absolute hotspots increased by 1% and 5%, depending on species.

For Case 2 versus Case 1, estimated weight and $\overline{LPD}_{12,t}$ increased by 22% and 21%, respectively. One Hz and segment-average FUERs were estimated to increase between 4% and 18%, respectively, depending on species. The estimated number of absolute hotspots increased between 2% and 9%, depending on species. Typically, energy intensity, defined as the energy consumed per unit passenger-mile decreases with the addition of passenger cars (Dick and DiDomenico, 2016; Elgowainy et al., 2018). However, the maximum number of passenger cars that can be added is determined by the capacity of the locomotive to propel the train for the desired speed trajectory (AREMA, 2020; Hay, 1982).

Table B-23. Comparison of Average Trip Total Fuel Use, Emissions, and Estimated Number of Absolute Hotspots for Double-Powered Push/Pull and Tandem Consists Each Assumed to Operate on the 45 Real-World Trajectories that Met Data Completeness Criteria.

Case	Number of Passenger Cars	LCF ID	Train Weight (tons)	Trip Fuel Use and Emissions						Number of Absolute Hotspots					
				Fuel (kg)	CO ₂ (kg)	CO (g)	HC (g)	NO _x (g)	PM (g)	Fuel	CO ₂	CO	HC	NO _x	PM
Base	6	4	630	674	2150	5050	6580	40200	1590	179	180	144	115	95	153
	4	7	500	520	1660	5570	7150	56400	1610	121	122	180	154	183	230
	5	9	570	602	1900	6160	8040	49100	2540	155	154	203	137	154	287
	Average			599	1903	5593	7257	48567	1913	152	152	176	135	144	223
1	6	4	630	674	2150	5050	6580	40200	1590	179	180	144	115	95	153
		7	630	589	1880	6310	8180	69490	1840	141	143	190	162	195	240
		9	630	639	2020	6540	8450	51580	2720	165	162	209	146	157	297
	Average			634	2020	634	2017	5967	7737	53757	2050	162	162	181	141
2	8	4	770	755	2410	5760	7240	45020	1760	202	203	161	135	113	177
		7	770	654	2090	6820	9320	75740	2010	163	160	196	167	203	245
		9	770	715	2260	7380	9540	58810	2990	185	183	212	177	159	303
	Average			708	2253	708	2253	6653	8700	59857	2253	183	182	190	160
Difference of Case 2 versus Case 1 (%)				12	12	12	12	12	12	11	10	13	13	5	13

B.7 Delayed versus On-Time Trips

Table B-24. Estimated Percentage Increase in Trip Total Fuel Use and Emissions for Delayed versus On-Time Trips for the Case of **Delays at Stations. Aggressive On-Time Trajectories^a** are used as the Baseline for Estimating the Delay-Associated Fuel Use and Emissions Increment.

Trajectory ID ^b	Percentage Increase in Trip Total Fuel Use and Emissions for Delayed versus On-Time Trips (%)					
	Fuel Use	CO ₂	CO	HC	NO _x	PM
1	0.03%	0.04%	0.77%	0.11%	0.12%	0.34%
2	0.03%	0.04%	0.75%	0.11%	0.12%	0.34%
3	0.03%	0.04%	0.73%	0.11%	0.12%	0.34%
4	0.03%	0.04%	0.75%	0.11%	0.11%	0.34%
5	0.03%	0.04%	0.71%	0.11%	0.11%	0.34%
6	0.03%	0.04%	0.71%	0.11%	0.11%	0.34%
7	0.03%	0.04%	0.70%	0.11%	0.11%	0.33%
9	0.03%	0.04%	0.69%	0.11%	0.11%	0.33%
10	0.03%	0.04%	0.67%	0.11%	0.11%	0.32%
11	0.03%	0.04%	0.70%	0.10%	0.10%	0.31%
12	0.03%	0.04%	0.67%	0.11%	0.11%	0.32%
13	0.03%	0.04%	0.67%	0.11%	0.10%	0.31%
14	0.03%	0.03%	0.51%	0.11%	0.10%	0.30%
15	0.03%	0.03%	0.48%	0.11%	0.10%	0.29%
16	0.03%	0.03%	0.44%	0.11%	0.10%	0.29%
17	0.02%	0.03%	0.39%	0.12%	0.10%	0.28%
19	0.02%	0.03%	0.44%	0.10%	0.08%	0.26%
21	0.02%	0.03%	0.35%	0.11%	0.09%	0.26%
23	0.02%	0.03%	0.35%	0.11%	0.09%	0.25%
24	0.02%	0.03%	0.35%	0.10%	0.08%	0.25%
25	0.02%	0.03%	0.37%	0.11%	0.08%	0.25%
27	0.02%	0.03%	0.40%	0.10%	0.08%	0.24%
28	0.02%	0.03%	0.35%	0.10%	0.08%	0.24%
29	0.02%	0.03%	0.32%	0.11%	0.08%	0.25%
31	0.02%	0.02%	0.33%	0.11%	0.08%	0.24%
32	0.02%	0.02%	0.35%	0.11%	0.08%	0.24%
33	0.02%	0.02%	0.34%	0.10%	0.08%	0.24%
34	0.02%	0.02%	0.32%	0.11%	0.08%	0.24%
35	0.02%	0.02%	0.33%	0.10%	0.08%	0.24%
36	0.02%	0.02%	0.33%	0.10%	0.08%	0.24%
38	0.02%	0.02%	0.32%	0.10%	0.08%	0.24%
39	0.02%	0.02%	0.30%	0.11%	0.08%	0.24%
40	0.02%	0.02%	0.32%	0.10%	0.08%	0.23%
42	0.02%	0.02%	0.24%	0.10%	0.07%	0.20%
43	0.02%	0.02%	0.24%	0.10%	0.07%	0.20%
Average	0.02%	0.03%	0.48%	0.11%	0.09%	0.28%

Note: ^a Aggressive on-time trajectories include Trajectory IDs 31, 42, and 43.

^b Trajectory ID is defined in Table B-19.

Table B-25. Estimated Percentage Increase in Trip Total Fuel Use and Emissions for Delayed versus On-Time Trips for the Case of **Delays at Stations. Non-Aggressive On-Time Trajectories** ^a are used as the Baseline for Estimating the Delay-Associated Fuel Use and Emissions Increment.

Trajectory ID ^b	Percentage Increase in Trip Total Fuel Use and Emissions for Delayed versus On-Time Trips (%)					
	Fuel Use	CO ₂	CO	HC	NO _x	PM
1	0.13%	0.14%	0.02%	0.30%	0.18%	0.34%
2	0.13%	0.14%	0.02%	0.32%	0.17%	0.34%
3	0.13%	0.14%	0.02%	0.33%	0.17%	0.35%
4	0.13%	0.13%	0.02%	0.32%	0.17%	0.34%
5	0.13%	0.13%	0.02%	0.32%	0.17%	0.34%
6	0.13%	0.13%	0.02%	0.32%	0.17%	0.34%
7	0.13%	0.13%	0.02%	0.30%	0.17%	0.33%
9	0.12%	0.13%	0.02%	0.32%	0.16%	0.33%
10	0.12%	0.12%	0.02%	0.31%	0.16%	0.32%
11	0.12%	0.12%	0.02%	0.29%	0.16%	0.31%
12	0.12%	0.12%	0.02%	0.31%	0.16%	0.32%
13	0.12%	0.12%	0.02%	0.30%	0.16%	0.32%
14	0.11%	0.11%	0.01%	0.31%	0.15%	0.30%
15	0.10%	0.11%	0.01%	0.31%	0.15%	0.29%
16	0.10%	0.11%	0.01%	0.31%	0.14%	0.29%
17	0.09%	0.10%	0.01%	0.34%	0.14%	0.28%
19	0.09%	0.09%	0.01%	0.28%	0.13%	0.26%
21	0.09%	0.09%	0.01%	0.31%	0.13%	0.26%
23	0.08%	0.09%	0.01%	0.31%	0.13%	0.25%
24	0.08%	0.09%	0.01%	0.29%	0.12%	0.25%
25	0.08%	0.09%	0.01%	0.31%	0.12%	0.25%
27	0.08%	0.09%	0.01%	0.27%	0.12%	0.24%
28	0.08%	0.09%	0.01%	0.29%	0.12%	0.24%
29	0.08%	0.09%	0.01%	0.32%	0.13%	0.25%
31	0.08%	0.08%	0.01%	0.30%	0.12%	0.24%
32	0.08%	0.08%	0.01%	0.30%	0.12%	0.24%
33	0.08%	0.08%	0.01%	0.30%	0.12%	0.24%
34	0.08%	0.08%	0.01%	0.30%	0.12%	0.24%
35	0.08%	0.08%	0.01%	0.30%	0.12%	0.24%
36	0.08%	0.08%	0.01%	0.30%	0.12%	0.24%
38	0.08%	0.08%	0.01%	0.29%	0.12%	0.24%
39	0.08%	0.08%	0.01%	0.32%	0.12%	0.24%
40	0.08%	0.08%	0.01%	0.29%	0.12%	0.23%
42	0.06%	0.07%	0.01%	0.29%	0.10%	0.20%
43	0.06%	0.07%	0.01%	0.28%	0.10%	0.20%
Average	0.10%	0.10%	0.01%	0.30%	0.14%	0.28%

Note: ^a Non-aggressive on-time trajectories include all on-time trajectories except for Trajectory IDs 31, 42, and 43.

^b Trajectory ID is defined in Table B-19.

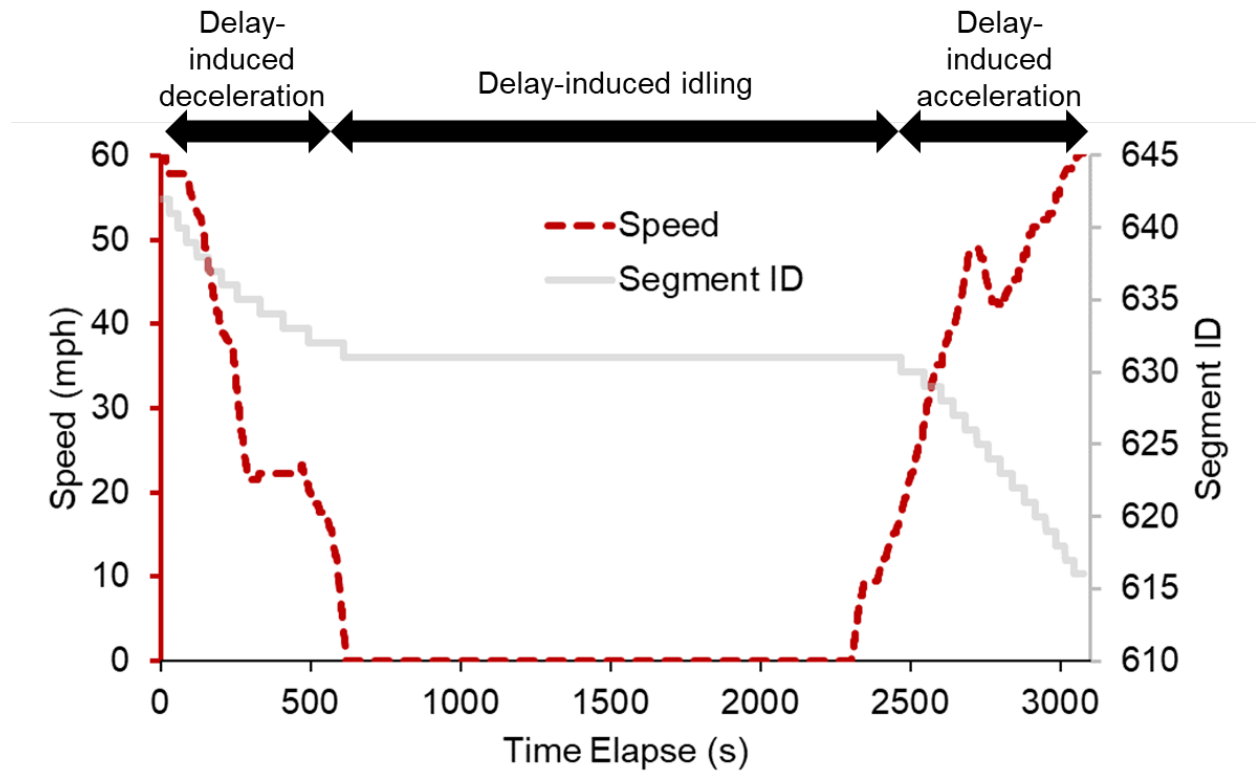


Figure B-17. An Illustration of Identification of Delay-Induced Deceleration, Idling, and Acceleration Trajectories and Associated Segments for a Trip with Delay between Stations. Trajectory ID 45 is given in this example. Trajectory ID is defined in Table B-19.

Table B-26. Estimated Percentage Increase in Trip Total Fuel Use and Emissions for Delayed versus On-Time Trips for the Case of **Delays between Stations. Aggressive On-Time Trajectories** ^a are used as the Baseline for Estimating the Delay-Associated Fuel Use and Emissions Increment.

Trajectory ID ^b	Percentage Increase in Trip Total Fuel Use and Emissions for Delayed versus On-Time Trips (%)					
	Fuel Use	CO ₂	CO	HC	NO _x	PM
1	1.4%	1.4%	0.8%	0.9%	3.0%	5.2%
2	1.3%	1.3%	0.8%	0.9%	2.9%	5.3%
3	1.3%	1.3%	0.8%	0.9%	2.9%	5.3%
4	1.3%	1.3%	0.8%	0.9%	2.9%	5.2%
5	1.3%	1.3%	0.8%	0.9%	2.9%	5.2%
6	1.3%	1.3%	0.8%	0.9%	2.9%	5.2%
7	1.3%	1.3%	0.8%	0.9%	2.9%	5.1%
9	1.3%	1.3%	0.8%	0.9%	2.9%	5.1%
10	1.3%	1.3%	0.8%	0.9%	2.8%	5.0%
11	1.3%	1.3%	0.8%	0.9%	2.8%	4.9%
12	1.3%	1.3%	0.8%	0.9%	2.8%	5.0%
13	1.3%	1.3%	0.8%	0.9%	2.8%	4.9%
14	1.3%	1.3%	0.8%	0.9%	2.8%	4.7%
15	1.2%	1.2%	0.8%	0.9%	2.8%	4.6%
16	1.2%	1.2%	0.8%	0.9%	2.7%	4.5%
17	1.2%	1.2%	0.8%	0.9%	2.7%	4.5%
19	1.2%	1.2%	0.8%	0.9%	2.6%	4.2%
21	1.2%	1.2%	0.8%	0.9%	2.6%	4.2%
23	1.2%	1.2%	0.8%	0.9%	2.6%	4.1%
24	1.2%	1.2%	0.8%	0.9%	2.6%	4.1%
25	1.2%	1.2%	0.8%	0.9%	2.6%	4.1%
27	1.2%	1.2%	0.8%	0.9%	2.5%	4.0%
28	1.2%	1.2%	0.8%	0.9%	2.6%	4.0%
29	1.2%	1.2%	0.8%	0.9%	2.6%	4.1%
31	1.2%	1.2%	0.8%	0.9%	2.6%	4.0%
32	1.2%	1.2%	0.8%	0.9%	2.6%	4.0%
33	1.2%	1.2%	0.8%	0.9%	2.6%	3.9%
34	1.1%	1.2%	0.8%	0.9%	2.6%	4.0%
35	1.1%	1.1%	0.8%	0.9%	2.6%	3.9%
36	1.1%	1.1%	0.8%	0.9%	2.5%	3.9%
38	1.1%	1.1%	0.8%	0.9%	2.5%	3.9%
39	1.1%	1.1%	0.8%	0.9%	2.6%	4.0%
40	1.1%	1.1%	0.8%	0.9%	2.5%	3.8%
42	1.1%	1.1%	0.8%	0.9%	2.4%	3.4%
43	1.1%	1.1%	0.8%	0.9%	2.4%	3.4%
Average	1.2%	1.2%	0.8%	0.9%	2.7%	4.4%

Note: ^a Aggressive on-time trajectories include Trajectory IDs 31, 42, and 43.

^b Trajectory ID is defined in Table B-19.

Table B-27. Estimated Percentage Increase in Trip Total Fuel Use and Emissions for Delayed versus On-Time Trips for the Case of **Delays between Stations. Non-Aggressive On-Time Trajectories** ^a are used as the Baseline for Estimating the Delay-Associated Fuel Use and Emissions Increment.

Trajectory ID ^b	Percentage Increase in Trip Total Fuel Use and Emissions for Delayed versus On-Time Trips (%)					
	Fuel Use	CO ₂	CO	HC	NO _x	PM
1	4.0%	4.0%	2.6%	2.8%	8.6%	14%
2	4.0%	4.0%	2.6%	2.8%	8.5%	14%
3	4.0%	4.0%	2.6%	2.8%	8.6%	14%
4	3.9%	4.0%	2.6%	2.8%	8.5%	14%
5	3.9%	3.9%	2.6%	2.8%	8.5%	14%
6	3.9%	3.9%	2.6%	2.8%	8.5%	14%
7	3.9%	3.9%	2.6%	2.8%	8.5%	13%
9	3.9%	3.9%	2.6%	2.8%	8.4%	14%
10	3.8%	3.9%	2.6%	2.8%	8.3%	13%
11	3.8%	3.8%	2.6%	2.8%	8.2%	13%
12	3.8%	3.8%	2.6%	2.8%	8.3%	13%
13	3.8%	3.8%	2.6%	2.8%	8.2%	13%
14	3.7%	3.7%	2.6%	2.8%	8.2%	13%
15	3.7%	3.7%	2.6%	2.8%	8.1%	12%
16	3.7%	3.7%	2.6%	2.8%	8.0%	12%
17	3.6%	3.6%	2.6%	2.8%	8.0%	12%
19	3.5%	3.6%	2.6%	2.8%	7.7%	11%
21	3.5%	3.5%	2.6%	2.8%	7.8%	11%
23	3.5%	3.5%	2.6%	2.8%	7.7%	11%
24	3.5%	3.5%	2.6%	2.8%	7.7%	11%
25	3.5%	3.5%	2.6%	2.8%	7.6%	11%
27	3.5%	3.5%	2.6%	2.8%	7.5%	11%
28	3.5%	3.5%	2.6%	2.8%	7.6%	11%
29	3.5%	3.5%	2.6%	2.8%	7.7%	11%
31	3.5%	3.5%	2.6%	2.8%	7.6%	11%
32	3.5%	3.5%	2.6%	2.8%	7.6%	11%
33	3.5%	3.5%	2.6%	2.8%	7.6%	11%
34	3.5%	3.5%	2.6%	2.8%	7.6%	11%
35	3.4%	3.5%	2.6%	2.8%	7.6%	11%
36	3.4%	3.5%	2.6%	2.8%	7.5%	11%
38	3.4%	3.4%	2.6%	2.8%	7.5%	10%
39	3.4%	3.4%	2.6%	2.8%	7.6%	11%
40	3.4%	3.4%	2.6%	2.8%	7.5%	10%
42	3.3%	3.3%	2.6%	2.8%	7.2%	9%
43	3.3%	3.3%	2.6%	2.8%	7.1%	9%
Average	3.6%	3.6%	2.6%	2.8%	7.9%	12%

Note: ^a Non-aggressive on-time trajectories include all on-time trajectories except for Trajectory IDs 31, 42, and 43.

^b Trajectory ID is defined in Table B-19.

B.8 References Cited in Appendix B

- 40 CFR 1033, 1998. Control of Emissions from Locomotives. Fed. Regist. 63, 18978–19084.
- 40 CFR 1065, S.J., 2005. Field Testing and Portable Emission Measurement Systems. Fed. Regist. 70, 40599–40604.
- Amtrak, 2018. Amtrak Sustainability Report 2016-17. National Passenger Rail Corporation (Amtrak).
- AREMA, 2020. American Railway Engineering and Maintenance-of-way Association Manual for Railway Engineering. Lanham, MD.
- Bergin, M., Harrell, M., Janssen, M., 2012. ERTAC Rail Emissions Inventory Part 1: Class I Line-Haul Locomotives.
- Boroujeni, B.Y., Frey, H.C., 2014. Road grade quantification based on global positioning system data obtained from real-world vehicle fuel use and emissions measurements. Atmos. Environ. 85, 179–186.
- Boroujeni, B.Y., Frey, H.C., Sandhu, G.S., 2013. Road grade measurement using in-vehicle, stand-alone GPS with barometric altimeter. J. Transp. Eng. 139, 605–611.
- Butler, J., Gierczak, C., Liscombe, P., Lesko, J., New, D., 1995. Factors Affecting the NDIR Measurement of Exhaust Hydrocarbons, in: Published by the Coordinating Research Council, Published for the CRC 5th On-Road Vehicle Emissions Workshop.
- Caretto, L., 2008. Revised Inventory Guidance for Locomotive Emissions. Prep. Sierra Res. Inc Southeast. State Air Resour. Manag. Inc Www Metro4-Sesarm OrgpubsrailroadFinalGuidance Pdf Accessed Oct 20.
- Drish, W.F., 1992. Train energy model version 2.0 technical manual. Publication SD-040, Association of American Railroads, Washington, D.C.
- Elgowainy, A., Vyas, A., Biruduganti, M., Shurland, M., 2018. Railroad Energy Intensity and Criteria Air Pollutant Emissions (No. DOT/FRA/ORD-18/34). Argonne National Laboratory, Argonne, IL United States 60439.
- EPA, 2002. A comprehensive analysis of biodiesel impacts on exhaust emissions (No. Prepared for US EPA. 420-P-02-001), US Environmental Protection Agency. Washington DC.
- EPA, 1998. Locomotive Emission Standards: Regulatory Support Document (No. EPA/98-04). U.S. Environmental Protection Agency, Ann Arbor, MI.
- Flagan, R.C., Seinfeld, J.H., 2012. Fundamentals of air pollution engineering. Courier Corporation.
- Frey, H.C., Graver, B.M., 2012. Measurement and evaluation of fuels and technologies for passenger rail service in North Carolina. Prepared by North Carolina State University for North Carolina Department of Transportation.
- Frey, H.C., Hu, J., 2015. Measurement of Locomotive Head End Power Engine Fuel and Emissions (Technical Report No. 0704–0188). Prepared by North Carolina State University for North Carolina Department of Transportation, Raleigh, NC.

- Frey, H.C., Hu, J., Graver, B.M., 2016. Locomotive Biofuel Study (Technical Report No. DOT/FRA/ORD-16/04). Prepared by North Carolina State University for Federal Railroad Administration.
- Frey, H.C., Rastogi, N., 2019. Managing Energy and Emissions for Rail Operations (No. FHWA/NC/2018-09). Prepared by North Carolina State University for North Carolina Department of Transportation, Raleigh, NC.
- Frey, H.C., Rastogi, N., 2018. Evaluation of Locomotive Emissions Reduction Strategies (No. FHWA/NC/2016-20). Prepared by North Carolina State University for North Carolina Department of Transportation, Raleigh, NC.
- Fritz, S.G., 2000. Diesel fuel effects on locomotive exhaust emissions. Prepared for California Air Resources Board by Southwest Research Institute, San Antonio, TX; Sacramento, CA.
- Gbologah, F.E., Xu, Y., Rodgers, M.O., Guensler, R., 2014. Demonstrating a Bottom-Up Framework for Evaluating Energy and Emissions Performance of Electric Rail Transit Options. *Transp. Res. Rec.* 2428, 10–17. <https://doi.org/10.3141/2428-02>
- General Motors of Canada Limited, 1994. F59PH Locomotive Service Manual, Third Edition. Ontario, Canada.
- GlobalMRV, 2014. Axion R/S™ Basic User's Manual.
- Graver, B.M., Frey, H., 2013. Comparison of Locomotive Emissions Measured During Dynamometer Versus Rail Yard Engine Load Tests. *Transp. Res. Rec. J. Transp. Res. Board* 23–33.
- Graver, B.M., Frey, H.C., 2016. Highway Vehicle Emissions Avoided by Diesel Passenger Rail Service Based on Real-World Data. *Urban Rail Transit* 2, 153–171.
- Graver, B.M., Frey, H.C., 2015. Comparison of Over-the-Rail and Rail Yard Measurements of Diesel Locomotives. *Environ. Sci. Technol.* 49, 13031–13039.
- Graver, B.M., Frey, H.C., Hu, J., 2016. Effect of Biodiesel Fuels on Real-World Emissions of Passenger Locomotives. *Environ. Sci. Technol.* 50, 12030–12039.
- Hay, W.W., 1982. *Railroad engineering*. John Wiley & Sons, New York.
- Kim, S.W., Kwon, H.B., Kim, Y.G., Park, T.W., 2006. Calculation of resistance to motion of a high-speed train using acceleration measurements in irregular coasting conditions. *Proc. Inst. Mech. Eng. Part F J. Rail Rapid Transit* 220, 449–459.
- Lukaszewicz, P., 2009. Running resistance and energy consumption of ore trains in Sweden. *Proc. Inst. Mech. Eng. Part F J. Rail Rapid Transit* 223, 189–197.
- Miller, J.W., Durbin, T., Johnson, K., Cocker III, D., 2006. Evaluation of Portable Emissions Measurement Systems (PEMS) for Inventory Purposes and the Not-To-Exceed Heavy-Duty Diesel Engine Regulation (No. 03–345). Prepared for California Air Resources Board by University of California Riverside, Riverside, CA.
- Nakamura, H., Kihara, N., Adachi, M., Nakamura, S., Ishida, K., 2003. Development of hydrocarbon analyzer using heated-NDIR method and its application to on-board mass emission measurement system. *JSAE Rev.* 24, 127–133.

- Norfolk Southern, Center for Alternative Fuels Engines and Emissions, n.d. Locomotive Emissions Testing Facility. Altoona, Pennsylvania.
- Pang, S.-H., Frey, H.C., Rasdorf, W.J., 2009. Life cycle inventory energy consumption and emissions for biodiesel versus petroleum diesel fueled construction vehicles. *Environ. Sci. Technol.* 43, 6398–6405.
- Profillidis, V.A., 2014. *Railway management and engineering*. Ashgate Publishing, Ltd., Burlington, VT.
- Rastogi, N., Frey, H.C., 2021. Characterizing Fuel Use and Emissions Hotspots for a Diesel-operated Passenger Rail Service. *Submitt. Environ. Sci. Technol.*
- Rastogi, N., Frey, H.C., 2018. Estimation of Rail Grade and Horizontal Curvature from Non-Proprietary Data Sources, in: *Proceedings of the Transportation Research Board 97th Annual Meeting*, 18-06366. Washington, D.C.
- Sandhu, G., Frey, H., 2013. Effects of errors on vehicle emission rates from portable emissions measurement systems. *Transp. Res. Rec. J. Transp. Res. Board* 10–19.
- Sensors Inc., 2011. SEMTECH-DS: On Board Vehicle Emissions Analyzer User Manual (No. 9510–086), Revision 2.02. Saline, MI.
- Singer, B.C., Harley, R.A., Littlejohn, D., Ho, J., Vo, T., 1998. Scaling of infrared remote sensor hydrocarbon measurements for motor vehicle emission inventory calculations. *Environ. Sci. Technol.* 32, 3241–3248.
- Stephens, R.D., Cadle, S.H., Qian, T.Z., 1996a. Analysis of remote sensing errors of omission and commission under FTP conditions. *J. Air Waste Manag. Assoc.* 46, 510–516.
- Stephens, R.D., Mulawa, P.A., Giles, M.T., Kennedy, K.G., Grobiicki, P.J., Cadle, S.H., Knapp, K.T., 1996b. An experimental evaluation of remote sensing-based hydrocarbon measurements: A comparison to FID measurements. *J. Air Waste Manag. Assoc.* 46, 148–158.
- SwRI, 2016. *SwRI Upgrades Locomotive Technology Center to Meet EPA Certification Guidelines*. San Antonio, TX.
- Tsay, R.S., 2010. *Analysis of financial time series*, 3rd ed. Wiley, Hoboken, N.J.
- Tsolakis, A., Megaritis, A., Wyszynski, M.L., Theinnoi, K., 2007. Engine performance and emissions of a diesel engine operating on diesel-RME (rapeseed methyl ester) blends with EGR (exhaust gas recirculation). *Energy* 32, 2072–2080.
- Vojtisek, M., Kotek, M., 2014. Estimation of Engine Intake Air Mass Flow Using a Generic Speed-Density Method. *J. Middle Eur. Constr. Des. Cars* 12, 7–15.
- Vojtisek-Lom, M., Allsop, J.E., 2001. Development of Heavy-Duty Diesel Portable, On-Board Mass Exhaust Emissions Monitoring System with NO_x, CO₂ and Qualitative PM Capabilities. SAE Technical Paper.
- Vu, D., Szente, J., Loos, M., Maricq, M., 2020. How Well Can mPEMS Measure Gas Phase Motor Vehicle Exhaust Emissions? SAE Technical Paper.

- Weaver, C.S., Balam-Almanza, M.V., 2001. Development of the 'RAVEM' Ride-Along Vehicle Emission Measurement System for Gaseous and Particulate Emissions. SAE Technical Paper.
- Weaver, C.S., Petty, L.E., 2004. Reproducibility and accuracy of on-board emission measurements using the RAVEM™ System. SAE Technical Paper.
- Wong, T.-T., 2015. Performance evaluation of classification algorithms by k-fold and leave-one-out cross validation. *Pattern Recognit.* 48, 2839–2846.
<https://doi.org/10.1016/j.patcog.2015.03.009>
- Wooldridge, J.M., 2016. *Introductory econometrics: A modern approach*. Nelson Education.

Appendix C. User Manual for Piedmont Passenger Train Fuel Use and Emission Estimator Software

C.1. Introduction

C.1.1 What is this Software?

The Piedmont Passenger Train Fuel Use and Emission Estimator Software is used to estimate trip and station-to-station segment based fuel use and emissions for Piedmont passenger trains. This software tool was developed based on data collected by the Mobile Air Pollutant Emissions Laboratory at North Carolina State University using Portable Emission Measurement Systems from 2013 to 2019 (1–5). The software tool is applicable to passenger trains with no more than 2 locomotives, no more than 6 passenger cars, and fueled with ultra-low sulfur diesel or 20% blend of biodiesel (B20), for speed limit of no more than 79 mph, for track grade within $\pm 2\%$, and for track curvature within 5 degrees.

C.1.2 Purpose

The purpose is to develop a planning-level software for estimating the fuel use and emissions of a typical Piedmont train operation based on second-by-second train speed, track grade, and track curvature.

C.1.3 System Requirements

This software requires the following configurations:

- An computer running Microsoft Windows 10 and 11
- A Microsoft Excel 2016 and newer (macro-enabled spreadsheet)
- At least 300 Megabytes of free hard disk space

For users whose macros in Excel have been enabled, no action is needed. For users whose macros in Excel have not been enabled, please follow the procedure below to enable macros:

- Open an Excel workbook
- Click the **File** tab
- Click **Options**
- Click **Trust Center**, and then click **Trust Center Settings**
- In the **Trust Center**, click **Macro Settings**
- In the **Macro Settings**, click **Enable all macros**
- Click **OK**

C.1.4 Copyright Notice

Microsoft Excel, Copyright © 2016, Microsoft Corporation. All Rights Reserved.

C.2 Introduction to Software Worksheet

C.2.1 Cover Page

This worksheet includes the name, authors, authors' affiliation, version number, release date, brief introduction, and key references for this software.

C.2.2 Input

This worksheet includes the only two required model inputs from users – a locomotive, consist, and fuel (LCF) ID and a train speed trajectory ID (Table 1 of the software). Users can confirm their selection of LCF ID and speed trajectory ID in Tables 2 and 3, respectively. Users can visualize the selected speed trajectory in Figure 1 of the software. A reference table for 12 LCF IDs (Table 4 of the software) is provided in this worksheet for users. A reference table for 45 train speed trajectory IDs (Table 5 of the software) is provided in this worksheet for users. This worksheet is also the user interface to run the software.

C.2.3 Output

This worksheet includes results based on running the software, including train information (Table 6 of the software), trip information (Table 7 of the software), as well as train activity (Table 8 of the software), total fuel use and emissions (Table 9, Figures 2 to 7 of the software for fuel use, carbon dioxide [CO₂] emissions, carbon monoxide [CO] emissions, hydrocarbons [HC] emissions, nitrogen oxides [NO_x] emissions, and particulate matter [PM] emissions, respectively), distance-based fuel use and emission rates (Table 10, Figures 8 to 13 of the software for fuel economy, CO₂ emission rates, CO emission rates, HC emission rates, NO_x emission rates, and PM emission rates, respectively), time-based fuel use and emission rates (Table 11, Figures 14 to 19 of the software for fuel use rates, CO₂ emission rates, CO emission rates, HC emission rates, NO_x emission rates, and PM emission rates, respectively), and fuel-based emission rates (Table 12, Figures 20 to 24 of the software for CO₂ emission rates, CO emission rates, HC emission rates, NO_x emission rates, and PM emission rates, respectively) for each station-to-station segment and whole trip.

C.2.4 Diagnostics

This worksheet includes diagnostics for travel time, fuel use, and emissions for each pollutant species by sub-models based on running the software. Sub-models were developed based on engine load, such as locomotive power demand (LPD). There are four sub-models. Sub-models corresponding to negative, zero, and peak engine load include Sub-Model 1, Sub-Model 2, and Sub-Model 4, respectively. Sub-Model 3 accounts for all other engine loads. Table C-1 below shows the definition of sub-models based on LPD.

Table C-1. Locomotive Power Demand Sub-Model Definition

Sub-Model	Speed (v_t mph)	12-Second Backwards Moving Average Locomotive Power Demand ($LPD_{12,t}$ kW)
1	> 0	< 0
2	$= 0$	$= 0$
3	> 0	$0 < LPD_{12,t} < 2519$
4	> 0	≥ 2519

Notes: 1. v_t : locomotive speed at time t ;

2. $LPD_{12,t}$: 12-second backwards moving average locomotive power demand at time t .

The Diagnostics worksheet includes results for:

- Travel time, fuel use, and emissions for the whole trip for each sub-model (Table 13 of the software);
- Travel time for each station-to-station segment and whole trip for each mode in Sub-Model 3 (Table 14 of the software);
- Travel time for each station-to-station segment and whole trip for each sub-model (Table 15 of the software);
- Percent of travel time spent in each sub-model for each station-to-station segment and whole Trip (Table 16, Figure 25 of the software);
- Fuel use for each station-to-station segment and whole trip for each sub-model (Table 17 of the software);
- Percent of fuel use in each sub-model for each station-to-station segment and whole trip (Table 18, Figure 26 of the software);
- CO₂ emissions for each station-to-station segment and whole trip for each sub-model (Table 19 of the software);
- Percent of CO₂ emissions in each sub-model for each station-to-station segment and whole trip (Table 20, Figure 27 of the software);
- CO emissions for each station-to-station segment and whole trip for each sub-model (Table 21 of the software);
- Percent of CO emissions in each sub-model for each station-to-station segment and whole trip (Table 22, Figure 28 of the software);
- HC emissions for each station-to-station segment and whole trip for each sub-model (Table 23 of the software);
- Percent of HC emissions in each sub-model for each station-to-station segment and whole trip (Table 24, Figure 29 of the software);
- NO_x emissions for each station-to-station segment and whole trip for each sub-model (Table 25 of the software);
- Percent of NO_x emissions in each sub-model for each station-to-station segment and whole trip (Table 26, Figure 30 of the software);
- PM emissions for each station-to-station segment and whole trip for each sub-model (Table 27 of the software); and
- Percent of PM emissions in each sub-model for each station-to-station segment and whole trip (Table 28, Figure 31 of the software);

C.2.5 1 Hz LPD Estimation

This worksheet includes second-by-second train activity data and estimated LPD based on the selected train speed trajectory ID (Table 29 of the software). The train activity data include speed, acceleration, track grade, and track curvature. The estimated second-by-second LPD is estimated by based on resistive forces opposing train motion, including starting, journal, flange, drag, acceleration, grade, and curvature. The second-by-second 12-second backwards moving average LPD is also quantified.

C.2.6 Grade Curve Spec Elevation Data

This worksheet includes model default input data for track grade and curvature by quarter-mile segments (Table 30 of the software), train specification (Tables 31 and 32 of the software), and

cumulative elevation gain for each station-to-station segment and whole trip (Table 33 of the software).

C.2.7 Sub-Model 1

This worksheet is the basis to quantify train fuel use and emission rates in Sub-Model 1. This worksheet default model default input data for train fuel use and emission rates for each LCF ID for Sub-Model 1 (Table 34 of the software).

C.2.8 Sub-Model 2

This worksheet is the basis to quantify train fuel use and emission rates in Sub-Model 2. This worksheet includes model default input data for train fuel use and emission rates for each LCF ID for Sub-Model 2 (Table 35 of the software).

C.2.9 Sub-Model 3 Regression

This worksheet is the basis to quantify Sub-Model 3 train fuel use and emission rates for LCFs and pollutants that were calibrated using quadratic regression models. This worksheet includes model default input data for Sub-Model 3 quadratic regression parameters to estimate fuel use rates for all LCF IDs (Table 36 of the software), CO₂ emission rates for all LCF IDs (Table 37 of the software), and NO_x emission rates for all LCF IDs except for LCF IDs 1 and 10 (Table 38 of the software).

C.2.10 Sub-Model 3 Modal

This worksheet is the basis to quantify Sub-Model 3 train fuel use and emission rates for LCFs and pollutants that were calibrated using modal models. This worksheet includes model default input data for Sub-Model 3 modal emission rates for CO for all LCF IDs (Table 39 of the software), for HC for all LCF IDs (Table 40 of the software), for PM for all LCF IDs (Table 41 of the software), and for NO_x for LCF IDs 1 and 10 (Table 42 of the software).

C.2.11 Sub-Model 4

This worksheet is the basis to quantify train fuel use and emission rates in Sub-Model 4. This worksheet includes default model input data for train fuel use and emission rates for each LCF ID for Sub-Model 4 (Table 43 of the software).

C.2.12 Trajectory Library

This worksheet includes second-by-second train activity data (e.g., speed, track grade, and track curvature) for all 45 speed trajectory IDs (Table 44 of the software). These activity data were collected and quantified based on over-the-rail measurements for Piedmont passenger trains between Raleigh and Charlotte.

C.3 Data Input, Running the Software, and Results Output

C.3.1 Data Input

In this section, users will learn how to enter data in the software. To enter input data, users need to go to the Input worksheet. Users only need to provide two inputs to the software, including a LCF ID and a train speed trajectory ID (Table 1 of the software).

Table 1. Model Inputs

Please Select a Locomotive, Consist, and Fuel (LCF) ID	1	<div style="border: 1px solid black; padding: 5px;"> Please click this cell and select a LCF ID from the drop-down list. Please refer to Table 4 to review details regarding LCF options. </div>
Please Select a Train Speed Trajectory ID	15	<div style="border: 1px solid black; padding: 5px;"> Please click this cell and select a Train Speed Trajectory ID from the drop-down list. Please refer to Table 5 to review details regarding speed trajectory options. </div>

There are 12 LCF IDs. Table 4 in the Input worksheet of the software shows a reference table for each LCF ID, including locomotive name, locomotive consist type, fuel type, blended after-treatment system used or not, number of passenger cars, train weight, and train length.

LCF ID	Locomotive	Locomotive Consist Type	Fuel Type	Blended After-Treatment System	Number of Passenger Cars	Train Weight (metric ton)	Train Length (m)
1	NC1797	Single Locomotive	Ultra-Low Sulfur Diesel	No	3	310	100
2	NC1810	Single Locomotive	Ultra-Low Sulfur Diesel	No	3	310	100
3	NC1859	Single Locomotive	Ultra-Low Sulfur Diesel	No	3	310	100
4	NC1859	Double-Powered Tandem	Ultra-Low Sulfur Diesel	No	6	630	190
5	NC1893	Single Locomotive	Ultra-Low Sulfur Diesel	No	3	310	100
6	NC1871	Single-Powered Push/Pull	Ultra-Low Sulfur Diesel	No	4	500	140
7	NC1871	Double-Powered Push/Pull	Ultra-Low Sulfur Diesel	No	4	500	140
8	NC1984	Single-Powered Push/Pull	Ultra-Low Sulfur Diesel	No	5	570	170
9	NC1984	Double-Powered Push/Pull	Ultra-Low Sulfur Diesel	No	5	570	170
10	NC1797	Single Locomotive	B20	No	3	310	100
11	NC1810	Single Locomotive	B20	No	3	310	100
12	NC1859	Single Locomotive	B20	No	3	310	100

Users can select a LCF ID from the drop-down list when clicking the cell.

Table 1. Model Inputs

Please Select a Locomotive, Consist, and Fuel (LCF) ID	1	<div style="border: 1px solid black; padding: 5px;"> Please click this cell and select a LCF ID from the drop-down list. Please refer to Table 4 to review details regarding LCF options. </div>
Please Select a Train Speed Trajectory ID	<div style="border: 1px solid black; padding: 2px;"> 1 2 3 4 5 6 7 8 </div>	<div style="border: 1px solid black; padding: 5px;"> Please click this cell and select a Train Speed Trajectory ID from the drop-down list. Please refer to Table 5 to review details regarding speed trajectory options. </div>

There are 45 train speed trajectory IDs. Table 5 in the Input worksheet of the software shows a reference table for each trajectory ID, including origin, destination, travel time, distance, and trip average speed. Users can select a speed trajectory ID from the drop-down list when clicking the cell.

Table 1. Model Inputs

Please Select a Locomotive, Consist, and Fuel (LCF) ID	1	<div style="border: 1px solid black; padding: 5px; margin-bottom: 5px;">Please click this cell and select a LCF ID from the drop-down list. Please refer to Table 4 to review details regarding LCF options.</div> <div style="border: 1px solid black; padding: 5px;">Please click this cell and select a Train Speed Trajectory ID from the drop-down list. Please refer to Table 5 to review details regarding speed trajectory options.</div>
Please Select a Train Speed Trajectory ID	15	

Click Here to Run

15
16
17
18
19
20
21
22

ow several minutes to run the model

Table 5. Reference Table for Train Speed Trajectory ID

Speed Trajectory ID	Origin	Destination	Travel Time (min)	Distance (mile)	Average Speed (mph)
1	Raleigh	Charlotte	173	163	57
2	Raleigh	Charlotte	174	160	55
3	Raleigh	Charlotte	174	164	56
4	Raleigh	Charlotte	178	168	56
5	Raleigh	Charlotte	179	164	55
6	Raleigh	Charlotte	180	169	56
7	Raleigh	Charlotte	180	160	53
8	Raleigh	Charlotte	180	159	53
9	Raleigh	Charlotte	180	159	53
10	Raleigh	Charlotte	181	157	52
11	Raleigh	Charlotte	182	160	53
12	Raleigh	Charlotte	187	171	55
13	Raleigh	Charlotte	188	169	54
14	Raleigh	Charlotte	188	171	54
15	Raleigh	Charlotte	190	173	55
16	Raleigh	Charlotte	196	168	51
17	Raleigh	Charlotte	197	166	51
18	Raleigh	Charlotte	197	167	51
19	Raleigh	Charlotte	200	168	50
20	Raleigh	Charlotte	203	162	48
21	Raleigh	Charlotte	204	173	51
22	Raleigh	Charlotte	204	169	50
23	Raleigh	Charlotte	224	170	45
24	Raleigh	Charlotte	242	170	42
25	Charlotte	Raleigh	173	156	54
26	Charlotte	Raleigh	174	156	54
27	Charlotte	Raleigh	175	160	55
28	Charlotte	Raleigh	178	166	56
29	Charlotte	Raleigh	180	166	56
30	Charlotte	Raleigh	183	164	54
31	Charlotte	Raleigh	184	170	56
32	Charlotte	Raleigh	191	161	50
33	Charlotte	Raleigh	191	165	52
34	Charlotte	Raleigh	193	171	53
35	Charlotte	Raleigh	195	173	53
36	Charlotte	Raleigh	196	173	53
37	Charlotte	Raleigh	197	170	52
38	Charlotte	Raleigh	198	163	49
39	Charlotte	Raleigh	201	172	51
40	Charlotte	Raleigh	202	171	51
41	Charlotte	Raleigh	206	165	48
42	Charlotte	Raleigh	207	167	48
43	Charlotte	Raleigh	208	165	48
44	Charlotte	Raleigh	215	169	47
45	Charlotte	Raleigh	228	172	45

Users can verify their selections for LCF ID and trajectory ID in Tables 2 and 3 of the software, respectively.

Table 2. Confirmation of User Input Selection for Locomotive, Consist, and Fuel (LCF) ID

LCF ID	Locomotive	Locomotive Consist Type	Fuel Type	Blended After-Treatment System	Number of Passenger Cars
1	NC1797	Single Locomotive	Ultra-Low Sulfur Diesel	No	3

Table 3. Confirmation of User Input Selection for Train Speed Trajectory ID

Speed Trajectory ID	Origin	Destination	Travel Time (min)	Distance (mile)	Average Speed (mph)
15	Raleigh	Charlotte	190	173	55

Users can also visualize the time series profile for the selected speed trajectory in the Input worksheet.



Figure 1. Second-by-Second Speed Trajectory for Trajectory ID 15

C.3.2 Running the Software

In this section, users will learn how to run the software. To run the software, users need to go to the Input worksheet. After entering required input data (i.e., LCF ID and trajectory ID), users can single-click “Click Here to Run the Model” button to run the software. The button is located under Table 1 in the Input worksheet. Please allow several minutes processing time to run the software.

Please Select a Locomotive, Consist, and Fuel (LCF) ID	1	← Please click this cell and select a LCF ID from the drop-down list. Please refer to Table 4 to review details regarding LCF options.
Please Select a Train Speed Trajectory ID	15	← Please click this cell and select a Train Speed Trajectory ID from the drop-down list. Please refer to Table 5 to review details regarding speed trajectory options.

Click Here to Run the Model
← Allow several minutes to run the model

C.3.3 Results Output

In this section, users will learn how to review results for model outputs after the software run is completed. To review results for model outputs, users need to go to the Output worksheet. Tables 6 and 7 in the Output worksheet of the software show the train and trip information, respectively, based on the user's selection.

Table 6. Train Information		Table 7. Trip Information	
Locomotive, Consist, and Fuel (LCF) ID	1	Trajectory ID	15
Locomotive	NC1797	Origin	Raleigh
Locomotive Consist Type	Single Locomotive	Destination	Charlotte
Fuel Type	Ultra-Low Sulfur Diesel	Travel Time (minute)	190
Blended After-Treatment System	No	Distance (mile)	173
Number of Baggage/Café and Passenger Cars	3	Average Speed (mph)	55
Train Weight (metric ton)	310		
Train Length (m)	100		

Table 8 in the Output worksheet of the software quantifies train activities for each station-to-station segment and whole trip, including travel time, distance, maximum speed, average speed, average positive acceleration, average negative acceleration, idle duration at stations, idle duration during train operations, total idle duration, cumulative elevation gain, cumulative positive elevation gain, and cumulative negative elevation gain.

Train Activity	Station-to-Station Segments								Whole Trip
	Raleigh-Cary	Cary-Durham	Durham-Burlington	Burlington-Greensboro	Greensboro-High Point	High Point-Salisbury	Salisbury-Kannapolis	Kannapolis-Charlotte	
Travel Time (minute)	13	19	39	20	15	32	15	27	190
Distance (mile)	8	18	33	21	15	34	16	27	173
Maximum Speed (mph)	78	82	77	80	79	81	79	81	82
Average Speed (mph)	40	56	52	63	63	64	64	60	55
Average Positive Acceleration (mph/s)	1.04	0.68	0.50	0.63	0.38	0.37	0.47	0.47	0.51
Average Negative Acceleration (mph/s)	-1.03	-0.95	-0.66	-0.75	-0.89	-0.68	-0.61	-0.63	-0.75
Idle duration at stations (minute) *	2	2	1	3	1	1	1	0	10
Idle duration during train operations (minute)	0	0	0	0	0	0	0	0	0
Total idle duration (minute)	2	2	1	3	1	1	1	0	11
Cumulative Elevation Gain (feet)	149	-111	271	154	83	-147	80	-100	365
Cumulative Positive Elevation Gain (feet)	314	470	1110	837	457	756	404	594	5093
Cumulative Negative Elevation Gain (feet)	-165	-581	-839	-683	-373	-903	-323	-695	-4729

*Note: Idle duration at stations refers to idling at Cary station for Raleigh-Cary, Durham station for Cary-Durham, Burlington station for Durham-Burlington, Greensboro station for Burlington-Greensboro, High Point station for Greensboro-High Point, Kannapolis station for Salisbury-Kannapolis, and Charlotte station for Kannapolis-Charlotte.

Table 9 in the Output worksheet of the software quantifies total fuel use and emissions for CO₂, CO, HC, NO_x, and PM for each station-to-station segment and whole trip.

Table 9. Total Fuel Use and Emissions for Each Station-to-Station Segment and Whole Trip

Species (unit)	Station-to-Station Segments								Whole Trip
	Raleigh-Cary	Cary-Durham	Durham-Burlington	Burlington-Greensboro	Greensboro-High Point	High Point-Salisbury	Salisbury-Kannapolis	Kannapolis-Charlotte	
Fuel (gallon)	14	20	44	26	20	37	18	31	210
CO ₂ (kg)	137	197	440	262	203	370	179	308	2,106
CO (g)	197	303	670	394	311	572	256	494	3,259
HC (g)	702	1,003	2,054	1,097	774	1,695	846	1,320	9,868
NO _x (g)	4,111	5,603	12,180	6,945	5,122	10,094	5,239	7,932	57,597
PM (g)	26	42	98	61	51	86	37	76	478

Users can also visualize total fuel use and emissions for each station-to-station segment under Table 9 of the software. Figures 2 to 7 of the software are station-to-station segment total fuel use and emissions of CO₂, CO, HC, NO_x, and PM, respectively, for a selected LCF ID and trajectory ID.

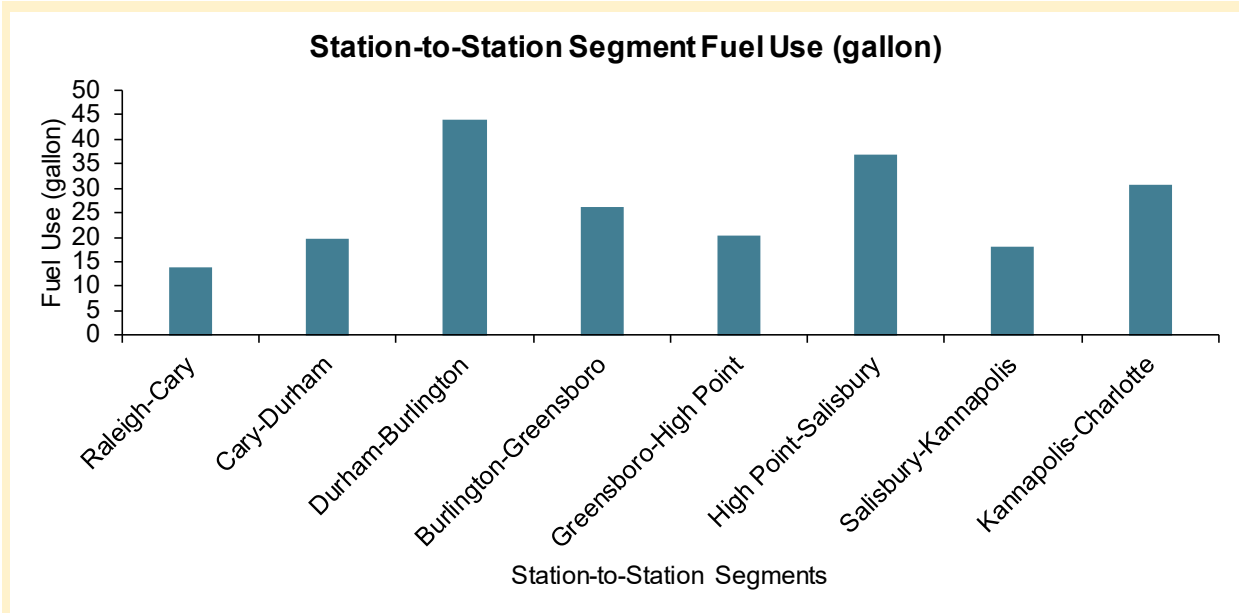


Figure 2. Station-to-Station Segment Total Fuel Use for LCF ID 1 and Trajectory ID 15

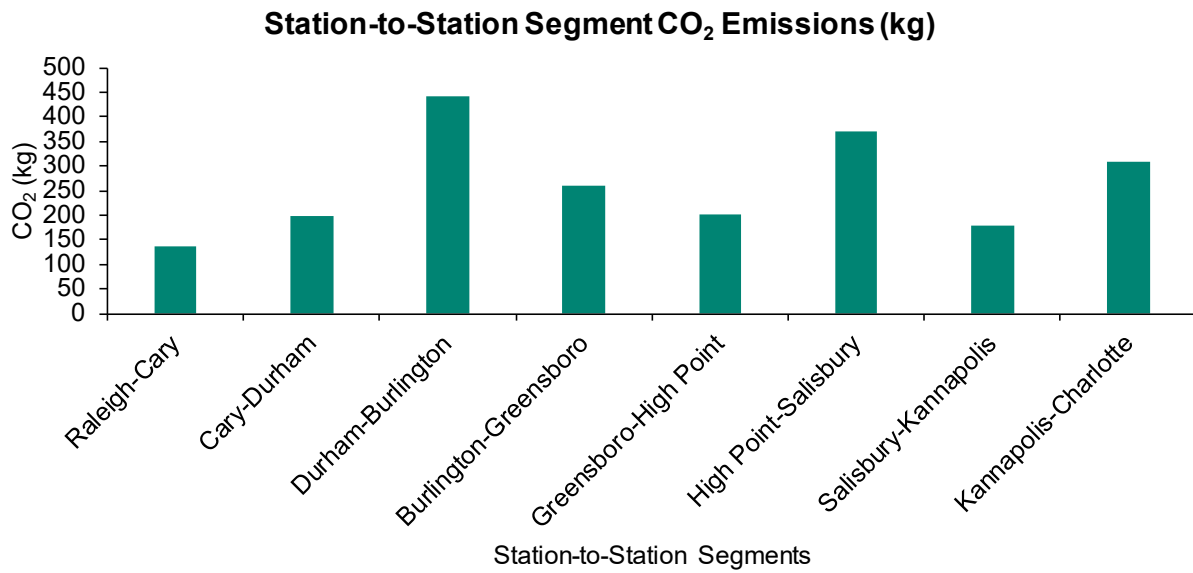


Figure 3. Station-to-Station Segment Total CO₂ Emissions for LCF ID 1 and Trajectory ID 15

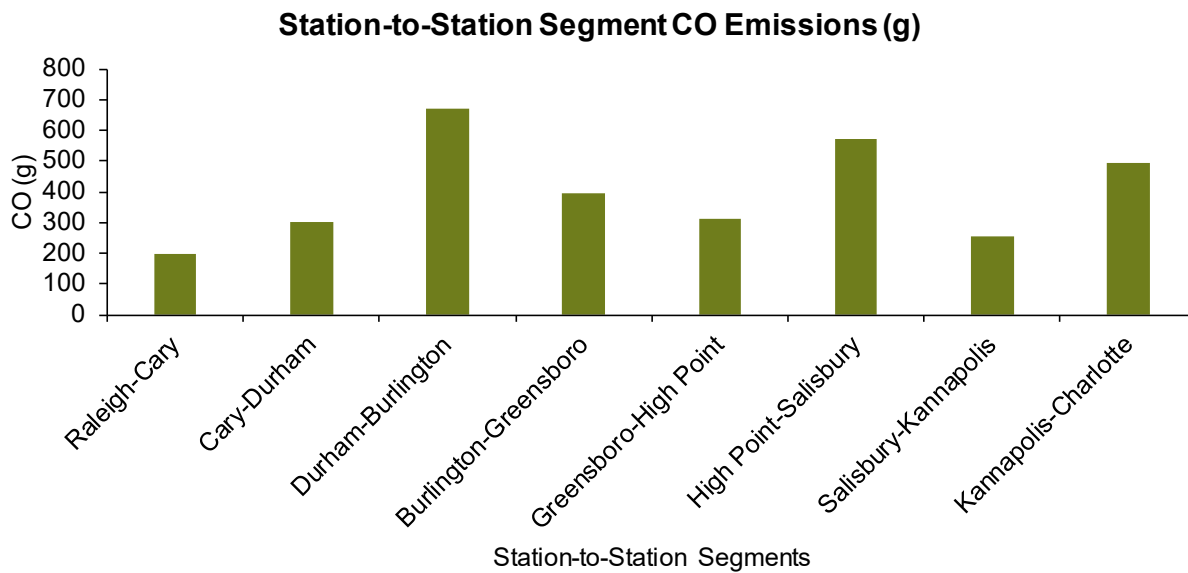


Figure 4. Station-to-Station Segment Total CO Emissions for LCF ID 1 and Trajectory ID 15

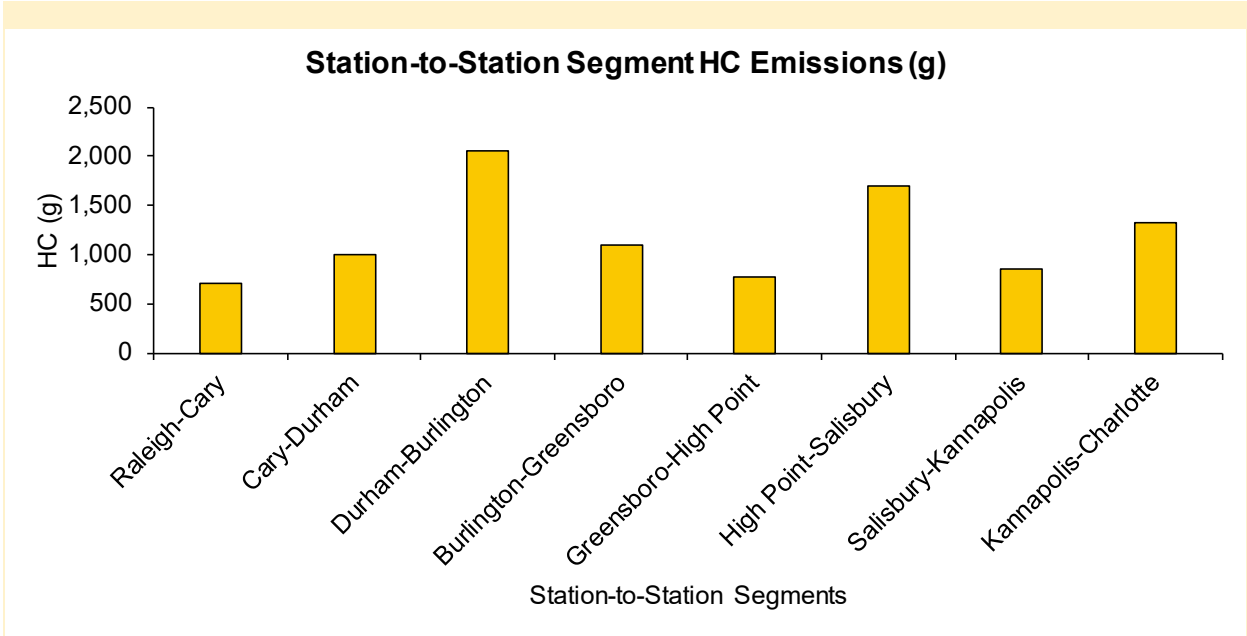


Figure 5. Station-to-Station Segment Total HC Emissions for LCF ID 1 and Trajectory ID 15

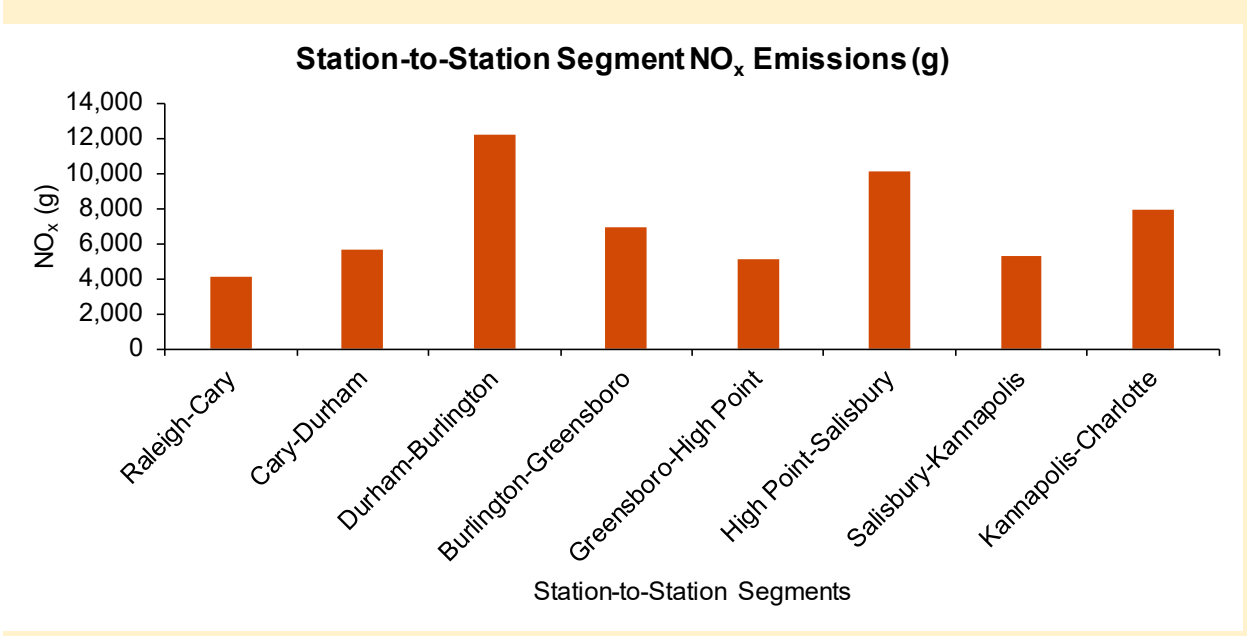


Figure 6. Station-to-Station Segment Total NO_x Emissions for LCF ID 1 and Trajectory ID 15

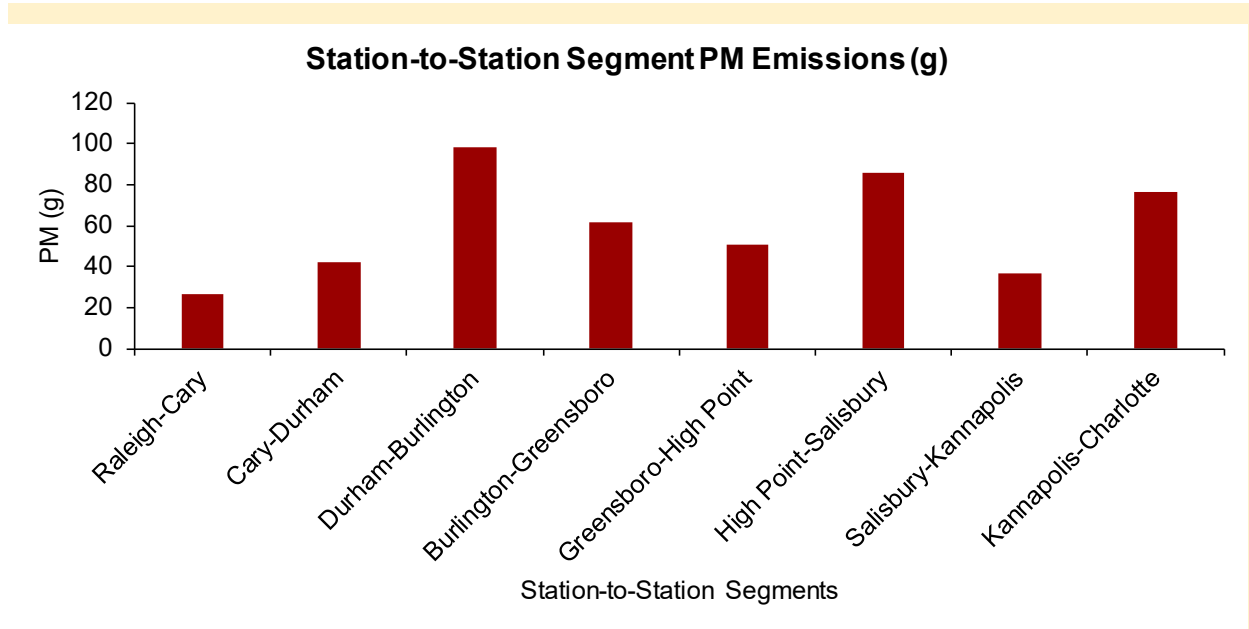


Figure 7. Station-to-Station Segment Total PM Emissions for LCF ID 1 and Trajectory ID 15

Table 10 in the Output worksheet of the software quantifies fuel economy (mpg) as well as distance-based emission rates (e.g., g/mile) for CO₂, CO, HC, NO_x, and PM for each station-to-station segment and whole trip.

Table 10. Distance-based Segment Average Fuel Use and Emission Rates for Each Station-to-Station Segment and Whole Trip

Species (unit)	Station-to-Station Segments								Whole Trip
	Raleigh-Cary	Cary-Durham	Durham-Burlington	Burlington-Greensboro	Greensboro-High Point	High Point-Salisbury	Salisbury-Kannapolis	Kannapolis-Charlotte	
Fuel Economy (mpg)	0.6	0.9	0.8	0.8	0.8	0.9	0.9	0.9	0.8
CO ₂ (kg/mile)	16.2	10.9	13.3	12.2	13.2	10.8	11.4	11.6	12.2
CO (g/mile)	23.2	16.8	20.2	18.4	20.2	16.7	16.3	18.6	18.8
HC (g/mile)	83.0	55.6	61.8	51.3	50.2	49.4	54.0	49.8	57.0
NO _x (g/mile)	486	311	366	325	332	294	334	299	333
PM (g/mile)	3.1	2.3	3.0	2.9	3.3	2.5	2.4	2.9	2.8

Users can also visualize fuel economy and distance-based emission rates for each station-to-station segment and whole trip under Table 10 of the software. Figures 8 to 13 of the software are fuel economy and distance-based emission rates of CO₂, CO, HC, NO_x, and PM, respectively, for each station-to-station segment and whole trip for a selected LCF ID and trajectory ID.

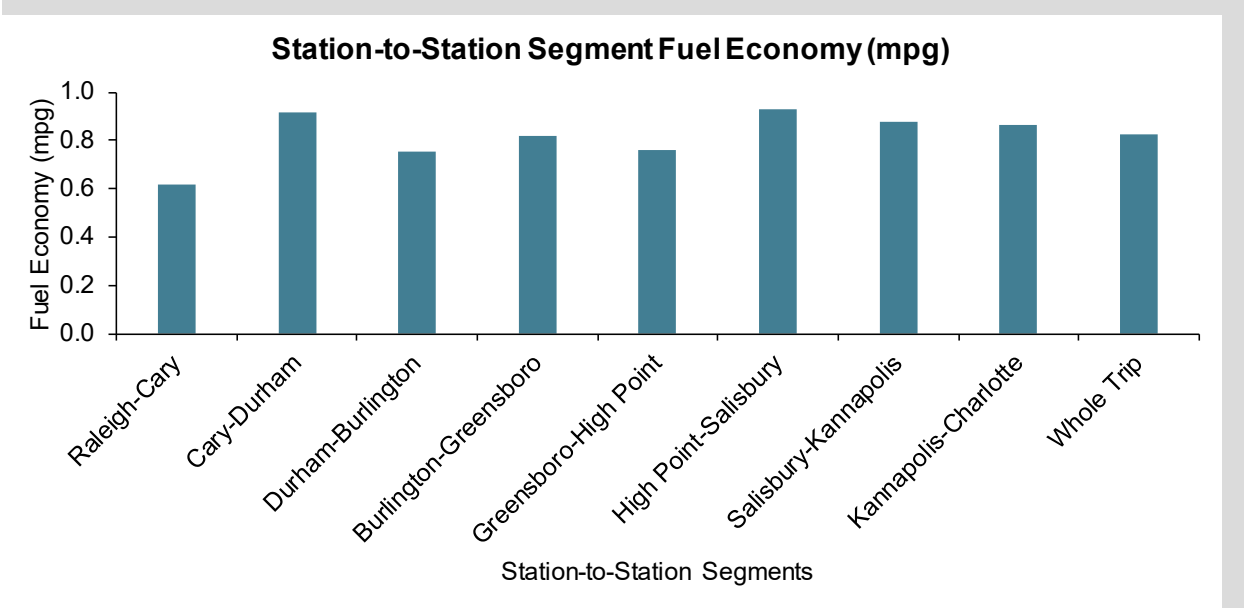


Figure 8. Station-to-Station Segment and Whole Trip Fuel Economy for LCF ID 1 and Trajectory ID 15

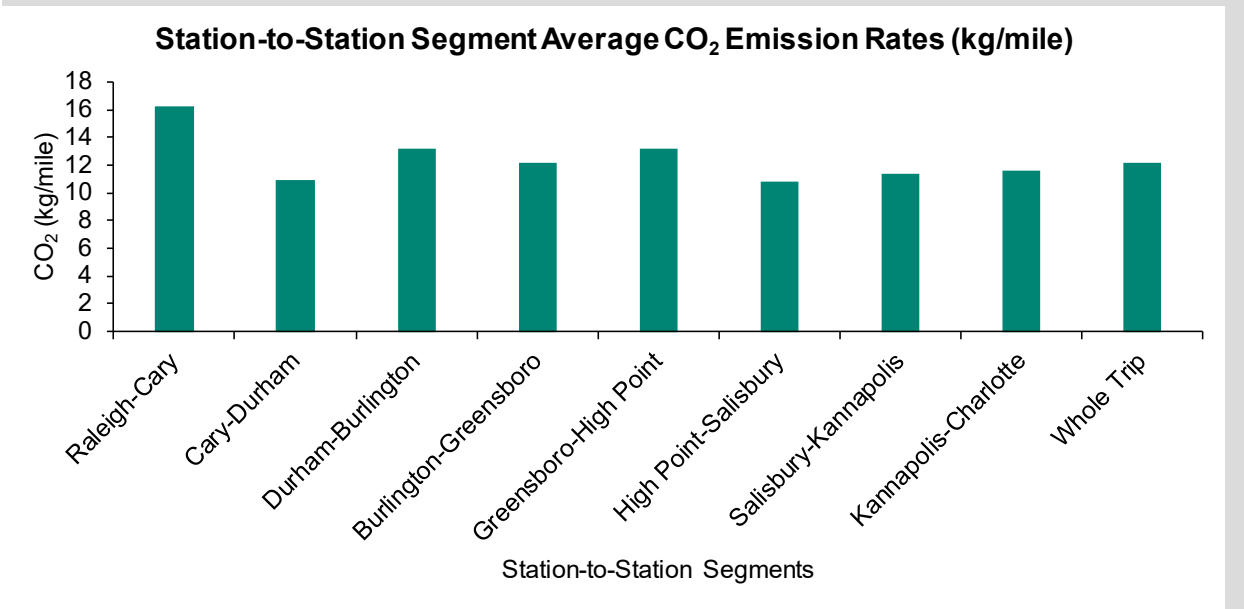


Figure 9. Distance-Based Station-to-Station Segment Average and Whole Trip Average CO₂ Emission Rates for LCF ID 1 and Trajectory ID 15

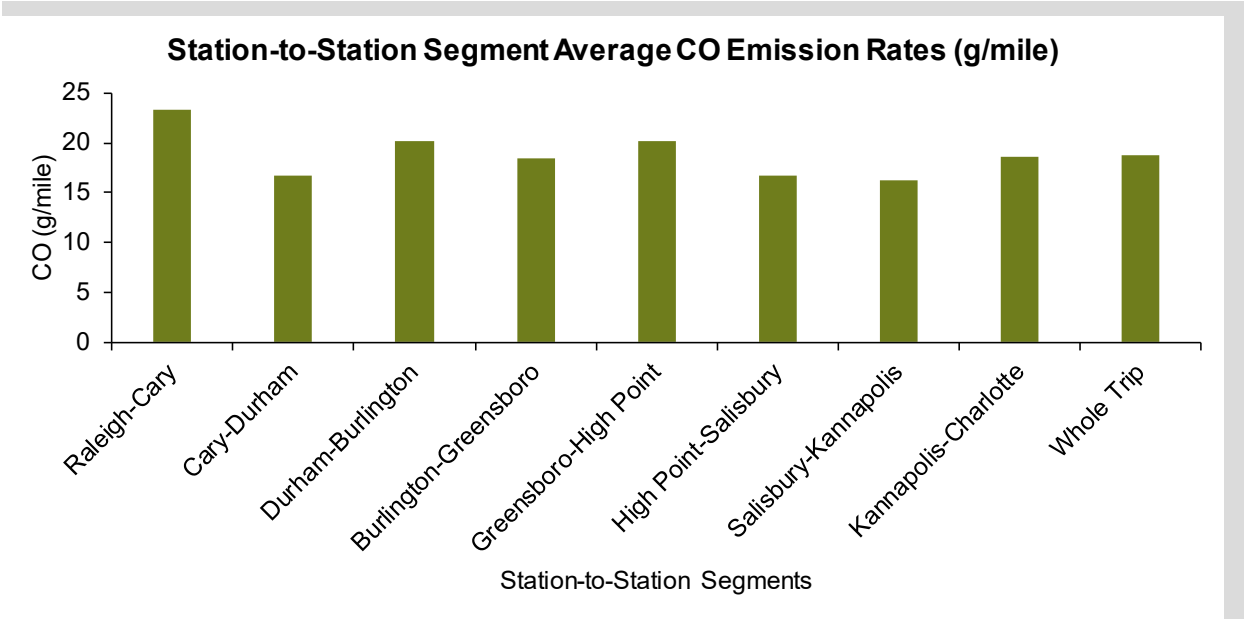


Figure 10. Distance-Based Station-to-Station Segment Average and Whole Trip Average CO Emission Rates for LCF ID 1 and Trajectory ID 15

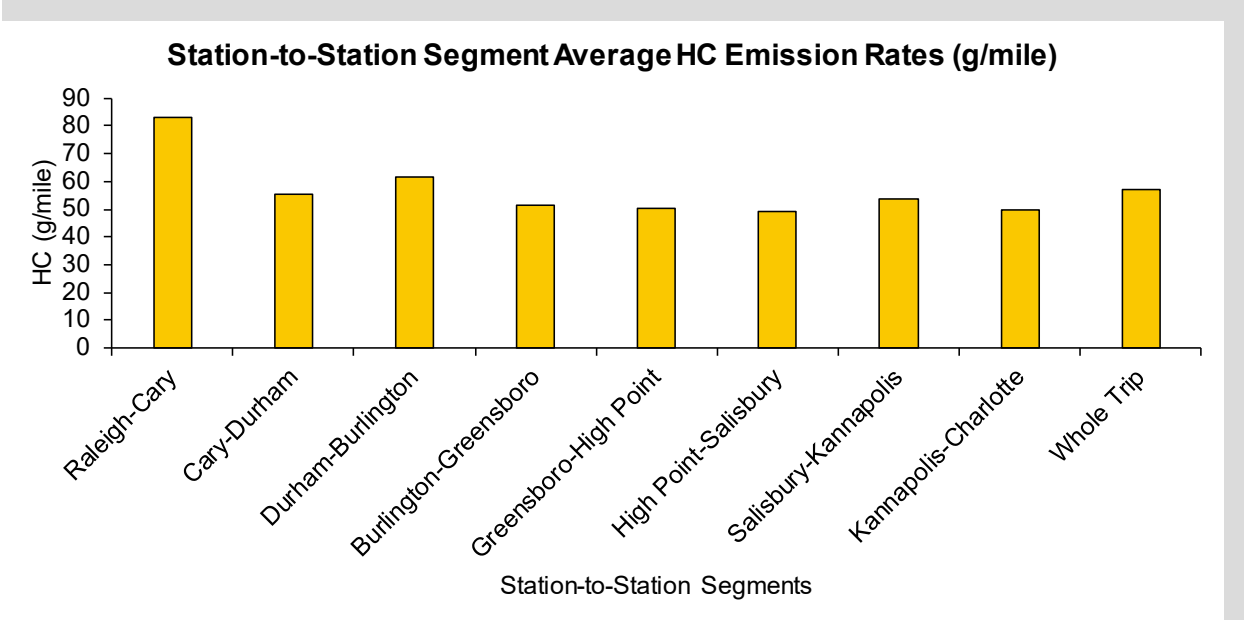


Figure 11. Distance-Based Station-to-Station Segment Average and Whole Trip Average HC Emission Rates for LCF ID 1 and Trajectory ID 15

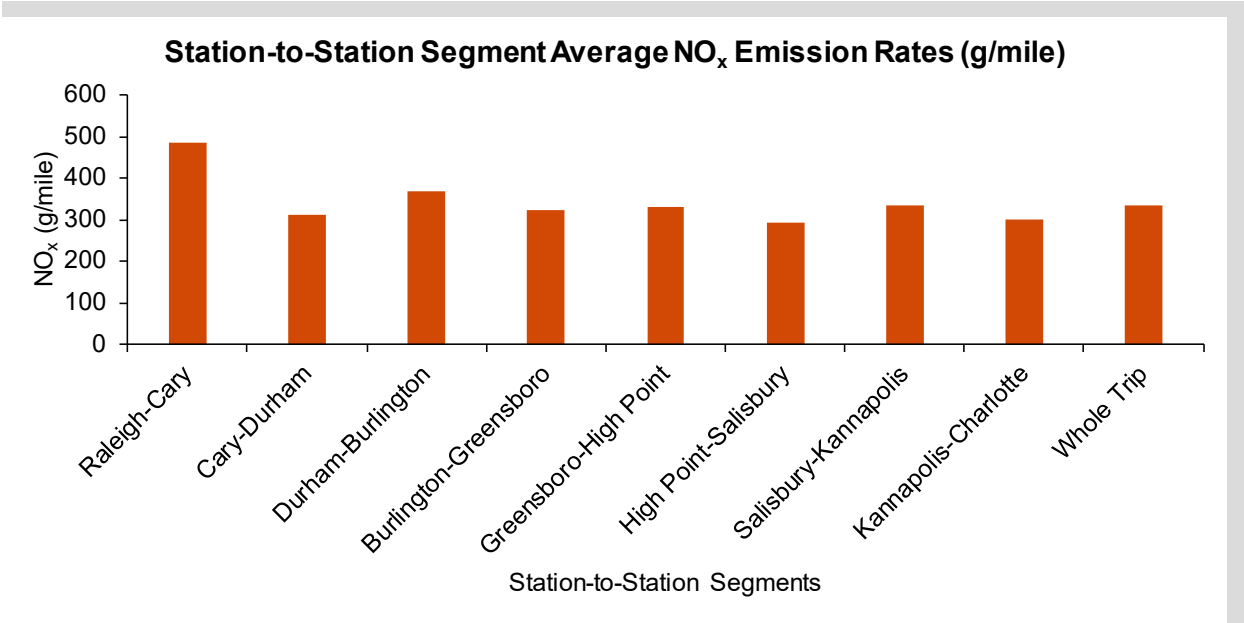


Figure 12. Distance-Based Station-to-Station Segment Average and Whole Trip Average NO_x Emission Rates for LCF ID 1 and Trajectory ID 15

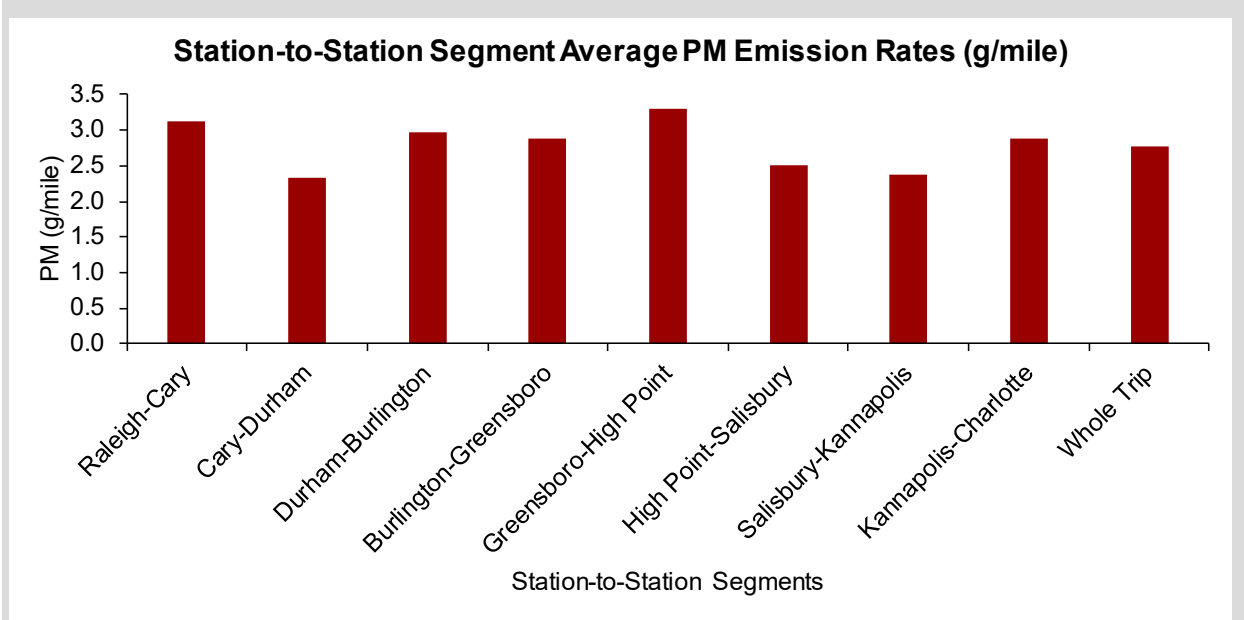


Figure 13. Distance-Based Station-to-Station Segment Average and Whole Trip Average PM Emission Rates for LCF ID 1 and Trajectory ID 15

Table 11 in the Output worksheet of the software quantifies time-based fuel use and emission rates (e.g., g/s) for CO₂, CO, HC, NO_x, and PM for each station-to-station segment and whole trip.

Table 11. Time-based Segment Average Fuel Use and Emission Rates for Each Station-to-Station Segment and Whole Trip

Species (unit)	Station-to-Station Segments								Whole Trip
	Raleigh-Cary	Cary-Durham	Durham-Burlington	Burlington-Greensboro	Greensboro-High Point	High Point-Salisbury	Salisbury-Kannapolis	Kannapolis-Charlotte	
Fuel (g/s)	57	54	60	67	73	61	64	61	58
CO ₂ (g/s)	181	170	190	213	230	192	202	194	185
CO (mg/s)	259	260	289	320	352	296	288	310	286
HC (mg/s)	923	861	884	893	876	878	952	829	866
NO _x (mg/s)	5,402	4,814	5,243	5,651	5,800	5,230	5,893	4,983	5,053
PM (mg/s)	35	36	42	50	57	44	42	48	42

Users can also visualize time-based fuel use and emission rates for each station-to-station segment and whole trip under Table 11 of the software. Figures 14 to 19 are time-based fuel use and emission rates of CO₂, CO, HC, NO_x, and PM, respectively, for each station-to-station segment and whole trip for a selected LCF ID and trajectory ID.

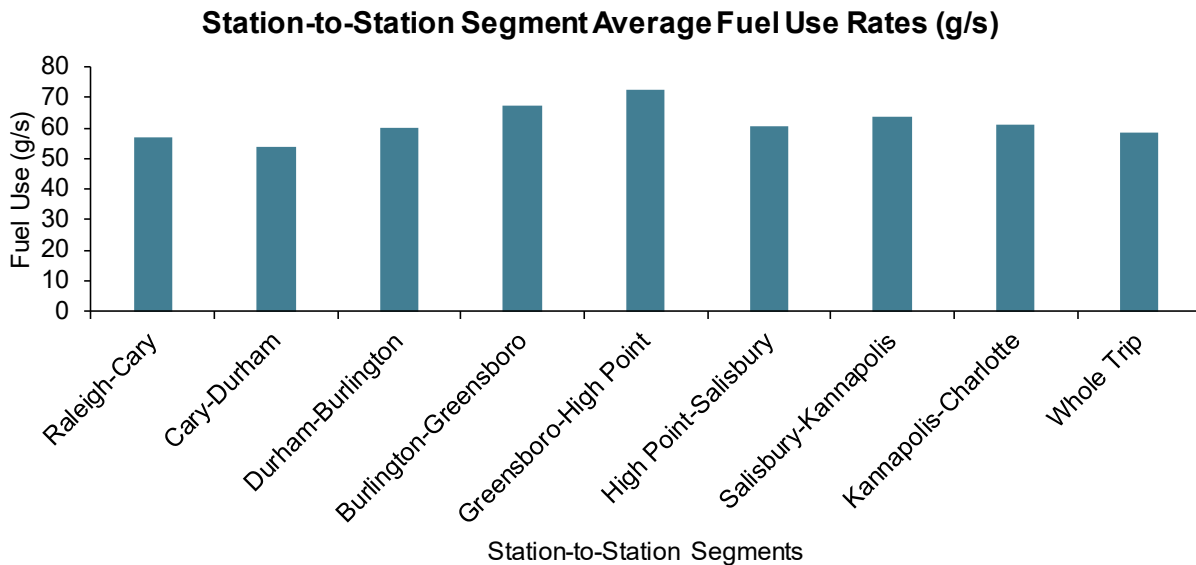


Figure 14. Time-Based Station-to-Station Segment Average and Whole Trip Average Fuel Use Rates for LCF ID 1 and Trajectory ID 15

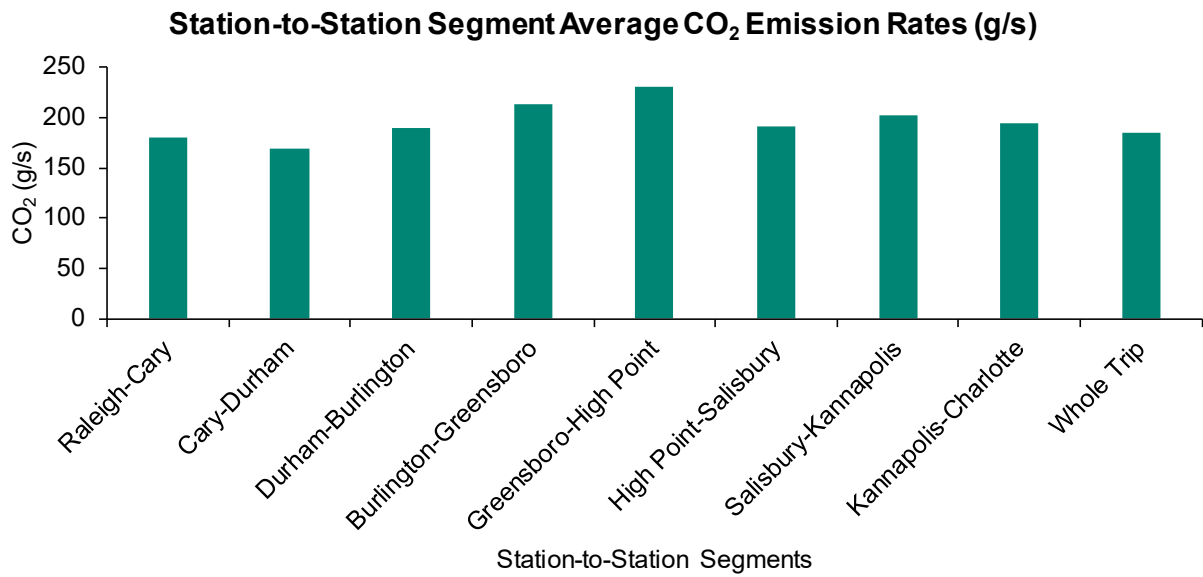


Figure 15. Time-Based Station-to-Station Segment Average and Whole Trip Average CO₂ Emission Rates for LCF ID 1 and Trajectory ID 15

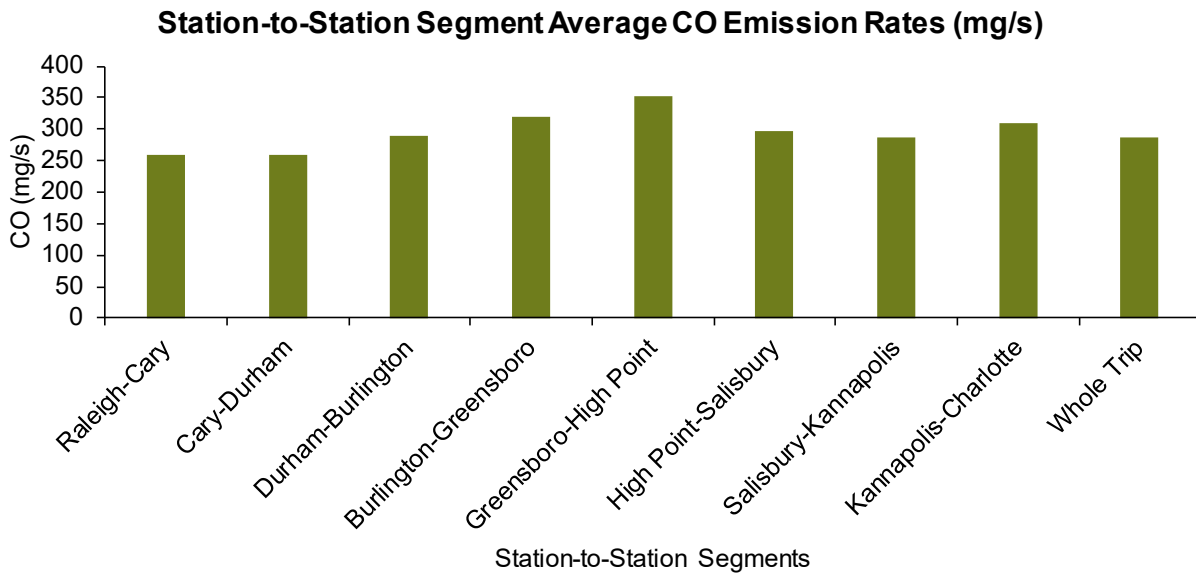


Figure 16. Time-Based Station-to-Station Segment Average and Whole Trip Average CO Emission Rates for LCF ID 1 and Trajectory ID 15

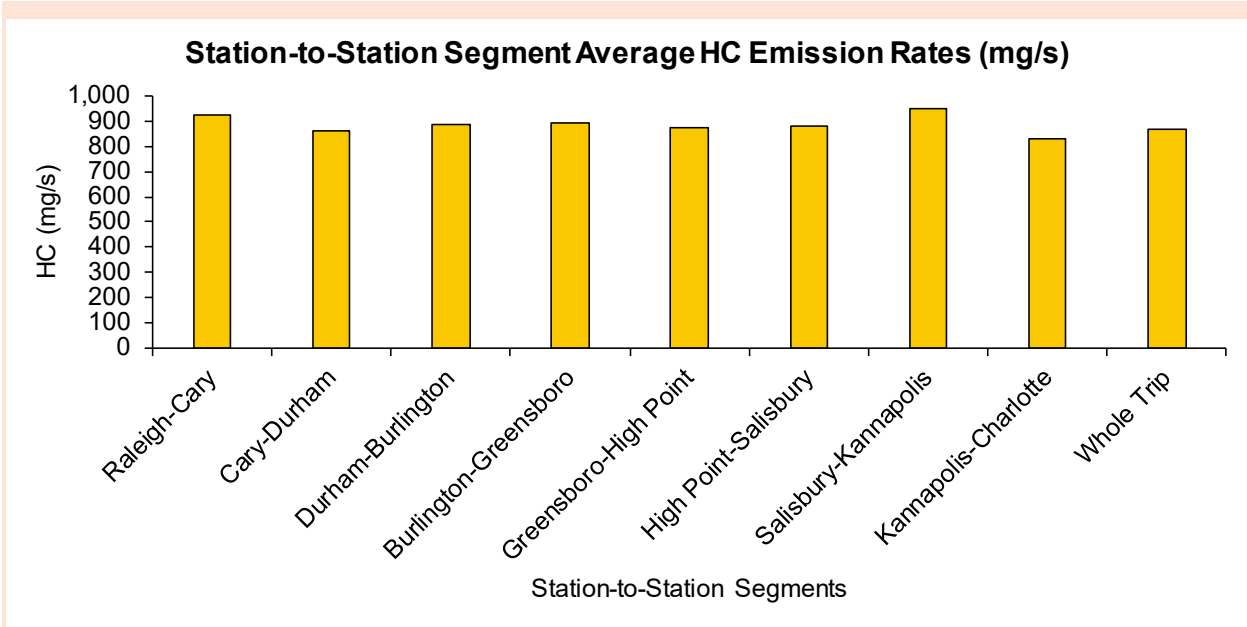


Figure 17. Time-Based Station-to-Station Segment Average and Whole Trip Average HC Emission Rates for LCF ID 1 and Trajectory ID 15

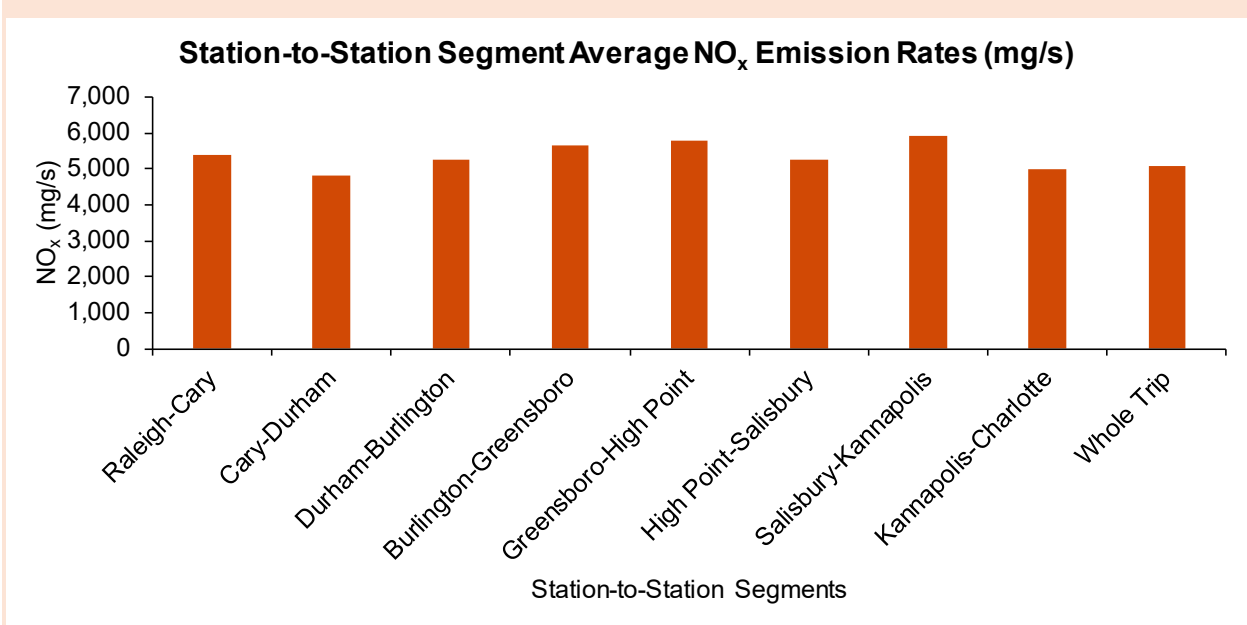


Figure 18. Time-Based Station-to-Station Segment Average and Whole Trip Average NO_x Emission Rates for LCF ID 1 and Trajectory ID 15

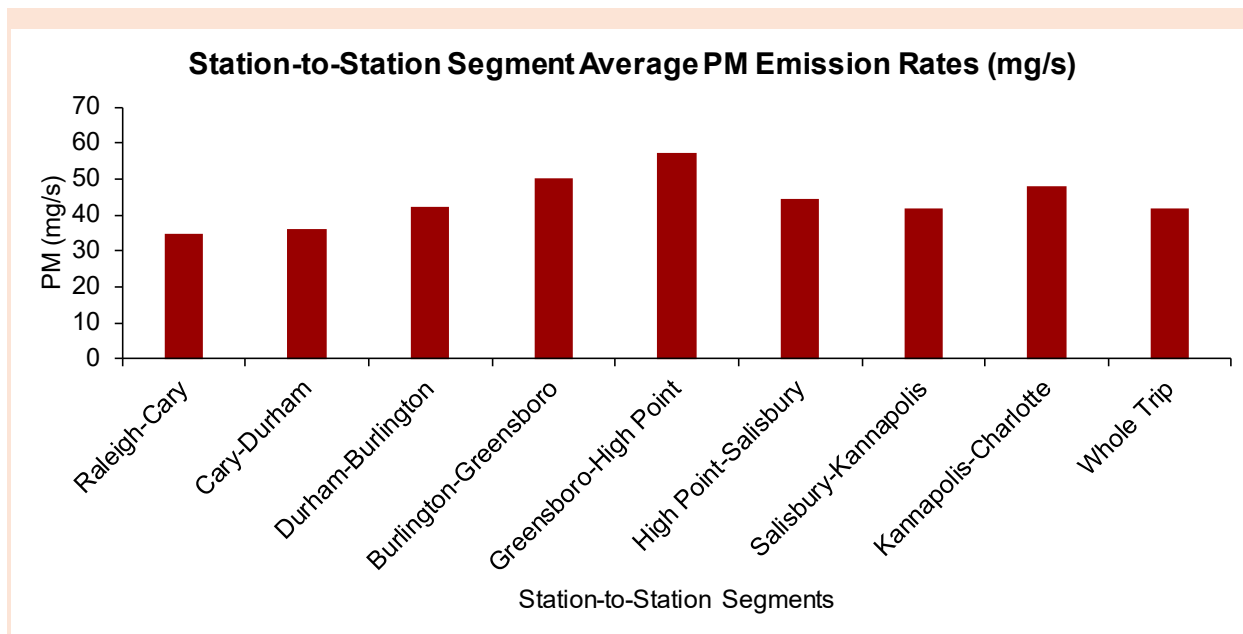


Figure 19. Time-Based Station-to-Station Segment Average and Whole Trip Average PM Emission Rates for LCF ID 1 and Trajectory ID 15

Table 12 in the Output worksheet of the software quantifies fuel-based emission rates (e.g., g/gallon) for CO₂, CO, HC, NO_x, and PM for each station-to-station segment and whole trip.

Table 12. Fuel-based Segment Average Emission Rates for Each Station-to-Station Segment and Whole Trip

Species (unit)	Station-to-Station Segments								Whole Trip
	Raleigh-Cary	Cary-Durham	Durham-Burlington	Burlington-Greensboro	Greensboro-High Point	High Point-Salisbury	Salisbury-Kannapolis	Kannapolis-Charlotte	
CO ₂ (kg/gallon)	10.0	10.0	10.0	10.0	10.0	10.0	10.0	10.0	10.0
CO (g/gallon)	14.3	15.4	15.2	15.1	15.3	15.5	14.3	16.1	15.5
HC (g/gallon)	51.1	50.8	46.7	42.0	38.2	45.9	47.2	42.9	46.9
NO _x (g/gallon)	299	284	277	266	253	273	292	258	274
PM (g/gallon)	1.9	2.1	2.2	2.4	2.5	2.3	2.1	2.5	2.3

Users can also visualize fuel-based emission rates for each station-to-station segment and whole trip under Table 12 of the software. Figures 20 to 24 of the software are fuel-based emission rates of CO₂, CO, HC, NO_x, and PM, respectively, for each station-to-station segment and whole trip for a selected LCF ID and trajectory ID.

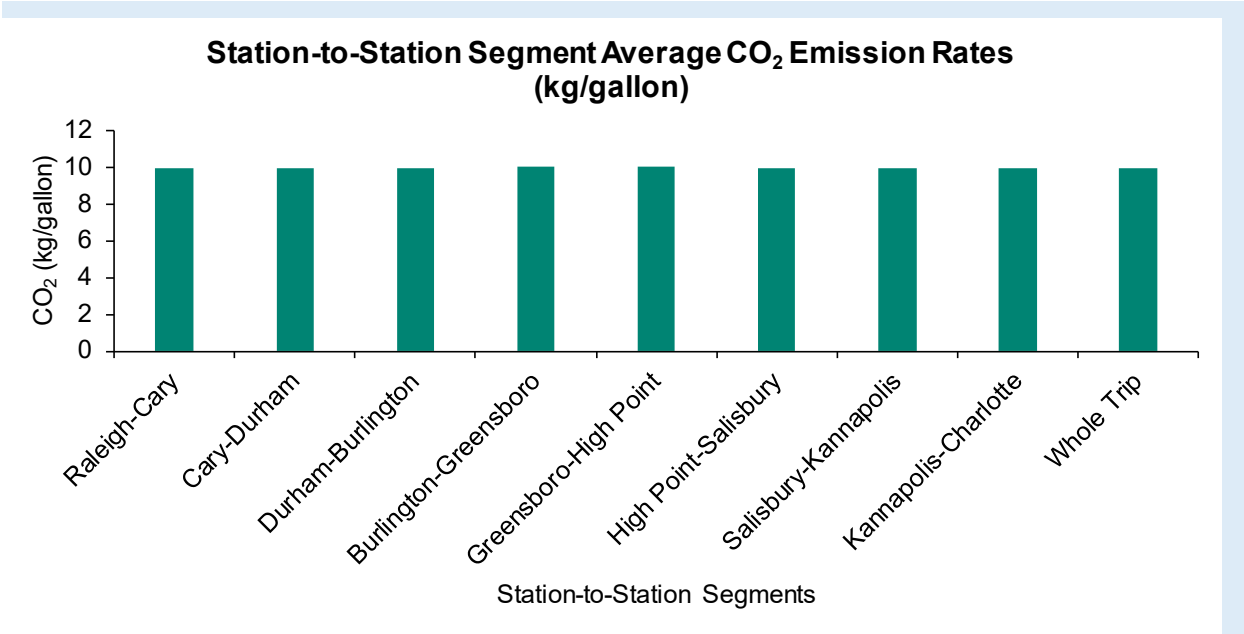


Figure 20. Fuel-Based Station-to-Station Segment Average and Whole Trip Average CO₂ Emission Rates for LCF ID 1 and Trajectory ID 15

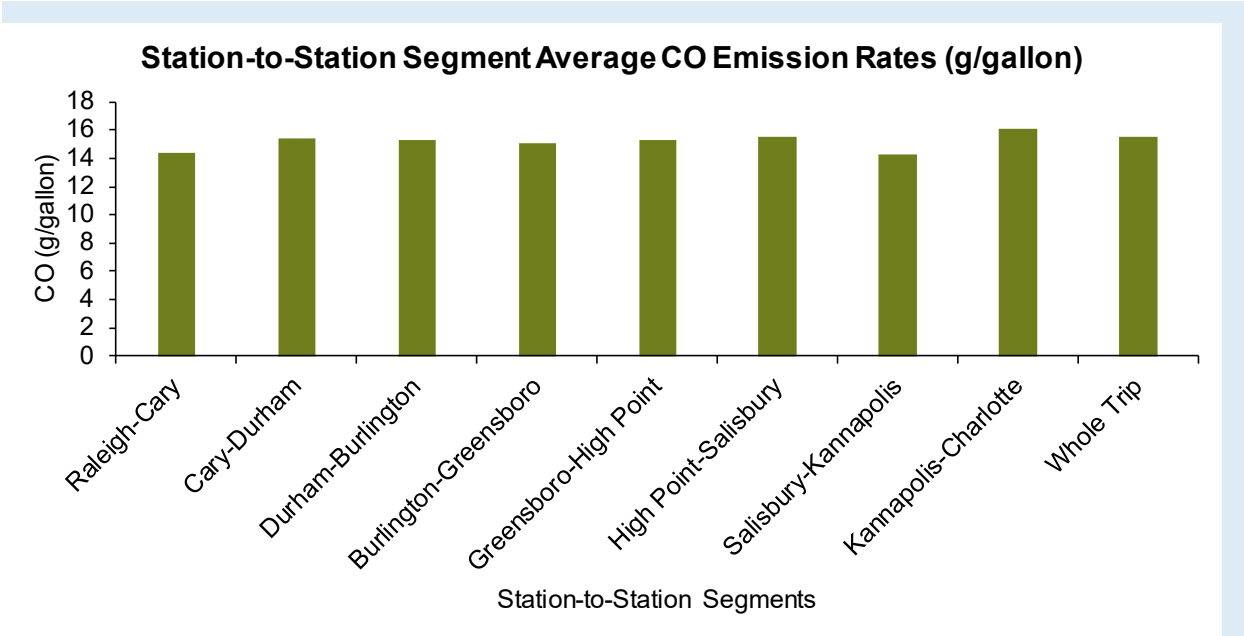


Figure 21. Fuel-Based Station-to-Station Segment Average and Whole Trip Average CO Emission Rates for LCF ID 1 and Trajectory ID 15

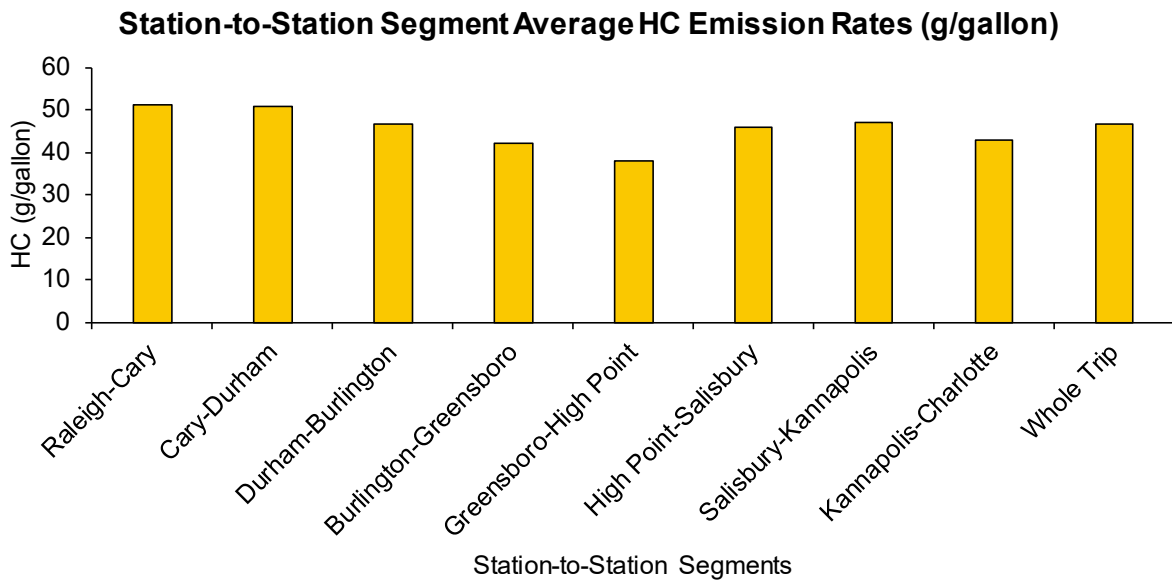


Figure 22. Fuel-Based Station-to-Station Segment Average and Whole Trip Average HC Emission Rates for LCF ID 1 and Trajectory ID 15

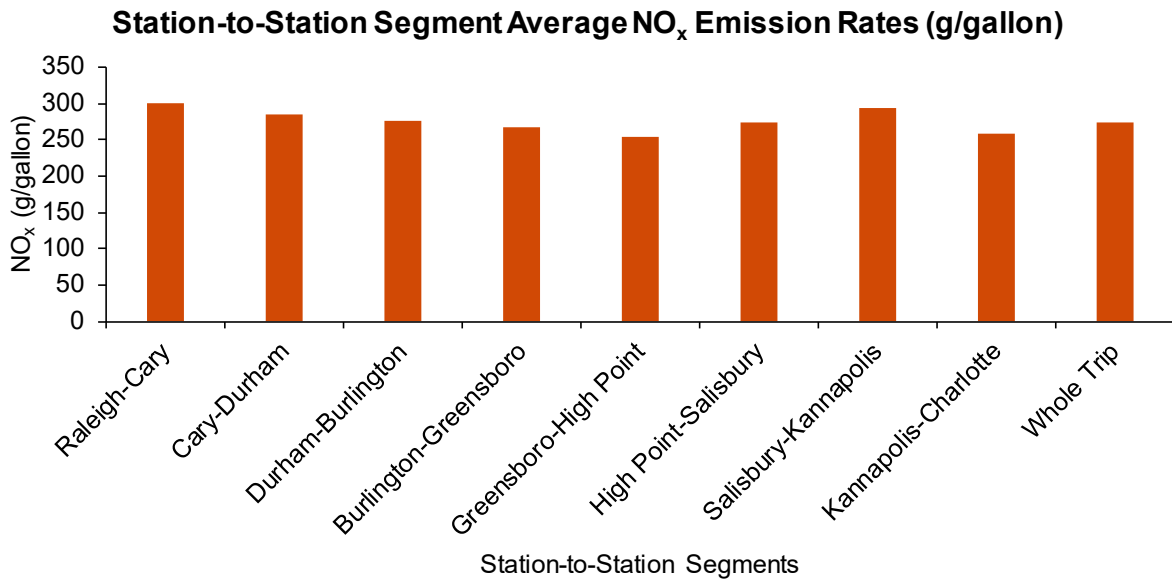


Figure 23. Fuel-Based Station-to-Station Segment Average and Whole Trip Average NO_x Emission Rates for LCF ID 1 and Trajectory ID 15

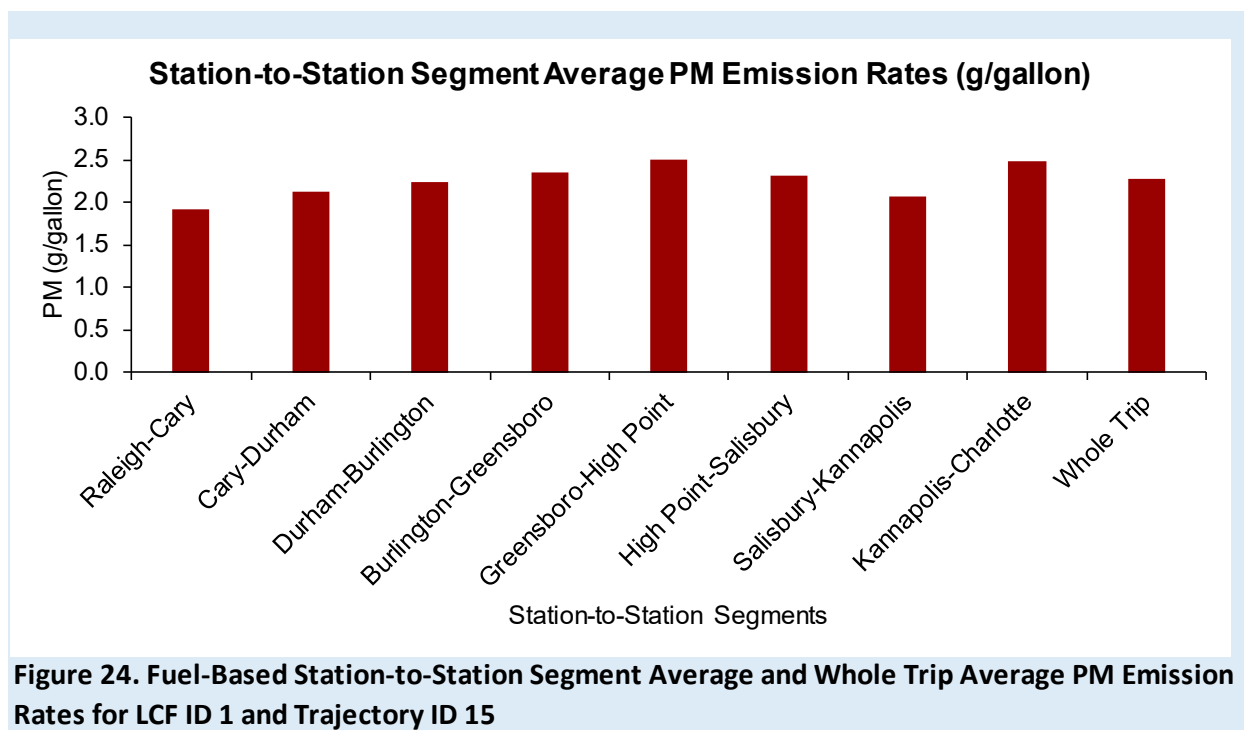


Figure 24. Fuel-Based Station-to-Station Segment Average and Whole Trip Average PM Emission Rates for LCF ID 1 and Trajectory ID 15

C.4 References Cited in Appendix C

1. Rastogi, N., and H. C. Frey. Characterizing Fuel Use and Emission Hotspots for a Diesel-Operated Passenger Rail Service. *Environmental Science & Technology*, Vol. 55, No. 15, 2021, pp. 10633–10644. <https://doi.org/10.1021/acs.est.1c00273>.
2. Rastogi, N., and H. C. Frey. Estimation of Rail Grade and Horizontal Curvature from Non-Proprietary Data Sources. Proceedings of Transportation Research Board 97th Annual Meeting. Paper No. TRB 18-06366. Transportation Research Board, Washington, D.C., 2018, pp. 1-17. <https://trid.trb.org/view/1497239>
3. Graver, B. M., H. C. Frey, and J. Hu. Effect of Biodiesel Fuels on Real-World Emissions of Passenger Locomotives. *Environmental Science & Technology*, Vol. 50, No. 21, 2016, pp. 12030–12039. <https://doi.org/10.1021/acs.est.6b03567>.
4. Graver, B. M., and H. C. Frey. Comparison of Over-the-Rail and Rail Yard Measurements of Diesel Locomotives. *Environmental Science & Technology*, Vol. 49, No. 21, 2015, pp. 13031–13039. <https://doi.org/10.1021/acs.est.5b02497>.
5. Graver, B. M., and H. C. Frey. Comparison of Locomotive Emissions Measured during Dynamometer versus Rail Yard Engine Load Tests. *Transportation Research Record*, Vol. 2341, No. 1, 2013, pp. 23–33. <https://doi.org/10.3141/2341-03>.

Appendix D. Supporting Information for Chapter 5

D.1 Introduction

This work included rail yard (RY) measurements on the prime mover engine (PME) of the locomotive NC 1984 conducted on 11/17/2020. Fuel use and emission rates (FUERs) were estimated for NC 1984. FUERs were benchmarked to prior baseline RY measurements of NC 1984 conducted on 1/25/2018. This work was to update the baseline fuel use and emissions for NC 1984, and also to benchmark two PEMS to each other using long exhaust sample lines.

This RY measurement also served to test the viability of new over-the-rail (OTR) measurement protocols. New OTR measurement protocols were devised in light of restrictions imposed by the Amtrak. The new measurement protocols were presented to the NCDOT in a progress report for the quarter ending in March 2020 (Frey and Rastogi, 2020). The proposed plan included installing the portable emissions measurement system (PEMS) in the baggage compartment of a baggage/café car adjacent to the locomotive. Consequently, the exhaust hoses must be re-routed to the baggage compartment. Therefore, this RY measurement was conducted using a newly devised PEMS placement and exhaust hose routing plan.

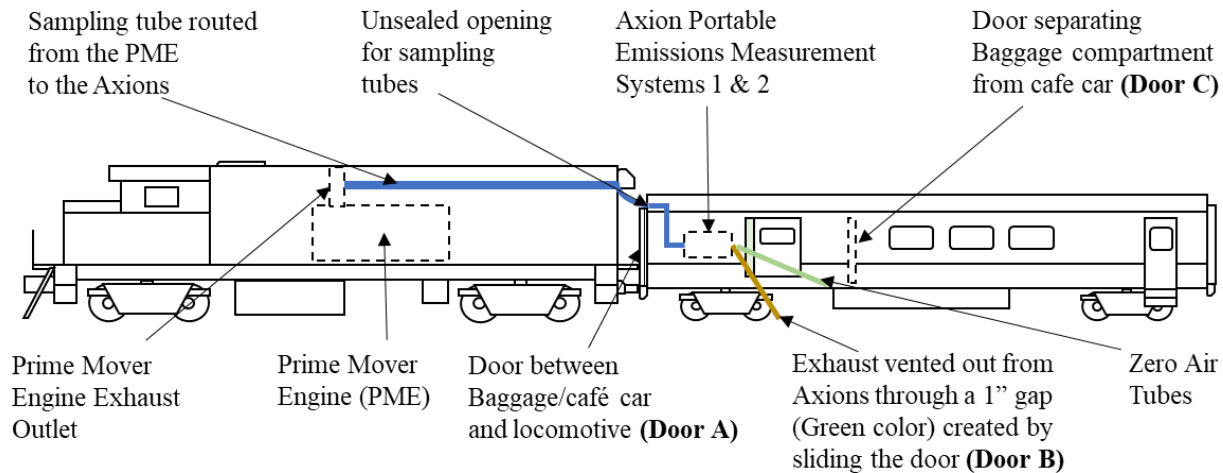
In the future, NCDOT and NCSU need to quantify the efficacy of a blended exhaust after-treatment system (BATS) for OTR operation. The BATS is an exhaust-treatment system based on selective catalytic reduction to reduce NO_x emission rates. The BATS treats the blended exhaust from the PME and head end power engine before releasing the exhaust to the atmosphere. To quantify BATS efficacy, exhaust gas composition measurements are required upstream and downstream of the BATS. Therefore, NCSU needs to use two PEMS for future measurements with BATS. In this work, two Axion PEMS were benchmarked based on simultaneous exhaust gas and PM measurements.

The objectives of the work here are to: (1) benchmark FUERs to prior measurements; and (2) benchmark two PEMS to each other. The background information on locomotives, locomotive FUERs, and locomotive FUERs measurements were previously given in a progress report for the quarter ending in June 2019 (Frey and Rastogi, 2019).

D.2 Measurement methods

In this section, the placement of PEMS and the routing of the exhaust hoses are discussed. The PEMS-based exhaust gas composition measurement, bias correction factors, engine activity variables measurement, PEMS benchmarking to a reference instrument, measurement schedule, engine output, quality assurance, and estimation of FUERs are detailed in a progress report for the quarter ending in June 2019 (Frey and Rastogi, 2019).

A schematic diagram of the measurement setup is given in Figure D-1. The measurement setup included the placement of PEMS, and routing of exhaust hoses, sensor array cables, and zero air hoses. Two PEMS were placed on the luggage rack inside the baggage compartment. Engine out exhaust hoses and sensor array cables were routed into the baggage car through a small opening created above Door A [Figure D-1(a)] and connected to the PEMS. PEMS exhaust outlet hoses and zero air inlet hoses were routed outwards from Door B [Figure D-1(a)] on one side of the baggage compartment. Door B was slid open to create a 1” gap to let the exhaust outlet and zero air hoses outside the compartment.



(a) A schematic layout of the rail yard measurement



(b) Exhaust hoses and sensor array cables from prime mover engine entering the baggage car



(c) PEMS exhaust outlet hoses and zero air inlet hoses exiting the baggage car

Figure D-1. A Schematic Diagram of the Measurement Setup Including: (a) PEMS Placement and Routing of Exhaust and Zero Air Sample Hoses; (b) Exhaust Hoses and Sensor Array Cables Entering the Baggage Car; and (c) Exhaust Hoses and Zero Air Inlet Hoses Exiting the Baggage Car

D.3 Results

RY measurements on the PME of locomotive NC 1984 were conducted on 11/17/2020. Three replicates were conducted. Simultaneous exhaust gas and PM concentration measurements were conducted using two Axion PEMS. Engine activity variables, including engine revolutions per minute (RPM), intake air temperature (IAT), and manifold absolute pressure (MAP) were measured using an engine sensor array connected to one of the Axion PEMS. This section provides a summary of notch-average measured concentrations and engine activity variables for each replicate measured with Axion 1. FUERs are also shown based on Axion 1. Cycle average emission rates (CAERs) were estimated for the EPA line-haul cycle. FUERs were benchmarked to FUERs from prior RY measurement of NC 1984. Prior RY measurements were also based on Axion 1. The two Axions were benchmarked to each other.

D.3.1 Notch-average engine activity and exhaust concentrations

The engine activity variables, including RPM, IAT, and MAP measured with the Axion PEMS for the three replicates, are summarized in Table D-1(a), (b), and (c), respectively. Engine RPM varied from 268 rpm at idle and notch 1 to 903 rpm at notch 8. The notch-average RPM was consistent among the replicates with the highest inter-replicate coefficient of variation (CV) for a given notch position being 0.001. CV is the ratio of standard deviation divided by the mean. Thus, the RPM measurements were highly repeatable.

The IAT varied from 73 C° at Notch 1 to 89 C° at Notch 7. In general, IAT increased with increasing notch position. However, IAT at the adjacent notch positions differed by less than 2 C°. IAT measurements were repeatable for a given notch position with the highest inter-replicate CV being 0.13. IAT varies with notch position, increasing by approximately 9 C° to 10 C° from notch 1 to notch 8, but also varies with replicate because of increasing engine warmup, increasing by typically 2 C° to 17 C° for a given notch from the first to last replicate.

MAP varied from 101 kPa at Idle to 208 kPa at Notch 8. MAP increased with an increase in engine RPM. MAP measurements were also highly repeatable for a given notch position with the highest inter-replicate CV being 0.007.

Table D-1. Notch-Average Engine Activity Variables for the Prime Mover Engine of Locomotive NC 1984 Measured Using Engine Sensor Array (a) Engine Revolutions per Minute; (b) Intake Air Temperature; and (c) Manifold Absolute Pressure.

(a) Engine Revolutions Per Minute (RPM)

Throttle Notch Position	Engine Speed (RPM)					
	17 Nov	17 Nov	17 Nov	3 Rep	3 Rep	3 Rep
	RY Rep1	RY Rep2	RY Rep3	Avg	Std Dev	CV
Idle	268	268	268	268	0.02	0.000
1	268	268	268	268	0.03	0.000
2	389	389	389	389	0.21	0.001
3	509	509	509	509	0.24	0.000
4	702	702	702	702	0.35	0.000
5	728	728	728	728	0.07	0.000
6	819	819	819	819	0.12	0.000
7	859	859	859	859	0.06	0.000
8	903	903	903	903	0.21	0.000

^a CV = Coefficient of Variation (Ratio of standard deviation and mean of three replicates)

(b) Intake Air Temperature

Throttle Notch Position	Intake Air Temperature (C°)					
	17 Nov	17 Nov	17 Nov	3 Rep	3 Rep	3 Rep
	RY Rep1	RY Rep2	RY Rep3	Avg	Std Dev	CV
Idle	63	80	79	74	9.8	0.13
1	63	78	78	73	8.2	0.11
2	68	78	77	74	5.9	0.08
3	74	79	78	77	2.6	0.03
4	80	82	81	81	0.8	0.01
5	82	84	82	83	1.0	0.01
6	84	86	84	85	1.1	0.01
7	88	89	87	88	1.1	0.01
8	90	91	88	89	1.4	0.02

^a CV = Coefficient of Variation (Ratio of standard deviation and mean of three replicates)

Table D-1 Continued on next page.

Table D-1 Continued from previous page.

(c) Manifold Absolute Pressure

Throttle Notch Position	Manifold Absolute Pressure (kPa)					
	17 Nov	17 Nov	17 Nov	3 Rep	3 Rep	3 Rep
	RY Rep1	RY Rep2	RY Rep3	Avg	Std Dev	CV
Idle	101	101	101	101	0.01	0.000
1	101	100	100	101	0.22	0.002
2	110	109	109	109	0.37	0.003
3	123	122	122	122	0.62	0.005
4	155	153	153	153	1.05	0.007
5	161	159	159	160	1.08	0.007
6	184	182	182	183	0.85	0.005
7	196	195	196	196	0.44	0.002
8	208	207	207	208	0.61	0.003

^a CV = Coefficient of Variation (Ratio of standard deviation and mean of three replicates).

Notch-average exhaust concentrations of CO₂, CO, HC, NO, and PM measured using Axion 1 are summarized in Table D-2. Notch-average CO₂ concentration varied from 0.80 vol% at idle to 6.18 vol% at notch 7. Notch-average CO₂ concentration increased with increasing notch position except for notch 8, which had CO₂ concentrations comparable to or slightly lower than those of notch 7. Notch-average CO₂ concentration measurements were highly repeatable with inter-replicate CVs of typically 0.01 or lower except at idle and notch 1 for which CO₂ emission rates (as shown later in Table 3(b)), are relatively low.

Notch-average CO concentrations were below the detection limit of the Axion PEMS except at notch 7. Notch-average HC concentrations were below the detection limit of the Axion PEMS.

Notch-average NO concentration varied between 206 ppm at idle and 1661 ppm at notch 7. Notch-average NO concentration typically increased with increasing notch position from idle through notch 7 and decreased for notch 8. Notch-average NO concentration measurements were highly repeatable based on inter-replicate CVs of 0.05 or lower, except for idle and notch 1. NO_x emission rates [as shown later in Table D-3(e)] at idle and notch 1 were relatively low.

Notch-average PM concentration varied between 4.7 mg/m³ and 15.9 mg/m³. On average, notch-average PM concentrations were within ±1 mg/m³ each other for idle through notch 5, ranging from 5.5 mg/m³ to 6.6 mg/m³. Notch 6 had a higher notch-average PM concentration compared to lower notch positions. The highest PM concentrations were measured for notch 7. Notch-average PM concentration measurements were repeatable with inter-replicate CVs of 0.10 or lower, except for idle.

Table D-2. Notch-Average Prime Mover Engine Exhaust Concentrations of Locomotive NC 1984 Measured Using Axion 1 (a) CO₂; (b) CO; (c) HC; (d) NO; and (e) PM.

(a) CO₂ concentration

Throttle Notch Position	Exhaust CO ₂ Concentration (vol %)					
	17 Nov	17 Nov	17 Nov	3 Rep	3 Rep	3 Rep
	RY Rep1	RY Rep2	RY Rep3	Avg	Std Dev	CV
Idle	0.75	0.77	0.88	0.80	0.07	0.09
1	1.69	1.18	1.18	1.35	0.30	0.22
2	2.51	2.48	2.49	2.49	0.02	0.01
3	3.45	3.45	3.48	3.46	0.02	0.00
4	3.67	3.74	3.74	3.72	0.04	0.01
5	4.48	4.54	4.56	4.53	0.04	0.01
6	5.51	5.53	5.52	5.52	0.01	0.00
7	6.19	6.17	6.18	6.18	0.01	0.00
8	5.99	6.06	6.00	6.02	0.04	0.01

^a CV = Coefficient of Variation (Ratio of standard deviation and mean of three replicates)

(b) CO concentration

Throttle Notch Position	Exhaust CO Concentration (vol %)					
	17 Nov	17 Nov	17 Nov	3 Rep	3 Rep	3 Rep
	RY Rep1	RY Rep2	RY Rep3	Avg	Std Dev	CV
Idle	<0.0005	<0.0005	0.001	<0.0005	<0.0005	1.80
1	0.001	<0.0005	<0.0005	<0.0005	0.001	2.26
2	<0.0005	<0.0005	<0.0005	<0.0005	<0.0005	0.92
3	<0.0005	<0.0005	<0.0005	<0.0005	<0.0005	1.22
4	<0.0005	<0.0005	<0.0005	<0.0005	<0.0005	1.00
5	<0.0005	<0.0005	<0.0005	<0.0005	<0.0005	0.45
6	<0.0005	<0.0005	<0.0005	<0.0005	<0.0005	1.12
7	0.012	0.008	0.010	0.010	0.002	0.18
8	0.006	0.007	0.007	0.007	0.001	0.10

^a CV = Coefficient of Variation (Ratio of standard deviation and mean of three replicates)
The values in italics are below the detection limit of the instrument (0.008 vol % for CO).

Table D-2 Continued on next page.

Table D-2 Continued from previous page.

(c) HC concentration

Throttle Notch Position	Exhaust HC Concentration (ppm)					
	17 Nov	17 Nov	17 Nov	3 Rep	3 Rep	3 Rep
	RY Rep1	RY Rep2	RY Rep3	Avg	Std Dev	CV
Idle	<i>1.0</i>	<i>1.7</i>	<i>1.6</i>	<i>1.4</i>	<i>0.37</i>	<i>0.25</i>
1	3.0	3.8	8.8	5.2	3.15	0.60
2	2.6	3.0	7.9	4.5	2.94	0.66
3	6.0	7.4	6.5	6.6	0.69	0.10
4	5.4	8.0	7.0	6.8	1.28	0.19
5	4.8	7.3	6.3	6.1	1.25	0.20
6	6.2	5.5	6.0	5.9	0.36	0.06
7	6.1	6.8	5.9	6.3	0.50	0.08
8	2.6	0.9	1.1	1.5	0.95	0.63

^a CV = Coefficient of Variation (Ratio of standard deviation and mean of three replicates)
The values in italics are below the detection limit of the instrument (13 ppm for HC).

(d) NO concentration

Throttle Notch Position	Exhaust NO Concentration (ppm)					
	17 Nov	17 Nov	17 Nov	3 Rep	3 Rep	3 Rep
	RY Rep1	RY Rep2	RY Rep3	Avg	Std Dev	CV
Idle	206	228	289	241	43	0.18
1	488	375	381	415	64	0.15
2	739	807	816	787	42	0.05
3	1103	1186	1212	1167	57	0.05
4	1083	1159	1174	1139	49	0.04
5	1405	1474	1514	1464	55	0.04
6	1606	1636	1639	1627	18	0.01
7	1632	1661	1640	1644	15	0.01
8	1551	1599	1555	1568	27	0.02

^a CV = Coefficient of Variation (Ratio of standard deviation and mean of three replicates)

Table D-2 Continued on next page.

Table D-2 Continued from previous page.

(e) PM Concentration

Throttle Notch Position	Exhaust PM Concentration ($\mu\text{g}/\text{m}^3$)					
	17 Nov	17 Nov	17 Nov	3 Rep	3 Rep	3 Rep
	RY Rep1	RY Rep2	RY Rep3	Avg	Std Dev	CV
Idle	5.1	6.8	4.7	5.5	1.1	0.20
1	5.6	6.6	5.9	6.0	0.5	0.08
2	6.3	7.2	6.3	6.6	0.5	0.08
3	5.6	6.1	5.9	5.9	0.2	0.04
4	5.5	6.2	5.7	5.8	0.4	0.06
5	6.4	7.0	6.3	6.6	0.4	0.06
6	9.2	11.0	9.3	9.9	1.0	0.10
7	15.9	15.8	13.4	15.0	1.4	0.09
8	11.4	12.6	12.3	12.1	0.6	0.05

^a CV = Coefficient of Variation (Ratio of standard deviation and mean of three replicates)

D.3.2 Fuel use and emission rates

Notch-average fuel use and emission rates were estimated for locomotive NC 1984 based on Axion PEMS measurements of engine activity and exhaust concentrations of selected gases and PM. Mass per time-based and engine output-based emission rates were estimated. Engine-output based emission rates were weighted to the EPA Line-haul cycle to estimate cycle average emission rates. The mass per time-based fuel use rate and emission rates of CO₂, CO, THC, NO_x, and PM are shown in Table D-3.

Notch-average fuel use rate increased monotonically with increasing notch position for all the replicates. Notch-average fuel use rates were highly repeatable at a given notch position. The inter-replicate CV for each of the notch positions was 0.08 or lower for all notch positions except for notch 1. Notch-average CO₂ emission rates have the same trend as fuel use rate because approximately 99 percent of the carbon in fuel is emitted as CO₂. Notch-average CO₂ emission rates were highly repeatable at a given notch position. The inter-replicate CV for each of the notch positions was 0.08 or lower, except for notch 1.

Notch-average CO emission rates were based on CO concentrations below the detection limit of the Axion PEMS for all notch positions except for notch 7. These notch positions had high CVs but CO emission rates were low. Notch-average THC emission rates were based on HC concentrations below the detection limit of the PEMS, resulting in CVs of 0.06 or higher and large inter-replicate variability. However, the THC emission rates were low.

Notch-average NO_x emission rates increased monotonically from idle through notch 8. Notch-average NO_x emission rates were highly repeatable at a given notch position. The inter-replicate CV for each of the notch positions was 0.04 or lower, except for idle and notch 1. Notch-average PM emission rates increased monotonically from idle through notch 7 and decreased for notch 8. Notch-average PM emission rates were repeatable at a given notch position. The inter-replicate CV for each of the notch positions was 0.1 or lower, except for idle.

Table D-3. Notch-Average Mass Per Time-Based Fuel Use and Emission Rates Based on Axion 1 Measured Concentrations for the Prime Mover Engine of Locomotive NC 1984: (a) Fuel Use Rate; (b) CO₂ Emission Rate; (c) CO Emission Rate; (d) THC Emission Rate; (e) NO_x Emission Rate; and (f) PM Emission Rate.

(a) Mass per time-based fuel use rate

Throttle Notch Position	Time-Based Fuel Use Rate (g/s)					
	17 Nov	17 Nov	17 Nov	3 Rep	3 Rep	3 Rep
	RY Rep1	RY Rep2	RY Rep3	Avg	Std Dev	CV ^a
Idle	3.4	3.4	3.9	3.6	0.3	0.08
1	7.7	5.1	5.2	6.0	1.5	0.24
2	15.6	15.0	15.2	15.3	0.3	0.02
3	27.9	27.5	27.9	27.8	0.2	0.01
4	43.6	44.2	44.4	44.0	0.4	0.01
5	56.4	56.5	57.1	56.7	0.4	0.01
6	82.1	81.9	82.2	82.1	0.1	0.00
7	100	98.9	100	100	0.5	0.01
8	102	102	103	103	0.8	0.01

^aCV = Coefficient of Variation (Ratio of standard deviation and mean of three replicates).

(b) Mass per time-based CO₂ emission rate

Throttle Notch Position	Time-based CO ₂ Emission Rate (g/s)					
	17 Nov	17 Nov	17 Nov	3 Rep	3 Rep	3 Rep
	RY Rep1	RY Rep2	RY Rep3	Avg	Std Dev	CV ^a
Idle	11	11	12	11	0.9	0.08
1	24	16	16	19	4.5	0.24
2	49	47	47	48	1.0	0.02
3	87	86	87	87	0.6	0.01
4	136	138	139	138	1.2	0.01
5	176	177	179	177	1.1	0.01
6	257	256	257	257	0.4	0.00
7	312	309	311	311	1.6	0.01
8	320	318	323	320	2.6	0.01

^a CV = Coefficient of Variation (Ratio of standard deviation and mean of three replicates).

Table D-3 Continued on next page.

Table D-3 Continued from previous page.

(c) Mass per time-based CO emission rate

Throttle Notch Position	Time-based CO Emission Rate (g/s)					
	17 Nov	17 Nov	17 Nov	3 Rep	3 Rep	3 Rep
	RY Rep1	RY Rep2	RY Rep3	Avg	Std Dev	CV ^a
Idle	<i><0.005</i>	<i><0.005</i>	<i>0.01</i>	<i><0.005</i>	<i><0.005</i>	<i>1.80</i>
1	<i>0.01</i>	<i><0.005</i>	<i><0.005</i>	<i><0.005</i>	<i>0.01</i>	<i>2.24</i>
2	<i><0.005</i>	<i><0.005</i>	<i><0.005</i>	<i><0.005</i>	<i><0.005</i>	<i>0.93</i>
3	<i><0.005</i>	<i><0.005</i>	<i><0.005</i>	<i><0.005</i>	<i><0.005</i>	<i>0.45</i>
4	<i><0.005</i>	<i><0.005</i>	<i><0.005</i>	<i><0.005</i>	<i><0.005</i>	<i>1.00</i>
5	<i><0.005</i>	<i><0.005</i>	<i><0.005</i>	<i><0.005</i>	<i><0.005</i>	<i>1.34</i>
6	<i><0.005</i>	<i>0.01</i>	<i><0.005</i>	<i><0.005</i>	<i><0.005</i>	<i>1.12</i>
7	<i>0.37</i>	<i>0.26</i>	<i>0.31</i>	<i>0.31</i>	<i>0.06</i>	<i>0.18</i>
8	<i>0.21</i>	<i>0.24</i>	<i>0.25</i>	<i>0.23</i>	<i>0.02</i>	<i>0.10</i>

^a CV = Coefficient of Variation (Ratio of standard deviation and mean of three replicates).
 Values in italics correspond to estimates based on concentrations below-detection limit.

(d) Mass per time-based THC emission rate

Throttle Notch Position	Time-based HC Emission Rate ^b (g/s)					
	17 Nov	17 Nov	17 Nov	3 Rep	3 Rep	3 Rep
	RY Rep1	RY Rep2	RY Rep3	Avg	Std Dev	CV ^a
Idle	<i>0.01</i>	<i>0.01</i>	<i>0.01</i>	<i>0.01</i>	<i>0.00</i>	<i>0.25</i>
1	<i>0.02</i>	<i>0.03</i>	<i>0.06</i>	<i>0.04</i>	<i>0.02</i>	<i>0.59</i>
2	<i>0.02</i>	<i>0.03</i>	<i>0.07</i>	<i>0.04</i>	<i>0.03</i>	<i>0.65</i>
3	<i>0.07</i>	<i>0.09</i>	<i>0.08</i>	<i>0.08</i>	<i>0.01</i>	<i>0.10</i>
4	<i>0.10</i>	<i>0.14</i>	<i>0.13</i>	<i>0.12</i>	<i>0.02</i>	<i>0.18</i>
5	<i>0.09</i>	<i>0.14</i>	<i>0.12</i>	<i>0.12</i>	<i>0.02</i>	<i>0.20</i>
6	<i>0.14</i>	<i>0.12</i>	<i>0.14</i>	<i>0.13</i>	<i>0.01</i>	<i>0.06</i>
7	<i>0.15</i>	<i>0.17</i>	<i>0.15</i>	<i>0.15</i>	<i>0.01</i>	<i>0.07</i>
8	<i>0.07</i>	<i>0.02</i>	<i>0.03</i>	<i>0.04</i>	<i>0.02</i>	<i>0.64</i>

^a CV = Coefficient of Variation (Ratio of standard deviation and mean) of three replicates).

^b HC concentrations measured with Axion PEMS were multiplied with a bias-correction factor estimated in prior work to obtain THC concentrations.

Table D-3 Continued on next page.

Table D-3 Continued from previous page.

(e) Mass per time-based NO_x emission rate

Throttle Notch Position	Time-Based NO _x Emission Rate ^b (g/s)					
	17 Nov	17 Nov	17 Nov	3 Rep	3 Rep	3 Rep
	RY Rep1	RY Rep2	RY Rep3	Avg	Std Dev	CV ^a
Idle	0.32	0.35	0.44	0.37	0.06	0.17
1	0.76	0.56	0.57	0.63	0.11	0.18
2	1.59	1.68	1.71	1.66	0.06	0.04
3	3.07	3.25	3.34	3.22	0.14	0.04
4	4.43	4.71	4.79	4.64	0.19	0.04
5	6.09	6.32	6.52	6.31	0.22	0.03
6	8.23	8.34	8.40	8.32	0.09	0.01
7	9.05	9.15	9.10	9.10	0.05	0.01
8	9.11	9.24	9.22	9.19	0.07	0.01

^a CV = Coefficient of Variation (Ratio of standard deviation and mean of three replicates).

^b NO concentrations measured with the Axion PEMS were multiplied with a bias-correction factor estimated in prior work to estimate NO_x concentrations.

(f) Mass per time-based PM emission rate

Throttle Notch Position	Time based PM Emission Rate ^b (g/s)					
	17 Nov	17 Nov	17 Nov	3 Rep	3 Rep	3 Rep
	RY Rep1	RY Rep2	RY Rep3	Avg	Std Dev	CV ^a
Idle	0.02	0.03	0.02	0.02	0.00	0.20
1	0.02	0.03	0.02	0.02	0.00	0.07
2	0.03	0.04	0.03	0.04	0.00	0.07
3	0.04	0.04	0.04	0.04	0.00	0.03
4	0.06	0.06	0.06	0.06	0.00	0.06
5	0.07	0.08	0.07	0.07	0.00	0.05
6	0.12	0.14	0.12	0.13	0.01	0.10
7	0.23	0.22	0.19	0.21	0.02	0.09
8	0.17	0.19	0.19	0.18	0.01	0.05

^a CV = Coefficient of Variation (Ratio of standard deviation and mean of three replicates).

^b PM emission rates estimated with Axion measurements were multiplied by a factor of 5 to account for total PM.

Mass per time-based notch-average emission rates were divided by notch-average net engine output corresponding to each notch to estimate notch-average engine output-based emission rates. Engine output-based notch-average emission rates were weighted to the EPA line-haul duty cycle to estimate cycle average emission rates. The results are shown in Table D-4. The measured cycle average NO_x emission rates were higher than the Tier 0+ standard for each of the three replicates. Cycle average CO and HC emission rates were lower than the Tier 2+ standard. The estimated cycle average PM emission rates were higher than the Tier 0+ standard.

Table D-4. EPA Line-Haul Duty Cycle-Based Average Emission Rates for the Prime Mover Engine of Locomotive NC 1984

Results	NO _x ^b	CO	HC ^b	PM ^c
	[g/bhp-hr]	[g/bhp-hr]	[g/bhp-hr]	[g/bhp-hr]
Replicate 1	15.3	0.2	0.20	0.31
Replicate 2	15.6	0.2	0.20	0.35
Replicate 3	15.9	0.2	0.22	0.32
Average	15.6	0.2	0.21	0.33
CV ^d	0.02	0.02	0.05	0.06
Tier 0+	8.0	5.0	1.00	0.22
Tier 1+	7.4	2.2	0.55	0.22
Tier 2+	5.5	1.5	0.30	0.10

^a EPA Line-Haul includes dynamic brake. Since dynamic brake measurements were not conducted due to the unavailability of the dynamic braking grid, time spent in the dynamic brake is assigned to idle.

^b NO_x and HC emission rates have been estimated from bias-corrected Axion PEMS measured NO and HC concentrations using factors estimated in prior work.

^c PM emission rates estimated with Axion measurements have been multiplied by a factor of 5 to account for total PM.

^d CV = Coefficient of Variation (Ratio of standard deviation and mean of three replicates).

D.3.3 Comparison with prior rail yard measurements

Notch-average engine activity variables and FUEP estimated here were compared to prior rail yard measurements of the same locomotive to determine whether there are differences between the prior and most recent measurements. Notch-average engine activity variables for each of these measurements are given in Figure D-2. Notch-average engine RPM was comparable among the measurements. IAT is affected by ambient temperature and notch position. The ambient temperature on 1/25/2018 and 11/17/2020 was 35 F° and 38 F°, respectively. Given varying ambient conditions between the two measurements, it was expected that IAT would vary. However, based on the use of absolute temperature, IAT was within 2 to 5 percent of each other for a given notch position.

Notch-average MAP was within $\pm 1\%$ of each other for all notch positions, except for notches 7 and 8. For notches 7 and 8, the average MAP for the current measurement was 4.5% and 2.5% lower than the prior measurement. FUEs are directly related to MAP. A 4.5% and 2.5% decrease in MAP results in a decrease of 3.4% and 1.6% in FUEs, respectively, if other variables remain the same. Relative trends of notch-average RPM, IAT, and MAP were similar among the two measurements.

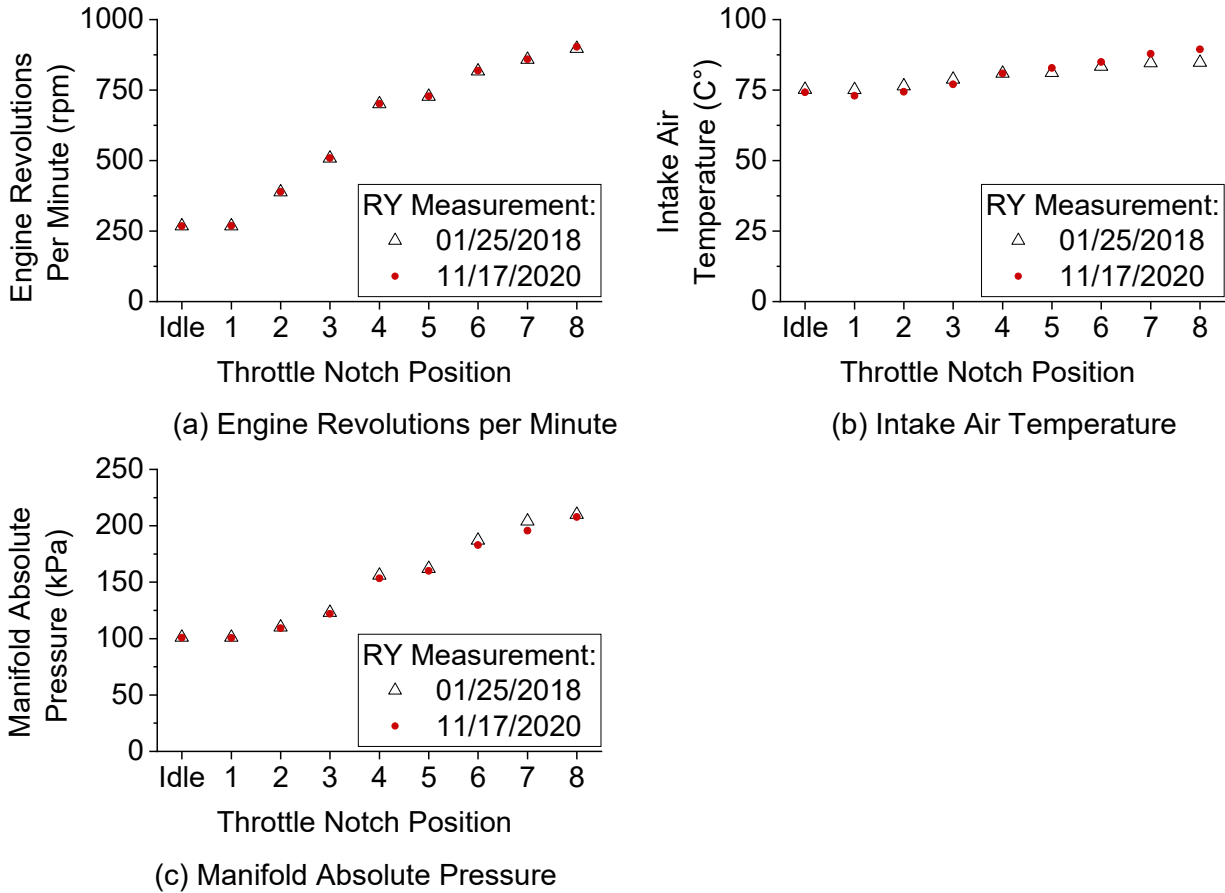


Figure D-2. Comparison of Notch-Average Engine Activity Variables Measured Based on Axion 1 for the Prime Mover Engine of Locomotive NC 1984 Among Rail Yard Measurements Conducted on 11/17/2020 versus 01/25/2018: (a) Engine Revolutions per Minute; (b) Intake Air Temperature; and (c) Manifold Absolute Pressure.

Notch-average measured concentrations of CO₂, CO, HC, NO, and PM are compared to the prior RY measurement in Figure D-3. For idle and notches 1 through, average CO₂ concentrations were approximately similar. For notch 7 and notch 8, CO₂ concentrations for the most recent measurements were up to 16% higher. However, the relative trends in notch-average concentrations among the two measurements were similar to each other. Compared to the previous measurement, an increase in CO₂ concentration indicates an increase in fuel use rate. For example, at notch 8, a 10% increase in CO₂ concentration versus the previous measurement would lead to a 4.1% increase in fuel use rate and a 5.1% decrease in emission rates if all other factors are held constant. This difference in measured concentrations is not because of an error

because the Axion 1 was properly calibrated and inspected for malfunctions before each measurement. Thus, this increase in CO₂ concentrations indicative of increased fuel use rate since prior measurement.

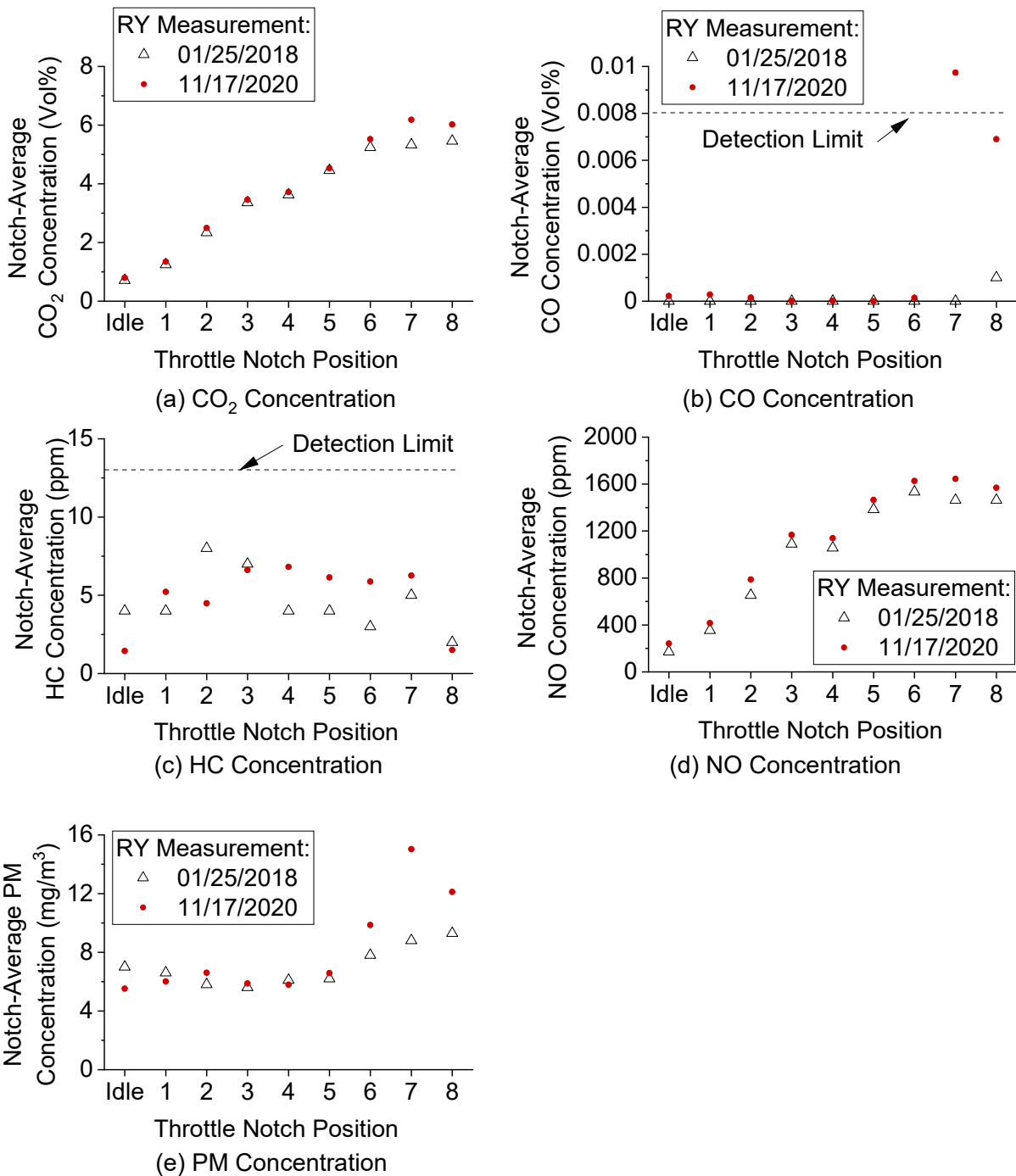


Figure D-3. Comparison of Notch-Average Prime Mover Engine-Out Exhaust Concentrations Based on Axion 1 for Locomotive NC 1984 Among Rail Yard Measurements Conducted on 11/17/2020 versus 01/25/2018: (a) CO₂; (b) CO; (c) HC; (d) NO; and (e) PM.

Notch-average CO concentrations were approximately similar to those of the prior measurements for idle and notches 1 through 6. For notches 7 and 8, average CO concentrations differed between measurements. Average CO concentrations for notches 7 and 8 in the prior measurement were below the detection limit. In the recent measurement, average CO concentration at notch 7 was only 13% higher than the detection limit, and at notch 8 was below the detection limit. Therefore, the differences between notch-average concentrations were not significant. Notch-average CO concentrations were similar among measurements.

Notch-average HC concentrations were below the detection limit of the Axion 1 for each notch position for recent and prior measurements. Therefore, the differences between notch-average concentrations were not significant.

Notch-average NO concentrations were approximately similar to those of the prior measurements for idle and notches 1 through 6. Average NO concentration for notches 7 and 8 for the recent measurements were consistently higher by 7% to 12% compared to the prior measurements. However, the relative trends in notch-average NO concentrations were similar.

Notch-average PM concentrations in the recent measurements were approximately constant for idle and notches 1 through 5, and increased monotonically at higher notches. Similar relative trends were measured previously. For notches 6 through 8, average PM concentrations measured recently were higher by 23% to 70%. An increase in PM concentrations indicates a potential increase in PM emission rates.

Time-based notch-average FUEs are compared for the recent and prior measurements in Figure D-4. Notch-average fuel use rates for the recent measurements were approximately similar to those of the prior measurements for idle and notches 1 through 6. For notches 7 and 8, fuel use rates were 16% and 7% higher, respectively. The increases in fuel use rates for each notch position were not the same as the increases in notch-average CO₂ concentrations. As explained earlier in this Section, an example 10% increase in CO₂ concentration leads to a 4.1% increase in fuel use rate if other factors are held constant. For notches 7 and 8, lower average MAP partly compensated for higher CO₂ concentrations. The highest increase in fuel use rate was measured for notch 7. However, in real-world operations, very little time (typically less than one percent) is spent in notch 7. Therefore, an increase in average fuel use rate at notch 7 will have an insignificant effect on trip fuel use and cycle average fuel use rates. The relative trends in fuel use rate among the measurements were similar to each other.

Notch-average CO and HC emission rates were mostly based on concentrations below the detection limit of the PEMS. However, in general, CO and HC emission rates for recent measurements were higher than for prior measurements, especially for notches 7 and 8.

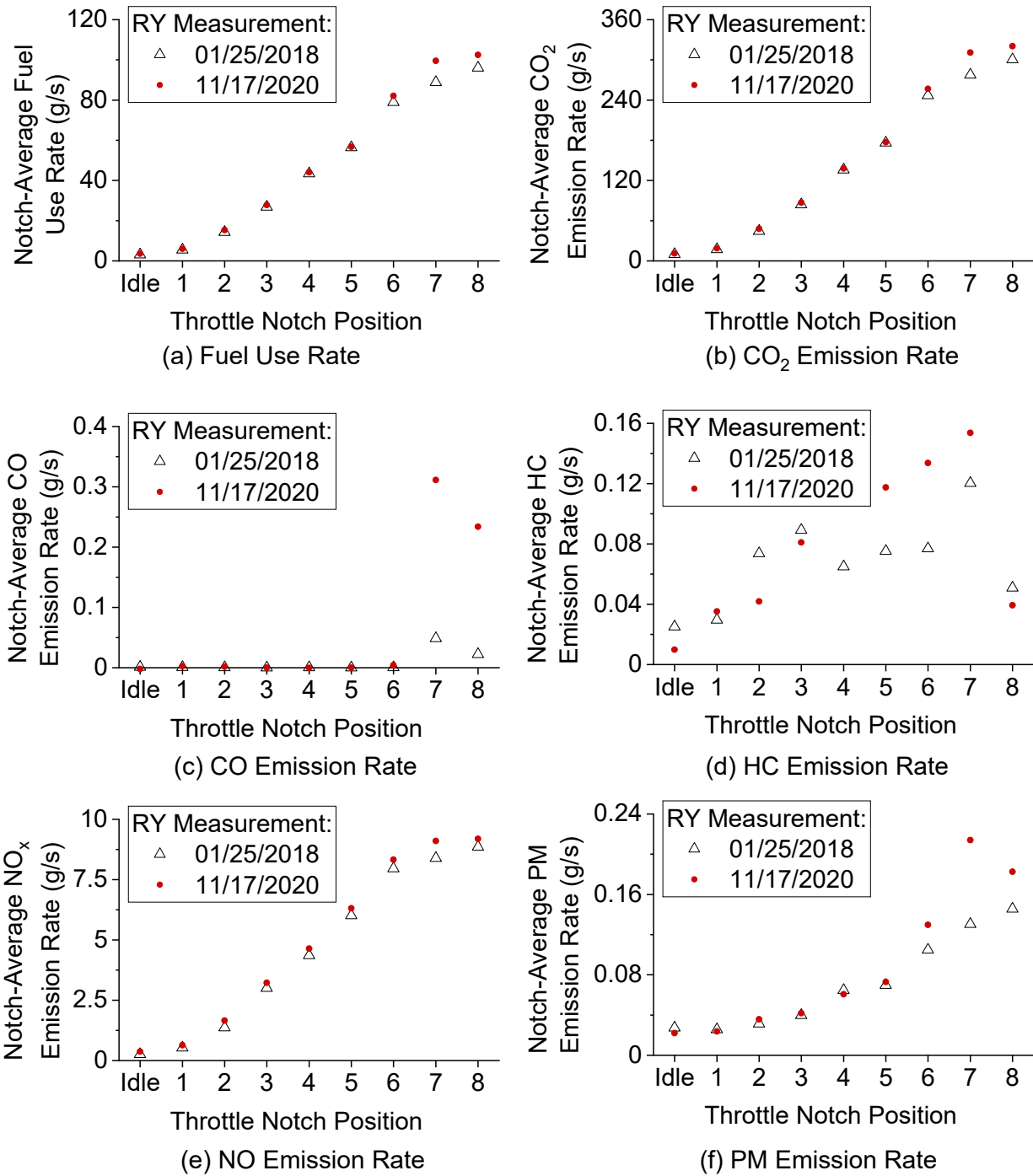


Figure D-4. Comparison of Notch-Average Prime Mover Engine-Out Fuel Use and Emission Rates Based on Axion 1 for Locomotive NC 1984 Among Rail Yard Measurements Conducted on 11/17/2020 versus 01/25/2018: (a) Fuel Use; (b) CO₂; (c) CO; (d) HC; (e) NO; and (f) PM.

Notch-average NO_x emission rates for recent measurements were approximately similar to those for prior measurements for idle and notches 1 through 6. For notches 7 and 8, NO_x emission rates were 8% and 4% higher, respectively. Higher NO_x emission rates were due to higher measured NO concentrations. However, the differences in NO_x emission rates were not the same as the differences in NO concentrations because of differences in notch-average CO₂ concentrations and MAP, which negated some of the effects of increased NO concentrations. The relative trends in NO_x emission rates were similar among the measurements.

Notch-average PM emission rates for the recent measurements were generally similar to those of the prior measurements for idle and notches 1 through 5, and 24% to 64% higher for notches 6 through 8. The highest difference of 64% was measured for notch 7. Likewise compared to fuel use rates, this difference has an insignificant effect on trip PM emissions and cycle average PM emission rates. The relative trends in notch-average PM emission rates were similar among recent and prior measurements.

Overall, FUERs in recent measurements were typically similar to those of the prior measurements for idle and notches 1 through 6. Higher FUERs were measured for notches 7 and 8 in the recent measurements. The highest difference in FUERs among measurements was measured for notch 7, and the difference at notch 8 was typically less than 10%. Consistently measured similar FUERs for notches 6 and lower indicate that the measurement was robust for these notches. Differences in notch-average engine activity variables, notch-average exhaust gas and PM concentrations, and FUERs for notches 7 and 8 indicate an underlying change in the PME operation. However, the difference in notch 7 will have a low impact on cycle-average FUERs and trip total fuel use and emissions as operators typically spend less than one percent of trip duration in notch 7. Most time is spent in idle and notch 8.

D.3.4 Benchmarking two Axion PEMS

Two Axions were benchmarked to each other. Pollutant concentrations measured with Axion 1 were benchmarked to Axion 2. The comparison is presented in Figure D-5.

The plot of notch-average CO₂ concentrations is well described by the line $y=x$. Hence, notch-average CO₂ concentrations measured with both PEMS were comparable to each other. The notch-average CO₂ concentrations were similar to within $\pm 18\%$ for idle and notch 1 and within $\pm 3\%$ for notches 2 and higher. The notch-average CO₂ concentrations at idle and notch 1 were relatively lower than for other notch positions. Therefore, the absolute differences in notch-average CO₂ concentrations were low.

Notch-average CO and HC concentrations were typically below the detection limit of both the Axions. Therefore, differences between the average CO and HC concentrations were insignificant.

The notch-average NO concentrations were similar to the line $y=x$, except for Replicate 3. The NO concentrations from Axion 2 were systematically underestimated for this replicate, indicating drift or malfunction of Axion 2. Excluding Replicate 3, measured concentrations were typically similar to within $\pm 6\%$ for both Axions.

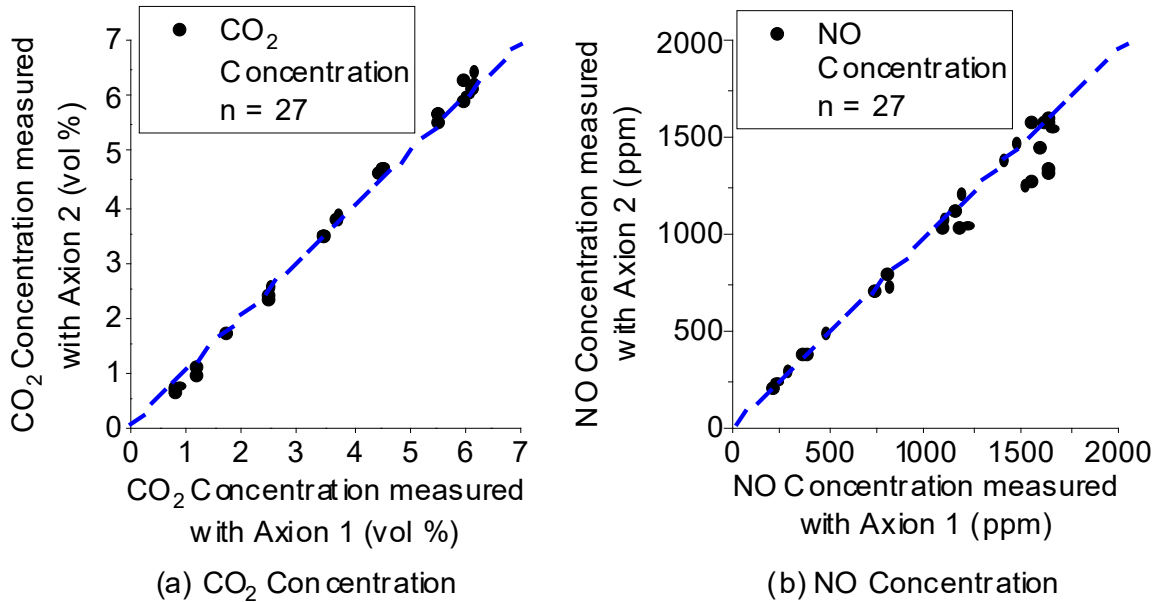


Figure D-5. Benchmarking Axion PEMS Concentration Measurements for Bias-Correction for Future Planned Measurements with Two PEMS: (a) CO₂; and (b) NO.

The blue dashed line in each panel indicates the line $y = x$.

CO and HC concentrations were typically below the detection limit of both the Axions. Therefore, the differences between the two Axions were insignificant. PM concentrations were noisy indicating a need for maintenance or repair of the PM sensor.

Notch-average PM concentrations measured with Axion 2 were noisy and did not show a typical trend of monotonically increasing PM concentrations with notch position that was measured for each Replicate of Axion 1, indicating a need for maintenance or repair of the Axion 2 PM sensor.

In general, the concentrations measured with both PEMS were similar to each other, except for PM. Thus, there is no bias in measurements of CO₂, CO, HC, and NO concentrations. A need for maintenance of the PM sensor of Axion 2 was identified.

D.4 Conclusions

A revised baseline for NC 1984 was quantified based on railyard measurements. The most recent baseline results indicate that the current NO_x and PM emission rates for locomotive NC 1984 are higher than the Tier 0+ standard. Thus, interventions to reduce these emissions should be considered, such as retrofit of an emission control system.

Compared to a prior RY measurement, engine RPM, IAT, and MAP variables were similar. Average concentrations and FUERs for idle and notches 1 through 6 were also similar. For notches 7 and 8, average concentrations and FUERs were higher for recent measurements. These differences were because of changes in the exhaust composition. However, the relative trends of notch-average pollutant concentrations and FUERs were similar among measurements, indicating that the measurements were robust. Changes in the condition of the PME can lead to changes in FUER. The underlying changes in locomotive PME indicate that a PME should be measured periodically to assess the impact of such changes and to quantify FUER representative of the current PME operation.

The notch-average concentrations measured with both PEMS were typically similar to each other, except for PM. Thus, there is no bias in measurements of CO₂, CO, HC, and NO concentrations. A need for maintenance of the PM sensor of Axion 2 was identified.

D.5 References Cited in Appendix D

Frey, H.C., Rastogi, N., 2020. Quarterly Progress Report: Development of New Over-the-Rail Measurement Protocols Considering Restrictions Imposed by Amtrak. Prepared by North Carolina State University for North Carolina Department of Transportation.

Frey, H.C., Rastogi, N., 2019. Quarterly Progress Report: Baseline Rail Yard Fuel Use and Emission Rates for the Prime Mover Engine of Locomotive NC 1871. Prepared by North Carolina State University for North Carolina Department of Transportation.